Synthesis methods for multi-band coupled resonator filters

by

Tobias Gerhardus Brand

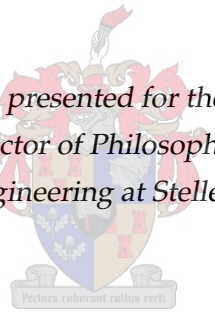

Dissertation presented for the degree of
Doctor of Philosophy
in the Faculty of Engineering at Stellenbosch University

Promoters:

Prof. Petrie Meyer
Department of Electrical and Electronic Engineering
University of Stellenbosch

Prof. Riana Geschke
Department of Electrical and Electronic Engineering
University of Cape Town

December 2014

Declaration

By submitting this dissertation electronically, I declare that the entirety of the work contained therein is my own, original work, that I am the sole author thereof (save to the extent explicitly otherwise stated), that reproduction and publication thereof by Stellenbosch University will not infringe any third party rights and that I have not previously in its entirety or in part submitted it for obtaining any qualification.

December 2014

Abstract

In this dissertation a number of techniques to design multi-band filters, with specific focus on coupled resonator implementations, is presented. Multi-band transfer functions are constructed from single-band transfer functions using frequency mapping methods. A general class of rational mapping functions is presented that can accommodate arbitrary bandwidth specifications. Multi-band circuits are synthesised directly from multi-band transfer functions and are obtained by applying reactance transformations to single-band prototype circuits. For the direct synthesis of multi-band filters from multi-band transfer functions coupling matrix synthesis methods are employed. The circuits that result from matrix synthesis methods tend to have topologies that are undesirable from a practical perspective and must be simplified using rotations of the coupling matrix. The synthesis of multi-band filters through reactance transformations is both simple and result in filters that have practical topologies for realisation as coupled resonator circuits. Multiple filters are designed using different design methodologies and different transmission line technologies to illustrate the various design possibilities. The designs include both all-pole and cross-coupled filters and employ single-layer stripline, multi-layer stripline as well as coaxial resonators as transmission line technologies for the implementations.

Uittreksel

In hierdie proefskrif word verskeie ontwerpstegnieke vir multi-band filters aangebied en word daar spesifiek klem gelê op filters wat as gekoppelde resoneerder strukture geïmplimenteer kan word. Multi-band oordragsfunksies word geskep uit enkelband oordragsfunksies deur gebruik te maak van wiskundige afbeeldingstegnieke. 'n Spesiale klas van rasionale funksies word voorgestel wat spesifiek gebruik kan word om multi-band funksies te skep wat 'n arbitrêre bandwydte spesifikasie het. Multi-band stroombane word direk gesintetiseer vanuit multi-band oordragsfunksies en word ook verkry deur die toepassing van reaktansietransformasies op enkelband stroombane. Vir die direkte sintese van multi-band stroombane vanuit multi-band oordragsfunksies word stroombane gesintetiseer as koppelmatrikse. Stroombane wat op hierdie wyse gesintetiseer word is geneig om topologieë te hê wat nie baie gesog is vanuit 'n praktiese perspektief nie en matriks rotasies word dan hier ingespan om die stroombane se topologieë te vereenvoudig. Die sintese van multi-band stroombane deur gebruik te maak van reaktansietransformasies is beide eenvoudig en lei tot stroombane wat praktiese topologieë het vir implimentering as gekoppelde resoneerder strukture. Die ontwerpsmoontlikhede wat die verskillende metodieke bied word geïllustreer deur die ontwerp van verskeie filters op verskillende maniere waar daar gebruik gemaak word van verskeie transmissielyn tegnologië. Die filter ontwerpe sluit filters in waar alle transmissienulle by oneidige frekwensies is, sowel as gevalle waar somige transmissienulle by eindige frekwensies is. Die filters word geïmplimenteer deur gebruik te maak van koaksiale resoneerders sowel as enkellaag en multilaag strooklyn.

Acknowledgements

I would like to express my sincere gratitude to the following individuals or entities who directly or indirectly contributed to the completion of this project:

- God
- The University of Stellenbosch, for financial aid and the usage of their facilities.
- My family, for their continued love and unfailing support.
- Prof. Riana Geschke for her optimism and valuable insight.
- Prof. Petrie Meyer for his support and enthusiasm.

"There but for the grace of God, go I" – John Bradford

Contents

List of Figures

List of Tables

Nomenclature

Acronyms

SIR	Stepped Impedance Resonator.
RLC	Resistors, Inductors and Capacitors.
TEM	Transverse Electromagnetic.
TE	Transverse Electric.
TM	Transverse Magnetic.
LTI	Linear Time-Invariant.
FIR	Frequency Invariant Reactance.
LTCC	Low-temperature cofired ceramic.

Mathematical conventions

j	The complex number $\sqrt{-1}$.
$\Re\{z\}$	Real part of complex number z.
$\Im\{z\}$	Imaginary part of complex number z.
z^*	Complex conjugate of z.
$\|z\|$	Modulus/Absolute value of complex number z.
$\mathbf{A}$	Bold capital letters represent matrices.
$\mathbf{A}^T$	Transpose of the matrix $\mathbf{A}$.
$\|\mathbf{A}\|$	Determinant of the matrix $\mathbf{A}$.
$\mathbf{A}_{i\,j}$	The j-th element in the i-th row of matrix $\mathbf{A}$.
$(\cdot)_{i\,j}$	The j-th element in the i-th row of matrix enclosed in parenthesis.
$\mathbf{U}$	The identity matrix.
$k \in \mathbb{Z}$	The variable k is an integer.
$k \in \mathbb{N}$	The variable k is a natural number.
$\mathcal{F}\{h(t)\}$	The Fourier transform of $h(t)$.
$\mathcal{F}^{-1}\{H(s)\}$	The inverse Fourier transform of $H(s)$.
$F(s) = \mathcal{L}\{f(t)\}$	The Laplace transform of $f(t)$.
$f(t) = \mathcal{L}^{-1}\{F(s)\}$	The inverse Laplace transform of $F(s)$.
$f(t) * g(t)$	The convolution product of $f(t)$ and $g(t)$.
$\vec{v_i} \cdot \vec{v_j}$	The dot product of the vectors $\vec{v_i}$ and $\vec{v_j}$.

$\|\|\vec{v_i}\|\|$	The magnitude of the vector $\vec{v_i}$.
$\det\|\mathbf{A}\|$	The determinant of the matrix $\mathbf{A}$.
$A^{'}(x)$	The derivative of the function $A(x)$ with respect to x.

Circuit symbols

f_0	Centre frequency in Hertz.
N	Order of a filter response. Numerically equal to the number of reactive elements in the prototype domain.
n_{fz}	The number of transmission zeros located at finite frequencies.
ω_0	Centre frequency in radians per second.
Δ	Fractional bandwidth.
$\mathbf{Z}$	Impedance parameters of a two-port.
$\mathbf{Y}$	Admittance parameters of a two-port.
Z_{DP}	Driving point impedance function.
$\mathbf{M}$	The coupling matrix.
x	The reactance slope of a series resonator.
b	The susceptance slope of a shunt resonator.
q_e	The external quality factor of a resonator.
λ_g	The guided wavelength.
θ	Electrical length in radians.
$\angle H(S)$	The phase of the transfer function $H(S)$.
Ω'	The single-band prototype frequency variable in rad/s.
Ω	The multi-band prototype frequency variable in rad/s.
ω	The actual frequency variable of a final filter in rad/s.
S'	The complex single-band prototype frequency variable ($S' = j\Omega'$).
S	The complex multi-band prototype frequency variable ($S = j\Omega$).
s	The actual complex frequency variable of a final filter ($s = j\omega$).

Chapter 1

Introduction

1.1 Motivation for research

The closing decades of the twentieth century saw a massive increase in global communication traffic. The dawn of the computer age and the subsequent birth of the Internet has resulted in an unrivalled increase in communication products and services. Advances in technology has made it possible to produce mobile devices that have enough computational power to run operating systems with various application programs. Most of these, so called *Smart devices*, can connect to the Internet and can therefore offer the user a myriad of communication services. When the mobile market emerged in the eighties, the total number of mobile subscribers numbered in the tens of thousands. That number has increased into the billions in less than two decades, with congestion of the spectrum as a result. In order to remedy this situation, engineers have developed various network access technologies and protocols that define how information must be send and received to maximise the usage of the spectrum. However there is no international consensus on spectrum usage and different access technologies often have different spectrum allocations in different countries [1].

The absence of a standard spectrum allocation presents a problem for hardware designers. They must either develop a different device for each spectrum allocation or develop a single device that can operate in multiple frequency bands. For mass production purposes, it would be financially better to have a single communication device that could operate in multiple frequency bands. From a hardware perspective, there are two ways to achieve this:

1. Multiplex multiple single-band RF-chains inside the device. Each RF-chain is responsible for a different frequency band.

2. Include a single multi-band RF-chain inside a device.

Including multiple RF-chains inside a device is unrealistic for mobile devices because it would greatly increase the size of the device. A multi-band RF-chain is an elegant solution to the problem. RF-chains generally consist of a combination of filters, antennas, amplifiers, mixers and oscillators. Designing a multi-band RF-chain implies that one must adapt each of these subsystems for multi-band operation.

This dissertation presents a number of design techniques and physical implementations of one of these subcircuits, namely multi-band filters, with a specific focus on coupled resonator filters.

1.2 A brief history of filter synthesis

The literature study will be conducted in three separate parts. First we shall provide a historic overview of filter synthesis. Then we shall discuss the origins of coupled resonator filters and the associated concept of a coupling matrix. This will be followed by an investigation into the various approaches to the design of multi-band filters. From the conducted literature study we shall draw conclusions and define the context of the contributions made in this dissertation. The literature study does not serve as an exhaustive list of publications, but rather provides an overview of the major relevant developments.

1.2.1 The development of filter synthesis

Filter design is a well-established field. It indirectly emerged from general electromagnetic theory in the nineteenth century. Oliver Heaviside was an English researcher who simplified Maxwell's original equations using vector calculus. He introduced a mathematical model for transmission lines and is credited with introducing concepts such as impedance and admittance [2]. Heaviside postulated that the distortion of electric signals on transmission lines could be reduced if the transmission lines were periodically loaded with inductors. The periodic loading of transmission lines with inductors would increase the unloaded quality factor of the distributed inductance (this is usually lower than the unloaded quality factor of the distributed capacitance). This idea was not originally accepted because researchers assumed increased inductance would retard signals. In reality signals do experience an increase in time delay but a decrease in distortion [3]. Heaviside's ideas where practically implemented by Campbell at the AT&T telephone company. Periodic loading greatly increased the operational range of telephone lines. Campbell also discovered that loaded transmission lines would attenuate signals if they had frequencies higher than a certain cuttoff frequency. The cutoff frequency was dependant on the spacing and size of the coils. Cambell realised that should the loading coils be moved closely together, the transmission line structure would reduce to an iterative ladder structure consisting of capacitors and inductors. These structures were the first electric filters [3].

Cambell designed his filters from a transmission line perspective. He assumed that a filter consists of an infinite chain of transmission line sections. He would then design the propagation constants of the sections to obtain a passband. The first and last sections must be terminated in an *image impedance* in order to obtain the correct transfer characteristics. The image impedance is just the characteristic impedance of the line. Unfortunately the image impedance is usually complex and it was mathematically shown that it is impossible to construct the impedance using a discrete number of components [3]. Nonetheless the image impedance can be approximated and practical filters can be designed. Cambell's filter design technique became known as the *image parameter method*. The image parameter method was simple to use because the nett propagation constant of the entire filter would just be the sum of the propagation constants of the various sections (if the terminations were close to the required image impedance). Zobel (also from AT&T) extended Cambell's ideas and introduced various filter sections that can be cascaded to obtain desired frequency characteristics. By the 1920's an entire catalogue of filter sections were available that could be used to obtain filters for most practical specifications [4]. The image parameter technique did not result in exact designs but the results obtained were adequate.

In 1924 Foster introduced an alternative view on the analysis of filters. He introduced the concept of a driving point impedance function – the impedance connected to the generator. He showed that a filter could be realised if the driving point impedance is expanded as a sum of inductors and capacitors. He also introduced the idea that filter characteristics are described by the zeros and poles of the driving point impedance [5]. Cauer recognised the significance of Foster's work and formulated a general design technique for one-port circuits

consisting out of two elements. He showed that it is possible to design a desired driving point impedance function, gave conditions for its realisability and showed that the network could be extracted using continued fractions [3]. The synthesis of one-port networks in two types of elements was now solved. In 1931 Brune extended the technique for general one-port circuits. He also discovered that the driving point impedance of all realisable networks are positive real (rational) functions. The problem with Brune's synthesis technique was that it employed ideal transformers. It was later shown in 1949 by Bott and Duffin that any positive real driving point impedance could be synthesised using only resistors, capacitors and inductors [4].

At this stage researchers started to discover that certain mathematical functions are well-suited to approximate user specifications. In 1930 Butterworth applied the maximally flat condition to the design of amplifiers. In 1931 Cauer realised that Chebyshev polynomials have agreeable characteristics and approximated the desired frequency responses for a class of image parameter filters using said polynomials [3]. Between 1937 and 1939 Norton and Darlington introduced the *insertion loss method*. This is an extension of Foster, Cauer and Brune's work to accommodate two-port networks. The insertion loss method consists of two primary stages. During the first stage designers specify the required insertion loss as a function of frequency. This is the insertion loss an input signal experiences as it propagates through the network. It is common practice to use Butterworth or Chebyshev functions to approximate the required insertion loss function. Consequently, this stage of the design is referred to as the approximation problem. During the next stage of the design a doubly terminated circuit is extracted that has the required insertion loss. This part of the design is referred to as the synthesis problem. Darlington provided a theorem that stated that the only resistors necessary to synthesise certain networks are the source and load resistors. The rest of the elements can be purely reactive. Reactive networks with equal resistive terminations are ideally suited for filter applications. This is because the networks themselves do not dissipate any energy. Maximum power transfer can be obtained as the load impedance and the source impedance can be chosen as complex conjugates of each other [4].

The problem with the insertion loss method is that it is mathematically intensive. Researchers tried to overcome this problem by tabulating design values for reference filters. These reference filters were traditionally referred to as *prototype filters*. They were usually lowpass filters with a cutoff frequency of 1 rad/s and operated in a 1 Ω environment. Designers can use them as a starting point for a design. Using a prototype filter for a design is a two step process. First the prototype is transformed into a bandpass, bandstop or highpass filter depending on the specification. This is accomplished by replacing all the reactive components with well-defined subcircuits. This process is dubbed *reactance mapping*. The prototype must then be denormalised with respect to impedance, bandwidth and centre frequency [2]. This will result in a RLC circuit that has the required insertion loss function. The final circuit is referred to as the denormalised filter. The insertion loss method forms the basis of most of the later filter design techniques. This includes the design of coupled resonator filters. Next we shall investigate the origins of coupled resonator filters and the associated concept of a coupling matrix.

1.2.2 The origins of coupled resonator filters and coupling matrices

World War II started in 1939 and this signalled the start of an era of rapid development in microwave engineering. Researchers developed high-frequency electronic systems for military applications. Great strides were made in the design of microwave filters. In most design techniques the insertion loss method is first used to obtain an initial circuit consisting out of inductors, capacitors and resistors. A microwave filter is then constructed by finding a distributed structure that behaves like the synthesised network over a finite bandwidth. There are numerous physical structures available that can be used to implement filters. The choice of structure depends on the centre frequency of the filter and the bandwidth of the filter. Wider bandwidth filters are gener-

ally designed using Richard's transformation and narrowband filters are generally designed using the coupled resonator approach [2]. Coupled resonator circuits can be fully described using three fundamental parameters: the centre frequency of each resonator, the coupling between adjacent resonators and the external quality factors of the resonators connected to the source and to the load [6]. Milton Dishal was the first researcher to note that narrowband filters are in essence a group of resonators that are connected in a string between the source and the load (initially resonators were not coupled to non-adjacent resonators). This configuration is referred to as an inline configuration. Numerous realisations of coupled resonator filters were then published, each with its own design formulas to relate the insertion loss prototypes to the microwave devices [7, 8].

The next major breakthrough was when researchers realised that it is not necessary to have a set of unique formulas to design every different type of coupled resonator filter. Matthaei, Young and Jones introduced the susceptance/reactance slope parameter to completely generalise coupled resonator filter design. With the use of the susceptance/reactance slope parameter it was possible to use the same formulas for all coupled resonator filters irrespective of the type of resonator used in the circuit [9].

In the 1960's and 1970's the demands on filter performance in satellite communication systems became more stringent. Conventional coupled resonator filters, connected in the inline topology, had to contain too many elements to reach the selectivity requirements. Researchers realised that elliptic filter functions can be approximated if couplings between non-adjacent resonators are allowed. Couplings between non-adjacent resonators are referred to as cross-couplings. Filters could be realised in smaller structures and have better selectivity if cross-couplings are included. It must however be stated that filters in the inline topology have a flatter group delay response than those containing cross-couplings. The introduction of cross-couplings results in better selectivity at the cost of increased group delay distortion.

The synthesis of coupled resonator circuits containing cross-couplings is however a nontrivial problem. In 1970 Williams published an article on the design of a fourth-order cross-coupled waveguide filter [10]. In this article he introduced the concept of a *coupling matrix*. This idea was novel because both a filter's response and its topology could be described by a single matrix. The synthesis technique Williams proposed was laborious and revolved around the idea of equating the coefficients of two transmission polynomials. The one polynomial was generated using the circuit and the other was the result of the approximation problem (a step in the insertion loss method). Even though the technique worked, it was impractical for higher order designs and/or any design containing more cross-couplings. Fortunately researchers soon realised that matrices that represent circuits have some mathematical properties that could be exploited to greatly simplify their synthesis. A general synthesis technique for an N-th order coupled resonator filter, producing a maximum of $N-2$ finite frequency transmission zeros, was developed and published by Atia and Williams [11, 12]. Atia's technique is based on the insertion loss method. The technique was simple to apply but the topologies of the synthesised circuits were generally undesirable. Atia and Williams solved this problem by developing a coupling matrix reduction technique. Their technique is to apply successive similarity transformations on the coupling matrix to obtain new topologies. They would perform successive matrix rotations where each rotation would eliminate a redundant coupling. The ultimate goal is to minimise the number of couplings and to obtain a physically realisable circuit. An early example of coupling matrix reduction can be found in [13].

In order to cope with the increasing demand for capacity in the overcrowded spectrum, asymmetric frequency responses have become popular [1]. The original coupling matrix synthesis technique introduced by Atia could not accommodate filters with asymmetric frequency responses. Cameron published a technique to generate asymmetric transfer functions with prescribed transmission zeros in 1999 [14]. In the same article

[1] An asymmetric frequency response is a frequency response that is geometrically asymmetric with respect to the centre frequency.

he also showed how to synthesise a coupling matrix that could support asymmetric frequency responses and provided an algorithm to transform the synthesised coupling matrix into the folded canonical topology. A canonical topology is a topology where the minimum number of cross-couplings is present. Cameron later extended Atia's original $N \times N$ coupling matrix to obtain a $N+2 \times N+2$ coupling matrix. Cameron did this by incorporating the source and the load into matrix. This enabled him to synthesise N-th degree coupled resonator filters that can accommodate a maximum of N finite frequency transmission zeros [15]. The contributions of Cameron are significant. His extended coupling matrix enables designers to create a wide variety of different topologies for a given frequency response. We shall next investigate the various approaches to the design of multi-band filters.

1.3 An overview of design techniques for multi-band filters

There is no standard design technique for multi-band filters. There are however numerous, seemingly unique, publications available in the literature on the design of multi-band microwave filters. Fortunately, close inspection of these publications reveal that they can all be characterised as belonging to one of three main design methodologies. Next follows an overview of the available literature and definitions of said design methodologies.

Table 1.1 contains a list of published articles on the design of multi-band filters listed per year. The columns separate the different design methodologies. The list is not exhaustive. The methodologies are as follows:

1. **Interconnection of single-band filters:**
   A multi-band filter can be created by connecting multiple single-band filters in parallel using multiplexers. Such an approach was followed by Yu et al.[53]. Generally this technique results in physically large structures. An alternative possibility is to connect a wideband filter and a stopband filter in cascade. Such an approach was followed by Tsai et al. [18]. Their technique had the significant advantage that one could specifically design the bandwidths and centre frequencies of the different passbands by carefully choosing the individual bandwidths of the wideband and stopband filters. Each filter could be designed individually and then cascaded. Unfortunately numerical optimisation was required throughout the design. We can assume that if we create multi-band filters through the combination of single-band filters, we shall always obtain a physically larger structure than the one we could have obtained by designing a single structure multi-band filter. We thus focus on the design of single structure multi-band filters.

2. **Higher order resonant modes:**
   The impedance of a transmission line is a periodic function of frequency. As a consequence distributed resonators have higher order resonant modes. Some researchers have exploited this quality to create multi-band filters. The general idea is to centre the first passband on the first resonant frequency and the second passband on the second resonant frequency of the resonator. The obvious problem is that if the first passband is centred on f_0 Hz, one does not necessarily want the second passband to be centred on $2f_0$ Hz. This problem is overcome if one uses a perturbed resonator, such as the stepped impedance resonator (SIR). A SIR is a transmission line resonator that consists of three cascaded transmission line sections. The first and last sections are generally the same length and have the same characteristic impedance. The second resonant frequency can be designed by appropriately choosing the ratio of the characteristic impedance of the first section to the characteristic impedance of the second section. An design example of such a filter is given in [17]. A problem of the dual-band SIR filter is that designers

	Extend insertion loss method	Higher order resonant modes	Interconnection of single-band filters
2004	Lee [16]	Chang et al. [17]	Tsai et al. [18]
2005	Guan et al. [19] Macchiarella et al. [20] Lee [21]		
2006	Mokhtaari et al. [22] Guan et al. [23] Cameron et al. [24] Salazar-Palma et al. [25]		
2007	Sarabandi et al. [26] Lamperez [28] Deslandes et al.[30] Lee et al. [31] Macchiarella et al. [32] Seyfert et al. [33]	Han et al. [27] Mokhtaari et al. [29]	
2008	Liu et al. [34] Seyfert et al. [36] Mao et al. [37] Sarabandi et al. [38]	Singh et al. [35]	
2009	Deslandes et al. [39] Wu et al. [40]	Karpuz et al. [41, 42]	
2010	Zhao et al. [43] Chang et al. [45]	Chuang et al. [44] Guan et al. [46] Luo et al. [47]	
2011	Garcia-Lamperez et al. [48]	Wang et al. [49] Yang et al.[50]	
2012	Mohan et al. [51] Yang et al. [54] Lancaster et al. [56]	Doan et al. [52] Wu et al.[55] Xiao et al. [57] Wang et al. [58]	Yu et al. [53]
2013		Genc et al. [59] Hsu et al. [60]	

Table 1.1: Publications on the design of multi-band filters can be characterised as belonging to one of three design methodologies. The methodologies differ mainly on the mechanism used to obtain multi-band behaviour. The table above contains a list of publications on multi-band design listed per year and grouped according to the methodology followed.

	Extend insertion loss method		
	Extend approximation problem		Extend synthesis problem
	Iterative approximation technique	Frequency mapping technique	
2004	Lee [16]		
2005	Lee [21]	Macchiarella et al. [20]	Guan et al. [19]
2006		Cameron et al. [24]	Mokhtaari et al. [22] Guan et al. [23] Salazar-Palma et al. [25]
2007	Seyfert et al. [33] Deslandes et al. [30]	Macchiarella et al. [32] Sarabandi et al. [26]	Lamperez [28] Lee et al. [31]
2008	Seyfert et al. [36]	Sarabandi et al. [38]	Liu et al. [34] Mao et al. [37]
2009	Deslandes et al. [39]		Wu et al. [40]
2010	Zhao et al. [43]	Chang et al. [45]	
2011			Garcia-Lamperez et al. [48]
2012	Lancaster et al. [56]	Mohan et al. [51]	Yang et al. [54]

Table 1.2: Publications based on the extension of the insertion loss method can further be grouped as those extending the approximation problem and those extending the synthesis problem. Publications where the approximation problem is extended can again be separated into those employing mapping functions and those employing direct iterative methods.

cannot specify the bandwidths of the different passbands. It is only possible to specify the centre frequency and bandwidth of the first passband. The bandwidths of the other passbands must be designed using optimisation. Unfortunately the convergence of optimisation procedures are usually not guaranteed. That being said, this technique has the advantages that it usually results in relatively small filters and can accommodate cases where there is a wide separation between the passbands in the spectrum (due to resonant frequencies).

3. **Extension of insertion loss method:**
   Multi-band filters can also be designed by extending the insertion loss method. Table 1.2 contains a list of publications on this matter. The insertion loss method consists of the approximation problem and the synthesis problem, and either of these can be extended in order to accommodate multi-band designs.

   a) **Extension of synthesis problem:**
   Whether stated explicitly or not, the publications that fall into this category all initially design a single-band lowpass/prototype filter using the insertion loss method. All the reactive elements in the single-band prototype circuit are then replaced by a transformation subcircuit. This concept is illustrated in figures 1.1 and 1.2. In figure 1.1 we introduce the concept of extending the synthesis problem by using the well-known concept of transforming a prototype circuit into a single-band filter. In figure 1.2 we illustrate that this idea can be extended to filters with multiple passbands. Conceptually the transformation subcircuits transform the prototype frequency variable into a multi-band frequency variable. Naturally the structure of the transformation subcircuit is determined by a single-band to multi-band transformation. Garcia and Lamperez presented a general method to construct N-band coupled resonator filters through the extension of the synthesis problem [48]. The distinct advantage of extending the synthesis problem is that it is possible to design multi-band filters with complex frequency responses that have desirable topologies - i.e. that are suitable to be realised using distributed resonators at microwave frequencies. The disadvantage of extend-

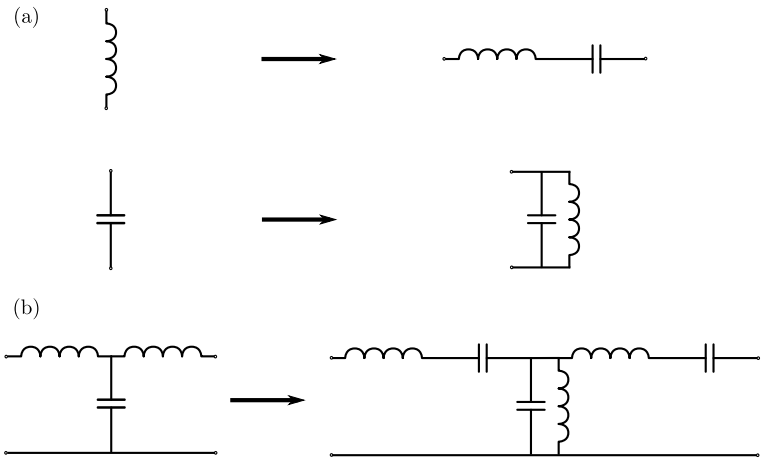

Figure 1.1: The concept of extending the synthesis problem, to transform a circuit accommodating a single passband, into a circuit accommodating multiple passbands is illustrated above. The circuit on the left in (b) is a lowpass circuit and has a single passband centred around 0 Hz. This is referred to as the prototype circuit. Each reactive element in the prototype circuit is replaced with a transformation subcircuit as shown in (a). The result is the circuit on the right in (b). This circuit has two pass bands (one for positive frequencies and one for negative frequencies)

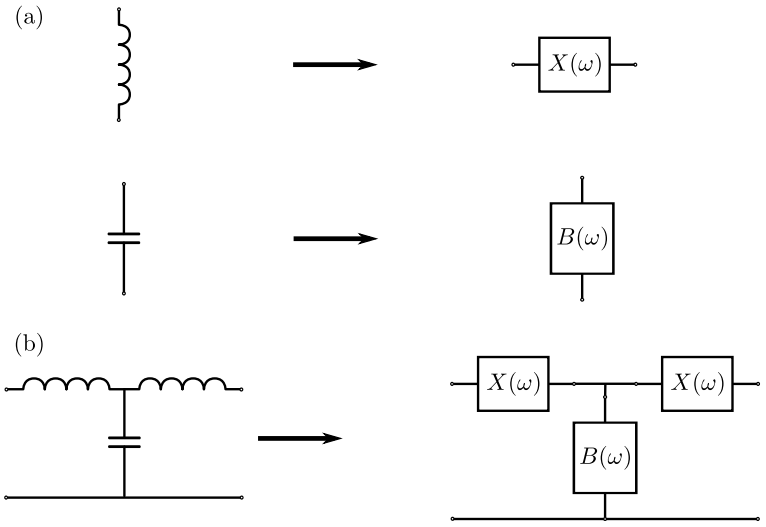

Figure 1.2: The concept introduced in figure 1.1 is extended to the general multi-band case. In (a) we show that each reactive/susceptive element in the prototype circuit must be replaced by a subcircuit. The form of the subcircuits are defined by an appropriate reactance/susceptance transformation function. The circuit on the right in (b) is the final multi-band filter.

ing the synthesis problem is that the set of realisable multi-band frequency responses depend on the topology of the initial single-band prototype. Essentially, the technique is limited in that it can only produce multi-band filters where each passband is an exact bandwidth-scaled and frequency-translated copy the original prototype frequency response.

b) **Extension of approximation problem:**
There are multiple techniques to extend the approximation problem. Fortunately, all the published techniques can be classified as either exploiting frequency mapping functions or employing iterative techniques. The approximation problem is solved by first finding a valid filtering function and then constructing transfer functions from said filtering function. In order to extend the approximation problem to accommodate multi-band responses, one must find a multi-band filtering function.

It is common practice to employ Butterworth or Chebyshev functions as single-band filtering functions [61]. The only group of functions that have been used as multi-band filtering functions are Zolotarev functions [67]. These functions have properties similar to Chebyshev polynomials but have the freedom that the equal-ripple condition is not enforced on all of the turning points. This property enables one to design dual-band filters with poor selectivity between the bands. Unfortunately there is no known group of functions that are ideally suited to be used as multi-band filtering functions *in general*. Multi-band filtering functions must be obtained through other means. Numerous approaches have been published in the literature. Fortunately all of them can be classified as either employing frequency mapping functions or employing some iterative approximation technique. Once a valid multi-band filtering function is found, the transfer functions can be constructed from said filtering function and a circuit can be synthesised using one of the numerous available synthesis procedures [62]. The circuit can then in turn be realised as a distributed structure. The design of multi-band filters is now exactly the same as the design of single-band filters, except for the approximation problem.

For the specific case of coupled resonator circuits the synthesis procedure is performed by constructing a coupling matrix from the transfer functions [11, 12]. The disadvantage of this approach is that the synthesised circuits do not necessarily have topologies that are well-suited for realisation as microwave circuits. This problem has been addressed by simplifying the synthesised circuit using similarity transformations [63, 14, 64, 61]. In the following subsections we discuss methods of extending the approximation problem.

i. **Frequency mapping techniques:**
A multi-band filtering function is constructed from a single-band filtering function by mapping the poles and zeros of the single-band filtering function from a single-band frequency plane onto a multi-band frequency plane using an appropriate mapping function. The crux of the matter is the definition of the mapping function. The frequency mapping technique was first proposed by Macchiarella as design method A in [20]. Cameron published a virtually identical technique for the design of stopband filters in [65]. The approximation problem is generally solved in a normalised frequency domain (the lowpass prototype domain). Macchiarella and Cameron both introduced an additional frequency domain and called it the multi-band prototype domain. They proposed the idea to map the solution of the single-band approximation problem onto the multi-band prototype plane. Macchiarella and Cameron both used second order polynomials as their mapping functions. Their technique is however limited because their mapping functions are only capable of producing symmetric dual-band prototypes [2]. They did not provide any method to construct general asymmetric N-band mapping functions nor did they consider the conditions for a mapping function to be valid. Researchers have also attempted to employ rational functions as mapping functions. In 2007 Lee and Sarabandi introduced a new dual-band mapping function [26]. They adapted the traditional lowpass-to-bandpass transformation to obtain a single-band to dual-band transformation that could accommodate symmetric and asymmetric dual-band filters. In 2008 Lee and Sarabandi extended their technique to accommodate symmetric and asymmetric triple-band filters [38]. A problem with their technique is that the calculation of the coefficients of the mapping functions can be quite cumbersome as it involves the simultaneous solution of multiple coupled equations. Their technique is also

[2]Symmetric in this context means that the transmission zeros, the outer passband limits and the inner passband limits of the prototype filter are all symmetric with respect to the zero frequency of the filter. Vice versa for the definition of asymmetric

not scalable to filters with more passbands because the associated calculations become intractable. Garcia and Lamperez further extended the concept to accommodate N bands [48]. Their solution is limited to filters based on the coupled resonator principles, but is complete for this subset.

ii. **Iterative approximation techniques:**
An initial multi-band filtering function is constructed directly on the multi-band frequency plane by arbitrarily placing poles and zeros on the multi-band frequency plane. The poles and zeros are then iteratively adjusted, in a converging manner, until an optimal set is found that meets the design specifications. We here distinguish between techniques employing blind optimisation that do not necessarily converge and those that are guaranteed to converge. An early example of a technique that uses blind optimisation is given in [16]. Lee et al. solved the multi-band approximation problem using direct numerical optimisation of the poles and zeros of the filtering function. Due to the obvious issue of convergence, their technique is not considered ideal. An alternative iterative approximation technique was presented by Deslandes and Boone in 2007 [30]. Their technique guaranteed that zeros and poles generated with each subsequent iteration would provide a closer approximation of the ideal response. Deslandes and Boone initially only solved the problem for all-pole filters. Zhang et al. then extended the technique for generalised multi-band filters with prescribed passbands, stopbands and transmission zeros [66].

It is clear that there is no standard design method for multi-band filters. Numerous approaches have been presented. The most promising approach exploits the wealth of filter synthesis theory by extending the insertion loss method to accommodate multi-band designs. This is achieved by either extending the approximation problem to accommodate multi-band transfer functions, or by extending the synthesis problem by transforming single-band prototype circuits into multi-band circuits using frequency transformation subcircuits. Both the approximation problem and the synthesis problem can be extended using frequency mapping functions. The approximation problem is extended by employing frequency mapping functions to construct multi-band filtering functions from single-band filtering functions. The synthesis problem is extended by synthesising frequency transformation subcircuits from suitable frequency mapping functions. The other school of thought is to directly construct multi-band filtering functions using iterative techniques and to then synthesise multi-band filters directly from the obtained transfer functions using standard synthesis methods. Frequency mapping functions therefore play a central role in the multi-band design techniques that are not based on optimisation. To date, no standard method of constructing arbitrary mapping functions has been presented. It is the aim of this work to address this issue.

1.4 Original contributions

This dissertation presents new techniques for the design of multi-band filters, specifically filters that can be implemented using coupled resonators. Original methods to construct polynomial and rational mapping functions are proposed.

The polynomial mapping functions are constructed using Lagrange basis functions. The Lagrange functions were chosen as they are generally well-behaved for low-order interpolation problems. The polynomial mapping functions are used to construct multi-band filtering functions, and in turn multi-band transfer functions, from single-band filtering functions. Multi-band circuits are then synthesised directly from the obtained

multi-band transfer functions. The polynomial mapping functions are suitable to design filters containing two or three passbands.

A special class of rational mapping functions is presented. A simple procedure to construct a mapping function from a bandwidth specification is presented. There are two formulations of the rational mapping functions – a general formulation suitable for all multi-band filters and a narrowband formulation suitable for coupled resonator filters. In both cases the rational functions are used to construct one-port frequency transformation subcircuits. These subcircuits are then used to transform single-band prototype circuits into multi-band circuits. The rational mapping functions can also be used to construct multi-band filtering functions, and in turn multi-band transfer functions, from single-band filtering functions. The multi-band transfer functions can then be used to synthesise multi-band circuits directly. The method of constructing frequency transformation one-port subcircuits is however simpler to apply and result in circuits with desirable topologies for implementation as coupled resonator circuits. The rational mapping functions can always be synthesised as frequency transformation subcircuits and can be used to design filters that have any number of bands and that have any bandwidth specification. The presented rational mapping functions therefore solve the outstanding problem associated with mapping functions as described in the previous section.

The main original contributions are as follows:

1. A general technique which utilises high-order reactance mapping functions to design multi-band filters is presented. The technique is rigorous and does not require any optimisation, is unlimited in the number of bands which can be created, allows the passband frequencies of each band to be chosen completely arbitrarily, and results in a set of passbands of which each is an exact bandwidth-scaled and frequency-translated copy of the original lowpass function. The technique is not limited in its application to any type of technology (i.e. waveguide, planar transmission lines etc.). The reader is referred to chapters 4 and 6.

2. A narrowband formulation of the general theory is presented for application to multi-band coupled resonator filters [68, 69]. The reader is referred to sections 4.3 and 6.1.

3. The use of Lagrange polynomials to construct polynomial mapping functions is proposed. Refer to chapter 3.

The theory is validated in all cases through the design and manufacture of multi-band coupled resonator filters using different implementation technologies.

1.5 Contents of dissertation

Chapter 2 serves as a summary of fundamental concepts and provides a basis for the theory presented in this dissertation. Part I deals with the approximation of multi-band transfer functions and multi-band filtering functions using mapping functions. Polynomial mapping functions are presented in chapter 3 and rational mapping functions in chapter 4. Part II provides techniques to obtain electric circuits from transfer functions and consists of chapters 5 and 6. Chapter 5 serves as a summary of established theory on filter synthesis methods using coupling matrices. Chapter 6 presents the synthesis of multi-band filters through reactance transformations. The reactance transformations are defined by the rational mapping functions. Chapter 7 serves as a summary of well-known literature on the realisation of lumped element circuits at microwave frequencies using distributed structures. The methods contained therein are used extensively in the practical

designs in chapters 8 through 10. Chapter 8 presents the design of a dual-band all-pole filter in stripline. Chapter 9 presents the design of a dual-band cross-coupled filter in stripline. The designs in chapters 8 and 9 were performed using polynomial mapping functions. Chapter 10 presents the design of a three-band coaxial resonator filter using rational mapping functions. All of the filters were manufactured and the measurements corresponded well with the theoretical predictions. Chapter 11 gives a summary of all the work presented in this dissertation. Some conclusions are drawn and possible future research directions are mentioned.

Chapter 2

Fundamental concepts

This chapter serves as a summary of well-known and important concepts in the field of filter design that is considered relevant to the theory presented in this dissertation [9, 14, 15, 61, 70]. The chapter does not contain original contributions. We introduce network functions that are generally employed to model electric circuits and illustrate how they are related to filtering functions. We also describe the construction of the generalised Chebyshev polynomials as these are commonly employed as filtering functions in the design of quasi-elliptic single-band filters. The generalised Chebyshev polynomials are presented as they are later used in conjunction with mapping functions to design multi-band filters.

2.1 Network functions for linear, time-invariant and lossless passive networks

A two-port circuit is generally described by four network functions – two transfer functions and two driving point functions. This section describes the use of scattering parameters as network functions. We specifically consider purely reactive two-port circuits with equal resistive terminations. Suppose an unknown reactive two-port device is connected between two voltage sources as shown in figure 2.1. Here E_1 and E_2 are two ideal voltage sources and R_1 and R_2 are their associated internal resistances. The incident and reflected voltage waves associated with ports one and two are indicated as a_1, a_2, b_1 and b_2 respectively. The net voltages and currents at ports one and two are indicated as V_1, V_2, I_1 and I_2 respectively. Scattering parameters are used to define the relationship between the incident and reflected voltage waves at the ports of the circuit as follows:

$$\begin{bmatrix} b_1(s) \\ b_2(s) \end{bmatrix} = \begin{bmatrix} s_{11}(s) & s_{12}(s) \\ s_{21}(s) & s_{22}(s) \end{bmatrix} \begin{bmatrix} a_1(s) \\ a_2(s) \end{bmatrix} \tag{2.1}$$

Here s is the complex frequency variable [1]. If we assume that the two-port device in figure 2.1 is a passive, lossless, linear and time-invariant circuit, it can be shown that the associated scattering parameter matrix is a unitary matrix, therefore $\mathbf{I} = (\mathbf{S}^*)^T \mathbf{S}$ [2]. The fact that $\mathbf{S}$ is a unitary matrix ensures the following relationships between the scattering parameters:

$$\begin{aligned} &(1) \quad s_{11}^*(s)s_{11}(s) + s_{21}^*(s)s_{21}(s) = 1 \\ &(2) \quad s_{12}^*(s)s_{11}(s) + s_{22}^*(s)s_{21}(s) = 0 \\ &(3) \quad s_{11}^*(s)s_{12}(s) + s_{21}^*(s)s_{22}(s) = 0 \\ &(4) \quad s_{12}^*(s)s_{12}(s) + s_{22}^*(s)s_{22}(s) = 1 \end{aligned} \tag{2.2}$$

[1] In this work we denote the single-band prototype complex frequency variable as $S' = j\Omega'$ and the multi-band prototype complex frequency variable as $S = j\Omega$. The actual complex frequency variable in a final filter design is denoted as $s = j\omega$.

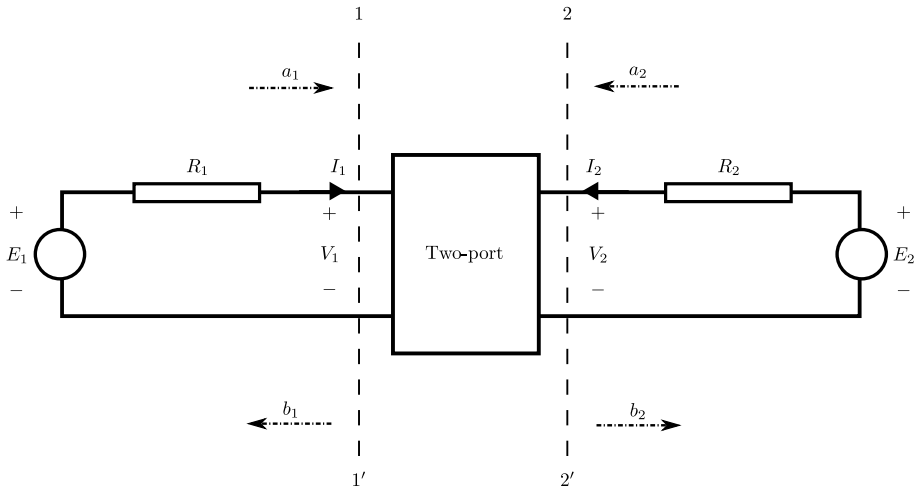

Figure 2.1: A reactive two-port circuit connected between two sources. The voltage sources are indicated as E_1 and E_2. The input resistances of the voltage sources are R_1 and R_2. V_1, V_2, I_1 and I_2 are the net voltages and currents at the ports. The incident and reflected voltage waves associated with ports one and two are indicated as a_1, a_2, b_1 and b_2 respectively.

The relationships above are referred to as the unitary conditions of the scattering parameters.

We can expand the scattering parameter matrix of a linear, time-invariant network as a set of rational functions:

$$\mathbf{S} = \begin{bmatrix} \frac{a}{b} & \frac{c}{d} \\ \frac{e}{f} & \frac{g}{h} \end{bmatrix} \tag{2.3}$$

Here a, b, c, d, e, f, g and h are polynomials in s. It is therefore possible to rewrite $\mathbf{S}$ in the following form:

$$\mathbf{S} = \frac{1}{bdfh} \begin{bmatrix} adfh & cbhf \\ ebdh & gfbd \end{bmatrix} \tag{2.4}$$

It is clear that scattering parameters can be factorised in such a manner that $s_{11}(s)$, $s_{12}(s)$, $s_{21}(s)$ and $s_{22}(s)$ all share a single common denominator polynomial. If a two-port is reciprocal, an electromagnetic wave propagating from port one to port two will be influenced in exactly the same manner as a wave propagating from port two to port one. Such a circuit can be described as follows:

$$\mathbf{S} = \frac{1}{E(s)} \begin{bmatrix} F_{11}(s) & P(s) \\ P(s) & F_{22}(s) \end{bmatrix} \tag{2.5}$$

If we substitute equation 2.5 into the third unitary condition in equation 2.2, we arrive at the following:

$$F_{22}(s) = \frac{-F_{11}^*(s)P(s)}{P^*(s)} \tag{2.6}$$

Our factorisation in equation 2.4 showed that all the scattering parameters share a single common denominator and therefore $F_{11}(s)$ cannot be a rational fraction in s. Thus $P(s)$ and $P^*(s)$ must cancel. This knowledge of $P(s)$ will be used to investigate its zero positions. Suppose:

$$P(s) = p_0 + p_1 s + p_2 s^2 + \ldots + p_{n_{fz}} s^{n_{fz}}$$

Here $P(s)$ is an n_{fz}-th order polynomial and has p_0, p_1, $\ldots p_{n_{fz}}$ as its complex coefficients. Remembering that $s = 0 + j\omega$ and evaluating α as ± 1, $P(s)$ and $P^*(s)$ will cancel when:

$$\begin{aligned} P(s) &= \alpha P^*(s) \\ p_0 + p_1 s + p_2 s^2 + \ldots + p_{n_{fz}} s^{n_{fz}} &= \alpha \left(p_0 + p_1 s + p_2 s^2 + \ldots + p_{n_{fz}} s^{n_{fz}} \right)^* \end{aligned} \tag{2.7}$$

Depending on the value of α, the coefficients are related as follows:

$\alpha = 1$		$\alpha = -1$	
Coefficient relationship	Implication	Coefficient relationship	Implication
$p_0 \equiv p_0^*$	$\Im\{p_0\} = 0$	$p_0 \equiv -p_0^*$	$\Re\{p_0\} = 0$
$p_1 \equiv -p_1^*$	$\Re\{p_1\} = 0$	$p_1 \equiv p_1^*$	$\Im\{p_1\} = 0$
$p_2 \equiv p_2^*$	$\Im\{p_2\} = 0$	$p_2 \equiv -p_2^*$	$\Re\{p_2\} = 0$
$\vdots$	$\vdots$	$\vdots$	$\vdots$

We can conclude that for $F_{22}(s)$ to be a polynomial, the coefficients of $P(s)$ must alternate between purely real and purely imaginary numbers. This is equivalent to requiring that $P(s)$ must either be a complex-even or a complex-odd function. The definition of complex-even and complex-odd functions is as follows:

$$\begin{aligned} &\text{Complex-even:} \quad P(s) = P^*(-s) \\ &\text{Complex-odd:} \quad P(s) = -P^*(-s) \end{aligned} \tag{2.8}$$

We can therefore conclude that the roots of $P(s)$ are all located either on the imaginary axis, or as mirror-image pairs symmetrically arranged about the imaginary axis on the complex s-plane [61]. The value of α can be related to the value of n_{fz} by observing that p_0 is only purely real when α is equal to $+1$ and when n_{fz} is an even number. Therefore $\alpha = (-1)^{n_{fz}}$. Hence equation 2.6 is rewritten as[61]:

$$F_{22}(s) = (-1)^{n_{fz}+1} F_{11}^*(s) \tag{2.9}$$

If we assume that $F_{11}(s)$ is an N-th order polynomial, equation 2.9 can be used to relate the roots of $F_{22}(s)$ to those of $F_{11}(s)$ as follows:

$$\begin{aligned} F_{22}(s) &= (-1)^{nfz+1} \textstyle\prod_{k=1}^{N} (s - s_{11k})^* \\ &= (-1)^{nfz+1} \textstyle\prod_{k=1}^{N} (-s - s_{11k}^*) \\ &= (-1)^{N+nfz+1} \textstyle\prod_{k=1}^{N} (s - (-s_{11k}^*)) \\ &= (-1)^{N+nfz+1} \textstyle\prod_{k=1}^{N} (s - s_{22k}) \end{aligned} \tag{2.10}$$

The roots of $F_{22}(s)$ are therefore given as:

$$s_{22k} = -s_{11k}^* \quad \text{for} \quad k \in [1, N] \tag{2.11}$$

It is said that the roots of $F_{22}(s)$ are the *para-conjugates* of the roots of $F_{11}(s)$. The roots of $F_{11}(s)$ and $F_{22}(s)$ are either coincident on the imaginary axis or arranged in mirror-image pairs about the imaginary axis [15]. Due to the known relationship between $F_{11}(s)$ and $F_{22}(s)$, it is possible to define $F(s) = F_{11}(s)$.

The relative phase differences between the scattering parameters can easily be investigated if we represent the scattering parameters as vectors in the complex plane:

$$\begin{aligned} s_{11} &= |s_{11}|e^{j\theta_{11}} \\ s_{22} &= |s_{22}|e^{j\theta_{22}} \\ &= |s_{11}|e^{j\theta_{22}} \\ s_{21} &= |s_{21}|e^{j\theta_{21}} = s_{12} \end{aligned} \tag{2.12}$$

Substitution of 2.12 into the first unitary condition in equation 2.2 reveals that:

$$|s_{21}|^2 = 1 - |s_{11}|^2 \tag{2.13}$$

Further substitution of equations 2.12 and 2.13 into the second unitary condition in equation 2.2 reveals that:

$$\begin{aligned} &|s_{11}|e^{j\theta_{11}}|s_{21}|e^{-j\theta_{21}} + |s_{21}|e^{j\theta_{21}}|s_{11}|e^{-j\theta_{22}} = 0 \\ \Longrightarrow\ &|s_{21}||s_{11}|\left(e^{j(\theta_{11}-\theta_{21})} + e^{j(\theta_{21}-\theta_{22})}\right) = 0 \end{aligned} \tag{2.14}$$

For the above statement to be true, the following phase relationship is required:

$$\tfrac{\theta_{11}+\theta_{22}}{2} - \theta_{21} = \tfrac{\pi}{2}(2k \pm 1) \quad k \in \mathbb{Z} \tag{2.15}$$

The identity in 2.15 states that the difference between the phase of the s_{21} vector and the average of the phases of the s_{11} and s_{22} vectors must be an odd multiple of $\pi/2$ radians. Note also that this phase relationship must hold at all frequencies. All the scattering parameters share a singular denominator polynomial. Therefore the phase relationship refers to $P(s)$, $F_{11}(s)$ and $F_{22}(s)$. The roots of $P(s)$ appear either as symmetric complex pairs about the imaginary axis or are located at any position on the imaginary axis. Consequently the phase of the s_{21} vector could be written as:

$$\theta_{21} = n_{fz}\tfrac{\pi}{2} + k_1\pi \qquad \begin{matrix} k_1 \in \mathbb{Z} \\ n_{fz} \in \mathbb{N} \end{matrix} \tag{2.16}$$

The roots of $F_{11}(s)$ and $F_{22}(s)$ are para-conjugates of each other. Both functions have N roots, consequently the sum of their phases should be

$$\theta_{11} + \theta_{22} = N\pi \tag{2.17}$$

Substitution of equations 2.17 and 2.16 into equation 2.15 results in the following:

$$\tfrac{\pi}{2}(N - n_{fz}) = \tfrac{\pi}{2}(2k \pm 1) + k_1\pi \quad k, k_1 \in \mathbb{Z} \tag{2.18}$$

The identity in equation 2.18 is only true if $(N - n_{fz})$ equates to an uneven number. This will obviously not always be true. Therefore if $(N - n_{fz})$ is an even number, $P(s)$ must be multiplied by j to increase its phase by $\pi/2$ radians [15]. Generally the constants ϵ_r and ϵ are used to normalise the leading coefficients of $F(s)$ and $P(s)$ respectively. If we now express the first unitary condition in equation 2.2 in terms of the polynomial definitions in equation 2.5, we arrive at the following:

$$\frac{F^*(s)F(s)}{\epsilon_r^2} + \frac{P^*(s)P(s)}{\epsilon^2} = E^*(s)E(s) \tag{2.19}$$

Equation 2.19 is known as the *Feldtkeller* equation and governs the relationship between $E(s)$, $F(s)$ and $P(s)$. If two of the polynomials are known, the third can be calculated. From the discussion above it is clear that the transfer functions of passive, lossless and reciprocal two-ports are defined as follows:

$$\mathbf{S} = \frac{1}{E(s)}\begin{bmatrix} \frac{1}{\epsilon_r}F(s) & \frac{1}{\epsilon}P(s) \\ \frac{1}{\epsilon}P(s) & \frac{1}{\epsilon_r}(-1)^{n_{fz}+1}F^*(s) \end{bmatrix} \tag{2.20}$$

Here ϵ_r and ϵ are constants used to normalise the leading coefficients of $F(s)$ and $P(s)$ respectively. The $P(s)$, $E(s)$ and $F(s)$ polynomials are collectively referred to as the *characteristic polynomials* of the filter.

In the next section we shall introduce the concept of a filtering function. Filtering functions are closely related the to characteristic polynomials and play a central role in the design of transfer functions.

2.2 Filtering functions

The magnitude of the transmission coefficient $|s_{21}(s)|$ of a filter must approximate 1 inside passbands and values close to 0 inside stopbands. The synthesis of such a function proves to be a mathematical challenge.

Researchers introduced the concept of a filtering function to remedy this. A filtering function is a function that has a mathematical relationship with the transmission coefficient, but has characteristics that makes it easier to synthesise. A filtering function is a rational function in a real frequency variable, its roots are the reflection zeros of a filter and its poles are the transmission zeros of a filter. For simplicity it common practice to define the function using the normalised frequency variable Ω [2]. Once a desired filtering function is found, it can be related to the transmission coefficient to identify the characteristic polynomials. In order to find an expression for the filtering function, we start with the following definitions of the scattering parameters on the Ω-plane:

$$s_{21}(\Omega) = \frac{P(\Omega)}{\epsilon E(\Omega)} \qquad s_{11}(\Omega) = \frac{F(\Omega)}{\epsilon_r E(\Omega)} \tag{2.21}$$

The calculations are performed on the Ω-plane as this simplifies the mathematics and makes the filtering function simpler to synthesise. Applying the unitary conditions yield:

$$\begin{aligned} \frac{F^*(\Omega)F(\Omega)}{\epsilon_r^2 E^*(\Omega)E(\Omega)} + \frac{P^*(\Omega)P(\Omega)}{\epsilon^2 E^*(\Omega)E(\Omega)} &= 1 \\ \frac{|F(\Omega)|^2}{\epsilon_r^2 |E(\Omega)|^2} + \frac{|P(\Omega)|^2}{\epsilon^2 |E(\Omega)|^2} &= 1 \end{aligned} \tag{2.22}$$

Defining $C_N(\Omega) = \frac{F(\Omega)}{P(\Omega)}$ yields:

$$|s_{21}(\Omega)|^2 = \frac{1}{1 + \frac{\epsilon^2}{\epsilon_r^2}\frac{|F(\Omega)|^2}{|P(\Omega)|^2}} \tag{2.23}$$

$$= \frac{1}{1 + c_o^2 |C_N(\Omega)|^2}$$

$$= \frac{1}{[1 + jc_o C_N(\Omega)][1 - jc_o C_N(\Omega)]} \tag{2.24}$$

Here $C_N(\Omega)$ is called the *filtering function*, or the *characteristic function* [61]. As we would expect, the zeros of $C_N(\Omega)$ are the reflection zeros of the filter and the poles of $C_N(\Omega)$ are the transmission zeros of the filter. $C_N(\Omega)$ is said to define the shape of a frequency response and is regularly encountered in approximation procedures. $C_N(\Omega)$ has N transmission zeros and N reflection zeros. The number of transmission zeros located at finite frequencies is $n_{fz} \leq N$. Table 2.1 summarises the various properties of the various functions discussed in this chapter. In the next section we describe a simple procedure to obtain the characteristic polynomials from a filtering function.

2.3 Calculation of the characteristic polynomials from filtering functions

In this section we present a method to construct $F(S)$, $P(S)$, $E(S)$, ϵ and ϵ_r from a filtering function.

The roots of the numerator and denominator polynomials of a filtering function can be mapped to the complex frequency plane using the relation $S = j\Omega$ and then used to construct $F(S)$ and $P(S)$ respectively. The normalisation constants of the $P(S)$ and $F(S)$ polynomials are calculated from a minimum passband return loss figure. The return loss of a filter is measured in decibels and is defined as follows:

$$\text{RL} = 10 \log \frac{1}{|s_{11}(s)|^2} \tag{2.25}$$

A filtering function is scaled with a normalisation factor, that is a combination of ϵ_r and ϵ, to obtain the required return loss inside a passband. Refer to equation 2.23 for the definition of said normalisation factor. The

[2] Filtering functions can be defined using single-band or multi-band variables. The filtering functions are usually constructed using normalised/prototype variables.

$P(s)$	$P(s)$ is the numerator of the transmission coefficient. It is an n_{fz}-th order monic polynomial where n_{fz} is the number of finite frequency transmission zeros. The roots of $P(s)$ are the transmission zeros – the frequency points of no transmission. These are located in the stopbands of a filter. $P(s)$ is allowed have multiple roots at any position on the imaginary axis. However, when roots are not located on the imaginary axis, they must present as symmetric pairs about the imaginary axis. When $N-n_{fz}$ is an even number, $P(s)$ must be multiplied by j to ensure that its phase stay orthogonal to the average phases of $F_{11}(s)$ and $F_{22}(s)$. For $P(s)$ to be a monic polynomial, it is normalised using the real constant ϵ.
$F(s)$	$F(s)$ is the numerator polynomial of the reflection coefficient. We define $F(s)$ as being equal to $F_{11}(s)$. It is an N-th order monic polynomial where N is the order of the filter. The roots of $F(s)$ are the reflection zeros of the filter – the frequency points of perfect transmission. The roots of $F(s)$ are usually purely complex and are located inside the passbands of the filter. They are however allowed to be located on the complex plane (as is the case for pre-distorted filters). For $F(s)$ to be a monic polynomial, it is normalised using the real constant ϵ_r.
$E(s)$	$E(s)$ is the common denominator of all the scattering parameters. It is an N-th order monic polynomial where N is the order of the filter. In order to describe stable systems, it must be a Hurwitz polynomial. Consequently all its zeros are located on the negative real side of the complex plane. $E(s)$ is related to $P(s)$ and $F(s)$ through the Feldtkeller equation.
$C_N(\omega) = \frac{F(\omega)}{P(\omega)}$	$C_N(\omega)$ is known as the filtering function. It is constructed out of $P(\omega)$ and $F(\omega)$. These polynomials are in turn constructed out of transmission zeros and reflection zeros of the filter respectively. The filtering function was introduced to simplify the design of transfer functions. $C_N(\omega)$ has the property that it evaluates to small values inside passbands and large values inside stopbands. The function is also completely real that simplifies the process considerably. All the zeros of the function are located inside passbands and all the poles are located inside stopbands. $C_N(\omega)$ is said to define the shape of a filter response. If $C_N(\omega)$ is known, $P(s)$ and $F(s)$ can be constructed by remembering that $s = j\omega$. The Feldtkeller equation can then be used to construct $E(s)$. All the characteristic polynomials are then known and the approximation problem is considered solved.

Table 2.1: A description of the characteristic polynomials and their allowable zero locations are provided above. The properties of the filtering function are also summarised.

minimum return loss figure of a passband for an equal-ripple filtering function is calculated at a local maxima of the filtering function and one such maxima point is always located at the edge of a passband. We shall now illustrate how to calculate a value for ϵ using the minimum passband return loss figure for an equal-ripple filtering function. The process starts with the first unitary condition in equation 2.2:

$$|s_{21}(j\Omega)|^2 + |s_{11}(j\Omega)|^2 = 1 \tag{2.26}$$

Suppose the passband edge is indicated as Ω_c rad/s. We now substitute equation 2.25 into equation 2.26 at $\Omega = \Omega_c$:

$$\begin{aligned}
\left|\frac{P(j\Omega_c)}{E(j\Omega_c)}\right|^2 &= 1 - 10^{-\mathrm{RL}/10} \\
\implies \qquad \epsilon &= \frac{1}{\sqrt{1-10^{-\mathrm{RL}/10}}}\left|\frac{P(j\Omega_c)}{E(j\Omega_c')}\right| \\
&= \frac{\sqrt{10^{\mathrm{RL}/10}}}{\sqrt{10^{\mathrm{RL}/10}-1}}\left|\frac{P(j\Omega_c)}{E(j\Omega_c)}\right| \\
&= \frac{1}{\sqrt{10^{\mathrm{RL}/10}-1}}\left|\frac{P(j\Omega_c)}{E(j\Omega_c)}\frac{E(j\Omega_c)}{F(j\Omega_c)}\right| \\
\implies \qquad \epsilon &= \frac{1}{\sqrt{10^{\mathrm{RL}/10}-1}}\left|\frac{P(j\Omega_c)}{F(j\Omega_c)}\right|
\end{aligned} \tag{2.27}$$

Here RL is the minimum return loss in the passband. We next consider how to calculate ϵ_r. An N-th order filter has N-transmission zeros. A transmission zero is allowed to be located at any frequency point. The filter has $N - n_{fz}$ transmission zeros located at infinity. We can obtain an expression for ϵ_r by investigating the behaviour of the first unitary condition (equation 2.2) in the following limit:

$$\lim_{j\Omega\to\pm j\infty}\left\{\frac{F(j\Omega)F^*(j\Omega)}{\epsilon_r^2 E(j\Omega)E^*(j\Omega)} + \frac{P(j\Omega)P^*(j\Omega)}{\epsilon^2 E(j\Omega)E^*(j\Omega)}\right\} = 1 \tag{2.28}$$

From equation 2.28 we can derive the following expressions for ϵ_r:

$$\epsilon_r = \begin{cases} 1 & n_{fz} < N \\ \frac{\epsilon}{\sqrt{\epsilon^2-1}} & n_{fz} = N \end{cases} \tag{2.29}$$

Filtering functions where all the transmission zeros are located at finite frequency points are called *canonical* filtering functions. For canonical filtering functions all the polynomials are of degree N and consequently $\epsilon_r \neq 1$. The remaining characteristic polynomial, $E(S)$, can be calculated from the other characteristic polynomials using the Feldtkeller equation, as shown in equation 2.19. One typically finds an expression for $E(-S)E(S)$ and then separates the $2N$ complex roots into the roots of $E(S)$ and $E(-S)$ by exploiting that fact that $E(S)$ is a Hurwitz polynomial and all its roots would therefore be located on the left half of the complex plane. Even though this technique is completely general and works for any filter specification, it does involve working with double-degree polynomials. The roots of $E(-S)E(S)$ tend to cluster together and for high order filters it becomes a numerical challenge to accurately determine all the roots [61]. Fortunately there is an alternative method to find $E(S)$ for transfer functions where all of the reflection zeros are located on the imaginary frequency axis. This method is dubbed the alternating pole/singularity method and is attributed to Rhodes and Alseyab [71, 61].

We shall next give an overview of this technique. For the cases where $N - n_{fz}$ is odd, we can expand the Feldtkeller equation as follows:

$$\begin{aligned}
\epsilon^2\epsilon_r^2 E(S)E(S)^* = &\left[\epsilon_r P(S) + \epsilon F(S)\right]\left[\epsilon_r P(S)^* + \epsilon F(S)^*\right] \\
&- \epsilon\epsilon_r\left[P(S)^*F(S) + P(S)F(S)^*\right]
\end{aligned} \tag{2.30}$$

For the term on the extreme right to evaluate to zero, we require that:

$$P(S)^*F(S) + P(S)F(S)^* = 0 \tag{2.31}$$

The second unitary condition in equation 2.2 can be expressed for the cases where $N - n_{fz}$ is odd as:

$$P(S)^*F_{11}(S) + P(S)F_{22}(S)^* = 0 \tag{2.32}$$

Clearly the term on the extreme right in equation 2.30 will only evaluate to zero if $F_{11}(S) = F_{22}(S)$. A similar argument can be constructed for the cases where $N - n_{fz}$ is even and exactly the same conclusion is drawn. This implies that all the roots of $F_{11}(S)$ and the roots of $F_{22}(S)$ must be located on the imaginary axis and must be coincident. We can therefore state that in general, if all the reflection zeros of a filter are located on the imaginary axis, the following relationship is valid:

$$\epsilon^2\epsilon_r^2 E(S)E(S)^* = \begin{cases} [j\epsilon_r P(S) + \epsilon F(S)]\,[j\epsilon_r P(S) + \epsilon F(S)]^* & , N - n_{fz} \quad \text{even} \\ [\epsilon_r P(S) + \epsilon F(S)]\,[\epsilon_r P(S) + \epsilon F(S)]^* & , N - n_{fz} \quad \text{odd} \end{cases} \tag{2.33}$$

The expressions in equation 2.33 enables us to calculate $E(S)$ from the other characteristic polynomials without having to first calculate the roots of a double-degree polynomial. This resolves the numerical accuracy problem. The process to find $E(S)$ is as follows:

1. If $N - n_{fz}$ is even, calculate $Q(S) = j\epsilon_r P(S) + \epsilon F(S)$. If $N - n_{fz}$ is odd, calculate $Q(S) = \epsilon_r P(S) + \epsilon F(S)$. Note that $Q(S)$ is of degree N.

2. Find the roots of $Q(S)$. These roots will alternate between the left half of the complex plane and the right half of the complex plane. Take the para-conjugates of all the roots of $Q(S)$ that are located on the right half of the complex plane (mirror them in the imaginary axis to obtain roots in the left half of the complex plane). This results in a combined set of N roots on the left half of the complex plane. These are the roots of $E(S)$.

This technique provides an efficient way to accurately calculate the roots of $E(S)$ in the cases where all of the reflection zeros of a filter are located on the imaginary axis. Fortunately, for the work presented in this dissertation, this condition always holds and therefore this methodology will be followed throughout this dissertation.

2.4 Filter design using prototypes

The Insertion Loss Method can be divided into Approximation and Synthesis, where Approximation is the process of finding a mathematical description of the desired frequency response, and Synthesis is the process of obtaining the filter circuit from said mathematical description.

The first step in the approximation procedure is to identify a valid filtering function. Typical functions that are regularly employed as filtering functions include Chebyshev functions and Butterworth functions [9]. A designer would usually deduce the type and minimum order of the filtering function from a minimum attenuation requirement. There are numerous design tables available in the literature for this purpose [9]. Both the filtering function and the characteristic polynomials are generally defined in a normalised frequency domain. The use of denormalisation functions imply that one can arbitrarily choose the passband and stopband limits in the prototype domain. Usually the passband is defined as $\Omega \in [-1; 1]$ and the stopbands are defined as $\Omega \in [-\infty; 1) \cap (1; \infty]$.

The next step in the design procedure is to synthesise an electric circuit from the characteristic polynomials. There are numerous classic methods available that can be used to synthesise an electric circuit from the characteristic polynomials as well as numerous design tables that provide circuit element values for various filtering functions of various orders [62, 9]. The last step is denormalisation. Here a designer would transform a prototype circuit into a final circuit using a circuit transformation. The type of transformation depends on the final circuit – bandpass, bandstop, highpass etc.

The design method outlined above does not accommodate multi-band filters. The reason for this is that there is no known group of filtering functions that are ideally suited to serve as multi-band filtering functions. In this dissertation we address this problem by constructing multi-band filtering functions from single-band filtering functions using frequency mapping functions. We elaborate on frequency mapping functions in part I. Although we can construct multi-band filtering functions from any single-band filtering function, we specifically employ equal-ripple filtering functions (colloquially called equiripple) as they provide excellent selectivity for filtering functions of reasonable orders. In [14] Cameron introduces a general technique for the development of single-band generalised Chebyshev filtering functions. As this technique is one of the most widely used methods of constructing equal-ripple single-band filtering functions, and as it is used in this work to design single-band prototypes, a detailed exposition of Cameron's theory is supplied in the next section.

2.5 The generalised Chebyshev filtering function

An N-th order Chebyshev polynomial of the first kind can be written in trigonometric form as follows:

$$C_N(\Omega') = \cosh\left(\sum_{n=1}^{N} \operatorname{arccosh}\left(x_n(\Omega')\right)\right) \tag{2.34}$$

For the case where $x_n(\Omega') = \Omega'$ the function in equation 2.34 reduces to the classic Chebyshev polynomial. Chebyshev polynomials have the property that $T_N(\Omega')$ oscillates between $T_N(\Omega') = +1$ and $T_N(\Omega') = -1$ when $\Omega' \in [-1, 1]$. The characteristics of the Chebyshev polynomials are illustrated in figure 2.2. All the roots of a Chebyshev polynomial are located inside a domain that corresponds to the passband of a single-band filter. Consequently the polynomial oscillates a maximum number of times inside the passband and has a constant gradient outside the passband. These properties make Chebyshev polynomials ideally suited to serve as single-band filtering functions. It has been proven that Chebyshev polynomials provide the optimum selectivity for any given order of filter if all the transmission zeros of that filter are located at infinity [70]. The only filters with higher selectivity for a given order are those that have an equal ripple response in both the passband and the stopbands. Functions that exhibit this property is referred to as elliptic functions. Cameron generalised the Chebyshev polynomial by artificially introducing transmission zeros into the function so that it exhibits a quasi-elliptic behaviour (almost elliptic). He achieved this by defining $x_n(\Omega')$ in such a way as to allow for finite frequency transmission zeros.

2.5.1 The functon $x_n(\Omega')$

We mentioned in section 2.2 that the zeros of a filtering function are the reflection zeros of a filter and that the poles of a filtering function are the transmission zeros of a filter. The form of $x_n(\Omega')$ must be chosen in such a manner that $C_N(\Omega')$ still behaves like a Chebyshev function whether finite frequency transmission zeros are specified or not. The following conditions are therefore imposed $x_n(\Omega')$:

1. Condition for transmission zeros:
   Ω'_n is defined as the n-th transmission zero. Transmission zeros are allowed to be located at positive

infinity, negative infinity or at some finite frequency point. At these frequency points we require that $x_n(\Omega') = \pm\infty$. This condition ensures that $C_N(\Omega')$ exhibits a pole at a transmission zero.

2. Condition for passband edges:
   At the passband edges when $\Omega' = \pm 1$, it is required that $x_n(\Omega') = \pm 1$.

3. Condition for equal ripple in passband:
   When $-1 \leq \Omega' \leq 1$, it is required that $-1 \leq x_n(\Omega') \leq 1$. Under such conditions the filtering function reduces to $C_N(\Omega') = \cos\left(\sum_{n=1}^{N} \arccos\left(x_n(\Omega')\right)\right)$. This function has an equal ripple passband.

For finite frequency transmission zeros we require for $x_n(\Omega')$ to be a rational function:

$$x_n(\Omega') = \frac{f(\Omega')}{\Omega' - \Omega'_n}$$

For the passband edges we require that:

$$x_n(\Omega' = \pm 1) = \left.\frac{f(\Omega')}{\Omega' - \Omega'_n}\right|_{\Omega'=\pm 1} = \pm 1$$

Thus $f(1) = 1 - \Omega'_n$ and $f(-1) = 1 + \Omega'_n$. Consequently $f(\Omega') = 1 - \Omega'\Omega'_n$. The form of $x_n(\Omega')$ is now as follows:

$$x_n(\Omega') = \frac{1 - \Omega'\Omega'_n}{\Omega' - \Omega'_n} \tag{2.35}$$

In order to ensure an equal ripple response in the passband, $x_n(\Omega')$ must be bounded. Cameron showed that $-1 \leq x_n(\Omega') \leq 1$ when $-1 \leq \Omega' \leq 1$ by proving that $x_n(\Omega')$ always has a positive gradient in the passband and noting that $x_n(\Omega' = \pm 1) = \pm 1$. Consequently $x_n(\Omega')$ is a monotonically increasing function on the domain $\Omega' \in [-1, 1]$ proving the bounded condition. The gradient of $x_n(\Omega')$ is calculated as follows:

$$\frac{\mathrm{d}x_n(\Omega')}{\mathrm{d}\Omega'} = \frac{(\Omega'_n)^2 - 1}{(\Omega' - \Omega'_n)^2}$$

Considering that the finite frequency transmission zeros are always located outside the passband, the gradient of $x_n(\Omega')$ is always positive. Lastly the definition of $x_n(\Omega')$ is adjusted to accommodate transmission zeros at infinity. This is done by dividing the numerator and the denominator of equation 2.35 with Ω'_n to arrive at:

$$x_n(\Omega') = \frac{\Omega' - \frac{1}{\Omega'_n}}{1 - \frac{\Omega'}{\Omega'_n}} \tag{2.36}$$

Equation 2.36 is the final form of $x_n(\Omega')$. Note that the filtering function simplifies to the standard Chebyshev definition when all transmission zeros are placed at infinity:

$$\lim_{\Omega'_n \to \infty} \{x_n(\Omega')\} = \cosh\left(\sum_{n=1}^{N} \operatorname{arccosh}(\Omega')\right)$$

The adapted form of the filtering function is thus a generalisation of the standard Chebyshev filtering function. Next we illustrate how to express equation 2.34 as a rational function defined in terms of the transmission zeros of the filtering function.

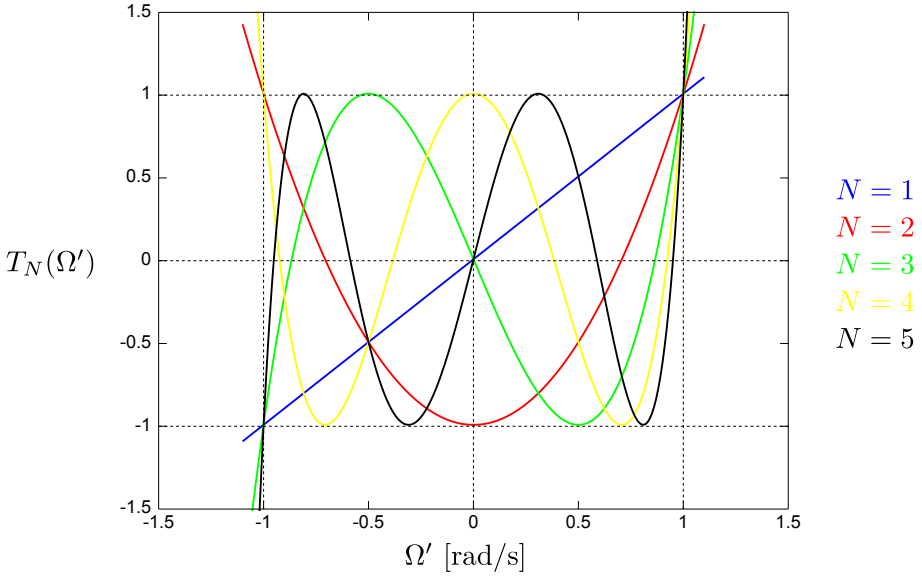

Figure 2.2: The first few Chebyshev polynomials of the first kind are shown above. The Chebyshev polynomials have the property that $-1 \leq T_N(\Omega') \leq 1$ when $\Omega' \in [-1, 1]$. All the roots of a Chebyshev polynomial of the first kind are located in the domain $\Omega' \in [-1, 1]$.

2.5.2 $C_N(\Omega')$ expressed as a rational function

It is known that $\text{arccosh}(x) = \log\left(x + \sqrt{x^2 - 1}\right)$ and $\cosh(x) = \frac{1}{2}\left(e^x + e^{-x}\right)$. As a consequence one can rewrite equation 2.34 as follows:

$$\begin{aligned} C_N(\Omega') &= \cosh\left(\sum_{n=1}^{N} \text{arccosh}\left(x_n(\Omega')\right)\right) \\ &= \frac{1}{2}\exp\left(\sum_{n=1}^{N} \ln\left(x_n(\Omega') + \sqrt{x_n(\Omega')^2 - 1}\right)\right) \\ &+ \quad \frac{1}{2}\exp\left(-\sum_{n=1}^{N} \ln\left(x_n(\Omega') + \sqrt{x_n(\Omega')^2 - 1}\right)\right) \end{aligned} \tag{2.37}$$

An exponential function raised to a sum of exponents, is the same as the product of the individual exponential functions each raised to a single exponent. Equation 2.37 can therefore be simplified as follows:

$$C_N(\Omega') = \frac{1}{2}\left[\prod_{n=1}^{N}\left(x_n(\Omega') + \sqrt{x_n(\Omega')^2 - 1}\right) + \prod_{n=1}^{N}\left(\frac{1}{x_n(\Omega') + \sqrt{x_n(\Omega')^2 - 1}}\right)\right] \tag{2.38}$$

Multiplying the numerator and denominator of the second term with $\prod_{n=1}^{N}\left(x_n(\Omega') - \sqrt{x_n(\Omega')^2 - 1}\right)$, equation 2.38 can be simplified to:

$$C_N(\Omega') = \frac{1}{2}\left[\prod_{n=1}^{N}\left(x_n(\Omega') + \sqrt{x_n(\Omega')^2 - 1}\right) + \prod_{n=1}^{N}\left(x_n(\Omega') - \sqrt{x_n(\Omega')^2 - 1}\right)\right] \tag{2.39}$$

Next we substitute equation 2.36 into equation 2.39. To save space, the substitution is performed in steps. The $\sqrt{x_n(\Omega')^2-1}$ terms can be expanded as follows:

$$\begin{aligned}\sqrt{x_n(\Omega')^2-1} &= \sqrt{\frac{\left(\Omega'-\frac{1}{\Omega'_n}\right)^2-\left(1-\frac{\Omega'}{\Omega'_n}\right)^2}{\left(1-\frac{\Omega'}{\Omega'_n}\right)^2}} \\ &= \sqrt{(\Omega')^2-1}\frac{\sqrt{1-\frac{1}{(\Omega'_n)^2}}}{1-\frac{\Omega'}{\Omega'_n}} \\ &= \hat{\Omega}\frac{\sqrt{1-\frac{1}{(\Omega'_n)^2}}}{1-\frac{\Omega'}{\Omega'_n}} \end{aligned} \tag{2.40}$$

Here $\hat{\Omega}$ is a transformed frequency variable and is equal to $\sqrt{\Omega'^2-1}$. Using equation 2.40, equation 2.39 is expressed as the following rational function:

$$C_N(\Omega') = \frac{1}{2}\left[\frac{\prod_{n=1}^{N}\left(\Omega'-\frac{1}{\Omega'_n}+\hat{\Omega}\sqrt{1-\frac{1}{(\Omega'_n)^2}}\right)+\prod_{n=1}^{N}\left(\Omega'-\frac{1}{\Omega'_n}-\hat{\Omega}\sqrt{1-\frac{1}{(\Omega'_n)^2}}\right)}{\prod_{n=1}^{N}\left(1-\frac{\Omega'}{\Omega'_n}\right)}\right] \tag{2.41}$$

The filtering function was defined as $C_N(\Omega') = \frac{F(\Omega')}{P(\Omega')}$ (refer to table 2.1). Therefore, the numerator of $C_N(\Omega')$ in equation 2.41 is an expression for $F(\Omega')$ in terms of the transmission zeros. Likewise the denominator of $C_N(\Omega')$ in equation 2.41 is an expression for $P(\Omega')$ in terms of the transmission zeros. In the next subsection we present Cameron's recursive method to quickly generate $F(\Omega')$ using the expression in equation 2.41 [14].

2.5.3 Recursive procedure to construct $F(\Omega')$

The presence of $\hat{\Omega}$ in equation 2.41 makes it seem that the numerator of equation 2.41 is not a polynomial. For a function to be classified as a polynomial, its variables must have non-negative integer exponents. If the numerator of equation 2.41 is however expanded, the resulting expression is always a polynomial in Ω'. This is the case as the $\hat{\Omega}$ variable is always raised to an even power. This is illustrated by assuming that N is a small number and then expanding the numerator of equation 2.41. In order to simplify notation equation 2.41 is written as follows:

$$C_N(\Omega') = \frac{1}{2}\left[\frac{\prod_{n=1}^{N}(c_n+d_n)+\prod_{n=1}^{N}(c_n-d_n)}{\prod_{n=1}^{N}\left(1-\frac{\Omega'}{\Omega'_n}\right)}\right] \tag{2.42}$$

Here $c_n = \Omega' - \frac{1}{\Omega'_n}$ and $d_n = \hat{\Omega}\sqrt{1-\frac{1}{(\Omega'_n)^2}}$. For the cases $N \in [1,3]$, we the numerator of equation 2.42 is expanded as follows:

$$\begin{aligned}\text{Num}\{C_1(\Omega')\} &= \frac{1}{2}[2c_1] = c_1 \\ \text{Num}\{C_2(\Omega')\} &= \frac{1}{2}[2c_1c_2+2d_1d_2] = c_1c_2+d_1d_2 \\ \text{Num}\{C_3(\Omega')\} &= \frac{1}{2}[2c_1c_2c_3+2c_1d_2d_3+2c_2d_1d_3+2c_3d_1d_2] = c_1c_2c_3+c_1d_2d_3+c_2d_1d_3+c_3d_1d_2\end{aligned}$$

In each case the transformed frequency variable is raised to an even power. This pattern persists for any N. The numerator of equation 2.42 thus evaluates to a polynomial. Cameron realised that $F(\Omega')$ can be systematically constructed in a recursive fashion. He introduced the polynomials $G_N(\Omega')$ and $G'_N(\Omega')$ to illustrate the

recursive technique:

$$F(\Omega') = \frac{1}{2}\left[\prod_{n=1}^{N}(c_n + d_n) + \prod_{n=1}^{N}(c_n - d_n)\right] = \frac{1}{2}\left[G_N(\Omega') + G_N^{'}(\Omega')\right] \tag{2.43}$$

Here $G_N(\Omega') = \prod_{n=1}^{N}(c_n + d_n)$ and $G_N^{'}(\Omega') = \prod_{n=1}^{N}(c_n - d_n)$. The polynomial $G_N(\Omega')$ can be separated into $U_N(\Omega')$ and $V_N(\Omega')$. Similarly one can separate $G_N^{'}(\Omega')$ into $U_N^{'}(\Omega')$ and $V_N^{'}(\Omega')$. The $V_N(\Omega')$ and $V_N^{'}(\Omega')$ polynomials contain terms that are influenced by the transformed frequency variable $\hat{\Omega}$. The $U_N(\Omega')$ and $U_N^{'}(\Omega')$ polynomials are pure polynomials in Ω', as follows:

$$\begin{aligned}
U_N(\Omega') &= u_0 + u_1\Omega' + \ldots + u_N\Omega'^N \\
V_N(\Omega') &= \hat{\Omega}\left[v_0 + v_1\Omega' + \ldots + v_N\Omega'^N\right] \\
U_N^{'}(\Omega') &= u_0^{'} + u_1^{'}\Omega' + \ldots + u_N^{'}\Omega'^N \\
V_N^{'}(\Omega') &= \hat{\Omega}\left[v_0^{'} + v_1^{'}\Omega' + \ldots + v_N^{'}\Omega'^N\right]
\end{aligned}$$

It is possible to construct these polynomials by starting with the terms associated with the first transmission zero, and then systematically introducing the remaining transmission zeros one at a time. After each iteration the resulting polynomial must again be separated into the new U and V polynomials. This is to separate the terms dependent on both Ω' and $\hat{\Omega}$ from the terms only dependent on Ω'. We next show the first two cycles of the construction of $G_N(\Omega')$. The process starts with the first transmission zero:

$$\begin{aligned}
G_1(\Omega') &= c_1 + d_1 \\
&= \left(\Omega' - \frac{1}{\Omega_1'}\right) + \left(\hat{\Omega}\sqrt{1 - \frac{1}{(\Omega_1')^2}}\right) \\
&= U_1(\Omega') + V_1(\Omega')
\end{aligned} \tag{2.44}$$

The terms associated with the second transmission zero are then multiplied with $G_1(\Omega')$. The resulting polynomial is then separated into $U_2(\Omega')$ and $V_2(\Omega')$ as follows:

$$\begin{aligned}
G_2(\Omega') &= G_1(\Omega')\,(c_2 + d_2) \\
&= (U_1(\Omega') + V_1(\Omega'))\left(\Omega' - \frac{1}{\Omega_2'} + \hat{\Omega}\sqrt{1 - \frac{1}{(\Omega_2')^2}}\right) \\
&= \left(\Omega' U_1(\Omega') - \frac{U_1(\Omega')}{\Omega_2'} + \hat{\Omega}V_1(\Omega')\sqrt{1 - \frac{1}{(\Omega_2')^2}}\right) + \left(\Omega' V_1(\Omega') - \frac{V_1(\Omega')}{\Omega_2'} + \hat{\Omega}U_1(\Omega')\sqrt{1 - \frac{1}{(\Omega_2')^2}}\right) \\
&= U_2(\Omega') + V_2(\Omega')
\end{aligned} \tag{2.45}$$

The term containing $\hat{\Omega}V_1(\Omega')$ is grouped into the $U_2(\Omega')$ polynomial. This is because $\hat{\Omega}^2$ is a polynomial in only Ω'. For similar reasons the term containing $\hat{\Omega}U_1(\Omega')$ is grouped into the $V_2(\Omega')$ polynomial. This process is continued for the remaining transmission zeros. The process is completed once N prescribed transmission zeros have been used to obtain $G_N(\Omega')$. The N transmission zeros include the finite frequency transmission zeros and those located at infinity. When the procedure above is performed for $G_N^{'}(\Omega')$, it becomes apparent that $U_N^{'}(\Omega') = U_N(\Omega')$ and $V_N^{'}(\Omega') = -V_N(\Omega')$. It is then possible to express $F(\Omega')$ as follows:

$$F(\Omega') = \frac{1}{2}\left[U_N(\Omega') + V_N(\Omega') + U_N^{'}(\Omega') + V_N^{'}(\Omega')\right] = U_N(\Omega')$$

Clearly the polynomial that results out of the recursive algorithm in equations 2.44 and 2.45 is $F(\Omega')$. We are now able to construct generalised Chebyshev filtering functions from prescribed transmission zeros.

2.5.4 Examples

This subsection contains two numerical examples of the construction of generalised Chebyshev polynomials. The specific examples are included because the resulting single-band filtering functions are later used as base functions from which we construct multi-band filtering functions. Most of the examples presented in this dissertation are linked to one another and form part of the design of the practical filters in chapters 8 to 10.

Example 1:

Generate the characteristic polynomials of a prototype filter of order four. The transmission zeros are all located at infinity. The return loss in the passband is 20 dB. We start by constructing $U_4(\Omega')$ from the prescribed transmission zeros. The recursive technique outlined in equations 2.44 and 2.45 is used and the following results are obtained:

$$\begin{aligned}
U_1(\Omega') &= \Omega' \\
V_1(\Omega') &= \hat{\Omega} \\
U_2(\Omega') &= 2(\Omega')^2 - 1 \\
V_2(\Omega') &= \hat{\Omega}(2\Omega') \\
U_3(\Omega') &= 4(\Omega')^3 - 3\Omega' \\
V_3(\Omega') &= \hat{\Omega}(4(\Omega')^2 - 1) \\
U_4(\Omega') &= 8(\Omega')^4 - 8(\Omega')^2 + 1 \\
V_4(\Omega') &= \hat{\Omega}(8(\Omega')^3 - 4(\Omega'))
\end{aligned}$$

Next we can construct $F(\Omega')$ by remembering that it has the same roots as $U_4(\Omega')$:

$$F(\Omega') = (\Omega')^4 - (\Omega')^2 + 0.125$$

Next we can map the roots of $F(\Omega')$ and $P(\Omega')$ (specified) to the S'-plane using $S' = j\Omega'$. We can then construct the associated S'-plane polynomials. Also note that $N - n_{fz}$ is even. Consequently we need to increase the phase of $P(S')$ with $\frac{\pi}{2}$ radians. The result is as follows:

$$\begin{aligned}
F(S') &= (S')^4 + (S')^2 + 0.125 \\
jP(S') &= j
\end{aligned}$$

We can now use equations 2.27 and 2.29 to find the normalisation constants as:

$$\begin{aligned}
\epsilon_r &= 1 \\
\epsilon &= 0.804
\end{aligned}$$

In order to generate $E(S')$ we must first calculate the roots of the polynomial $Q(S') = j\epsilon_r P(S') + \epsilon F(S')$ (refer to equation 2.33). These are found to be $\pm 0.3138 \pm 1.1948j$ and $\pm 0.7577 \pm 0.4949j$. The roots of $E(S')$ are all the roots of $Q(S')$ that are located on the left half of the complex plane and the para-conjugates of all the roots of $Q(S')$ that are located on the right half of the complex plane. The roots of $E(S')$ are therefore $-0.3138 \pm 1.1948j$ and $-0.7577 \pm 0.4949j$. Therefore an expression for $E(S')$ is as follows:

$$E(S') = (S')^4 + 2.1431(S')^3 + 3.2964(S')^2 + 2.8268(S') + 1.25$$

The calculated characteristic polynomials were used to obtain the scattering parameters of this prototype filter. The frequency response is shown in figure 2.3.

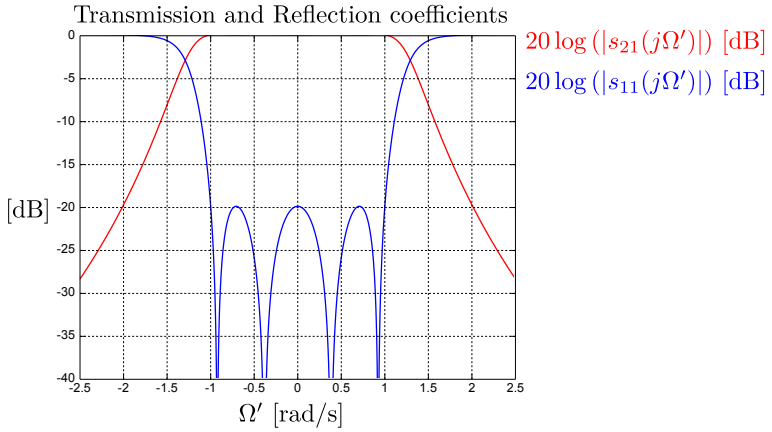

Figure 2.3: The transmission and reflection coefficients of the prototype filter in example 1. The figure was obtained using the polynomial definitions of the scattering parameters.

Example 2:

Generate the characteristic polynomials of a prototype filter of order two. The filter has one transmission zero located at $\Omega' = 2$ rad/s and one located at infinity. The return loss in the passband is 20 dB. We start by constructing $U_2(\Omega')$ from the prescribed transmission zeros. The recursive technique outlined in equations 2.44 and 2.45 is used and the following results are obtained:

$$\begin{aligned} U_1(\Omega') &= \Omega' - 0.5 \\ V_1(\Omega') &= 0.866\hat{\Omega} \\ U_2(\Omega') &= 1.866(\Omega')^2 - 0.5(\Omega') - 0.866 \\ V_2(\Omega') &= \hat{\Omega}(1.866\Omega' - 0.5) \end{aligned} \tag{2.46}$$

Next we can construct $F(\Omega')$ by remembering that it has the same roots as $U_2(\Omega')$:

$$F(\Omega') = (\Omega')^2 - 0.2679(\Omega') - 0.4641$$

Next we can map the roots of $F(\Omega')$ and $P(\Omega')$ (specified) to the S'-plane using $S' = j\Omega'$. We can then construct the associated S'-plane polynomials. The result is as follows:

$$\begin{aligned} F(S') &= (S')^2 - 0.2679j(S') + 0.4641 \\ P(S') &= (S') - 2j \end{aligned}$$

We can now use equations 2.27 and 2.29 to find the normalisation constants as:

$$\begin{aligned} \epsilon_r &= 1 \\ \epsilon &= 0.3751 \end{aligned}$$

In order to generate $E(S')$ we must first calculate the roots of the polynomial $Q(S')$. The quantity $N - n_{fz}$ is odd, so $Q(S') = \epsilon_r P(S') + \epsilon F(S')$ (refer to equation 2.33). The roots of $Q(S')$ are $-3.1269 - 1.2527j$ and $0.4608 + 1.5207j$. The roots of $E(S')$ are all the roots of $Q(S')$ that are located on the left half of the complex plane and the para-conjugates of all the roots of $Q(S')$ that are located on the right half of the complex plane. The roots of $E(S')$ are therefore $-3.1269 - 1.2527j$ and $-0.406 + 1.5207j$. Therefore an expression for $E(S')$ is

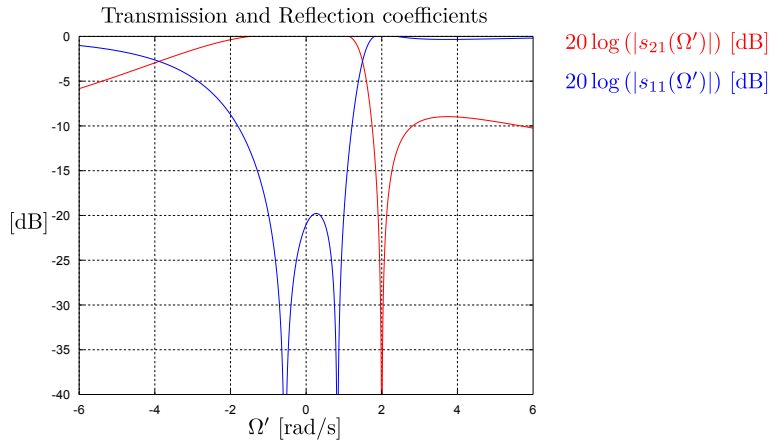

Figure 2.4: The transmission and reflection coefficients of the prototype filter in example 2. The figure was obtained using the polynomial definitions of the scattering parameters.

as follows:

$$E(S') = (S')^2 + (3.5877 - 0.2679j)(S') + 3.3458 - 4.1776j$$

The calculated characteristic polynomials were used to obtain the scattering parameters of this prototype filter. The frequency response is shown in figure 2.4.

2.6 Summary

In this chapter we introduced general definitions for the transfer functions of passive, lossless and reciprocal two-port networks. The transfer functions are constructed using scattering parameters as they are the most reliable measurements at microwave frequencies. The transfer functions are completely defined in terms of three characteristic polynomials and their normalisation constants. The characteristic polynomials are mathematically related to filtering functions. Approximation is usually performed by first finding a valid filtering function and then calculating the characteristic polynomials from said function. In section 2.5 we presented Cameron's method to construct generalised Chebyshev polynomials [14]. The generalised Chebyshev polynomials are used in this dissertation as the filtering functions of single-band prototype filters.

In part I we present new contributions on the theory of frequency mapping functions. The theory can be used to construct multi-band filtering functions and/or multi-band transfer functions from single-band filtering functions. Later in part II we present methods to synthesise multi-band circuits.

Part I

Approximation

Chapter 3

Polynomial mapping functions

Multi-band network functions can be constructed from single-band network functions using mapping functions. As any frequency mapping function must be constrained by the requirement that the resulting multi-band network function must be a realisable LC-function, only polynomials or rational polynomials can be used as mapping functions. In this chapter we propose the use of specific polynomials as frequency mapping functions. In chapter 4 we introduce a class of rational functions that are ideally suited to serve as frequency mapping functions. In this chapter however multi-band filtering functions, and their associated multi-band characteristic polynomials, are constructed from single-band filtering functions using polynomial mapping functions. The obtained characteristic polynomials can be used to design multi-band circuits using the methods presented in chapter 5.

3.1 Frequency mapping principle

In this section we briefly introduce the basic principle of frequency mapping that is used to construct multi-band functions from single-band functions. In section 2.4 we introduced the concept of designing a filter using prototype functions. Unfortunately the methodology described in section 2.4 is limited to the design of single-band filters. In this section we describe how the design technique can be extended to accommodate multi-band designs using frequency mapping functions. A frequency mapping function is defined as follows:

$$\Omega' = T(\Omega) \tag{3.1}$$

The function relates the single-band prototype frequency variable Ω', to the multi-band prototype frequency variable Ω. The multi-band prototype frequency variable is then related to the actual frequency variable ω through a denormalisation function [1]. There are now three frequency domains associated with a filter design – the two prototype frequency domains and the actual frequency domain [2]. A bandwidth specification is provided in the actual frequency domain. The specification is then transformed into a bandwidth specification in the multi-band prototype domain. A mapping function is then constructed to transform a single-band prototype into a multi-band prototype that has the desired bandwidth specification. Once a mapping function has been found, a multi-band filter can be designed through one of the following methods:

[1] The function that relates the actual frequency variable to the multi-band prototype variable is referred to as a normalisation function when it transforms the actual frequency variable into the prototype variable and a denormalisation function when it transforms the prototype variable back into the actual frequency variable.

[2] The single-band prototype complex frequency variable is $S' = j\Omega'$. The multi-band prototype complex frequency variable is $S = j\Omega$. The actual complex frequency variable is $s = j\omega$.

1. Multi-band filtering functions can be constructed from single-band filtering functions through the application of the following mapping procedure:

$$C_m(\Omega) = C_s(T(\Omega)) \tag{3.2}$$

Here $C_m(\Omega)$ is the multi-band filtering function and $C_s(\Omega')$ is the single-band filtering function. The multi-band filtering function can be used to find expressions for multi-band network functions and these can be used to synthesise multi-band circuits using established theory [62, 9, 61]. This methodology is followed in this chapter using polynomial mapping functions in conjunction with the method described in section 2.3. Well-known coupling matrix synthesis procedures are then employed in chapter 5 to synthesise multi-band coupled resonator circuits and actual filter designs using this technique are presented in chapters 8 and 9.

2. Frequency mapping functions can be synthesised as one-port impedance or admittance circuits. Single-band prototype circuits can then be transformed into multi-band prototype circuits by substituting frequency-dependent elements in the single-band prototype circuit with scaled versions of the mentioned impedance or admittance one-port. The single-band and multi-band circuit elements are related as follows:

	Single-band prototype circuit	Multi-band prototype circuit
Impedance	$Z(j\Omega') = j\Omega' L$	$Z(j\Omega) = jT(\Omega) L$
Admittance	$Y(j\Omega') = j\Omega' C$	$Y(j\Omega) = jT(\Omega) C$

The multi-band prototype circuit is now transformed into the actual multi-band filter through frequency and impedance scaling. The impedance scaling is performed in the traditional manner and the frequency scaling is performed using the dernormalisation function mentioned above [2]. This methodology is followed in chapters 4 and 6 where we present the rational mapping functions and the associated synthesis procedures respectively. An actual filter design using this methodology is presented in chapter 10.

3.2 Introduction to polynomial mapping functions

A polynomial is used to relate the single-band prototype frequency variable to the multi-band prototype frequency variable. The multi-band prototype frequency variable is then in turn related to the actual frequency variable through a standard lowpass-to-bandpass transformation (the denormalisation function)[2].

The idea of using a polynomial mapping function, followed by a standard lowpass-to-bandpass transformation as denormalisation function, was first illustrated (independently) by Macchiarella and Cameron in 2005 [20, 65]. Their method was limited to filters containing two passbands and they provided no indication of how one could extend their method to accommodate filters that have more passbands. The bandwidths of the passbands of their filters could also not be specified individually.

In this chapter we propose a technique for the design of filters that can contain more than two passbands. The technique presented here differs from others in the literature in the method that is followed to construct the polynomials and in the number of bands that can be accommodated. Polynomial mapping functions are constructed from a bandwidth specification in the multi-band prototype domain using Lagrange basis functions. The Lagrange functions were chosen as they are generally well-behaved for low-order interpolation problems. The polynomial mapping functions presented here are suitable to design filters containing two or three passbands.

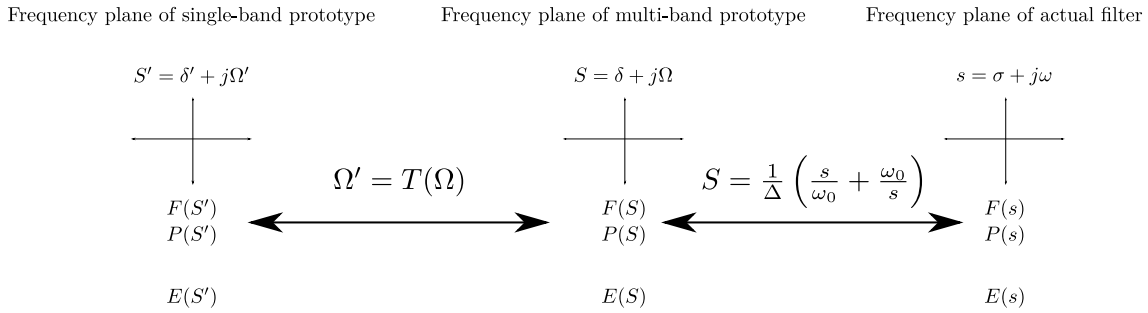

Figure 3.1: The multi-band prototype frequency domain is related to the actual frequency domain through the lowpass-to-bandpass transformation. The multi-band prototype frequency domain is again related to the single-band prototype frequency domain through a polynomial mapping function $\Omega' = T(\Omega)$.

3.3 Denormalisation using the standard lowpass-to-bandpass transformation

The lowpass-to-bandpass transformation relevent to this discussion is defined as follows [2]:

$$\Omega = \frac{1}{\Delta}\left[\frac{\omega}{\omega_0} - \frac{\omega_0}{\omega}\right] \tag{3.3}$$

$$\omega_0 = \sqrt{\omega_2\omega_1} \tag{3.4}$$

$$\Delta = \frac{\omega_2 - \omega_1}{\omega_0} \tag{3.5}$$

For multi-band filters ω_1 and ω_2 are the lowest frequency in the lowest passband and the highest frequency in the highest passband respectively. For single-band filters ω_1 and ω_2 are the lower and upper passband edge frequencies. Also ω_0 and Δ are defined as the centre frequency and fractional bandwidth respectively. The various relevant frequency domains are illustrated in figure 3.1. Equation 3.3 is a well-known denormalisation function and is frequently used to design bandpass filters from single-band prototype filters. We shall first discuss the case where equation 3.3 is used to design single-band filters. We shall then investigate the implications when equation 3.3 is used to design multi-band filters.

3.3.1 Single-band filters

A single-band filter has a single passband on the positive frequency axis and a single passband on the negative frequency axis. The magnitude of the frequency response is always symmetric and the phase of the frequency response asymmetric with respect to the zero-frequency. If these conditions are not met, it is impossible to synthesise a physically realisable circuit that has the desired frequency response [62]. Equation 3.3 therefore maps the two passbands of a single-band filter in the actual frequency domain to the one passband of the filter in the prototype frequency domain. A graphical illustration of the two frequency domains and the mentioned passbands is provided in figure 3.2. Figure 3.3 contains a plot of equation 3.3. The y-axis is the single-band prototype frequency variable and the x-axis is the actual frequency variable. As mentioned earlier, single-band prototypes usually have the property that the passband is defined as $\Omega' \in [-1, 1]$ and the stopbands as $\Omega' \in (-\infty, -1] \cap [1, \infty)$. Consequently, $\Omega' = \pm 1$ maps to the passband edge frequencies, here indicated as ω_2 and ω_1. The centre frequencies are the zeros of the lowpass-to-bandpass transformation. An important observation to be made is that equation 3.3 is not a linear function. The non-linearity is a function of the fractional bandwidth and the effect is more pronounced for higher fractional bandwidths.

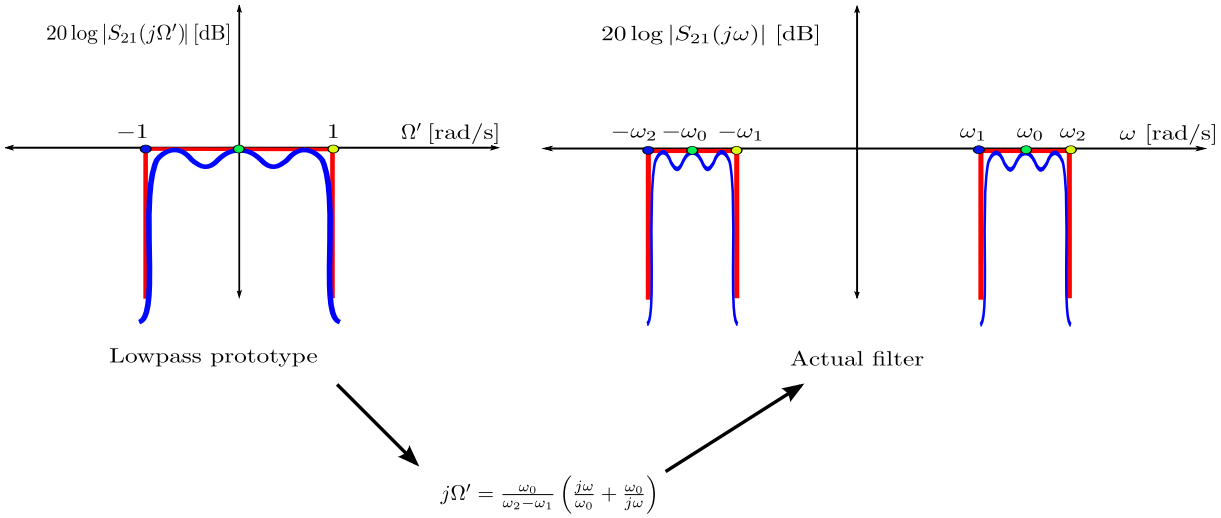

Figure 3.2: The relationship between the single-band prototype domain and the actual frequency domain is illustrated above. Left: The single-band prototype response. Right: The actual frequency response. Note the symmetry of the two passbands with respect to the zero-frequency. The red squares illustrate the ideal response and the blue functions illustrate an arbitrary approximated response.

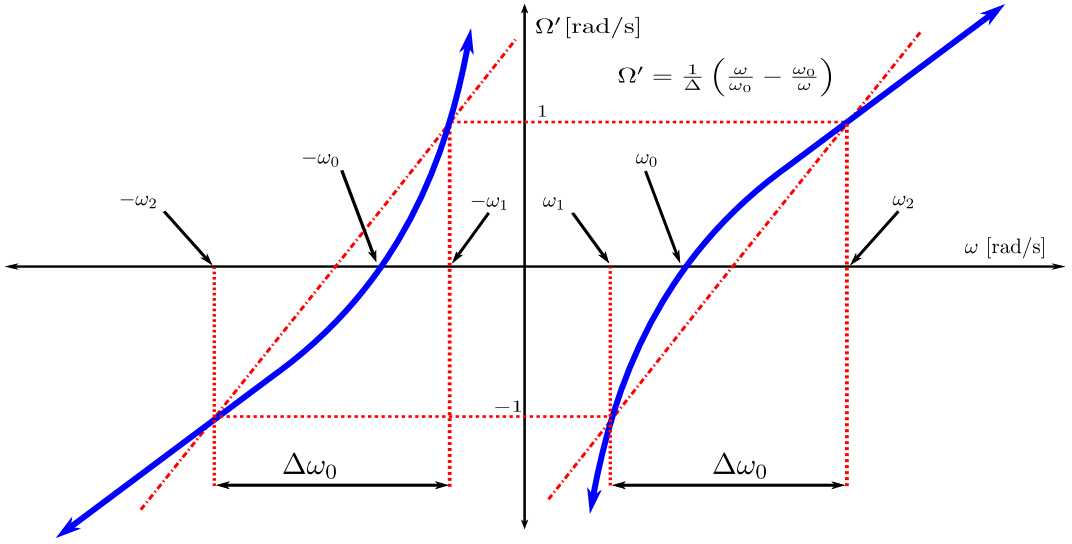

Figure 3.3: The lowpass-to-bandpass transformation is shown in blue. The y-axis contains the prototype frequency variable. The x-axis contains the actual frequency variable. It is clear that $\Omega' = \pm 1$ map to the passband edge frequencies in the actual frequency domain. Also $\Omega' = 0$ maps to the centre frequency in the actual frequency domain. An important observation is that the transformation is non-linear. The degree of non-linearity is a function of the fractional bandwidth.

3.3.2 Multi-band filters

For multi-band filters the centre frequency is defined as the geometric mean of the upper edge frequency of the highest passband and the lower edge frequency of the lowest passband. Note that the centre frequency is therefore not necessarily located inside one of the passbands. We can now deduce the required form of the multi-band prototype characteristic polynomials by normalising the edge frequencies of the passbands of a multi-band frequency response using equation 3.3. This procedure is graphically illustrated for the case of a dual-band filter in figure 3.4. From figure 3.4 we can conclude that equation 3.3 would normalise an arbitrary selection of passbands and stopbands in the actual frequency domain to a prototype where the passbands and the stopbands are not necessarily symmetrically positioned with respect to the zero frequency. We shall refer to these prototypes as *asymmetric multi-band prototypes*. A graphical illustration of the passband specification for a dual-band filter is provided in figure 3.5. Note that all the passbands are located within the region defined as $\Omega \in [-1, 1]$. Also note that the number of passbands in the prototype domain is equal to the number of passbands on the positive frequency axis of the final filter response. Asymmetric multi-band prototypes have transfer functions in s with complex coefficients. Inspection of table 2.1 show that the characteristic polynomials are indeed allowed to have complex coefficients. The problem is that if a circuit is entirely constructed from inductors, capacitors and resistors, the transfer function of the circuit will always be a rational function with real coefficients. Prototype filters with asymmetric frequency responses will therefore contain non-physical electrical components. Fortunately this is not a problem as they are merely intermediary circuits. If all of the reactive elements in the intermediary circuits are denormalised using equation 3.3, the resulting filter circuit would still contain non-physical electrical components. We shall later show in part II that the frequency responses of non-physical electrical components can be approximated over narrow bandwidths using normal capacitors and inductors. As a consequence, when we denormalise prototype circuits that contain non-physical electrical components, the resulting final filter circuits will only be valid over narrow bandwidths around the centre frequency. We can thus conclude that if we design multi-band filters using the lowpass-to-bandpass transformation in equation 3.3 as our denormalisation function, we must ensure that all the passbands are located in a narrow bandwidth around the overall centre frequency of the total frequency response. We shall provide more detail on the realisation of circuits containing non-ideal electrical components in part II.

In the next subsection we discuss the required form of the mapping function $T(\Omega)$.

3.4 Requirements of a polynomial mapping function

In this section we discuss the requirements of the polynomial mapping function. The range of the mapping function must be equal to the domain of the characteristic polynomials of the single-band prototype. The domain of the mapping function must be equal to the domain of the characteristic polynomials of the multi-band prototype. Passbands in the single-band prototype plane must map to passbands in the multi-band prototype plane. Likewise stopbands in the single-band prototype plane must map to stopbands in the multi-band prototype plane. The requirements can be summarised as follows:

- $|\Omega'| \leq 1$ should map to passbands.
- $|\Omega'| > 1$ should not map to passbands.
- $|\Omega'| = 0$ should map to the centre frequencies of the various passbands.

A graphical representation of an arbitrary mapping function that relates the single-band and multi-band prototype planes is shown in figure 3.6. The blue sections of $T(\Omega)$ are sections when passbands are mapped.

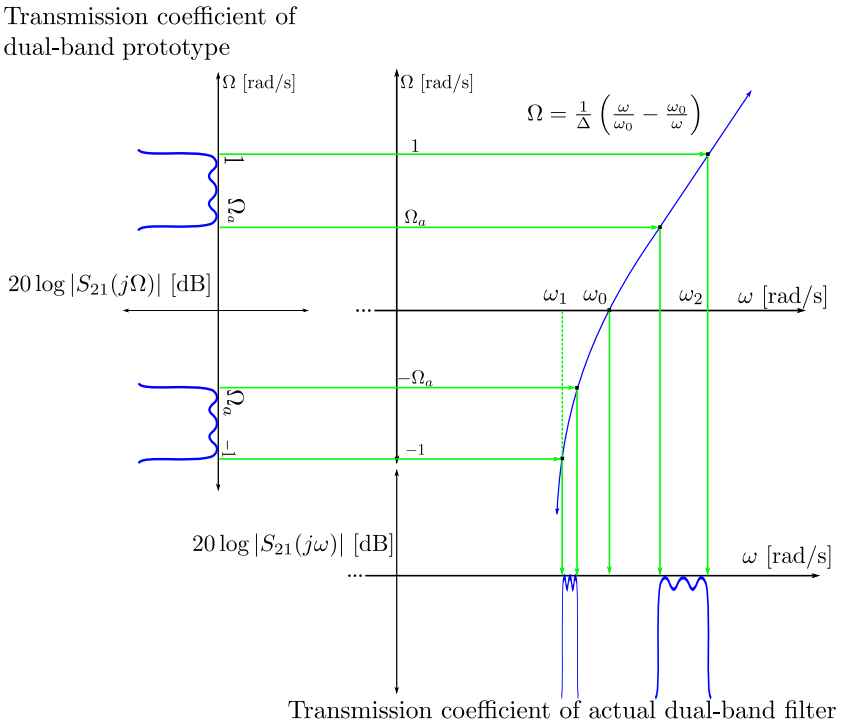

Figure 3.4: The transformation of the dual-band prototype frequency variable into the actual frequency variable is illustrated above. The y-axis is the dual-band prototype frequency variable and the x-axis is the actual frequency variable. Only the positive part of the actual frequency axis is shown. Top left: The dual-band prototype response. Top right: The lowpass-to-bandpass transformation for $\omega > 0$. Bottom: The actual frequency response.

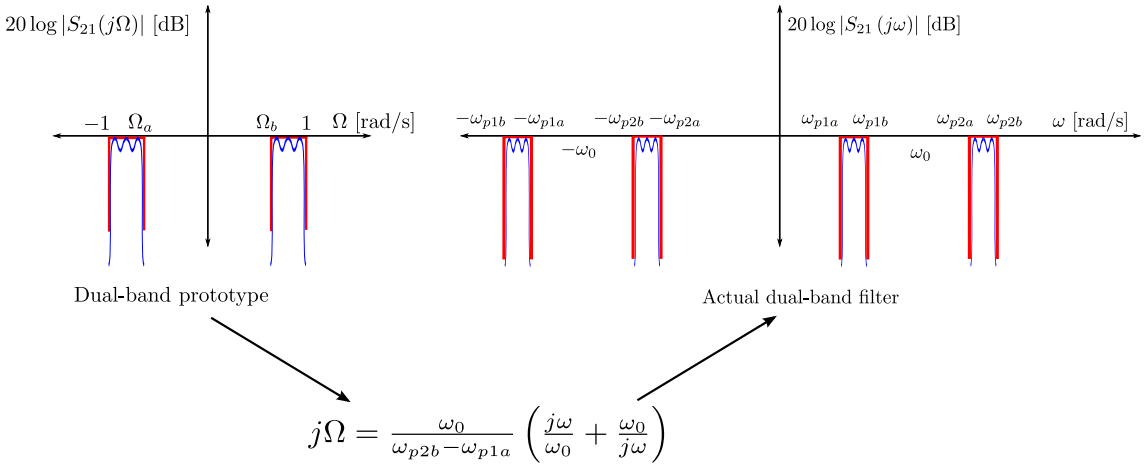

Figure 3.5: The relationship between the dual-band prototype domain and the actual frequency domain is illustrated above. Left: The dual-band prototype response. Right: The denormalised actual dual-band response. Note that the red squares illustrate the ideal response and the blue functions illustrate an arbitrary approximated response.

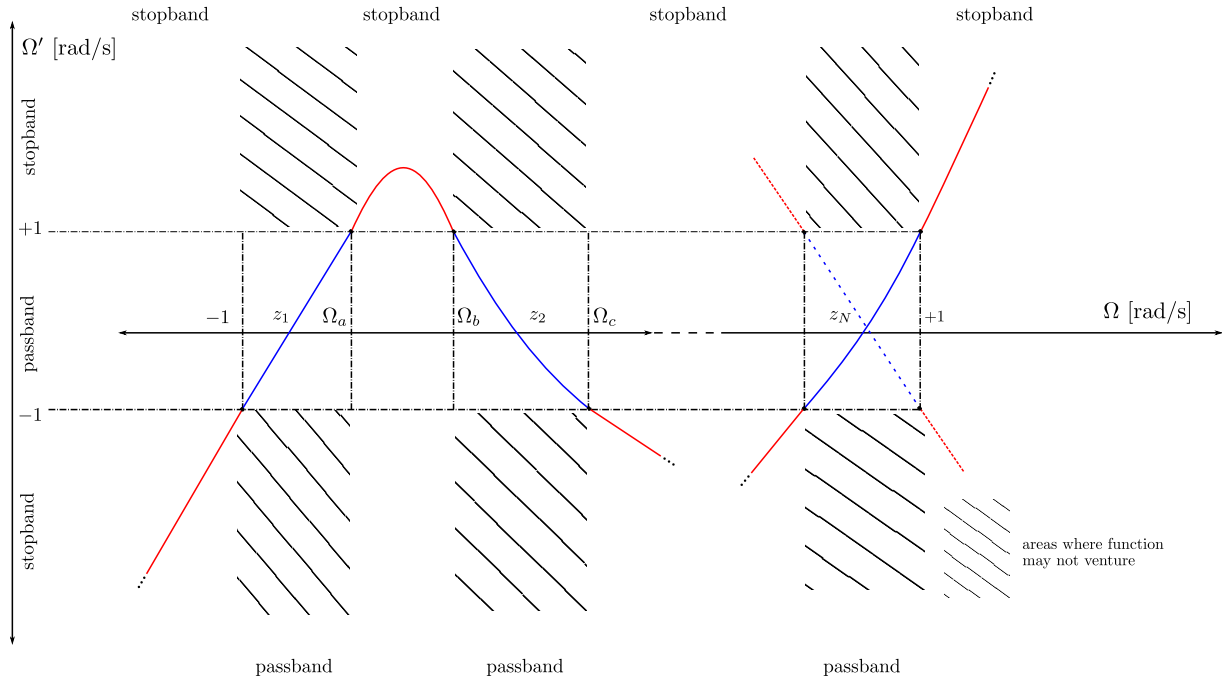

Figure 3.6: A graphical representation of the frequency mapping function $\Omega' = T(\Omega)$. The range of $T(\Omega)$ corresponds to the domain of the characteristic polynomials of the single-band prototype. The domain of $T(\Omega)$ corresponds to the domain of the characteristic polynomials of the multi-band prototype. The edges of the passbands of the multi-band prototype are indicated as $\{-1, \Omega_a, \ldots, \Omega_N, 1\}$. The blue sections of $T(\Omega)$ correspond to regions where passbands are mapped. The red sections of $T(\Omega)$ correspond to regions where stopbands are mapped.

The red sections of $T(\Omega)$ are sections when stopbands are mapped. Figure 3.6 also highlights the areas where the mapping function should not venture. This requirement ensures that the mapping function does not map parts of the stopbands into the passbands and vice versa. The multi-band passband edges are defined as $\{-1, \Omega_a, \ldots, \Omega_N, 1\}$. The mapping function must always evaluate to either $+1$ or -1 at a passband edge. The knowledge of the passband edge frequencies in the prototype domain can be used to generate a set of coordinates that are definitely located on the function $T(\Omega)$:

$$C_1 = \{(x_i, T(x_i))\} = \{(-1, -1)\,;(\Omega_a, 1)\,;(\Omega_b, 1)\,;(\Omega_c, -1)\,;\ldots(\pm 1, \pm 1)\} \tag{3.6}$$

These coordinates will be used to generate $T(\Omega)$ using a Lagrange interpolation method. The mapping function can evaluate to either $+1$ or -1 at a passband edge and the best results occurs if the following pattern is used: $-1; +1; +1; -1; -1; +1; +1 \ldots$. This pattern ensures that the interpolation is performed using the minimum number of zeros. The coordinates in figure 3.6 illustrate this notion. We shall next discuss how $T(\Omega)$ can be constructed using Lagrange basis functions.

3.5 Construction of polynomial

The mapping function $T(\Omega)$ is a Lagrange interpolation polynomial and is defined as follows:

$$T(\Omega) = \sum_{j=1}^{n} P_j(\Omega) \tag{3.7}$$

The polynomial $T(\Omega)$ is of degree $\leq (n-1)$ and is guaranteed to pass through the n points:

$$(\Omega_1, T(\Omega_1)), (\Omega_2, T(\Omega_2)), \ldots, (\Omega_k, T(\Omega_k)), \ldots, (\Omega_n, T(\Omega_n))$$

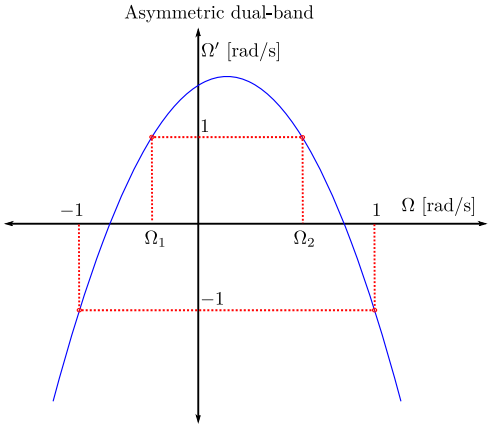

$$\Omega' = -\frac{(2\,\Omega_2 + 2\,\Omega_1)\,\Omega^3 + \left(-2\,{\Omega_2}^2 - 2\,\Omega_1\,\Omega_2 - 2\,{\Omega_1}^2 + 2\right)\,\Omega^2 + (-2\,\Omega_2 - 2\,\Omega_1)\,\Omega + \left({\Omega_1}^2 + 1\right)\,{\Omega_2}^2 + 2\,\Omega_1\,\Omega_2 + {\Omega_1}^2 - 1}{\left({\Omega_1}^2 - 1\right)\,{\Omega_2}^2 - {\Omega_1}^2 + 1}$$

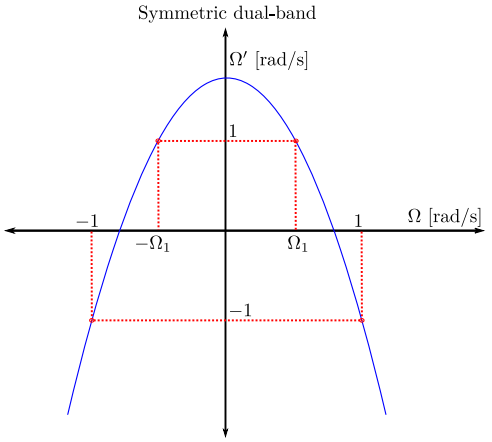

$$\Omega' = \frac{2\,\Omega^2 - {\Omega_1}^2 - 1}{{\Omega_1}^2 - 1}$$

Figure 3.7: Frequency mapping functions for symmetric and asymmetric dual-band prototypes are shown above. These functions were synthesised using Lagrange basis functions as shown in equation 3.7.

The polynomial $T(\Omega)$ is a linear combination of n Lagrange basis functions. Each basis function is defined as follows [72]:

$$P_j(\Omega) = T(\Omega_j) \prod_{\substack{k=1 \\ k \neq j}}^{n} \frac{\Omega - \Omega_k}{\Omega_j - \Omega_k} \tag{3.8}$$

The desired mapping function can now be generated from the coordinate set C_1 in equation 3.6 using a Lagrange polynomial. Figure 3.7 contains two example polynomial mapping functions for dual-band filters. The one example can generate an asymmetric dual-band prototype from a single-band prototype. The other example can generate a symmetric dual-band prototype from a single-band prototype.

We are now in a position to define a general frequency mapping procedure using polynomial mapping functions. The general procedure is presented in the next section.

3.6 General application of technique

A general technique to construct the characteristic polynomials of multi-band prototypes using polynomial mapping functions is described in this section. The procedure is as follows:

1. Determine the passband edge frequencies and the positions of the finite frequency transmission zeros in the multi-band prototype domain by mapping the actual frequency domain information to the multi-band prototype domain using the lowpass-to-bandpass transformation as shown in equation 3.3. Here the first passband edge frequency must map to -1 and the last passband edge frequency must map to 1.

2. Construct a coordinate set, C_1, from the multi-band prototype specification. An arbitrary coordinate set is shown in equation 3.6. All the passband edge frequencies must be included inside the coordinate set. One can also include frequency points in the stopband if certain transmission zero positions are required (illustrated in the example in section 3.7.1).

3. Construct the mapping function $\Omega' = T(\Omega)$ from the coordinate set C_1. This is achieved using equations 3.7 and 3.8.

4. An appropriate single-band prototype can now be found. The design specifications that must be chosen is the order of the single-band prototype, the minimum return loss in the passband as well as the positions of its finite frequency transmission zeros. If we want to construct an N-th order M-band filter, we require an N/M-th order single-band prototype. This is because the frequency mapping technique forces all the passbands to be of the same order. The single-band stopband is defined as $\Omega' \notin [-1, 1]$. The positions of the finite frequency transmission zeros must be determined from $T(\Omega)$. Transmission zeros cannot be placed arbitrarily inside the stopband of the single-band prototype. This is because only a part of the stopband is mapped from the single-band prototype domain to the multi-band prototype domain. The minimum return loss of the single-band prototype must be the same as the return loss figure for the multi-band prototype. A single-band prototype can now be constructed using the technique presented in chapter 2.5.

5. The roots of the $F(S')$ and $P(S')$ must be mapped to the multi-band domain using the relation $\Omega' = T(\Omega)$ and then used to construct $F(S)$ and $P(S)$ respectively. For high-order mapping functions the designer must discard the roots of $F(S)$ that are located outside of the wanted passbands and the roots of $P(S)$ that are located outside of the wanted stopbands. Note that if $N - n_{fz}$ is even, $P(S)$ must be multiplied by j to correct its phase.

6. The normalisation constants ϵ_r and ϵ is then calculated for the multi-band prototype. The technique shown in section 2.3 can be used.

7. The denominator polynomial $E(S)$ is constructed using alternating pole method presented in section 2.3.

We shall now clarify the presented theory by providing a couple of complete examples of the use of mapping functions to obtain multi-band characteristic polynomials.

3.7 Examples

This section contains three examples of the synthesis of the characteristic polynomials of multi-band filters using polynomial mapping functions. The first two examples presented here employ the single-band characteristic polynomials synthesised in section 2.5.4 and are included because they form part of the design of the

practical filters in chapters 8 and 9. The third example is included to illustrate how a three-band filter can be designed using the proposed method.

Example 1: Symmetric dual-band prototype

Suppose we want to obtain the characteristic polynomials of a dual-band prototype that has the following specifications:

- Passband 1: $\Omega \in [-1\ ;\ -0.5822]$.
- Passband 2: $\Omega \in [0.5822\ ;\ 1]$.
- Minimum return loss in passband 1: 20 dB.
- Order of dual-band filter: 8.
- The filter should be an all-pole filter. All the transmission zeros must be located at infinity.

This prototype specification is symmetric around $\Omega = 0$. We therefore know that our characteristic polynomials will have real coefficients. We start by choosing an appropriate coordinate set for our mapping function:

$$C_1 = \{(-1,-1)\ ;\ (-0.5822,1)\ ;\ (0.5822,1)\ ;\ (1,-1)\}$$

From C_1 we generate an appropriate mapping function $T(\Omega)$ using equations 3.7 and 3.8:

$$\Omega' = T(\Omega) = -3.0257\Omega^2 + 2.0257$$

Next we need to construct the single-band characteristic polynomials. We know that an eighth order dual-band filter requires a fourth order single-band prototype. The minimum return loss specification of the single-band prototype is also 20 dB. The characteristic polynomials of a single-band prototype with these specifications were derived in example 1 in section 2.5.4. The characteristic polynomials and their normalisation constants are as follows:

$$\begin{aligned} F(S') &= (S')^4 + (S')^2 + 0.125 \\ jP(S') &= j \\ E(S') &= (S')^4 + 2.1431(S')^3 + 3.2964(S')^2 + 2.8268(S') + 1.25 \\ \epsilon_r &= 1 \\ \epsilon &= 0.804 \end{aligned}$$

The single-band reflection zeros are given as:

$$\Omega' = \pm\{0.9239\ ;\ 0.3827\}$$

The transmission zeros of both the single-band and dual-band prototypes are all located at infinity, therefore only $F(\Omega')$ needs to be mapped to the dual-band domain. The single-band reflection zeros are mapped to the dual-band domain using $T(\Omega)$. The dual-band reflection zeros are then found to be:

$$\Omega = \pm\{0.9873\ ;\ 0.8922\ ;\ 0.7369\ ;\ 0.6035\}$$

From this we are able to construct two of the dual-band characteristic polynomials as follows:

$$\begin{aligned} F(S) &= S^8 + 2.678\,S^6 + 2.5802\,S^4 + 1.0541\,S^2 + 0.1534 \\ jP(S) &= j \end{aligned}$$

Next we can find the normalisation constants using equations 2.27 and 2.29. The result is as follows:

$$\epsilon = 67.3889$$
$$\epsilon_r = 1$$

Lastly we can find $E(S)$ using the alternating pole method presented in section 2.3. We start by finding the auxiliary function $Q(S)$ as follows:

$$\begin{aligned} Q(S) &= j\epsilon_r P(S) + \epsilon F(S) \\ &= 67.3889\,S^8 + 180.4676\,S^6 + 173.8738\,S^4 + 71.0349S^2 + 10.349 + j \end{aligned}$$

The roots of $Q(S)$ are obtained as follows:

$$S = \pm\{0.0502 + 1.0329j\ ;\ 0.1357 - 0.9228j\ ;\ 0.1711 + 0.7316j\ ;\ 0.0973 - 0.544j\}$$

The roots of $E(S)$ are all the roots of $Q(S)$ that are located on the left half of the complex plane and the para-conjugates of all the roots of $Q(S)$ that are located on the right half of the complex plane. The roots of $E(S)$ are therefore as follows:

$$S = \{-0.0502 \pm 1.0329j\ ;\ -0.1357 \pm 0.9228j\ ;\ -0.1711 \pm 0.7316j\ ;\ -0.0973 \pm 0.544j\}$$

An expression for $E(S)$ can now be found as follows:

$$\begin{aligned} E(S) = S^8 &+ 0.9087\,S^7 + 3.0909\,S^6 + 1.9876\,S^5 + 3.1954\,S^4 \\ &+ 1.3239\,S^3 + 1.2655\,S^2 + 0.2582\,S + 0.1542 \end{aligned}$$

All the dual-band characteristic polynomials are now known. The approximation problem is therefore solved. A graphical representation of the frequency mapping procedure is shown in figure 3.8. The figure shows how the two passbands of the dual-band filter are created using the frequency mapping function.

3.7.1 Example 2: Asymmetric dual-band prototype

Suppose we want to obtain the characteristic polynomials of a dual-band prototype that has the following specifications:

- Passband 1: $\Omega \in [-1\ ;\ -0.5476]$.
- Passband 2: $\Omega \in [0.7575\ ;\ 1]$.
- Minimum return loss in passband 1: 20 dB.
- Order of dual-band filter: 4.
- The filter should have finite frequency transmission zeros at $\Omega = 0.1752$ and $\Omega = 0.3725$.

This prototype specification is asymmetric around $\Omega = 0$. We therefore know that our characteristic polynomials will have complex coefficients. The first step is to find an appropriate coordinate set (C_1) for the mapping function. As usual, coordinates associated with the passband edges must be included in C_1. We want to place transmission zeros in the stopband between the two passbands at specific frequencies. We therefore include two coordinates in C_1 that control the two transmission zeros inside the inner stopband. The Ω-value of these

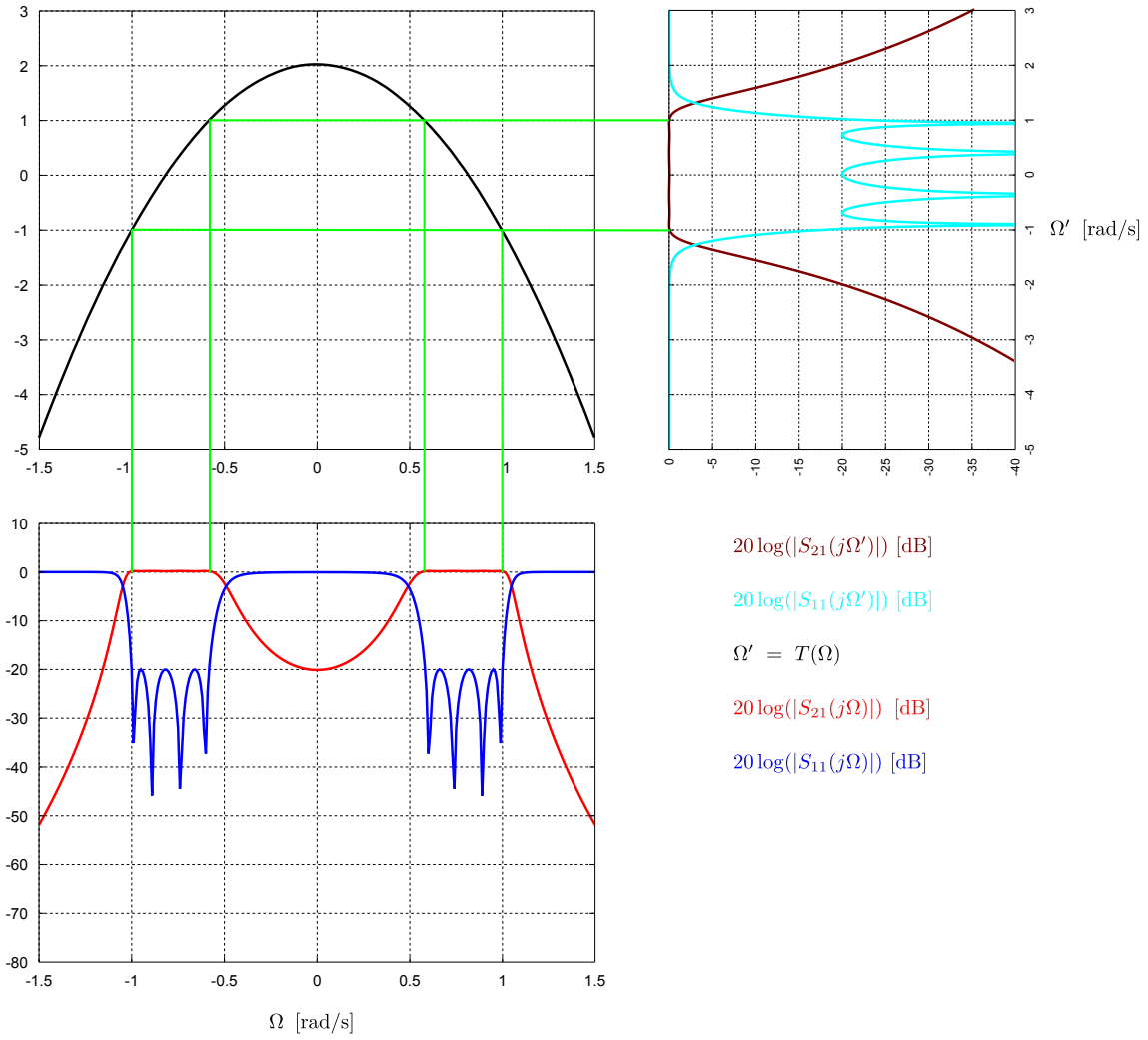

Figure 3.8: A graphical representation of the synthesis of multi-band prototypes using frequency mapping functions. Top right: Frequency response of single-band prototype. Top left: The frequency mapping function $T(\Omega)$. Bottom: Frequency response of the dual-band prototype. The passband of the single-band prototype is mapped to the two passbands of the dual-band prototype.

coordinates must correspond to the positions of the transmission zeros in the dual-band prototype. The $T(\Omega)$ value of the coordinates is equal to the location of the transmission zero in the single-band prototype domain. We employ the single-band prototype derived in example 2 in section 2.5.4, that has a finite frequency transmission zero at $\Omega' = 2$, as our base function and therefore use $(0.1752, 2)$; $(0.3725, 2)$ as the coordinate points to control the transmission zero placement. The complete coordinate set is given as follows:

$$C_1 = \{(-1,-1)\ ;\ (-0.5476, 1)\ ;\ (0.1752, 2)\ ;\ (0.3725, 2)\ ;\ (0.7575, 1)\ ;\ (1,-1)\}$$

From C_1 we generate an appropriate mapping function $T(\Omega)$ using equations 3.7 and 3.8:

$$\Omega' = T(\Omega) = -0.1791\,\Omega^5 - 1.7807\,\Omega^4 - 0.7719\,\Omega^3 - 1.0921\,\Omega^2 + 0.9509\,\Omega + 1.8728$$

The characteristic polynomials of a single-band prototype were derived in example 2 in section 2.5.4. The characteristic polynomials and their normalisation constants are as follows:

$$\begin{aligned} F(S') &= (S')^2 - 0.2679j\,(S') + 0.4641 \\ P(S') &= (S') - 2j \\ E(S') &= (S')^2 + (3.5877 - 0.2679j)(S') + 3.3458 - 4.1776j \\ \epsilon_r &= 1 \\ \epsilon &= 0.3751 \end{aligned}$$

The single-band reflection zeros are as follows:

$$\Omega' = \{0.8283\ ;\ -0.5604\}$$

The single-band reflection zeros are mapped to the dual-band domain using $T(\Omega)$. The dual-band reflection zeros, that are located inside of the desired bands, are as follows:

$$\Omega = \{0.9598\ ;\ 0.787\ ;\ -0.9329\ ;\ -0.6106\}$$

In a similar fashion the single-band transmission zeros are mapped to the dual-band domain. There is only one single-band transmission zero at $\Omega' = 2$. The dual-band transmission zeros that are located inside the desired bands are given as:

$$\Omega = \{0.1752\ ;\ 0.3725\}$$

From this we are able to construct two of the dual-band characteristic polynomials as follows:

$$\begin{aligned} F(S) &= S^4 - 0.2038j\,S^3 + 1.3716\,S^2 - 0.1713jS + 0.4306 \\ jP(S) &= j\,S^2 + 0.5477\,S - 0.0653j \end{aligned}$$

Note that $N - n_{fz}$ is even for the dual-band filter. We therefore had to adjust the phase of $P(S)$. Next we can find the normalisation constants using equations 2.27 and 2.29. The result is as follows:

$$\begin{aligned} \epsilon &= 1.9568 \\ \epsilon_r &= 1 \end{aligned}$$

Lastly we can find $E(S)$ using the alternating pole method presented in section 2.3. We start by finding the auxiliary function $Q(S)$ as follows:

$$\begin{aligned} Q(S) &= j\epsilon_r P(S) + \epsilon F(S) \\ &= 1.9568\,S^4 - 0.3987j\,S^3 + (2.6839 + j)\,S^2 + (0.5477 - 0.3352j)\,S + 0.8426 - 0.0653j \end{aligned}$$

The roots of $Q(S)$ are obtained as:

$$S = \{0.3661 - 1.1196j\ ;\ -0.2522 + 1.0633j\ ;\ 0.1058 + 0.6886j\ ;\ -0.2197 - 0.4286j\}$$

The roots of $E(S)$ are all the roots of $Q(S)$ that are located on the left half of the complex plane and the para-conjugates of all the roots of $Q(S)$ that are located on the right half of the complex plane. The roots of $E(S)$ are therefore given as:

$$S = \{-0.3661 - 1.1196j\ ;\ -0.2522 + 1.0633j\ ;\ -0.1058 + 0.6886j\ ;\ -0.2197 - 0.4286j\}$$

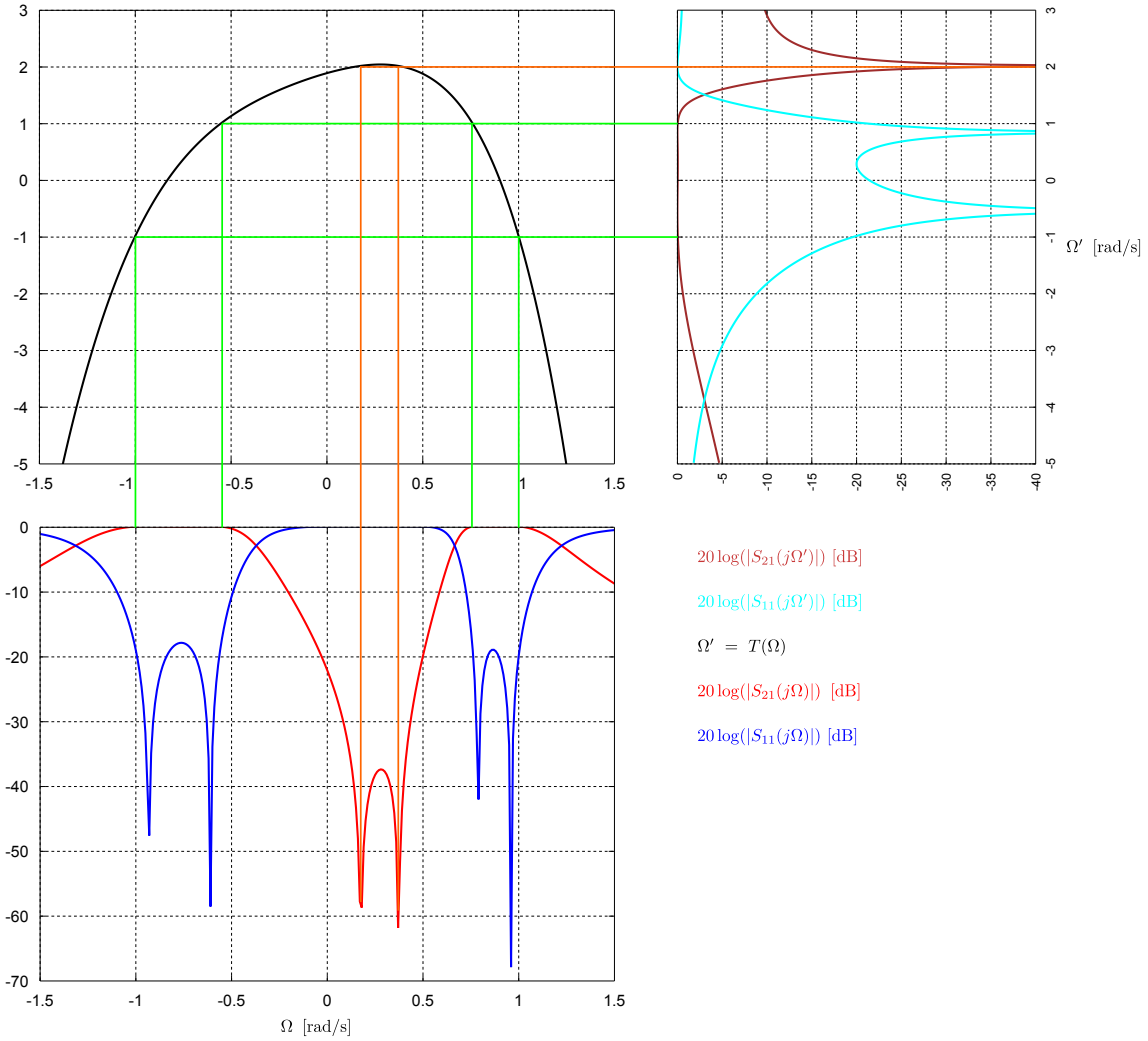

Figure 3.9: A graphical representation of the synthesis of multi-band prototypes using frequency mapping functions. Top right: Frequency response of single-band prototype. Top left: The frequency mapping function $T(\Omega)$. Bottom: Frequency response of the dual-band prototype. The passband of the single-band prototype is mapped to the two passbands of the dual-band prototype. A single single-band transmission zero is mapped to two specific frequencies in the dual-band domain inside the inner stopband.

An expression for $E(S)$ can now be found as follows:

$$E(S) = S^4 + (0.9439 - 0.2038j)\,S^3 + (1.8170 - 0.3554j)\,S^2 + (0.5926 - 0.4160j)\,S + 0.3970 - 0.1700j$$

All the dual-band characteristic polynomials are now known. The approximation problem is therefore solved. A graphical representation of the frequency mapping procedure is shown in figure 3.9. Note that the return loss in the two passbands are not equal to the return loss of the original single-band prototype. This is because we discarded poles and zeros that fall outside of the desired bands. The synthesised dual-band transfer functions however still meets our design specifications.

3.7.2 Example 3: Symmetric three-band prototype

This example is included to illustrate the design of a three-band filter. Suppose we want to obtain the characteristic polynomials of prototype filter that has the following specifications:

- Passband 1: $\Omega \in [-1\ ;\ -0.8]$.
- Passband 2: $\Omega \in [-0.1\ ;\ 0.1]$.
- Passband 3: $\Omega \in [0.8\ ;\ 1]$.
- Minimum return loss in passband 1: 20 dB.
- Order of three-band filter: 9.
- Adjacent passbands should be separated with two finite frequency transmission zeros.

We start by finding an appropriate coordinate set (C_1) for the mapping function. As usual, coordinates associated with the passband edges must be included in C_1. Adjacent passbands should be separated with two finite frequency transmission zeros. The exact positions of the transmission zeros were not specified, therefore we do not include coordinates for them in C_1. The coordinate set is given as follows:

$$C_1 = \{(-1,-1)\ ;\ (-0.8,1)\ ;\ (-0.1,1)\ ;\ (0.1,-1)\ ;\ (0.8,-1)\ ;\ (1,1)\}$$

From C_1 we generate an appropriate mapping function $T(\Omega)$ using equations 3.7 and 3.8:

$$\Omega' = T(\Omega) = -7.7160\,\Omega^5 + 18.9043\,\Omega^3 - 10.1883\Omega$$

Next we need to construct the single-band characteristic polynomials. We know that a ninth order three-band filter requires a third order single-band prototype. The minimum return loss specification of the single-band prototype is 20 dB. A plot of the mapping function $T(\Omega)$ is shown in the top left of figure 3.10. If a single-band prototype has a transmission zero in the region $\Omega' \in (1.55; 3.0056]$, the function $T(\Omega)$ can map that transmission zero to two positions in the three-band domain between the first and second passbands and to one position below the first passband. In a similar fashion, if a single-band prototype has a transmission zero in the region $\Omega' \in [-3.0056; -1.55)$, the function $T(\Omega)$ can map that transmission zero to two positions in the three-band domain between the second and third passbands and to one position above the third passband. The single-band prototype for this design is a third-order generalised Chebyshev polynomial with 20 dB minimum return loss in the passband and finite frequency transmission zeros at $\Omega' = 3.0056$ and $\Omega' = -3.0056$. The characteristic polynomials of a single-band prototype with these specifications were derived using the methods presented in section 2.5 and the resulting characteristic polynomials and their normalisation constants are as follows:

$$\begin{aligned} F(S') &= (S')^3 + 0.7644(S') \\ P(S') &= (S')^2 + 9.0336 \\ E(S') &= E(S') = (S')^3 + 2.2835(S')^2 + 3.3291(S') + 2.6355 \\ \epsilon_r &= 1 \\ \epsilon &= 3.4277 \end{aligned}$$

The single-band reflection zeros are given as:

$$\Omega' = \{\pm 0.8743\ ;\ 0\}$$

There are two single-band transmission zeros at $\Omega' = \pm 3.0056$. The single-band reflection zeros are mapped to the three-band domain using $T(\Omega)$. Note that there are now multiple solutions. Only the solutions that are located inside the passbands are valid solutions. The three-band reflection zeros are given as:

$$\Omega = \{\pm 0.9848\ ;\ \pm 0.8947\ ;\ \pm 0.8121\ ;\ \pm 0.0870\ ;\ 0\}$$

Next the single-band transmission zeros are mapped to the three-band domain. We are only interested in placing transmission zeros between adjacent passbands. We therefore discard the zeros that map to the outer stopbands. The three-band transmission zeros are $\Omega = \{\pm 0.4580 \ ; \ \pm 0.4574\}$. From this we are able to construct two of the three-band characteristic polynomials as follows:

$$F(S) = S^9 + 2.4373\,S^7 + 1.9622\,S^5 + 0.5267\,S^3 + 0.0039\,S$$
$$P(S) = S^4 + 0.4190\,S^2 + 0.0439$$

Next we can find the normalisation constants using equations 2.27 and 2.29. The result is as follows:

$$\epsilon = 30.7840$$
$$\epsilon_r = 1$$

Lastly we can find $E(S)$ using the alternating pole method presented in section 2.3. We start by finding the auxiliary function $Q(S)$ as follows:

$$\begin{aligned} Q(S) &= j\epsilon_r P(S) + \epsilon F(S) \\ &= 30.7840\,S^9 + 75.0303\,S^7 + 60.4033\,S^5 + S^4 \\ &\qquad + 16.2135\,S^3 + 0.4190\,S^2 + 0.1194\,S + 0.0439 \end{aligned}$$

The roots of $Q(S)$ are obtained as follows:

$$S = \{-0.0647 \pm 1.0375j \ ; \ -0.1276 \ ; \ 0.1256 \pm 0.8906j \ ; \ 0.0557 \pm 0.1368j \ ; \ -0.0529 \pm 0.7636j\}$$

The roots of $E(S)$ are all the roots of $Q(S)$ that are located on the left half of the complex plane and the para-conjugates of all the roots of $Q(S)$ that are located on the right half of the complex plane. The roots of $E(S)$ are therefore given as:

$$S = \{-0.0647 \pm 1.0375j \ ; \ -0.1276 \ ; \ -0.1256 \pm 0.8906j \ ; \ -0.0557 \pm 0.1368j \ ; \ -0.0529 \pm 0.7636j\}$$

An expression for $E(S)$ can now be found as follows:

$$\begin{aligned} E(S) &= S^9 + 0.7255\,S^8 + 2.7005\,S^7 + 1.4319\,S^6 \\ &\qquad + 2.3250\,S^5 + 0.8365\,S^4 + 0.6627\,S^3 + 0.1394\,S^2 + 0.0193\,S + 0.0014 \end{aligned}$$

All the three-band characteristic polynomials are now known. The approximation problem is therefore solved. A graphical representation of the frequency mapping procedure is shown in figure 3.10. The green lines indicate how the reflection zeros are mapped from the single-band prototype to the three passbands of the three-band prototype. The orange lines show how the single-band transmission zeros are mapped to positions between adjacent passbands in the three-band domain. Again, due to the discarded poles and zeros, the passbands of the three-band transfer functions are not bandwidth-scaled and frequency-translated copies of the original single-band transfer functions. The three-band transfer functions however still meet the design specifications.

It is now appropriate to elaborate on the limitations of the polynomial mapping technique.

3.8 Limitations of polynomial mapping functions

In this section we shall provide reasons why polynomials are not ideally suited to serve as mapping functions. A polynomial of order N can interpolate $N + 1$ points. An M-band filter has $2M$ passband edge frequencies.

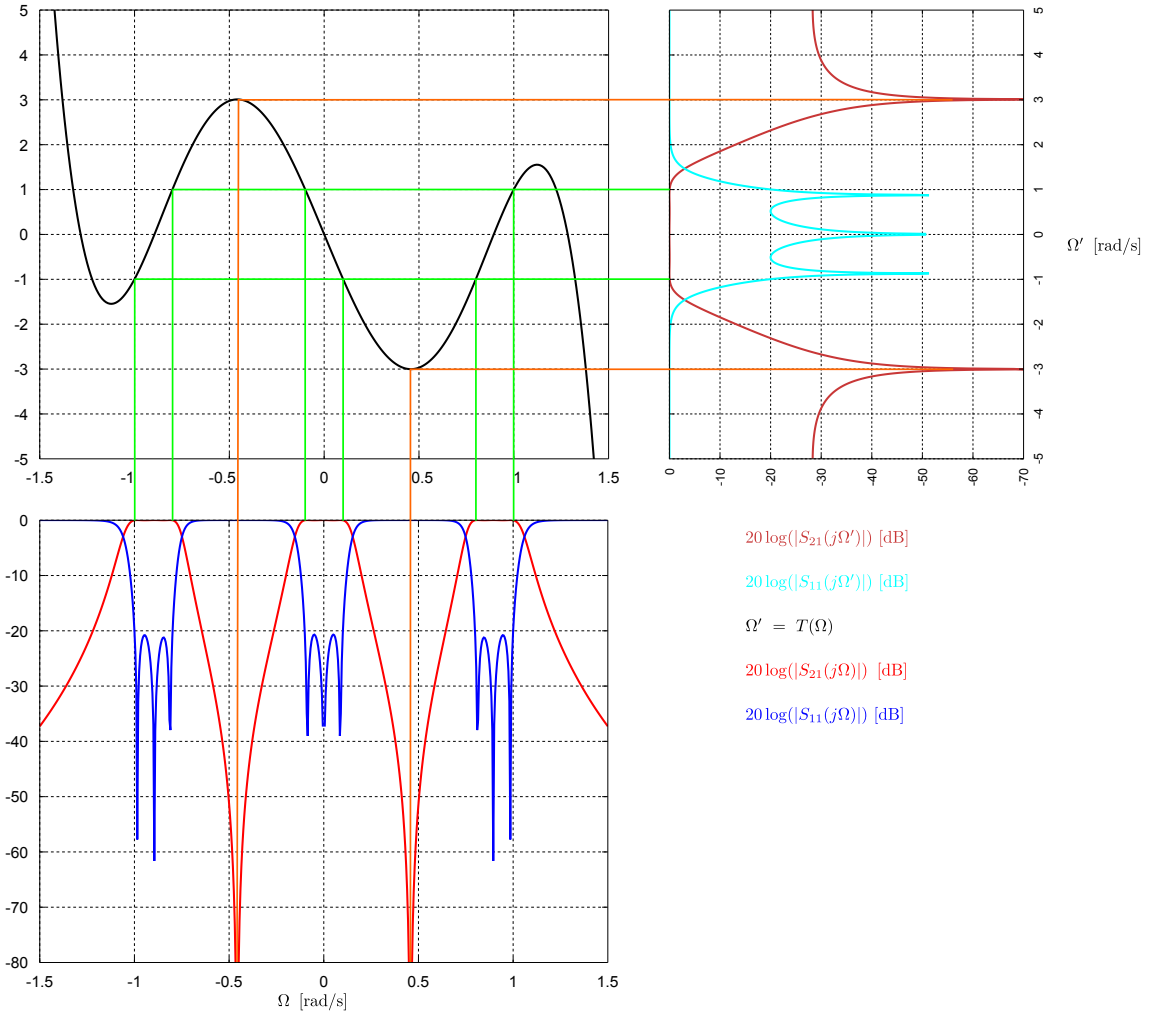

Figure 3.10: A graphical representation of the synthesis of multi-band prototypes using frequency mapping functions. Top right: Frequency response of single-band prototype. Top left: The frequency mapping function $T(\Omega)$. Bottom: Frequency response of the three-band prototype. The passband of the single-band prototype is mapped to the three passbands of the three-band prototype. The transmission zeros of the single-band prototype are mapped to positions between adjacent passbands in the three-band domain.

All of the edge frequencies must be interpolated by the mapping function. An M-band filter would therefore require a polynomial mapping function of order $2M - 1$ to ensure that all the passband edge frequencies are interpolated. An issue now arises as the zeros of the mapping function coincide with passband centre frequencies. A polynomial of order $2M - 1$ would therefore generate $M - 1$ unwanted passbands. One can partly circumvent this problem by consciously ignoring the poles and zeros of the multi-band filtering function that are located outside of the desired passbands and stopbands. The issue with this method is that the bandwidths and ripple levels of the remaining passbands start to distort. The limitation does not render the technique useless as the unwanted passbands only really become a problem if they are located close to the desired passbands.

The serious problem with polynomial mapping functions is that one cannot control the positions of the zeros of the polynomial and situations can arise where parts of the stopband will be mapped to areas inside the passband. This situation is illustrated in figure 3.11. A related issue is that the stopbands are not adequately mapped to the area between adjacent passbands. All of the mentioned limitations only really become a problem for filters with a high number of passbands. Polynomial mapping functions are more than adequate to

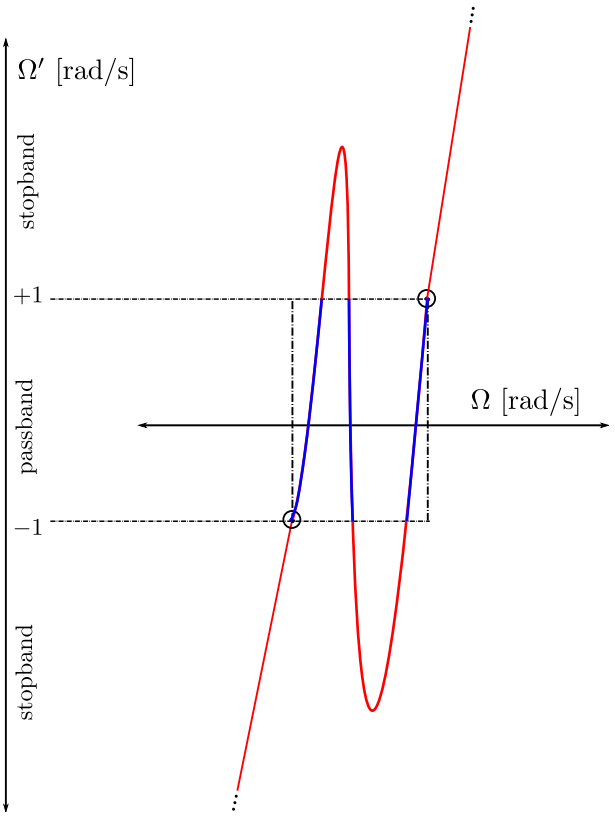

Figure 3.11: A limitation of polynomial mapping functions is that one cannot control the positions of the zeros. It is possible that more than one zero can be positioned between two interpolation points and thus resulting in cases where the single-band stopband is mapped into a multi-band passband. This situation is illustrated above.

design filters with up to three passbands. Later in chapter 4 we present mapping functions that have none of the issues associated with polynomial mapping functions.

3.9 Summary

In this chapter we considered the use of polynomials as mapping functions. The polynomials were used to construct multi-band characteristic polynomials from single-band characteristic polynomials. We defined the lowpass-to-bandpass function listed as equation 3.3 as our denormalisation function. We illustrated that multi-band filters designed using the lowpass-to-bandpass transformation as denormalisation function generally have characteristic polynomials with complex coefficients. Circuits such as these contain non-physical electrical components. Fortunately one can approximate these circuits over finite bandwidths using equivalent circuits. The important point to note is that when a circuit is designed using an asymmetric prototype and then denormalised using the lowpass-to-bandpass transformation, the circuit immediately becomes a narrowband circuit.

We illustrated the construction of polynomial mapping functions using Lagrange basis functions and outlined the general technique that can be followed to design filters using this method. We provided various examples to illustrate the application of the technique.

From the discussion in section 3.8 we conclude that polynomials are not ideally suited to serve as mapping functions. In the next chapter we present rational mapping functions. These functions solve all of the inherent problems associated with polynomial mapping functions. Even though polynomials are not ideally suited

to serve as mapping functions they can still be used in designs. The theory presented in this chapter, in conjunction with the theory in chapters 5 and 7, were employed to design the filters in chapters 8 and 9.

Chapter 4

Rational mapping functions

From chapter 3 it is clear that the use of polynomials as mapping functions involve fundamental limitations as the main problem, i.e. that of mapping the stopband, is a direct consequence of the polynomial approach. This chapter proposes the use of rational functions as frequency mapping functions. Specifically the reactance function of a lossless one-port circuit. The theory can be used to construct N-band mapping functions, which can in turn be used to design N-band filters. The theory is rigorous and the procedure is general. There is no limitation with respect to the number of bands which can be created. Likewise, there is no limitation with respect to the centre frequencies and bandwidths of the passbands – these can be chosen completely arbitrarily. The resulting multi-band filters have frequency responses where each band is an exact bandwidth-scaled and frequency-translated copy of the original single-band low-pass function. The synthesis procedures associated with the theory presented in this chapter are simple and elegant, and are treated in detail in chapter 6.

4.1 Introduction

Rational functions have been applied to the design of multi-band filters by Macchiarella et al. and later by Lee et al. [20, 38]. Their methods were limited to filters containing two or three bands and the associated calculations were tedious. At a later stage progress was made by Garcia et al. when they presented a method to design filters containing N-passbands [48]. Their method did not directly employ rational mapping functions but nonetheless enabled designers to design N-band coupled resonator filters. Their method is however limited to narrowband coupled resonator circuits. To the author's knowledge, no technique to design general N-band filters using rational mapping functions have been presented to date. In this chapter we present a general approach to the design of N-band filters using rational mapping functions. The theory presented here is based on the insertion loss method and applies to all filters and can accommodate any bandwidth specification. The theory enables one to construct a lumped element multi-band filter circuit for any passband specification where each passband is a bandwidth-scaled and frequency-translated copy of a single-band prototype circuit.

Two different formulations of the same theory is presented. In the first formulation the standard lowpass-to-bandpass transformation is used in conjunction with a rational mapping function to relate the single-band prototype frequency variable to the actual multi-band frequency variable. This formulation is only valid for narrowband filters and is intended to be used for the design of coupled resonator filters. In the second formulation a linear denormalisation function is used in conjunction with a rational mapping function to relate the single-band prototype frequency variable directly to the actual multi-band frequency variable. This formulation is completely general and can be used to design lumped element multi-band filter circuits that are valid at all frequencies. The method can be used to design filter circuits that operate at any frequencies and that have

any bandwidth specification.

The synthesis procedures associated with both presented mapping functions result in circuit topologies that are very well suited for coupled resonator implementations. This is because each reactive element in the original single-band prototype circuit is simply expanded into a separate coupled resonator chain consisting of inverter coupled resonators (refer to chapter 6). The mapping functions therefore do not introduce any additional cross-couplings that were not present in the original single-band prototype.

4.2 Ideal properties of rational mapping functions

As in chapter 3, a mapping function transforms the single-band prototype frequency variable (Ω') into the multi-band prototype frequency variable (Ω). We define the rational mapping function as $T = \Omega'(\Omega)$. Ideally, a rational mapping function should have the following properties:

- $|\Omega'(\Omega)| \leq 1$ should map to passbands.
- $|\Omega'(\Omega)| > 1$ should not map to passbands.
- $|\Omega'(\Omega)| = 0$ should map to the centre frequency of every band.
- $|\Omega'(\Omega)| = \pm\infty$ should preferably map to frequencies between every passband and to $\pm\infty$. Such a mapping would ensure a point of infinite isolation between each adjacent set of passbands for a lowpass function with attenuation poles at $\pm\infty$.

The list of ideal properties where formulated in an attempt to remedy the limitations of polynomial mapping functions.

4.3 Narrowband rational mapping functions using an intermediate frequency axis

We propose to transform the single-band prototype frequency variable (Ω'), into the actual multi-band frequency variable (ω), through the successive application of first a rational mapping function and then the lowpass-to-bandpass transformation. Both the rational mapping function and the low-pass-to-bandpass transformation are defined in terms of the passband edge frequencies in the actual frequency domain. In the next subsection we discuss the use of the lowpass-to-bandpass transformation as normalisation function. Then in section 4.3.2 we discuss the rational mapping function.

4.3.1 Relationship between the actual frequency domain and the multi-band prototype frequency domain

The denormalisation function defines the relationship between the multi-band prototype frequency variable (Ω) and the actual frequency variable (ω). For narrowband rational mapping functions we use the relationship defined in equations 3.3 through 3.5 to relate the actual frequency variable to the multi-band prototype frequency variable. Here ω_1 and ω_2 constitute the lowest frequency in the lowest passband and the highest frequency in the highest passband respectively. The function in equation 3.3 maps ω_1 to $\Omega = -1$ and ω_2 to $\Omega = 1$. The multi-band prototype frequency domain is an intermediary frequency domain and the highest frequency of the highest passband and the lowest frequency of the lowest passband could in reality have been mapped to any frequency points in the multi-band prototype frequency domain. The choice of $\Omega = \pm 1$ is merely made for convenience.

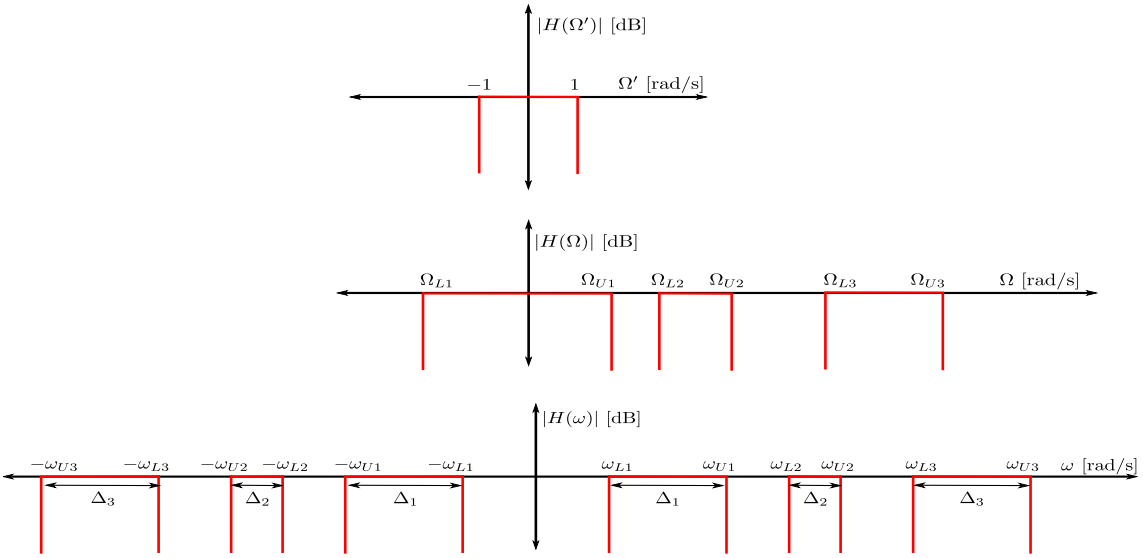

Figure 4.1: Passband bandwidth specifications for the three frequency domains associated with the mapping procedure are illustrated above. Here Ω', Ω and ω signify the single-band prototype frequency variable, the multi-band prototype frequency variable and the actual frequency variable respectively. The multi-band prototype frequency variable is related to the actual frequency variable through equation 3.3. The multi-band prototype frequency variable is related to the single-band prototype frequency variable through equation 4.1.

The passband specification for an N-band filter is a set of $2N$ passband edge frequencies in the actual frequency domain. If one now maps these frequencies to the multi-band prototype frequency domain, using equation 3.3, one obtains a set of $2N$ passband edge frequencies that are all located within the band $\Omega \in [-1, 1]$. This situation is graphically illustrated in figure 4.1. In the next subsection we discuss the relationship between the single-band prototype frequency domain and the multi-band prototype frequency domain.

4.3.2 Relationship between the multi-band prototype frequency domain and the single-band prototype frequency domain

The narrowband rational mapping function transforms the single-band prototype frequency variable (Ω') into the multi-band prototype frequency variable (Ω). A graphical representation of the allowed and disallowed regions for the mapping function, in accordance with the properties listed in section 4.2, are provided in figure 4.2 as unshaded and shaded regions respectively. The stringent requirement to avoid all shaded regions does place quite severe restrictions on possible mapping functions, especially the requirement of poles between adjacent passbands. A classical function that does satisfy all of the requirements is a rational polynomial fraction with single poles and zeros interspersed on the Ω axis. Such a function is known to rise monotonically, and when plotted on the same axis system in Figure 4.2, can be seen to yield the required mapping function. In polynomial form, such a function is given by equation 4.1 where all coefficients are real.

$$\Omega'(\Omega) = \frac{\alpha_N \Omega^N + \alpha_{N-1}\Omega^{N-1} + \alpha_{N-2}\Omega^{N-2} + \ldots + \alpha_2\Omega^2 + \alpha_1\Omega + \alpha_0}{\beta_{N-1}\Omega^{N-1} + \beta_{N-2}\Omega^{N-2} + \beta_{N-3}\Omega^{N-3} + \ldots + \beta_1\Omega + 1} = \frac{\rho_1(\Omega)}{q_1(\Omega)} \tag{4.1}$$

The rational mapping function in equation 4.1 has N zeros, $z_1, \ldots, z_N$, and $N+1$ poles, $p_1, \ldots, p_{N-1}, \pm\infty$. The poles and zeros are interspersed on the frequency axis such that $z_1 < p_1 < z_2 < p_2 < \ldots z_{N-1} < p_{N-1} < z_n$. A single-band prototype filtering function evaluated at its centre frequency would map to the N zeros of the function in equation 4.1. Likewise a single-band prototype filtering function evaluated at $\Omega' = \pm\infty$ would map to the $N+1$ poles of the function in equation 4.1. As a consequence, each $p_i \rightarrow z_i \rightarrow p_{i+1}$ region on

the multi-band frequency axis is a bandwidth-scaled and frequency-translated replica of the original lowpass filtering function. It is clear that the function in equation 4.1 meets the mapping function requirements.

Calculation of rational function coefficients

The coefficients of the rational mapping function in equation 4.1 can be calculated directly from the passband frequency specification in the actual frequency domain. The passband edge frequencies in the actual frequency domain can be normalised using equation 3.3 to obtain a set of $2N$ passband edge frequencies in the prototype domain. These are signified as $\Omega \in [-1, a] \cap [b, \ldots 1]$. The mapping function is required to map each of these frequencies to either $\Omega' = 1$ or $\Omega' = -1$ – the passband edge frequencies in the single-band prototype domain. It is therefore possible to construct the following set of $2N$ coordinate pairs that must be located on the mapping function:

$$\{\Omega_i, \Omega'(\Omega_i)\} = \{(-1,-1), (a,1), (b,-1), (c,1), \ldots, (1,1)\} \quad i \in [1, 2N] \tag{4.2}$$

Note that the set of coordinates in equation 4.2 are also indicated on the mapping function in figure 4.2. The coordinate set in equation 4.2 can now be applied to equation 4.1 to obtain a set of $2N$ linear equations in terms of the unknown coefficients:

$$\rho_1(\Omega_i) - \Omega'(\Omega_i)\, q_1(\Omega_i) = 0 \quad i \in [1, 2N] \tag{4.3}$$

The expression in equation 4.3 can now be presented in matrix notation as

$$\mathbf{AX} = \mathbf{B} \tag{4.4}$$

and solved for $\mathbf{X}$. The individual matrices in equation 4.4 are defined as follows:

$$\mathbf{A} = \begin{bmatrix} \Omega_1^N & \Omega_1^{N-1} & \ldots & \Omega_1 & 1 & -\Omega'(\Omega_1)\,\Omega_1^{N-1} & -\Omega'(\Omega_1)\,\Omega_1^{N-2} & \ldots & -\Omega'(\Omega_1)\,\Omega_1 \\ \Omega_2^N & \Omega_2^{N-1} & \ldots & \Omega_1 & 1 & -\Omega'(\Omega_2)\,\Omega_2^{N-1} & -\Omega'(\Omega_2)\,\Omega_2^{N-2} & \ldots & -\Omega'(\Omega_2)\,\Omega_2 \\ \vdots & \vdots & & \vdots & \vdots & \vdots & & \vdots & \vdots \\ \Omega_{2N}^N & \Omega_{2N}^{N-1} & \ldots & \Omega_1 & 1 & -\Omega'(\Omega_{2N})\,\Omega_{2N}^{N-1} & -\Omega'(\Omega_{2N})\,\Omega_{2N}^{N-2} & \ldots & -\Omega'(\Omega_{2N})\,\Omega_{2N} \end{bmatrix} \tag{4.5}$$

$$\mathbf{B} = \begin{bmatrix} \Omega'(\Omega_1) \\ \Omega'(\Omega_2) \\ \vdots \\ \Omega'(\Omega_{2N}) \end{bmatrix} \tag{4.6}$$

$$\mathbf{X} = \begin{bmatrix} \alpha_N \\ \alpha_{N-1} \\ \alpha_{N-2} \\ \vdots \\ \alpha_0 \\ \beta_{N-1} \\ \beta_{N-2} \\ \vdots \\ \beta_1 \end{bmatrix} \tag{4.7}$$

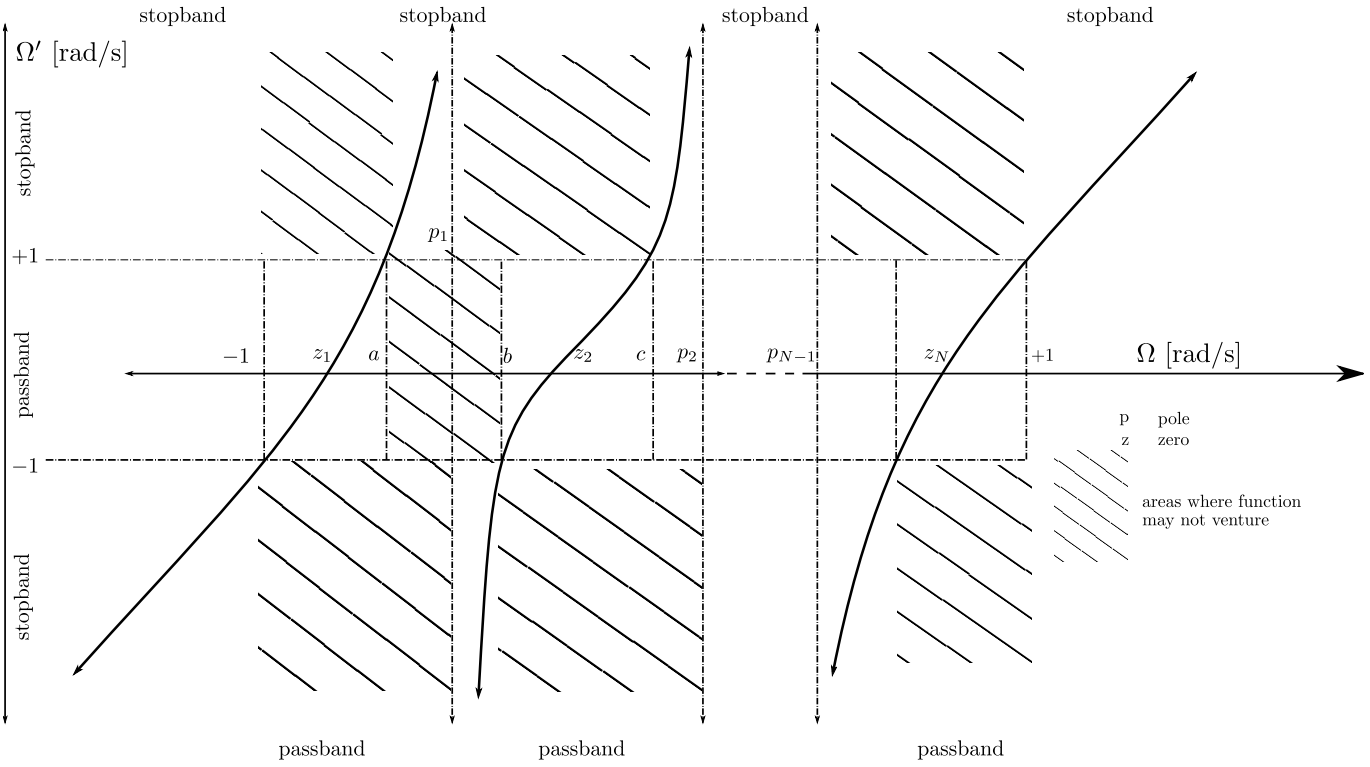

Figure 4.2: Graphical representation of the ideal rational mapping function for narrowband applications.

Naturally $\mathbf{A} \in \mathbb{R}^{2N\times 2N}$, $\mathbf{B} \in \mathbb{R}^{2N\times 1}$ and $\mathbf{X} \in \mathbb{R}^{2N\times 1}$. The necessary and sufficient condition for a solution to the matrix equation in 4.4 is that the rank of $\mathbf{A}$, and that of the augmented matrix $\mathbf{A}|\mathbf{B}$, must be $2N$. This condition is always true as both $\mathbf{A}$ and $\mathbf{A}|\mathbf{B}$ always have $2N$ linearly independent row vectors. One can confirm this by constructing the following vector sum:

$$c_1\mathbf{A}_{1,1:2N} + c_2\mathbf{A}_{2,1:2N} + \ldots + c_{2N}\mathbf{A}_{2N,1:2N} = \mathbf{0} \tag{4.8}$$

Equation 4.8 only holds if $\Omega_i \neq \Omega_j$ for $i \neq j$ and $c_1 = 0, c_2 = 0, \ldots, c_{2N} = 0$. Hence $\mathbf{A}$ is always of rank $2N$. A similar argument holds for the augmented matrix $\mathbf{A}|\mathbf{B}$. We can therefore conclude that a solution to the coefficients of equation 4.1 always exists. Due to the nature of the mapping function in equation 4.1, the successive combination of the two transformations in equations 4.1 and 3.3, when applied to applied to a valid lowpass network function, will again result in a valid network function showing N bands with identical amplitude and phase responses, but arbitrary centre frequencies and bandwidths. We illustrate the application of the theory with an example in the following subsection.

4.3.3 Examples

This subsection contains examples to illustrate the construction of rational mapping functions for narrowband multi-band filters.

Example 1: Three-band filter

In this example we illustrate how to construct a narrowband rational mapping function for a three-band filter with the following bandwidth specification:

- Passband 1: 1.50 GHz to 1.53 GHz.

- Passband 2: 1.56 GHz to 1.59 GHz.
- Passband 3: 1.62 GHz to 1.65 GHz.

Note that one could use the transformation that we construct in this example for any three-band filter of any order. The transformation merely maps a single-band filter to a three-band filter that has the desired bandwidth specification. The three passbands are bandwidth-scaled and frequency-translated copies of the original passband of the single-band filter. The single-band filter can be considered an input to the rational mapping function.

The first step in the procedure is to map the actual passband edge frequencies to the prototype frequency domain using the relationship defined in equations 3.3 through 3.5. We therefore calculate the centre frequency and fractional bandwidth using equations 3.4 and 3.5 as follows:

$$f_0 = \sqrt{1.5 * 1.65} = 1.573 \text{ GHz} \qquad \Delta = 0.095346$$

The passband edge frequencies in the prototype frequency domain can then be found using equation 3.3. The prototype passband edge frequencies are found as follows:

- Passband 1: $\Omega \in [-1; -0.584313]$.
- Passband 2: $\Omega \in [-0.176923; 0.222642]$
- Passband 3: $\Omega \in [0.614815; 1]$

We are constructing a mapping function for a three-band filter. Therefore $N = 3$. From the prototype passband specification we can now construct the following set of $2N$ coordinate pairs that must be located on the mapping function:

$$\{\Omega_i, \Omega_i'\} = \{(-1,-1), (-0.584313, 1), (-0.176923, -1), (0.222642, 1), (0.614815, -1), (1,1)\}$$

Using equation 4.3 we can construct the matrices $\mathbf{A}$ and $\mathbf{B}$ as follows:

$$\mathbf{A} = \begin{bmatrix} -1.0000 & 1.0000 & -1.0000 & 1.0000 & 1.0000 & -1.0000 \\ -0.1995 & 0.3414 & -0.5843 & 1.0000 & -0.3414 & 0.5843 \\ -0.0055 & 0.0313 & -0.1769 & 1.0000 & 0.0313 & -0.1769 \\ 0.0110 & 0.0496 & 0.2226 & 1.0000 & -0.0496 & -0.2226 \\ 0.2324 & 0.3780 & 0.6148 & 1.0000 & 0.3780 & 0.6148 \\ 1.0000 & 1.0000 & 1.0000 & 1.0000 & -1.0000 & -1.0000 \end{bmatrix}, \quad \mathbf{B} = \begin{bmatrix} -1.0000 \\ 1.0000 \\ -1.0000 \\ 1.0000 \\ -1.0000 \\ 1.0000 \end{bmatrix}$$

The coefficient matrix $\mathbf{X}$ is now found as follows:

$$\mathbf{X} = \begin{bmatrix} -8.372845537969210 \\ 0.319087141653249 \\ 4.347312742067144 \\ -0.089244322963917 \\ -5.025532795902067 \\ 0.229842818689351 \end{bmatrix}$$

From equations 4.7 and 4.1 we can now construct the required mapping function as follows:

$$\Omega'(\Omega) = \frac{-8.3728455379692 10\Omega^3 + 0.3190871416532 49\Omega^2 + 4.347312742067144\Omega - 0.089244322963917}{-5.025532795902067\Omega^2 + 0.229842818689351\Omega + 1} \tag{4.9}$$

A plot of equation 4.9 is provided in figure 4.3. It is clear that the function performs the mapping as required.

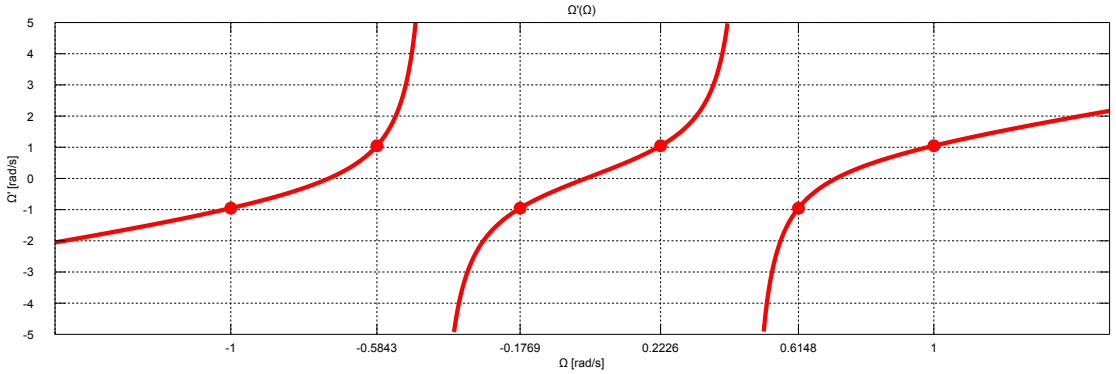

Figure 4.3: A plot of the three-band rational mapping function constructed in example 1 in section 4.3.3 is shown above.

Example 2: Five-band filter

In this example we illustrate how to construct a narrowband rational mapping function for a five-band filter with the following bandwidth specification:

- Passband 1: 1.78 GHz to 1.80 GHz.
- Passband 2: 1.85 GHz to 1.92 GHz.
- Passband 3: 1.98 GHz to 2.02 GHz.
- Passband 4: 2.05 GHz to 2.07 GHz.
- Passband 5: 2.1 GHz to 2.12 GHz.

Note that one could use the transformation that we construct in this example for any five-band filter of any order. The transformation merely maps a single-band filter to a five-band filter that has the desired bandwidth specification. The five passbands are bandwidth-scaled and frequency-translated copies of the original passband of the single-band filter. The single-band filter can be considered an input to the rational mapping function.

The first step in the procedure is to map the actual passband edge frequencies to the prototype frequency domain using the relationship defined in equations 3.3 through 3.5. We therefore calculate the centre frequency and fractional bandwidth using equations 3.4 and 3.5 as follows:

$$f_0 = \sqrt{1.78 * 2.12} = 1.9425 \text{ GHz} \qquad \Delta = 0.1750253$$

The passband edge frequencies in the prototype frequency domain can then be found using equation 3.3. The prototype passband edge frequencies are found as follows:

- Passband 1: $\Omega \in [-1; -0.8718]$.
- Passband 2: $\Omega \in [-0.5582; -0.1336]$
- Passband 3: $\Omega \in [0.2181; 0.4467]$
- Passband 4: $\Omega \in [0.6154; 0.7265]$
- Passband 5: $\Omega \in [0.8913; 1]$

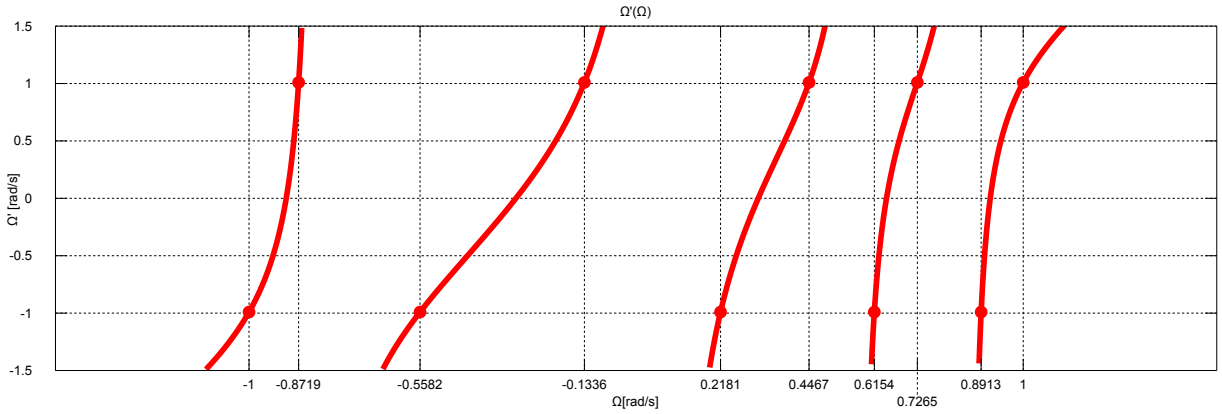

Figure 4.4: A plot of the five-band rational mapping function constructed in example 2 in section 4.3.3 is shown above.

We are constructing a mapping function for a five-band filter. Therefore $N = 5$. From the prototype pass-band specification we can now construct the following set of $2N$ coordinate pairs that must be located on the mapping function:

$$\{\Omega_i, \Omega_i'\} = \left\{ \begin{array}{c} (-1,-1), (-0.8718, 1), (-0.5582, -1), (-0.1336, 1), (0.2181, -1), \\ (0.4467, 1), (0.6154, -1), (0.7265, 1), (0.8913, -1), (1, 1) \end{array} \right\}$$

Using equation 4.3 we can construct the matrices $\mathbf{A}$ and $\mathbf{B}$. We can then calculate the coefficient matrix $\mathbf{X}$ and from equations 4.7 and 4.1 construct the required mapping function as follows:

$$\Omega'(\Omega) = \frac{-69.05221\Omega^5 + 46.06693\Omega^4 + 62.94617\Omega^3 - 41.86384\Omega^2 - 5.22418\Omega + 3.60994}{-34.56674\Omega^4 + 23.52414\Omega^3 + +22.23652\Omega^2 - 15.71112\Omega + 1} \tag{4.10}$$

A plot of equation 4.10 is provided in figure 4.4. It is clear that the function performs the mapping as required.

In the next section we introduce the general formulation for rational mapping functions.

4.4 General rational mapping functions

The rational mapping functions developed in the previous section had the limitation that they could only accommodate the design of narrowband multi-band filters. The reason for this is that if the mentioned mapping functions are used to construct multi-band prototype circuits, those circuits always contain frequency-invariant reactive elements. These elements are not physically realisable on their own, but they can be approximated in the actual frequency domain over a finite bandwidth using detuned resonators. Hence the narrowband limitation.

This leads to the question of how to obtain a general mapping function that does not lead to prototype circuits that might require the use of frequency-invariant reactive elements. In order for a transfer function to have the possibility of being physically realisable using only positive inductors and capacitors, the transfer function must have an amplitude response that is symmetric with respect to the zero frequency and a phase response that is asymmetric with respect to the zero frequency. Symmetric amplitude responses are therefore indicative of circuits that do not contain frequency-invariant reactances. From the discussion in section 3.3 it is apparent that the use of the lowpass-to-bandpass transformation as denormalisation function is the primary cause for the presence of frequency-invariant reactances in the multi-band prototype circuits. As a consequence, and in order to remedy this issue, we propose to substitute the non-linear lowpass-to-bandpass transformation for a linear denormalisation function. We therefore propose to employ the reactance function

of a passive, lossless, LC-network that is transformed through a linear transformation, as a general rational mapping function.

The procedure to transform the single-band prototype frequency variable (Ω') into the actual multi-band frequency variable (ω), is therefore the successive application of first the reactance function of a lossless LC-network (the rational mapping function) and then a linear frequency transformation. Both the rational mapping function and the linear frequency transformation are defined in terms of the passband edge frequencies in the actual frequency domain. In the next subsection we discuss the use of a linear frequency transformation as a normalisation function. Then in section 4.4.2 we discuss the rational mapping function.

4.4.1 Relationship between the actual frequency domain and the multi-band prototype frequency domain

The denormalisation function defines the relationship between the multi-band prototype frequency variable (Ω) and the actual frequency variable (ω). We define the linear frequency transformation function as follows:

$$\Omega = \frac{\omega}{\omega_{UN}} \tag{4.11}$$

As before, the the multi-band prototype frequency domain is an intermediary frequency domain and that any normalisation constant could have been used. The choice of ω_{UN} is merely made for convenience. An important difference between the narrowband formulation and the general formulation is that the multi-band prototype for the general formulation contains $2N$ passbands opposed to the N passbands for the narrowband case. The passband specification for an N-band filter is a set of $4N$ passband edge frequencies in the actual frequency domain ($2N$ on the positive frequency axis and $2N$ on the negative frequency axis). If one now maps these points to the multi-band prototype frequency domain, using equation 4.11, one obtains a set of $2N$ passband edge frequencies on the positive frequency axis and a mirrored set of $2N$ passband edge frequencies on the negative frequency axis. All of the passband edge frequencies are located within the band $\Omega \in [-1, 1]$. This situation is graphically illustrated in figure 4.5. In the next subsection we discuss the relationship between the single-band prototype frequency domain and the multi-band prototype frequency domain.

4.4.2 Relationship between the multi-band prototype frequency domain and the single-band prototype frequency domain

The exact methodology followed in section 4.3.2 will be followed here again. The general rational mapping function transforms the single-band prototype frequency variable (Ω') into the multi-band prototype frequency variable (Ω). A graphical representation of the allowed and disallowed regions for the mapping function, in accordance with the properties listed in section 4.2, are provided in figure 4.6 as unshaded and shaded regions respectively. In this case the reactance function of a passive, lossless LC-circuit is directly used as mapping function. From [62] the function is:

$$\Omega'(\Omega) = \frac{\alpha_{2N}\Omega^{2N} + \alpha_{2N-1}\Omega^{2N-1} + \alpha_{2N-2}\Omega^{2N-2} + \ldots + \alpha_2\Omega^2 + \alpha_1\Omega + 1}{\beta_{2N-1}\Omega^{2N-1} + \beta_{2N-2}\Omega^{2N-2} + \beta_{2N-3}\Omega^{2N-3} + \ldots + \beta_1\Omega + \beta_0} = \frac{\rho_2(\Omega)}{q_2(\Omega)} \tag{4.12}$$

All of the coefficients are positive and real. Also $|\Omega'(\Omega)| = |\Omega'(-\Omega)|$. The rational mapping function in equation 4.12 has $2N$ zeros, $z_1, \ldots, z_{2N}$, and $2N+1$ poles, $p_1, \ldots, p_{2N-1}, \pm\infty$. The poles and zeros are interspersed on the frequency axis such that $z_1 < p_1 < z_2 < p_2 < \ldots z_{2N-1} < p_{2N-1} < z_{2N}$. A single-band prototype filtering function evaluated at its centre frequency would map to the $2N$ zeros of the function in equation 4.12. Likewise a single-band prototype filtering function evaluated at $\Omega' = \pm\infty$ would map to the $2N+1$ poles of the

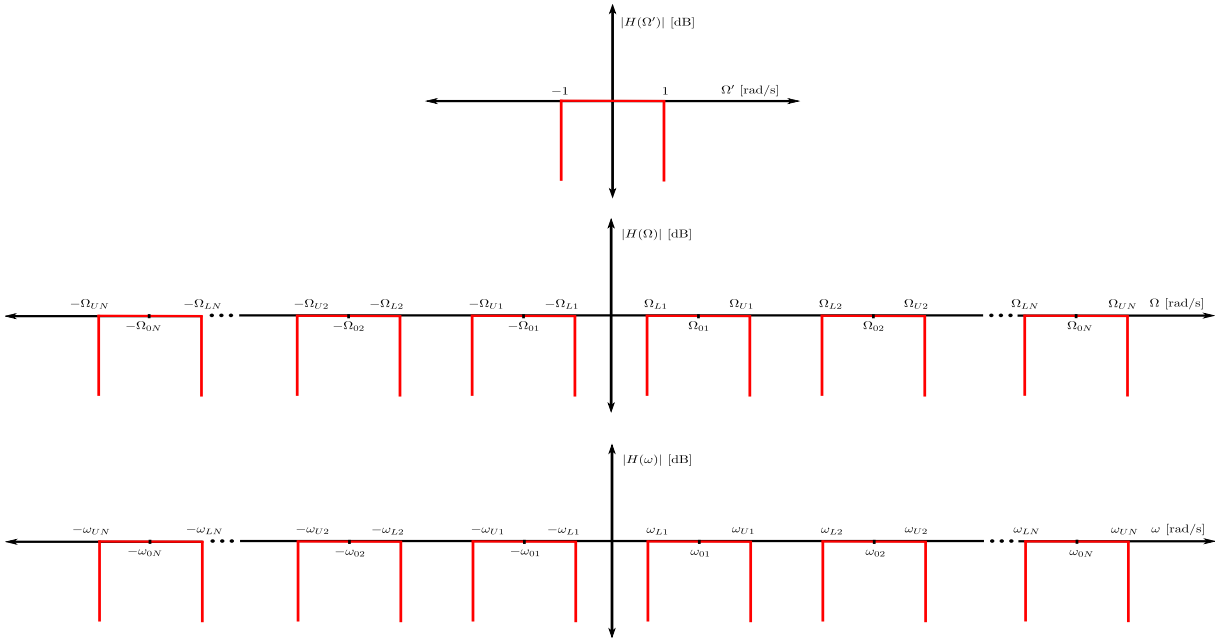

Figure 4.5: The passband bandwidth specifications for the three frequency domains associated with the mapping procedure are illustrated above. Here Ω', Ω and ω signify the single-band prototype frequency variable, the multi-band prototype frequency variable and the actual frequency variable respectively. The multi-band prototype frequency variable is related to the actual frequency variable through equation 4.11. The multi-band prototype frequency variable is related to the single-band prototype frequency variable through equation 4.12.

function in equation 4.12. Again, as a consequence, each $p_i \rightarrow z_i \rightarrow p_{i+1}$ region on the multi-band frequency axis is a bandwidth-scaled and frequency-translated replica of the original lowpass filtering function. It is clear that the function in equation 4.12 meets the mapping function requirements.

Calculation of rational function coefficients

The coefficients of the rational mapping function in equation 4.12 can be calculated directly from the passband frequency specification in the actual frequency domain. The passband edge frequencies in the actual frequency domain can be normalised using equation 4.11 to obtain a set of $4N$ passband edge frequencies in the prototype domain. These are signified as $\Omega \in [-\Omega_{UN}, -\Omega_{LN}] \cap \left[-\Omega_{U(N-1)}; \ldots \Omega_{UN}\right]$. Where $\pm\Omega_{UN} = \pm 1$. The mapping function is required to map each of these frequencies to either $\Omega' = 1$ or $\Omega' = -1$. These frequencies correspond to the passband edge frequencies in the single-band prototype domain. It is therefore possible to construct the following set of $4N$ coordinate pairs that must be located on the mapping function:

$$\{\Omega_i, \Omega'(\Omega_i)\} = \left\{(-1,-1), \left(-\Omega_{U(N-1)}, 1\right), \left(-\Omega_{U(N-2)}, -1\right), \left(-\Omega_{U(N-3)}, 1\right), \ldots, (1,1)\right\} \quad i \in [1, 4N] \tag{4.13}$$

Note that the set of coordinates in equation 4.13 are also indicated on the mapping function in figure 4.6. The coordinate set in equation 4.13 can now be applied to equation 4.14 to obtain a set of $4N$ linear equations in terms of the unknown coefficients:

$$\rho_2(\Omega_i) - q_2(\Omega_i)\,\Omega'(\Omega_i) = 0 \qquad i \in [1, 4N] \tag{4.14}$$

The expression in equation 4.14 can now be presented in matrix notation as:

$$\mathbf{AX} = \mathbf{B} \tag{4.15}$$

Equation 4.15 can then be solved for$\mathbf{X}$. The individual matrices in equation 4.15 are defined as follows:

$$\mathbf{A} = \begin{bmatrix} \Omega_1^{2N} & \Omega_1^{2N-1} & \dots & \Omega_1 & -\Omega'(\Omega_1)\Omega_1^{2N-1} & -\Omega'(\Omega_1)\Omega_1^{2N-2} & \dots & -\Omega'(\Omega_1)\Omega_1 & -\Omega'(\Omega_1) \\ \Omega_2^{2N} & \Omega_2^{2N-1} & \dots & \Omega_1 & -\Omega'(\Omega_2)\Omega_2^{2N-1} & -\Omega'(\Omega_2)\Omega_2^{2N-2} & \dots & -\Omega'(\Omega_2)\Omega_2 & -\Omega'(\Omega_2) \\ \vdots & \vdots & & \vdots & \vdots & \vdots & & \vdots & \vdots \\ \Omega_{4N}^{2N} & \Omega_{4N}^{2N-1} & \dots & \Omega_1 & -\Omega'(\Omega_{4N})\Omega_{4N}^{2N-1} & -\Omega'(\Omega_{4N})\Omega_{4N}^{2N-2} & \dots & -\Omega'(\Omega_{4N})\Omega_{4N} & -\Omega'(\Omega_{4N}) \end{bmatrix}, \tag{4.16}$$

$$\mathbf{B} = -\begin{bmatrix} 1 \\ 1 \\ \vdots \\ 1 \end{bmatrix} \tag{4.17}$$

and

$$\mathbf{X} = \begin{bmatrix} \alpha_{2N} \\ \alpha_{2N-1} \\ \alpha_{2N-2} \\ \vdots \\ \alpha_1 \\ \beta_{2N-1} \\ \beta_{2N-2} \\ \vdots \\ \beta_0 \end{bmatrix}. \tag{4.18}$$

Naturally $\mathbf{A} \in \mathbb{R}^{4N\times 4N}$, $\mathbf{B} \in \mathbb{R}^{4N\times 1}$ and $\mathbf{X} \in \mathbb{R}^{4N\times 1}$. The necessary and sufficient condition for a solution to the matrix equation in 4.15 is that the rank of $\mathbf{A}$, and that of the augmented matrix $\mathbf{A}|\mathbf{B}$, must be $4N$. This condition is always true as both $\mathbf{A}$ and $\mathbf{A}|\mathbf{B}$ always have $4N$ linearly independent row vectors. One can confirm this by constructing the following vector sum:

$$c_1\mathbf{A}_{1,1:4N} + c_2\mathbf{A}_{2,1:4N} + \ldots + c_{4N}\mathbf{A}_{4N,1:4N} = \mathbf{0} \tag{4.19}$$

Equation 4.19 only holds if $\Omega_i \neq \Omega_j$ for $i \neq j$ and $c_1 = 0, c_2 = 0, \ldots, c_{4N} = 0$. Hence $\mathbf{A}$ is always of rank $4N$. A similar argument holds for the augmented matrix $\mathbf{A}|\mathbf{B}$. We can therefore conclude that a solution to the coefficients of equation 4.12 always exists.

Due to the nature of the mapping function in equation 4.12, the successive combination of the two transformations in equations 4.12 and 4.11, when applied to a valid lowpass network function, will again result in a valid network function showing N bands with identical amplitude and phase responses, but arbitrary centre frequencies and bandwidths. We illustrate the application of the theory with an example in the following subsection.

4.4.3 Examples

This subsection contains three examples that illustrate how to construct general rational mapping functions to design multi-band filters. The first example is for a narrowband multi-band filter and the second example is for a wideband multi-band filter. The third example uses the same bandwidth specification as the second example, but illustrates how one can construct a rational mapping function suitable for the design of multi-band TEM filters.

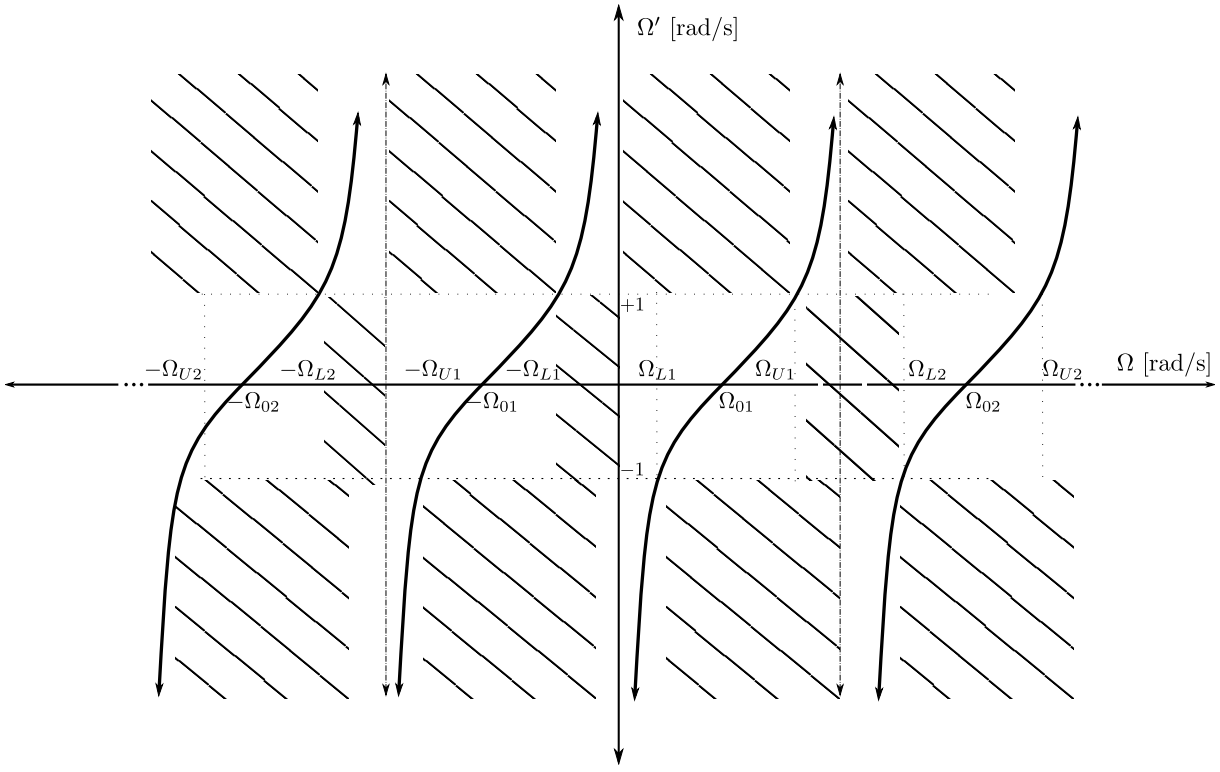

Figure 4.6: Graphical representation of the ideal general rational mapping function.

Example 1: Three-band narrowband filter

In this example we illustrate how to construct a general rational mapping function for a three-band filter with the following bandwidth specification:

- Passband 1: 1.50 GHz to 1.53 GHz.
- Passband 2: 1.56 GHz to 1.59 GHz.
- Passband 3: 1.62 GHz to 1.65 GHz.

Note that one could use the transformation that we construct in this example for any three-band filter of any order. The transformation merely maps a single-band filter to a three-band filter that has the desired bandwidth specification. The three passbands are bandwidth-scaled and frequency-translated copies of the original passband of the single-band filter. The single-band filter can be considered an input to the rational mapping function. The mapping provided here is not only valid in the vicinity of the filter passband, but everywhere on the frequency axis.

The first step in the procedure is to map the actual passband edge frequencies to the prototype frequency domain using the relationship defined in equation 4.11. The prototype passband edge frequencies are found as follows:

- Passband 1: $\Omega \in [0.909090909090909; 0.927272727272727]$.
- Passband 2: $\Omega \in [0.945454545454545; 0.963636363636364]$
- Passband 3: $\Omega \in [0.981818181818182; 1.000000000000000]$

We are constructing a mapping function for a three-band filter, therefore $N = 3$. Note that in total there are 6 passbands – three on the positive frequency axis and three on the negative frequency axis. The passbands on the negative axis are mirror images of the passbands in on the positive frequency axis. The symmetry is about the $\Omega = 0$ line. From the prototype passband specification we can now construct the following set of $4N$ coordinate pairs that must be located on the mapping function:

$$\{\Omega_i, \Omega_i'\} = \left\{ \begin{array}{c} (-1,-1), (-0.9818, 1), (-0.9636, -1), (-0.9455, 1), (-0.9273, -1), (-0.909, 1), \\ (0.909, -1), (0.9273, 1), (0.9455, -1), (0.9636, 1), (0.9818, -1), (1, 1) \end{array} \right\}$$

Using equation 4.14 we can construct the matrices $\mathbf{A}$ and $\mathbf{B}$ as follows:

$$\mathbf{A} = \begin{bmatrix} 1.000 & -1.000 & 1.000 & -1.000 & 1.000 & -1.000 & -1.000 & 1.000 & -1.000 & 1.000 & -1.000 & 1.000 \\ 0.896 & -0.912 & 0.929 & -0.946 & 0.964 & -0.982 & 0.912 & -0.929 & 0.946 & -0.964 & 0.982 & -1.000 \\ 0.801 & -0.831 & 0.862 & -0.895 & 0.929 & -0.964 & -0.831 & 0.862 & -0.895 & 0.929 & -0.964 & 1.000 \\ 0.714 & -0.755 & 0.799 & -0.845 & 0.894 & -0.946 & 0.755 & -0.799 & 0.845 & -0.894 & 0.946 & -1.000 \\ 0.636 & -0.686 & 0.739 & -0.797 & 0.860 & -0.927 & -0.686 & 0.739 & -0.797 & 0.860 & -0.927 & 1.000 \\ 0.565 & -0.621 & 0.683 & -0.751 & 0.826 & -0.909 & 0.621 & -0.683 & 0.751 & -0.826 & 0.909 & -1.000 \\ 0.565 & 0.621 & 0.683 & 0.751 & 0.826 & 0.909 & 0.621 & 0.680 & 0.751 & 0.826 & 0.909 & 1.000 \\ 0.636 & 0.686 & 0.739 & 0.797 & 0.860 & 0.927 & -0.686 & -0.739 & -0.797 & -0.860 & -0.927 & -1.000 \\ 0.714 & 0.755 & 0.799 & 0.845 & 0.894 & 0.946 & 0.755 & 0.799 & 0.845 & 0.894 & 0.946 & 1.000 \\ 0.801 & 0.831 & 0.862 & 0.895 & 0.929 & 0.964 & -0.831 & -0.862 & -0.895 & -0.929 & -0.964 & -1.000 \\ 0.896 & 0.912 & 0.929 & 0.946 & 0.964 & 0.982 & 0.912 & 0.929 & 0.946 & 0.964 & 0.982 & 1.000 \\ 1.000 & 1.000 & 1.000 & 1.000 & 1.000 & 1.000 & -1.000 & -1.000 & -1.000 & -1.000 & -1.000 & -1.000 \end{bmatrix}$$

$$\mathbf{B} = \begin{bmatrix} -1 \\ -1 \\ -1 \\ -1 \\ -1 \\ -1 \\ -1 \\ -1 \\ -1 \\ -1 \\ -1 \\ -1 \end{bmatrix}$$

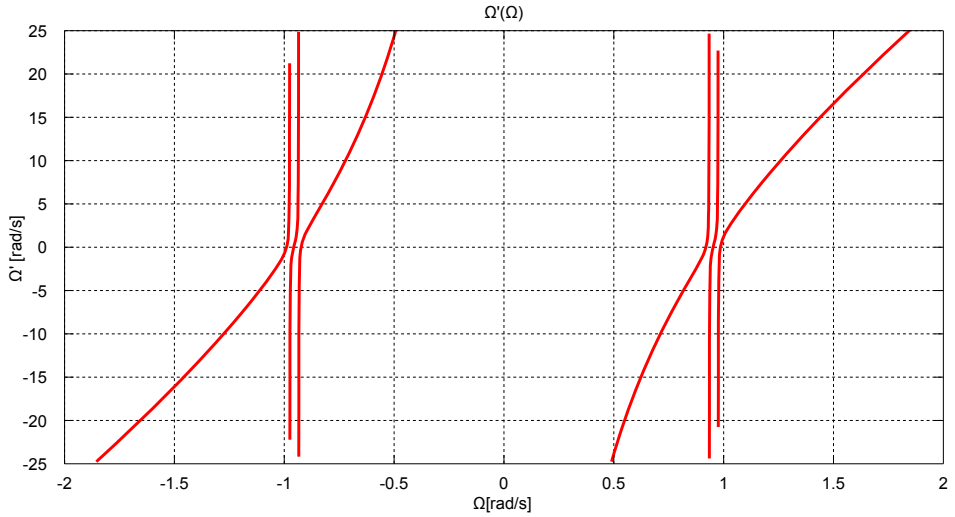

Figure 4.7: The three-band rational mapping function constructed in example 1 in in section 4.4.3 is shown above.

The coefficient matrix $\mathbf{X}$ is now found as follows:

$$\mathbf{X} = \begin{bmatrix} -1.326173342798413 \\ 0.000000000000004 \\ 3.626919690899577 \\ 0.000000000000007 \\ -3.301198836788956 \\ -0.000000000000004 \\ -0.072336727789001 \\ 0 \\ 0.131927843706407 \\ 0 \\ -0.060043604605202 \\ 0 \end{bmatrix}$$

From equations 4.18 and 4.12 we can now construct the required mapping function as follows:

$$\Omega'(\Omega) = \frac{-1.326173342798413\Omega^6 + 3.626919690899577\Omega^4 - 3.301198836788956\Omega^2 + 1}{-0.072336727789001\Omega^5 + 0.131927843706407\Omega^3 - 0.0600436046052020\Omega} \tag{4.20}$$

A wideband plot of equation 4.20 is provided in figure 4.7. Narrowband plots of the passband regions on the positive and negative frequency axis are provided in figures 4.8 and 4.9 respectively. It is clear that the function performs the mapping as required. The mapping function in equation 4.20 is employed to synthesise a multi-band filter in example 1 in section 6.2.5. In the next example we illustrate that the technique is also suitable for wide-band filters.

Example 2: Three-band wideband filter

The goal is to design a three-band filter with the following bandwidth specification:

- Passband 1: 1.0 GHz to 5.0 GHz.
- Passband 2: 6.0 GHz to 6.1 GHz.

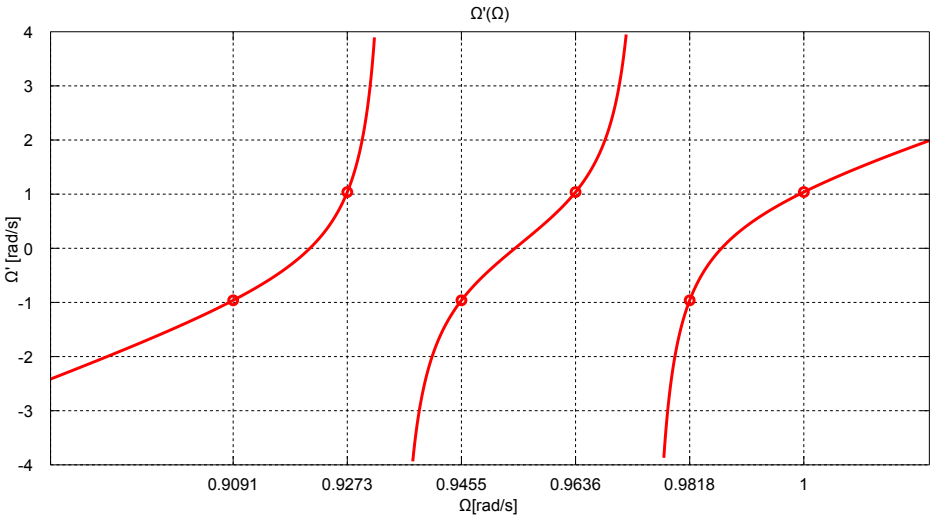

Figure 4.8: A region on the positive frequency axis of the three-band rational mapping function constructed in example 1 in in section 4.4.3 is shown above. The three passbands on the positive frequency axis are visible.

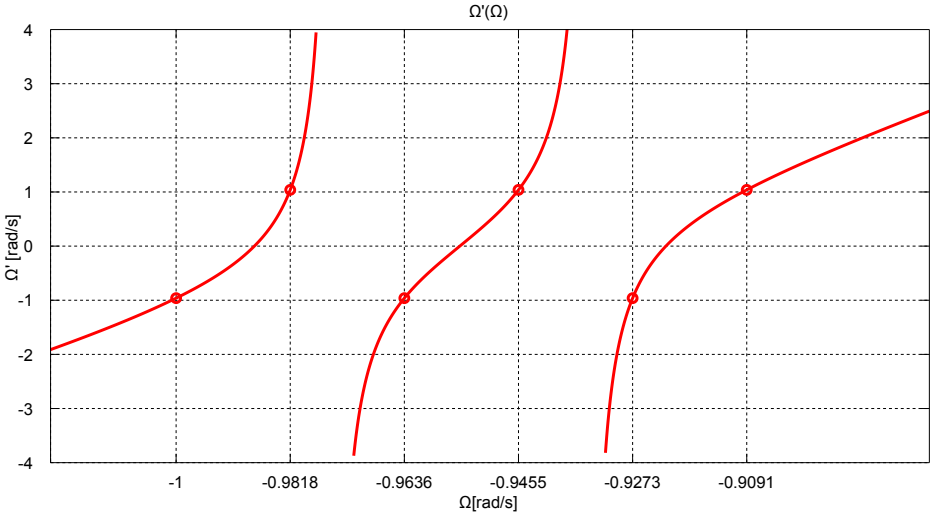

Figure 4.9: A region on the negative frequency axis of the three-band rational mapping function constructed in example 1 in in section 4.4.3 is shown above. The three passbands on the negative frequency axis are visible.

- Passband 3: 7.0 GHz to 8.0 GHz.

The actual passband edge frequencies are mapped to the prototype frequency domain using the relationship defined in equation 4.11 to obtain the following:

- Passband 1: $\Omega \in [0.1250; 0.6250]$.
- Passband 2: $\Omega \in [0.7500; 0.7625]$
- Passband 3: $\Omega \in [0.8750; 1.0000]$

The mapping function is for a three-band filter, therefore $N = 3$. From the prototype passband specification one can construct the following set of $4N$ coordinate pairs that must be located on the mapping function:

$$\{\Omega_i, \Omega_i'\} = \left\{ \begin{array}{c} (-1,-1), (-0.8750, 1), (-0.7625, -1), (-0.7500, 1), (-0.6250, -1), (-0.1250, 1), \\ (0.1250, -1), (0.6250, 1), (0.7500, -1), (0.7625, 1), (0.8750, -1), (1, 1) \end{array} \right\} \tag{4.21}$$

We can now use the coordinates in equation 4.21 to construct matrices $\mathbf{A}$ and $\mathbf{B}$ as follows:

$$\mathbf{A} = \begin{bmatrix} 1.000 & -1.000 & 1.000 & -1.000 & 1.000 & -1.000 & -1.000 & 1.000 & -1.000 & 1.000 & -1.000 & 1.000 \\ 0.449 & -0.513 & 0.586 & -0.670 & 0.766 & -0.875 & 0.513 & -0.586 & 0.670 & -0.766 & 0.875 & -1.000 \\ 0.197 & -0.258 & 0.338 & -0.443 & 0.581 & -0.763 & -0.258 & 0.338 & -0.443 & 0.581 & -0.763 & 1.000 \\ 0.178 & -0.237 & 0.316 & -0.422 & 0.563 & -0.750 & 0.237 & -0.316 & 0.422 & -0.563 & 0.750 & -1.000 \\ 0.060 & -0.095 & 0.153 & -0.244 & 0.391 & -0.625 & -0.095 & 0.153 & -0.244 & 0.391 & -0.625 & 1.000 \\ 0.000 & 0.000 & 0.000 & -0.002 & 0.016 & -0.125 & 0.000 & 0.000 & 0.002 & -0.016 & 0.125 & -1.000 \\ 0.000 & 0.000 & 0.000 & 0.002 & 0.016 & 0.125 & 0.000 & 0.000 & 0.002 & 0.016 & 0.125 & 1.000 \\ 0.060 & 0.095 & 0.153 & 0.244 & 0.391 & 0.625 & -0.095 & -0.153 & -0.244 & -0.391 & -0.625 & -1.000 \\ 0.178 & 0.237 & 0.316 & 0.422 & 0.563 & 0.750 & 0.237 & 0.316 & 0.422 & 0.563 & 0.750 & 1.000 \\ 0.197 & 0.258 & 0.338 & 0.443 & 0.581 & 0.763 & -0.258 & -0.338 & -0.443 & -0.581 & -0.763 & -1.000 \\ 0.449 & 0.513 & 0.586 & 0.670 & 0.766 & 0.875 & 0.513 & 0.586 & 0.670 & 0.766 & 0.875 & 1.000 \\ 1.000 & 1.000 & 1.000 & 1.000 & 1.000 & 1.000 & -1.000 & -1.000 & -1.000 & -1.000 & -1.000 & -1.000 \end{bmatrix}$$

$$\mathbf{B} = \begin{bmatrix} -1 \\ -1 \\ -1 \\ -1 \\ -1 \\ -1 \\ -1 \\ -1 \\ -1 \\ -1 \\ -1 \\ -1 \end{bmatrix}$$

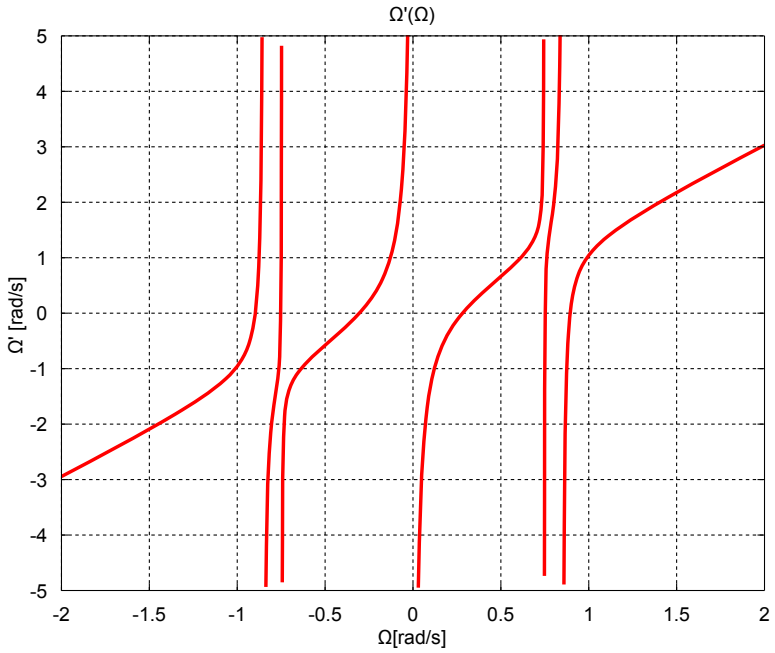

Figure 4.10: The three-band rational mapping function constructed in example 2 in in section 4.4.3 is shown above.

The coefficient matrix $\mathbf{X}$ is now found as follows:

$$\mathbf{X} = \begin{bmatrix} -25.580015612802494 \\ -0.000000000000001 \\ 37.210928961748650 \\ -0.000000000000001 \\ -14.634192037470729 \\ -0.000000000000000 \\ -16.307259953161580 \\ -0.000000000000001 \\ 20.868696330991408 \\ -0.000000000000000 \\ -6.564715066354411 \\ -0.000000000000000 \end{bmatrix}$$

We can now construct the required mapping function as follows:

$$\Omega'(\Omega) = \frac{-25.5800156128024940\Omega^6 + 37.2109289617486500\Omega^4 - 14.6341920374707290\Omega^2 + 1}{-16.3072599531615800\Omega^5 + 20.8686963309914080\Omega^3 - 6.5647150663544110\Omega} \tag{4.22}$$

A wideband plot of equation 4.22 is provided in figure 4.10. Narrowband plots of the passband regions on the positive and negative frequency axis are provided in figures 4.11 and 4.12 respectively. It is clear that the function performs the mapping as required. The mapping function in equation 4.22 is employed to synthesise a multi-band filter in example 2 in section 6.2.5. The mapping functions constructed in this section in examples 1 and 2 are suitable for lumped element filters. In the next example we illustrate how one can adapt the technique so that it can accommodate transmission line filters.

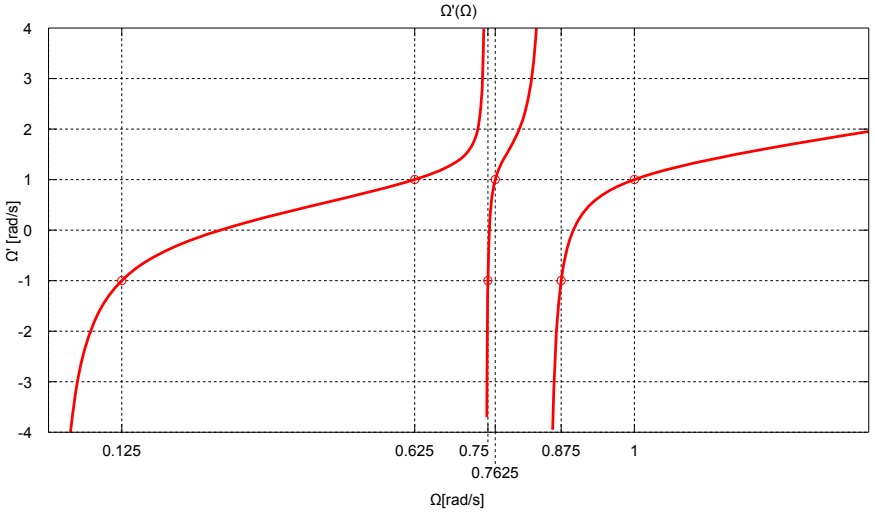

Figure 4.11: A region on the positive frequency axis of the three-band rational mapping function constructed in example 2 in in section 4.4.3 is shown above. The three passbands on the positive frequency axis are visible.

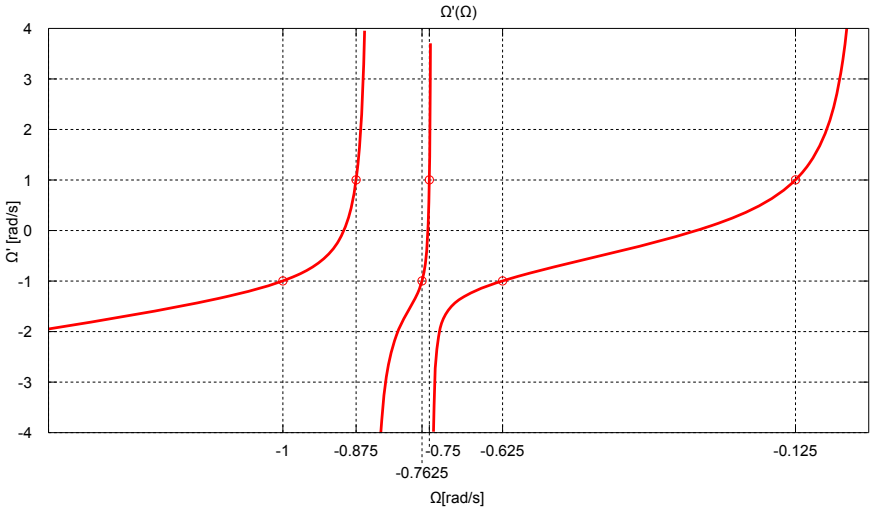

Figure 4.12: A region on the negative frequency axis of the three-band rational mapping function constructed in example 2 in in section 4.4.3 is shown above. The three passbands on the negative frequency axis are visible.

Example 3: Three-band wideband TEM filter

The goal is to design a three-band TEM filter with the following bandwidth specification:

- Passband 1: 1.0 GHz to 5.0 GHz.
- Passband 2: 6.0 GHz to 6.1 GHz.
- Passband 3: 7.0 GHz to 8.0 GHz.

The first step is to construct the frequency mapping function from the bandwidth specification. We can map the actual passband edge frequencies to the prototype frequency domain using the following relationship:

$$\Omega = \tan\left(\frac{\pi}{4}\frac{\omega}{\omega_{UN}}\right) \tag{4.23}$$

Note that the normalisation function in equation 4.23 incorporates the Richard's transformation ensuring that the mapping produces the correct bandwidths for transmission line elements. Again ω_{UN} is the highest frequency in the highest passband. The prototype passband edge frequencies are the following:

- Passband 1: $\Omega \in [0.098491403357164; 0.534511135950792]$.
- Passband 2: $\Omega \in [0.668178637919299; 0.682473483187274]$
- Passband 3: $\Omega \in [0.820678790828660; 1.0000]$

Again we are constructing a mapping function for a three-band filter, therefore $N = 3$. From the prototype passband specification we can now construct the following set of $4N$ coordinate pairs that must be located on the mapping function:

$$\{\Omega_i, \Omega_i'\} = \left\{ \begin{array}{c} (-1,-1), (-0.8207, 1), (-0.6825, -1), (-0.6682, 1), (-0.5345, -1), (-0.0985, 1), \\ (0.0985, -1), (0.5345, 1), (0.6682, -1), (0.6825, 1), (0.8207, -1), (1, 1) \end{array} \right\} \tag{4.24}$$

We can now use the coordinates in equation 4.24 to construct matrices $\mathbf{A}$ and $\mathbf{B}$ as follows:

$$\mathbf{A} = \begin{bmatrix} 1.000 & -1.000 & 1.000 & -1.000 & 1.000 & -1.000 & -1.000 & 1.000 & -1.000 & 1.000 & -1.000 & 1.000 \\ 0.306 & -0.372 & 0.454 & -0.553 & 0.674 & -0.821 & 0.372 & -0.454 & 0.553 & -0.674 & 0.821 & -1.000 \\ 0.101 & -0.148 & 0.217 & -0.318 & 0.466 & -0.682 & -0.148 & 0.217 & -0.318 & 0.466 & -0.682 & 1.000 \\ 0.089 & -0.133 & 0.199 & -0.298 & 0.446 & -0.668 & 0.133 & -0.199 & 0.298 & -0.446 & 0.668 & -1.000 \\ 0.023 & -0.044 & 0.082 & -0.153 & 0.286 & -0.535 & -0.044 & 0.082 & -0.153 & 0.286 & -0.535 & 1.000 \\ 0.000 & 0.000 & 0.000 & -0.001 & 0.010 & -0.098 & 0.000 & 0.000 & 0.001 & -0.010 & 0.098 & -1.000 \\ 0.000 & 0.000 & 0.000 & 0.001 & 0.010 & 0.098 & 0.000 & 0.000 & 0.001 & 0.010 & 0.098 & 1.000 \\ 0.023 & 0.044 & 0.082 & 0.153 & 0.286 & 0.535 & -0.044 & -0.082 & -0.153 & -0.286 & -0.535 & -1.000 \\ 0.089 & 0.133 & 0.199 & 0.298 & 0.446 & 0.668 & 0.133 & 0.199 & 0.298 & 0.446 & 0.668 & 1.000 \\ 0.101 & 0.148 & 0.217 & 0.318 & 0.466 & 0.682 & -0.148 & -0.217 & -0.318 & -0.466 & -0.682 & -1.000 \\ 0.306 & 0.372 & 0.454 & 0.553 & 0.674 & 0.821 & 0.372 & 0.454 & 0.553 & 0.674 & 0.821 & 1.000 \\ 1.000 & 1.000 & 1.000 & 1.000 & 1.000 & 1.000 & -1.000 & -1.000 & -1.000 & -1.000 & -1.000 & -1.000 \end{bmatrix}$$

$$\mathbf{B} = \begin{bmatrix} -1 \\ -1 \\ -1 \\ -1 \\ -1 \\ -1 \\ -1 \\ -1 \\ -1 \\ -1 \\ -1 \\ -1 \end{bmatrix}$$

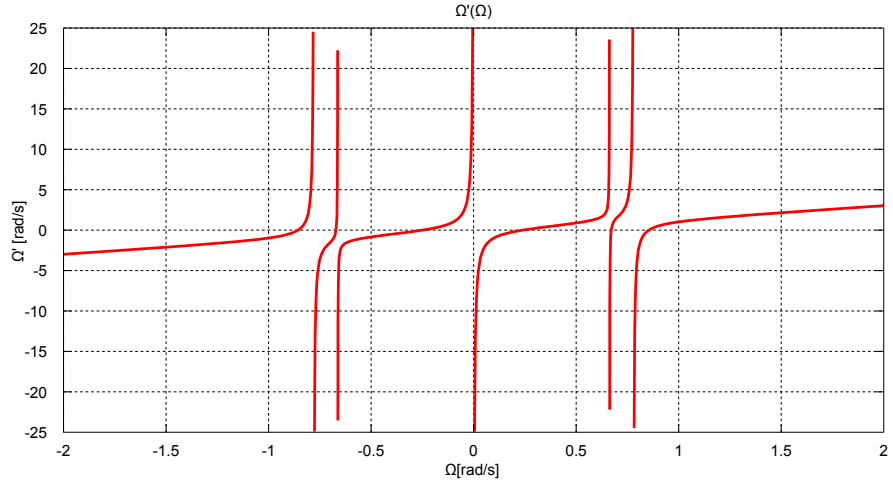

Figure 4.13: The three-band rational mapping function constructed in example 3 in in section 4.4.3 is shown above.

The coefficient matrix $\mathbf{X}$ is now found as follows:

$$\mathbf{X} = \begin{bmatrix} -50.756695301874259 \\ -0.000000000000028 \\ 63.057781197189911 \\ 0.000000000000037 \\ -20.330473374962409 \\ -0.000000000000009 \\ -31.958231793586798 \\ 0.000000000000002 \\ 33.460997183899671 \\ -0.000000000000005 \\ -8.532152869959482 \\ 0.000000000000001 \end{bmatrix}$$

We can now construct the required mapping function from $\mathbf{X}$:

$$\Omega'(\Omega) = \frac{-50.75669530187425 9\Omega^6 + 63.057781197189911\Omega^4 - 20.330473374962409\Omega^2 + 1}{-31.958231793586798\Omega^5 + 33.460997183899671\Omega^3 - 8.532152869959482\Omega} \tag{4.25}$$

A wideband plot of equation 4.25 is provided in figure 4.13. Narrowband plots of the passband regions on the positive and negative frequency axis are provided in figures 4.14 and 4.15 respectively. It is clear that the function performs the mapping as required. The mapping function in equation 4.25 is employed to synthesise a multi-band filter in example 3 in section 6.2.5.

In the next section we list the advantages of designing multi-band filters by using rational mapping functions.

4.5 Advantages and disadvantages of using rational mapping functions

The use of the reactance function of a passive, lossless, LC-network, as a mapping function, has the following advantages:

- There is no theoretical limit on the number of passbands that can be obtained using this transformation.

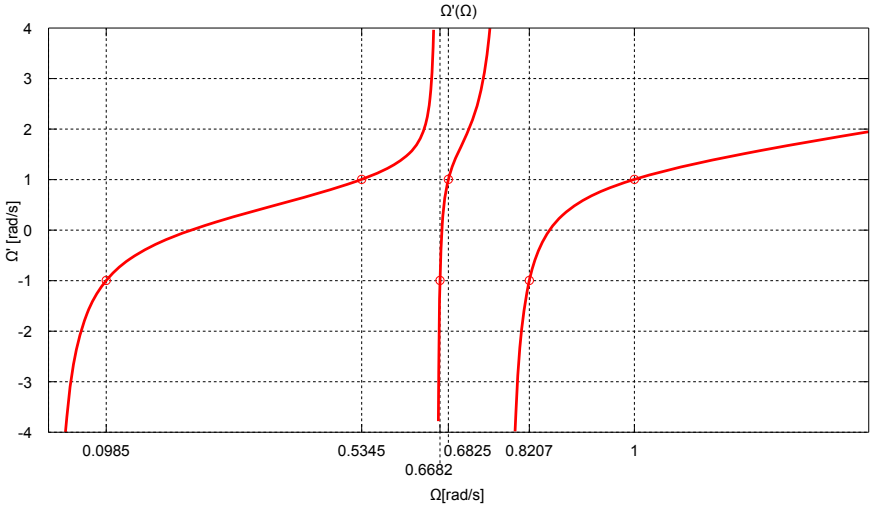

Figure 4.14: A region on the positive frequency axis of the three-band rational mapping function constructed in example 3 in in section 4.4.3 is shown above. The three passbands on the positive frequency axis are visible.

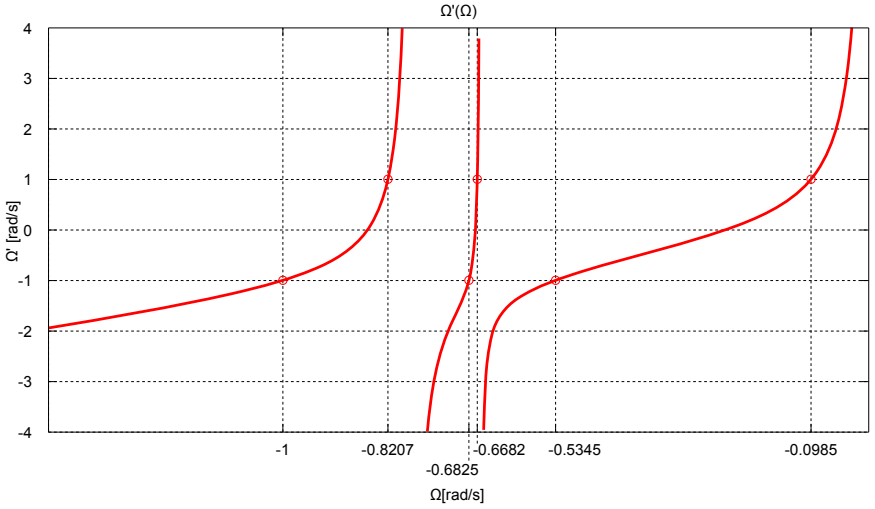

Figure 4.15: A region on the negative frequency axis of the three-band rational mapping function constructed in example 3 in in section 4.4.3 is shown above. The three passbands on the negative frequency axis are visible.

- Each passband in the final multi-band filter will have the exact same reflection and transmission responses as the original lowpass transfer function in terms of amplitude and phase.
- The centre frequency and bandwidth of each passband can be chosen completely arbitrarily.
- By simply choosing the correct poles and zeros, or equivalently choosing the passband edges for each band, a valid mapping function can be obtained using a single matrix equation. No optimisation of the final transfer functions are required.
- Given a lowpass filter function that can be realised with a circuit containing only positive inductors and capacitors, the application of the mapping function, followed by the application of the appropriate denormalisation function, will result in a classical reactance function transformation, and will, therefore, guarantee, a multi-band filter function, which can also be realised with positive value inductors and capacitors.

- The multi-band circuit can simply be realised by replacing each reactive element of any lowpass network with a network obtained by synthesising the mapping function as a scaled impedance or admittance one-port. The process places no restrictions on the lowpass function, therefore any lowpass network can be used.
- No complicated cross-couplings are incurred by the lowpass to multi-band mapping as each reactive element is realised in isolation.
- The final multi-band function needs never be synthesised as a whole on its own. The only functions that need to be synthesised are the original lowpass function and the mapping function, in isolation, as a one-port impedance or admittance.
- The only disadvantage of designing multi-band filters using rational mapping functions is that the topology of the multi-band filter is dependent on the topology of the single-band base filter [1].

4.6 Summary

In this chapter we considered the use of rational functions as mapping functions. Rational mapping functions are superior to polynomial mapping functions as they overcome all of the inherent limitations of polynomial mapping functions. Rational mapping functions can be used to design N-band filters from a single-band prototype filters. Each of the passbands of the multi-band filter is an exact bandwidth-scaled and frequency-translated copy of the passband of the original single-band prototype.

We presented two formulations for the design of N-band filters using rational mapping functions. The first employed multi-band prototypes that contained N-passbands. In this formulation the mapping was an N-th order rational function in conjunction with the lowpass-to-bandpass transformation. This formulation was intended for the design of narrowband filters. The second formulation employed multi-band prototypes that contained $2N$-passbands. In this formulation the mapping was an $2N$-th order rational function in conjunction with a linear transformation. This formulation can be used to design general multi-band filters that are valid at all frequencies.

As was the case with polynomial mapping functions, rational mapping functions can be used to construct multi-band characteristic polynomials from single-band characteristic polynomials. These polynomials can then be used to directly synthesise multi-band filters. Multi-band filters are generally high-order filters and the direct synthesis of these filters from the characteristic polynomials tend to be tedious and to result in circuits with complex topologies. The rational mapping functions however lend themselves to a much simpler synthesis procedure. A rational mapping function can directly be synthesised as a one-port impedance or admittance network. Capacitors and inductors in single-band prototype circuits can then be substituted by scaled versions of the one-port networks synthesised from the mapping function in order to obtain final multi-band filters. This is the preferred synthesis methodology for rational mapping functions that will be followed in this dissertation. We shall further elaborate on this synthesis procedure in chapter 6.

The next chapter concerns the synthesis of coupled resonator circuits using coupling matrices. The chapter provides a summary of well-known circuit synthesis and circuit simplification methods and therefore does not contain a new contribution. The theory is intended to be used to directly synthesise multi-band filters from multi-band characteristic polynomials.

[1] Note that this is only true if the multi-band filter is synthesised using reactance transformations and not true if the multi-band filter is directly synthesised from multi-band transfer functions.

Part II

Synthesis

Chapter 5

Synthesis of multi-band filters through coupling matrix techniques

This chapter serves as a summary of well-known and important theory on the synthesis and simplification of coupled resonator filters using coupling matrices [14, 15, 61]. The chapter does not contain original contributions. The theory is presented in great detail as it is used to directly synthesise coupled resonator circuits from the multi-band characteristic polynomials that were constructed using mapping functions. The theory is used extensively in the designs presented in chapters 8 and 9.

We start this chapter by introducing some of the fundamental principles of synthesis. We illustrate that filters can be modelled using two-port immittance parameters. Expressions for the immittance parameters are found using the prescribed characteristic polynomials. The immittance parameters thus relate our desired frequency response with a mathematical model of a circuit that could realise that frequency response. Obviously not all transfer functions can be realised as circuits. We therefore investigate conditions for the realisability of a transfer function. We then consider how to synthesise coupled resonator circuits from the prescribed immittance parameters. We present the synthesis techniques of both the $N \times N$ and $N+2 \times N+2$ coupled resonator circuits. We later show how the different formulations are related to each other. Circuit simplification techniques are later presented that can be used to obtain desirable filter topologies. We conclude the chapter with a summary of the most important results.

5.1 Introduction to synthesis

Synthesis is the process of finding an electrical circuit from a prescribed transfer function. Virtually any electrical parameter can be used to define a transfer function. One-port circuits are usually designed by relating the desired transfer function to the driving point impedance function of the circuit. The driving point impedance function is the impedance observed at the port of the circuit. Synthesis is performed by expanding the driving point impedance function as a sum of partial fractions. One can identify the network functions of individual S-plane components and their interconnections from the partial fraction expansion. The result is thus a prototype circuit with a frequency response corresponding to the transfer function. Filters are however two-port devices. They are modelled using four two-port parameters. Two of the parameters are driving point functions and the other two are transfer functions. For reciprocal networks the two transfer parameters are equivalent. A reciprocal two-port circuit can be designed by synthesising a circuit that satisfies one of the driving point parameters and one of the transfer parameters simultaneously. In order to design multi-band filters,

we require a relationship between the characteristic polynomials and the two-port parameters of a prototype circuit. In this dissertation we employ admittance parameters for this purpose. A design is performed by first finding the desired characteristic polynomials and then the associated admittance parameters. A circuit is then synthesised from the admittance parameters. In the following sections we relate the characteristic polynomials to the admittance parameters and then illustrate how to synthesise circuits from the mentioned parameters.

5.2 Admittance parameters in terms of characteristic polynomials

The goal of this section is to relate the admittance parameters of an arbitrary two-port circuit to the characteristic polynomials of a desired frequency response. Figure 2.1 shows the two-port circuit under consideration. Ports one and two are defined as the input and output ports respectively. Both the input and the output ports are terminated in finite impedances. The relationship between voltages and currents at the input and output ports can be expressed using the following two-port parameters:

$$\begin{bmatrix} V_1 \\ V_2 \end{bmatrix} = \begin{bmatrix} z_{11} & z_{12} \\ z_{21} & z_{22} \end{bmatrix} \begin{bmatrix} I_1 \\ I_2 \end{bmatrix} \quad \text{and} \quad \begin{bmatrix} I_1 \\ I_2 \end{bmatrix} = \begin{bmatrix} y_{11} & y_{12} \\ y_{21} & y_{22} \end{bmatrix} \begin{bmatrix} V_1 \\ V_2 \end{bmatrix} \tag{5.1}$$

In section 5.4 we shall synthesise a coupling matrix from the admittance parameters. Only y_{21} and y_{22} are needed for the synthesis procedure. In the next subsection we determine y_{22} from the characteristic polynomials. We consider how to obtain y_{21} in subsection 5.2.2.

5.2.1 The driving point admittance y_{22}

The driving point impedance function is used as an intermediary function to relate the characteristic polynomials to y_{22}. We first calculate an expression for the driving point impedance of a network in terms of its two-port parameters. We then calculate the driving point impedance using the characteristic polynomials. This enables us to relate y_{22} to our desired characteristic polynomials.

Driving point impedance in terms of two-port parameters

In this section we derive an expression for the driving point impedance of a reactive two-port circuit. Using the notation above, we can find a relation between the impedance and admittance parameters as follows:

$$\begin{aligned} V_2 z_{11} - V_1 z_{21} &= z_{11} I_1 z_{21} + z_{11} z_{22} I_2 - z_{21} I_1 z_{11} - z_{12} I_2 z_{21} \\ &= |\mathbf{Z}|\ I_2 \\ \iff I_2 &= -\frac{z_{21}}{|\mathbf{Z}|} V_1 + \frac{z_{11}}{|\mathbf{Z}|} V_2 \\ &= y_{21} V_1 + y_{22} V_2 \end{aligned} \tag{5.2}$$

Clearly $y_{21} = -\frac{z_{21}}{|\mathbf{Z}|}$ and $y_{22} = \frac{z_{11}}{|\mathbf{Z}|}$. Port two is terminated in an impedance R_2. We can express the voltage at port two as follows:

$$V_2 = z_{21} I_1 + z_{22} I_2 = -I_2 R_2 \tag{5.3}$$

We can now find an expression for the current at port two by factorising equation 5.3 as follows:

$$I_2 = \frac{-z_{21}}{z_{22} + R_2} I_1 \tag{5.4}$$

An expression for the voltage at port one is as follows:

$$V_1 = z_{11}I_1 + z_{12}I_2 \tag{5.5}$$

The driving point impedance at port one can be calculated by substituting equation 5.4 into equation 5.5:

$$\begin{aligned} Z_{\text{DP}} &= \frac{V_1}{I_1} \\ &= z_{11} + \frac{z_{12}}{I_1}I_2 \end{aligned} \tag{5.6}$$

Substitution of equation 5.4 into equation 5.6 results in the following:

$$\begin{aligned} Z_{\text{DP}} &= z_{11} - \frac{z_{12}z_{21}}{z_{22} + R_2} \\ &= \frac{|\mathbf{Z}| + z_{11}R_2}{z_{22} + R_2} \\ &= \frac{z_{11}\left(\frac{|\mathbf{Z}|}{z_{11}} + R_2\right)}{z_{22} + R_2} \end{aligned} \tag{5.7}$$

Remembering the definition of y_{22} in equation 5.2, we can factorise equation 5.7 to obtain the final expression for the driving point impedance at port one:

$$Z_{\text{DP}} = \frac{z_{11}\left(\frac{1}{y_{22}} + R_2\right)}{z_{22} + R_2} \tag{5.8}$$

Next we find derive an expression for the driving point impedance in terms of the characteristic polynomials.

Driving point impedance in terms of characteristic polynomials

The characteristic polynomials describe normalised networks. If we assume that the source impedance at port one is $1\,\Omega$, we can express the reflection coefficient at port one as follows:

$$s_{11}(S) = \frac{Z_{\text{in}}(S) - 1}{Z_{\text{in}}(S) + 1} \tag{5.9}$$

We can find an expression for the input impedance by factorising equation 5.9 as follows:

$$Z_{\text{in}}(S) = \frac{1 + s_{11}(S)}{1 - s_{11}(S)} \tag{5.10}$$

The driving point impedance at port one is equal to the input impedance at port one, we can therefore rewrite equation 5.10 as follows:

$$Z_{\text{DP}}(S) = \frac{\epsilon_r E(S) + F(S)}{\epsilon_r E(S) - F(S)} \tag{5.11}$$

If one compares equations 5.8 and 5.11, it becomes apparent that one could identify y_{22} in terms of the characteristic polynomials. In order to separate the numerator of equation 5.11 appropriately, it is necessary to investigate the mathematical character of y_{22}. The filter prototypes used throughout this dissertation are reactive circuits with real terminations. The two-port parameters therefore describe a purely reactive circuit. The two-port immittance parameters of a reactive circuit are in general rational functions with odd symmetry [73]. A rational function can only have odd symmetry in the following cases:

1. The numerator polynomial is even and the denominator polynomial is odd.

2. The numerator polynomial is odd and the denominator polynomial is even.

We want to factorise the numerator of equation 5.11 into even and odd parts to identify y_{22}. In section 3.3 we showed that the characteristic polynomials of multi-band filters necessarily have complex coefficients. Consequently $Z_{\text{DP}}(S)$ is a rational function with complex coefficients. If m_i constitutes a complex even polynomial and n_i constitutes a complex odd polynomial, we can express equation 5.11 as follows:

$$Z_{\text{DP}}(S) = \frac{m_1 + n_1}{m_2 + n_2} \tag{5.12}$$

Note that $m_i(S)$ is complex even if $m_i(S) = m_i^*(-S)$. Also, $n_i(S)$ is complex odd if $n_i(S) = -n_i^*(-S)$. We can separate the numerator of equation 5.12 into m_1 and n_1 as follows [61]:

$$m_1 = \Re\{e_0 + f_0\} + jS\,\Im\{e_1 + f_1\} + S^2\,\Re\{e_2 + f_2\} + \dots \tag{5.13}$$

$$n_1 = j\,\Im\{e_0 + f_0\} + S\,\Re\{e_1 + f_1\} + jS^2\,\Im\{e_2 + f_2\} + \dots \tag{5.14}$$

Here e_i and $f_i, i = 0, 1, \dots N$ are the complex coefficients of $E(S)$ and $F(S)$ respectively. Note that if N is even, the order of m_1 is one higher than that of n_1. Similarly, if N is odd, the order of n_1 is one higher than that of m_1. We therefore have to distinguish between the cases where N is even and odd to ensure that y_{22} is a proper rational function. We can now factorise equation 5.12 so that it resembles equation 5.8:

$$Z_{\text{DP}}(S) = \begin{cases} m_1 \frac{n_1/m_1+1}{m_2+n_2} & \text{when} \quad N \text{ is even} \\ n_1 \frac{m_1/n_1+1}{m_2+n_2} & \text{when} \quad N \text{ is odd} \end{cases} \tag{5.15}$$

The driving point admittance, $y_{22}(S)$, is found through the comparison of equations 5.8 and 5.15 as follows:

$$y_{22}(S) = \begin{cases} \frac{n_1(S)}{m_1(S)} & \text{when} \quad N \text{ is even} \\ \frac{m_1(S)}{n_1(S)} & \text{when} \quad N \text{ is odd} \end{cases} \tag{5.16}$$

In the next subsection we shall relate y_{21} to the characteristic polynomials.

5.2.2 The transfer admittance y_{21}

From equation 5.1 we can see that y_{12} and y_{22} share a denominator polynomial. We only consider reciprocal two-ports, therefore $y_{12} = y_{21}$. We can therefore state that y_{21} and y_{22} share the same denominator polynomial. Transmission zeros occur when the output of a two-port is zero for a finite, non-zero input. All the transfer functions that describe a filter therefore have the same zeros and these zeros are the transmission zeros of the filter. As a consequence, y_{21} and $P(S)$ have the same zeros and thus share a numerator polynomial [73]. The transfer admittance, y_{21}, is therefore defined as follows:

$$y_{21}(S) = \begin{cases} \frac{P(S)/\epsilon}{m_1(S)} & \text{when} \quad N \text{ is even} \\ \frac{P(S)/\epsilon}{n_1(S)} & \text{when} \quad N \text{ is odd} \end{cases} \tag{5.17}$$

Note that $P(S)$ must be multiplied by j to correct its phase if $N - n_{\text{fz}}$ is an even number (refer to section 2.1). In part I we showed how design specifications can be approximated with transfer functions. These functions are completely defined by a set of characteristic polynomials. In this section we related the characteristic polynomials to y_{22} and y_{21}. It is important to state that not all transfer functions can be successfully synthesised as circuits. Also, an important point to note is that the driving point functions are rational functions with complex coefficients. Should the driving point admittance parameters be expanded as partial fractions, it becomes

apparent that they represent prototype circuits containing frequency-invariant reactive elements (FIR). Such elements are non-physical. Before we show how to synthesise circuits from y_{22} and y_{21}, we shall briefly diverge and show in the next section how FIR elements can be included in the prototype domain and how they can be used to obtain physically realisable filters. We shall also investigate the conditions that must be imposed on transfer functions to ensure that they represent realisable circuits.

5.3 Asymmetric prototype circuits and their realisation conditions

In this section we investigate the conditions that must be met for a transfer function to always be realisable as an electrical circuit. We start by investigating the traditional conditions imposed on transfer functions to ensure realisability. We find that prototype circuits consisting of only ideal elements cannot accommodate asymmetric frequency responses. We remedy this problem by including FIR elements in the prototype domain. Unfortunately the traditional conditions for realisation cannot be applied to circuits containing these new elements. We then discuss realisation conditions that can accommodate the new circuit elements and can thus be used for the design of multi-band filters [61].

5.3.1 Traditional conditions for realisability

The realisability of electrical circuits depends on the mathematical character of their driving point immittance functions. Brune investigated the necessary and sufficient conditions for a driving point immittance function to be realisable as an electrical circuit. He realised that the first law of thermodynamics must hold true for all electrical circuits. He investigated the flow of energy in electrical circuits that consist entirely of ideal components and imposed the first law of thermodynamics – the conservation of energy [3]. Brune arrived at the following startling conclusion:

> If a rational function is a positive real function, there exists a one-port network, consisting entirely of physical electrical components, whose driving point impedance or admittance function is this rational function.

A positive real function is a function that is analytic in the right half of the complex plane and evaluates to real values on the real axis. The mathematical requirements for a driving point function, $A(S)$, to be positive real is as follows:

$$\begin{aligned} \Re\{A(S)\} &\geq 0 \quad \text{if} \quad \Re\{S\} \geq 0 \\ \Im\{A(S)\} &= 0 \quad \text{if} \quad \Im\{S\} = 0 \end{aligned}$$

Using the maximum modulus principle, it can be shown that $A(S)$ will meet the abovementioned requirements if the following conditions are met [73]:

- The coefficients of the numerator and denominator polynomials of $A(S)$ must be real.
- The denominator polynomial of $A(S)$ must be a Hurwitz polynomial – i.e. all the poles of $A(S)$ must be located on the left half of the complex plane.
- $\Re\{A(j\Omega)\} \geq 0$ for all values of Ω.

Electrical circuits consisting entirely of physical components have the following properties:

- A transfer function of a circuit consisting entirely of physical components is always a rational function with real coefficients.
- The denominator polynomial of said transfer function is always a Hurwitz polynomial.
- Resistance in circuits consisting entirely of physical components can only assume real values.

From these properties we can conclude that, for circuits consisting of only physical elements, that the driving point immittance function, associated with the transfer function, will always be a positive real function. Thus, to ensure the realisability of a transfer function, the associated driving point immittance function must be positive real.

The investigation in section 3.3 revealed that the transfer functions of circuits with symmetric frequency responses are rational functions with real coefficients. The transfer functions of prototype circuits with asymmetric frequency responses are rational functions with complex coefficients. Thus, the only prototype circuits that can have positive real driving point functions are those with symmetric frequency responses. We thus conclude that Brune's conditions for realisability are limited to prototype circuits where the frequency response is symmetric with respect to zero frequency. This does not mean that it is impossible to construct filters with asymmetric frequency responses. It is well-known that bandpass filters with asymmetric frequency responses can be constructed by appropriately arranging resonant circuits [61]. These asymmetric bandpass filters will have driving point functions that are positive real. The problem is thus that although filters with asymmetric frequency responses are realisable, they cannot be described by prototype circuits with positive real driving point functions. It is impossible to obtain driving point functions that are not positive real if only ideal elements are used. It is necessary to include additional circuit elements in the prototype domain to ensure that the driving point functions can have complex coefficients. We next consider how adapt prototype circuits to ensure that they can accommodate asymmetric frequency responses.

5.3.2 Prototype circuits with asymmetric frequency responses

The only way to accommodate asymmetric frequency responses is to extend the set of prototype circuit elements. Baum was the first researcher to suggest this solution by introducing a new fictitious electrical component – the frequency-invariant reactance (FIR) [74]. The nomenclature for describing FIR elements is as follows [61]:

$$\text{Frequency-invariant inductive element: } X \geq 0\ ,\ V(S) = jXI(S)$$
$$\text{Frequency-invariant capacitive element:} B \geq 0\ ,\ I(S) = jBV(S)$$

Considering the voltage and current relationships presented above, it is clear that the transfer functions of prototype circuits consisting of ideal components and FIR elements are rational functions with complex coefficients. These prototypes can therefore accommodate asymmetric frequency responses. An obvious problem is that FIR elements do not really exist. Fortunately, FIR elements in the prototype domain must also be mapped to the actual frequency domain through the lowpass-to-bandpass transformation. We know that filters with asymmetric frequency responses can be obtained using resonant circuits. It is therefore plausible to map the combination of a reactive element and a FIR element in the prototype domain, to a resonant circuit in the actual frequency domain. The resonant frequencies of these resonant circuits will be dependent on the value of the FIR element. The result will be an actual filter that consist entirely of ideal components and therefore physically realisable. We shall next derive equations that describe how FIR elements are mapped from the prototype

domain to the actual frequency domain. Figure 5.1 illustrates the two types of FIR elements that can be found in prototype circuits. Their associated actual frequency-domain resonant circuits are also shown. We shall start by analysing the capacitive case. The input admittance of the prototype circuit can be expressed as follows:

$$Y_{LP}(S) = SC + jB \tag{5.18}$$

The prototype domain is related to the actual frequency domain through the lowpass-to-bandpass transformation. We can map the input admittance in equation 5.18 to the actual frequency domain as follows:

$$Y_{BP}(S) = \frac{C}{\Delta}\left(\frac{s}{\omega_0} + \frac{\omega_0}{s}\right) + jB \tag{5.19}$$

We want expression 5.19 to represent the input admittance of a shunt resonator. We will now calculate the resonant frequency, ω_i, of this resonator. This is done by enforcing a resonant condition – the input susceptance of a resonator should evaluate to zero at the resonant frequency:

$$Y_{BP}(j\omega_i) = 0 + jB(\omega_i) = j\left[\frac{C}{\Delta}\left(\frac{\omega_i}{\omega_0} - \frac{\omega_0}{\omega_i}\right) + B\right] = 0 \tag{5.20}$$

From equation 5.20 we can calculate the resonant frequency of the equivalent shunt resonator in the actual frequency domain as follows:

$$\omega_i = \frac{\omega_0}{\frac{\Delta B}{2C} + \sqrt{\left(\frac{-\Delta B}{2C}\right)^2 + 1}} \tag{5.21}$$

The inductive FIR elements can be mapped from the prototype domain to the actual frequency domain using a similar approach. The resonant frequency of the equivalent series resonator in the actual frequency domain is given as follows:

$$\omega_i = \frac{\omega_0}{\frac{\Delta X}{2L} + \sqrt{\left(\frac{-\Delta X}{2L}\right)^2 + 1}} \tag{5.22}$$

Equations 5.21 and 5.22 can be used to relate FIR elements in prototype circuits with ideal components in actual circuits. It is thus possible to obtain realisable circuits with asymmetric frequency responses. We are now left with the problem of finding a realisation condition for filters with asymmetric frequency responses. We shall investigate this problem in the next subsection.

5.3.3 Conditions for realisation of circuits with asymmetric frequency responses

We want to identify the realisation conditions for transfer functions describing asymmetric frequency responses. These transfer functions must be realisable as prototype circuits that can in turn be mapped to bandpass filters consisting only of ideal components. As mentioned above, Brune's realisation condition cannot be applied to this special case. Brune's original realisation conditions were derived by enforcing the conservation of energy principle in a circuit. Belevitch realised that the conservation of energy principle must also hold for prototype circuits containing ideal and FIR elements [75]. The characteristic polynomials derive their form from the assumption that the scattering parameter matrix is a unitary matrix. The scattering parameter matrix must always be a unitary matrix for the conservation of energy principle to hold [61]. Therefore, if the characteristic polynomials are constructed using the rules listed in table 2.1, the resulting transfer function will describe a network that adheres to the conservation of energy principle. We can thus conclude that all frequency responses that can be approximated using the characteristic polynomials can be realised as electrical networks. Table 2.1 thus contains the required realisation conditions. In the next section we consider how to synthesise a circuit from the admittance parameters.

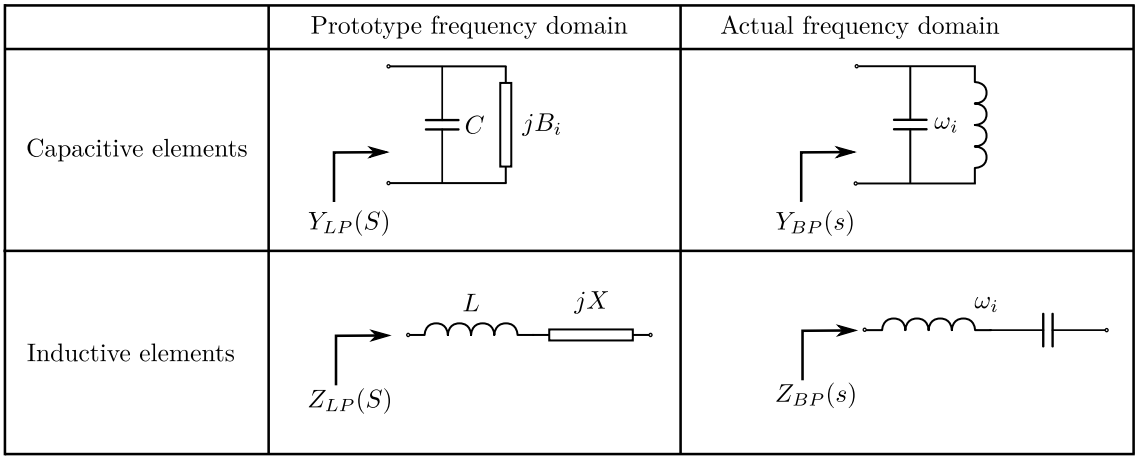

Figure 5.1: The prototype frequency domain is related to the actual frequency domain through the lowpass-to-bandpass transformation. Inductive and capacitive FIR elements in the prototype frequency domain, are mapped to resonators in the actual frequency domain. The resonant frequency of a resonator in the actual frequency domain is dependent on the FIR element in the prototype domain. Formulas to calculate the resonant frequencies are given in equations 5.21 and 5.22 for the capacitive and inductive cases respectively

5.4 Coupled resonator circuits

This section concerns the synthesis of coupled resonator filters from $y_{21}(S)$ and $y_{22}(S)$. An N-th order coupled resonator circuit is a circuit consisting of a minimum of two non-resonant nodes and N resonant nodes. The source and load are assumed to be non-resonant. We shall only consider circuits with a maximum of two non-resonant nodes – the source and the load. In a general coupled resonator circuit, any node in the circuit is theoretically coupled to any other node in the circuit. The topology of a general coupled resonator circuit is illustrated using a coupling routing diagram in figure 5.2. The squares represent non-resonant nodes and the circles represent resonant nodes. The blue lines are couplings between sequentially numbered nodes and are referred to as *mainline couplings*. The red lines represent all the other couplings and are referred to as *cross-couplings*. The general coupled resonator circuit can therefore have multiple signal propagation paths between the source and the load. Consequently, these circuits can accommodate multiple finite frequency transmission zeros (due to the possibility of destructive signal interference). The number of finite frequency transmission zeros that a given topology can realise is determined using the shortest path rule [61]:

> Suppose a network consists of N coupled resonators. The maximum number of finite frequency transmission zeros that can be realised by the network is $N - n_{\text{min}}$. Here n_{min} is the number of resonant nodes in the shortest route through the network between the source and load terminations.

The different nodes in a coupled resonator circuit are coupled to each other through either magnetic fields or electric fields. In the most general case nodes are coupled through a combination of magnetic and electric fields. We model magnetic field coupling by including mutual inductance in our circuits and electric field coupling by including mutual capacitance in our circuits. In order to simplify the modelling of coupled resonator filters and to make it mathematically simpler to synthesise these networks, we assume that the coupling between any two nodes is constant with respect to frequency. The values of the couplings are always calculated at f_0 Hz and are assumed to be constant over the entire operational band of the filter. This assumption is obviously only valid in a narrow bandwidth around f_0 Hz. Consequently, coupled resonator circuits are inherently narrow-band devices. If the frequency response of a coupled resonator circuit is geometrically symmetric with respect to f_0 Hz, the centre frequency of each resonator in the circuit is f_0 Hz. If the centre frequencies of the different

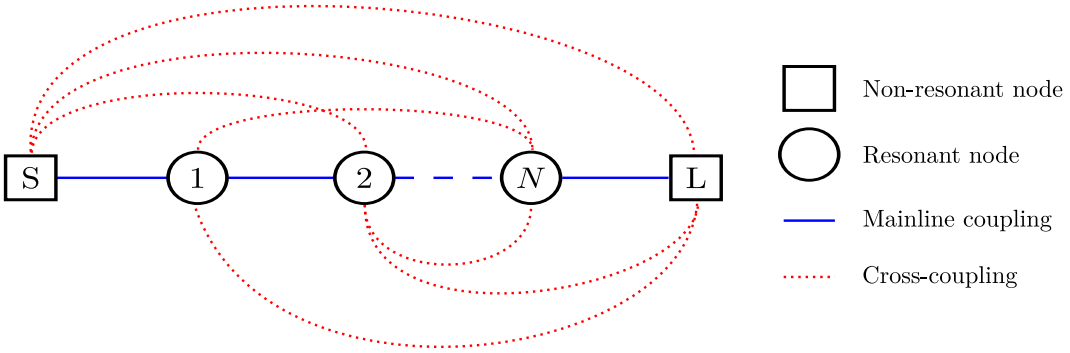

Figure 5.2: Routing diagram of a general N-th order coupled resonator circuit. Each node in the network is theoretically coupled to every other node in the network.

resonators are however not the same, it is possible to obtain frequency responses that are geometrically asymmetric with respect to f_0 Hz [61]. Coupled resonator circuits can accommodate any narrowband frequency response if the restriction on the maximum number of finite frequency transmission zeros is not violated. The restriction referred to here is the restriction imposed by the shortest path rule. We shall consider the general coupled resonator circuit as our target circuit during the synthesis procedure. The parameters that completely define a coupled resonator circuit are its topology, the centre frequencies of the resonators and the values of the couplings between the different nodes. In order to synthesise a transfer function as a coupled resonator circuit, it is necessary to relate the characteristic polynomials to the parameters of the coupled resonator circuit. We achieve this by first calculating the admittance parameters in terms of the characteristic polynomials and then calculating the same parameters using the coupled resonator circuit. In section 5.2 we calculated the admittance parameters using the characteristic polynomials. Our next goal is thus to calculate the admittance parameters in terms of the parameters of a coupled resonator circuit. There thus exist two sets of admittance parameters, one in terms of the characteristic polynomials and one in terms of the electrical parameters of a prototype circuit. These parameters can be related to each other to obtain synthesis equations. We are going to investigate the synthesis of two types of coupled resonator circuits. They differ in terms of allowable couplings. We shall later consider which representation is superior. In the next section we consider the $N \times N$ coupled resonator circuit. In this circuit there is a restriction on the couplings associated with the source and the load. The source can only couple to the first resonator and the load can only couple to the last resonator. All the other resonators have no restrictions on their allowable couplings. This topology is graphically illustrated by the coupling diagram given in figure 5.3. Later in this chapter we shall consider the $N+2 \times N+2$ coupled resonator circuit. In this circuit there will be no restrictions on the allowable couplings associated with any node.

5.5 The $N \times N$ coupled resonator circuit

This section starts by introducing the general $N \times N$ coupled resonator prototype circuit. Then expressions for $y_{21}(S)$ and $y_{22}(S)$ are derived in terms of the electrical parameters of said prototype circuit. These parameters shall then be related to the admittance parameters as obtained from the characteristic polynomials in section 5.2. From this relationship we obtain general synthesis equations. At the end of the section we shall clarify the presented theory through some application examples. The theory introduced in this section was originally introduced by Atia and Williams [10, 11, 12].

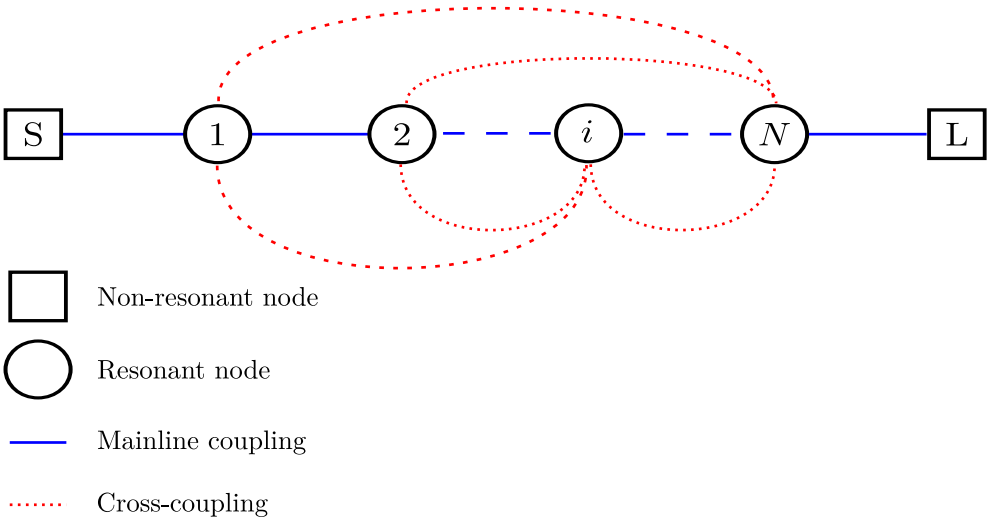

Figure 5.3: Routing diagram of a $N \times N$ coupled resonator circuit.

5.5.1 Admittance parameters of $N \times N$ prototype circuit

Figure 5.4 shows the general $N \times N$ coupled resonator circuit. All the resonators in the circuit are coupled to each other through mutual inductance. The source and load are connected to the input and output resonators via ideal transformers. The resonant frequencies of the different loops are not necessarily the same. The resonant frequency of loop i is calculated as $\omega_i = \frac{1}{\sqrt{L_i C_i}}$. Positive mutual inductance is associated with magnetic coupling. Negative mutual inductance is associated with capacitive coupling. Through the application of the shortest path rule, the network in figure 5.4 can accommodate a maximum of $N - 2$ finite frequency transmission zeros. This circuit can accommodate any asymmetric frequency response providing the restriction on the maximum number of finite frequency transmission zeros is not violated. Our goal is to use the circuit in figure 5.4 as our target during synthesis. We therefore need to relate the defining electrical parameters of this circuit to the characteristic polynomials. The defining electrical parameters are all the centre frequencies of the resonators, the coupling between the resonators and the input and output transformer windings. We employ the admittance parameters, y_{21} and y_{22}, as a link between the characteristic polynomials and the electrical parameters of our circuit. We must find expressions for y_{21} and y_{22} in terms of these electrical parameters. The first step is to map the circuit in figure 5.4 from the actual frequency domain to the prototype frequency domain. We assume that the inductive coupling does not vary with frequency:

$$j\omega M \approx j\omega_0 M$$

As a consequence only the resonators are mapped from the actual frequency domain to the prototype frequency domain. Each resonator is replaced by an inductor and a FIR element. The FIR element was included because the resonant frequencies of the different resonators in the actual frequency domain might differ from the centre frequency of the filter (refer to section 5.3.2). The total self inductance of a resonant loop in the prototype domain is 1 H. This ensures that the cutoff frequency is 1 rad/s in the prototype domain. The prototype circuit is shown in figure 5.5. We shall now proceed to analyse the circuit in figure 5.5. Through the application of Kirchhoff's voltage law, we can express the relationships between the different currents and voltages as

follows:

$$\begin{bmatrix} e_1 \\ 0 \\ \vdots \\ 0 \\ -e_N \end{bmatrix} = \begin{bmatrix} S+jX_1 & -jM_{1\,2} & -jM_{1\,3} & \dots & -jM_{1\,N} \\ -jM_{1\,2} & S+jX_2 & -jM_{2\,3} & \dots & -jM_{2\,N} \\ -jM_{1\,3} & -jM_{2\,3} & S+jX_3 & \dots & -jM_{3\,N} \\ \vdots & \vdots & \vdots & \ddots & \vdots \\ -jM_{1\,N} & -jM_{2\,N} & -jM_{3\,N} & \dots & S+jX_N \end{bmatrix} \begin{bmatrix} i_1 \\ i_2 \\ \vdots \\ i_{N-1} \\ i_N \end{bmatrix} \tag{5.23}$$

Note that the currents and voltages in equation 5.23 refer to frequency domain parameters. If we define $\mathbf{E}$ as our node voltage vector, $\mathbf{I}$ as our loop current vector and $\mathbf{Z}$ as our impedance matrix, we can express equation 5.23 as follows:

$$\begin{aligned} \mathbf{E} &= \mathbf{Z}\,\mathbf{I} \\ &= (S\mathbf{U} - j\mathbf{M})\,\mathbf{I} \end{aligned} \tag{5.24}$$

Here $\mathbf{U}$ is the identity matrix. $\mathbf{M}$ is referred to as the coupling matrix and is defined as follows:

$$\mathbf{M} = \begin{bmatrix} -X_1 & M_{1\,2} & M_{1\,3} & \dots & M_{1\,N} \\ M_{1\,2} & -X_2 & M_{2\,3} & \dots & M_{2\,N} \\ M_{1\,2} & M_{2\,3} & -X_3 & \dots & M_{3\,N} \\ \vdots & \vdots & \vdots & \ddots & \vdots \\ M_{1\,N} & M_{2\,N} & M_{3\,N} & \dots & -X_N \end{bmatrix} \tag{5.25}$$

A matrix entry $M_{i\,j}$ is the strength of the coupling between resonator i and resonator j. If this value is positive, it refers to magnetic field coupling. If the value is negative, it refers to electric field coupling. If the value is zero, it means that the resonators are uncoupled. $\mathbf{M}$ contains all the information concerning the topology of the filter and the coupling between different resonators. The only electrical parameters that are not contained inside the matrix are the windings of the input and output transformers. Note that it is possible to calculate the resonant frequency of each resonator in the actual frequency domain by remembering that the total self inductance is unity and substituting the main diagonal entries of $\mathbf{M}$ into equation 5.22 as follows:

$$\begin{aligned} \omega_i &= \frac{\omega_0}{\frac{\Delta X}{2C} + \sqrt{\left(\frac{-\Delta X}{2C}\right)^2 + 1}} \\ &= \frac{\omega_0}{-\frac{\Delta \mathbf{M}_{ii}}{2} + \sqrt{\left(\frac{\Delta \mathbf{M}_{ii}}{2}\right)^2 + 1}} \end{aligned} \tag{5.26}$$

Here $\mathbf{M}_{ii}$ is the i-th main diagonal entry of $\mathbf{M}_{N\times N}$ and corresponds to the negative-signed FIR element at the i-th resonant node. We shall now start to construct the admittance parameters. Consider the two-port circuit between planes $a - a'$ and $b - b'$ in figure 5.5. The currents and voltages associated with this two-port are related as follows:

$$\begin{bmatrix} i_1 \\ -i_N \end{bmatrix} = \begin{bmatrix} y'_{11} & y'_{12} \\ y'_{21} & y'_{22} \end{bmatrix} \begin{bmatrix} e_1 \\ e_N \end{bmatrix} \tag{5.27}$$

We can calculate the individual admittance parameters as follows:

$$\begin{aligned} y'_{11} &= \left.\frac{i_1}{e_1}\right|_{e_N=0} \quad ; \quad y'_{12} = \left.\frac{i_1}{e_N}\right|_{e_1=0} \\ y'_{21} &= \left.-\frac{i_N}{e_1}\right|_{e_N=0} \quad ; \quad y'_{22} = \left.-\frac{i_N}{e_N}\right|_{e_1=0} \end{aligned} \tag{5.28}$$

We shall now find expressions for i_1 and i_N from equation 5.24. Suppose we define $\mathbf{Z}_{\text{inv}} = \mathbf{Z}^{-1}$. Then, $\mathbf{Z}_{\text{inv},\,i\,j}$ is the j-th element in the i-th row of $\mathbf{Z}^{-1}$. We can rewrite equation 5.24 as follows:

$$\mathbf{I} = \mathbf{Z}^{-1}\,\mathbf{E} \tag{5.29}$$

$$\begin{bmatrix} i_1 \\ i_2 \\ i_3 \\ \vdots \\ i_N \end{bmatrix} = \begin{bmatrix} \mathbf{Z}_{\text{inv},\,1\,1} & \mathbf{Z}_{\text{inv},\,1\,2} & \mathbf{Z}_{\text{inv},\,1\,3} & \cdots & \mathbf{Z}_{\text{inv},\,1\,N} \\ \mathbf{Z}_{\text{inv},\,2\,1} & \mathbf{Z}_{\text{inv},\,2\,2} & \mathbf{Z}_{\text{inv},\,2\,3} & \cdots & \mathbf{Z}_{\text{inv},\,2\,N} \\ \mathbf{Z}_{\text{inv},\,3\,1} & \mathbf{Z}_{\text{inv},\,3\,2} & \mathbf{Z}_{\text{inv},\,3\,3} & \cdots & \mathbf{Z}_{\text{inv},\,3\,N} \\ \vdots & \vdots & \vdots & \ddots & \vdots \\ \mathbf{Z}_{\text{inv},\,N\,1} & \mathbf{Z}_{\text{inv},\,N\,2} & \mathbf{Z}_{\text{inv},\,N\,3} & \cdots & \mathbf{Z}_{\text{inv},\,N\,N} \end{bmatrix} \begin{bmatrix} e_1 \\ 0 \\ 0 \\ \vdots \\ -e_N \end{bmatrix} \tag{5.30}$$

From the expression above we can see that $e_j = 0$ for $j \in [2, N-1]$. Expressions for i_1 and i_N are as follows:

$$i_1 = (\mathbf{Z}_{\text{inv},\,1\,1})\,e_1 - (\mathbf{Z}_{\text{inv},\,1\,N})\,e_N \tag{5.31}$$

$$i_N = (\mathbf{Z}_{\text{inv},\,N\,1})\,e_1 - (\mathbf{Z}_{\text{inv},\,N\,N})\,e_N \tag{5.32}$$

From the definitions in equation 5.28 we can calculate the admittance parameters as follows:

$$\begin{aligned} y'_{11} &= \mathbf{Z}_{\text{inv},\,1\,1} \quad ; \quad y'_{12} = -\mathbf{Z}_{\text{inv},\,1\,N} \\ y'_{21} &= -\mathbf{Z}_{\text{inv},\,N\,1} \quad ; \quad y'_{22} = \mathbf{Z}_{\text{inv},\,N\,N} \end{aligned} \tag{5.33}$$

For reciprocal two-port circuits $y'_{12} = y'_{12}$. The synthesis of the coupling matrix requires one driving point function and one transfer function. We shall use y'_{21} and y'_{22}. Using the notation in equation 5.24, we can find an expression for the transfer admittance as follows:

$$\begin{aligned} y'_{21} &= -\mathbf{Z}_{\text{inv},\,N\,1} \\ &= -\left(S\mathbf{U} - j\mathbf{M}\right)^{-1}_{N\,1} \\ &= -\left(j\Omega\mathbf{U} - j\mathbf{M}\right)^{-1}_{N\,1} \\ &= -\left(j\right)^{-1}\left(\Omega\mathbf{U} - M\right)^{-1}_{N\,1} \\ \iff \quad y'_{21}(\Omega) &= j\left(\Omega\mathbf{U} - M\right)^{-1}_{N\,1} \end{aligned} \tag{5.34}$$

In a similar fashion we can find an expression for y'_{22} as follows:

$$\begin{aligned} y'_{22} &= \mathbf{Z}_{\text{inv},\,N\,N} \\ &= \left(S\mathbf{U} - j\mathbf{M}\right)^{-1}_{N\,N} \\ &= \left(j\Omega\mathbf{U} - j\mathbf{M}\right)^{-1}_{N\,N} \\ &= \left(j\right)^{-1}\left(\Omega\mathbf{U} - M\right)^{-1}_{N\,N} \\ \iff \quad y'_{22}(\Omega) &= -j\left(\Omega\mathbf{U} - M\right)^{-1}_{N\,N} \end{aligned} \tag{5.35}$$

Equations 5.34 and 5.35 can be further simplified if we exploit the mathematical properties of the coupling matrix. Consider the coupling matrix shown in equation 5.25. The matrix $\mathbf{M}$ is a $N \times N$ symmetric matrix and contains only real values. As a consequence $\mathbf{M}$ will have N distinct eigenvalues. The eigenvectors that correspond to distinct eigenvalues are orthogonal. We can therefore associate $\mathbf{M}$ with a set of N orthonormal eigenvectors. A sufficient condition for a matrix to be diagonalisable is that the matrix should have N linearly independent eigenvectors. As a consequence, $\mathbf{M}$ is always diagonalisable. We can diagonalise $\mathbf{M}$ as follows [76]:

$$\begin{aligned} \mathbf{\Lambda} &= \mathbf{T}^T\,\mathbf{M}\,\mathbf{T} \\ \iff \mathbf{M} &= \mathbf{T}\,\mathbf{\Lambda}\,\mathbf{T}^T \end{aligned} \tag{5.36}$$

Here $\mathbf{\Lambda}$ is a diagonal matrix containing all the eigenvalues of $\mathbf{M}$. $\mathbf{T}$ is a matrix with columns corresponding to the normalised eigenvectors of $\mathbf{M}$. Substitution of equation 5.36 into equations 5.34 and 5.35 yields the following expressions for $y'_{21}(\Omega)$ and $y'_{22}(\Omega)$:

$$y'_{21}(\Omega) = j\left(\Omega\mathbf{U} - \mathbf{T}\,\mathbf{\Lambda}\,\mathbf{T}^T\right)^{-1}_{N\,1} \tag{5.37}$$

$$y'_{22}(\Omega) = -j\left(\Omega\mathbf{U} - \mathbf{T}\,\mathbf{\Lambda}\,\mathbf{T}^T\right)^{-1}_{N\,N} \tag{5.38}$$

We know that $\mathbf{T}^T\mathbf{T} = \mathbf{U}$. Therefore $\mathbf{T}\mathbf{U}\mathbf{T}^T = \mathbf{U}$. We can factorise the matrix $\left(\Omega\mathbf{U} - \mathbf{T}\,\mathbf{\Lambda}\,\mathbf{T}^T\right)^{-1}$ as follows:

$$\begin{aligned}
\left(\Omega\mathbf{U} - \mathbf{T}\,\mathbf{\Lambda}\,\mathbf{T}^T\right)^{-1} &= \left(\Omega\mathbf{T}\,\mathbf{U}\,\mathbf{T}^T - \mathbf{T}\,\mathbf{\Lambda}\,\mathbf{T}^T\right)^{-1} \\
&= \left[\mathbf{T}\,\left(\Omega\mathbf{U} - \mathbf{\Lambda}\right)\,\mathbf{T}^T\right]^{-1} \\
&= \left(\mathbf{T}^T\right)^{-1}\left(\Omega\mathbf{U} - \mathbf{\Lambda}\right)^{-1}\,\mathbf{T}^{-1} \\
&= \left(\mathbf{T}^{-1}\right)^{-1}\left(\Omega\mathbf{U} - \mathbf{\Lambda}\right)^{-1}\mathbf{T}^T \\
&= \mathbf{T}\,\left(\Omega\mathbf{U} - \mathbf{\Lambda}\right)^{-1}\mathbf{T}^T \\
&= \begin{bmatrix} T_{11} & T_{12} & \dots & T_{1N} \\ T_{21} & T_{22} & \dots & T_{2N} \\ \vdots & \vdots & \ddots & \vdots \\ T_{N1} & T_{N2} & \dots & T_{NN} \end{bmatrix} \begin{bmatrix} \frac{1}{\Omega-\lambda_1} & 0 & \dots & 0 \\ 0 & \frac{1}{\Omega-\lambda_2} & \dots & 0 \\ \vdots & \vdots & \ddots & \vdots \\ 0 & 0 & \dots & \frac{1}{\Omega-\lambda_N} \end{bmatrix} \begin{bmatrix} T_{11} & T_{12} & \dots & T_{1N} \\ T_{21} & T_{22} & \dots & T_{2N} \\ \vdots & \vdots & \ddots & \vdots \\ T_{N1} & T_{N2} & \dots & T_{NN} \end{bmatrix}^T \\
&= \begin{bmatrix} T_{11} & T_{12} & \dots & T_{1N} \\ T_{21} & T_{22} & \dots & T_{2N} \\ \vdots & \vdots & \ddots & \vdots \\ T_{N1} & T_{N2} & \dots & T_{NN} \end{bmatrix} \begin{bmatrix} \frac{T_{11}}{\Omega-\lambda_1} & \frac{T_{12}}{\Omega-\lambda_1} & \dots & \frac{T_{1N}}{\Omega-\lambda_1} \\ \frac{T_{21}}{\Omega-\lambda_2} & \frac{T_{22}}{\Omega-\lambda_2} & \dots & \frac{T_{2N}}{\Omega-\lambda_2} \\ \vdots & \vdots & \ddots & \vdots \\ \frac{T_{N1}}{\Omega-\lambda_N} & \frac{T_{N2}}{\Omega-\lambda_N} & \dots & \frac{T_{NN}}{\Omega-\lambda_N} \end{bmatrix}^T
\end{aligned}$$

Through the expansion of the expression above, we can now write an expression for the j-th element in the i-th row of $\left(\Omega\mathbf{U} - \mathbf{T}\,\mathbf{\Lambda}\,\mathbf{T}^T\right)^{-1}$ as follows:

$$\left(\Omega\mathbf{U} - \mathbf{T}\,\mathbf{\Lambda}\,\mathbf{T}^T\right)^{-1}_{i\,j} = \sum_{k=1}^{N} \frac{T_{i\,k}T_{j\,k}}{\Omega - \lambda_k} \tag{5.39}$$

We can now rewrite equations 5.37 and 5.38 as follows:

$$y'_{21} = j\sum_{k=1}^{N} \frac{T_{N\,k}T_{1\,k}}{\Omega - \lambda_k} \tag{5.40}$$

$$y'_{22} = -j\sum_{k=1}^{N} \frac{T^2_{N\,k}}{\Omega - \lambda_k} \tag{5.41}$$

The admittance parameters calculated above only refer to N coupled resonators. The port terminations of the network are not taken into consideration. The source and load must be coupled to the first and last resonators through ideal transformers. The two-port circuit connected between reference planes $1-1'$ and $2-2'$ in figure 5.5 can be described using the following two-port expression:

$$\begin{bmatrix} I_1 \\ I_2 \end{bmatrix} = \begin{bmatrix} y_{11} & y_{12} \\ y_{21} & y_{22} \end{bmatrix} \begin{bmatrix} V_1 \\ V_2 \end{bmatrix} \tag{5.42}$$

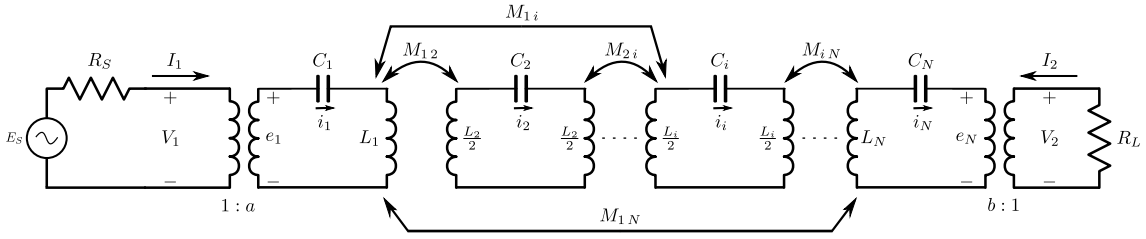

Figure 5.4: The general $N \times N$ coupled resonator circuit is shown above. The circuit is comprised of N lumped element series resonators. Each resonator is coupled to all the other resonators through mutual inductance. The source is coupled to the input resonator using an ideal transformer. Likewise, the load is coupled to the output resonator also using an ideal transformer. The resonant frequency of a resonator i is calculated as $\frac{1}{\sqrt{L_i C_i}}$.

Substitution of equation 5.27 into equation 5.42 results in the following:

$$\begin{aligned}
\begin{bmatrix} I_1 \\ I_2 \end{bmatrix} &= \begin{bmatrix} n_1 & 0 \\ 0 & n_2 \end{bmatrix} \begin{bmatrix} i_1 \\ -i_N \end{bmatrix} \\
&= \begin{bmatrix} n_1 & 0 \\ 0 & n_2 \end{bmatrix} \begin{bmatrix} y'_{11} & y'_{12} \\ y'_{21} & y'_{22} \end{bmatrix} \begin{bmatrix} e_1 \\ e_N \end{bmatrix} \\
&= \begin{bmatrix} n_1 & 0 \\ 0 & n_2 \end{bmatrix} \begin{bmatrix} y'_{11} & y'_{12} \\ y'_{21} & y'_{22} \end{bmatrix} \begin{bmatrix} n_1 & 0 \\ 0 & n_2 \end{bmatrix} \begin{bmatrix} V_1 \\ V_2 \end{bmatrix} \\
&= \begin{bmatrix} n_1^2\, y'_{11} & n_1 n_2\, y'_{12} \\ n_1 n_2\, y'_{21} & n_2^2\, y'_{22} \end{bmatrix} \begin{bmatrix} V_1 \\ V_2 \end{bmatrix}
\end{aligned} \tag{5.43}$$

Using equations 5.40 through 5.43, we can find an expression for $y_{21}(S)$ as follows:

$$\begin{aligned}
y_{21}(\Omega) &= j \sum_{k=1}^{N} \frac{n_1 n_2 T_{1\,k} T_{N\,k}}{\Omega - \lambda_k} \\
\iff y_{21}(S) &= -\sum_{k=1}^{N} \frac{n_1 n_2 T_{1\,k} T_{N\,k}}{S - j\lambda_k}
\end{aligned} \tag{5.44}$$

In a similar fashion we can derive an expression for $y_{22}(S)$ as follows:

$$\begin{aligned}
y_{22}(\Omega) &= -j \sum_{k=1}^{N} \frac{(n_2 T_{N\,k})^2}{\Omega - \lambda_k} \\
\iff y_{22}(S) &= \sum_{k=1}^{N} \frac{(n_2 T_{N\,k})^2}{S - j\lambda_k}
\end{aligned} \tag{5.45}$$

We now have expressions for the admittance parameters of the prototype circuit in figure 5.5. The next step is to relate the characteristic polynomials to the prototype circuit. We shall describe the synthesis procedure in the next subsection.

5.5.2 Derivation of synthesis expressions

The characteristic polynomials were related to the admittance parameters in section 5.2. The admittance parameters of the prototype circuit in figure 5.5 were calculated in the previous section. We are now able to link the characteristic polynomials (that define a desired frequency response) to the prototype circuit in figure 5.5 by equating the expressions for their admittance parameters. An expression for the driving admittance in terms

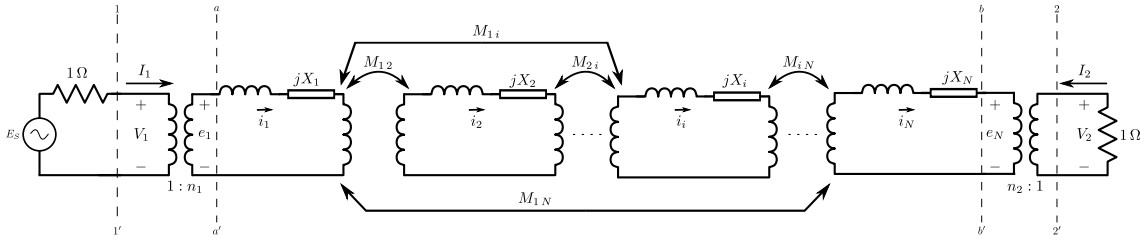

Figure 5.5: The general prototype associated with the $N \times N$ coupled resonator circuit is shown above. Note that the resonators in the actual frequency domain were mapped to the prototype frequency domain using the transformations provided in figure 5.1. The total inductance in each resonant loop evaluates to 1 H.

of the characteristic polynomials is given in equation 5.16. A partial fraction expansion for this expression is as follows:

$$y_{22}(S) = \sum_{k=1}^{N} \frac{K_{22,k}}{S - p_k} \tag{5.46}$$

Through the comparison of equations 5.45 and 5.46, we observe the following:

$$K_{22,k} = (n_2 T_{Nk})^2 \tag{5.47}$$

$$p_k = j\lambda_k \tag{5.48}$$

In a similar fashion we can express equation 5.17 as a partial fraction as follows:

$$y_{21}(S) = \sum_{k=1}^{N} \frac{K_{21,k}}{S - p_k} \tag{5.49}$$

Through the comparison of equations 5.17 and 5.49, we observe the following:

$$K_{21,k} = n_1 n_2 T_{1k} T_{NK} \tag{5.50}$$

$$p_k = j\lambda_k \tag{5.51}$$

We know that $\mathbf{T}$ is a orthonormal matrix. Thus $\mathbf{T}^T\mathbf{T} = \mathbf{T}\mathbf{T}^T = \mathbf{U}$. This implies the following:

$$\sum_{k=1}^{N} (T_{Nk})^2 = 1 \tag{5.52}$$

Substitution of equation 5.52 into equation 5.47 results in the following relationship:

$$\sum_{k=1}^{N} K_{22,k} = n_2^2 \tag{5.53}$$

Substitution of equation 5.53 into equation 5.47 results in the following equation for the k-th element in the N-th row of matrix $\mathbf{T}$:

$$T_{Nk} = \sqrt{\frac{K_{22,k}}{\sum_{k=1}^{N} K_{22,k}}} \tag{5.54}$$

In a similar fashion, because $\mathbf{T}$ is a orthonormal matrix, we can state the following:

$$\sum_{k=1}^{N} (T_{1k} T_{Nk})^2 = 1 \tag{5.55}$$

Substitution of equation 5.55 into equation 5.50 results in the following expression for n_1^2:

$$n_1^2 = \sum_{k=1}^{N} \frac{(K_{21,k})^2}{K_{22,k}} \tag{5.56}$$

We can now express the k-th element in the 1-th row of matrix $\mathbf{T}$ is as follows:

$$T_{1,k} = \frac{K_{21,k}}{n_1 n_2 T_{Nk}} \tag{5.57}$$

The circuit in figure 5.5 is fully described by the input and output transformer windings and by the coupling matrix $\mathbf{M}$. Equations 5.56 and 5.53 can be used to calculate the input and output transformer windings from the characteristic polynomials. The coupling matrix can be constructed from the matrix $\mathbf{T}$ and from the poles of y_{22} or y_{21}. The poles of y_{22} or y_{21} can be found from the characteristic polynomials as shown in section 5.2. The first and last rows of the matrix $\mathbf{T}$ can be calculated from the characteristic polynomials using equations 5.57 and 5.54 respectively. In order to construct $\mathbf{M}$, we still need to calculate rows 2 to $N-1$ of $\mathbf{T}$. It is possible to construct $\mathbf{T}$ if we remember that its columns are the orthogonal eigenvectors of $\mathbf{M}$. We can find the remaining entries in $\mathbf{T}$ through the application of the Gram-Schmidt orthogonalisation procedure. This procedure enables one to start with a set of linearly independent vectors, and then generate an additional set of vectors that are all orthogonal and that belong to the same subspace as the original set. We shall next introduce the Gram-Schmidt procedure and show how it can be utilised to construct $\mathbf{T}$. We then present coupling matrix synthesis examples.

The Gram-Schmidt orthogonalisation process

Suppose $B = \{\vec{u_1}; \vec{u_2}; \ldots; \vec{u_m}\}$, $m \leq n$ is a basis for a subspace W_m of $\mathcal{R}^n$. Then $\{\vec{v_1}; \vec{v_2}; \ldots; \vec{v_m}\}$, where

$$\begin{aligned}
\vec{v_1} &= \vec{u_1} \\
\vec{v_2} &= \vec{u_2} - \left(\frac{\vec{u_2}\cdot\vec{v_1}}{\vec{v_1}\cdot\vec{v_1}}\right)\vec{v_1} \\
\vec{v_3} &= \vec{u_3} - \left(\frac{\vec{u_3}\cdot\vec{v_1}}{\vec{v_1}\cdot\vec{v_1}}\right)\vec{v_1} - \left(\frac{\vec{u_3}\cdot\vec{v_2}}{\vec{v_2}\cdot\vec{v_2}}\right)\vec{v_2} \\
&\vdots \\
\vec{v_m} &= \vec{u_m} - \left(\frac{\vec{u_m}\cdot\vec{v_1}}{\vec{v_1}\cdot\vec{v_1}}\right)\vec{v_1} - \left(\frac{\vec{u_m}\cdot\vec{v_2}}{\vec{v_2}\cdot\vec{v_2}}\right)\vec{v_2} \ldots - \left(\frac{\vec{u_m}\cdot\vec{v_{m-1}}}{\vec{v_{m-1}}\cdot\vec{v_{m-1}}}\right)\vec{v_{m-1}},
\end{aligned} \tag{5.58}$$

is an orthogonal basis for W_m. A orthonormal basis for W_m is then
$B' = \{\vec{w_1}; \vec{w_2}; \ldots; \vec{w_m}\} = \left\{\frac{\vec{v_1}}{||\vec{v_1}||}; \frac{\vec{v_2}}{||\vec{v_2}||}; \ldots; \frac{\vec{v_m}}{||\vec{v_m}||}\right\}$.
The Gram-Schmidt procedure can be utilised to construct $\mathbf{T}$ by choosing B as follows:

$$B = \{T_1; <1,0,\ldots,0>; <0,1,0,\ldots,0>; \ldots; <0,0,\ldots,1,0,0>; T_N\}$$

Here we define B as being a set of N linearly independent vectors belonging to the same subspace as the vectors contained in $\mathbf{T}$. Note that the vectors in B are all linearly independent but not necessarily orthogonal. The Gram-Schmidt procedure then produces a set of orthogonal vectors, B', that correspond to the rows of $\mathbf{T}$. With the matrix $\mathbf{T}$ now known, we are able to construct the $N \times N$ coupling matrix using equation 5.36. Note that $\mathbf{\Lambda}$ in the mentioned equation is a diagonal matrix with the poles of $y_{22}(S)$ or $y_{21}(S)$ as its diagonal entries. The synthesis procedure described above highlights the fact that there is not a one-to-one mapping between characteristic polynomials and prototype circuits. The Gram-Schmidt orthogonalisation process implies that there

are multiple possible definitions for $\mathbf{T}$ and therefore multiple possible definitions of $\mathbf{M}$. Each of these circuits produces the same frequency response. The goal is to find the prototype circuit that would be amendable for realisation as a microwave circuit.

We now have the necessary theoretical background to construct $N \times N$ coupled resonator circuits from the characteristic polynomials. In the next subsection we shall clarify the presented theory by providing complete synthesis examples.

5.5.3 Examples

This section contains two examples. The examples are a continuation of the examples presented in section 2.5.4 and in section 3.7 and form part of the practical designs presented in chapters 8 and 9.

Example 1: Symmetric dual-band prototype

Suppose we want to find a dual-band prototype that has the following specifications:

- Passband 1: $\Omega \in [-1\ ;\ -0.5822]$.
- Passband 2: $\Omega \in [0.5822\ ;\ 1]$.
- Minimum return loss in passband 1: 20 dB.
- Order of dual-band filter: 8.
- The filter should be an all-pole filter, i.e. all the transmission zeros must be located at infinity.

The approximation problem for these specifications was solved in section 3.7 using the frequency mapping technique. The following characteristic polynomials were obtained:

$$\begin{aligned} F(S) &= S^8 + 2.678\,S^6 + 2.5802\,S^4 + 1.0541\,S^2 + 0.1534 \\ E(S) &= S^8 + 0.9088\,S^7 + 3.0909\,S^6 + 1.9878\,S^5 + 3.1953\,S^4 \\ &\quad + 1.324\,S^3 + 1.2655\,S^2 + 0.2582\,S + 0.1541 \\ jP(S) &= j \\ \epsilon &= 67.3703 \\ \epsilon_r &= 1 \end{aligned}$$

The crux of the synthesis procedure is to relate the characteristic polynomials to the prototype circuit using the admittance parameters. The first step is to calculate the numerator of the driving point impedance function using equation 5.11 as follows:

$$\begin{aligned} \text{Numerator}\left\{Z_{\text{DP}(S)}\right\} &= 2\,S^8 + 0.9089\,S^7 + 5.7688\,S^6 + 1.9880\,S^5 + 5.7753\,S^4 \\ &\quad + 1.3241\,S^3 + 2.3193\,S^2 + 0.2583\,S + 0.3075 \end{aligned}$$

The numerator polynomial above can be separated into its complex even and complex odd parts using equations 5.13 and 5.14 respectively. The result is as follows:

$$\begin{aligned} m_1(S) &= 2\,S^8 + 5.7688\,S^6 + 5.7753\,S^4 + 2.3193\,S^2 + 0.3075 \\ n_1(S) &= 0.9089\,S^7 + 1.9880\,S^5 + 1.3241\,S^3 + 0.2583\,S \end{aligned}$$

We can now identify $y_{22}(S)$ using equation 5.16 as follows:

$$\begin{aligned} y_{22}(S) &= \frac{n_1(S)}{m_1(S)} = \frac{0.9089\,S^7 + 1.9880\,S^5 + 1.3241\,S^3 + 0.2583\,S}{2\,S^8 + 5.7688\,S^6 + 5.7753\,S^4 + 2.3193\,S^2 + 0.3075} \\ &= \frac{0.0337}{S + 1.0673j} + \frac{0.0337}{S - 1.0673j} + \frac{0.0706}{S + 0.9713j} + \frac{0.0706}{S - 0.9713j} \\ &\quad + \frac{0.0771}{S + 0.7306j} + \frac{0.0771}{S - 0.7306j} + \frac{0.0459}{S + 0.5177j} + \frac{0.0459}{S - 0.5177j} \end{aligned} \tag{5.59}$$

We can also identify $y_{21}(S)$ using equation 5.17 as follows:

$$\begin{aligned} y_{21}(S) &= \frac{P(S)/\epsilon}{m_1(S)} = \frac{0.0148j}{2\,S^8 + 5.7688\,S^6 + 5.7753\,S^4 + 2.3193\,S^2 + 0.3075} \\ &= \frac{0.0337}{S + 1.0673j} - \frac{0.0337}{S - 1.0673j} + \frac{0.0706}{S - 0.9713j} - \frac{0.0706}{S + 0.9713j} \\ &\quad + \frac{0.0771}{S + 0.7306j} - \frac{0.0771}{S - 0.7306j} + \frac{0.0459}{S - 0.5177j} - \frac{0.0459}{S + 0.5177j} \end{aligned} \tag{5.60}$$

We can next calculate the input transformer windings using equation 5.56 as follows:

$$n_1 = \sqrt{\sum_{k=1}^{N} \frac{(K_{21,k})^2}{K_{22,k}}} = 0.674166 \tag{5.61}$$

Similarly the output transformer windings are calculated using equation 5.53 as follows:

$$n_2 = \sqrt{\sum_{k=1}^{N} K_{22,k}} = 0.674166 \tag{5.62}$$

We can use equation 5.57 to calculate the first row of $\mathbf{T}$. Similarly we can use equation 5.54 to calculate the last row of $\mathbf{T}$. We shall now apply the Gram-Schmidt orthogonalisation procedure to construct $\mathbf{T}$. We choose our initial basis vectors as follows:

$$B = \left\{ \begin{array}{l} \vec{u_1} = T_1 \\ \vec{u_2} \\ \vec{u_3} \\ \vec{u_4} \\ \vec{u_5} \\ \vec{u_6} \\ \vec{u_7} \\ \vec{u_8} = T_8 \end{array} \right\} = \left\{ \begin{array}{llllllll} < 0.2723 & -0.2723 & 0.3941 & -0.3941 & 0.4119 & -0.4119 & 0.3177 & -0.3177 > \\ < 1 & 0 & 0 & 0 & 0 & 0 & 0 & 0 > \\ < 0 & 1 & 0 & 0 & 0 & 0 & 0 & 0 > \\ < 0 & 0 & 1 & 0 & 0 & 0 & 0 & 0 > \\ < 0 & 0 & 0 & 1 & 0 & 0 & 0 & 0 > \\ < 0 & 0 & 0 & 0 & 1 & 0 & 0 & 0 > \\ < 0 & 0 & 0 & 0 & 0 & 1 & 0 & 0 > \\ < 0.2723 & 0.2723 & 0.3941 & 0.3941 & 0.4119 & 0.4119 & 0.3177 & 0.3177 > \end{array} \right\}$$

These vectors are all linearly independent but not necessarily orthogonal. They are contained in the same subspace as the vectors in $\mathbf{T}$. The procedure shown in equation 5.58 can now be applied to obtain B'. The vectors in B' can be used to construct the matrix $\mathbf{T}$ as follows:

$$\mathbf{T} = \begin{bmatrix} 0.2723 & -0.2723 & 0.3941 & -0.3941 & 0.4119 & -0.4119 & 0.3177 & -0.3177 \\ 0.9229 & 0.0000 & -0.2326 & 0.0000 & -0.2431 & 0.0000 & -0.1875 & 0.0000 \\ -0.0000 & 0.9229 & 0.0000 & -0.2326 & 0.0000 & -0.2431 & 0.0000 & -0.1875 \\ 0.0000 & 0.0000 & 0.7971 & 0.0000 & -0.4782 & 0.0000 & -0.3688 & 0.0000 \\ -0.0000 & -0.0000 & -0.0000 & 0.7971 & 0.0000 & -0.4782 & 0.0000 & -0.3688 \\ 0.0000 & 0.0000 & 0.0000 & 0.0000 & 0.6108 & -0.0000 & -0.7918 & 0.0000 \\ -0.0000 & 0.0000 & -0.0000 & 0.0000 & -0.0000 & 0.6108 & -0.0000 & -0.7918 \\ 0.2723 & 0.2723 & 0.3941 & 0.3941 & 0.4119 & 0.4119 & 0.3177 & 0.3177 \end{bmatrix}$$

We can construct the diagonal matrix $\mathbf{\Lambda}$ using the poles of $y_{21}(S)$ or $y_{22}(S)$ as follows:

$$\mathbf{\Lambda} = \begin{bmatrix} -1.0673 & 0 & 0 & 0 & 0 & 0 & 0 & 0 \\ 0 & 1.0673 & 0 & 0 & 0 & 0 & 0 & 0 \\ 0 & 0 & 0.9713 & 0 & 0 & 0 & 0 & 0 \\ 0 & 0 & 0 & -0.9713 & 0 & 0 & 0 & 0 \\ 0 & 0 & 0 & 0 & -0.7306 & 0 & 0 & 0 \\ 0 & 0 & 0 & 0 & 0 & 0.7306 & 0 & 0 \\ 0 & 0 & 0 & 0 & 0 & 0 & 0.5177 & 0 \\ 0 & 0 & 0 & 0 & 0 & 0 & 0 & -0.5177 \end{bmatrix}$$

We can finally construct the $N \times N$ coupling matrix using equation 5.36 as follows:

$$\begin{aligned} \mathbf{M} &= \mathbf{T}\,\mathbf{\Lambda}\,\mathbf{T}^T \\ &= \begin{bmatrix} 0.0000 & -0.3150 & -0.3150 & 0.3883 & 0.3883 & -0.3140 & -0.3140 & 0.0000 \\ -0.3150 & -0.8814 & 0.0000 & -0.2292 & -0.0000 & 0.1853 & 0.0000 & -0.3150 \\ -0.3150 & 0.0000 & 0.8814 & 0.0000 & 0.2292 & -0.0000 & -0.1853 & 0.3150 \\ 0.3883 & -0.2292 & 0.0000 & 0.5205 & -0.0000 & 0.3645 & 0.0000 & 0.3883 \\ 0.3883 & -0.0000 & 0.2292 & -0.0000 & -0.5205 & 0.0000 & -0.3645 & -0.3883 \\ -0.3140 & 0.1853 & -0.0000 & 0.3645 & 0.0000 & 0.0521 & 0.0000 & -0.3140 \\ -0.3140 & 0.0000 & -0.1853 & 0.0000 & -0.3645 & 0.0000 & -0.0521 & 0.3140 \\ 0.0000 & -0.3150 & 0.3150 & 0.3883 & -0.3883 & -0.3140 & 0.3140 & 0.0000 \end{bmatrix} \end{aligned}$$

The input and output transformer windings and the coupling matrix are now known. The synthesis procedure is thus complete. Note that coupling matrix above does not correspond to a circuit with a practical topology. Almost all the resonators are coupled to each other and this makes the realisation of the filter a challenging task. Also, the resonators are still asynchronously tuned even though the prototype specification is symmetric. Symmetric frequency responses do not require asynchronously tuned resonators. The coupling matrix is thus not in an optimal topology. In section 5.7 we illustrate how the coupling matrix can be transformed to obtain more practical filter topologies that have identical frequency responses.

Example 2: Asymmetric dual-band prototype

Suppose we want to find a dual-band prototype that has the following specifications:

- Passband 1: $\Omega \in [-1\ ;\ -0.5476]$.
- Passband 2: $\Omega \in [0.7575\ ;\ 1]$.
- Minimum return loss in passband 1: 20 dB.
- Order of dual-band filter: 4.
- The filter should have finite frequency transmission zeros at $\Omega = 0.1752$ and $\Omega = 0.3725$.

The approximation problem for these specifications was solved in section 3.7.1 using the frequency mapping technique. The following characteristic polynomials were obtained:

$$\begin{aligned} F(S) &= S^4 - 0.2122j\,S^3 + 1.3531\,S^2 - 0.1749jS + 0.4195 \\ jP(S) &= j\,S^2 + 0.5477\,S - 0.0653j \\ E(S) &= S^4 + (1.0701 - 0.2122j)\,S^3 + (1.9257 - 0.4080j)\,S^2 \\ &\qquad + (0.6604 - 0.4899j)\,S + 0.3762 - 0.1903j \\ \epsilon &= 1.5615 \\ \epsilon_r &= 1 \end{aligned}$$

The crux of the synthesis procedure is to relate the characteristic polynomials to the prototype circuit using the admittance parameters. The first step is to calculate the numerator of the driving point impedance function using equation 5.11 as follows:

$$\begin{aligned} \text{Numerator}\left\{Z_{\text{DP}(S)}\right\} &= 2\,S^4 + (1.0701 - 0.4244j)\,S^3 + (3.2787 - 0.4080j)\,S^2 \\ &\qquad + (0.6604 - 0.6648j)\,S + (0.7958 - 0.1903j) \end{aligned}$$

The numerator polynomial above can be separated into its complex even and complex odd parts using equations 5.13 and 5.14 respectively. The result is as follows:

$$\begin{aligned} m_1(S) &= 2\,S^4 - 0.4244j\,S^3 + 3.2787\,S^2 - 0.6648j\,S + 0.7958 \\ n_1(S) &= 1.0701\,S^3 - 0.4080j\,S^2 + 0.6604\,S - 0.1903j \end{aligned}$$

We can now identify $y_{22}(S)$ using equation 5.16 as follows:

$$\begin{aligned} y_{22}(S) = \frac{n_1(S)}{m_1(S)} &= \frac{1.0701\,S^3 - 0.4080j\,S^2 + 0.6604\,S - 0.1903j}{2\,S^4 - 0.4244j\,S^3 + 3.2787\,S^2 - 0.6648j\,S + 0.7958} \\ &= \frac{0.2090}{S + 1.1768j} + \frac{0.1478}{S - 1.1272j} + \frac{0.0585}{S - 0.6940j} + \frac{0.1197}{S + 0.4322j} \end{aligned}$$

We can also identify $y_{21}(S)$ using equation 5.17 as follows:

$$\begin{aligned} y_{21}(S) = \frac{P(S)/\epsilon}{m_1(S)} &= \frac{0.6404j\,S^2 + 0.3508\,S - 0.0418j}{2\,S^4 - 0.4244j\,S^3 + 3.2787\,S^2 - 0.6648j\,S + 0.7958} \\ &= -\frac{0.2090}{S + 1.1768j} + \frac{0.1478}{S - 1.1272j} - \frac{0.0585}{S - 0.6940j} + \frac{0.1197}{S + 0.4322j} \end{aligned} \tag{5.63}$$

We can next calculate the input transformer windings using equation 5.56 as follows:

$$n_1 = \sqrt{\sum_{k=1}^{N} \frac{(K_{21,k})^2}{K_{22,k}}} = 0.7315$$

Similarly the output transformer windings are calculated using equation 5.53 as follows:

$$n_2 = \sqrt{\sum_{k=1}^{N} K_{22,k}} = 0.7315$$

We can use equation 5.57 to calculate the first row of $\mathbf{T}$. Similarly we can use equation 5.54 to calculate the last row of $\mathbf{T}$. We shall now apply the Gram-Schmidt orthogonalisation procedure to construct $\mathbf{T}$. We choose our

initial basis vectors as follows:

$$B = \left\{ \begin{array}{l} \vec{u_1} = T_1 \\ \vec{u_2} \\ \vec{u_3} \\ \vec{u_4} = T_4 \end{array} \right\} = \left\{ \begin{array}{llll} < -0.6250 & 0.5256 & -0.3307 & 0.4730 > \\ < 1 & 0 & 0 & 0 > \\ < 0 & 1 & 0 & 0 > \\ < 0.6250 & 0.5256 & 0.3307 & 0.4730 > \end{array} \right\}$$

These vectors are all linearly independent but not necessarily orthogonal. They are contained in the same subspace as the vectors in $\mathbf{T}$. The procedure shown in equation 5.58 can now be applied to obtain B'. The vectors in B' can be used to construct the matrix $\mathbf{T}$ as follows:

$$\mathbf{T} = \begin{bmatrix} -0.6250 & 0.5256 & -0.3307 & 0.4730 \\ 0.4677 & -0.0000 & -0.8839 & -0.0000 \\ 0.0000 & 0.6689 & 0.0000 & -0.7433 \\ 0.6250 & 0.5256 & 0.3307 & 0.4730 \end{bmatrix}$$

We can construct the diagonal matrix $\mathbf{\Lambda}$ using the poles of $y_{21}(S)$ or $y_{22}(S)$ as follows:

$$\mathbf{\Lambda} = \begin{bmatrix} -1.1768 & 0 & 0 & 0 \\ 0 & 1.1272 & 0 & 0 \\ 0 & 0 & 0.6940 & 0 \\ 0 & 0 & 0 & -0.4322 \end{bmatrix}$$

We can finally construct the $N \times N$ coupling matrix using equation 5.36 as follows:

$$\begin{aligned} \mathbf{M} &= \mathbf{T}\,\mathbf{\Lambda}\,\mathbf{T}^T \\ &= \begin{bmatrix} -0.1690 & 0.5469 & 0.5483 & 0.5984 \\ 0.5469 & 0.2847 & -0.0000 & -0.5469 \\ 0.5483 & -0.0000 & 0.2655 & 0.5483 \\ 0.5984 & -0.5469 & 0.5483 & -0.1690 \end{bmatrix} \end{aligned}$$

The input and output transformer windings and the coupling matrix are now known. The synthesis procedure is thus complete. Note that coupling matrix above does not correspond to a circuit with a practical topology. Almost all the resonators are coupled to each other and this makes the realisation of the filter a challenging task. In section 5.7 we illustrate how the coupling matrix can be transformed to obtain more practical filter topologies that have identical frequency responses. We next introduce the synthesis of the general $N+2 \times N+2$ coupled resonator circuit.

5.6 The $N+2 \times N+2$ coupled resonator circuit

In this section we introduce the general $N+2 \times N+2$ coupled resonator circuit. The $N+2 \times N+2$ coupled resonator circuit is a relatively new development and has considerable advantages over the classical $N \times N$ coupled resonator circuit [15]. The $N+2 \times N+2$ coupled resonator circuit has no restrictions with respect to the allowable couplings. Each node in the network can theoretically be coupled to every other node in the network. A direct coupling between the source and the load is also possible. If one considers the shortest path rule (refer to section 5.4), it becomes apparent that the general $N+2 \times N+2$ coupled resonator circuit can accommodate a maximum of N finite frequency transmission zeros. The characteristic polynomials can also

accommodate a maximum of N transmission zeros. Circuits that have the ability to accommodate N transmission zeros at finite frequencies are referred to as fully canonical circuits [15].

The section starts by introducing the prototype circuit associated with the $N+2\times N+2$ coupled resonator circuit. We then calculate expressions for $y_{21}(S)$ and $y_{22}(S)$ in terms of the electrical parameters of said prototype circuit. These parameters will then be related to the admittance parameters as obtained from the characteristic polynomials in section 5.2. From this relationship we obtain general synthesis equations. At the end of this section we shall clarify the presented theory through some application examples. The theory presented in this section was originally introduced by Cameron in [15].

5.6.1 Admittance parameters of $N+2\times N+2$ prototype circuit

The topology of a circuit is directly influenced by the number of finite frequency transmission zeros. There are three known circuit topologies that can accommodate full canonical frequency responses, these are presented in section 5.7.2. The $N\times N$ coupling matrix, introduced in section 5.5, can only describe the interconnection of N resonators. Cameron extended the coupling matrix by appending two additional rows and two additional columns. The new rows and columns are included in the matrix to model the coupling of the source and the load to any other node inside the network. The new extended coupling matrix is referred to as the $N+2\times N+2$ coupling matrix and is used to model the general $N+2\times N+2$ coupled resonator circuit.

In order for the synthesis technique to be able to accommodate canonical frequency responses, Cameron employed a canonical prototype circuit during the synthesis procedure. Cameron chose the transversal canonical network as the prototype circuit for the synthesis procedure. The coupling routing diagram of a coupled resonator structure in the transversal topology is shown in figure 5.6. The resonant nodes are modelled using lumped element resonators. The couplings between different nodes can again be modelled using frequency invariant mutual inductances. Cameron however employed ideal admittance inverters to model the coupling between different nodes. We discuss the modelling of coupling using immittance inverters in appendix B.

The values of the immittance inverters associated with a $N+2\times N+2$ matrix are the same as the values of the mutual inductances associated with an $N\times N$ matrix. The immittance inverters are equivalent to the mutual inductances/transformers with respect to energy exchange and phase shift. A circuit can be constructed using either series resonators with impedance inverters or parallel resonators with admittance inverters. The $N+2\times N+2$ coupling matrices that describe both cases are identical. This property is due to electrical duality [61]. Following the same technique introduced in section 5.5.1, the transversal circuit in the actual frequency domain can be mapped to the prototype frequency domain using the relationships given in figure 5.1. The resulting transversal prototype circuit, in the shunt configuration, is shown in figure 5.7. The extended coupling matrix that fully describes this circuit only contains elements on the outer peripheral and on the main diagonal of the matrix. All the other entries are zero. This is a direct result of the individual resonant nodes being uncoupled. The described coupling matrix is as follows:

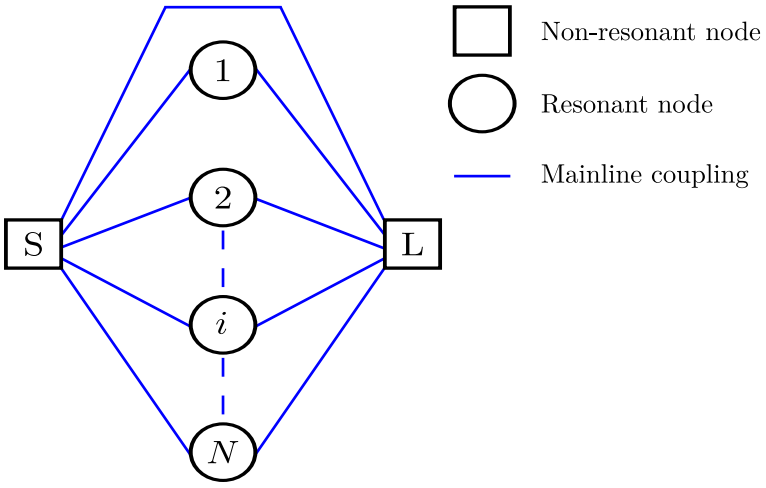

Figure 5.6: The coupling routing diagram of a coupled resonator circuit in the transversal topology. Note that all the resonant nodes are uncoupled. This greatly simplifies the synthesis procedure for this group of circuits.

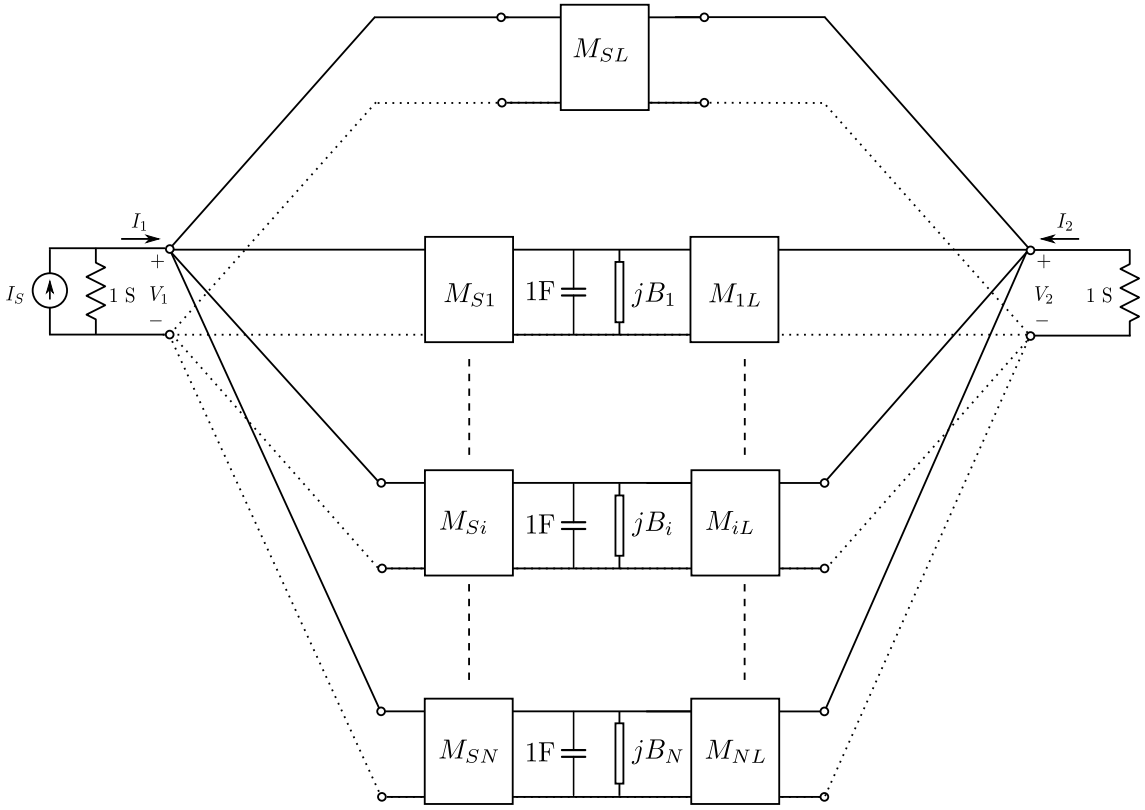

Figure 5.7: The general prototype associated with the $N + 2 \times N + 2$ coupled resonator circuit is shown above. The circuit above is an admittance inverter and shunt resonator realisation of the coupling routing diagram shown in figure 5.6.

$$\mathbf{M}_{N+2\times N+2} = \begin{array}{c} \\ S \\ 1 \\ \vdots \\ i \\ \vdots \\ N \\ L \end{array} \begin{array}{c} \begin{array}{ccccccc} S & 1 & \dots & i & \dots & N & L \end{array} \\ \begin{bmatrix} & M_{S\,1} & \dots & M_{S\,i} & \dots & M_{S\,N} & M_{S\,L} \\ M_{1\,S} & B_1 & & & & & M_{1\,L} \\ \vdots & & \ddots & & & & \vdots \\ M_{i\,S} & & & B_i & & & M_{i\,L} \\ \vdots & & & & \ddots & & \vdots \\ M_{N\,S} & & & & & B_N & M_{N\,L} \\ M_{L\,S} & M_{L\,1} & \dots & M_{L\,i} & \dots & M_{L\,N} & \end{bmatrix} \end{array} \tag{5.64}$$

Inspection of equation 5.64 shows that both the source and the load are coupled to every resonator inside the circuit. The existence of frequency invariant reactive elements allows each resonator to be resonant at a different frequency. Note that it is possible to calculate the resonant frequency of each resonator by remembering that the total self capacitance is unity and substituting the main diagonal entries of $\mathbf{M}_{N+2\times N+2}$ into equation 5.21 as follows:

$$\omega_i = \frac{\omega_0}{\frac{\Delta\mathbf{M}_{ii}}{2} + \sqrt{\left(\frac{\Delta\mathbf{M}_{ii}}{2}\right)^2 + 1}} \tag{5.65}$$

Here $\mathbf{M}_{ii}$ is the i-th main diagonal entry of $\mathbf{M}_{N+2\times N+2}$. The properties of the coupling matrix enable the transversal topology to accommodate fully canonical asymmetric frequency responses. The synthesis of the general $N+2\times N+2$ coupled resonator circuit is conceptually similar to the synthesis of the general $N\times N$ coupled resonator circuit. In both cases expressions for the admittance parameters are first found in terms of the electrical parameters of the prototype circuit. Expressions for the admittance parameters are then also found using the characteristic polynomials. The admittance parameters can then be used to relate the characteristic polynomials to the prototype circuit and thus produce a set of synthesis equations. Expressions for the admittance parameters for the two-port network in figure 5.7 can by found through the summation of the admittance parameters of the individual parallel sections. An expression for the admittance parameters of a parallel section can be found by first calculating the ABCD-parameters of said section and then converting these parameters into an equivalent set of admittance parameters. The ABCD-parameters of the i-th parallel resonant section is calculated as follows:

$$\begin{aligned}
\begin{bmatrix} V_1 \\ I_1 \end{bmatrix} &= \begin{bmatrix} 0 & \frac{1}{jM_{S\,i}} \\ -jM_{S\,i} & 0 \end{bmatrix} \begin{bmatrix} 1 & 0 \\ (SC_i + jB_i) & 1 \end{bmatrix} \begin{bmatrix} 0 & \frac{1}{jM_{i\,L}} \\ -jM_{i\,L} & 0 \end{bmatrix} \begin{bmatrix} V_2 \\ -I_2 \end{bmatrix} \\
&= \begin{bmatrix} \frac{SC_i+jB_i}{jM_{S\,i}} & \frac{1}{jM_{S\,i}} \\ -jM_{S\,i} & 0 \end{bmatrix} \begin{bmatrix} 0 & \frac{1}{jM_{i\,L}} \\ -jM_{i\,L} & 0 \end{bmatrix} \begin{bmatrix} V_2 \\ -I_2 \end{bmatrix} \\
&= -\begin{bmatrix} \frac{M_{L\,i}}{M_{S\,i}} & \frac{SC_i+jB_i}{M_{S\,i}M_{L\,i}} \\ 0 & \frac{M_{S\,i}}{M_{i\,L}} \end{bmatrix} \begin{bmatrix} V_2 \\ -I_2 \end{bmatrix}
\end{aligned}$$

The admittance parameters can be obtained from the ABCD-parameters using the following relationships [2]:

$$\begin{aligned}
y_{11} &= \tfrac{D}{B} & y_{12} &= \tfrac{BC-AD}{B} \\
y_{21} &= -\tfrac{1}{B} & y_{22} &= \tfrac{A}{B}
\end{aligned}$$

The admittance parameters of the i-th parallel resonant section is therefore given as follows:

$$\mathbf{Y}_i = \frac{1}{SC_i + jB_i} \begin{bmatrix} M_{S\,i}^2 & M_{S\,i}M_{i\,L} \\ M_{S\,i}M_{i\,L} & M_{i\,L}^2 \end{bmatrix}$$

The admittance parameters of the direct source-load coupling can be obtained using a similar technique. An expression for the admittance parameters of the transversal circuit in figure 5.7 is found through the summation of the admittance parameters of all the individual parallel sections. The final expression for the admittance parameters of the $N+2 \times N+2$ coupled resonator prototype circuit is therefore as follows:

$$\begin{aligned} \mathbf{Y} &= \begin{bmatrix} y_{11}(S) & y_{12}(S) \\ y_{21}(S) & y_{22}(S) \end{bmatrix} \\ &= j \begin{bmatrix} 0 & M_{S\,L} \\ M_{S\,L} & 0 \end{bmatrix} + \sum_{i=0}^{N} \frac{1}{SC_i + jB_i} \begin{bmatrix} M_{S\,i}^2 & M_{S\,i}M_{i\,L} \\ M_{S\,i}M_{i\,L} & M_{i\,L}^2 \end{bmatrix} \end{aligned} \tag{5.66}$$

We now have expressions for the admittance parameters of the prototype circuit in figure 5.7. The next step is to relate the characteristic polynomials to the prototype circuit. We shall describe the synthesis procedure in the next subsection.

5.6.2 Derivation of synthesis expressions

The characteristic polynomials were related to the admittance parameters in section 5.2. The admittance parameters of the prototype circuit in figure 5.7 were calculated in the previous subsection. We are now able to link a set of characteristic polynomials, that define a desired frequency response, to a prototype circuit with the topology shown in figure 5.7. This is achieved by equating the expressions for their admittance parameters. Through partial fraction expansion, we can express the admittance parameters in terms of the characteristic polynomials as follows:

$$\begin{aligned} \mathbf{Y} &= \begin{bmatrix} y_{11}(S) & y_{12}(S) \\ y_{21}(S) & y_{22}(S) \end{bmatrix} \\ &= j \begin{bmatrix} 0 & K_0 \\ K_0 & 0 \end{bmatrix} + \sum_{i=0}^{N} \frac{1}{S - j\lambda_i} \begin{bmatrix} K_{11\,i} & K_{12\,i} \\ K_{21\,i} & K_{22\,i} \end{bmatrix} \end{aligned} \tag{5.67}$$

Here the constant K_0 was introduced to accommodate fully canonical filter responses. For the fully canonical case there are N finite frequency transmission zeros and as a consequence the degree of $P(S)$ is equal to the degree of $E(S)$. Consequently, K_0 must be extracted to ensure that $y_{12}(S)$ and $y_{21}(S)$ are proper rational functions. If K_0 is known, we can calculate the new numerator polynomial of $y_{21\,n}(S)$ as follows:

$$y'_{21\,n}(S) = y_{21\,n}(S) - jK_0\, y_{21\,d}(S)$$

Here $y_{21\,n}(S)$ and $y_{21\,d}(S)$ are the old numerator and denominator polynomials of $y_{21}(S)$ respectively. Once K_0 has been extracted, the admittance parameters can be expanded as a sum of partial fractions as shown in equation 5.67. We shall now consider how to calculate K_0 from the characteristic polynomials. The complex constant K_0 must be extracted from the transfer admittance functions when they are associated with fully

canonical filtering functions. These are cases when $n_{\text{fz}} = N$. For fully canonical cases the following holds true:

$$jK_0 = \lim_{S\to\pm j\infty} y_{21}(S) = \begin{cases} \lim\limits_{S\to\pm j\infty} \frac{jP(S)}{\epsilon m_1} & N \text{ is even} \\ \lim\limits_{S\to\pm j\infty} \frac{jP(S)}{\epsilon n_1} & N \text{ is odd} \end{cases}$$
$$= \frac{j/\epsilon}{1+1/\epsilon_r}$$
$$\iff \qquad K_0 = \frac{\epsilon}{\epsilon_r}(\epsilon_r - 1)$$

If the number of finite frequency transmission zeros are less than N, K_0 must assume the value of 0. Synthesis equations can be obtained through the comparison of equations 5.66 and 5.67:

$$\begin{aligned} M_{S\,L} &= K_0 \\ C_i &= 1 \\ B_i &= -\lambda_i \\ M_{i\,L} &= \sqrt{K_{22\,i}} \\ M_{S\,i} &= \frac{K_{21\,i}}{\sqrt{K_{22\,i}}} \qquad i = 1, 2, \ldots, N \end{aligned} \tag{5.68}$$

Clearly the entire electrical network is now specified. Note that the direct source-load coupling is equal to K_0. This completes the synthesis procedure of the general $N+2 \times N+2$ coupled resonator circuit. The synthesis procedure presented in this section is much simpler than the original technique presented in section 5.5 as the Gram-Schmidt orthogonalisation process is not required. It must be stated that the $N \times N$ and $N+2 \times N+2$ coupled resonator representations of an arbitrary set of characteristic polynomials are not the same. They represent two different electrical networks that have the same frequency response. Neither of these networks is in general suited to be realised as microwave circuits. This is because they contain numerous cross-couplings. In section 5.7 we illustrate how the coupling matrix can be simplified using matrix rotations. We shall next clarify the presented theory by providing some complete synthesis examples.

5.6.3 Examples

This section contains two examples. The examples are a continuation of the examples presented in section 2.5.4 and in section 3.7 and form part of the practical designs presented in chapters 8 and 9. The examples also highlight the differences between the $N \times N$ and $N+2 \times N+2$ synthesis procedures.

Example 1: Symmetric dual-band prototype

Suppose we want to find a dual-band prototype that has the following specifications:

- Passband 1: $\Omega \in [-1\ ;\ -0.5822]$.
- Passband 2: $\Omega \in [0.5822\ ;\ 1]$.
- Minimum return loss in passband 1: 20 dB.
- Order of dual-band filter: 8.
- The filter should be an all-pole filter, i.e. all the transmission zeros must be located at infinity.

The approximation problem for these specifications was solved in section 3.7 using the frequency mapping technique. The following characteristic polynomials were obtained:

$$\begin{aligned} F(S) &= S^8 + 2.678\,S^6 + 2.5802\,S^4 + 1.0541\,S^2 + 0.1534 \\ E(S) &= S^8 + 0.9088\,S^7 + 3.0909\,S^6 + 1.9878\,S^5 + 3.1953\,S^4 \\ &\quad + 1.324\,S^3 + 1.2655\,S^2 + 0.2582\,S + 0.1541 \\ jP(S) &= j \\ \epsilon &= 67.3703 \\ \epsilon_r &= 1 \end{aligned}$$

The crux of the synthesis procedure is to relate the characteristic polynomials to the prototype circuit using the admittance parameters. The first step is to calculate the numerator of the driving point impedance function using equation 5.11 as follows:

$$\begin{aligned} \text{Numerator}\left\{Z_{\text{DP}(S)}\right\} &= 2\,S^8 + 0.9089\,S^7 + 5.7688\,S^6 + 1.9880\,S^5 + 5.7753\,S^4 \\ &\quad + 1.3241\,S^3 + 2.3193\,S^2 + 0.2583\,S + 0.3075 \end{aligned}$$

The numerator polynomial above can be separated into its complex even and complex odd parts using equations 5.13 and 5.14 respectively. The result is as follows:

$$\begin{aligned} m_1(S) &= 2\,S^8 + 5.7688\,S^6 + 5.7753\,S^4 + 2.3193\,S^2 + 0.3075 \\ n_1(S) &= 0.9089\,S^7 + 1.9880\,S^5 + 1.3241\,S^3 + 0.2583\,S \end{aligned}$$

We can now identify $y_{22}(S)$ using equation 5.16 as follows:

$$\begin{aligned} y_{22}(S) &= \frac{n_1(S)}{m_1(S)} = \frac{0.9089\,S^7 + 1.9880\,S^5 + 1.3241\,S^3 + 0.2583\,S}{2\,S^8 + 5.7688\,S^6 + 5.7753\,S^4 + 2.3193\,S^2 + 0.3075} \\ &= \frac{0.0337}{S + 1.0673j} + \frac{0.0337}{S - 1.0673j} + \frac{0.0706}{S + 0.9713j} + \frac{0.0706}{S - 0.9713j} \\ &\quad + \frac{0.0771}{S + 0.7306j} + \frac{0.0771}{S - 0.7306j} + \frac{0.0459}{S + 0.5177j} + \frac{0.0459}{S - 0.5177j} \end{aligned} \tag{5.69}$$

We can also identify $y_{21}(S)$ using equation 5.17 as follows:

$$\begin{aligned} y_{21}(S) &= \frac{P(S)/\epsilon}{m_1(S)} = \frac{0.0148j}{2\,S^8 + 5.7688\,S^6 + 5.7753\,S^4 + 2.3193\,S^2 + 0.3075} \\ &= \frac{0.0337}{S + 1.0673j} - \frac{0.0337}{S - 1.0673j} + \frac{0.0706}{S - 0.9713j} - \frac{0.0706}{S + 0.9713j} \\ &\quad + \frac{0.0771}{S + 0.7306j} - \frac{0.0771}{S - 0.7306j} + \frac{0.0459}{S - 0.5177j} - \frac{0.0459}{S + 0.5177j} \end{aligned} \tag{5.70}$$

With the admittance parameters known, it is now possible to synthesise the coupling matrix directly using the equations in 5.68. All the transmission zeros are located at infinity, thus $M_{SL} = K_0 = 0$. The $N + 2 \times N + 2$ coupling matrix is entirely described by the poles and residues of its admittance parameters. The synthesis equations in 5.68 can be used in conjunction with the expressions for the admittance parameters in equations

5.69 and 5.70 to construct the following $N+2 \times N+2$ coupling matrix:

$$\mathbf{M} = \begin{array}{c} \\ S \\ 1 \\ 2 \\ 3 \\ 4 \\ 5 \\ 6 \\ 7 \\ 8 \\ L \end{array} \begin{array}{c} \begin{array}{ccccccccccc} S & 1 & 2 & 3 & 4 & 5 & 6 & 7 & 8 & L \end{array} \\ \left[\begin{array}{ccccccccccc} 0 & 0.1836 & -0.2656 & 0.2777 & -0.2142 & 0.2142 & -0.2777 & 0.2656 & -0.1836 & 0 \\ 0.1836 & 1.0673 & 0 & 0 & 0 & 0 & 0 & 0 & 0 & 0.1836 \\ -0.2656 & 0 & 0.9713 & 0 & 0 & 0 & 0 & 0 & 0 & 0.2656 \\ 0.2777 & 0 & 0 & 0.7306 & 0 & 0 & 0 & 0 & 0 & 0.2777 \\ -0.2142 & 0 & 0 & 0 & 0.5177 & 0 & 0 & 0 & 0 & 0.2142 \\ 0.2142 & 0 & 0 & 0 & 0 & -0.5177 & 0 & 0 & 0 & 0.2142 \\ -0.2777 & 0 & 0 & 0 & 0 & 0 & -0.7306 & 0 & 0 & 0.2777 \\ 0.2656 & 0 & 0 & 0 & 0 & 0 & 0 & -0.9713 & 0 & 0.2656 \\ -0.1836 & 0 & 0 & 0 & 0 & 0 & 0 & 0 & -1.0673 & 0.1836 \\ 0 & 0.1836 & 0.2656 & 0.2777 & 0.2142 & 0.2142 & 0.2777 & 0.2656 & 0.1836 & 0 \end{array}\right] \end{array}$$

The $N+2 \times N+2$ coupling matrix describes the entire prototype circuit. With the coupling matrix known, the synthesis procedure is now complete.

Example 2: Asymmetric dual-band prototype

Suppose we want to find a dual-band prototype that has the following specifications:

- Passband 1: $\Omega \in [-1\ ;\ -0.5476]$.
- Passband 2: $\Omega \in [0.7575\ ;\ 1]$.
- Minimum return loss in passband 1: 20 dB.
- Order of dual-band filter: 4.
- The filter should have finite frequency transmission zeros at $\Omega = 0.1752$ and $\Omega = 0.3725$.

The approximation problem for these specifications was solved in section 3.7.1 using the frequency mapping technique. The following characteristic polynomials were obtained:

$$\begin{aligned} F(S) &= S^4 - 0.2122j\,S^3 + 1.3531\,S^2 - 0.1749jS + 0.4195 \\ jP(S) &= j\,S^2 + 0.5477\,S - 0.0653j \\ E(S) &= S^4 + (1.0701 - 0.2122j)\,S^3 + (1.9257 - 0.4080j)\,S^2 \\ &\qquad + (0.6604 - 0.4899j)\,S + 0.3762 - 0.1903j \\ \epsilon &= 1.5615 \\ \epsilon_r &= 1 \end{aligned}$$

The crux of the synthesis procedure is to relate the characteristic polynomials to the prototype circuit using the admittance parameters. The first step is to calculate the numerator of the driving point impedance function using equation 5.11 as follows:

$$\begin{aligned} \text{Numerator}\left\{Z_{\text{DP}(S)}\right\} = 2\,S^4 &+ (1.0701 - 0.4244j)\,S^3 + (3.2787 - 0.4080j)\,S^2 \\ &+ (0.6604 - 0.6648j)\,S + (0.7958 - 0.1903j) \end{aligned}$$

The numerator polynomial above can be separated into its complex even and complex odd parts using equations 5.13 and 5.14 respectively. The result is as follows:

$$m_1(S) = 2\,S^4 - 0.4244j\,S^3 + 3.2787\,S^2 - 0.6648j\,S + 0.7958$$
$$n_1(S) = 1.0701\,S^3 - 0.4080j\,S^2 + 0.6604\,S - 0.1903j$$

We can now identify $y_{22}(S)$ using equation 5.16 as follows:

$$\begin{aligned} y_{22}(S) &= \frac{n_1(S)}{m_1(S)} = \frac{1.0701\,S^3 - 0.4080j\,S^2 + 0.6604\,S - 0.1903j}{2\,S^4 - 0.4244j\,S^3 + 3.2787\,S^2 - 0.6648j\,S + 0.7958} \\ &= \frac{0.2090}{S + 1.1768j} + \frac{0.1478}{S - 1.1272j} + \frac{0.0585}{S - 0.6940j} + \frac{0.1197}{S + 0.4322j} \end{aligned} \tag{5.71}$$

We can also identify $y_{21}(S)$ using equation 5.17 as follows:

$$\begin{aligned} y_{21}(S) &= \frac{P(S)/\epsilon}{m_1(S)} = \frac{0.6404j\,S^2 + 0.3508\,S - 0.0418j}{2\,S^4 - 0.4244j\,S^3 + 3.2787\,S^2 - 0.6648j\,S + 0.7958} \\ &= -\frac{0.2090}{S + 1.1768j} + \frac{0.1478}{S - 1.1272j} - \frac{0.0585}{S - 0.6940j} + \frac{0.1197}{S + 0.4322j} \end{aligned} \tag{5.72}$$

With the admittance parameters known, it is now possible to synthesise the coupling matrix directly using the equations in 5.68. The filtering function is not fully canonical, thus $M_{S\,L} = K_0 = 0$. The $N+2 \times N+2$ coupling matrix is entirely described by the poles and residues of its admittance parameters. The synthesis equations in 5.68 can be used in conjunction with the expressions for the admittance parameters in equations 5.71 and 5.72 to construct the following $N+2 \times N+2$ coupling matrix:

$$\mathbf{M} = \begin{array}{c} \\ S \\ 1 \\ 2 \\ 3 \\ 4 \\ L \end{array} \begin{array}{c} \begin{array}{cccccc} S & 1 & 2 & 3 & 4 & L \end{array} \\ \begin{bmatrix} 0 & -0.4572 & 0.3460 & -0.2419 & 0.3845 & 0 \\ -0.4572 & 1.1768 & 0 & 0 & 0 & 0.4572 \\ 0.3460 & 0 & 0.4322 & 0 & 0 & 0.3460 \\ -0.2419 & 0 & 0 & -0.6940 & 0 & 0.2419 \\ 0.3845 & 0 & 0 & 0 & -1.1272 & 0.3845 \\ 0 & 0.4572 & 0.3460 & 0.2419 & 0.3845 & 0 \end{bmatrix} \end{array}$$

The $N+2 \times N+2$ coupling matrix describes the entire prototype circuit. With the coupling matrix known, the synthesis procedure is now complete. The coupling matrices synthesised thus far do not describe circuit topologies that are especially amenable for realisation as microwave filters. We shall next introduce a technique to simplify circuit topologies using matrix operations.

5.7 Circuit simplification through similarity transformations

In the previous sections we introduced the idea that narrowband microwave filters can be modelled using coupling matrices. Modelling a circuit as a matrix is particularly useful because the topology of the circuit can be changed using matrix operations. The goal is to find multiple coupling matrices that all produce the same frequency response. Some of these matrices should be more amenable for realisation as microwave circuits. Whether a topology is desirable for realisation depends on the technology used. We want to find a group of similarity transformations that can be used to simplify the topology of a circuit without changing the frequency response of the circuit. We therefore need to define a criterion to identify the group of valid similarity transformations. Cameron stated that if the matrix $\mathbf{M_1}$ is obtained through the application of a

similarity transformation on the matrix $\mathbf{M_0}$, the matrices $\mathbf{M_1}$ and $\mathbf{M_0}$ will have identical frequency responses if their eigenvalues and eigenvectors are also identical [61]. Our criterion for a valid similarity transformation is therefore that the eigenvalues and eigenvectors of the initial coupling matrix are preserved after the application of the transformation. In the next subsection we introduce a set of matrix rotations that are considered to be valid similarity transformations according to the mentioned criterion. These transformations will then be used to transform any coupling matrix into one of the canonical topologies. The canonical topologies are standard forms for the coupling matrix that can accommodate any frequency response. We end the section by presenting a technique to design cascaded triplet filters using matrix rotations and the canonical forms. The theoretical techniques presented in this section shall later be validated through design examples.

5.7.1 Matrix rotations

A similarity transformation is carried out on the matrix $\mathbf{M_{r-1}}$ by pre- and postmultiplying it by a rotation matrix $\mathbf{R}$ and its transpose $\mathbf{R}^T$. The resultant matrix $\mathbf{M_r}$ is calculated as follows:

$$\mathbf{M_r} = \mathbf{R_r}\mathbf{M_{r-1}}\mathbf{R_r}^T \tag{5.73}$$

Note that if $\mathbf{M_{r-1}}$ is an $a \times a$ matrix, the rotation matrix $\mathbf{R_r}$ must also be an $a \times a$ matrix. A rotation matrix is fully defined by its size and by a parameter referred to as the pivot. The pivot is a set of coordinates and is defined as $\tau = (i, j)$. The pivot defines four elements inside the rotation matrix:

$$\begin{aligned}
\mathbf{R}_{i\,i} &= \cos\theta_r \\
\mathbf{R}_{i\,j} &= -\sin\theta_r \\
\mathbf{R}_{j\,j} &= \cos\theta_r \\
\mathbf{R}_{j\,i} &= \sin\theta_r
\end{aligned}$$

Here θ_r is referred to as the angle or rotation. All the other principal diagonal entries inside $\mathbf{R}$ are equal to one. All the other off-diagonal entries in $\mathbf{R}$ are equal to zero. The general $a \times a$ rotation matrix can therefore

be expressed as follows:

$$\mathbf{R} = \begin{array}{c|cccccccccccc} & 1 & 2 & \dots & i-1 & i & i+1 & \dots & j-1 & j & j+1 & \dots & a-1 & a \\ \hline 1 & 1 & & & & & & & & & & & & \\ 2 & & 1 & & & & & & & & & & & \\ \vdots & & & \ddots & & & & & & & & & & \\ i-1 & & & & 1 & & & & & & & & & \\ i & & & & & c_r & & & & -s_r & & & & \\ i+1 & & & & & & 1 & & & & & & & \\ \vdots & & & & & & & \ddots & & & & & & \\ j-1 & & & & & & & & 1 & & & & & \\ j & & & & & s_r & & & & c_r & & & & \\ j+1 & & & & & & & & & & 1 & & & \\ \vdots & & & & & & & & & & & \ddots & & \\ a-1 & & & & & & & & & & & & 1 & \\ a & & & & & & & & & & & & & 1 \end{array}$$

Here $c_r = \cos\theta_r$ and $s_r = \sin\theta_r$. The rotation formula in equation 5.73 will always produce a new coupling matrix that has the same size as the original matrix and is also associated with the same frequency response as the original matrix. It is thus possible to perform an arbitrarily long sequence of rotations in order to obtain a desired topology. The similarity transformation in equation 5.73 has the following important properties:

1. If the pivot of the rotation matrix is $\tau = (i, j)$, only elements in rows i and j and columns i and j are influenced by the rotation. These are the only elements in matrices $\mathbf{M_{r-1}}$ and $\mathbf{M}_r$ that can differ in value. We refer to these elements as the *affected region*.

2. If elements in the affected region are zero before the application of the transformation, they will remain zero after the transformation has occurred.

The following restrictions are imposed on the pivot:

$$i \in [2, a-1]$$
$$j \in [2, a-1]$$

These restrictions are imposed on the pivot to ensure that the termination nodes are excluded from the affected region. If the terminations nodes where to be included inside the affected region, similarity transformations could influence the transfer- and reflection coefficients of the network [63]. We shall clarify the concept of an affected region using an example. Suppose a 7×7 coupling matrix $\mathbf{M_0}$ is rotated through an angle θ_r at a pivot

$(3, 5)$. An illustration of the matrix is shown below. The affected region is shaded.

$\mathbf{M_0} =$

	1	2	3	4	5	6	7
1	x	x	x	x	x	x	x
2	x	x	x	x	x	x	x
3	x	x	x	x	x	x	x
4	x	x	x	x	x	x	x
5	x	x	x	x	x	x	x
6	x	x	x	x	x	x	x
7	x	x	x	x	x	x	x

Only elements in the affected region are influenced during the similarity transformation. We shall now provide formulas that describe how elements in the affected region change during the similarity transformation. The general relationship between the values in matrices $\mathbf{M_{r-1}}$ and $\mathbf{M_r}$ is as follows [61]:

$$\mathbf{M'}_{i\,k} = c_r\mathbf{M}_{i\,k} + s_r\mathbf{M}_{j\,k} \qquad \text{for the } k\text{-th element in row } i \tag{5.74}$$

$$\mathbf{M'}_{j\,k} = s_r\mathbf{M}_{i\,k} + c_r\mathbf{M}_{j\,k} \qquad \text{for the } k\text{-th element in row } j \tag{5.75}$$

$$\mathbf{M'}_{k\,i} = c_r\mathbf{M}_{k\,i} - s_r\mathbf{M}_{k\,j} \qquad \text{for the } k\text{-th element in column } i \tag{5.76}$$

$$\mathbf{M'}_{k\,j} = s_r\mathbf{M}_{k\,i} + c_r\mathbf{M}_{k\,j} \qquad \text{for the } k\text{-th element in column } j \tag{5.77}$$

Here the dashed matrix elements belong to $\mathbf{M_r}$ and the undashed elements belong to $\mathbf{M_{r-1}}$. Equations 5.74 through 5.77 are valid for elements that are not located on the cross-points of the pivot, i.e. $k \neq i, j$. For the elements located on the cross-points, the following equations are valid [61]:

$$\begin{aligned}
\mathbf{M'}_{i\,i} &= c_r^2\mathbf{M}_{i\,i} - 2s_rc_r\mathbf{M}_{i\,j} + s_r^2\mathbf{M}_{j\,j} \\
\mathbf{M'}_{j\,j} &= s_r^2\mathbf{M}_{i\,i} + 2s_rc_r\mathbf{M}_{i\,j} + c_r^2\mathbf{M}_{j\,j} \\
\mathbf{M'}_{i\,j} &= \mathbf{M}_{i\,j}(c_r^2 - s_r^2) + s_rc_r(\mathbf{M}_{i\,i} - \mathbf{M}_{j\,j})
\end{aligned} \tag{5.78}$$

Our goal is to use the matrix rotations to simplify circuit topologies. It is desirable to construct filters using a minimum number of cross-couplings. It is therefore beneficial to obtain formulas that can be used to annihilate specific unwanted couplings. Equations 5.74 through 5.78 can now be used to find expressions for the rotation angle required to force a specific element in $\mathbf{M_r}$ to become equal to zero. We shall next provide a listing of the formulas that describe how to annihilate a specific coupling inside a matrix. In each case the required rotation angle is provided on the left with a description of the target coupling on the right (the target coupling here meaning the coupling that must become equal to zero after the application of the rotation). Note that the target coupling is in each case defined in terms of the pivot. Formulas for the couplings located inside the affected region, but not on the cross-points of the pivot, are as follows [61]:

$$\theta_r = \arctan\left(\frac{\mathbf{M}_{i\,k}}{\mathbf{M}_{j\,k}}\right) \qquad \text{for the } k\text{-th element in row } i\ (\mathbf{M}_{i\,k}) \tag{5.79}$$

$$\theta_r = -\arctan\left(\frac{\mathbf{M}_{j\,k}}{\mathbf{M}_{i\,k}}\right) \qquad \text{for the } k\text{-th element in row } j\ (\mathbf{M}_{j\,k}) \tag{5.80}$$

$$\theta_r = \arctan\left(\frac{\mathbf{M}_{k\,i}}{\mathbf{M}_{k\,j}}\right) \qquad \text{for the } k\text{-th element in column } i\ (\mathbf{M}_{i\,k}) \tag{5.81}$$

$$\theta_r = -\arctan\left(\frac{\mathbf{M}_{k\,j}}{\mathbf{M}_{k\,i}}\right) \qquad \text{for the } k\text{-th element in column } j\ (\mathbf{M}_{k\,j}) \tag{5.82}$$

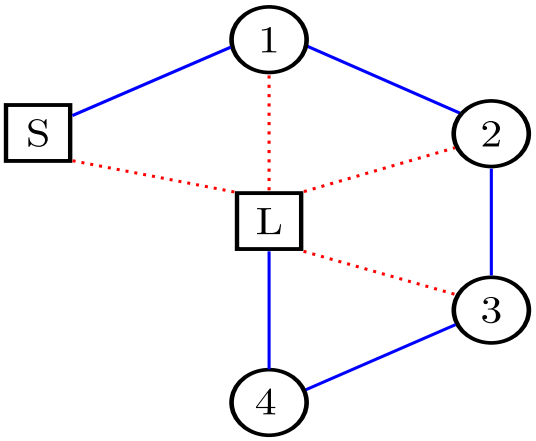

	S	1	2	3	4	L
S		×				×
1	×	×	×			×
2		×	×	×		×
3			×	×	×	×
4				×	×	×
L	×	×	×	×	×	

Figure 5.8: Left: Coupling diagram of a fourth order fully canonical circuit in the wheel/arrow topology. Right: The associated $N+2 \times N+2$ coupling matrix. The coupling diagram resembles a wheel and the coupling matrix resembles an arrow. Note that mainline couplings are indicated in blue. The cross-couplings are indicated in red. The spokes of the wheel are cross-couplings. These cross-couplings are responsible for the creation of finite frequency transmission zeros.

Formulas for the elements located on the cross-points of the pivot are as follows [61]:

$$\theta_r = \arctan\left(\frac{-\mathbf{M}_{i\,j} \pm \sqrt{\mathbf{M}_{i\,j}^2 - \mathbf{M}_{i\,i}\mathbf{M}_{j\,j}}}{\mathbf{M}_{j\,j}}\right) \quad \text{for the cross-pivot element } \mathbf{M}_{i\,i} \tag{5.83}$$

$$\theta_r = \arctan\left(\frac{\mathbf{M}_{i\,j} \pm \sqrt{\mathbf{M}_{i\,j}^2 - \mathbf{M}_{i\,i}\mathbf{M}_{j\,j}}}{\mathbf{M}_{i\,i}}\right) \quad \text{for the cross-pivot element } \mathbf{M}_{j\,j} \tag{5.84}$$

$$\theta_r = \frac{1}{2}\arctan\left(\frac{2\mathbf{M}_{i\,j}}{\mathbf{M}_{j\,j} - \mathbf{M}_{i\,i}}\right) \quad \text{for the cross-pivot element } \mathbf{M}_{j\,j} \tag{5.85}$$

In the next subsection we shall introduce the canonical filter topologies. Algorithms will then be provided that can be used to transform any coupling matrix into one of the canonical topologies using the presented similarity transformations.

5.7.2 Canonical forms

Bell defines a canonical filter topology as a topology that employs the minimum number of couplings to produce a specific frequency response [63]. There are three standard canonical topologies. They are the wheel/arrow form, the folded form and the transversal form. These filter topologies can accommodate the most general group of frequency responses – asymmetric frequency responses with a maximum of N finite frequency transmission zeros [61]. As a consequence, any coupling matrix can always be transformed into each of the different canonical topologies. The couplings that are present in the transformed topology depend on the filtering function. The number of cross-couplings in the network decreases as the number of finite frequency transmission zeros decreases. The canonical topologies can be used to realise microwave filters directly, or can be used as intermediary forms during the synthesis procedure. We shall now discuss the three canonical topologies and provide algorithms to obtain them.

Wheel/Arrow form

The wheel/arrow form was originally suggested by Bell [63]. A fourth order fully canonical circuit in the wheel topology is shown in figure 5.8. The figure contains both the coupling routing diagram and the $N+2 \times N+2$

coupling matrix. The filter in figure 5.8 accommodates four finite frequency transmission zeros. The coupling diagram resembles a wheel and the entries in the coupling matrix resemble an arrow. The mainline couplings are indicated using blue and the cross-couplings are indicated using red. Note that the main-diagonal entries are shown in black inside the coupling matrix and correspond to FIR elements. As mentioned in section 5.3.2, FIR elements in the prototype domain are mapped to resonators with frequency offsets in the actual frequency domain. The following properties characterise the prototype:

1. The only non-zero entries in the coupling matrix are located on the main diagonal, on the first two subdiagonals, in the last row and in the last column.

2. The load is coupled to the resonators $N, N-1, \ldots, m$. Here $m = N - n_{\text{fz}}$. The number of finite frequency transmission zeros therefore correspond to the number of resonators that are cross-coupled to the load. As a consequence the first $N - n_{\text{fz}}$ elements in the last row and the last column of the coupling matrix will be zero.

We shall now provide an algorithm to describe how an arbitrary coupling matrix can be transformed into the wheel topology. The algorithm is as follows:

Data: $\mathbf{M}_{\text{full}}$ is a generic $N+2 \times N+2$ coupling matrix with rows and columns numbering $1, 2, \ldots, N+2$.

Result: $\mathbf{M}_{\text{wheel}}$ is a $N+2 \times N+2$ coupling matrix where all the cross-couplings are located in the last row and the last column of the matrix.

$\mathbf{M} = \mathbf{M}_{\text{full}}$;
$row = 2$;
while $row \leq N$ **do**
  $column = row + 1$;
  while $column \leq N + 1$ **do**
    // Annihilate $\mathbf{M}_{row-1,row}$ using $\mathbf{M}_{row,column}$ as the;
    // pivot;
    $pivot\_x = row$;
    $pivot\_y = column$;
    $\theta_r = -\arctan\left(\frac{\mathbf{M}_{row-1,column}}{\mathbf{M}_{row-1,row}}\right)$;
    $\mathbf{R}_{\text{pivot\_x,pivot\_y}} = -sin(\theta_r)$;
    $\mathbf{R}_{\text{pivot\_x,pivot\_x}} = cos(\theta_r)$;
    $\mathbf{R}_{\text{pivot\_y,pivot\_y}} = cos(\theta_r)$;
    $\mathbf{R}_{\text{pivot\_y,pivot\_x}} = sin(\theta_r)$;
    $\mathbf{M} = \mathbf{R}\,\mathbf{M}\,\mathbf{R}^T$;
  end
  $row = row + 1$;
end
$\mathbf{M}_{\text{wheel}} = \mathbf{M}$;

Algorithm 1: The reduction of an arbitrary coupling matrix to the wheel topology.

We shall now illustrate the execution of algorithm 1 using an example.

Example: Asymmetric dual-band prototype

We shall use the result of example 2 in section 5.6.3 as our initial coupling matrix. The initial matrix is in the transversal form and is indicated as $\mathbf{M_0}$. Note that the algorithm can reduce a coupling matrix with any arbitrary topology to the wheel/arrow form. We shall now show the different iterations of algorithm 1 as it executes. In each case the affected region is shaded. The colour green is used to indicate the position of a pivot. Red is used to indicate the position of a target element. Due to symmetry there are two pivots and two target elements in each matrix. The target element is the element that is forced to assume the value of zero after the rotation. The initial matrix with the first pivots and target elements is as follows:

$\mathbf{M_0} =$

	S	1	2	3	4	L
S	0	−0.4572	0.3460	−0.2419	0.3845	0
1	−0.4572	1.1768	0	0	0	0.4572
2	0.3460	0	0.4322	0	0	0.3460
3	−0.2419	0	0	−0.6940	0	0.2419
4	0.3845	0	0	0	−1.1272	0.3845
L	0	0.4572	0.3460	0.2419	0.3845	0

The angle of rotation required to force $\mathbf{M}_{S\,2} = 0$ is calculated as $\theta_r = 0.6478$ rad using equation 5.82. The following matrix was obtained after the similarity transformation:

$\mathbf{M_1} =$

	S	1	2	3	4	L
S	0	−0.5733	0	−0.2419	0.3845	0
1	−0.5733	0.9056	0.3583	0	0	0.1557
2	0	0.3583	0.7034	0	0	0.5518
3	−0.2419	0	0	−0.6940	0	0.2419
4	0.3845	0	0	0	−1.1272	0.3845
L	0	0.1557	0.5518	0.2419	0.3845	0

The pivots in $\mathbf{M}_1$ are again indicated using green and the target elements are indicated using red. The angle of rotation required to force $\mathbf{M}_{S\,3} = 0$ is calculated as $\theta_r = -0.3993$ rad using equation 5.82. The following matrix was obtained after the similarity transformation:

$\mathbf{M_2} =$

	S	1	2	3	4	L
S	0	−0.6223	0	0	0.3845	0
1	−0.6223	0.6638	0.3301	−0.5730	0	0.2376
2	0	0.3301	0.7034	−0.1393	0	0.5518
3	0	−0.5730	−0.1393	−0.4522	0	0.1623
4	0.3845	0	0	0	−1.1272	0.3845
L	0	0.2376	0.5518	0.1623	0.3845	0

The pivots in $\mathbf{M}_2$ are again indicated using green and the target elements are indicated using red. The angle of rotation required to force $\mathbf{M}_{S\,4} = 0$ is calculated as $\theta_r = 0.5534$ rad using equation 5.82. The following matrix

was obtained after the similarity transformation:

$$\mathbf{M_3} = \begin{array}{c|cccccc} & S & 1 & 2 & 3 & 4 & L \\ \hline S & 0 & -0.7315 & 0 & 0 & 0 & 0 \\ 1 & -0.7315 & 0.1690 & 0.2808 & -0.4875 & 0.8008 & 0 \\ 2 & 0 & 0.2808 & 0.7034 & -0.1393 & 0.1735 & 0.5518 \\ 3 & 0 & -0.4875 & -0.1393 & -0.4522 & -0.3012 & 0.1623 \\ 4 & 0 & 0.8008 & 0.1735 & -0.3012 & -0.6323 & 0.4520 \\ L & 0 & 0 & 0.5518 & 0.1623 & 0.4520 & 0 \end{array}$$

The pivots in $\mathbf{M}_3$ are again indicated using green and the target elements are indicated using red. The angle of rotation required to force $\mathbf{M}_{1\,3} = 0$ is calculated as $\theta_r = 1.0482$ rad using equation 5.82. The following matrix was obtained after the similarity transformation:

$$\mathbf{M_4} = \begin{array}{c|cccccc} & S & 1 & 2 & 3 & 4 & L \\ \hline S & 0 & -0.7315 & 0 & 0 & 0 & 0 \\ 1 & -0.7315 & 0.1690 & 0.5626 & 0 & 0.8008 & 0 \\ 2 & 0 & 0.5626 & -0.0438 & 0.5697 & 0.3476 & 0.1347 \\ 3 & 0 & 0 & 0.5697 & 0.2949 & 0 & 0.5592 \\ 4 & 0 & 0.8008 & 0.3476 & 0 & -0.6323 & 0.4520 \\ L & 0 & 0 & 0.1347 & 0.5592 & 0.4520 & 0 \end{array}$$

The pivots in $\mathbf{M}_4$ are again indicated using green and the target elements are indicated using red. The angle of rotation required to force $\mathbf{M}_{1\,4} = 0$ is calculated as $\theta_r = -0.9584$ rad using equation 5.82. The following matrix was obtained after the similarity transformation:

$$\mathbf{M_5} = \begin{array}{c|cccccc} & S & 1 & 2 & 3 & 4 & L \\ \hline S & 0 & -0.7315 & 0 & 0 & 0 & 0 \\ 1 & -0.7315 & 0.1690 & 0.9787 & 0 & 0 & 0 \\ 2 & 0 & 0.9787 & -0.1109 & 0.3275 & -0.3947 & 0.4473 \\ 3 & 0 & 0 & 0.3275 & 0.2949 & -0.4662 & 0.5592 \\ 4 & 0 & 0 & -0.3947 & -0.4662 & -0.5652 & 0.1495 \\ L & 0 & 0 & 0.4473 & 0.5592 & 0.1495 & 0 \end{array}$$

The pivots in $\mathbf{M}_5$ are again indicated using green and the target elements are indicated using red. The angle of rotation required to force $\mathbf{M}_{2\,4} = 0$ is calculated as $\theta_r = 0.8782$ rad using equation 5.82. The following matrix was obtained after the similarity transformation:

$$\mathbf{M_6} = \begin{array}{c|cccccc} & S & 1 & 2 & 3 & 4 & L \\ \hline S & 0 & -0.7315 & 0 & 0 & 0 & 0 \\ 1 & -0.7315 & 0.1690 & 0.9787 & 0 & 0 & 0 \\ 2 & 0 & 0.9787 & -0.1109 & 0.5129 & 0 & 0.4473 \\ 3 & 0 & 0 & 0.5129 & 0.2436 & 0.5088 & 0.2419 \\ 4 & 0 & 0 & 0 & 0.5088 & -0.5139 & 0.5258 \\ L & 0 & 0 & 0.4473 & 0.2419 & 0.5258 & 0 \end{array}$$

The algorithm now terminates as $\mathbf{M_6}$ is in the wheel/arrow form. We shall now introduce the folded canonical form and also provide an algorithm to transform any arbitrary coupling matrix into this form.

Folded form

We now introduce the folded canonical form. The coupling routing diagram and the $N+2 \times N+2$ coupling matrix of a fourth order fully canonical filter in the folded topology is shown in figure 5.9. The mainline couplings are indicated using blue and the cross-couplings are indicated using red. A coupling matrix is synthesised from the characteristic polynomials and therefore exists in a normalised domain (a coupling matrix represents a prototype circuit). The main diagonal entries of the coupling matrix represent FIR elements in the prototype frequency domain. As mentioned in section 5.3.2, FIR elements in the prototype domain are mapped to resonators with frequency offsets in the actual frequency domain. Cohn illustrated as early as 1957 that the lowpass ladder networks derived from Chebyshev polynomials can be realised as a set of cascaded synchronously tuned resonators. This topology is referred to as the inline topology. These filters have all their transmission zeros located at infinity and therefore do not require cross-coupling between resonators. The folded topology is an adaptation of the inline topology and was developed to introduce cross-coupling between non-sequential resonators to accommodate finite frequency transmission zeros. This topology has found many applications in the communications industry over the last couple of decades [61]. Algorithm 2 provides a description of the sequence of matrix rotations required to transform the topology of an arbitrary coupling matrix into the folded form. The sequence involves alternately annihilating elements left to right in the rows and top to bottom in the columns. The elements in the rows are annihilated using equation 5.82 and the elements in the columns are annihilated using equation 5.79. Note that the pivot is continuously positioned in such a manner that annihilated couplings cannot be reintroduced by later rotations. The algorithm takes advantage of the property that elements inside the affected region that are initially zero would remain zero after a rotation has been applied. We shall now clarify algorithm 2 by providing an example of its execution in the next subsection.

Example: Symmetric dual-band prototype

We shall use the result of example 1 in section 5.6.3 as our initial coupling matrix. The initial matrix is in the transversal form and is indicated as $\mathbf{M_0}$. Note that the algorithm can reduce a coupling matrix with any arbitrary topology to the folded form. We shall now show the different iterations of algorithm 2 as it executes. In each case the affected region is shaded. The colour green is used to indicate the position of a pivot. Red is used to indicate the position of a target element. Due to symmetry there are two pivots and two target elements in each matrix. The target element is the element that is forced to assume the value of zero after the rotation. The initial matrix with the first pivots and target elements is as follows:

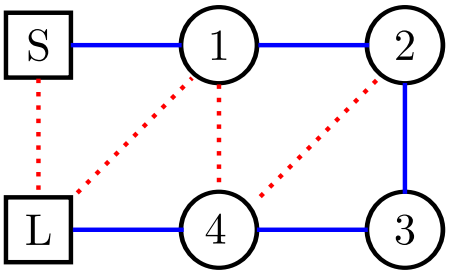

	S	1	2	3	4	L
S		×				×
1	×	×	×		×	×
2		×	×	×	×	
3			×	×	×	
4		×	×	×	×	×
L	×	×			×	

Figure 5.9: Left: Coupling diagram of a fourth order fully canonical circuit in the folded topology. Right: The associated $N+2 \times N+2$ coupling matrix. Note that mainline couplings are indicated in blue. The cross-couplings are indicated in red. The cross-couplings are responsible for the creation of finite frequency transmission zeros.

Annihilate elements in horizontal direction ←

$\mathbf{M_0} =$

	S	1	2	3	4	5	6	7	8	L
S	0	0.184	−0.266	0.278	−0.214	0.214	−0.278	0.266	−0.184	0
1	0.184	1.067	0	0	0	0	0	0	0	0.184
2	−0.266	0	0.971	0	0	0	0	0	0	0.266
3	0.278	0	0	0.731	0	0	0	0	0	0.278
4	−0.214	0	0	0	0.518	0	0	0	0	0.214
5	0.214	0	0	0	0	−0.518	0	0	0	0.214
6	−0.278	0	0	0	0	0	−0.731	0	0	0.278
7	0.266	0	0	0	0	0	0	−0.971	0	0.266
8	−0.184	0	0	0	0	0	0	0	−1.067	0.184
L	0	0.184	0.266	0.278	0.214	0.214	0.278	0.266	0.1840	0

We do not show matrices $\mathbf{M_1}$ through $\mathbf{M_6}$. We do however show the direction of the annihilation sequence. First $\mathbf{M}_{S\,8}$ is annihilated, then $\mathbf{M}_{S\,7}$, then $\mathbf{M}_{S\,6}$ etc. In each case the pivot is moved up along the first subdiagonal and equation 5.82 is used to find the required angle of rotation. When the first annihilation cycle is complete, we obtain $\mathbf{M_7}$ as follows:

$\mathbf{M_7} =$

	S	1	2	3	4	5	6	7	8	L
S	0	0.674	0	0	0	0	0	0	0	0
1	0.674	0	0.302	−0.456	0.480	−0.385	0.105	−0.085	0.022	0
2	0	0.302	0.982	0.129	−0.136	0.109	−0.030	0.024	−0.006	0.191
3	0	−0.456	0.129	0.758	0.224	−0.180	0.049	−0.040	0.010	0.268
4	0	0.480	−0.136	0.224	0.440	0.233	−0.063	0.051	−0.013	0.281
5	0	−0.385	0.109	−0.180	0.233	0.294	0.0610	−0.049	0.012	0.200
6	0	0.105	−0.030	0.049	−0.063	0.061	−0.592	0.060	−0.015	0.234
7	0	−0.085	0.024	−0.040	0.051	−0.049	0.060	−0.846	0.029	0.285
8	0	0.022	−0.006	0.010	−0.013	0.012	−0.015	0.029	−1.036	0.302
L	0	0	0.191	0.268	0.281	0.200	0.234	0.285	0.302	0

Annihilate elements in vertical direction ↓

We now annihilate elements in the last column. Again the direction of the annihilation sequence is shown. Equation 5.79 is used to calculate the required angle of rotation for each annihilation. After each rotation the pivot is shifted down along the first subdiagonal. We do not show matrices $\mathbf{M_8}$ through $\mathbf{M_{12}}$. After the completion of this annihilation cycle we obtain $\mathbf{M_{13}}$ as follows:

Annihilate elements in horizontal direction ←

$\mathbf{M_{13}} =$

	S	1	2	3	4	5	6	7	8	L
S	0	0.674	0	0	0	0	0	0	0	0
1	0.674	0	0.511	−0.492	0.418	−0.100	0.091	−0.024	0	0
2	0	0.511	0.784	0.279	−0.194	0.065	−0.031	0.024	0.024	0
3	0	−0.492	0.279	0.556	0.310	−0.004	0.109	0.031	0.091	0
4	0	0.418	−0.194	0.310	0.323	0.125	0.004	0.065	0.100	0
5	0	−0.100	0.065	−0.004	0.125	−0.323	0.310	0.194	0.418	0
6	0	0.091	−0.031	0.109	0.004	0.310	−0.556	0.279	0.492	0
7	0	−0.024	0.024	0.031	0.065	0.194	0.279	−0.784	0.511	0
8	0	0	0.024	0.091	0.100	0.418	0.492	0.511	0	0.674
L	0	0	0	0	0	0	0	0	0.674	0

The process now repeats itself. All the elements in the second row are now annihilated. After the cycle is complete we obtain $\mathbf{M_{18}}$ as follows:

$\mathbf{M_{18}} =$

	S	1	2	3	4	5	6	7	8	L
S	0	0.674	0	0	0	0	0	0	0	0
1	0.674	0	0.835	0	0	0	0	0	0	0
2	0	0.835	0	0.261	−0.164	0.197	−0.026	0.009	0	0
3	0	0	0.261	0.850	0.167	−0.142	0.043	0.013	0.030	0
4	0	0	−0.164	0.167	0.649	0.319	0.050	0.086	0.115	0
5	0	0	0.197	−0.142	0.319	−0.588	0.223	0.012	0.098	0
6	0	0	−0.026	0.043	0.050	0.223	−0.280	0.401	0.537	0
7	0	0	0.009	0.013	0.086	0.012	0.401	−0.631	0.620	0
8	0	0	0	0.030	0.115	0.098	0.537	0.620	0	0.674
L	0	0	0	0	0	0	0	0	0.674	0

Annihilate elements in vertical direction ↓

The elements in column 8 are now annihilated. After the cycle is complete we obtain $\mathbf{M_{22}}$ as follows:

Annihilate elements in horizontal direction ←

$\mathbf{M_{22}} =$

	S	1	2	3	4	5	6	7	8	L
S	0	0.674	0	0	0	0	0	0	0	0
1	0.674	0	0.835	0	0	0	0	0	0	0
2	0	0.835	0	0.295	−0.211	0.059	−0.013	0	0	0
3	0	0	0.295	0.754	0.293	0.003	0.029	0.013	0	0
4	0	0	−0.211	0.293	−0.316	0.616	−0.003	0.059	0	0
5	0	0	0.059	0.003	0.616	0.316	0.293	0.211	0	0
6	0	0	−0.013	0.029	−0.003	0.293	−0.754	0.295	0	0
7	0	0	0	0.013	0.059	0.211	0.295	0	0.835	0
8	0	0	0	0	0	0	0	0.835	0	0.674
L	0	0	0	0	0	0	0	0	0.674	0

The elements in the third row are now annihilated. After the cycle is complete we obtain $\mathbf{M_{25}}$ as follows:

$\mathbf{M_{25}} =$

	S	1	2	3	4	5	6	7	8	L
S	0	0.674	0	0	0	0	0	0	0	0
1	0.674	0	0.835	0	0	0	0	0	0	0
2	0	0.835	0	0.367	0	0	0	0	0	0
3	0	0	0.367	0	0.730	−0.170	0.029	0	0	0
4	0	0	0	0.730	0.153	0.358	0.009	0.022	0	0
5	0	0	0	−0.170	0.358	0.426	0.509	0.153	0	0
6	0	0	0	0.029	0.009	0.509	−0.579	0.333	0	0
7	0	0	0	0	0.022	0.153	0.333	0	0.835	0
8	0	0	0	0	0	0	0	0.835	0	0.674
L	0	0	0	0	0	0	0	0	0.674	0

Annihilate elements in vertical direction

The elements in column 7 are now annihilated. After the cycle is complete we obtain $\mathbf{M_{27}}$ as follows:

Annihilate elements in horizontal direction

$\mathbf{M_{27}} =$

	S	1	2	3	4	5	6	7	8	L
S	0	0.674	0	0	0	0	0	0	0	0
1	0.674	0	0.835	0	0	0	0	0	0	0
2	0	0.835	0	0.367	0	0	0	0	0	0
3	0	0	0.367	0	0.747	−0.070	0	0	0	0
4	0	0	0	0.747	0.058	0.303	0.070	0	0	0
5	0	0	0	−0.070	0.303	−0.058	0.747	0	0	0
6	0	0	0	0	0.070	0.747	0	0.367	0	0
7	0	0	0	0	0	0	0.367	0	0.835	0
8	0	0	0	0	0	0	0	0.835	0	0.674
L	0	0	0	0	0	0	0	0	0.674	0

Lastly $\mathbf{M}_{35}$ is annihilated to complete the procedure. The final $N+2 \times N+2$ coupling matrix in the folded form is as follows:

$\mathbf{M_{28}} =$

	S	1	2	3	4	5	6	7	8	L
S	0	0.674	0	0	0	0	0	0	0	0
1	0.674	0	0.835	0	0	0	0	0	0	0
2	0	0.835	0	0.367	0	0	0	0	0	0
3	0	0	0.367	0	0.750	0	0	0	0	0
4	0	0	0	0.750	0	0.309	0	0	0	0
5	0	0	0	0	0.309	0	0.750	0	0	0
6	0	0	0	0	0	0.750	0	0.367	0	0
7	0	0	0	0	0	0	0.367	0	0.835	0
8	0	0	0	0	0	0	0	0.835	0	0.674
L	0	0	0	0	0	0	0	0	0.674	0

(5.86)

We shall now illustrate the equivalence of the $N \times N$ and $N+2 \times N+2$ coupling matrix synthesis procedures. We shall illustrate the equivalence by transforming an equivalent $N \times N$ coupling matrix into the folded form using algorithm 2. The $N \times N$ coupling matrix in example 1 in section 5.5.3 was synthesised using exactly the

same characteristic polynomials as the $N+2\times N+2$ coupling matrix in example 1 in section 5.6.3. The $N\times N$ coupling matrix is as follows.

$$\mathbf{M_{N\times N,\,0}} = \begin{vmatrix} 0 & -0.3150 & -0.3150 & 0.3883 & 0.3883 & -0.3140 & -0.3140 & 0 \\ -0.3150 & -0.8814 & 0 & -0.2292 & 0 & 0.1853 & 0 & -0.3150 \\ -0.3150 & 0 & 0.8814 & 0 & 0.2292 & 0 & -0.1853 & 0.3150 \\ 0.3883 & -0.2292 & 0 & 0.5205 & 0 & 0.3645 & 0 & 0.3883 \\ 0.3883 & 0 & 0.2292 & 0 & -0.5205 & 0 & -0.3645 & -0.3883 \\ -0.3140 & 0.1853 & 0 & 0.3645 & 0 & 0.0521 & 0 & -0.3140 \\ -0.3140 & 0 & -0.1853 & 0 & -0.3645 & 0 & -0.0521 & 0.3140 \\ 0 & -0.3150 & 0.3150 & 0.3883 & -0.3883 & -0.3140 & 0.3140 & 0 \end{vmatrix}$$

After the application of algorithm 2 the $N\times N$ coupling matrix in the folded topology is as follows:

$$\mathbf{M_{N\times N,\,15}} = \begin{vmatrix} 0 & 0.835 & 0 & 0 & 0 & 0 & 0 & 0 \\ 0.835 & 0 & 0.367 & 0 & 0 & 0 & 0 & 0 \\ 0 & 0.367 & 0 & 0.750 & 0 & 0 & 0 & 0 \\ 0 & 0 & 0.750 & 0 & 0.309 & 0 & 0 & 0 \\ 0 & 0 & 0 & 0.309 & 0 & 0.750 & 0 & 0 \\ 0 & 0 & 0 & 0 & 0.750 & 0 & 0.367 & 0 \\ 0 & 0 & 0 & 0 & 0 & 0.367 & 0 & 0.835 \\ 0 & 0 & 0 & 0 & 0 & 0 & 0.835 & 0 \end{vmatrix} \tag{5.87}$$

The equivalence between the $N+2\times N+2$ and $N\times N$ synthesis procedures becomes apparent if one compares the results in equations 5.86 and 5.87. The only difference is that the $N+2\times N+2$ coupling matrix contains immittance inverters in the outside rows and columns to couple the source and the load to the first and last resonators respectively. The $N\times N$ synthesis procedure in section 5.5.3 employed ideal transformers to couple the source and the load to the first and last resonators. The input and output transformer windings are given in equations 5.61 and 5.62 respectively. The number of windings are numerically equal to the values of the inverters in the $N+2\times N+2$ prototype. The two synthesis techniques are therefore equivalent. It must be stated that the $N+2\times N+2$ technique is more versatile as it allows the source and load to be coupled to multiple resonators inside the network. In the next subsection we shall discuss the transversal topology.

Transversal form

The transversal topology was used as the basis prototype circuit for the synthesis of the $N+2\times N+2$ coupled resonator filter in section 5.6. The topology has thus already been introduced and we just list it in this section for the sake of completeness. The transversal topology can be obtained directly from the characteristic polynomials without the use of matrix rotations. The coupling routing diagram and the $N+2\times N+2$ coupling matrix of a fourth order fully canonical filter in the transversal topology is shown in figure 5.10. The following properties characterise the prototype:

1. Both the source and the load are coupled to every resonator inside the network.
2. For fully canonical networks there is a direct source-load coupling.
3. None of the resonators are coupled to each other.

This completes our investigation into the canonical topologies. In the next section we shall use our knowledge of the canonical topologies and the matrix rotations to design cascaded triplet filters.

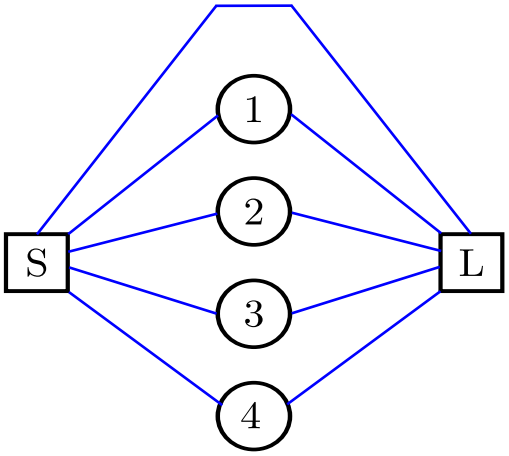

	S	1	2	3	4	L
S		×	×	×	×	×
1	×	×				×
2	×		×			×
3	×			×		×
4	×				×	×
L	×	×	×	×	×	

Figure 5.10: Left: Coupling diagram of a fourth order fully canonical circuit in the transversal topology. Right: The associated $N+2 \times N+2$ coupling matrix in the transversal topology. Note that all the resonant nodes are only coupled to the source and the load – there are no cross-couplings.

5.7.3 Cascaded triplet circuits

In this section we present a technique to design cascaded triplet filters. A triplet is a modular block inside a coupled resonator circuit that consists of three nodes. Each node inside a triplet is coupled to the other two nodes inside the group. A triplet is capable of producing a single finite frequency transmission zero. Not all the nodes inside a triplet are necessarily resonant nodes. The source and the load are also allowed to form part of a triplet [61]. An N-th order frequency response with n_{fz} finite frequency transmission zeros can be accommodated in a coupled resonator filter consisting of a cascade of n_{fz} triplets and a total of N resonant nodes. Each triplet is responsible for a single finite frequency transmission zero. Such a topology is illustrated in figure 5.11.

The synthesis of cascaded triplet circuits was originally performed using optimisation procedures. These procedures are incapable of associating a specific transmission zero with a specific triplet. Macchiarella was the first to present a fully analytical synthesis technique. His technique enables designers to associate specific transmission zeros with specific triplets. The theory presented in this section is based on Macchiarella's work [64]. Macchiarella developed an analytical technique to extract triplets from a coupling matrix that is in the wheel/arrow form. We shall present his technique in the next subsection. The presented theory shall then be used to define a general synthesis procedure for cascaded triplet circuits. We shall then conclude this section by illustrating the presented synthesis procedure using an example.

The extraction of triplets from the wheel/arrow topology

The coupling diagram of an N-th order $N+2 \times N+2$ coupled resonator circuit that is in the wheel form is shown in figure 5.12. This circuit has n_{fz} finite frequency transmission zeros. Resonators M through N are coupled to the load and the value of M is equal to $N - n_{\text{fz}}$. Suppose the coupling matrix $\mathbf{M_0}$, that is initially in the wheel topology, is rotated through an arbitrary angle θ_r to obtain $\mathbf{M_1}$. Macchiarella showed that if the pivot is defined as $\tau = (k, k+1)$, where $k \in [M+1, \ldots, N-1]$, all the generated non-zero couplings in $\mathbf{M_1}$ will be concentrated in the matrix in such a manner that for every coupling $|\text{rows} - \text{columns}| = 2$. This implies that all the generated couplings will be located on the main diagonal and on the first two subdiagonals. For the specific case where the pivot is defined as $\tau = (N-1, N)$, the only new coupling in $\mathbf{M_1}$ will be $(\mathbf{M_1})_{N-2,N}$ [64]. This new coupling is generated irrespective of the angle of rotation. Resonators $N, N-1$ and $N-2$ are

now connected to form a triplet. This triplet is shown figure 5.12 where $(\mathbf{M_1})_{N-2,N}$ is indicated with a solid red line. This triplet is however associated with an unknown finite frequency transmission zero. It is desirable to relate the angle of rotation required to generate a triplet with the value of the transmission zero produced by the triplet. Macchiarella and Cameron both showed that the value of the determinant of the self and mutual couplings of any triplet evaluated at $\Omega = \Omega_z$, the position of the transmission zero associated with the triplet, is zero [64, 61]. Mathematically, if a triplet is formed between resonators N, $N-1$ and $N-2$, the mentioned condition is expressed as follows:

$$\det \begin{vmatrix} (\mathbf{M_r})_{N-2,N-1} & (\mathbf{M_r})_{N-2,N} \\ \Omega_z + (\mathbf{M_r})_{N-1,N-1} & (\mathbf{M_r})_{N-1,N} \end{vmatrix} = 0 \tag{5.88}$$

Equation 5.88 can be used to relate the couplings inside a triplet with the position of the finite frequency transmission zero associated with the triplet. Equation 5.88 can be substituted into equations 5.74 through 5.77 in order to relate the angles of rotation of similarity transformations with the positions of finite frequency transmission zeros. Macchiarella and Cameron both used this principle to derive the following formula for the creation and repositioning of triplets [61, 64]:

$$\begin{aligned} \theta_{r-1,r} &= \arctan\left(\frac{(\mathbf{M_{r-1}})_{N-r,N+1-r}}{\Omega_z + (\mathbf{M_{r-1}})_{N+1-r,N+1-r}}\right) \\ \tau &= (N-r, N+1-r) \\ r &= 1, \ldots, N-1 \end{aligned} \tag{5.89}$$

Here $\theta_{r-1,r}$ is the angle or rotation that transforms a matrix $\mathbf{M_{r-1}}$ into a matrix $\mathbf{M_r}$. The pivot associated with the rotation is defined as τ. The finite frequency transmission zero associated with the generated triplet is indicated as Ω_z. If $r = 1$ when a similarity transformation is performed, the generated matrix $\mathbf{M_{r-1}}$ contains a triplet consisting of resonators N, $N-1$ and $N-2$. The generated triplet can be shifted up the main diagonal by systematically incrementing r and then performing additional similarity transformations. In each case the associated triplet consists of resonators $N-r$, $N+1-r$ and $N-1-r$. The process of shifting a triplet towards the source is illustrated in figure 5.12. We shall now define a general procedure for the synthesis of cascaded triplet circuits.

General procedure for the synthesis of cascaded triplet circuits

The design procedure for a cascaded triplet filter is as follows:

1. Generate expressions for the multi-band characteristic polynomials from the design specifications using the techniques presented in part I.

2. Synthesise a coupling matrix from the characteristic polynomials. Either the $N \times N$ or the $N+2 \times N+2$ coupling matrices can be used. The $N+2 \times N+2$ coupling matrix is however preferred as the source and load nodes can be included inside the triplets. The synthesis procedure for the $N \times N$ matrix is discussed in section 5.5. The synthesis procedure for the $N+2 \times N+2$ matrix is discussed in section 5.6.

3. Algorithm 1 must now be used to transform the obtained coupling matrix into a matrix with the wheel topology. The number of triplets that are contained inside the wheel is equal to the number of finite frequency transmission zeros.

4. It is now possible to construct a circuit with the topology illustrated in figure 5.11. Triplets must be extracted from the wheel and shifted towards the source until they are positioned correctly. Equation

5.89 defines the pivot and the required angle of rotation to extract a triplet from the wheel. The triplet is associated with a specific transmission zero. A rotation with $r = 1$ generates the initial triplet. The triplet can then be shifted towards the source by incrementing r and then performing additional rotations. This process must be performed for all the triplets inside the wheel.

We shall now illustrate the synthesis of a cascaded triplet filter using a design example. The example is included as it forms part of the practical design presented in chapter 9.

Example

Our example is the synthesis of a cascaded triplet filter from a set of characteristic polynomials. The characteristic polynomials describe a fourth order asymmetric dual-band frequency response where the passbands are separated by two finite frequency transmission zeros. The initial approximation problem was solved in section 3.7.1 using the frequency mapping technique. An $N+2 \times N+2$ coupled resonator circuit was then synthesised from the characteristic polynomials in section 5.6.3. The obtained circuit was in the folded topology. This matrix was then transformed into the wheel form in the example in section 5.7.2. The obtained coupling matrix will serve as our initial coupling matrix for the extraction of triplets. The initial matrix in the wheel form is as follows:

$$\mathbf{M_0} = \begin{array}{c|cccccc} & S & 1 & 2 & 3 & 4 & L \\ \hline S & 0 & -0.7315 & 0 & 0 & 0 & 0 \\ 1 & -0.7315 & 0.1690 & 0.9787 & 0 & 0 & 0 \\ 2 & 0 & 0.9787 & -0.1109 & 0.5129 & 0 & 0.4473 \\ 3 & 0 & 0 & 0.5129 & 0.2436 & 0.5088 & 0.2419 \\ 4 & 0 & 0 & 0 & 0.5088 & -0.5139 & 0.5258 \\ L & 0 & 0 & 0.4473 & 0.2419 & 0.5258 & 0 \end{array}$$

Our cascaded triplet circuit will consist of two triplets. We want the first triplet to consist of the source, resonator one and resonator two. We want the second triplet to consist of resonator three, resonator four and the load. It is only necessary to extract one triplet from the wheel and to then shift it towards the source. The remainder of the wheel will constitute the other triplet. We choose the transmission zero associated with the first triplet as $\Omega_z = 0.1752$. Our algorithm starts with $r = 1$. The initial pivot is thus $\tau = (N - r, N + 1 - r) = (3, 4)$. The area in $\mathbf{M_0}$ that is affected by a similarity transformation using this pivot is shaded. The colour green is used to indicate the position of a pivot. Due to symmetry there are two pivots in each matrix. Equation 5.89 is used to calculate the first angle of rotation as follows:

$$\begin{aligned} \theta_{r-1,r} = \theta_{0,1} &= \arctan\left(\frac{(\mathbf{M_0})_{3,4}}{0.1752 + (\mathbf{M_0})_{4,4}}\right) \\ &= \arctan\left(\frac{0.5088}{0.1752 - 0.5139}\right) \\ &= -0.9835 \end{aligned}$$

After the application of the similarity transformation defined in equation 5.73 we obtain $\mathbf{M_1}$ as follows:

$$\mathbf{M_1} = \begin{array}{c|cccccc} & S & 1 & 2 & 3 & 4 & L \\ \hline S & 0 & -0.7315 & 0 & 0 & 0 & 0 \\ 1 & -0.7315 & 0.1690 & 0.9787 & 0 & 0 & 0 \\ 2 & 0 & 0.9787 & -0.1109 & 0.2842 & -0.4269 & 0.4473 \\ 3 & 0 & 0 & 0.2842 & 0.1881 & -0.5458 & 0.5718 \\ 4 & 0 & 0 & -0.4269 & -0.5458 & -0.4584 & 0.0900 \\ L & 0 & 0 & 0.4473 & 0.5718 & 0.0900 & 0 \end{array}$$

This process is illustrated in figure 5.13 a and b using coupling diagrams. We now increment r. The new pivot is $\tau = (N - r, N + 1 - r) = (2, 3)$. The affected area inside $\mathbf{M_1}$ is shaded. The new angle of rotation is

$$\begin{aligned} \theta_{r-1,r} = \theta_{1,2} &= \arctan\left(\frac{(\mathbf{M_1})_{2,3}}{0.1752 + (\mathbf{M_1})_{3,3}}\right) \\ &= \arctan\left(\frac{0.2842}{0.1752 + 0.1881}\right) \\ &= 0.6638 \end{aligned}$$

After the application of the similarity transformation defined in equation 5.73 we obtain $\mathbf{M_2}$ as follows:

$$\mathbf{M_2} = \begin{array}{c|cccccc} & S & 1 & 2 & 3 & 4 & L \\ \hline S & 0 & -0.7315 & 0 & 0 & 0 & 0 \\ 1 & -0.7315 & 0.1690 & 0.7709 & 0.6030 & 0 & 0 \\ 2 & 0 & 0.7709 & -0.2732 & -0.0767 & 0 & 0 \\ 3 & 0 & 0.6030 & -0.0767 & 0.3504 & -0.6929 & 0.7259 \\ 4 & 0 & 0 & 0 & -0.6929 & -0.4584 & 0.0900 \\ L & 0 & 0 & 0 & 0.7259 & 0.0900 & 0 \end{array}$$

This process is illustrated in figure 5.13 b and c using coupling diagrams. We again increment r. The new value for r is 2. The new pivot is $\tau = (N - r, N + 1 - r) = (1, 2)$. The new angle of rotation is

$$\begin{aligned} \theta_{r-1,r} = \theta_{2,3} &= \arctan\left(\frac{(\mathbf{M_2})_{1,2}}{0.1752 + (\mathbf{M_1})_{2,2}}\right) \\ &= \arctan\left(\frac{0.7709}{0.1752 - 0.2732}\right) \\ &= -1.444 \end{aligned}$$

Why apply the similarity transformation defined in equation 5.73 to obtain $\mathbf{M_3}$ as follows:

$$\mathbf{M_3} = \begin{array}{c|cccccc} & S & 1 & 2 & 3 & 4 & L \\ \hline S & 0 & -0.0923 & 0.7256 & 0 & 0 & 0 \\ 1 & -0.0923 & -0.0733 & -0.8017 & 0 & 0 & 0 \\ 2 & 0.7256 & -0.8017 & -0.0310 & -0.6078 & 0 & 0 \\ 3 & 0 & 0 & -0.6078 & 0.3504 & -0.6929 & 0.7259 \\ 4 & 0 & 0 & 0 & -0.6929 & -0.4584 & 0.0900 \\ L & 0 & 0 & 0 & 0.7259 & 0.0900 & 0 \end{array}$$

The triplet associated with the transmission zero $\Omega_z = 0.1752$ now consists of the source, resonator 1 and resonator 2. The remainder of the wheel is already a triplet consisting of the load, resonator 3 and resonator 4.

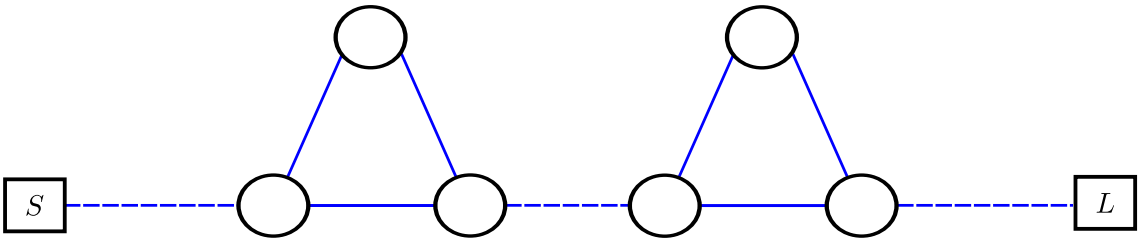

Figure 5.11: The general coupling routing diagram of a cascaded triplet circuit is shown above. Each triplet produces a single finite frequency transmission zero.

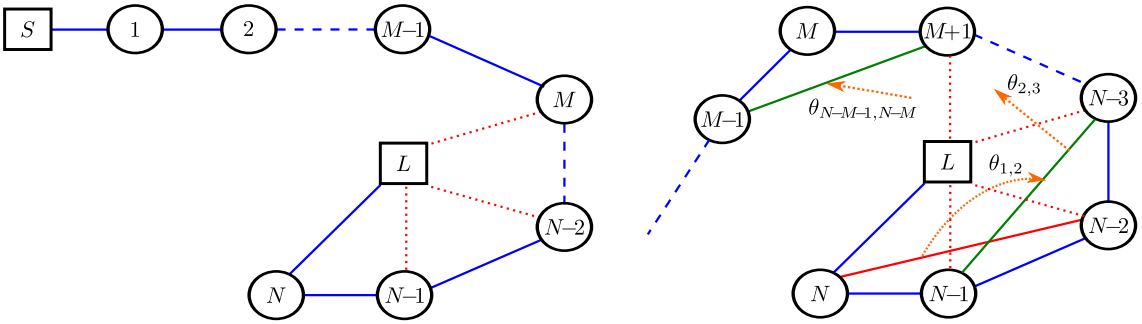

Figure 5.12: Left: The coupling diagram of an N-th order $N+2\times N+2$ coupled resonator circuit in the wheel form is shown. Resonators M through N are coupled to the load and form the spokes of the wheel. M is defined as $M=N-n_{\text{fz}}$ where n_{fz} is the number of finite frequency transmission zeros. Right: The process of extracting a triplet, associated with a specific transmission zero, from the wheel portion of the coupling diagram is shown. The triplet is initially created and then systematically shifted towards the source. This is achieved using the similarity transformation defined in equation 5.73 and the angle of rotation and pivot defined in equation 5.89.

This triplet is associated with the final transmission zero $\Omega_z = 0.3725$. The last transformation is illustrated in figure 5.13 c, d and e using coupling diagrams. In $\mathbf{M_3}$ the orange couplings constitute the first triplet and the pink couplings constitute the second triplet. The matrix $\mathbf{M_3}$ is thus the final coupling matrix. The frequency response associated with this circuit is shown in figure 5.13 f. In the next section we provide a summary of this chapter.

5.8 Summary

This chapter considered the synthesis of coupled resonator circuits from the characteristic polynomials. We started the chapter by introducing the basic concept of synthesis. We showed how the characteristic polynomials can be transformed into admittance parameters that could be used to synthesise circuits. These circuits would then produce the desired frequency response. We next considered the dilemma of accommodating asymmetric frequency responses in filter design. The FIR element was introduced to solve this problem. We also considered the conditions that must be imposed on the characteristic polynomials to ensure that they can be synthesised as an electrical circuit. We realised that any frequency response that can be approximated by the characteristic polynomials can be synthesised as prototype circuits. We next introduced synthesis techniques for two types of coupled resonator circuits. We started with the traditional $N\times N$ coupled resonator circuit and then introduced the more modern $N+2\times N+2$ coupled resonator circuit. These circuits are fully described using coupling matrices. We illustrated using examples that both techniques can produce equivalent results. The $N+2\times N+2$ coupled resonator circuit is however more flexible as it allows the source, the load and any other resonant node to be coupled. This enables the $N+2\times N+2$ coupled resonator circuit to accommodate

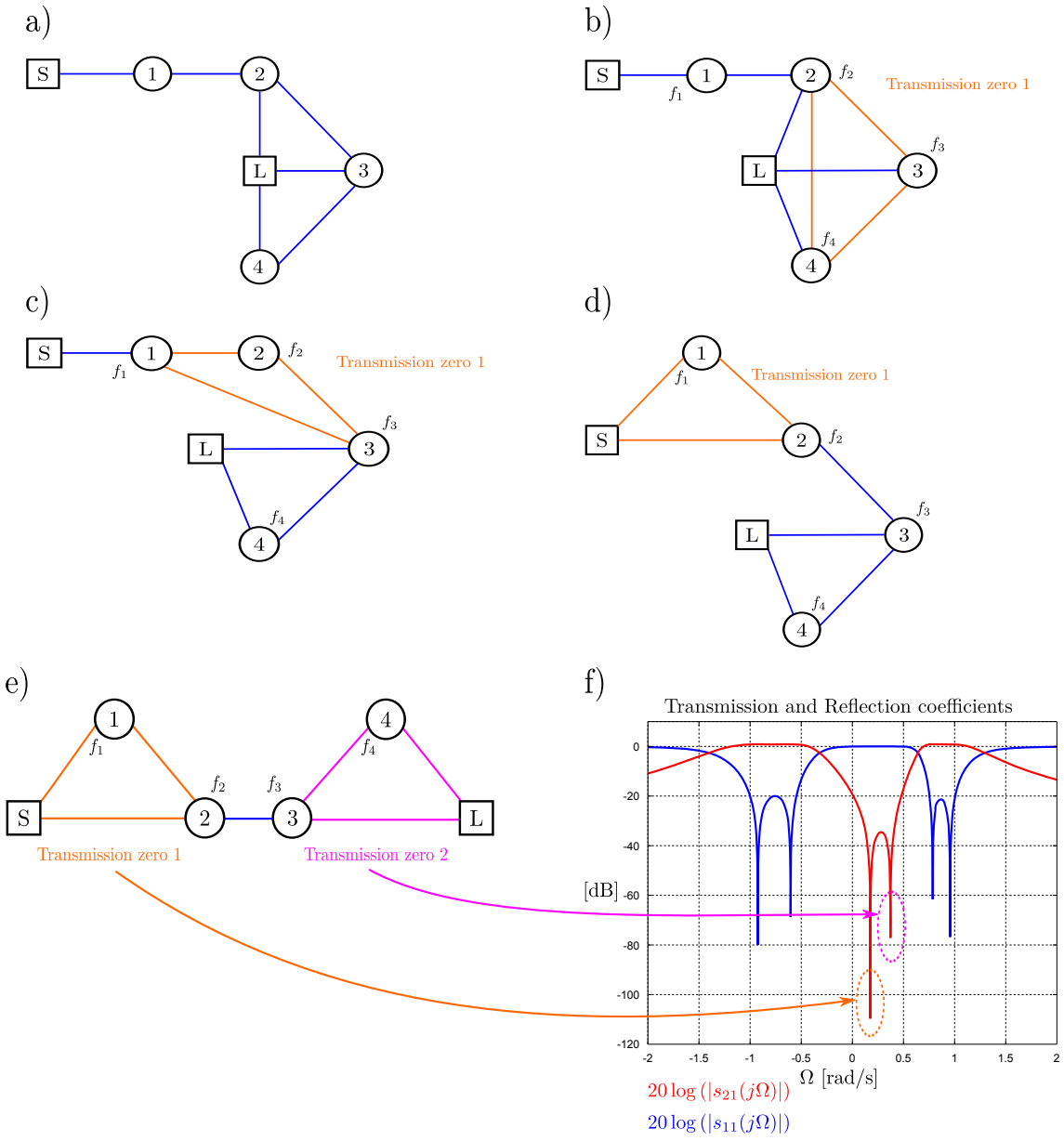

Figure 5.13: A graphical representation of the synthesis of a circuit with the cascaded triplet topology is shown above. Coupling diagrams are used to illustrate the effects of the similarity transformations. Circles are resonant nodes and squares are non-resonant nodes. The presence of a FIR element is indicated by including a f_i symbol next to the resonant node. a) The initial circuit in the wheel topology. b) The application of equation 5.89 results in a triplet being separated from the wheel. c) The triplet is shifted one position towards the source through a subsequent similarity transformation. d) The triplet is shifted onto the source through a final similarity transformation. e) The remainder of the wheel forms the second triplet. The synthesis procedure is now complete. f) The frequency response of the prototype circuit is shown. Note that each transmission zero is associated with a specific triplet.

fully canonical frequency responses. We then introduced the concept of using similarity transformations to simplify filter topologies. We introduced the three standard canonical topologies that can accommodate any frequency response and we provided algorithms to transform any coupling matrix into any one of these forms. We then used the canonical forms and the similarity transformations to define a general design technique for cascaded triplet filters. A triplet is an arrangement of three intercoupled nodes inside a coupled resonator circuit. A triplet can produce a single finite frequency transmission zero. In a cascaded triplet filter specific finite frequency transmission zeros are associated with specific triplets. Throughout the chapter we provided examples to clarify the theoretical work.

We are now capable of obtaining the multi-band characteristic polynomials from user specifications using the techniques presented in part I. In this chapter we illustrated how the characteristic polynomials can be used to synthesise circuits. Multi-band circuits that are directly synthesised from the characteristic polynomials using coupling matrices tend to have complex topologies that are generally unsuitable to be implemented as practical coupled resonator circuits.

Fortunately the similarity transformations presented in section 5.7 can be used to simplify the circuits to obtain more desirable topologies. That being said, there is an alternative synthesis procedure that circumvents the use of multi-band characteristic polynomials. In the next chapter we present one of the original contributions, the synthesis of multi-band circuits using reactance transformations. The synthesis procedure employs rational mapping functions to obtain frequency transformation subcircuits. Frequency-dependent elements in single-band prototype circuits can then be substituted with the frequency transformation subcircuits to obtain multi-band prototype filters. We shall discuss this synthesis procedure in detail in the following chapter.

Data: $\mathbf{M}_{\text{full}}$ is a generic $N+2 \times N+2$ coupling matrix with rows and columns numbering $1, 2, \ldots, N+2$.

Result: $\mathbf{M}_{\text{folded}}$ is a $N+2 \times N+2$ coupling matrix arranged in the folded topology.

$\mathbf{M} = \mathbf{M}_{\text{full}}$;
$lim\_column = 3$;
$lim\_row = N - 2$;
$ref\_x = 1$;
$ref\_y = N$;
// Annihilate unwanted row;
while $ref\_x \leq floor\left(\frac{N}{2}\right) - 1$ **do**
  $elim\_x = ref\_x$;
  $elim\_y = ref\_y - 1$;
  $pivot\_x = ref\_y - 2$;
  $pivot\_y = ref\_y - 1$;
  while $elim\_y \geq lim\_column$ **do**
    $\theta_r = -\arctan\left(\frac{\mathbf{M}_{elim\_x,\, elim\_y}}{\mathbf{M}_{elim\_x, elim\_y-1}}\right)$;
    $\mathbf{R}_{\text{pivot\_x, pivot\_y}} = -sin(\theta_r)$;
    $\mathbf{R}_{\text{pivot\_x, pivot\_x}} = cos(\theta_r)$;
    $\mathbf{R}_{\text{pivot\_y, pivot\_y}} = cos(\theta_r)$;
    $\mathbf{R}_{\text{pivot\_y, pivot\_x}} = sin(\theta_r)$;
    $\mathbf{M} = \mathbf{R}\,\mathbf{M}\,\mathbf{R}^T$;
    $elim\_y = elim\_y - 1$;
    if $elim\_y \geq lim\_columns$ **then**
      $pivot\_x = pivot\_x - 1$;
      $pivot\_y = pivot\_y - 1$;
    end
  end
  // Annihilate unwanted column;
  $elim\_x = ref\_x + 2$;
  $elim\_y = ref\_y$;
  $pivot\_x = pivot\_x + 1$;
  $pivot\_y = pivot\_y + 1$;
  while $elim\_x \leq lim\_row$ **do**
    $\theta_r = \arctan\left(\frac{\mathbf{M}_{elim\_x,\, elim\_y}}{\mathbf{M}_{elim\_x+1, elim\_y}}\right)$;
    $\mathbf{R}_{\text{pivot\_x, pivot\_y}} = -sin(\theta_r)$;
    $\mathbf{R}_{\text{pivot\_x, pivot\_x}} = cos(\theta_r)$;
    $\mathbf{R}_{\text{pivot\_y, pivot\_y}} = cos(\theta_r)$;
    $\mathbf{R}_{\text{pivot\_y, pivot\_x}} = sin(\theta_r)$;
    $\mathbf{M} = \mathbf{R}\,\mathbf{M}\,\mathbf{R}^T$;
    $elim\_x = elim\_x + 1$;
    if $elim\_x \leq lim\_row$ **then**
      $pivot\_x = pivot\_x + 1$;
      $pivot\_y = pivot\_y + 1$;
    end
  end
  $ref\_x = ref\_x + 1$;
  $ref\_y = ref\_y - 1$;
  $lim\_row = lim\_row - 1$;
  $lim\_column = lim\_column + 1$;
end
$\mathbf{M}_{\text{folded}} = \mathbf{M}$;

Algorithm 2: The reduction of an arbitrary coupling matrix to the folded topology.

Chapter 6

Synthesis of multi-band filters through reactance transformations

This chapter concerns the synthesis of multi-band filters using reactance transformations. Multi-band filters are constructed from single-band prototype filters by replacing each frequency-dependent element in the prototype circuit with a frequency transformation subcircuit. The frequency transformation subcircuits are essentially scaled impedance or admittance one-port circuits, that are obtained by synthesising rational mapping functions as one-port impedances or admittances. The rational mapping functions are obtained using the theory presented in chapter 4. We shall again consider the design of narrowband filters, and that of general filters, as separate cases. For the narrowband case we present a synthesis method that can be used to design coupled resonator filters. For the general mapping function case we present a method that can be used for the design of multi-band filters in general.

6.1 Synthesis of narrowband multi-band filters using rational mapping functions

In this section we consider the synthesis of narrowband multi-band filters from rational mapping functions. The filters are narrowband because the frequency transformation subcircuits referred to in this section contain frequency-invariant reactive elements that can only be approximated over narrow bandwidths. We therefore specifically consider the design of coupled resonator filters.

6.1.1 Synthesis of a frequency transformation subcircuit

The frequency transformation subcircuit is obtained by synthesising a rational mapping function as a one-port impedance or admittance network. There are numerous classical techniques available in the literature to synthesise the required transformation subcircuit from the reactance/susceptance function, with two of the simplest forms being the Cauer I and II topologies [62]. The rational mapping function considered in this section is that shown in equation 4.1. For a network containing frequency-invariant reactances, a modified Cauer I expansion is shown in equation 6.1, with the circuit form in figure 6.1.

$$\begin{aligned} S' &= j\Omega' \\ &= j\Omega'(\Omega) \\ &= j\Omega k_1 + jh_1 + \frac{1}{j\Omega k_2 + jh_2 + \frac{1}{j\Omega k_3 + jh_3 + \frac{1}{\cdots}}} \end{aligned} \tag{6.1}$$

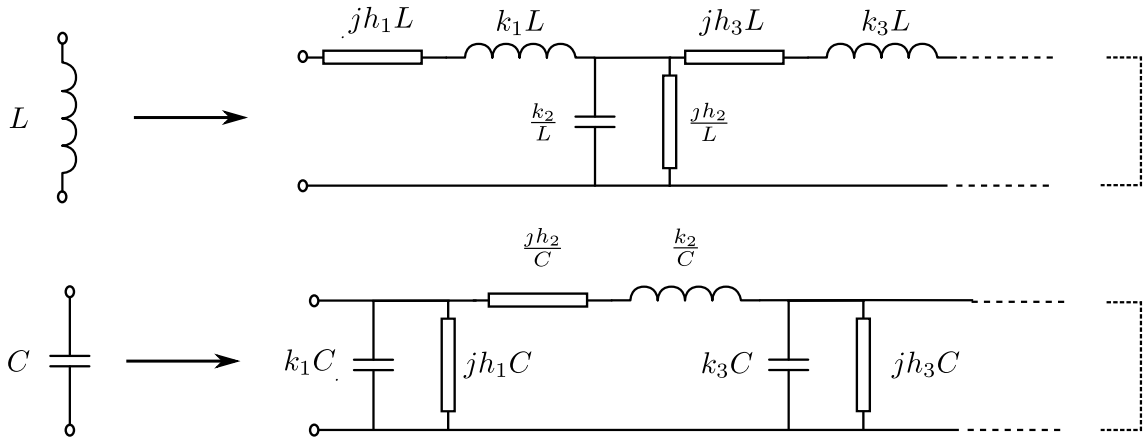

Figure 6.1: Modified Cauer I forms of the narrowband rational mapping functions introduced in section 4.3. The circuits can be used to transform single-band prototype filters into narrowband multi-band filters.

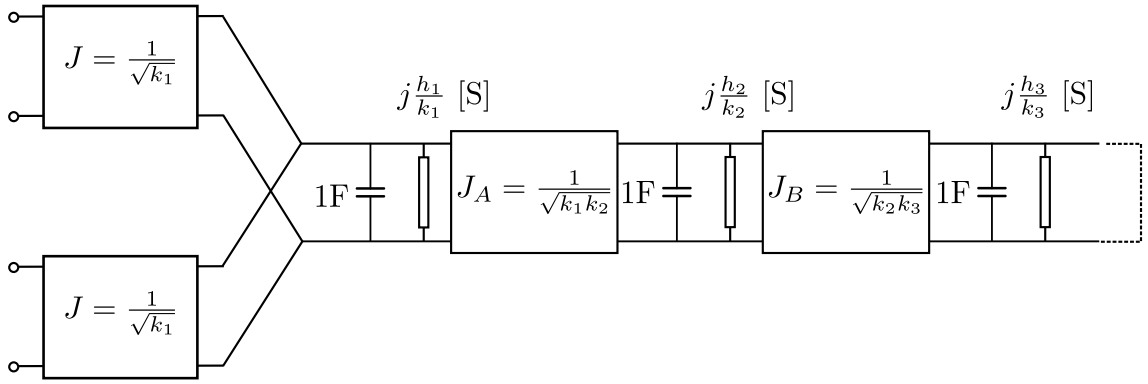

Figure 6.2: The circuits in figure 6.1 were transformed into a coupled reactance low-pass structure with equal shunt capacitance coupled by admittance inverters.

We refer to the k and h variables defined above as the frequency transformation parameters. Next we shall illustrate how to use the circuits in figure 6.1 to design coupled resonator filters.

6.1.2 Obtaining a multi-band prototype circuit

The modified Cauer I expansions in figure 6.1 can be transformed to a coupled reactance low-pass structure with equal shunt capacitance or series inductance values coupled by J or K inverters respectively. The transformation is illustrated in figure 6.3 (b) for the admittance version of the circuit for a three-band filter and the final circuit with element values is shown in figure 6.2. Note that the frequency-invariant reactance/susceptance values are also transformed using the same inverter constants. All of the inverters and frequency-invariant reactances are defined in terms of the frequency transformation parameters. Single-band prototype circuits can generally be transformed into circuits consisting of a source, a load and multiple reactances/susceptances that are coupled by impedance/admittance inverters. Such a transformation is illustrated in figure 6.3 (a) for a third-order all-pole single-band prototype. A single-band prototype circuit can be transformed into a multi-band prototype circuit by substituting all of the susceptances in the single-band circuit with the frequency transformation subcircuit provided in figure 6.2 [1]. This procedure is graphically illustrated in figure 6.3 for a three-band filter where a single-band prototype in (a), is transformed into a multi-band prototype in (c), by

[1] Due to duality similar solutions exist for impedance networks.

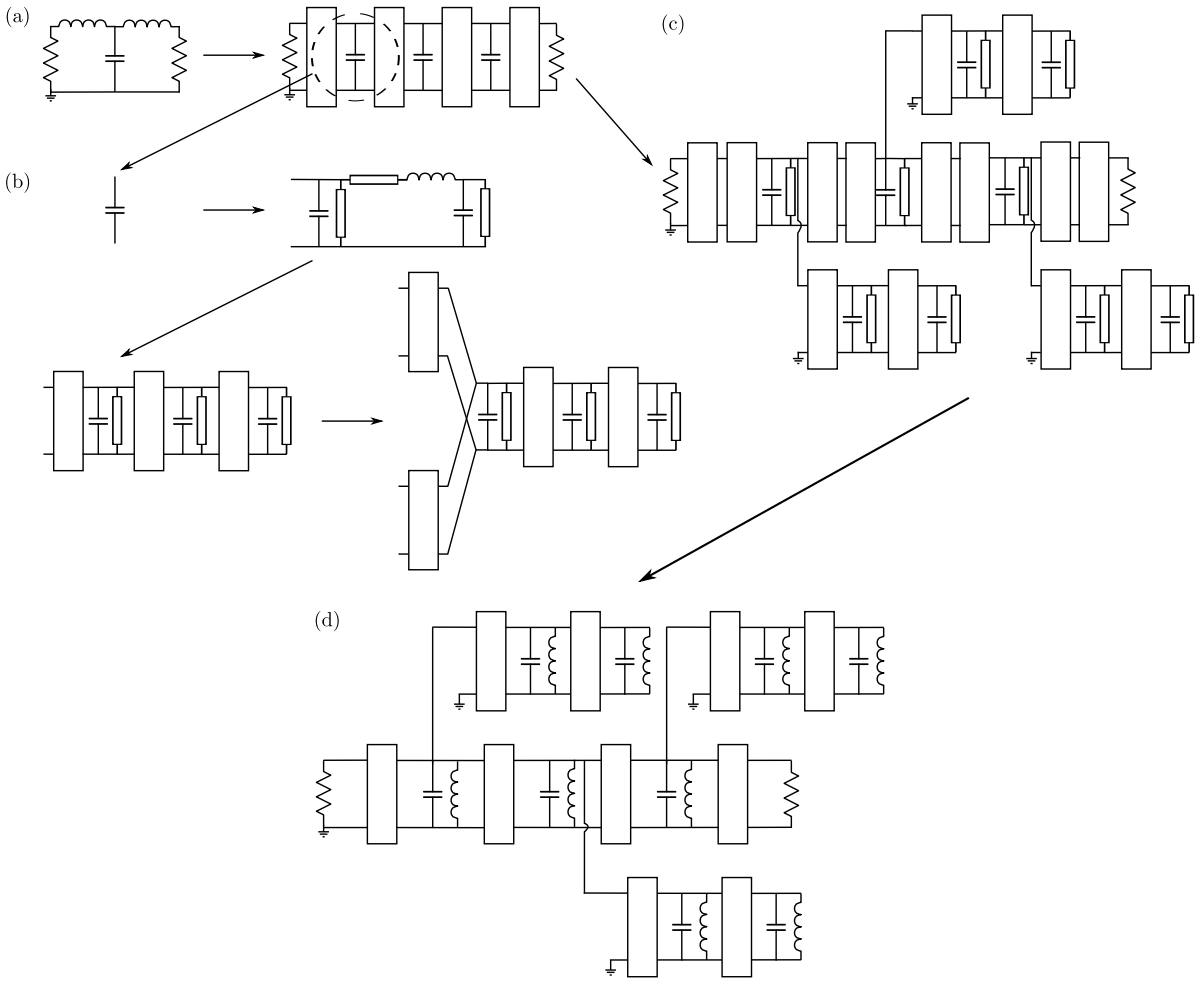

Figure 6.3: The design of a three-band narrowband filter using a rational mapping function is graphically illustrated above. The single-band prototype base filter, a third-order all-pole filter, is transformed into a coupled susceptance structure as shown in (a). Frequency dependent elements in the single-band prototype in (a), are substituted with the frequency transformation subcircuit in (b), to obtain the multi-band prototype in (c). The multi-band prototype is denormalised using the expressions provided in equation 6.2 and figure 6.4 to obtain the final filter in (d).

substituting all of the frequency-dependent elements in the single-band circuit with the frequency transformation subcircuits shown in (b).

6.1.3 Denormalisation to obtain a multi-band filter

From the theory presented in section 4.3.1 it should be clear that the multi-band prototype circuits discussed in this section need to be denormalised using equation 3.3 in order to obtain a final filter circuit. From the theory presented in section 5.3.2, equations 5.21 and 5.22 can be used for this purpose. When a normal reactance and a frequency-invariant reactance are denormalised from the prototype frequency domain to the actual frequency domain using the lowpass-to-bandpass transformation, a resonator and a frequency invariant reactance are obtained. The effect of the frequency invariant reactance can be compensated for by adjusting the centre frequency of the resonator. A new equivalent resonator is thus created, with the same resonance frequency as the resonator-reactance combination and the same Z_0 as the original resonator. Formulas that relate the combination of a frequency variant and a frequency-invariant reactance in the prototype domain, to equivalent resonators in the actual frequency domain, are summarised in figure 6.4. The coupling values of the inverters

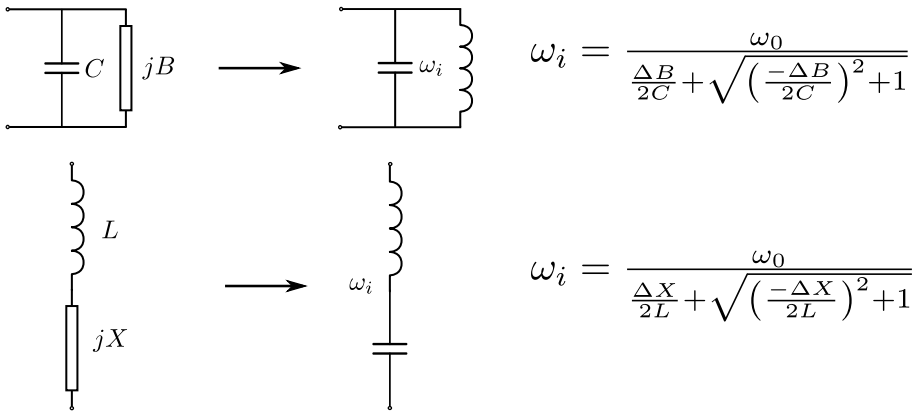

Figure 6.4: Prototype circuit elements and their equivalent resonators are shown above.

in the actual frequency domain are defined as follows:

$$\begin{array}{lll} \text{Original single-band couplings:} & J_{ij} = \frac{M_{ij}\Delta\sqrt{b_i b_j}}{k_1} & i,j \in \text{Single-band prototype} \\ \text{Branch couplings:} & J_x = J_X\Delta\sqrt{b_x b_{x+1}} & x \in \{a,b,c\ldots\} \\ \text{Input:} & J_{S1} = \sqrt{\frac{\Delta b_1 G_S}{k_1}}M_{S1} & \\ \text{Output:} & J_{LN} = \sqrt{\frac{\Delta b_N G_L}{k_1}}M_{LN} & \end{array} \tag{6.2}$$

Here M_{S1}, M_{LN} and M_{ij} are elements in the coupling matrix of an N-th order single-band prototype circuit. M_{S1} and M_{LN} are the input and output couplings respectively and M_{ij} refer to the coupling between resonators i and j. Δ is the fractional bandwidth and is defined in equation 3.5. The constant k_1 is defined in equation 6.1. Equations for the inverter values J_X where $x \in \{a,b,c\ldots\}$ are provided in figure 6.2 and the required constants in equation 6.1. The constant b_x is the susceptance slope of resonator x. Susceptance slopes are a well-known concept and also discussed in section 7.3 [9]. Next we define the general methodology that should be followed when designing a multi-band coupled resonator filter using the proposed narrowband rational mapping functions.

6.1.4 General application of the technique

The procedure is as follows:

1. Normalise the set of desired passband frequencies in the actual frequency domain using equations 3.3 through 3.5.
2. Construct the set of coordinates in equation 4.2 that must be located on the mapping function.
3. Construct matrices $\mathbf{A}$ and $\mathbf{B}$ and calculate $\mathbf{X}$ as shown in equation 4.7.
4. Calculate the frequency transformation parameters (k and h values) as defined in equation 6.1.
5. Choose a single-band prototype coupled resonator circuit to serve as a base for the multi-band filter. This circuit can have any topology.
6. In order to simplify the representation of complex circuits we introduce a set of symbols and their circuit equivalents in figure 6.5. Substitute all the sections in the single-band prototype circuit that correspond to figure 6.6 (a) with those corresponding to figure 6.6 (b). Note that the circuit in figure 6.6 (b) should take the form dictated by the constants present in the expansion in equation 6.1. Also note that the

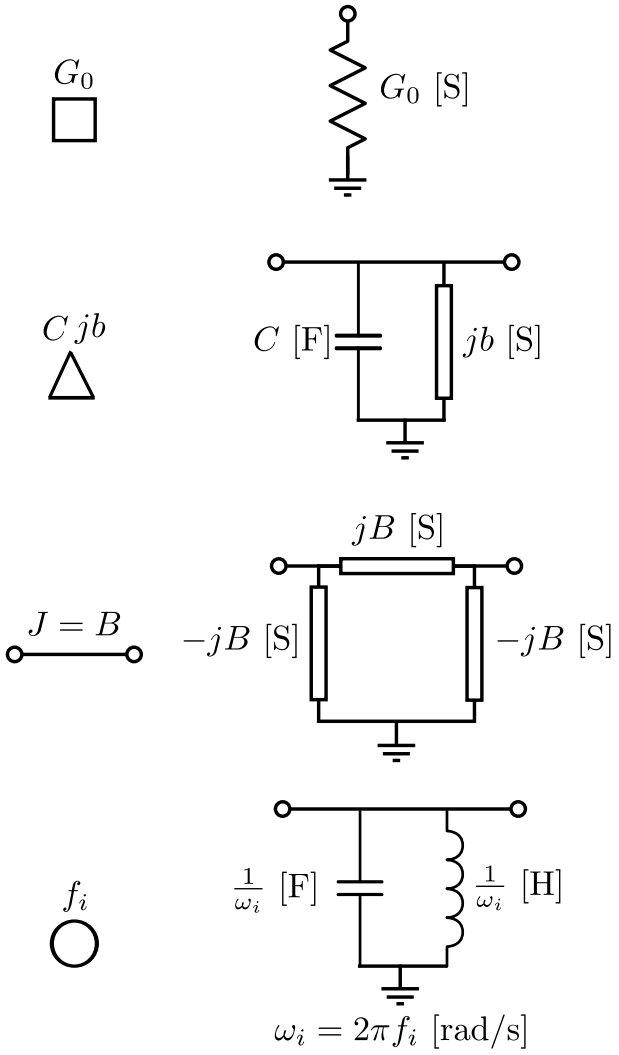

Figure 6.5: A list of symbols and their circuit representations are provided above. These symbols are used to simplify the representation of complex circuits.

single-band-to-multi-band transformation does not introduce any additional cross-couplings into the multi-band prototype that were not present in the original single-band prototype circuit.

7. Transform the multi-band prototype circuit into an actual filter circuit using the lowpass-to-bandpass transformation. This is achieved by substituting the lowpass nodes in the multi-band prototype circuit with resonators where the resonant frequencies are defined in terms of the frequency transformation parameters as shown in figure 6.4. Here the frequency invariant susceptance is defined in figure 6.6 and equation 6.1.

8. Calculate values for the couplings to ensure that the final filter has the desired port termination values and the correct bandwidth. The appropriate expressions are provided in equation 6.2.

We shall now illustrate the application of the theory using multiple examples.

6.1.5 Examples

In this section we present two examples. The first example is a three-band filter. This filter was fabricated and its design is covered in chapter 10. The next example is a five-band filter. This design is intended to serve as

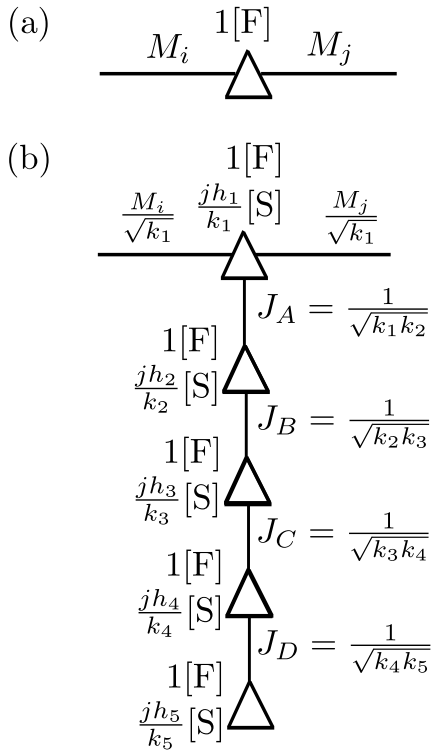

Figure 6.6: A single-band prototype circuit can be transformed into a multi-band prototype circuit by substituting the single-band prototype circuit elements for multi-band expansion circuits. (a) Single-band prototype element. (b) Multi-band expansion circuit for a five-band filter. The number of triangles indicate the number of bands. Refer to figure 6.5 for circuit symbol definitions and equation 6.1 for the definition of constants.

an illustration of the generality of the proposed theory.

Example 1:

The goal is to design a three-band filter, based on a fourth-order Chebyshev lowpass prototype with $|S_{11}| < -20$ dB in its passband, that has the following bandwidth specification:

- Passband 1: 1.50 GHz to 1.53 GHz.
- Passband 2: 1.56 GHz to 1.59 GHz.
- Passband 3: 1.62 GHz to 1.65 GHz.

A rational mapping function was constructed in example 1 in section 4.3.3. The mapping function is as follows:

$$\Omega'(\Omega) = \frac{-8.3728455379692 10\Omega^3 + 0.3190871416532 49\Omega^2 + 4.3473127420671 44\Omega - 0.0892443229639 17}{-5.0255327959020 67\Omega^2 + 0.2298428186893 51\Omega + 1} \quad (6.3)$$

The mapping function can now be expressed in the form illustrated in equation 6.1 to obtain the frequency transformation parameters as defined in table 6.1. The characteristic polynomials for the single-band base filter have been calculated in example 1 in section 2.5.4. From the characteristic polynomials, and using the theory presented in section 5.6, we can obtain an $N+2 \times N+2$ coupling matrix for the single-band prototype filter. The algorithm in section 5.7.2 can then be used to obtain the following coupling matrix for the single-

i	k_i	h_i
1	1.666061267135023	0.012704140772148
2	1.876366969318581	-0.014393322291461
3	2.674407155603390	-0.101799086088778

Table 6.1: The frequency transformation parameters associated with example 1 in section 6.1.5 are provided above.

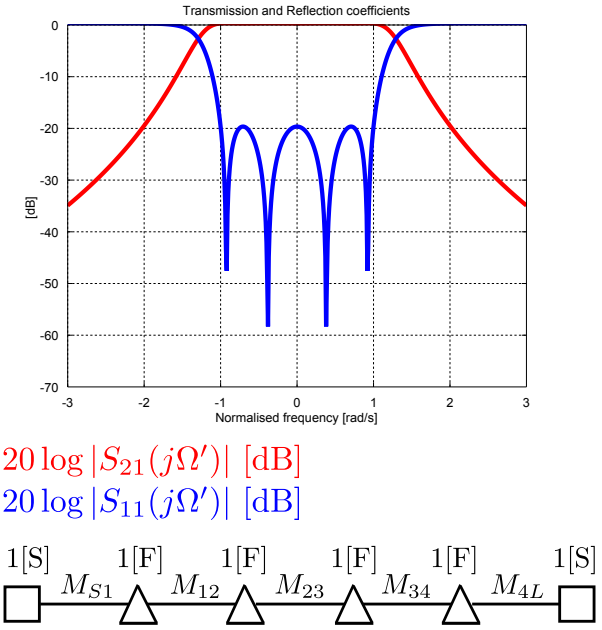

Figure 6.7: The single-band prototype filter circuit, with its associated frequency response, that is used in example 1 in section 6.1.5 is shown above. Refer to figure 6.5 for symbol definitions. The presented circuit is used as a base for the construction of a three-band filter.

band prototype filter:

$$\mathbf{M} = \begin{array}{c} \\ S \\ 1 \\ 2 \\ 3 \\ 4 \\ L \end{array} \begin{array}{c} \begin{array}{cccccc} S & 1 & 2 & 3 & 4 & L \end{array} \\ \begin{bmatrix} 0 & 1.0352 & 0 & 0 & 0 & 0 \\ 1.0352 & 0 & 0.9106 & 0 & 0 & 0 \\ 0 & 0.9106 & 0 & 0.6999 & 0 & 0 \\ 0 & 0 & 0.6999 & 0 & 0.9106 & 0 \\ 0 & 0 & 0 & 0.9106 & 0 & 1.0352 \\ 0 & 0 & 0 & 0 & 1.0352 & 0 \end{bmatrix} \end{array} \tag{6.4}$$

From equation 6.4 it is possible to directly construct the single-band prototype filter circuit. The prototype filter circuit and its associated frequency response is provided in figure 6.7. Using the frequency transformation parameters listed in table 6.1, and the circuit definitions provided in figure 6.6, the single-band prototype circuit in figure 6.7 can be transformed into a multi-band prototype circuit as shown in figure 6.8 The circuit can now be denormalised using the expressions presented in figure 6.4 for the centre frequencies and the expressions in equation 6.2 for the couplings. G_S and G_L can be used to define any port terminations. Any inductor and capacitor values can be used to realise the shunt resonators, providing that the resonator has the correct resonant frequency and that $b_i = \omega_i C_i$ [9]. The final filter circuit with its associated frequency response is provided in figure 6.9. Note that the circuit has the desired frequency response. Also note that the mapping procedure does not introduce any additional cross-couplings.

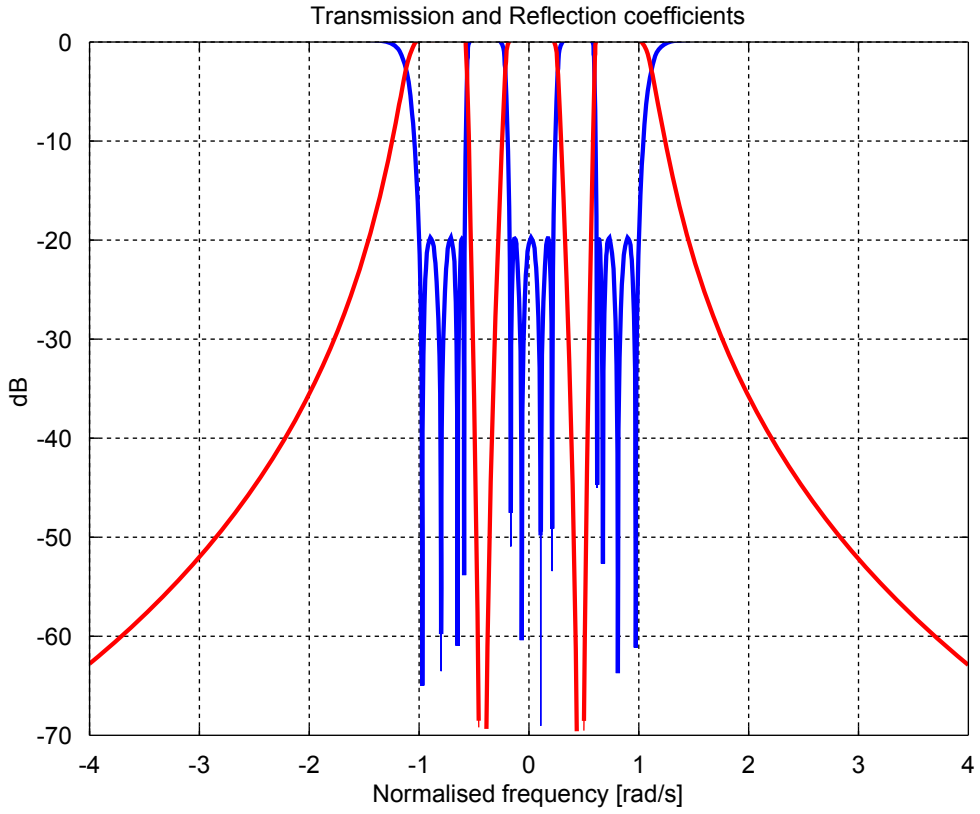

$20\log|S_{21}(j\Omega)|$ [dB]

$20\log|S_{11}(j\Omega)|$ [dB]

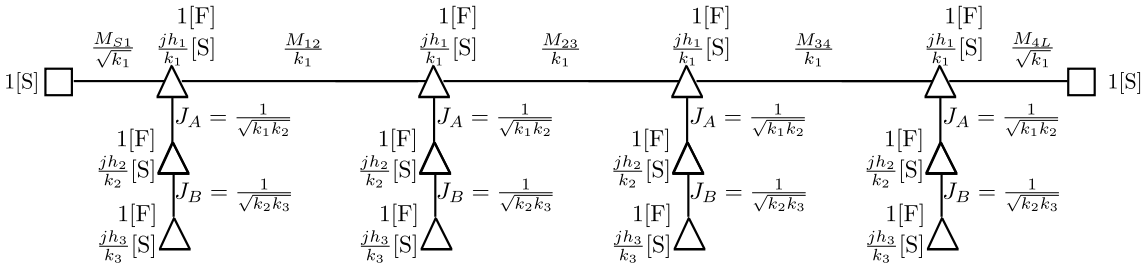

Figure 6.8: The three-band prototype circuit constructed in example 1 in section 6.1.5 is shown above. The circuit is shown with its frequency response. Refer to figure 6.5 for symbol definitions.

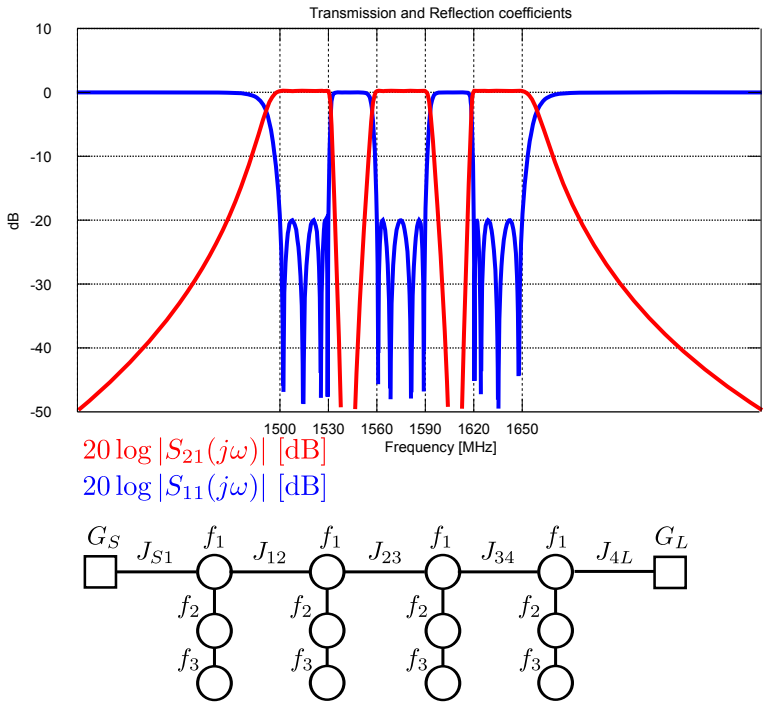

Figure 6.9: The final circuit for the three-band coupled resonator filter designed in example 1 in section 6.1.5 is shown above. Refer to figure 6.5 for symbol definitions. The circuit is provided with its frequency response.

Example 2:

The goal is to design a five-band filter, based on a fourth-order generalised Chebyshev lowpass prototype with finite frequency transmission zeros located at $\Omega' = \pm 3$ and $|S_{11}| < -20$ dB in its passband, that has the following bandwidth specification:

- Passband 1: 1.78 GHz to 1.80 GHz.
- Passband 2: 1.85 GHz to 1.92 GHz.
- Passband 3: 1.98 GHz to 2.02 GHz.
- Passband 4: 2.05 GHz to 2.07 GHz.
- Passband 5: 2.1 GHz to 2.12 GHz.

A rational mapping function was constructed in example 2 in section 4.3.3. The mapping function is as follows:

$$\Omega'(\Omega) = \frac{-69.05221\Omega^5 + 46.06693\Omega^4 + 62.94617\Omega^3 - 41.86384\Omega^2 - 5.22418\Omega + 3.60994}{-34.56674\Omega^4 + 23.52414\Omega^3 + +22.23652\Omega^2 - 15.71112\Omega + 1} \tag{6.5}$$

The mapping function can now be expressed in the form illustrated in equation 6.1 to obtain the frequency transformation parameters as defined in table 6.2. We employ the methods presented in section 2.5 to construct the characteristic polynomials for a fourth-order single-band prototype filter that has transmission zeros at

i	k_i	h_i
1	1.997648965022349	0.026790135341851
2	1.931621053078842	-0.119186280364041
3	1.717454185227932	0.252384832860504
4	1.805487331108606	-0.306876865152536
5	11.966439799456964	-7.129890329342206

Table 6.2: The frequency transformation parameters associated with example 2 in section 6.1.5 are provided above.

$\Omega' = \pm 3$. The characteristic polynomials and the normalisation constants are as follows:

$$\begin{aligned} F(S') &= (S')^4 + 1.01472(S') + 0.13247 \\ jP(S') &= j(S'^2) - 9j \\ E(S') &= (S')^4 + 2.12237(S')^3 + 3.26694(S')^2 + 2.82850(S') + 1.32468 \\ \epsilon_r &= 1 \\ \epsilon &= 6.82834 \end{aligned}$$

From the characteristic polynomials, and using the theory presented in section 5.6, we can obtain an $N+2 \times N+2$ coupling matrix for the single-band prototype filter. The algorithm in section 5.7.2 can then be used to obtain the following coupling matrix for the single-band prototype filter:

$$\mathbf{M} = \begin{array}{c} \\ S \\ 1 \\ 2 \\ 3 \\ 4 \\ L \end{array} \begin{array}{c} \begin{array}{cccccc} S & 1 & 2 & 3 & 4 & L \end{array} \\ \begin{bmatrix} 0 & 1.03014 & 0 & 0 & 0 & 0 \\ 1.03014 & 0 & 0.89630 & 0 & -0.06900 & 0 \\ 0 & 0.89630 & 0 & 0.72756 & 0 & 0 \\ 0 & 0 & 0.72756 & 0 & 0.89630 & 0 \\ 0 & -0.06900 & 0 & 0.89630 & 0 & 1.03014 \\ 0 & 0 & 0 & 0 & 1.03014 & 0 \end{bmatrix} \end{array} \tag{6.6}$$

From equation 6.6 it is possible to directly construct the single-band prototype filter circuit. The prototype filter circuit and its associated frequency response is provided in figure 6.10. Using the frequency transformation parameters listed in table 6.2, and the circuit definitions provided in figure 6.6, the single-band prototype circuit in figure 6.10 can be transformed into a multi-band prototype circuit as shown in figure 6.11 The circuit can now be denormalised using the expressions presented in figure 6.4 for the centre frequencies and the expressions in equation 6.2 for the couplings. G_S and G_L can be used to define any port terminations. Any inductor and capacitor values can be used to realise the shunt resonators, providing that the resonator has the correct resonant frequency and that $b_i = \omega_i C_i$ [9]. The final filter circuit with its associated frequency response is provided in figure 6.12. Note that the circuit has the desired frequency response.

6.2 Synthesis of general multi-band filters using rational mapping functions

In this section we consider the synthesis of general multi-band filters from rational mapping functions. As was the case in section 6.1, a multi-band filter can be constructed from a single-band prototype circuit by replacing each frequency dependent element in the prototype circuit with a frequency transformation subcircuit. For the narrowband case the frequency transformation subcircuits contained frequency-invariant reactances, for the case presented in this section the frequency transformation subcircuits only contain positive inductors and capacitors.

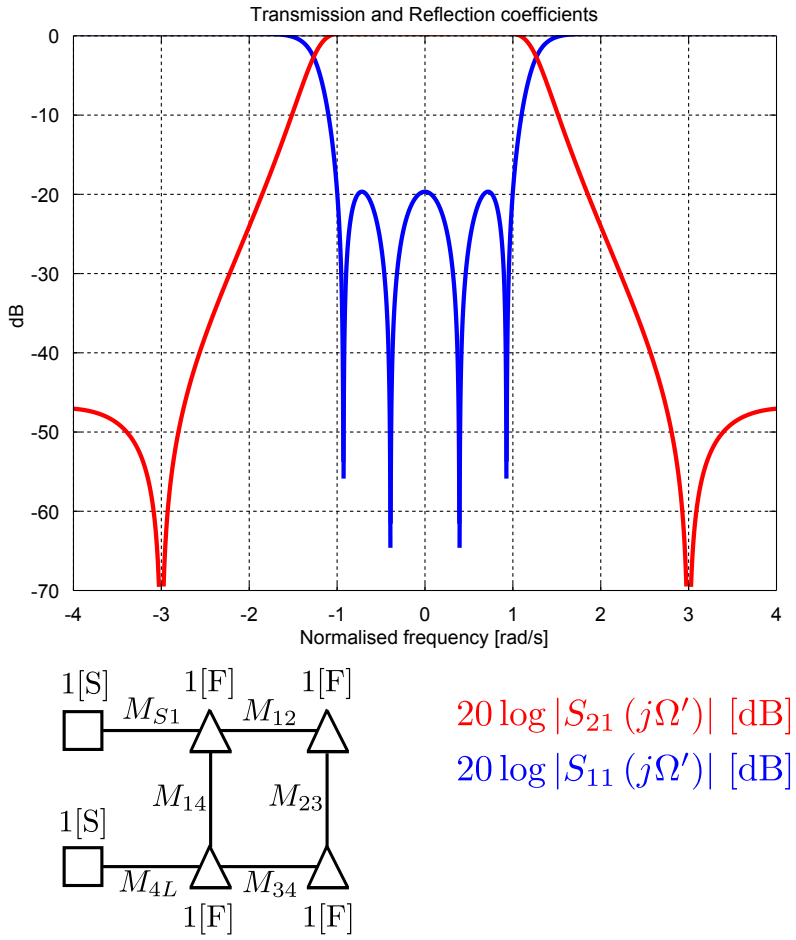

Figure 6.10: The single-band prototype filter circuit, with its associated frequency response, that is used in example 2 in section 6.1.5 is shown above. Refer to figure 6.5 for symbol definitions. The presented circuit is used as a base for the construction of a five-band filter.

6.2.1 Synthesis of a frequency transformation subcircuit

The rational mapping functions developed in section 4.4 describe the relationship between a single-band prototype frequency variable and a multi-band prototype frequency variable. Using complex frequency variables, we can relate a single-band prototype circuit to a multi-band prototype circuit as follows:

$$S' = j\Omega' = H(j\Omega) = H(S)$$

Here S' is the single-band prototype frequency variable, S is the multi-band prototype frequency variable and $\Omega'(\Omega)$ was defined in equation 4.12. The function $H(S)$ can be considered to be the driving point function of a unit reactance or a unit susceptance in a multi-band prototype circuit. Due to the structure of $\Omega'(\Omega)$, $H(S)$ will always be positive real and therefore realisable [62]. The driving point function can now be synthesised in order to obtain a frequency transformation subcircuit. Reactances and susceptances in a single-band prototype circuit can be substituted for by scaled versions of the frequency transformation subcircuit in order to obtain a multi-band prototype circuit. There are numerous classical techniques available in the literature to synthesise the required transformation subcircuits from the reactance/susceptance function and all of these methods can be used to design multi-band filters [62]. We shall now use established methods to synthesise various frequency transformation subcircuits from $H(S)$ [62]. Note that this is not an exhaustive list. For series inductors we shall use $H\left(\frac{s}{\omega_c}\right) R_0 L$ as the driving point impedance function and for parallel capacitors we shall

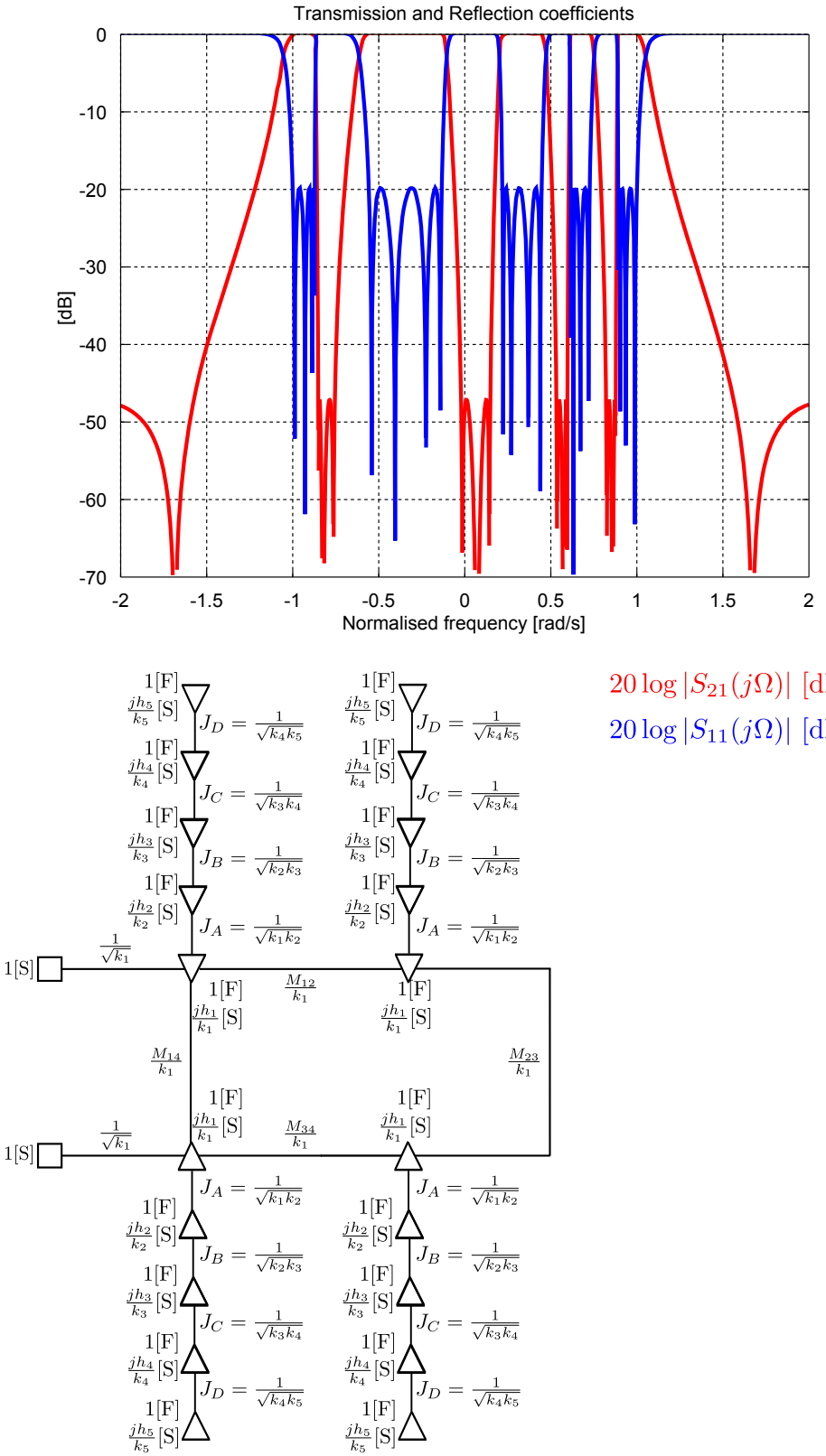

Figure 6.11: The five-band prototype circuit constructed in example 2 in section6.1.5 is shown above. The circuit is shown with its frequency response. Refer to figure 6.5 for symbol definitions.

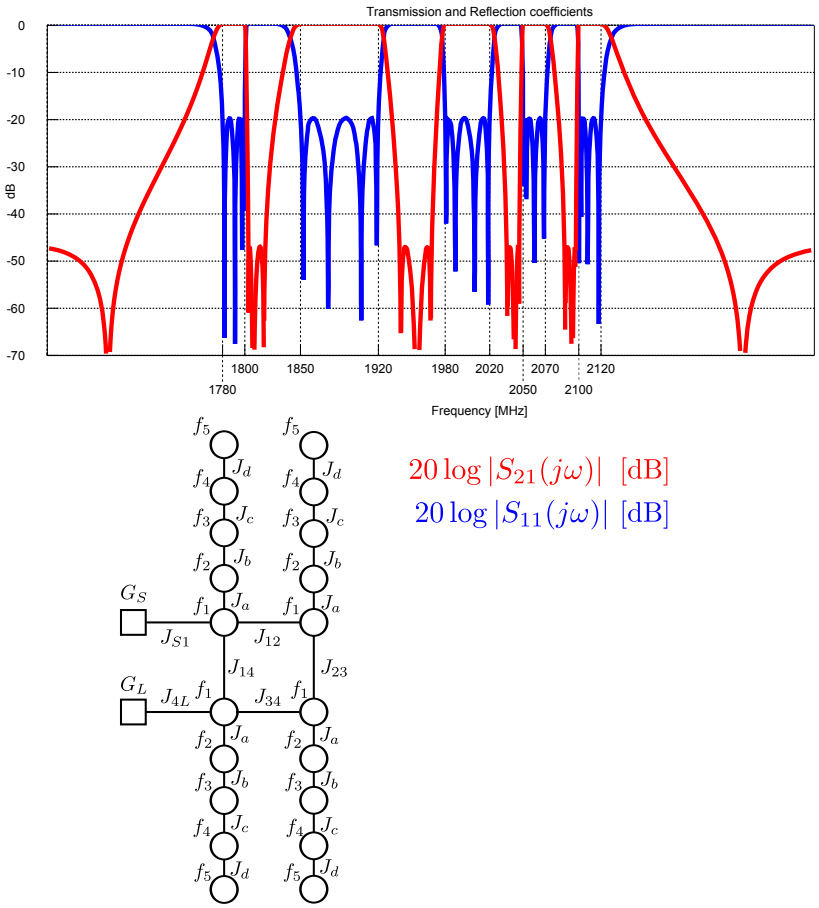

Figure 6.12: The final circuit for the three-band coupled resonator filter designed in example 2 in section 6.1.5 is shown above. Refer to figure 6.5 for symbol definitions. The circuit is provided with its frequency response.

use $H\left(\frac{s}{\omega_c}\right) G_0 C$ as the driving point admittance function. Here R_0 and G_0 scale resistance and susceptance respectively. The factor ω_c scales frequency and has the value of the highest passband edge frequency.

Foster topology

A driving point function can be expressed in the Foster topology by expressing the function as a sum of partial fractions. We can obtain the Foster form of the frequency transformation subcircuit as follows:

$$\begin{aligned} H(S) &= \frac{k_0}{S} + \frac{k_1}{S - j\omega_1} + \frac{k_1^*}{S + j\omega_1} + \frac{k_2}{S - j\omega_2} + \frac{k_2^*}{S + j\omega_2} + \ldots + k_\infty S \\ &= \frac{k_0}{S} + \sum_{i=1}^{N-1} \left(\frac{2k_i S}{S^2 + \omega_i^2} \right) + k_\infty S \end{aligned} \tag{6.7}$$

The expansion above describes a circuit. The topology of the circuit depend on whether the driving point function is an impedance function or an admittance function. If the driving point function is an impedance function we refer to the obtained topology as a Foster I topology. A Foster I topology consists of an interconnection of series elements. If the driving point function is an admittance function we refer to the obtained topology as a Foster II topology. A Foster II topology consists of an interconnection of parallel elements. This leads to two transformation subcircuits, one for series inductors and one for parallel capacitors. The two transformation subcircuits are shown in figure 6.13.

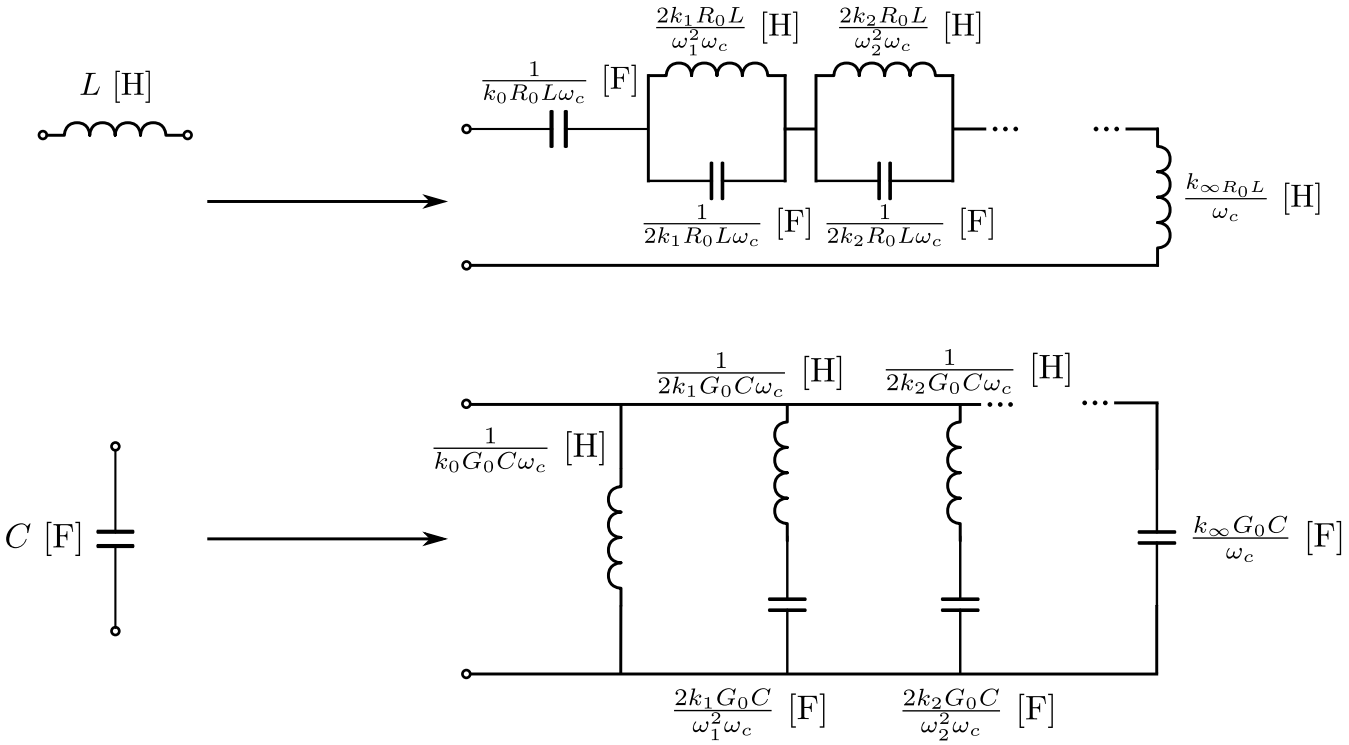

Figure 6.13: Multi-band filters can be obtained by replacing inductors and capacitors in prototype circuits with frequency transformation subcircuits. The frequency transformation subcircuits for series inductors and parallel capacitors are shown above. The subcircuit for the inductor is in a Foster I topology and the subcircuit for the capacitor is in a Foster II topology. Refer to equation 6.7 for circuit element values.

Cauer I topology

A driving point function can be synthesised in the Cauer I topology through the continued removal of poles at infinity. This can be achieved by first arranging the terms of the numerator and denominator polynomials in descending order according to the powers of S, and then expressing the rational function as a continued fraction. The continued fraction expansion can found through a series of polynomial division and inversion steps. The Cauer I form is therefore obtained as follows:

$$\begin{aligned} H(S) &= \frac{a_{2N}S^{2N} + a_{2N-2}S^{2N-2} + \ldots + 1}{b_{2N-1}S^{2N-1} + b_{2N-3}S^{2N-3} + \ldots + b_1S} \\ &= Sk_0 + \frac{1}{Sk_1 + \frac{1}{Sk_2 + \frac{1}{Sk_3 + \ldots}}} \end{aligned} \tag{6.8}$$

The expansion above describes a circuit. The topology of the circuit depend on whether the driving point function is an impedance function or an admittance function. We therefore have two possible circuit transformations as shown in figure 6.14.

Cauer II topology

A driving point function can be synthesised in the Cauer II topology through the continued removal of poles at zero. The Cauer II topology can be found in a fashion similar to the Cauer I topology. The difference between the techniques is that the terms of the numerator and denominator polynomials for the Cauer II case must be arranged in ascending order according to the powers of S, starting with the lowest power of S and ending

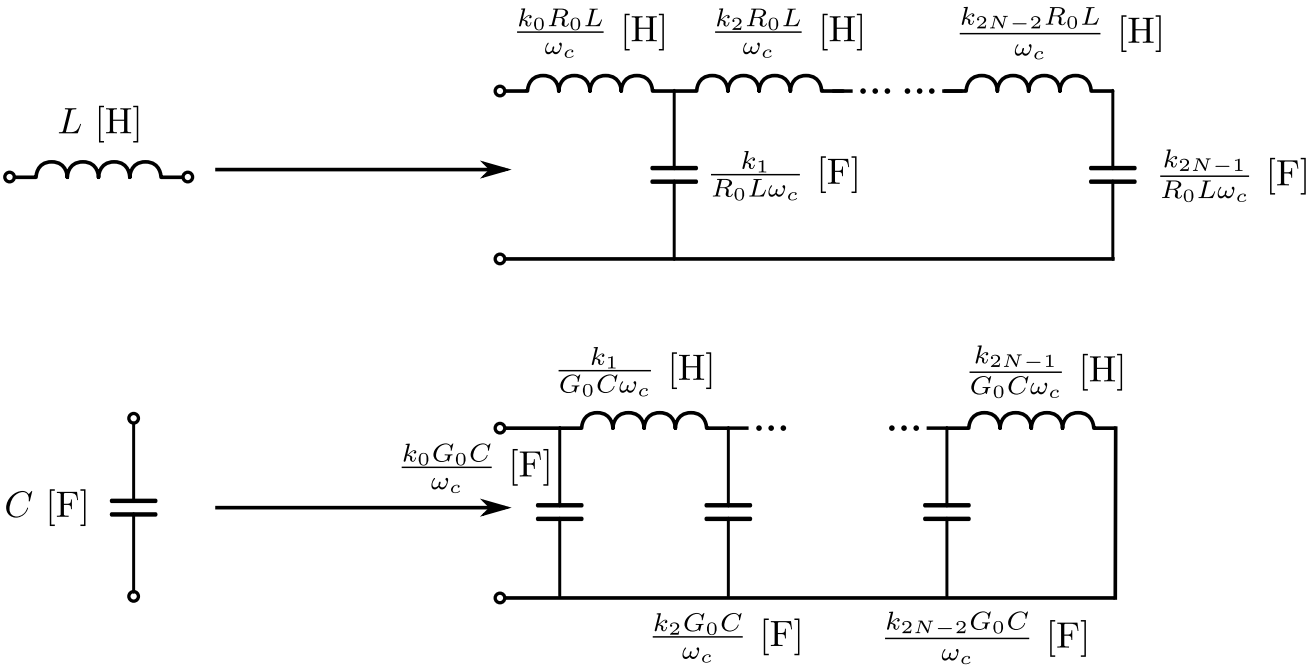

Figure 6.14: Multi-band filters can be obtained by replacing inductors and capacitors in prototype circuits with frequency transformation subcircuits. The frequency transformation subcircuits for series inductors and parallel capacitors are shown above. The subcircuits above are in the Cauer I topology. Refer to equation 6.8 for circuit element values.

with the leading coefficient. The Cauer II form is then obtained as follows:

$$\begin{aligned} H(S) &= \frac{1 + a_2 S^2 + a_4 S^4 + \ldots + a_{2N} S^{2N}}{b_1 S + b_3 S^3 + \ldots + b_{2N-1} S^{2N-1}} \\ &= \frac{k_0}{S} + \frac{1}{\frac{k_1}{S} + \frac{1}{\frac{k_2}{S} \ldots}} \end{aligned} \tag{6.9}$$

The expansion again describes a circuit. The topology of the circuit depend on whether the driving point function is an impedance function or an admittance function. The two possible circuit transformations are shown in figure 6.15.

Mixed Cauer I & II topology

Cauer I and II topologies can be mixed by by extracting one pole at zero and one pole at infinity at each level inside the continued fraction expansion. Essentially one extracts a complete resonator in each branch of the circuit. The continued fraction expansion can again be found through a series of polynomial division and inversion steps. Note that two components must be extracted between inversions. The continued fraction expansion is therefore as follows:

$$H(S) = k_0 S + \frac{k_1}{S} + \frac{1}{k_2 S + \frac{k_3}{S} + \frac{1}{k_3 S + \frac{k_4}{S} + \ldots}} \tag{6.10}$$

The expansion again describes a circuit. The topology of the circuit depend on whether the driving point function is an impedance function or an admittance function. The two possible circuit transformations are shown in figure 6.16.

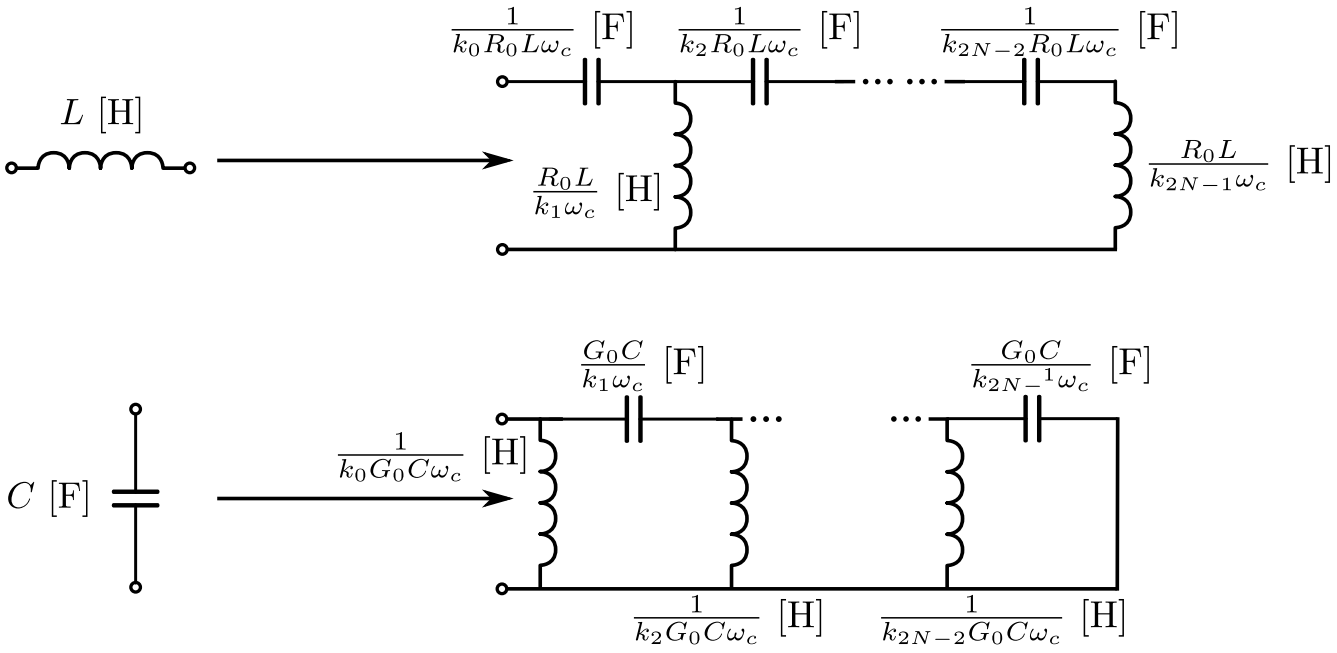

Figure 6.15: Multi-band filters can be obtained by replacing inductors and capacitors in prototype circuits with frequency transformation subcircuits. The frequency transformation subcircuits for series inductors and parallel capacitors are shown above. The subcircuits above are in the Cauer II topology. Refer to equation 6.9 for circuit element values.

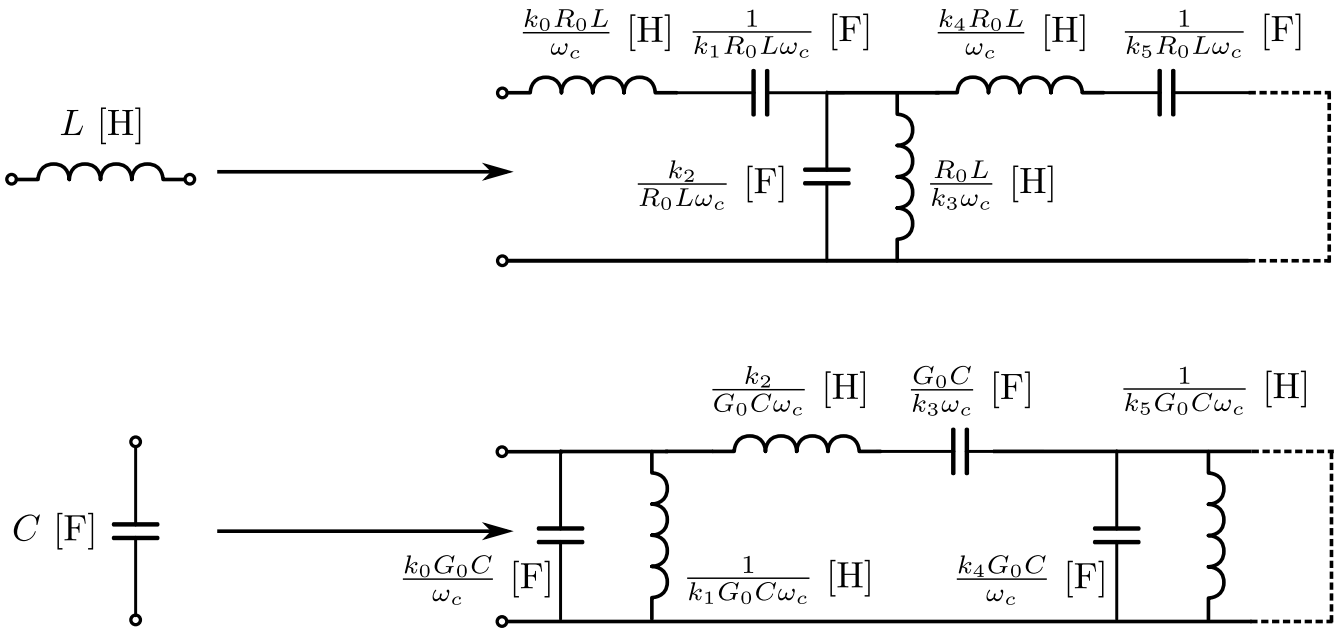

Figure 6.16: Multi-band filters can be obtained by replacing inductors and capacitors in prototype circuits with frequency transformation subcircuits. The frequency transformation subcircuits for series inductors and parallel capacitors are shown above. The subcircuits above are in the mixed Cauer I & II topology.

Coupled resonator topology

The Cauer I, Cauer II, mixed Cauer I & II and Foster forms are all complete realisations of the driving point function and valid at all frequencies. These subcircuits can therefore be used to design multi-band filters that have any passband specification providing that all of the bands are bandwidth-scaled and frequency-translated copies of the frequency response of the original single-band prototype. If we however limit ourselves to the design of narrowband filters, we can introduce perfect impedance or admittance inverters into the circuits in in figure 6.16 to transform them into a coupled resonator topology as shown in figure 6.17. For this discussion we shall only consider the admittance formulation of a coupled resonator circuit, though it should be apparent that the results are repeatable for the impedance case. Single-band coupled resonator circuits generally consist of unit capacitors that are coupled through admittance inverters. The property that all of the capacitors in a single-band coupled resonator prototype circuit are equal in value implies that all of the branches in a multi-band coupled resonator circuit would be identical. This property is beneficial for designs. Expressions for the couplings and centre frequencies for the coupled resonator frequency transformation subcircuit in figure 6.17 can be found by equating the driving point functions of the input admittance of the circuits in figures 6.16 and 6.17 and then equating the susceptance slopes. The resulting expressions are provided in figure 6.17 and will be discussed next. The resonant frequencies of the resonators inside the multi-band branches are defined as follows:

$$\begin{array}{ll} \text{First resonator in branch:} & f_1 = \sqrt{\frac{k_1}{k_0}} f_c \\ \text{Second resonator in branch:} & f_2 = \sqrt{\frac{k_3}{k_2}} f_c \\ \vdots & \vdots \end{array} \tag{6.11}$$

Here f_c is the frequency normalisation factor and has the value of the highest passband edge frequency. Any combination of inductor and capacitor can be used to construct the resonator providing that the resulting resonator has the correct centre frequency, according to equation 6.11, and that the effect of the choice of capacitor and inductor values are accounted for using a susceptance slope when calculating values for the couplings. The susceptance slope of an arbitrary resonator can be determined from equation 7.11. For the lumped element case in the parallel topology as shown in figure 6.17 the susceptance slope is calculated as follows:

$$b_i = \omega_i C_i \tag{6.12}$$

Here $\omega_i = 2\pi f_i$ where f_i is the resonant frequency of the resonator. Using equation 6.12 we define the couplings in a coupled resonator branch as follows:

$$\begin{array}{l} J_a = \frac{\sqrt{b_a b_b}}{\sqrt[4]{k_0 k_1 k_2 k_3}} \\ J_b = \frac{\sqrt{b_b b_c}}{\sqrt[4]{k_1 k_2 k_3 k_4}} \\ J_c = \frac{\sqrt{b_c b_d}}{\sqrt[4]{k_4 k_5 k_6 k_7}} \\ \vdots \end{array} \tag{6.13}$$

If one performs the substitution depicted in figure 6.17 to obtain a multi-band coupled resonator filter, the couplings in the original single-band prototype circuit also need to be scaled. For an N-th order single-band circuit the scaling is defined as follows:

$$\begin{array}{lll} \text{Original single-band couplings:} & J_{ij} = \frac{M_{ij} b_a}{\sqrt{k_0 k_1}} & i, j \in \text{Single-band prototype} \\ \text{Input:} & J_{S1} = \sqrt{\frac{G_S b_a}{\sqrt{k_0 k_1}}} M_{S1} & \\ \text{Output:} & J_{LN} = \sqrt{\frac{G_L b_a}{\sqrt{k_0 k_1}}} M_{LN} & \end{array} \tag{6.14}$$

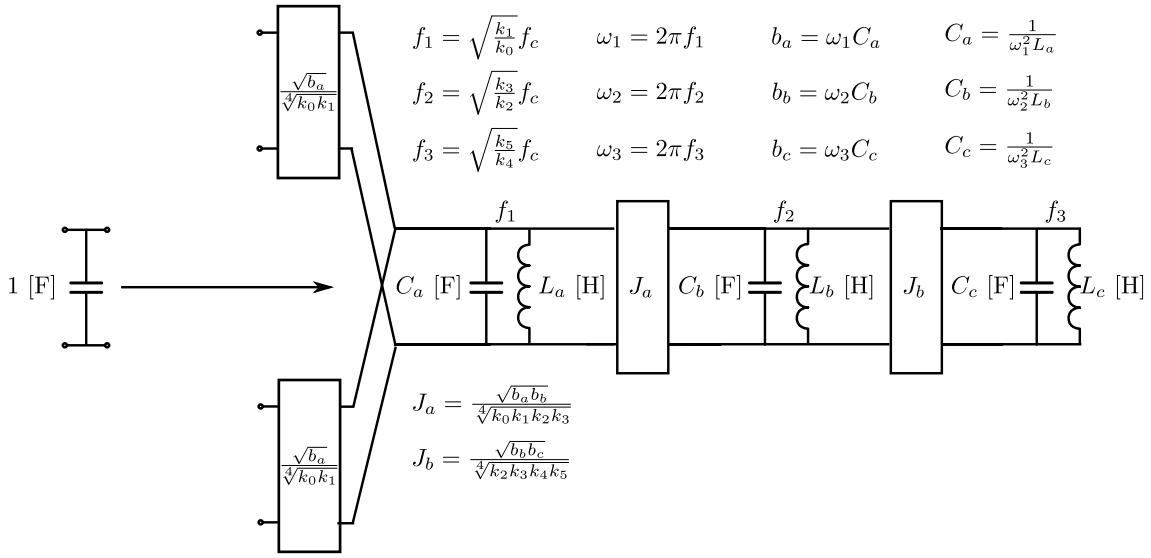

Figure 6.17: A coupled resonator implementation of a frequency transformation subcircuit is shown above. The circuit is in its admittance form and can be used to transform a single-band coupled resonator circuit into a multi-band coupled resonator circuit. Formulas for the couplings and centre frequencies are provided. A single-band prototype is transformed into a multi-band filter by simply replacing the capacitors with the provided subcircuit. Refer to equation 6.10 for the values of the frequency transformation constants.

Here M_{S1}, M_{LN} and M_{ij} are elements in the coupling matrix of an N-th order single-band prototype circuit. M_{S1} and M_{LN} are the input and output couplings respectively and M_{ij} refer to the coupling between resonators i and j.

6.2.2 Obtaining a multi-band prototype circuit

In the previous section we presented various realisations of frequency transformation subcircuits. All of these can be used to transform a single-band prototype circuit into a multi-band prototype circuit. In each case the procedure is to substitute all of the frequency-dependent elements in a single-band prototype with one of the frequency transformation subcircuits depicted in figures 6.13 through 6.17.

6.2.3 Denormalisation to obtain a multi-band filter

From the theory presented in section 4.4.1 the multi-band prototype circuits discussed in this section need to be denormalised using equation 4.11. The normalisation factor ω_c has been included in all of the frequency transformation subcircuits. This variable is equal to ω_{UN} in equation 4.11 and is essentially the highest passband edge frequency. The prototype circuit was synthesised assuming a $1\,\Omega$ source impedance. The impedance level of the prototype circuit can be scaled to an appropriate level in the final circuit using $R_0 = \frac{1}{G_0}$. We shall next describe a general method to design multi-band filters using the presented theory. We shall then substantiate the theory using some examples.

6.2.4 General application of the technique

The procedure is as follows:

1. Decide on a suitable single-band prototype circuit to use as a base filter. The frequency response of the final multi-band filter will be a bandwidth-scaled and frequency-translated copy of the frequency

response of the single-band prototype circuit.

2. Normalise the set of desired passband frequencies in the actual frequency domain using equation 4.11.
3. Construct the set of coordinates in equation 4.13 that must be located on the mapping function.
4. Construct matrices $\mathbf{A}$ and $\mathbf{B}$ and calculate $\mathbf{X}$ as shown in equations 4.15 through 4.18.
5. Decide on a topology for the frequency transformation subcircuit. We presented multiple options with their synthesis procedures in section 6.2.1. The entire body of knowledge for one-port reactance synthesis can be used for this purpose [62]. For the cases presented in this dissertation one should calculate the frequency transformation constants, indicated using the notation k_i in section 6.2.1.
6. Each frequency-dependent element in the single-band prototype circuit must be replaced by a scaled version of the frequency transformation subcircuit in either its reactance or susceptance forms. The scaling factor is equal to the single-band prototype element value in conjunction with a suitable arrangement of the impedance/admittance and frequency normalisation factors. For the cases discussed in this dissertation, the final element values are indicated in figures 6.13 through 6.17. The impedance/admittance factor should be equal to the port terminations (assumed equal valued ports) and the frequency normalisation factor ω_c should be equal to the highest passband edge frequency in the highest passband as discussed in section 4.4.1.

The result of the procedure is a multi-band lumped element circuit that has the desired passband specification. We shall now illustrate the application of the theory using multiple examples.

6.2.5 Examples

In this section we clarify the presented theory by presenting three design examples of three-band filters. The first design example is essentially a narrowband filter that has the same bandwidth specification as the filter designed in example 1 in section 6.1.5. The second design example is the design of a wideband multi-band filter. We design both narrowband and wideband filters using the presented theory to highlight its generality. We provide multiple synthesis solutions for both the first example and the second example, using all of the different frequency transformation subcircuits covered earlier, to illustrate the flexibility of the method. The last design example is that of a wideband transmission line filter. This example has been included to illustrate how Richard's transformation can be used in conjunction with the presented theory to design wideband multi-band transmission line filters.

The coupled resonator version of the filter in design example 1 was constructed to further substantiate the theory. The realisation and manufacturing of this filter is covered in chapter 10.

Example 1: Three-band narrowband filter

Specification

The goal is to design a three-band filter with the following bandwidth specification:

- Passband 1: 1.50 GHz to 1.53 GHz.
- Passband 2: 1.56 GHz to 1.59 GHz.
- Passband 3: 1.62 GHz to 1.65 GHz.

g_0	1 [Ω]
g_1	0.933232710550907 [Ω]
g_2	1.292330803106013 [S]
g_3	1.579515426018457 [Ω]
g_4	0.763554035905290 [S]
g_5	1.222222222222219 [Ω]

Table 6.3: The g-parameters of the single-band prototype circuit in figure 6.18 are provided above. Note that the prototype is normalised with respect to frequency and impedance and as a consequence g_1 is the inductance of the first inductor, g_2 is the capacitance of the first capacitor etc.

Each of these passbands must be fourth-order and have a minimum return loss figure of 20 dB. We shall now follow the procedure described in section 6.2.4 to complete the design. The first step is to find a single-band prototype base filter. We shall then find the required mapping function and synthesise multiple configurations for the frequency transformation subcircuit from it. The synthesised subcircuits will then be used to obtain multiple multi-band filters that all have the required frequency response.

Single-band prototype filter

The single-band prototype filter, that is used as a base filter for our multi-band design, is a fourth-order all-pole filter that has 20 dB return loss in its passband. The characteristic polynomials for this filter have been calculated in example 1 in section 2.5.4. We can synthesise a simple prototype circuit from the driving point impedance function using the characteristic polynomials. If we assume that the source has an input impedance of $g_0 = 1\ \Omega$, we can find a Cauer I expansion as follows:

$$\begin{aligned} Z_{DP}(S) &= \frac{g_0 - S_{11}(S)}{g_0 + S_{11}(S)} \\ &= \frac{\epsilon_r E(S) + F(S)}{\epsilon_r E(S) - F(S)} \\ &= \cfrac{1}{Sg_1 + \cfrac{1}{Sg_2 + \cfrac{1}{Sg_3 + \cfrac{1}{Sg_4 + \cfrac{1}{g_5}}}}} \end{aligned} \tag{6.15}$$

The characteristic polynomials are normalised with respect to frequency and impedance. Consequently the g-parameters in equation 6.15 that belong to impedance terms are numerically equal to the inductance of a series inductor and those that belong to susceptance terms refer directly to the capacitance of a shunt capacitor. The circuit and its frequency response is shown in figure 6.18. The g-parameters are provided in table 6.3. The next step in the design is to obtain a frequency mapping function and to then synthesise the necessary multi-band frequency transformation subcircuits from it.

Driving point function of frequency transformation subcircuit

The required mapping function was constructed in example 1 in section 4.4.3 and is repeated here for convenience:

$$\Omega'(\Omega) = \frac{-1.326173342798413\ \Omega^6 + 3.626919690899577\ \Omega^4 - 3.301198836788956\ \Omega^2 + 1}{-0.072336727789001\ \Omega^5 + 0.131927843706407\ \Omega^3 - 0.060043604605202\ \Omega}$$

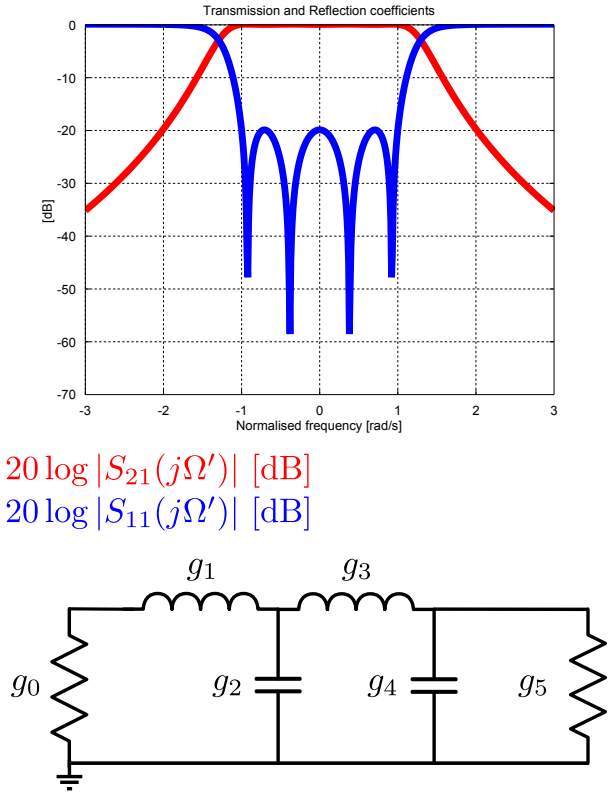

Figure 6.18: The single-band filter that is used as a basis for the three-band filter is shown above.

A driving point function for the frequency transformation subcircuit can now be found as follows:

$$\begin{aligned} S' &= j\Omega' = H(S) \\ &= \frac{1.326173342798413\ S^6 + 3.626919690899577\ S^4 + 3.301198836788956\ S^2 + 1}{0.072336727789001\ S^5 + 0.131927843706407\ S^3 + 0.060043604605202\ S} \end{aligned} \tag{6.16}$$

The driving point function can now be used to synthesise various frequency transformation subcircuits that can all in turn be used to transform the single-band prototype circuit into a multi-band filter. We shall now synthesise multiple possible frequency transformation subcircuits using equation 6.16. Capacitor and inductor values in single-band prototype circuits are substituted with the frequency transformation subcircuits to obtain multi-band prototype filters. The multi-band prototype circuits must then be denormalised using frequency and impedance scaling. We plan to design the filter in a $50\,\Omega$ environment and therefore choose $R_0 = 50$ and $G_0 = 0.02$. The frequency scaling for the various circuits are performed by choosing $\omega_c = 2\pi f_c$ where $f_c = 1.65$ GHz, the highest frequency in the highest passband (refer to example 1 in section 4.4.3). We shall now design a multi-band filter using a Foster topology for the frequency transformation subcircuits.

Multi-band filter using Foster topology

The driving point function of the frequency transformation subcircuit in equation 6.16 can be expressed in the Foster form as depicted in equation 6.7. The associated frequency transformation constants are listed in table 6.4. We can now obtain frequency transformation subcircuits for capacitors and inductors by applying the constants in table 6.4 to the general frequency transformation subcircuits depicted in figure 6.13. The frequency transformation subcircuits are now applied to the single-band prototype in figure 6.18 to obtain the three-band filter in figure 6.19. The frequency response of the multi-band filter is provided in figure 6.24.

k_0	16.654563072540121
k_1	0.011962177667602
k_2	0.012271437579326
ω_1	0.934195402164440
ω_2	0.269416412962130
k_∞	3.513513513513512

Table 6.4: Frequency transformation constants of the multi-band Foster topology for design example 1. Refer to equation 6.7 for a formal definition.

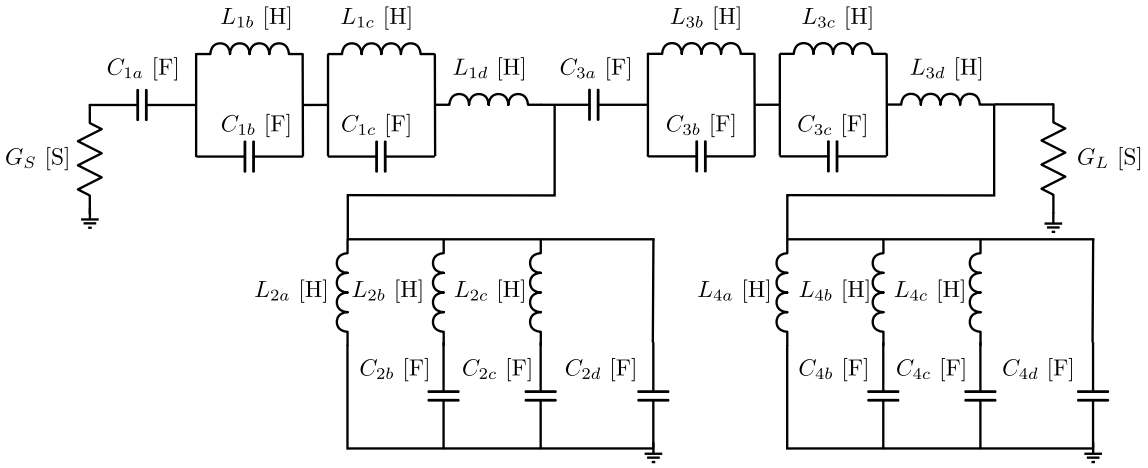

Figure 6.19: The single-band prototype in figure 6.18 was transformed into a three-band filter using Foster expansions (impedance and admittance) of the frequency transformation driving point function.

We shall next design a multi-band filter using a Cauer I topology for the frequency transformation subcircuits.

Multi-band filter using Cauer I topology

The driving point function of the frequency transformation subcircuit in equation 6.16 can be expressed in the Cauer I form as depicted in equation 6.8. The associated frequency transformation constants are listed in table 6.5. We can now obtain frequency transformation subcircuits for capacitors and inductors by applying the constants in table 6.5 to the general frequency transformation subcircuits depicted in figure 6.14. The frequency transformation subcircuits are now applied to the single-band prototype in figure 6.18 to obtain the three-band filter in figure 6.20. The frequency response of the multi-band filter is provided in figure 6.24.

We shall now design a multi-band filter using a Cauer II topology for the frequency transformation subcircuits.

Multi-band filter using Cauer II topology

The driving point function of the frequency transformation subcircuit in equation 6.16 can be expressed in the Cauer II form as depicted in equation 6.9. The associated frequency transformation constants are listed in

k_0	18.333333333334178
k_1	0.059869375907099
k_2	0.012271437579326
k_3	6315.833332904871
k_4	3478761.000115548
k_5	$3.162045337291503\ \ 10^{-7}$

Table 6.5: Frequency transformation constants of the multi-band Cauer I topology for design example 1. Refer to equation 6.8 for a formal definition.

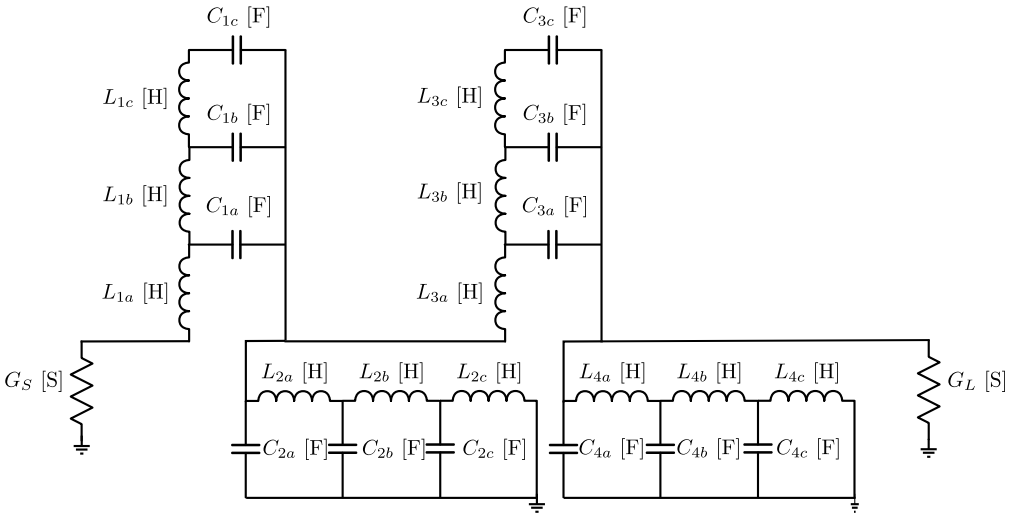

Figure 6.20: The single-band prototype in figure 6.18 was transformed into a three-band filter using Cauer I expansions (impedance and admittance) of the frequency transformation driving point function.

table 6.6. We can now obtain frequency transformation subcircuits for capacitors and inductors by applying the constants in table 6.6 to the general frequency transformation subcircuits depicted in figure 6.15. The frequency transformation subcircuits are now applied to the single-band prototype in figure 6.18 to obtain the three-band filter in figure 6.21. The frequency response of the multi-band filter is provided in figure 6.24.

We shall now design a multi-band filter using a mixed Cauer I & II topology for the frequency transformation subcircuits.

Multi-band filter using mixed Cauer I and II topology

The driving point function of the frequency transformation subcircuit in equation 6.16 can be expressed in the mixed Cauer I & II form as depicted in equation 6.10. The associated frequency transformation constants are listed in table 6.7. We can now obtain frequency transformation subcircuits for capacitors and inductors by applying the constants in table 6.7 to the general frequency transformation subcircuits depicted in figure 6.16. The frequency transformation subcircuits are now applied to the single-band prototype in figure 6.18 to obtain the three-band filter in figure 6.22. The frequency response of the multi-band filter is provided in figure 6.24.

We shall now design a multi-band filter using a coupled resonator topology for the frequency transforma-

k_0	16.654563072540238
k_1	0.054387409580735
k_2	5762.608162427217
k_3	$1.577606091141858\ 10^{-4}$
k_4	$3.220242916238307\ 10^{7}$
k_5	$2.843556030145810\ 10^{-7}$

Table 6.6: Frequency transformation constants of the multi-band Cauer II topology for design example 1. Refer to equation 6.9for a formal definition.

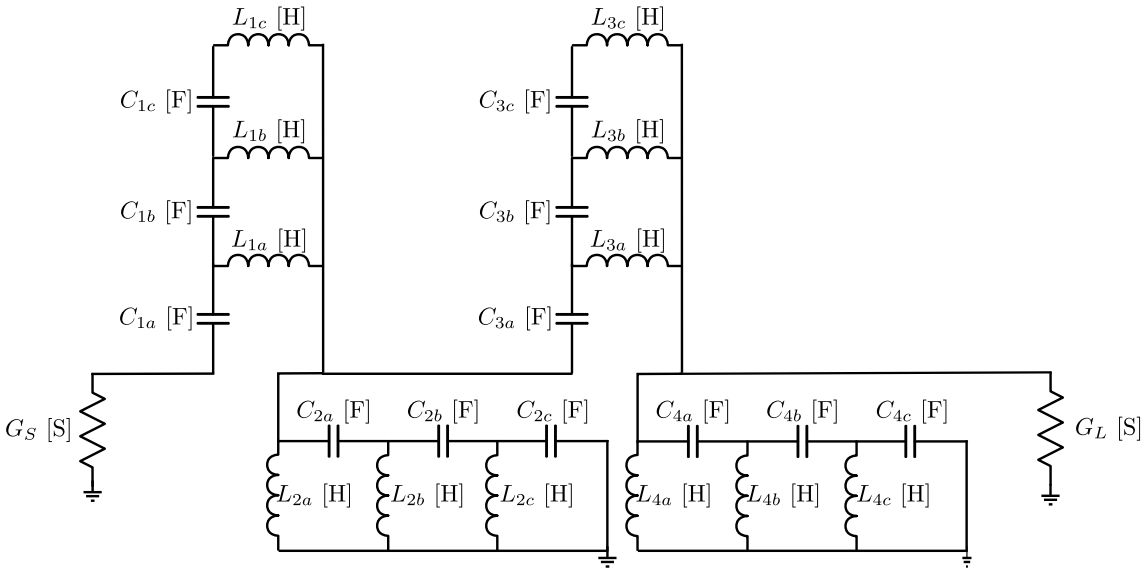

Figure 6.21: The single-band prototype in figure 6.18 was transformed into a three-band filter using Cauer II expansions (impedance and admittance) of the frequency transformation driving point function.

tion subcircuits.

Multi-band filter using coupled resonator topology

In order to design a multi-band coupled resonator filter using reactance transformations, we need to change the topology of the single-band prototype so that it consists of unit capacitances that are coupled using admittance inverters. To transform our fourth-order all-pole single-band base filter into a coupled capacitance structure we can either insert admittance inverters into the circuit in figure 6.18 or we can synthesise a coupling matrix as we did in example 1 in section 6.1.5. Whatever the case, a coupling matrix representation of the single-band prototype base filter is provided in equation 6.4 and the circuit with its frequency response is provided in figure 6.7. We must now synthesise the frequency transformation subcircuit in the coupled resonator topology as shown in figure 6.17. For this purpose we need to express the frequency transformation subcircuit in equation 6.16 in the mixed Cauer I & II form as depicted in equation 6.10. The associated frequency transformation constants are listed in table 6.7. These constants are the same for the mixed Cauer I & II and coupled resonator topologies. By applying the constants in table 6.7 to the expressions in figure 6.17 we obtain the frequency

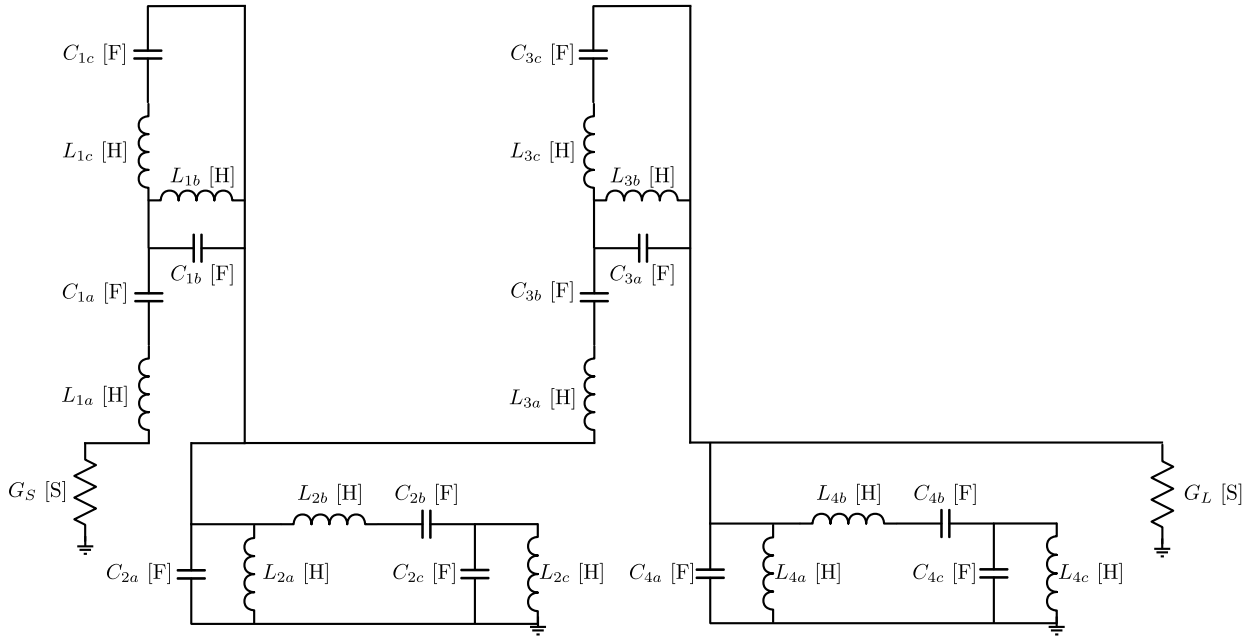

Figure 6.22: The single-band prototype in figure 6.18 was transformed into a three-band filter using mixed Cauer I and II expansions (impedance and admittance) of the frequency transformation driving point function.

k_0	18.333333333334284
k_1	16.654563072540238
k_2	20.632497252585164
k_3	18.770518772545945
k_4	29.365201855082802
k_5	26.792695479623539

Table 6.7: Frequency transformation constants of the multi-band mixed Cauer I and II topology for design example 1. Refer to equation 6.10 for a formal definition.

transformation subcircuit. All of the unit capacitances in the circuit in figure 6.7 can now be substituted with the circuit in figure 6.17 to obtain a final multi-band coupled resonator circuit as shown in figure 6.23. All of the circuit elements are defined by equations 6.12 through 6.14.

In this example we have synthesised five circuits that are all three-band filters and that all have exactly the same frequency response as shown in figure 6.24. The reason for the identical frequency responses is that all of the frequency transformation subcircuits were synthesised from the same driving point function.

In the next example we present the design of a wideband multi-band filter.

Example 2: Three-band wideband filter

Specification

The goal is to design a three-band wideband filter with the following bandwidth specification:

- Passband 1: 1.0 GHz to 5.0 GHz.

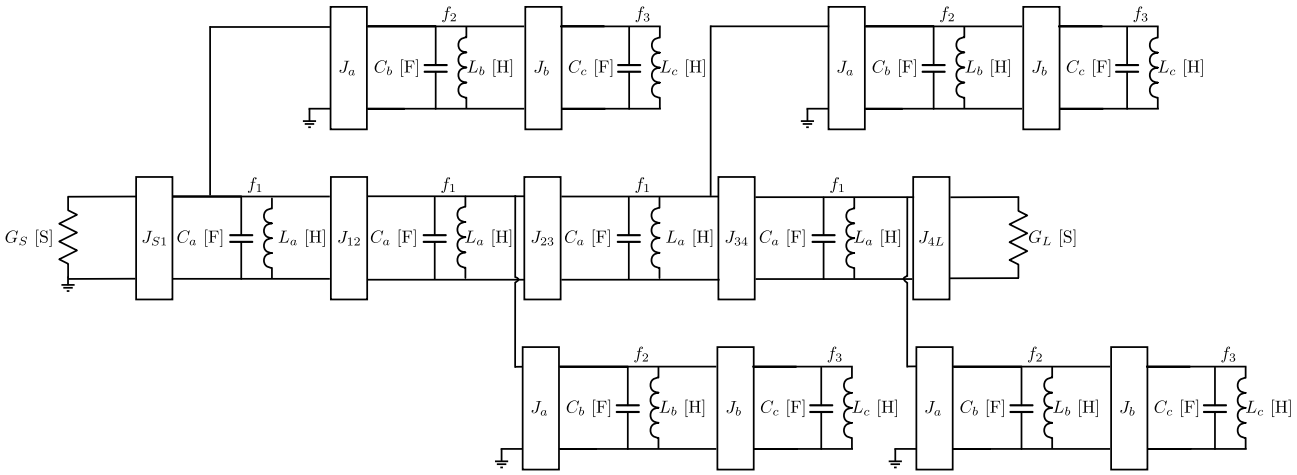

Figure 6.23: The single-band prototype in figure 6.18 was transformed into a three-band coupled resonator filter using the expansions depicted in figure 6.17. Expressions for the couplings and centre frequencies can be found in equation 6.12 through 6.14. The frequency transformation constants are the same ones used for the mixed Cauer I and II forms and are listed in table 6.7. The normalisation factors have the following values: $R_0 = 50\ \Omega$, $G_0 = 0.02$ S and $\omega_c = 2\pi f_c$ where $f_c = 1.65$ GHz. The obtained three-band filter is shown above and its frequency response is provided in figure 6.24.

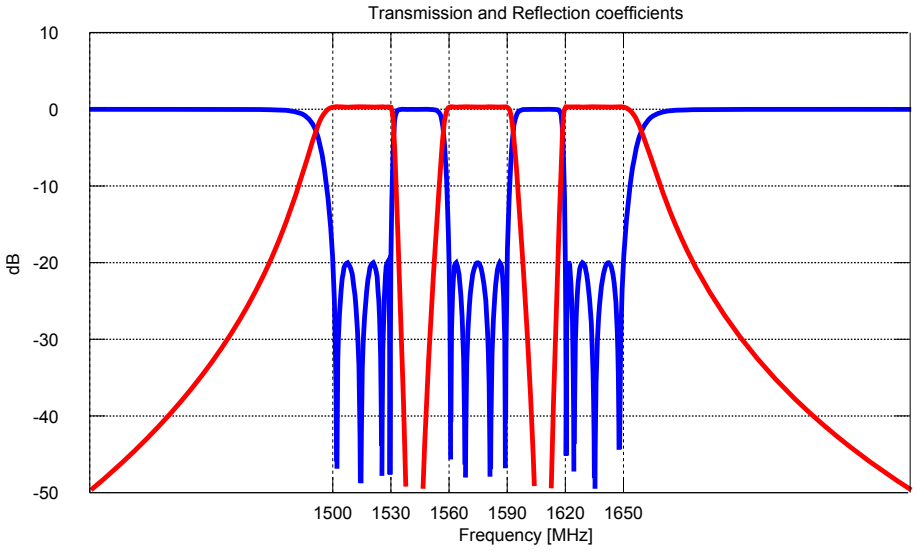

Figure 6.24: The frequency response of the three-band filter designed in example 1 section 6.2.5 is shown above.

k_0	0.152329535995434
k_1	0.052138540526214
k_2	0.008927564217322
ω_1	0.850092969478293854
ω_2	0.746364576127833
k_∞	1.568627450980393

Table 6.8: Frequency transformation constants of the multi-band Foster topology for design example 2. Refer to equation 6.7 for a formal definition.

- Passband 2: 6.0 GHz to 6.1 GHz.
- Passband 3: 7.0 GHz to 8.0 GHz.

Each of the passbands are fourth-order and have a minimum return loss figure of 20 dB. We shall use the same single-band base filter used in example 1. This example only differs from the previous example in that the bandwidth specification is now wideband and that we do not synthesise a coupled resonator circuit as they are inherently narrowband.

Driving point function of frequency transformation subcircuit

The required mapping function was constructed in example 2 in section 4.4.3 and is repeated here for convenience:

$$\Omega'(\Omega) = \frac{-25.5800156128024 94\Omega^6 + 37.2109289617486 50\Omega^4 - 14.6341920374707 29\Omega^2 + 1}{-16.3072599531615 80\Omega^5 + 20.8686963309914 08\Omega^3 - 6.5647150663544 11\Omega}$$

A driving point function for the frequency transformation subcircuit can now be found as follows:

$$H(S) = \frac{25.580015612802494\ S^6 + 37.210928961748650\ S^4 + 14.634192037470729\ S^2 + 1}{16.307259953161580\ S^5 + 20.868696330991408\ S^3 + 6.564715066354411\ S} \tag{6.17}$$

The driving point function can now be used to synthesise various frequency transformation subcircuits that can all in turn be used to transform the a single-band prototype circuit into a multi-band filter. We shall now synthesise multiple possible frequency transformation subcircuits using equation 6.17.

Multi-band filter in Foster topology

The driving point function in equation 6.17 can be expressed in the Foster form as depicted in equation 6.7. The associated frequency transformation constants are listed in table 6.8. We can now obtain frequency transformation subcircuits for capacitors and inductors by applying the constants in table 6.8 to the general frequency transformation subcircuits depicted in figure 6.13. The frequency transformation subcircuits are now applied to the single-band prototype in figure 6.18 to obtain the three-band filter in figure 6.19. The frequency response of the multi-band filter is provided in figure 6.26 (lumped element circuit).

We shall next design a multi-band filter using a Cauer I topology for the frequency transformation subcircuits.

k_0	1.568627450980393
k_1	3.643495009630535
k_2	0.883078013402952
k_3	2.884749817607770
k_4	48.174473617369280
k_5	0.036470239116107

Table 6.9: Frequency transformation constants of the multi-band Cauer I topology for design example 2. Refer to equation 6.8 for a formal definition.

Multi-band filter in Cauer I topology

The driving point function in equation 6.17 can be expressed in the Cauer I form as depicted in equation 6.8. The associated frequency transformation constants are listed in table 6.9. We can now obtain frequency transformation subcircuits for capacitors and inductors by applying the constants in table 6.9 to the general frequency transformation subcircuits depicted in figure 6.14. The frequency transformation subcircuits are now applied to the single-band prototype in figure 6.18 to obtain the three-band filter in figure 6.20. The frequency response of the multi-band filter is provided in figure 6.26 (lumped element circuit).

We shall now design a multi-band filter using a Cauer II topology for the frequency transformation subcircuits.

Multi-band filter in Cauer II topology

The driving point function in equation 6.17 can be expressed in the Cauer II form as depicted in equation 6.9. The associated frequency transformation constants are listed in table 6.10. We can now obtain frequency transformation subcircuits for capacitors and inductors by applying the constants in table 6.10 to the general frequency transformation subcircuits depicted in figure 6.15. The frequency transformation subcircuits are now applied to the single-band prototype in figure 6.18 to obtain the three-band filter in figure 6.21. The frequency response of the multi-band filter is provided in figure 6.26 (lumped element circuit).

We shall now design a multi-band filter using a mixed Cauer I & II topology for the frequency transformation subcircuits.

Multi-band filter in mixed Cauer I and II topology

The driving point function in equation 6.17 can be expressed in the mixed Cauer I & II form as depicted in equation 6.10. The associated frequency transformation constants are listed in table 6.11. We can now obtain frequency transformation subcircuits for capacitors and inductors by applying the constants in table 6.11 to the general frequency transformation subcircuits depicted in figure 6.16. The frequency transformation subcircuits are now applied to the single-band prototype in figure 6.18 to obtain the three-band filter in figure 6.22. The frequency response of the multi-band filter is provided in figure 6.26 (lumped element circuit).

In the next design example we illustrate the synthesis of a multi-band transmission line filter.

k_0	0.152329535995434
k_1	0.573073635769741
k_2	11.838200956310740
k_3	0.063589556043218
k_4	7.108978895920826 10^2
k_5	8.368081870407431 10^{-4}

Table 6.10: Frequency transformation constants of the multi-band Cauer II topology for design example 2. Refer to equation 6.9for a formal definition.

k_0	1.568627450980393
k_1	0.152329535995434
k_2	8.187848268689860
k_3	5.670573641211719
k_4	20.739888881369968
k_5	12.055468786713536

Table 6.11: Frequency transformation constants of the multi-band mixed Cauer I and II topology for design example 2. Refer to equation 6.10 for a formal definition.

Example 3: Three-band wideband transmission line filter

In this design example we design a three-band wideband filter that has the same bandwidth specification as the filter designed in example 2. We also use the same single-band base filter used in example 2. The difference between the two examples is that the filter designed in example 2 was a lumped element filter whereas the filter designed in this example is a transmission line filter. For transmission line filters one must adapt the normalisation function in equation 4.11 to incorporate Richard's transformation. The required mapping function was constructed in example 3 in section 4.4.3 and is repeated here for convenience:

$$H(S) = \frac{50.756695301874259\ S^6 + 63.057781197189911\ S^4 + 20.330473374962409\ S^2 + 1}{31.958231793586798\ S^5 + 33.460997183899671\ S^3 + 8.532152869959482\ S} \tag{6.18}$$

In this example we shall only synthesise a multi-band filter using the Cauer I topology. Note that there are many other synthesis possibilities.

Multi-band transmission line filter in Cauer I topology

The driving point function in equation 6.18 can be expressed in the Cauer I form as depicted in equation 6.8. The associated frequency transformation constants are listed in table 6.12. We can now obtain frequency transformation subcircuits for capacitors and inductors by applying the constants in table 6.12 to the general frequency transformation subcircuits depicted in figure 6.14. The frequency transformation subcircuits are now applied to the single-band prototype in figure 6.18 to obtain a three-band lumped element filter. Richard's

k_0	1.588219762272950
k_1	3.223427255126425
k_2	0.854123690799646
k_3	5.169910456128771
k_4	16.174251267168689
k_5	0.138815158704289

Table 6.12: Frequency transformation constants of the multi-band Cauer I topology for design example 3. Refer to equation 6.8 for a formal definition.

transformation can then be applied to the lumped element network to obtain a transmission line circuit [2]. In this example all transmission line sections have an electrical length of 45 degrees at 8000 MHz. We approximate inductors using short-circuited transmission lines where the characteristic impedance of the transmission line is equal to the inductance of the inductor. Likewise we approximate capacitors using open-circuited transmission lines where the characteristic admittance of the transmission line is equal to the capacitance of the capacitor. The final filter circuit is shown in figure 6.25 and its frequency response is provided in figure 6.26.

6.3 Summary

This chapter considered the synthesis of multi-band filters using rational mapping functions. The theory presented in this chapter is a continuation of the theory presented in chapter 4 that dealt with the approximation of multi-band transfer functions using rational mapping functions. In this chapter the rational mapping function was considered to be the driving point function of a unit reactance or susceptance in a multi-band circuit. The driving point function was then synthesised to obtain normalised lumped element circuits of multi-band reactances and susceptances. These circuits are said to be frequency transformation subcircuits and scaled versions of them can be substituted into single-band prototype filter circuits in order to obtain multi-band filter circuits. In chapter 4 we presented two formulations of the theory - one applicable to narrowband coupled resonator filters and one that is general and applicable to all filters. In this chapter we again considered these two cases separately. The design of a three-band filter was used as a design example throughout this chapter and both of the presented methods were clarified using this example. A coupled resonator version of the three-band filter was realised using coaxial resonators and the realisation and manufacturing of the filter is covered in chapter 10. For the general rational mapping function case we also included examples of the synthesis of wideband filters to highlight the capabilities of the design method.

It must be stated that the design method presented in section 6.1 for narrowband multi-band filters is merely a special case of the method presented in section 6.2 for general multi-band filters and that any design can be performed using the method in section 6.2. The narrowband formulation has the advantage that it employs lower order polynomials and smaller matrices and would therefore be less sensitive to numerical accuracy issues. That being said, the general formulation is superior as it encompasses the narrowband case and can be used to design filters that are valid at all frequencies.

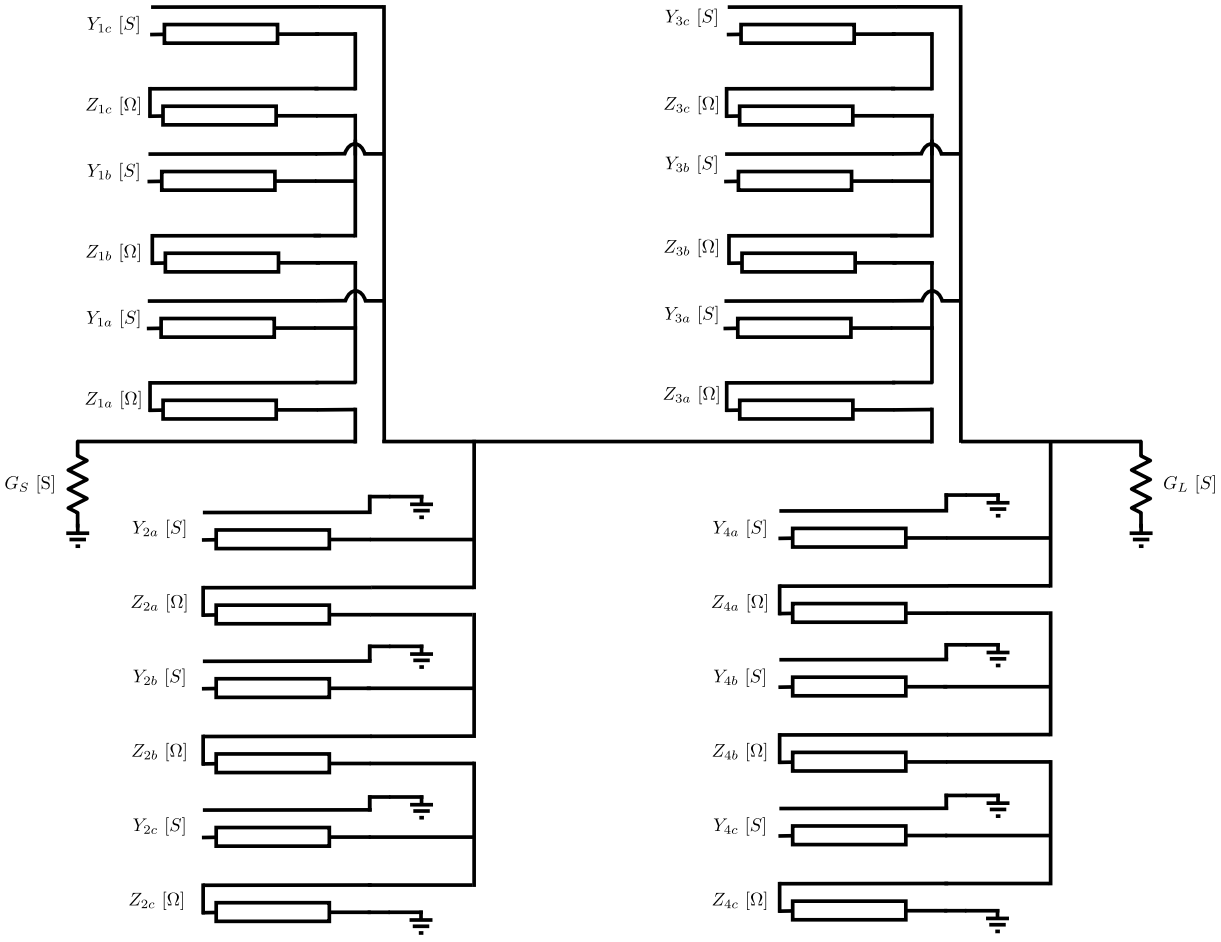

Figure 6.25: The single-band prototype in figure 6.18 was transformed into a three-band transmission line filter using Cauer I expansions (impedance and admittance) of the frequency transformation driving point function in equation 6.18. The expansions are defined in figure 6.14 and the frequency transformation constants are listed in table 6.12. The normalisation factors have the following values: $R_0 = 50\ \Omega$, $G_0 = 0.02$ S and $\omega_c = 2\pi f_c$ where $f_c = 8.0$ GHz. The Richard's transformation was then applied to obtain a transmission line circuit. The obtained three-band filter is shown above and its frequency response is provided in figure 6.26.

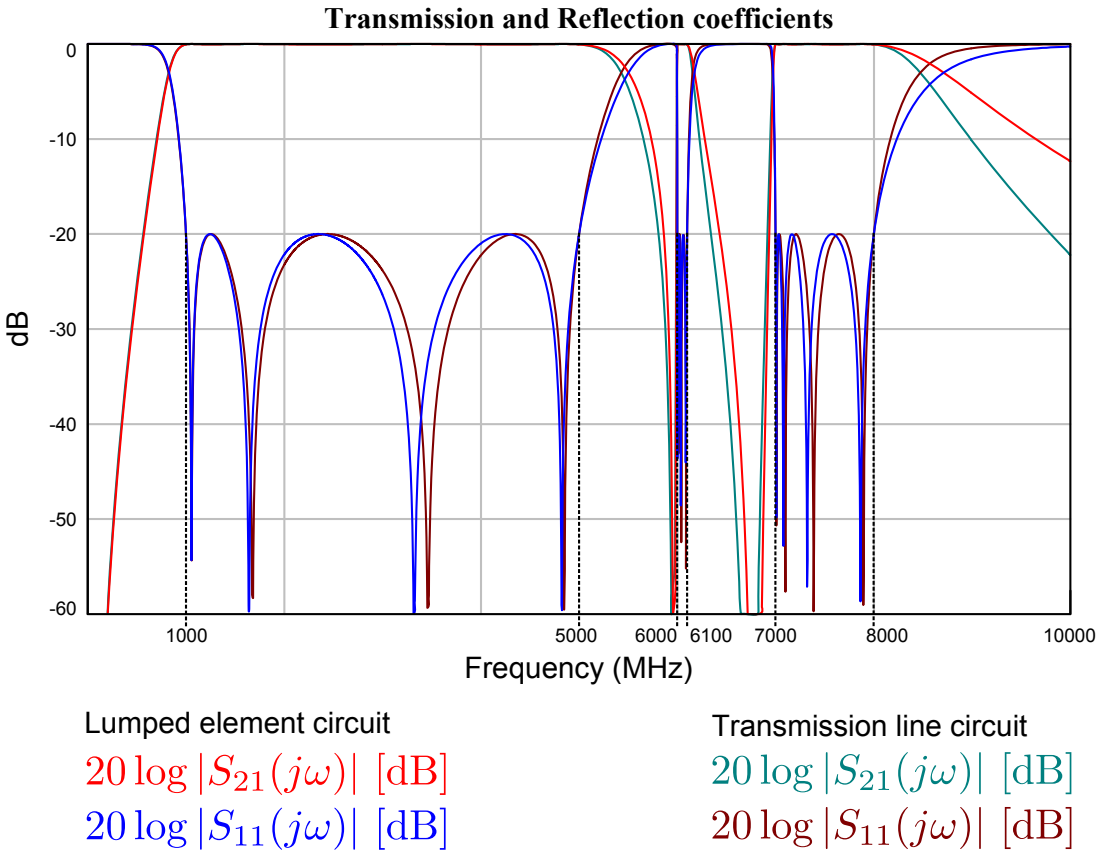

Figure 6.26: The frequency responses of the three-band filters designed in examples 2 and 3 are compared above. Multiple lumped element filters are designed in example 2 and a single transmission line filter is designed in example 3.

Part III

Realisation and practical verification

Chapter 7

Realisation techniques

This chapter serves as a summary of well-known and important theory on the realisation of coupled resonator circuits as distributed structures [9, 61, 77, 6, 78, 79, 10]. The chapter does not contain original contributions. The theory is presented in great detail as it is used extensively in chapters 8, 9 and 10 to design the practical filters.

This chapter deals with the physical realisation of coupled resonator circuits. In part I we presented techniques to construct transfer functions from design specifications. These functions are defined by a set of characteristic polynomials. In chapter 5 we presented two synthesis techniques that can be used to obtain coupling matrices from the characteristic polynomials. These matrices describe prototype circuits. We start this chapter by illustrating how a coupled resonator prototype circuit can be mapped from the prototype frequency domain to the actual frequency domain. The circuits in the actual frequency domain consist of ideal lumped elements. Filters are rarely constructed at microwave frequencies using lumped elements. We then show how coupled resonator theory can be generalised to use arbitrary resonators. The use of arbitrary resonators becomes important when one tries to design filters that operate at microwave frequencies. We then introduce the stepped impedance resonator (SIR). We present standard realisation techniques for both all-pole filters and cascaded triplet filters using stepped impedance resonators. Cross-couplings are introduced using delay lines. The design techniques result in filters that are defined in terms of transmission line parameters such as characteristic impedance and electrical length. We also discuss how the physical dimensions of transmission lines can be obtained from their electrical parameters. We then present tuning techniques for electromagnetic filters. These techniques can be used to fine tune the initial dimensions of electromagnetic filters in order to meet the design specifications. We conclude the chapter with a summary of the presented theory.

7.1 Denormalisation of coupled resonator circuits

Circuits in the prototype domain are normalised with respect to impedance, bandwidth and frequency. A circuit must be denormalised in order to operate in the actual frequency domain. This entails impedance scaling to ensure that the circuit is matched at its ports as well as frequency scaling to correct its bandwidth and centre frequency. The denormalisation procedure is graphically illustrated in figures 7.2 and 7.3. The procedure is performed systematically. For each step in the denormalisation procedure, both the impedance and admittance circuits together with the associated frequency response are shown. It is assumed that the filtering function is an equal ripple function. Consequently the bandwidth indicated here is the ripple bandwidth. The ripple level is indicated as L_r [dB]. Naturally the inverters in the impedance circuits are impedance inverters and those in the admittance circuits are admittance inverters. A third order filter with no cross-couplings is used to

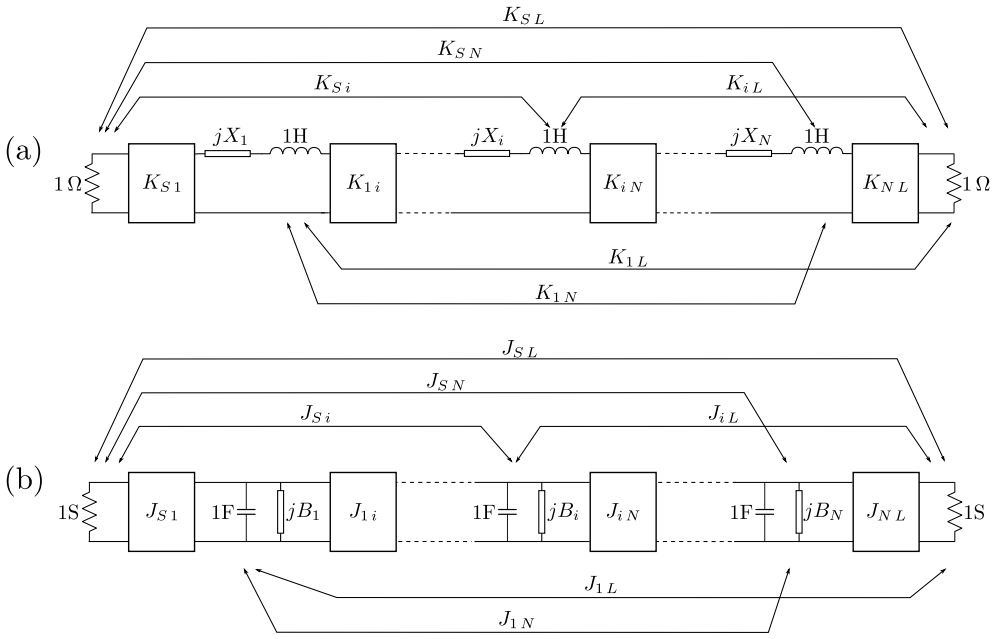

Figure 7.1: The two prototype circuits that are associated with any coupling matrix are shown above. The circuit in (a) is an impedance circuit consisting of series resonators and impedance inverters. The circuit in (b) is an admittance circuit consisting of shunt resonators and admittance inverters. Note that FIR elements are included in both circuits to accommodate asymmetric frequency responses.

illustrate the procedure. The illustrated procedure is however completely general as FIR elements are included and cross-couplings are scaled in exactly the same manner as their mainline counterparts.

The procedure starts with the general prototype circuits that were defined in figure 7.1. These are shown in figure 7.2 (a). Note that all the frequency dependent reactive elements are unity and the main diagonal entries of the coupling matrix is used to identify the values of the FIR elements. Also all the entries in the coupling matrix that are not on the main diagonal are precisely equal to the immittance inverter values. The presence of the FIR elements enables this circuit to accommodate asymmetric frequency responses. To illustrate this we defined the passband edges as Ω_a and Ω_b. The first step in the denormalisation procedure is bandwidth scaling. The bandwidth of the circuit is scaled by dividing all the frequency dependent elements with the fractional bandwidth Δ. This corresponds to the traditional approach found in the literature [2]. The resulting circuits with their associated frequency response are shown in figure 7.2 (b).

The next step is impedance scaling of the network. We scale the source of the impedance network with the factor Z_S and the source of the admittance network with the factor Y_S. We then include $\sqrt{Z_S}$ and $\sqrt{Y_S}$ in the expressions for the input and output immittance inverters to ensure that the circuit remains matched. We perform a similar operation at the load of the circuit. We then scale the direct source-load coupling in the impedance network with $\sqrt{Z_L Z_S}$ and in the admittance network with $\sqrt{Y_L Y_S}$ for similar reasons. The scaling factors that we have introduced enable us to design circuits that can operate under any port condition. Next we scale the impedance level of the entire network with the factor Δ. This is achieved by multiplying all the inner-inverter values, all the reactive elements and the port terminations with Δ. The port terminations are then scaled back to Z_S and Y_S by including $\sqrt{\Delta}$ in the expressions for the input and output immittance inverters. The direct source-load coupling is however not scaled with Δ. This is because the inverter is connected between two real elements. The impedance scaling with Δ is performed to force the frequency variant reactive

elements back to unity. This condition is required to ensure that a symmetric prototype circuit has a cutoff frequency of 1 rad/s. The effect of the impedance scaling procedure is illustrated in figure 7.2 (c).

The circuit in figure 7.2 (c) is still operates in the prototype frequency domain. The final step in the denormalisation procedure is to map the subcircuits between the inverters from the prototype frequency domain to the actual frequency domain. The procedure illustrated in figure 5.1 can be used to achieve this. The combination of a FIR element and a frequency dependent reactive element in the prototype domain is mapped to a resonator in the actual frequency domain. The circuits with their associated frequency response are shown in figure 7.3. For convenience we included the associated mapping formulas. Note that the circuit in figure 7.3 is the final denormalised circuit. Lumped element equivalent circuits for the immittance inverters are included in appendix B. This circuit can therefore entirely be fabricated using lumped elements. In the next section we discuss the limitations of lumped elements with respect to high frequency design.

7.2 Limitations of lumped elements

The circuits in section 7.1 consist entirely of lumped elements. Lumped element circuit theory does not take into consideration the propagation effects of electromagnetic waves. This is because one assumes that the physical dimensions of a circuit are negligible when compared to the shortest wavelength of the signals propagating through it. A result of this assumption is that the electrical parameters describing the lumped element circuits are governed by a set of simple and elegant equations. Lumped element circuit theory is not valid at microwave frequencies as the wavelengths become comparable to the dimensions of the circuit. There are two ways to construct circuits that can operate at microwave frequencies:

1. Construct lumped elements with dimensions that are insignificant when compared to a wavelength at the operating frequency. This approach is often followed when filters are designed using multi-layer technology such as LTCC [80].

2. Construct circuits using distributed elements. A common distributed element is the TEM transmission line. Using Richards' transform, one can approximate capacitors and inductors at microwave frequencies using TEM transmission lines. TEM propagation is only possible when there are two conductors. It is however possible to construct filters using waveguides - these structures consist of a single conductor. The design of waveguide filters is possible because waveguides can accommodate various other modes of propagation that can be exploited.

In this dissertation we shall only consider the design of coupled resonator circuits using TEM transmission line sections. A problem that is common to all distributed structures is that impedance is a periodic function of frequency. A transfer function can therefore only be approximated over a finite bandwidth. Lumped elements do not have this problem. The equations that describe the immittance inverters and the resonators in the circuits in section 7.1 are only applicable to the design of lumped element circuits. In the next section we shall generalise these equations so that they can be used to design coupled resonator circuits using distributed structures.

7.3 Coupled resonator circuits with arbitrary resonators

The goal of this section is to generalise the equations in figure 7.3 to enable us to design coupled resonator circuits that employ arbitrary resonators. We shall later use the general formulas to design microwave filters

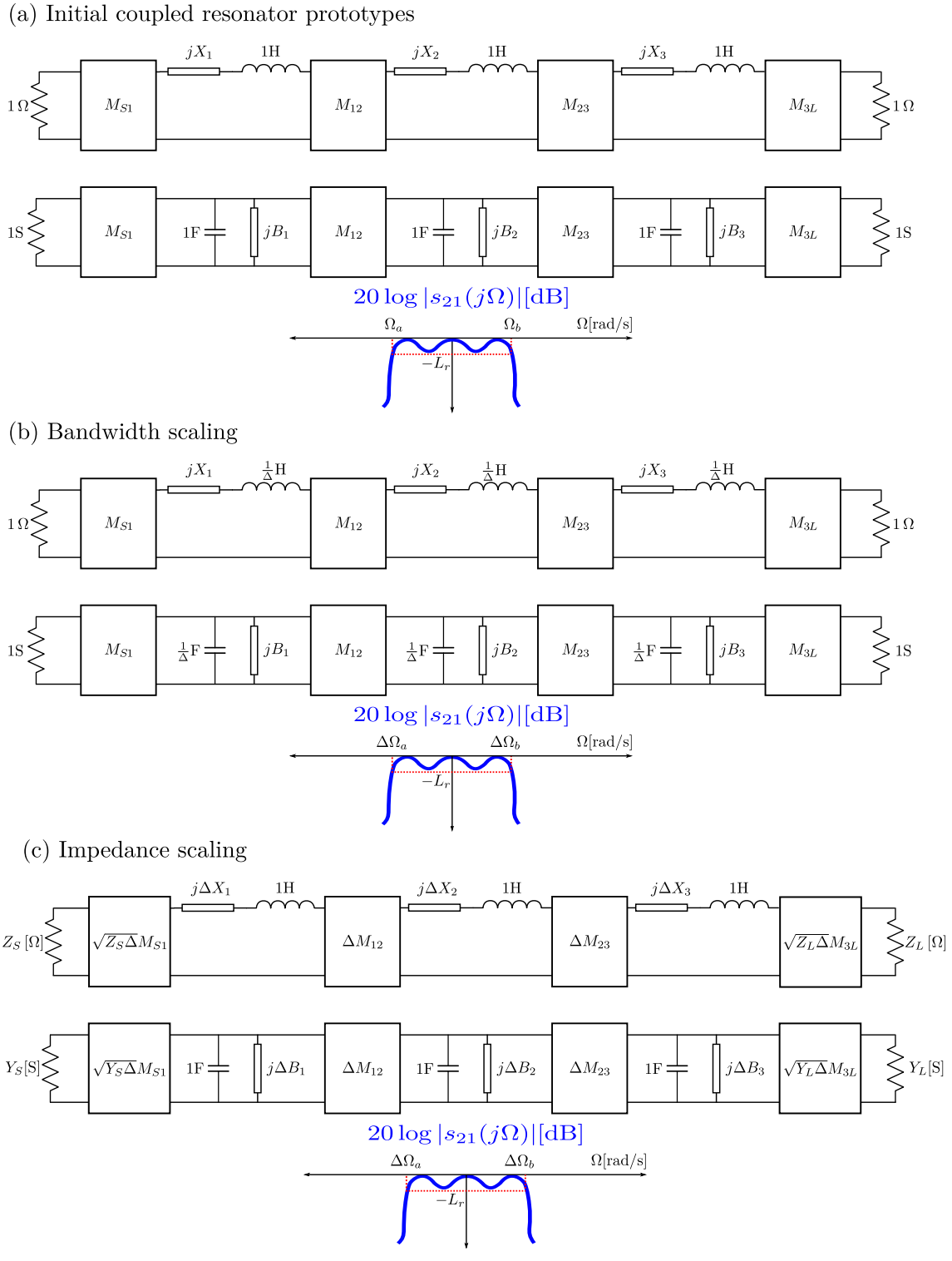

Figure 7.2: An initial coupled resonator prototype with its frequency response is shown in (a). The prototype after bandwidth scaling is shown in (b). The prototype after impedance scaling is shown in (c).

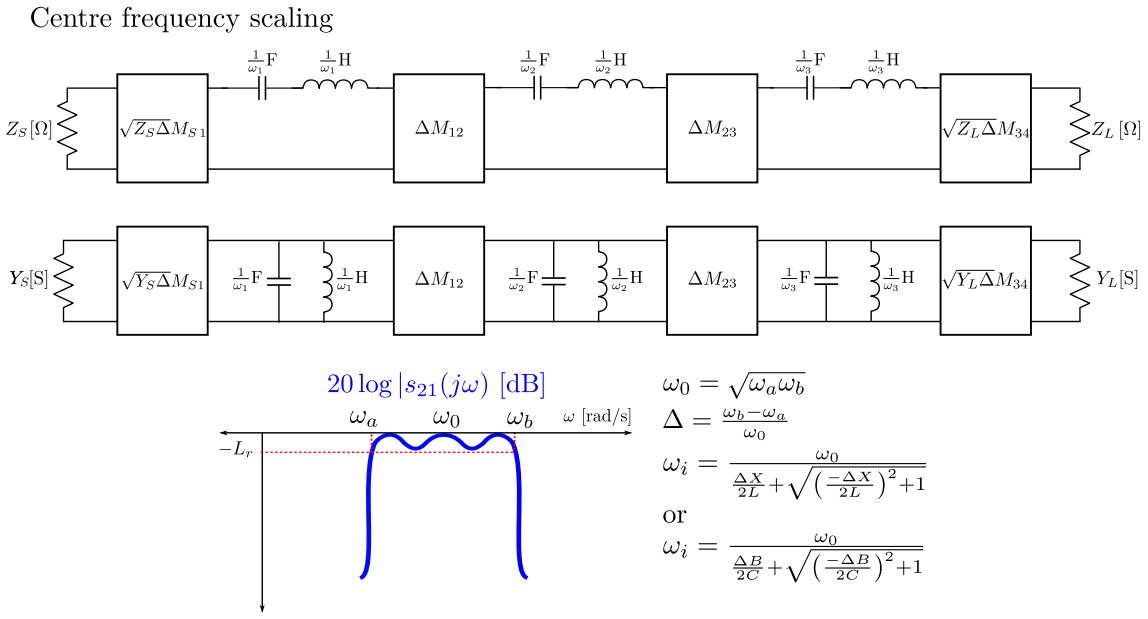

Figure 7.3: The reactive elements in the circuits in figure 7.2 (c) are mapped to resonators in the actual frequency domain using the techniques provided in figure 5.1. The formulas to perform the mapping are repeated here for convenience.

that use transmission line resonators. This generalisation is plausible as it is generally accepted that the filter constants, that define any narrowband filter, can always be reduced to three fundamental types: centre frequencies, coupling values and quality factors [77]. This is true irrespective of whether the filter under consideration is a low frequency lumped element filter or a high frequency distributed filter. The first step in the generalisation procedure is to relate a lumped element resonator to an arbitrary resonator. The relationship is then used to find expressions for the immittance inverters that define the couplings between the different nodes. In this section we shall derive the equations in terms of impedance inverters and series resonators. From the notion of electrical duality, these derivations are also applicable to shunt networks.

7.3.1 Equivalence of resonators

Figure 7.4 (a) is a lumped element series resonator. Figure 7.4 (b) is an arbitrary resonator exhibiting a series type resonance. The centre frequencies of both resonators is assumed to be $\omega_i = \frac{1}{\sqrt{L_i C_i}}$. We shall now find a relationship between the two resonators using Taylor polynomials. Any real or complex valued function, that is k times differentiable in the vicinity of a point x_0, can be approximated by a k-th order Taylor polynomial around x_0 as follows [81]:

$$T(x) = \sum_{n=0}^{k} \frac{f^{(n)}(x_0)}{n!}(x - x_0)^n \tag{7.1}$$

When a function is infinitely differentiable in the vicinity of x_0, equation 7.1 generalises to the well-known Taylor series. The input impedance of the lumped element resonator in figure 7.4 (a) can be expressed as follows:

$$\begin{aligned} Z_{LCi}(j\omega) &= 0 + jX_{LCi}(\omega) \\ &= j\left(\omega L_i - \frac{1}{\omega C_i}\right) \end{aligned} \tag{7.2}$$

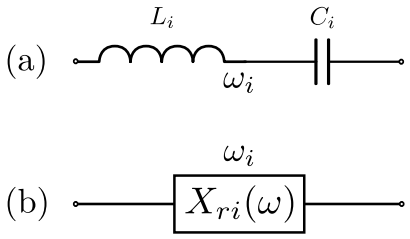

Figure 7.4: A lumped element series resonator is shown in (a). An arbitrary distributed resonator is shown in (b). Both resonators have a centre frequency of ω_i.

We can approximate the reactance function in equation 7.2 using a first order Taylor polynomial as follows:

$$\begin{aligned} X_{LCi}(\omega) &\approx X_{LCi}(\omega_i) + \frac{\mathrm{d}}{\mathrm{d}\omega} X_{LCi}(\omega)\bigg|_{\omega=\omega_i} (\omega - \omega_i) \\ &= 0 \; + \; \frac{\mathrm{d}}{\mathrm{d}\omega} X_{LCi}(\omega)\bigg|_{\omega=\omega_i} (\omega - \omega_i) \end{aligned} \tag{7.3}$$

The simplification in equation 7.3 is possible because we know that the reactance function evaluates to zero at the resonant frequency. Using equation 7.2, and the fact that $\omega_i = \frac{1}{\sqrt{L_i C_i}}$, we can factorise equation 7.3 as follows:

$$\begin{aligned} X_{LCi}(\omega) &= \left(L_i + \frac{1}{\omega_i^2 C_i} \right) (\omega - \omega_i) \\ &= 2L_i \, (\omega - \omega_i) \end{aligned} \tag{7.4}$$

We can now also approximate the input reactance of the arbitrary resonator in figure 7.4(b) using a first order Taylor polynomial. The expression is as follows:

$$\begin{aligned} X_{ri}(\omega) &\approx X_{ri}(\omega_i) + \frac{\mathrm{d}}{\mathrm{d}\omega} X_{ri}(\omega)\bigg|_{\omega=\omega_i} (\omega - \omega_i) \\ &= 0 + \frac{\mathrm{d}}{\mathrm{d}\omega} X_{ri}(\omega)\bigg|_{\omega=\omega_i} (\omega - \omega_i) \end{aligned} \tag{7.5}$$

If we compare equations 7.3 and 7.5, it is clear that resonator (b) in figure 7.4 would approximate resonator (a) in figure 7.4 if the following condition holds:

$$L_i = \frac{1}{2} \frac{\mathrm{d}}{\mathrm{d}\omega} X_{ri}(\omega)\bigg|_{\omega=\omega_i} \tag{7.6}$$

We shall now use the equivalence condition in equation 7.6 to calculate expressions for the impedance inverter values that model the couplings between resonant nodes.

7.3.2 Coupling between resonant nodes

Figure 7.5 (a) shows two lumped element series resonators that are coupled through an impedance inverter. Figure 7.5 (b) shows two arbitrary series resonators that are also coupled through an impedance inverter. We want to find an expression for the impedance inverter in figure 7.5 (b) when we impose the resonator equivalence condition given in equation 7.6. Under these conditions the coupled resonator circuits would be equal. In a coupled resonator prototype circuit the different resonant loops are coupled to each other through mutual inductance. The current in each loop is dependent on the self inductance of the loop and on the mutual inductances between the specific loop and the other loops in the network. The coupling coefficient between

two loops is a scalar quantity defined in terms of the self inductance of each loop and the mutual inductance between the two loops. Figure B.2 (a) contains an illustration of two coupled loops and also the definition of the coupling coefficient. When a coupling matrix is synthesised from the characteristic polynomials, the total self inductance in each loop is assumed to be 1H. The effect is that the coupling coefficient between two loops is equal to the mutual inductance between those loops evaluated at the centre frequency of the filter. Using the equation in figure B.2, the normalised coupling coefficient is calculated as:

$$k_{n\,ij} = \frac{M_{ij}}{\sqrt{L_i L_j}} = M_{ij} \tag{7.7}$$

Here M_{ij} is an entry in the coupling matrix. The coupling matrix entries are therefore considered to be normalised coupling coefficients. Due to impedance and bandwidth scaling, as discussed in section 7.1, the denormalised coupling coefficient is given as $k_{ij} = \Delta k_{n\,ij}$. Using the formula in figure B.3 (b), the value of the inverter in figure 7.5 (b) can be calculated as follows:

$$\begin{aligned} K_{ij} &= \omega M \\ &= \omega\sqrt{L_i L_j}k_{ij} \\ &= \omega\sqrt{L_i L_j}\Delta k_{n\,ij} \\ &= \omega\sqrt{L_i L_j}\Delta M_{ij} \end{aligned} \tag{7.8}$$

We can now force the resonators to become equivalent by substituting equation 7.6 into equation 7.8:

$$\begin{aligned} K_{ij} &= \omega\sqrt{\frac{1}{2}\frac{\mathrm{d}}{\mathrm{d}\omega}X_{ri}(\omega)\bigg|_{\omega=\omega_i}\frac{1}{2}\frac{\mathrm{d}}{\mathrm{d}\omega}X_{rj}(\omega)\bigg|_{\omega=\omega_j}}\Delta M_{ij} \\ &= \sqrt{\frac{\omega_i}{2}\frac{\mathrm{d}}{\mathrm{d}\omega}X_{ri}(\omega)\bigg|_{\omega=\omega_i}\frac{\omega_j}{2}\frac{\mathrm{d}}{\mathrm{d}\omega}X_{rj}(\omega)\bigg|_{\omega=\omega_j}}\Delta M_{ij} \\ &= \sqrt{x_i x_j}\ \Delta M_{ij} \end{aligned} \tag{7.9}$$

Equation 7.9 is the general expression for the impedance inverter between two arbitrary series resonators. Here x_i is die reactance slope of a resonator with a resonant frequency of ω_i. Through the concept of duality, shunt resonators have a similar parameter b that is referred to as the susceptance slope. Matthaei defines the reactance and susceptance slopes as follows [9]:

$$x_i = \frac{\omega_i}{2}\frac{\mathrm{d}}{\mathrm{d}\omega}X_{ri}(\omega)\bigg|_{\omega=\omega_i} \tag{7.10}$$

$$b_i = \frac{\omega_i}{2}\frac{\mathrm{d}}{\mathrm{d}\omega}B_{ri}(\omega)\bigg|_{\omega=\omega_i} \tag{7.11}$$

From our derivation process it is clear that two series resonators are considered equivalent if they have the same resonant frequency and the same reactance slope. Similarly two shunt resonators are equivalent if they have the same resonant frequency and the same susceptance slope. It can be shown using a similar derivation technique that the admittance inverter between two arbitrary shunt resonators is given as follows [9]:

$$J_{ij} = \sqrt{b_i b_j}\ \Delta M_{ij}$$

We are now able to calculate the values of the immittance parameters between arbitrary resonators. Next we shall calculate the coupling between resonant and non-resonant nodes.

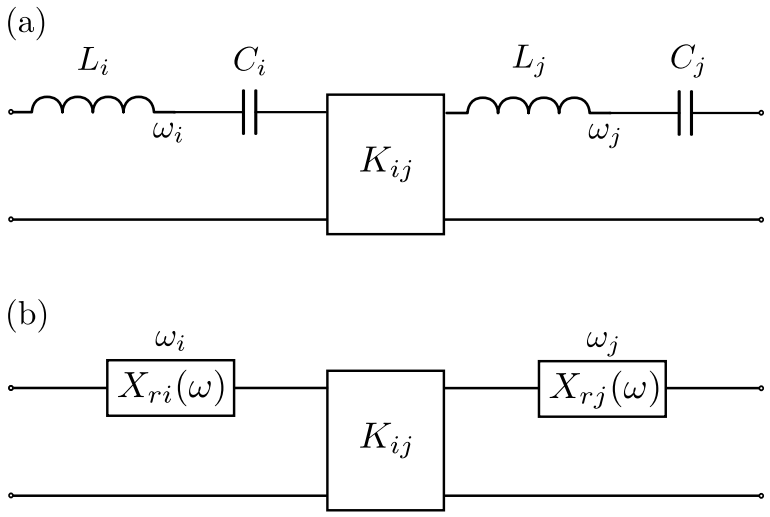

Figure 7.5: Two lumped element series resonators that are coupled with an impedance inverter is shown in (a). Two arbitrary series resonators that are coupled with an impedance inverter is shown in (b).

7.3.3 Coupling between a resonant node and a non-resonant node

The values of the immittance inverters that model the coupling between resonant and non-resonant nodes can be calculated using the concept of a quality factor. The quality factor is a measure of loss inside a resonator. When a resonator is not connected to any load, its quality factor is referred to as an unloaded quality factor and is defined as follows [2]:

$$Q_u = \omega \frac{\text{average energy stored per second}}{\text{energy dissipated per second}}$$

For lossless resonators the quality factor would be infinite. The coupling matrix synthesis technique assumes lossless resonators and therefore the unloaded quality factor of each resonator is assumed infinite. When a load is coupled to a resonator, i.e. coupling between a resonant and a non-resonant node, the coupling implies that the resonator has a finite resistance/conductance and therefore a finite quality factor. The quality factor under loaded conditions is referred to as the loaded quality factor and is indicated as Q_L. This factor is always lower than the unloaded quality factor. The relationship between a loaded and an unloaded quality factor is as follows [2]:

$$\frac{1}{Q_L} = \frac{1}{Q_U} + \frac{1}{Q_e}$$

Here Q_e is referred to as the external quality factor and is a numerical value that represents the loading effect of the external circuit on the resonator. Matthaei reports that the external quality factor is related to the reactance and susceptance slopes as follows [9]:

$$\text{Series resonator:} \quad Q_e = \tfrac{x}{R}$$

$$\text{Shunt resonator:} \quad Q_e = \tfrac{b}{G}$$

Here R is the loading resistance of a coupling on a resonator. Similarly G is the loading conductance. Note that these values are only finite if the coupling is between a resonant node and a non-resonant node. These are the couplings between the source/load terminations and other resonators. Figure 7.6 (a) illustrates the coupling between a source and a series lumped element resonator. Figure 7.6 (b) illustrates the coupling between a source and an arbitrary series resonator. Our goal is to find an expression for the impedance inverter in

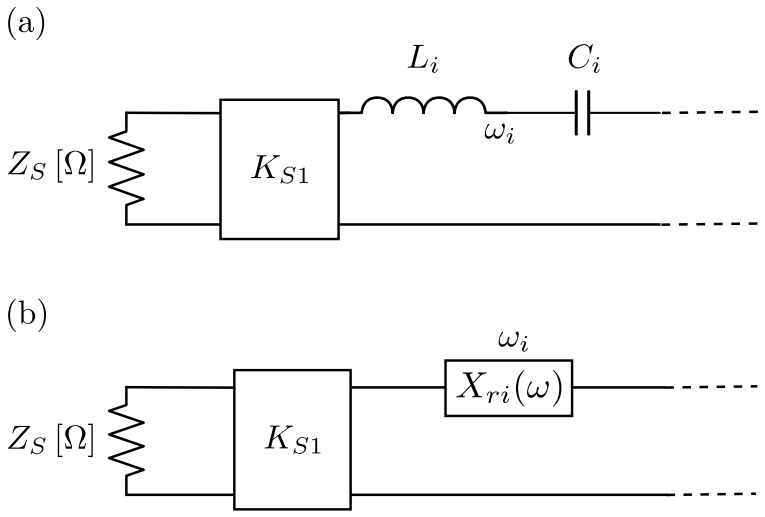

Figure 7.6: A real impedance is coupled to a lumped element series resonator in (a). A real impedance is coupled to an arbitrary series resonator in (b).

figure 7.6 (b). Note that the equations for coupling between the source and a resonator would the same as the equations for the coupling between the load and a resonator. The two circuits in figure 7.6 are equivalent if the resonators are equivalent and if their coupling circuits are equivalent. If we assume that the resonators are equivalent, the coupling circuits would be equivalent if they had the same external quality factors. The external quality factor for the circuit in 7.6 (a) can be calculated using the values in figure 7.3 as follows:

$$\begin{aligned} Q_e &= \frac{x}{R} \\ &= \frac{\omega_1 L_1}{(\sqrt{Z_S \Delta} M_{S1})^2 / Z_s} \\ &= \frac{\sqrt{\frac{1/\omega_1}{1/\omega_1}}}{M_{S1}^2 \Delta} \\ &= \frac{1}{M_{S1}^2 \Delta} \end{aligned}$$

By equating the external quality factors, we can find an expression for the impedance inverter value in figure 7.6 (b) as follows:

$$\begin{aligned} K_{S1} &= \sqrt{\frac{x}{Q_e}} \\ &= \sqrt{x Z_S \Delta} M_{S1} \end{aligned}$$

Using a similar derivation, we can find an expression the admittance inverter for a shunt resonator case as follows:

$$\begin{aligned} J_{S1} &= \sqrt{\frac{b}{Q_e}} \\ &= \sqrt{b Y_S \Delta} M_{S1} \end{aligned}$$

We now have expressions to calculate all the admittance and impedance inverters associated with the general circuits in figure 7.7. It was not necessary to alter the formula for the direct source-load coupling as it is not influenced by the type of resonator used in the circuit. The design formulas for the circuits in figure 7.7 are summarised in table 7.1.

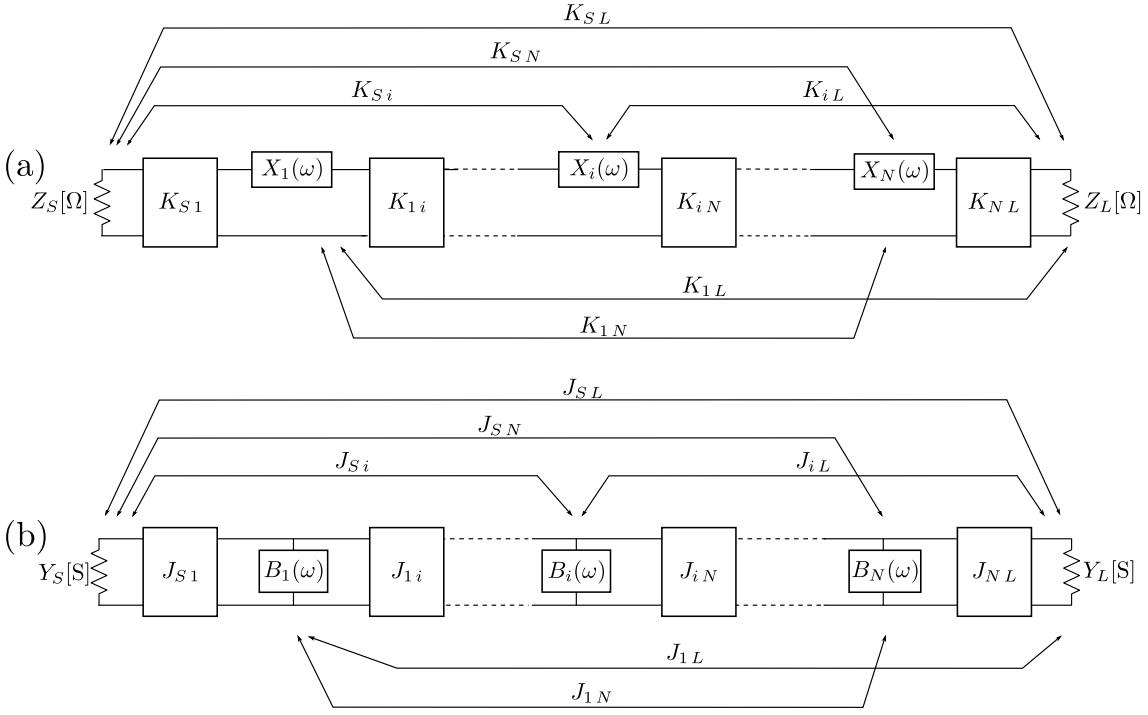

Figure 7.7: The impedance and admittance forms of a coupled resonator circuit that employs arbitrary resonators is shown above. The impedance circuit is shown in (a) and the admittance circuit is shown in (b).

Impedance circuit	Admittance circuit
$x_i = \frac{\omega_i}{2}\ \frac{\mathrm{d}}{\mathrm{d}\omega} X_i(\omega)\big\vert_{\omega=\omega_i}$	$b_i = \frac{\omega_i}{2}\ \frac{\mathrm{d}}{\mathrm{d}\omega} B_i(\omega)\big\vert_{\omega=\omega_i}$
$K_{Si} = \sqrt{x_i Z_S \Delta} M_{Si} \quad i \in [1, N]$	$J_{Si} = \sqrt{b_i Y_S \Delta} M_{Si} \quad i \in [1, N]$
$K_{ij} = \sqrt{x_i x_j}\ \Delta M_{ij} \quad i, j \in [1, N]$	$J_{ij} = \sqrt{b_i b_j}\ \Delta M_{ij} \quad i, j \in [1, N]$
$K_{iL} = \sqrt{x_i Z_L \Delta} M_{iL} \quad i \in [1, N]$	$J_{iL} = \sqrt{b_i Y_L \Delta} M_{iL} \quad i \in [1, N]$
$K_{SL} = \sqrt{Z_S Z_L} M_{SL}$	$J_{SL} = \sqrt{Y_S Y_L} M_{SL}$

Table 7.1: Design formulas for the circuit in figure 7.7 (a) is listed in the left column. Design formulas for the circuit in figure 7.7 (b) is listed in the right column. Note that M_{ij} is the j-th element in the i-th row of the coupling matrix and that Δ is the fractional bandwidth.

7.4 Coupling between arbitrary resonators

There have been numerous publications on the matter of calculation the coupling between two arbitrary resonators. The initial theory was developed by Dishal [6, 77] and then extensively used by Matthaei et al. [9]. Essentially one can calculate the coupling between two resonators by lightly coupling to the two of them using probes and then measuring the two observable resonant frequencies. The coupling between two identical coupled resonators is calculated as follows:

$$k = \frac{f_{p2}^2 - f_{p1}^2}{f_{p1}^2 + f_{p2}^2} \tag{7.12}$$

This formulation is only valid when the two resonators have the same resonant frequency, i.e. they are synchronously coupled. The method was later extended to accommodate the coupling between two resonators when they have different centre frequencies, i.e. asynchronously tuned. In the general case, the coupling between the two resonators can be calculated as follows [78]:

$$k = \pm\frac{1}{2}\left(\frac{f_{02}}{f_{01}} + \frac{f_{01}}{f_{02}}\right)\sqrt{\left(\frac{f_{p2}^2 - f_{p1}^2}{f_{p1}^2 + f_{p2}^2}\right)^2 - \left(\frac{f_{02}^2 - f_{01}^2}{f_{02}^2 - f_{01}^2}\right)^2} \tag{7.13}$$

Here f_{01} and f_{02} are the known self-resonant frequencies of the resonators. Also f_{p1} and f_{p2} are the observable resonant frequencies of the two coupled resonators. The formula in equation 7.13 can be used in conjunction with an electromagnetic simulator to design the couplings between arbitrary resonators. Note that a designer should ensure that the probes are decoupled to such a degree that their presence do not contribute to a shift in the measured frequencies. The expressions in equations 7.12 and 7.13 were derived by assuming that two arbitrary coupled resonators can be modelled by two coupled second order lumped element circuits (LC resonator circuits). This assumption is quite presumptuous and have been used extensively by researchers over the years. Fortunately Awai provided a theoretical grounding for the theory in 2006 and 2007 [82, 83]. In the next section we introduce the stepped impedance resonator (SIR). We shall later use this type of resonator to design multi-band filters.

7.5 Stepped impedance resonators

Close inspection of the formulas in table 7.1 reveal that it is possible to design a coupled resonator filter using an arbitrary resonator if the following is true:

- It is known whether the structure has a shunt type resonance or a series type resonance.
- It is possible to determine the centre frequency of the resonator.
- The susceptance slope or reactance slope of the resonator can be determined.
- It is possible to couple energy to and from a resonator and it is possible to quantify this coupling using an immittance inverter.

As a consequence, we shall proceed by first presenting the model of a stepped impedance resonator. We shall then determine its resonance condition and calculate its susceptance slope. Lastly we shall investigate how to relate coupling between stepped impedance resonators with immittance inverters. Once all of these topics have been covered, we shall consider the application of stepped impedance resonators to the design of coupled resonator circuits.

7.5.1 The stepped impedance resonator and its resonance condition

A stepped impedance resonator is a resonator where the characteristic admittance varies in discrete steps along the length of the resonator. The stepped impedance resonators considered in this dissertation are physically symmetric and consist of a cascade of three transmission line sections. A transmission line model of a stepped impedance resonator is shown in figure 7.8. The characteristic admittance of both the first and the last sections are Y_2 and the electrical length of both sections are θ_2.

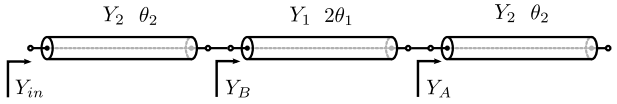

Figure 7.8: Transmission line model of a stepped impedance resonator. The electrical length and the characteristic admittance of the i-th transmission line section is denoted as θ_i and Y_i respectively.

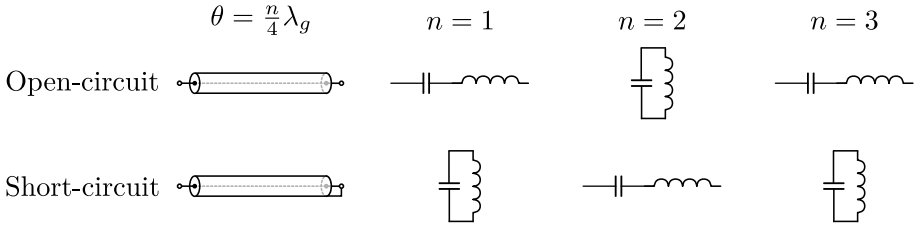

Figure 7.9: A segment of transmission line terminated in an open-circuit or a short-circuit can be modelled as a lumped element resonator. The type of resonance is determined by the electrical length and type of termination.

A length of transmission line that is terminated in either an open-circuit or a short-circuit can be used as a resonator. The transmission line resonator can be modelled as a lumped element resonator when the electrical length of the resonator is $\frac{n}{4}\lambda_g$. Here λ_g is the guided wavelength of a signal on the transmission line at the resonant frequency and n is a natural number. Whether a length of transmission line exhibits a series or a shunt resonance is determined by its terminating condition and by its electrical length. A summary of the applicable resonator models is given in figure 7.9 [9]. The stepped impedance resonator is an open circuited resonator. Our plan is to couple stepped impedance resonators in parallel. We prefer to use longer resonators to ensure that we can achieve strong couplings without requiring the resonators to be too close. We therefore decide on half wavelength resonators. Our stepped impedance resonators therefore exhibit a shunt type resonance. Our next step is to determine an expression for the input admittance of a stepped impedance resonator. We shall then use this expression to determine the condition for its resonance. Consider figure 7.8. Using the well-known input admittance formula for a transmission line, Y_A can be calculated as follows [2]:

$$\begin{aligned} Y_A &= \lim_{Y_L \to 0} \left(Y_2 \frac{Y_L + jY_2 \tan\theta_2}{Y_2 + jY_L \tan\theta_2} \right) \\ &= jY_2 \tan\theta_2 \end{aligned} \tag{7.14}$$

Next we derive an expression for Y_B. We start by remembering the following trigonometric identity [76]:

$$\tan(\theta_1 + \theta_2) = \frac{\tan\theta_1 + \tan\theta_2}{1 - \tan\theta_1 \tan\theta_2} \tag{7.15}$$

We then use the well-known input admittance formula for a transmission line and arrive at the following expression for Y_B:

$$\begin{aligned} Y_B &= Y_1 \frac{Y_A + jY_1 \tan(2\theta_1)}{Y_1 + jY_A \tan(2\theta_1)} \\ &= Y_1 \frac{Y_A - Y_A \tan^2\theta_1 + 2jY_1 \tan\theta_1}{Y_1 - Y_1 \tan^2\theta_1 + 2jY_A \tan\theta_1} \end{aligned} \tag{7.16}$$

Substituting equation 7.14 into equation 7.16, we arrive at the following expression for Y_B:

$$Y_B = Y_1 \frac{-jY_2 \tan^2\theta_1 \tan\theta_2 + jY_2 \tan\theta_2 + j2Y_1 \tan\theta_1}{Y_1 - 2Y_2 \tan\theta_1 \tan\theta_2 - Y_1 \tan^2\theta_1} \tag{7.17}$$

An expression for Y_{in} can be found using the input admittance formula for a transmission line and equation 7.17:

$$\begin{aligned} Y_{\text{in}} =\ & Y_2 \frac{Y_B + jY_2 \tan\theta_2}{Y_2 + jY_B \tan\theta_2} \\ =\ & \frac{2Y_2^3 j \tan\theta_1 \tan^2\theta_2 + Y_1 Y_2^2 \tan\theta_2 (2j \tan^2\theta_1 - 2j) - 2jY_1^2 Y_2 \tan\theta_1}{2Y_2^2 \tan\theta_1 \tan\theta_2 + Y_1 Y_2 (1 - \tan^2\theta_1)(\tan^2\theta_2 - 1) + 2Y_1^2 \tan\theta_1 \tan\theta_2} \end{aligned}$$

We can simplify the expression for Y_{in} by defining the constant $K = \frac{Y_1}{Y_2}$ as follows:

$$Y_{in} = jY_2 \frac{2(K \tan\theta_1 + \tan\theta_2)(K - \tan\theta_1 \tan\theta_2)}{K(1 - \tan^2\theta_1)(1 - \tan^2\theta_2) - 2\tan\theta_1 \tan\theta_2 (1 + K^2)} \tag{7.18}$$

We can now determine the resonance condition of a stepped impedance resonator. For any resonator, when at resonance, the imaginary part of the input immittance evaluates to zero. We can therefore define the resonance condition for a stepped impedance resonator as follows:

$$K = \tan\theta_1 \tan\theta_2 \tag{7.19}$$

From equation 7.19 it is clear that there is a direct link between the total electrical length of the resonator and the admittance ratio of its segments. The total length of a stepped impedance resonator is as follows:

$$\theta_T = 2\,(\theta_1 + \theta_2)$$

Using the resonance condition in equation 7.19 and the identity in equation 7.15, we can express the length of the stepped impedance resonator as a function of the admittance ratio K:

$$\theta_T = \begin{cases} 2 \arctan\left[\frac{1}{1-K}\,(K \cot\theta_1 + \tan\theta_1)\right] & K \neq 1 \\ \pi & K = 1 \end{cases}$$

We can now determine the value of θ_1, as a function of K, that would minimise the total length of the stepped impedance resonator. The following result can be obtained through differentiation [84]:

$$\theta_1 = \arctan\sqrt{K} \tag{7.20}$$

Substitution of equation 7.20 into equation 7.19 result in the following optimal values for θ_1 and θ_2:

$$\theta_1 = \theta_2 = \arctan\sqrt{K} \tag{7.21}$$

We can summarise the results of this subsection as follows:

- The stepped impedance resonator is a shunt resonator.
- K is defined as the admittance ratio of the inner to outer transmission line sections. K can be used to shorten or lengthen a resonator while keeping its resonant frequency constant.
- The electrical length of the stepped impedance resonator is $\theta_T = 2(\theta_1 + \theta_2) = 4 \arctan \sqrt{K}$. For the case $K = 1$, the electrical length of the stepped impedance resonator must be π radians at its centre frequency. When $K < 1$, the electrical length becomes shorter. When $K > 1$, the electrical length would be longer than π radians at the centre frequency.

There is also a relationship between the admittance ratio K and the positions of the higher order harmonics of the resonator. The governing equations can be found in the literature [84]. We did not investigate the suppression of spurious passbands in this dissertation and did therefore not investigate this further. We shall now use the expression for the input admittance function to calculate the susceptance slope of a stepped impedance resonator. This will enable us to derive design equations for coupled resonator filters using stepped impedance resonators.

7.5.2 Susceptance slope of a stepped impedance resonator

In this subsection we derive an expression for the susceptance slope of a stepped impedance resonator. From equation 7.21, it is appropriate to use a single electrical length parameter $\theta = \theta_1 = \theta_2$. An expression for the input susceptance of a stepped impedance resonator can be obtained from equation 7.18 as follows:

$$Y_{in} = jY_2 \frac{2(K+1)(K - \tan^2\theta)\tan\theta}{K - 2(1+K+K^2)\tan^2\theta + K\tan^4\theta} \tag{7.22}$$

We define θ_0 as the electrical length associated with the resonant frequency. Thus $Y_{in}(\theta_0) = 0$ and $K = \tan^2\theta_0$. The susceptance slope parameter can be generalised as follows [9]:

$$b = \frac{\omega_0}{2}\frac{\partial}{\partial\omega}B(\omega)\bigg|_{\omega=\omega_0} = \frac{\theta_0}{2}\frac{\partial}{\partial\theta}B(\theta)\bigg|_{\theta=\theta_0} \tag{7.23}$$

We shall now proceed to calculate b in a systematic fashion. Suppose $B(\theta) = \frac{N(\theta)}{D(\theta)}$. Then equation 7.23 becomes:

$$b = \frac{\theta_0}{2}\frac{N^{'}(\theta)D(\theta) - N(\theta)D^{'}(\theta)}{D^2(\theta)}$$

The individual parts of b can be calculated as follows:

$$N(\theta) = 2Y_2(K+1)(K - \tan^2\theta)\tan\theta \tag{7.24}$$

$$N^{'}(\theta) = 2Y_2(1+K)(\sec^2\theta(K - \tan^2\theta) - 2\tan^2\theta\sec^2\theta) \tag{7.25}$$

$$D(\theta) = K - 2(1+K+K^2)\tan^2\theta + K\tan^4\theta \tag{7.26}$$

$$D^{'}(\theta) = -4\tan\theta\sec^2\theta(1+K+K^2) + 4K\tan^3\theta\sec^2\theta \tag{7.27}$$

We can now use trigonometric identities and the resonance condition in equation 7.21 to derive the following relationships:

$$\tan^2\theta = K$$

$$\sec^2\theta = K + 1$$

We can now simplify equations 7.24 through 7.27 using the trigonometric relationships above. The susceptance slope can then be calculated as follows:

$$\begin{aligned} b &= \frac{\theta_0}{2}\frac{N^{'}(\theta_0)D(\theta_0) - N(\theta_0)D^{'}(\theta_0)}{D^2(\theta_0)} \\ &= \frac{\theta_0}{2}\frac{N^{'}(\theta_0)D(\theta_0) - (0)D^{'}(\theta_0)}{D^2(\theta_0)} \\ &= \frac{\theta_0}{2}\frac{N^{'}(\theta_0)}{D(\theta_0)} \\ &= \frac{2Y_2(1+K)((1+K)(K-K) - 2K(K+1))}{K - 2K(1+K+K^2) + 4K^2} \\ &= 2Y_2\theta_0 \end{aligned} \tag{7.28}$$

We now know the type of resonance a stepped impedance resonator exhibits. We also know how to calculate its resonance frequency and have an expression for its susceptance slope. Next we shall investigate how stepped impedance resonators can be coupled and find a way to relate the coupling to admittance inverters. Then we shall be able to present a design technique for coupled resonator filters using stepped impedance resonators.

7.5.3 Coupling between adjacent stepped impedance resonators

The stepped impedance resonator consists of a cascade of three transmission line sections. We want to use the first and last transmission line sections to couple energy to and from a resonator. For this purpose we want to relate parallel coupled transmission lines to admittance inverters. Figure 7.10 (a) provides the electrical model of two coupled transmission lines. Each line has an electrical length of θ radians. The lines are characterised by Z_{0e} and Z_{0o} that signify their even mode and odd mode characteristic impedances respectively. The even mode characteristic impedance is the characteristic impedance of one of the lines when the coupled lines are operated in the even mode - i.e. both lines have even polarity and both currents flow in the same direction. Likewise the odd mode characteristic impedance is the characteristic impedance of one of the lines when the coupled lines are operated in the odd mode - i.e. the lines have inverse polarity and the currents flow in opposing directions. An arbitrary excitation of coupled lines can be treated as a superposition of an even mode and an odd mode excitation [2]. Even and odd mode impedances is therefore a quantification of coupling. Figure 7.10 (b) contains an illustration of two transmission lines of electrical length θ and of characteristic impedance Z_0 that are coupled through an admittance inverter J. We shall now derive the conditions for the equivalence of the circuits in figure 7.10 (a) and (b). This equivalence will enable us to quantify the coupling between stepped impedance resonators and allow us to use the equations in table 7.1 design filters consisting of them.

We shall derive the equivalence using ABCD-parameters. The ABCD-parameters of the circuit in figure 7.10 (b) can be calculated as follows [84]:

$$\begin{aligned} \begin{bmatrix} V_1 \\ I_1 \end{bmatrix} &= \begin{bmatrix} \cos\theta & jZ_0\sin\theta \\ j\frac{1}{Z_0}\sin\theta & \cos\theta \end{bmatrix} \begin{bmatrix} 0 & \frac{-j}{J} \\ -jJ & 0 \end{bmatrix} \begin{bmatrix} \cos\theta & jZ_0\sin\theta \\ j\frac{1}{Z_0}\sin\theta & \cos\theta \end{bmatrix} \begin{bmatrix} V_2 \\ -I_2 \end{bmatrix} \\ &= \begin{bmatrix} \left(JZ_0 + \frac{1}{JZ_0}\right)\sin\theta\cos\theta & j\left(JZ_0^2\sin^2\theta - \frac{\cos^2\theta}{J}\right) \\ j\left(\frac{1}{JZ_0^2}\sin^2\theta - J\cos^2\theta\right) & \left(JZ_0 + \frac{1}{JZ_0}\right)\sin\theta\cos\theta \end{bmatrix} \begin{bmatrix} V_2 \\ -I_2 \end{bmatrix} \\ &= \begin{bmatrix} A & B \\ C & D \end{bmatrix} \begin{bmatrix} V_2 \\ -I_2 \end{bmatrix} \end{aligned} \tag{7.29}$$

We shall now calculate the ABCD-parameters of the circuit in figure 7.10 (a). The impedance matrix of two parallel coupled lines can be found in the literature as follows [9]:

$$\begin{bmatrix} V_1 \\ V_2 \end{bmatrix} = \begin{bmatrix} \frac{-j}{2}\left(Z_{0e}+Z_{0o}\right)\cot\theta & \frac{-j}{2}\left(Z_{0e}-Z_{0o}\right)\csc\theta \\ \frac{-j}{2}\left(Z_{0e}-Z_{0o}\right)\csc\theta & \frac{-j}{2}\left(Z_{0e}+Z_{0o}\right)\cot\theta \end{bmatrix} \begin{bmatrix} I_1 \\ I_2 \end{bmatrix} \tag{7.30}$$

We can transform the impedance parameters into the ABCD-parameters as follows [2]:

$$A = \frac{z_{11}}{z_{21}} = \left(\frac{Z_{0e}+Z_{0o}}{Z_{0e}-Z_{0o}}\right)\cos\theta \tag{7.31}$$

$$\begin{aligned} B &= \frac{z_{11}z_{22}-z_{12}z_{21}}{z_{21}} = j\left(\frac{1}{2}\left(Z_{0e}-Z_{0o}\right)\csc\theta - \frac{\cot^2\theta\left(Z_{0e}+Z_{0o}\right)^2}{2\csc\theta\left(Z_{0e}-Z_{0o}\right)}\right) \\ C &= \frac{1}{z_{21}} = \frac{2j}{\left(Z_{0e}-Z_{0o}\right)\csc\theta} \\ D &= \frac{z_{22}}{z_{21}} = \left(\frac{Z_{0e}+Z_{0o}}{Z_{0e}-Z_{0o}}\right)\cos\theta \end{aligned} \tag{7.32}$$

We shall now equate the ABCD-parameters of the circuits in figures 7.10 (a) and (b) to find the conditions for their equality. We start by equating equation 7.32 to the C-parameter in equation 7.29 as follows:

$$\begin{aligned} \frac{2\sin\theta}{Z_{0e}-Z_{0o}} &= \frac{\sin^2\theta}{JZ_0^2} - J\cos\theta \\ \iff \qquad Z_{0e} &= Z_{0o} + \frac{2JZ_0^2\sin\theta}{\sin^2\theta-\left(JZ_0\cos\theta\right)^2} \end{aligned} \tag{7.33}$$

We next equate equation 7.31 to the A-parameter in equation 7.29 as follows:

$$\begin{aligned} Z_{0e}+Z_{0o} &= \left(Z_{0e}-Z_{0o}\right)\sin\theta\left(JZ_0+\frac{1}{JZ_0}\right) \\ Z_{0e}\left(1-JZ_0\sin\theta-\frac{\sin\theta}{JZ_0}\right) &+ Z_{0o}\left(1+JZ_0\sin\theta+\frac{\sin\theta}{JZ_0}\right) = 0 \end{aligned} \tag{7.34}$$

We then substitute equation 7.33 into equation 7.34 and solve for Z_{0o} as follows:

$$\begin{aligned} &\left[Z_{0o}+\frac{2JZ_0^2\sin\theta}{\sin^2\theta-\left(JZ_0\cos\theta\right)^2}\right]\left(1-JZ_0\sin\theta-\frac{\sin\theta}{JZ_0}\right)+Z_{0o}\left(1+JZ_0\sin\theta+\frac{\sin\theta}{JZ_0}\right)=0 \\ Z_{0o} &= \frac{-2JZ_0^2\sin\theta\left(1-JZ_0\sin\theta-\frac{\sin\theta}{JZ_0}\right)}{\left(\sin^2\theta-J^2Z_0^2\cos^2\theta\right)\left(1-JZ_0\sin\theta-\frac{\sin\theta}{JZ_0}+1+JZ_0\sin\theta+\frac{\sin\theta}{JZ_0}\right)} \\ Z_{0o} &= \frac{-JZ_0^2\sin\theta\left(1-JZ_0\sin\theta-\frac{\sin\theta}{JZ_0}\right)}{\sin^2\theta-\left(JZ_0\cos\theta\right)^2} \\ Z_{0o} &= \frac{-JZ_0^2\csc\theta\left(1-JZ_0\sin\theta-\frac{\sin\theta}{JZ_0}\right)}{1-\left(JZ_0\cot\theta\right)^2} \\ Z_{0o} &= Z_0\frac{1-JZ_0\csc\theta+\left(JZ_0\right)^2}{1-\left(JZ_0\cot\theta\right)^2} \end{aligned} \tag{7.35}$$

Using equation 7.33 we can find Z_{0e} as follows:

$$Z_{0e} = Z_0\frac{1+JZ_0\csc\theta+\left(JZ_0\right)^2}{1-\left(JZ_0\cot\theta\right)^2} \tag{7.36}$$

Equations 7.35 and 7.36 enables us to quantify the coupling between two stepped impedance resonators using admittance inverters. We now know how to determine the resonant frequency of a stepped impedance resonator, we also have an expression for its susceptance slope and know how to relate coupled transmission lines to admittance inverters. In the next section we shall use the presented theory to define a realisation technique for all-pole coupled resonator filters using stepped impedance resonators. Later in section 7.8 we shall consider the realisation of cascaded triplet filters using stepped impedance resonators. Cascaded triplet filters can accommodate asymmetric frequency responses with finite frequency transmission zeros.

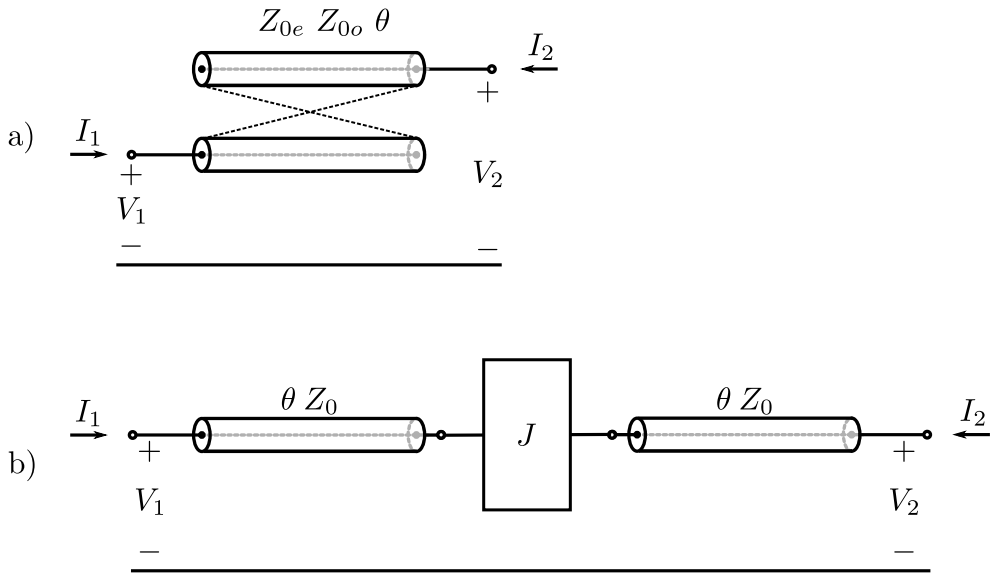

Figure 7.10: A section of two parallel coupled transmission lines of electrical length θ is shown in (a). The even and odd mode impedances of the coupled lines are Z_{0e} and Z_{0o} respectively. In (b) two identical transmission lines of electrical length θ and characteristic impedance Z_0 are coupled through an admittance inverter J. The circuits are equivalent over a narrow bandwidth if the circuit parameters adhere to equations 7.35 and 7.36.

7.6 The realisation of all-pole filters using stepped impedance resonators

The design procedure presented in this section is applicable to transfer functions where there are no finite frequency transmission zeros. The procedure is as follows:

1. Start with the design specifications and use the techniques in part I to generate a set of characteristic polynomials that describe the desired frequency response. These polynomials can be associated with a frequency response with any number of passbands and stopbands. The only requirement being that all the transmission zeros must be located at infinity.

2. Synthesise a coupling matrix using either the $N \times N$ or the $N+2 \times N+2$ coupling matrix synthesis procedures. The $N \times N$ synthesis procedure would result in a full $N \times N$ coupling matrix and a set of transformer windings that define the input and output couplings. The $N \times N$ synthesis procedure is described in section 5.5. The $N+2 \times N+2$ synthesis procedure would result in a $N+2 \times N+2$ coupling matrix that is in the transversal topology. The $N+2 \times N+2$ synthesis procedure is described in section 5.6. Irrespective of the synthesis technique used, the obtained coupling matrix will have to be reduced to the folded topology. This is achieved using the algorithm described in section 5.7.2. The coupling matrix

we obtain only contains mainline couplings as no cross-couplings are needed to produce finite frequency transmission zeros.

3. We shall now calculate the electrical parameters that define a coupled resonator circuit consisting of N stepped impedance resonators that are coupled through admittance inverters. The topology is graphically illustrated in figure 7.11. This circuit is completely defined by the admittance inverter values and the parameters that define the stepped impedance resonators themselves. For the design of the stepped impedance resonators one must start by choosing an admittance ratio K. For simplicity we choose $K = 1$. To achieve this we choose $Y_1 = Y_2 = Y_0$ where Y_0 is the characteristic admittance of the system. From equation 7.21 we know that the electrical length of the coupled sections (θ_1) are $\frac{\pi}{4}$ radians. We can calculate the centre frequency of each resonator using equation 5.65. The centre frequency of each resonator must be set by choosing θ_2 in such a manner that $\theta_T = 2\theta_1 + 2\theta_2$ is π radians at the resonant frequency. The resonators are now designed.

4. The next step in the design is the calculation of the admittance inverter values. This is achieved using the formulas in table 7.1. The susceptance slope was calculated as $2Y_2\theta_1$. The port terminations, fractional bandwidth and coupling matrix entries can now be used to calculate the required admittance inverters. The circuit in figure 7.11 is now completely specified. This circuit will have a periodic frequency response with one period corresponding to a denormalised coupled resonator lumped element circuit as specified in section 7.1. The periodic nature is contributed to the impedance of a distributed structure being a periodic function.

5. The last part of the design is to realise the admittance inverters as coupled transmission lines. Sections corresponding to the circuit in figure 7.10 (b) are replaced with coupled lines as shown in figure 7.10 (a). Equations 7.35 and 7.36 are used to obtain the even and odd mode impedances that define the coupled sections. The initial circuit with a topology illustrated in figure 7.11 is now transformed to a circuit with a topology illustrated in figure 7.12.

This completes the design procedure. The entire circuit is defined by the electrical lengths and characteristic impedances of the transmission line sections. In the next section we shall consider how to obtain the physical dimensions of filters from the mentioned transmission line properties. The resulting filter can then be manufactured. Later in section 7.8 we consider the realisation of cascaded triplet filters using stepped impedance resonators.

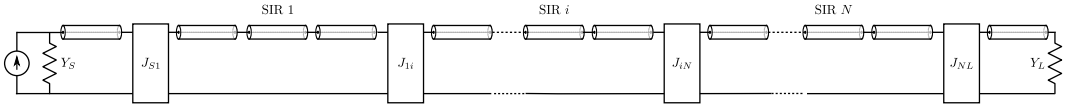

Figure 7.11: An N-th order all-pole coupled resonator circuit is shown above. Stepped impedance resonators are coupled through admittance inverters. Note that $i \in [1, N]$

7.7 Determining the physical dimensions of filters

The design techniques presented in parts I and II enable us to design lumped element coupled resonator filters. In order to design high frequency filters, we related the lumped elements to transmission lines. We now consider how to find the physical dimensions of the transmission lines. A simple transmission line section is

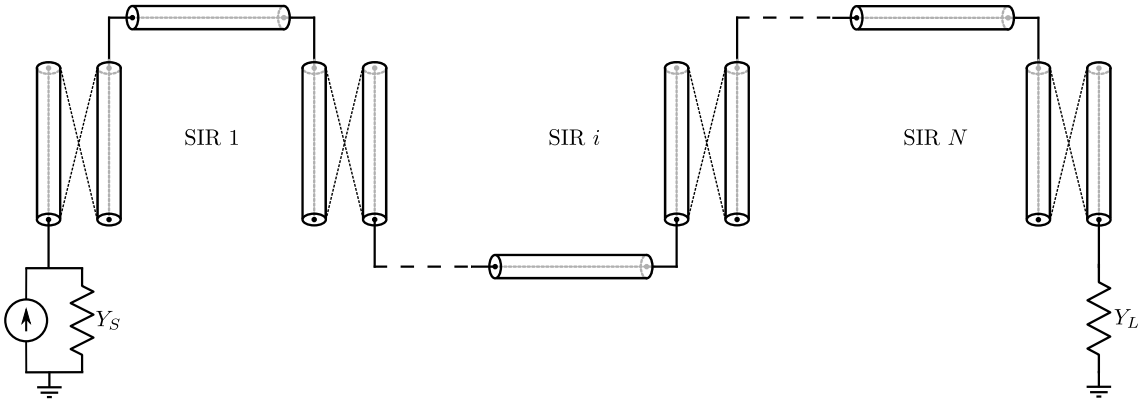

Figure 7.12: An N-th order all-pole coupled resonator circuit is shown above. The circuit consists of stepped impedance resonators that are coupled in a hairpin topology. The equivalence exhibited in figure 7.10 was used to transform the circuit in figure 7.11 into the topology above. Note that the resonators can also be arranged in a linear topology. The circuit above is completely defined by the electrical lengths of the transmission line sections, the even and odd mode impedances of the coupled sections and the characteristic impedances of the uncoupled sections.

defined by its characteristic impedance and by its electrical length at a specific frequency. A section of coupled transmission lines is defined by its electrical length and by its even and odd mode characteristic impedances. We refer to these properties as the electrical parameters of transmission lines. The electrical parameters define a general transmission line irrespective of its physical realisation. In order to construct a filter, one must first decide on an appropriate transmission line technology. The choice of technology is influenced by the frequency band under consideration and by design restrictions such as cost and size. The approximation and synthesis techniques presented in this dissertation are applicable to any narrowband filter operating in any frequency band. The realisation techniques we presented make use of stepped impedance resonators. These resonators assume TEM propagation and this places a restriction on the possible realisations. We shall specifically design filters using stripline and multi-layer stripline. It is possible to relate the electrical parameters of the coupled and uncoupled lines to the physical dimensions of striplines using transmission line theory. The calculation of these dimensions from first principles was considered outside the scope of this project. We rather exploited the wealth of available literature on the subject [85]. Modern design tools, such as AWR's Microwave Office, have incorporated the techniques published in the literature and have the capability to calculate the physical dimensions of transmission lines from their electrical parameters. We consider this the preferred technique to obtain initial dimensions for our circuits.

Circuits constructed using the initial dimensions rarely operate according to the design specifications. Fine tuning of the dimensions are now required. Microwave Office contains a set of closed form models for planar transmission lines. These models are parameterised with the physical dimensions of the transmission lines and with a definition of the electromagnetic environment. The electromagnetic environment being the definition of the substrates and the enclosure in which the device operates. Closed form models contain closed form mathematical formulas for the currents and voltages associated with physical transmission lines. These formulas were fitted on measured or simulated data and then normalised to be used in any network. Closed form models therefore offer a high degree of accuracy and are generally associated with fast simulation times. The next step in the design procedure is to use closed form models to construct a model of the circuit. The dimensions of the filter can then be tuned until the closed form model produces the desired frequency response. The circuit can then be constructed inside an electromagnetic simulator such as CST or Sonnet using the dimensions

obtained from the closed form models [1]. Additional tuning of the filter dimensions in the electromagnetic simulator is then usually required before a final design is obtained. We shall discuss tuning procedures in section 7.9. These procedures can be used with both closed form models and with electromagnetic models. We shall illustrate how to apply these techniques in the next two chapters where we present complete filter designs. In the next section we discuss the realisation of cascaded triplet filters using stepped impedance resonators.

7.8 The realisation of cascaded triplet filters using stepped impedance resonators

The general topology of a cascaded triplet filter is shown in figure 5.11. Each triplet is associated with one finite frequency transmission zero and contains one cross-coupling. In figure 7.10 we related the coupling between two parallel coupled transmission lines to an admittance inverter. The relationship we obtained can be used to model the coupling between two stepped impedance resonators. The limitation was that each resonator could only be coupled to two other nodes. This is because two of the four ports of the circuit in figure 7.10 (a) must have an open circuit as load. Even though this limitation exists, the relationship between the circuits in figure 7.10 (a) and (b) enables us to design all-pole filters.

Generally a triplet contains at least one node that must be coupled to three other nodes. This is excluding the case where a triplet is formed by the source, the load and one other resonator. We do not have a relationship between two admittance inverters and three coupled transmission lines. We are therefore unable to analytically calculate the couplings of a stepped impedance resonator when it is coupled to more than two other nodes. Consequently, we do not have a completely analytical technique to design triplets consisting of stepped impedance resonators. Fortunately we can solve the problem using a pseudo-analytical technique. We shall discuss the technique using an example.

Figure 7.13 contains an illustration of the coupling diagram and the $N+2 \times N+2$ coupling matrix of a fourth order cascaded triplet filter. It is possible to consider the main coupling path as an all-pole filter and to design it using the technique described in section 7.6. The frequency response of the main coupling path would in all likelihood not resemble a desirable filter response. The design would however be correct as the technique is fully analytical. It is then possible to artificially insert the cross-couplings. The final filter would have the desired frequency response if the cross-couplings are inserted correctly and their effects on the centre frequencies of the resonators are accounted for. We performed a literature survey to identify the standard techniques to design filters that contain cross-couplings. The goal was to identify a technique to artificially introduce cross-couplings into an all-pole stepped impedance resonator circuit. The standard techniques available in the literature are as follows [78, 86]:

1. A filter can be designed using the technique originally proposed by Dishal [77]. Here the coupling matrix is first synthesised. Then a resonator is chosen. There is decided on a layout for the filter to ensure that the correct signs for the couplings are obtained - i.e. one must ensure that one does not use the same type of coupling for both positive and negative entries in the coupling matrix. It is then necessary to adjust the distance and orientation of the neighbouring resonators two by two until the associated couplings have the correct magnitudes and signs. This procedure is time consuming and usually requires optimisation. The main problem is that it is difficult to control the unwanted couplings between resonators.

[1] Sonnet is a $2.5D$ electromagnetic simulator that employs the method of moments technique. CST is a $3D$ electromagnetic simulator that has the capability to solve Maxwell's equations using a variety of different techniques - these include the method of moments and the finite-difference time-domain method.

2. Hong proposed an alternative technique where delay lines are employed to facilitate cross-couplings [78]. Non-adjacent resonators are kept physically separate and are then coupled using delay lines. This minimises the possibility of introducing unwanted couplings. This technique is less time consuming but suffers from spurious frequency responses in its stopbands. The unwanted responses are generated because the delay lines appear as severely detuned resonant nodes inside the coupled resonator structure.

We want to insert the cross-couplings into a filter that we designed using the procedure in section 7.6. We are therefore unable to adjust the orientation of our resonators. Dishal's technique is therefore unsuited. We shall use delay lines to insert cross-couplings. Chang solved the problem of spurious responses in the stopband by noting that delay lines would not act as resonators if they are connected to the source or to the load. This is because the source and the load are per definition non-resonant [86]. We therefore limit our group of realisable cascaded triplet filters to those where the source or the load form part of each triplet. The coupling diagram of a valid cascaded triplet circuit is shown in figure 7.13. We shall now discuss the design of the delay lines. We shall again use the fourth order example to clarify the concepts.

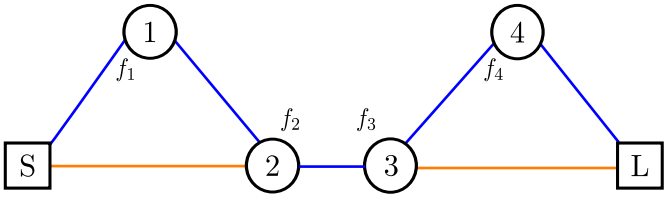

	S	1	2	3	4	L
S		×	×			
1	×	×	×			
2	×	×	×	×		
3			×	×	×	×
4				×	×	×
L				×	×	

Figure 7.13: The coupling routing diagram of a fourth order cascaded triplet filter is shown above. The general form of the associated $N + 2 \times N + 2$ coupling matrix is also shown. The blue couplings can be considered an all-pole filter and designed using the techniques in section 7.6. The orange couplings can be approximated using delay lines.

7.8.1 The length of the required delay line

As discussed in section 7.5, stepped impedance resonators exhibit a shunt type resonance. We therefore use shunt resonators in our coupled resonator circuit. A lumped element fourth order cascaded triplet filter is shown in figure 7.14 (a). The circuit in figure 7.14 (a) is realised using stepped impedance resonators and delay lines and is shown in figure 7.14 (b). The main coupling path of the lumped element circuit was realised as the blue part of the distributed circuit using the technique described in section 7.6. The orange transmission lines represent the cross-couplings. We want to calculate the required length of the orange transmission lines. Phase-reversing transformers have been added to the circuit in figure 7.14 (a) to ensure that it has a phase response similar to the circuit in figure 7.14 (b). These transformers do not influence the magnitude response of the filter but models the phase change over a half wavelength resonator. Note that the lumped element circuit only models the phase of the distributed circuit at the beginning of a resonator and at the end of a resonator. The phase in the middle of a distributed resonator is not modelled by the lumped element circuit. We can therefore only couple our delay lines to the beginning of a resonator or the end of a resonator as these are the only positions where the phase is known.

For this discussion we shall consider the triplet in figure 7.14 (a) that consist of the source, resonator one and resonator two. A triplet contains two signal paths. The first extends along the the main coupling path and second extends along the cross-coupling path. A finite frequency transmission zero is generated when the

phase change along the paths differ by $180°$. In order to design a cross-coupling path, one must measure the phase shift along the main coupling path from the source or the load to the resonator under consideration. Though it is possible to calculate the phase change along the main coupling path analytically, it is much simpler to measure it using a circuit simulator. The main coupling path of the circuit in figure 7.14 (a) is shown in figure 7.15. The triangles represent ports with real admittances. Two probe ports are included that each has a real admittance of zero. We want to create a cross-coupling between points A and B. We therefore measure the angle of the transfer admittance Y_{AB}. Our cross-coupling path must differ by $180°$ with $\angle Y_{AB}$ at the frequency of the transmission zero associated with the triplet. The cross-coupling is illustrated in figure 7.14 (b). Note that the phase change of the cross-coupling path is the phase change from A along the delay line and through the capacitive coupling to B. Note that the capacitive coupling already introduces a $-90°$ phase shift. From this discussion it is possible to calculate the length of the required delay line. The only parameter that is left to design is the capacitive gap at the end of the delay line. There is no analytical technique to calculate this gap. We shall discuss the design of the coupling gap in the next section where we present a general design technique for cascaded triplet filters using stepped impedance resonators.

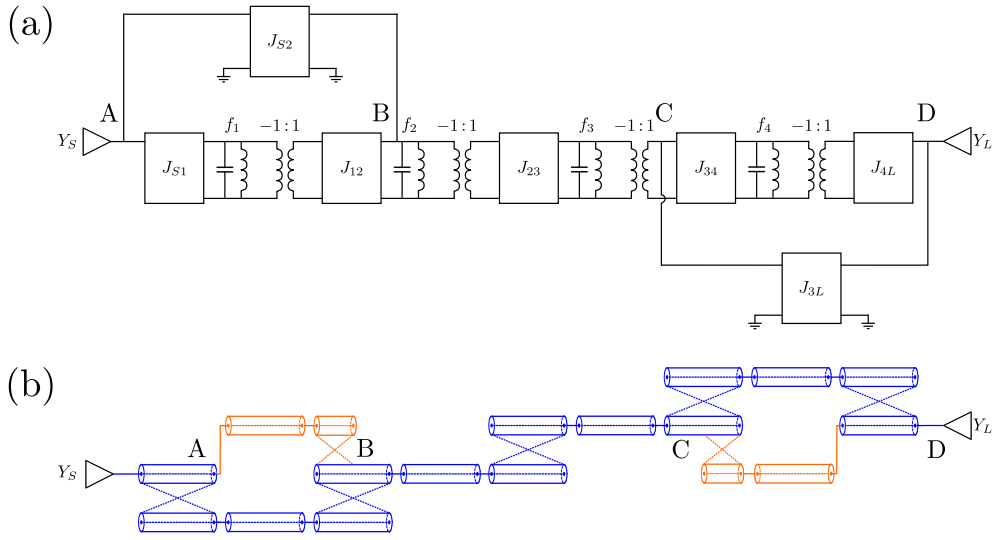

Figure 7.14: A lumped element cascaded triplet filter is shown in (a). Phase-reversing transformers are included in the model. The transformers do not change the magnitude response but ensures that the phase change for a lumped element resonator is similar to the phase change of a stepped impedance resonator. A cascaded triplet filter that was realised using stepped impedance resonators is shown in (b). The blue circuit constitutes the main coupling path and was realised using the technique presented in section 7.6. The orange transmission lines are the delay lines that are directly connected to the source and the load and that are capacitively coupled to resonators two and three respectively. The combined phase shift along the delay lines and through the capacitive coupling must differ by $180°$ from the phase shift along the main coupling path.

7.8.2 General design procedure

In this section we describe how to realise cascaded triplet filters using stepped impedance resonators. The design procedure presented here is applicable to cascaded triplet filters where either the source, or the load, or both the source and the load form part of triplets. Cascaded triplet filters consisting of a maximum of two triplets can therefore be designed. Consequently, transfer functions with a maximum of two finite frequency transmission zeros can be accommodated. The procedure is as follows:

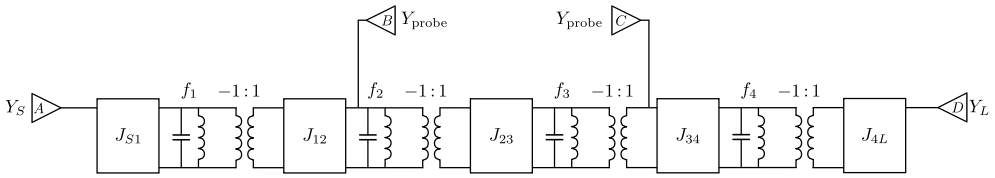

Figure 7.15: The main coupling path of the circuit in figure 7.14 (a) is shown above. Additional ports that serve as measurement probes have been inserted at the beginning of resonator two and at the end of resonator three. These ports each have an input admittance of zero. As a consequence they do not influence the circuit. These ports are used to measure the transfer admittances Y_{AB} and Y_{CD}. The phase of the transfer admittances can be used to design the cross-coupling paths.

1. Start with the design specifications and use the techniques in part I to generate a set of characteristic polynomials that describe the desired frequency response. The number of finite frequency transmission zeros must be equal to the number of triplets. A maximum of two triplets can be accommodated if the circuit is realised using stepped impedance resonators. The $N+2\times N+2$ synthesis procedure would result in a $N+2\times N+2$ coupling matrix that is in the transversal topology. The $N+2\times N+2$ synthesis procedure is described in section 5.6. The coupling matrix must now be transformed into the wheel topology using the algorithm defined in section 5.7.2. Next the wheel must be transformed into the cascaded triplet topology using the technique presented in section 5.7.3.

2. The main coupling path can now be realised using stepped impedance resonators as described in section 7.6.

3. The next step is to determine the required length of the delay lines that will be used to realise the cross-couplings. A lumped element circuit model with phase-reversing transformers is used for this. An example is shown in figure 7.14 (a). The phase of the transfer admittance between the source or the load and the resonator to be coupled to is measured along the main coupling path. The combined phase shift along the delay line and through the capacitive gap at the end of the delay line must then differ by 180° from the phase shift along the main coupling path. The capacitive gap on its own already introduces a -90° phase shift. From this the lengths of the different delay lines can be determined. All the transmission lines and coupled sections are now defined except for the capacitive gaps at the end of the delay lines.

4. The next step is to construct a closed from model of the main coupling path of the filter in a circuit simulator. The closed form model is defined in terms of the physical dimensions of the transmission lines. We discussed how to obtain the physical dimensions in section 7.7. We then include the first triplet in the closed form model. The dimensions of the capacitive gap and the characteristic impedance of the delay line can be arbitrarily chosen. We then tune the capacitive gap and the centre frequency of the resonator we are coupling to until the frequency response of our closed form model corresponds to the frequency response of our lumped element model. Here the lumped element model resembles the closed form model in that it only consists of the main coupling path and the triplet under consideration. This procedure can be sequentially performed for all the triplets. When the last triplet is tuned in, the closed form model should have the desired frequency response.

5. The entire circuit can now be simulated in an electromagnetic simulator. The filter dimensions will in all likelihood require additional fine tuning. The space mapping procedure discussed in section 7.9.2 can be employed for this purpose.

In the next section we shall discuss tuning procedures. These procedures can be used to fine tune the dimensions of electromagnetic models to meet the design specifications.

7.9 Tuning procedures

Design closure is the process of starting with an initial layout for a filter and then transforming it into a final layout. The final layout must meet all the design specifications when fabricated. A possible solution to this problem is to parameterise the dimensions of an electromagnetic structure and to then perform direct optimisation using an electromagnetic simulator. Although this approach is theoretically possible, it is practically infeasible to place an electromagnetic solver in an optimisation loop. This is because electromagnetic simulation is generally computationally intensive and the optimisation routine would in most cases require an unacceptably long time period to converge. In this section we introduce alternative techniques that can be used during the design closure procedure. We describe two tuning techniques. The first technique is only applicable to all-pole filters. The second technique is more general and can be applied to cross-coupled filters.

7.9.1 Group delay tuning of coupled resonator filters

In this section we present a systematic tuning procedure for all-pole coupled resonator circuits. The tuning procedure we present here is based on the s_{11} group delay technique proposed by Ness [87]. Suppose a bandpass filter was designed using a ladder prototype. The ladder prototype is defined by the traditional g-parameters [2]. Ness derived equations that relate the g-parameters of the prototype to the group delay of s_{11} of the bandpass filter. His equations can calculate the required value of the group delay at the centre frequency of the filter. He showed that the group delay measurement was always an even function about the centre frequency. He proposed a systematic procedure where a designer starts with a source and one resonator. The designer must then adjust the input coupling and the resonant frequency of the first resonator until it is tuned. The resonator is tuned when the group delay measurement is symmetric about the centre frequency and it also evaluates to the required value at that frequency. A second resonator is then coupled to the first resonator. The centre frequency of the new resonator and the coupling to the new resonator must now be tuned until the new group delay measurement is also symmetric and has the required value at the centre frequency. This procedure is continued until all the resonators are included in the circuit. Ness extended his theory by linking the group delay measurements to the coupling values and the external quality factors associated with the filter. The technique Ness proposed is however limited to synchronously tuned coupled resonator circuits. In asynchronously tuned coupled resonator circuits the group delay measurements are not necessarily symmetric about the centre frequency of the filter. This is usually not a problem as all-pole filters are rarely asynchronously tuned.

We however want to use this tuning technique to design the main coupling path of cascaded triplet filters. This means that our resonators will be asynchronously tuned. Consequently, the equations that Ness derived are no longer applicable. Fortunately a circuit simulator (Microwave Office) can be used to obtain the ideal group delay response for the asynchronously tuned case. The technique Ness described can still be applied, but the target response is now a group delay measurement from a circuit simulator and not one calculated using the g-parameters. We shall now describe the tuning procedure that is applicable to asynchronously tuned resonators. We shall describe how to tune an electromagnetic model. The technique is however applicable to closed form models as well. We assume that a lumped element coupled resonator circuit is available and that

the initial dimensions of an electromagnetic model have been derived using some transmission line design tool. We further assume that the electromagnetic model does not have the required frequency response. The tuning procedure is as follows:

1. In both the lumped element circuit and the electromagnetic model, include only the first coupling and the first resonator. Adjust the input coupling and the resonant frequency of the first resonator in the electromagnetic model until both circuits have the same group delay measurement. This situation is illustrated in figure 7.16 (a).

2. In both the lumped element circuit and the electromagnetic model, couple a second resonator to the first resonator. In the electromagnetic model, tune the resonant frequency of the second resonator and the coupling between the first and second resonators until the group delay of the model corresponds to that of the lumped element circuit. This situation is illustrated in figure 7.16 (b). This procedure is continued until all the resonators in the filter have been tuned.

In some cases the required group delay measurement cannot be obtained by only tuning the coupling to the new resonator and the resonant frequency of the new resonator. In such cases the second closest coupling and resonant frequency must also be used for tuning purposes. The rule is to keep the number of variables a minimum and to adjust the resonant frequencies and couplings that are closest to the new resonator the most. This completes the discussion on the sequential tuning of coupled resonator circuits using the group delay of s_{11}. In the next subsection we shall introduce the port tuning technique. This technique is based on space mapping and can be applied to any filter.

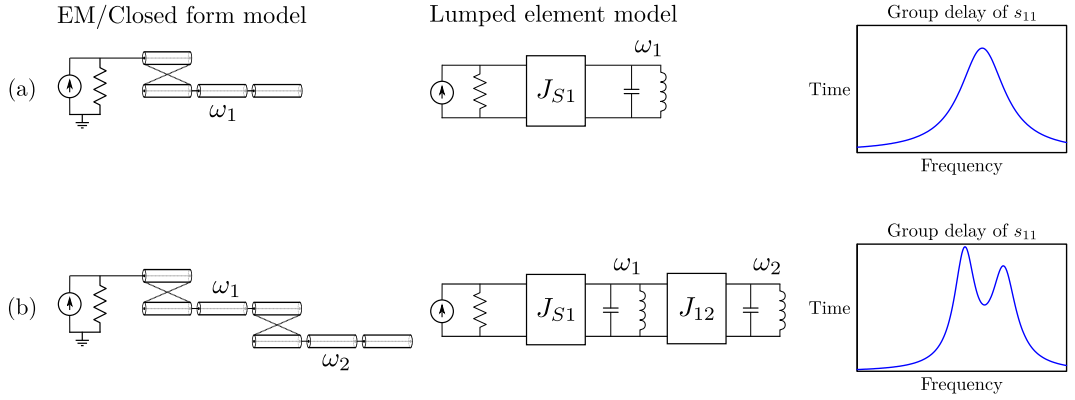

Figure 7.16: An all-pole filter can be tuned using the group delay of s_{11}. The s_{11} group delay of the electromagnetic/closed form model is systematically matched to the s_{11} group delay of the lumped element circuit. The lumped element circuit can be used as an optimisation goal as it is precisely obtained from the coupling matrix. The procedure starts with a single resonator. The dimensions corresponding to couplings and centre frequencies of the electromagnetic/closed form models are adjusted until the group delay measurements match. Once a match is found, an additional resonator can be appended and the procedure can repeat.

7.9.2 The port tuning procedure

Space mapping is an optimisation technique where the electromagnetic simulator is removed from the optimisation loop. The idea is to use two models for a filter. The one model is referred to as the fine model and is an accurate representation of reality. Due to the high degree of accuracy, the fine model is computationally expensive to simulate. The second model is referred to as a surrogate model and is constructed from the fine

model. The surrogate model does not model the filter as accurately as the fine model but is computationally inexpensive to simulate. The surrogate model is then placed inside an optimisation loop. The optimisation procedure would then fine tune the dimensions of the surrogate model until it has the desired frequency response. The procedure converges quickly as simulating the surrogate model is computationally inexpensive. The changes applied to the surrogate model are then applied to the fine model. The fine model is then executed again. If the fine model has the desired frequency response, the procedure terminates. If however the fine model still does not meet the design specifications, another surrogate model is constructed from the fine model and another optimisation iteration is performed [79].

Port tuning is a special case of space mapping. The name port tuning refers to the way the surrogate model is constructed. The fine model is identified as the electromagnetic model of a filter. A surrogate model is constructed from a fine model by including internal ports inside an electromagnetic simulation and then connecting circuit theory components to these ports. The circuit theory components can then be tuned to artificially change the dimensions of the electromagnetic model. Simulating the surrogate model is computationally inexpensive as the circuit consists of s-parameter matrices and circuit theory components.

In order to clarify the concepts, a fine model of a cascaded triplet filter is shown in figure 7.17. It is a fourth order filter and was realised using stepped impedance resonators and delay lines as discussed in section 7.8. We then subdivided the electromagnetic model into five smaller electromagnetic models. We chose the positions of the subdivision lines in such a manner that each resonator is split between two segments. We also ensured that both the delay lines and the cross-couplings are split over at least two segments. The subdivisions are illustrated in figure 7.18. Each segment is now a multi-port circuit. The segments can be represented with s-parameter matrices. We then connected the five smaller electromagnetic models together using closed form models in a circuit simulator (AWR's Microwave Office). The closed form models are now considered tuneable. We are therefore able to tune the centre frequencies of all the resonators, the lengths of the delay lines and the lengths of the coupled sections located at the ends of the delay lines. The combined circuit constitutes the surrogate model. Note that the we can now tune the dimensions of the filter using the surrogate model without performing additional electromagnetic simulations [79]. The port tuning procedure is summarised as an algorithm in figure 7.19. This completes our discussion on tuning techniques. We employ port tuning in chapters 8 and 9 where we present filter design examples. In the next section we shall provide a summary of this chapter.

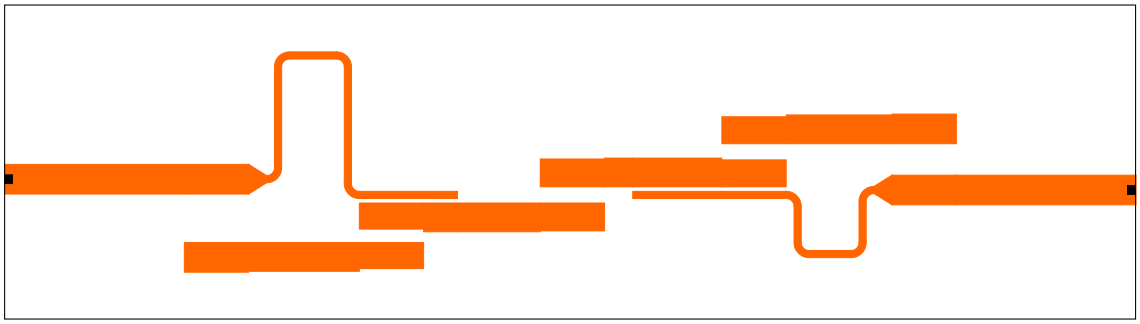

Figure 7.17: A cascaded triplet filter that was realised using stepped impedance resonators is shown above. The black squares represent ports. This circuit constitutes the fine model in our space mapping procedure.

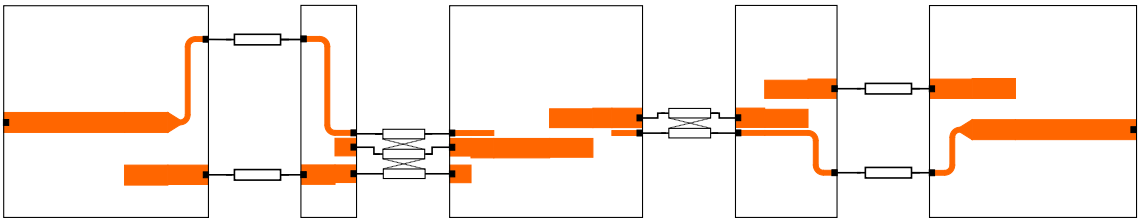

AWR title	Description	Symbol
GMCLIN	Multiple coupled lines on general multi-layer substrate	
GM1LIN	Single line on general multi-layer substrate	

Figure 7.18: A surrogate model associated with the fine model in figure 7.17 is shown above. The fine model was divided into five smaller electromagnetic models. These models were then connected together using closed form models. The electromagnetic models are presented by s-parameter matrices and are therefore computationally inexpensive in the optimisation loop. The circuit theory components are all considered tuneable and can be used to change the resonant frequencies of the resonators and alter the two cross-couplings.

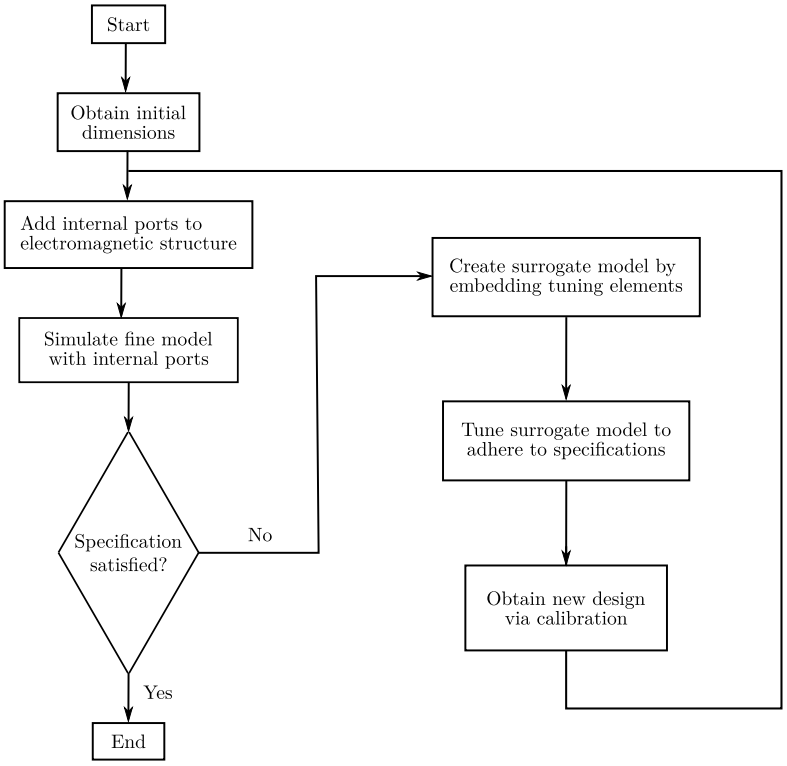

Figure 7.19: The general port tuning algorithm is illustrated above.

7.10 Summary

This chapter dealt with the problem of transforming coupled resonator circuits into physically manufacturable filters. The chapter started with a discussion on how a coupled resonator circuit can be denormalised to operate in the actual frequency domain. Next we discussed the limitations of lumped elements and highlighted the need for the generalisation of coupled resonator theory to accommodate arbitrary resonators. We then derived the general equations for coupled resonator circuits using arbitrary resonators. Next we introduced the

stepped impedance resonator and derived equations for its resonance condition and its susceptance slope. We then presented an analytical technique to model coupling between different stepped impedance resonators. A general design technique for all-pole filters using stepped impedance resonators was presented next. We also considered the design of cascaded triplet filters using stepped impedance resonators. The circuits one obtains consist entirely of transmission lines and are therefore described by characteristic impedances and electrical lengths. We next discussed how these transmission line parameters can be used to calculate the physical dimensions of filters. Lastly we concluded the chapter by presenting two tuning techniques that can be used during design closure.

At this point we are capable of obtaining the multi-band characteristic polynomials from user specifications using the techniques presented in part I. We can then synthesise the characteristic polynomials as lumped element coupled resonator circuits using the techniques presented in chapter 5. Alternatively we can construct rational mapping functions using the theory presented in chapter 4 and then transform any single-band prototype circuit into a lumped element multi-band filter using the methods presented in chapter 6. The techniques presented in this chapter can then be used to realise the lumped element circuits as distributed structures that can be fabricated. We therefore have all the necessary theory to design and manufacture test filters. In the next three chapters we shall validate the presented theory using design examples. In chapter 8 we shall design an all-pole filter. We shall then realise the filter in both single-layer and multi-layer stripline. In chapter 9 we shall design a cascaded triplet filter. We shall then realise the filter in both single-layer and multi-layer stripline. In chapter 10 we shall design a three-band filter using coaxial resonators. The filters that are designed in chapters 8 and 9 are designed using the methods presented in chapters 3 and 5. The filter designed in chapter 10 was designed using the methods presented in chapters 4 and 6.

Chapter 8

Designs: Dual-band all-pole filters

To validate the design techniques proposed in the earlier chapters, a number of multi-band filters were designed and tested. These include:

1. A dual-band all-pole filter:
   The filter is designed using a polynomial mapping function and has a prototype with a symmetric frequency response. The filter is synthesised using the well-known concepts summarised in chapter 5, and realised in both single-layer and multi-layer stripline using the established theory summarised in chapter 7. The design of the single-layer stripline filter is included in this chapter and serves as both a practical example and a validation of the theory presented in chapter 3. The filter was later realised in multi-layer stripline to reduce the passband loss. The multi-layer stripline design is included as appendix A.1.

2. Dual-band cascaded triplet filter:
   The design is included as a more complex example of the use of polynomial mapping functions to design multi-band filters. The filter, that has a prototype with an asymmetric frequency response, is synthesised using the well-known concepts summarised in chapter 5, and then realised in both single-layer and multi-layer stripline using the established theory presented in chapter 7. The single-layer design is included in chapter 9. The design serves as both a practical example and a validation of the theory presented in chapter 3. The filter was later realised in multi-layer stripline to reduce the passband loss and the multi-layer design is included as appendix A.2.

3. Three-band coaxial resonator filter:
   The design utilises a rational mapping function and is included in chapter 10. The design illustrates and validates the theory presented in chapters 4 and 6.

8.1 Specifications

Our goal is to design a dual-band filter, using a polynomial mapping function, with the following specifications:

- Half power passband 1: 2.4 GHz to 2.5 GHz.
- Half power passband 2: 2.688 GHz to 2.8 GHz.
- Return loss: 20 dB.
- Order of filter: 8.

The passband frequencies where chosen in such a manner that the required prototype filter would be symmetric with respect to the zero frequency. In the next sections we consider the approximation and synthesis procedures.

8.2 Approximation and synthesis

The design was carried out to validate the polynomial mapping procedure, as described in chapter 3. The passband specification was provided in terms of half power bandwidths and not ripple bandwidths to illustrate that half power bandwidths can easily be accommodated. As there is no simple relationship between the ripple bandwidth and the half power bandwidth of a multi-band filter, the polynomial mapping procedure was implemented as a computer program and the associated ripple bandwidth specification was found through an iterative procedure [1]. The following ripple bandwidths correspond to the desired half-power bandwidths:

- Passband 1: 2408.35 GHz to 2483.5 GHz.
- Passband 2: 2705.90 GHz to 2790.35 GHz.

Following the procedure in section 3.6, the ripple passbands were normalised to obtain the following multi-band prototype specification:

- Passband 1: $\Omega \in [-1\ ;\ -0.5822]$.
- Passband 2: $\Omega \in [0.5822\ ;\ 1]$.
- Return loss in passband: 20 dB.
- Order of dual-band filter: 8.
- All the transmission zeros must be located at infinity.

A polynomial mapping function for the bandwidth specification above was constructed in example 1 in section 3.7, and was then used to construct the required dual-band characteristic polynomials from a fourth-order all-pole generalised Chebyshev polynomial. The final dual-band characteristic polynomials are as follows:

$$\begin{aligned} E(S) &= S^8 + 0.9087\,S^7 + 3.0909\,S^6 + 1.9876\,S^5 + 3.1954\,S^4 \\ &\qquad + 1.3239\,S^3 + 1.2655\,S^2 + 0.2582\,S + 0.1542 \\ F(S) &= S^8 + 2.678\,S^6 + 2.5802\,S^4 + 1.0541\,S^2 + 0.1534 \\ jP(S) &= j \\ \epsilon &= 67.3889 \\ \epsilon_r &= 1 \end{aligned} \tag{8.1}$$

The methods presented in chapter 5 can now be employed to synthesise a prototype circuit from the characteristic polynomials in equation 8.1. An $N \times N$ coupled resonator circuit was synthesised from the polynomials in example 1 in section 5.5.3. The result was an $N \times N$ coupling matrix and the windings of the input and output transformers. The $N \times N$ coupling matrix describes a network where almost all of the nodes are coupled to one another. As this topology is undesirable for implementation, an $N+2 \times N+2$ coupling matrix was also

[1] Iteratively choose a ripple bandwidth specification for the filter until the generated characteristic polynomials have passbands that adhere to the specification in section 8.1.

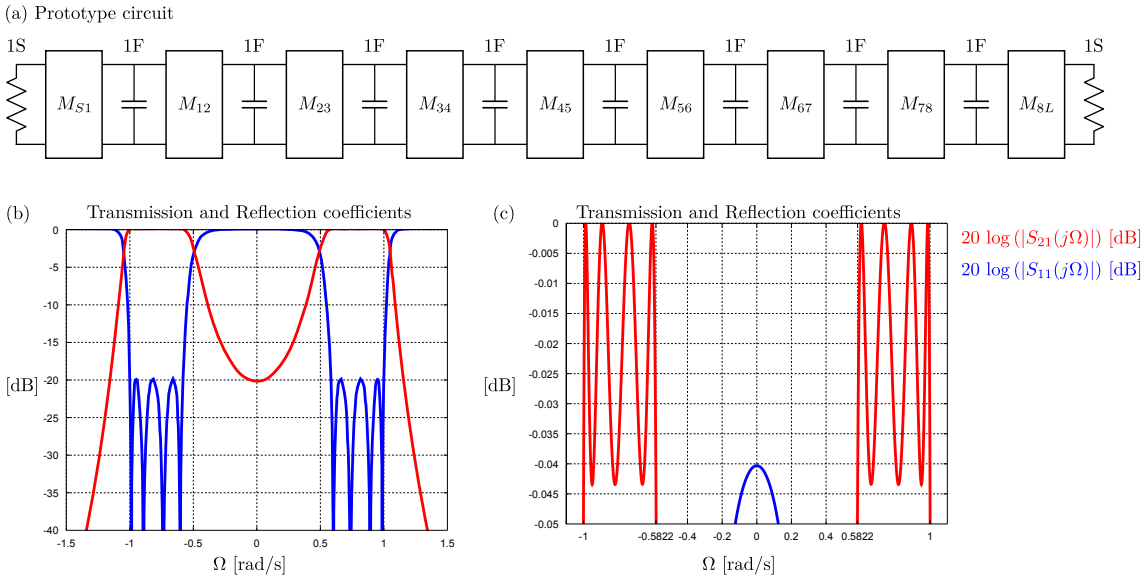

Figure 8.1: The coupling matrix represented as an admittance prototype is shown in (a). The values of the admittance inverters refer to the coupling matrix elements in equation 8.2. The frequency response in the prototype frequency domain is shown in (b). The ripple bandwidth is shown in (c). The ripple passbands are defined as $\Omega \in [-1; -0.5822] \cap [0.5822; 1]$

synthesised from the characteristic polynomials in example 1 in section 5.6.3. As the resulting $N+2 \times N+2$ coupling matrix in the transversal topology is also not well-suited for realisation, the coupling matrix was transformed into the folded topology. An all-pole filter in the folded topology would correspond to a simple ladder network. Both the $N \times N$ and $N+2 \times N+2$ coupling matrices, associated with this design, were transformed into the folded topology in the example in section 5.7.2. As one would expect, both matrices reduce to the same coupling matrix. The $N+2 \times N+2$ coupling matrix in the folded topology is as follows:

$$\mathbf{M} = \begin{array}{c|cccccccccc} & S & 1 & 2 & 3 & 4 & 5 & 6 & 7 & 8 & L \\ \hline S & 0 & 0.674 & 0 & 0 & 0 & 0 & 0 & 0 & 0 & 0 \\ 1 & 0.674 & 0 & 0.835 & 0 & 0 & 0 & 0 & 0 & 0 & 0 \\ 2 & 0 & 0.835 & 0 & 0.367 & 0 & 0 & 0 & 0 & 0 & 0 \\ 3 & 0 & 0 & 0.367 & 0 & 0.750 & 0 & 0 & 0 & 0 & 0 \\ 4 & 0 & 0 & 0 & 0.750 & 0 & 0.309 & 0 & 0 & 0 & 0 \\ 5 & 0 & 0 & 0 & 0 & 0.309 & 0 & 0.750 & 0 & 0 & 0 \\ 6 & 0 & 0 & 0 & 0 & 0 & 0.750 & 0 & 0.367 & 0 & 0 \\ 7 & 0 & 0 & 0 & 0 & 0 & 0 & 0.367 & 0 & 0.835 & 0 \\ 8 & 0 & 0 & 0 & 0 & 0 & 0 & 0 & 0.835 & 0 & 0.674 \\ L & 0 & 0 & 0 & 0 & 0 & 0 & 0 & 0 & 0.674 & 0 \end{array} \tag{8.2}$$

The circuit will be realised as a stepped impedance coupled resonator filter. As the stepped impedance resonators exhibit a shunt type resonance, the coupling matrix in equation 8.2 is represented as a prototype circuit in the admittance form as shown in figure 8.1.

The prototype circuit can now be denormalised using the technique presented in section 7.1. The centre frequency is calculated as $f_0 = 2.5923$ GHz, the fractional bandwidth as $\Delta = 0.1474$ and the impedance level at the ports were taken as $50\,\Omega$. The denormalised lumped element circuit is shown in figure 8.2. Both the ripple passbands and the half-power passbands are shown and it is clear that the lumped element filter adheres to the design specifications in section 8.1. Next we consider the realisation of the filter.

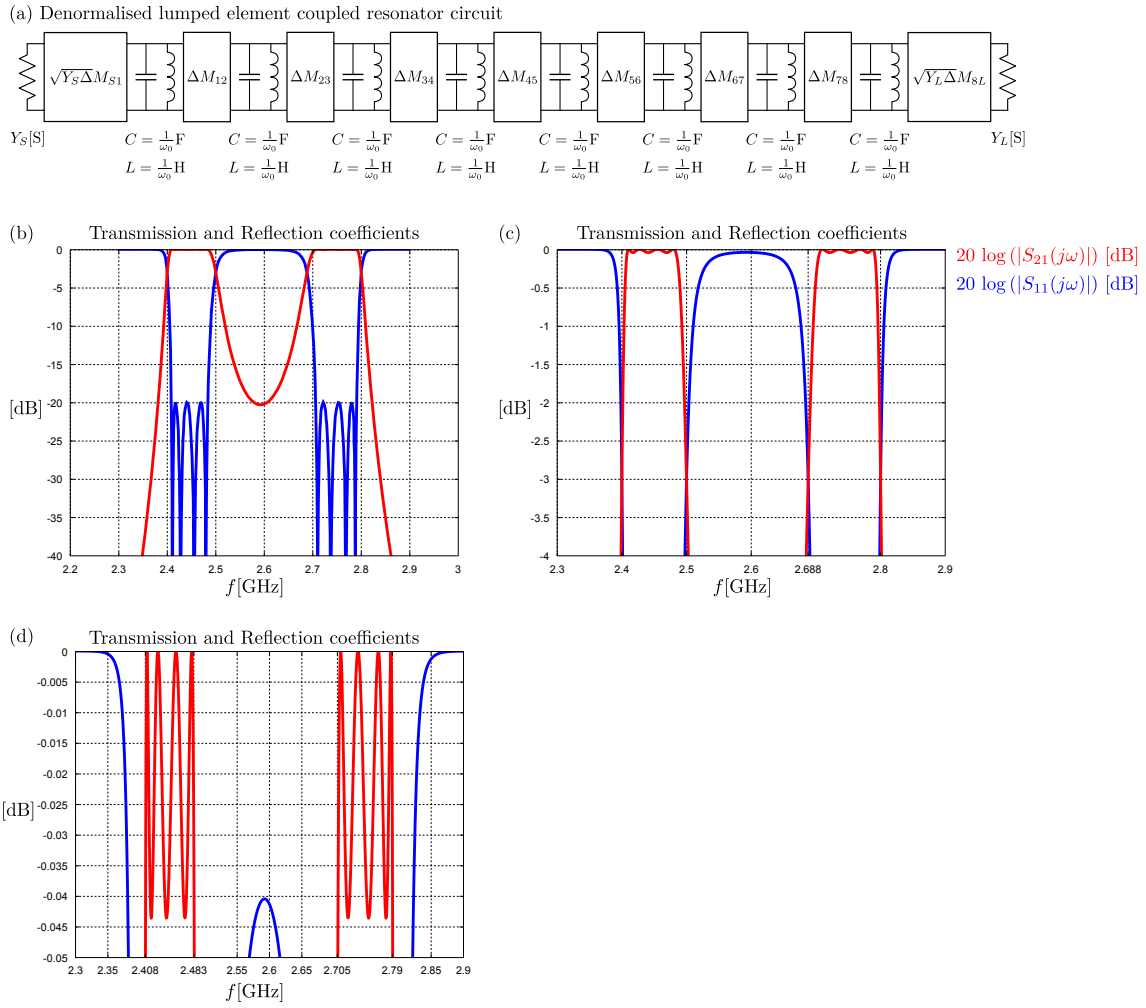

Figure 8.2: The denormalised lumped element coupled resonator circuit is shown in (a). The frequency response is shown in (b). The half-power bandwidth is shown in (c). The first half-power passband extends from 2.4 GHz to 2.5 GHz. The second half-power passband extends from 2.688 GHz to 2.8 GHz. The ripple bandwidth is shown in (d). The first ripple passband extends from 2.408 GHz to 2.483 GHz. The second ripple passband extends from 2.705 GHz to 2.790 GHz.

8.3 Realisation

This section concerns the realisation of the lumped element filter in figure 8.2 as a stepped impedance resonator filter in stripline. We shall systematically design the single-layer stripline filter using the technique described in section 7.6.

8.3.1 Ideal transmission line model

Figure 8.3 shows an all-pole filter that was realised using stepped impedance resonators. Each resonator consists of three ideal transmission line sections. The stepped impedance resonators exhibit a shunt type resonance and were therefore coupled to each other using admittance inverters. The entire circuit is defined by the characteristic impedances and electrical lengths of the transmission line sections and the values of the admittance inverters. These parameters can be calculated using the technique described in section 7.6. The presented theory is however limited to cases where the coupled sections are 45° in length. The coupled sections here refer to θ_2 in figure 7.8. For the stripline filter in this chapter each coupled section is 85° in length as the aim is to design a parallel coupled transmission line filter resembling those originally introduced by Cohn [8]. We how-

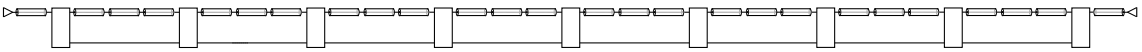

AWR title	Description	Symbol
TLIN	Section of ideal transmission line	
PORT	Port	
N/A	Admittance inverter circuit	

Figure 8.3: An all-pole filter using stepped impedance resonators is shown above. A table defining the Microwave Office elements is provided. The stepped impedance resonators exhibit a shunt type resonance and were coupled using admittance inverters. The admittance inverters where constructed using ideal admittance elements.

ever want to include a small transmission line section between the coupled sections to aid us with the tuning procedures. The inclusion of a 10° transmission line section between the coupled sections enables one to tune the centre frequencies of the resonators without influencing the couplings between adjacent resonators. For the case where the coupled sections are not equal to 45°, equation 7.28 is no longer valid. We can however use equation 7.28 with $\theta_0 = 45^\circ$ as an approximate value. Through minor adjustment of the centre frequency and fractional bandwidth of the circuit in figure 8.3, one can align its frequency response with that of the circuit in figure 8.2. The fractional bandwidth changes from 0.1474 to 0.1499 and the centre frequency changes from 2.5923 GHz to 2.5974 GHz. The frequency responses of the ideal model and the transmission line model is shown in figure 8.4. The circuit in figure 8.3 still contains the fictitious ideal admittance inverters. The circuit in figure 8.3 is now converted to the topology shown in figure 8.5. The technique described in section 7.6 is employed for this. The circuit in figure 8.5 contains physically realisable elements. The frequency responses of the circuits in figures 8.3 and 8.5 are virtually identical. The circuit in figure 8.5 is completely defined by electrical lengths and characteristic impedances. The next step is to convert the electrical parameters that define the circuit in figure 8.5 to physical dimensions of striplines. We shall consider this in the next subsection.

8.3.2 Closed form model of single-layer stripline filter

The filter was realised in the Rogers 4003C substrate with a thickness of 1.524 mm. The electrical properties of the substrate are listed in table 8.1. The substrates are combined using a RF bonding film. We used Arlon's CuClad 6250 as bonding film. The electrical properties of the bonding film are listed in table 8.2. Although the effects of the bonding film seem insignificant, care must be taken to accurately model its presence as it influences the resonant frequencies of the resonators and the coupling between them. The physical dimensions of each transmission line section can be calculated to obtain the initial dimensions of the filter. A closed form model of the filter can now be constructed. The closed form model is shown in figure 8.6. The initial simulation of the closed form model does not produce the desired frequency response. Filter dimensions need to be tuned. The group delay tuning procedure that we introduced in section 7.9.1 can be used to find a set of physical dimensions that produce to the desired frequency response. The frequency response of the tuned closed form model is compared to the ideal frequency response in figure 8.7. The ideal response here being the denormalised lumped element circuit in figure 8.2. The next step in the design procedure is to verify the filter dimensions using an electromagnetic simulator.

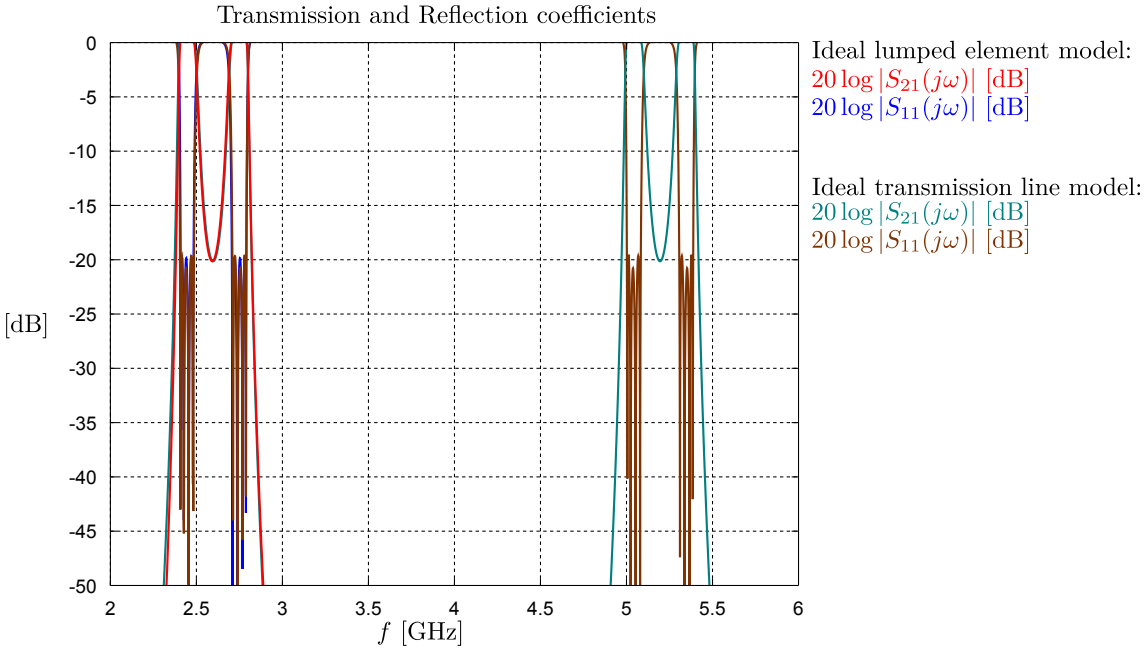

Figure 8.4: The frequency response of the ideal lumped element coupled resonator circuit (figure 8.2) is compared to the frequency response of the ideal transmission line model (figure 8.3). The two circuits have an identical frequency response over the band under consideration. The periodic nature of the input impedance of a transmission line results in the SIR circuit having a periodic frequency response. The lumped element circuit does not have a periodic frequency response.

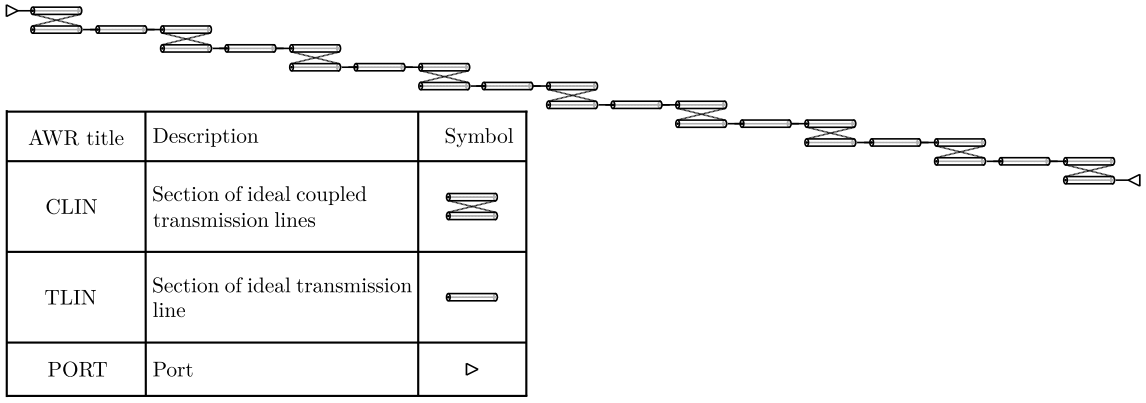

AWR title	Description	Symbol
CLIN	Section of ideal coupled transmission lines	
TLIN	Section of ideal transmission line	
PORT	Port	▷

Figure 8.5: An ideal transmission line model of the all-pole filter is shown above. A table defining the Microwave Office elements is provided. The model is completely defined by the characteristic impedances and electrical lengths of the transmission line sections.

Relative permittivity	3.55
Dissipation factor	0.0027
Copper cladding	35μm
Available thickness	1.524mm 0.508mm

Table 8.1: Properties of the Rogers 4003C substrate.

Relative permittivity	2.32
Dissipation factor	0.0013
Thickness	38.1μm

Table 8.2: Properties of Arlon's CuClad 6250 bonding film.

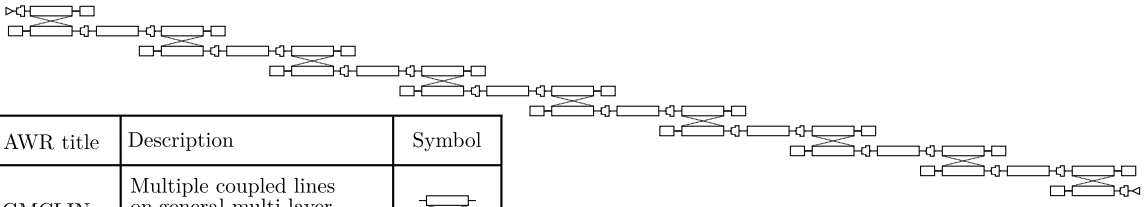

AWR title	Description	Symbol
GMCLIN	Multiple coupled lines on general multi-layer substrate	
GM1LIN	Single line on general multi-layer substrate	
PORT	Port	
SSTEP0	Stripline step in conductor width	
SLEF	Open stripline with end effect	

Figure 8.6: A closed form model of an all-pole stepped impedance resonator filter in stripline is shown above. A table identifying the Microwave Office components are provided. Note that the closed form models also require a general multi-layer substrate definition.

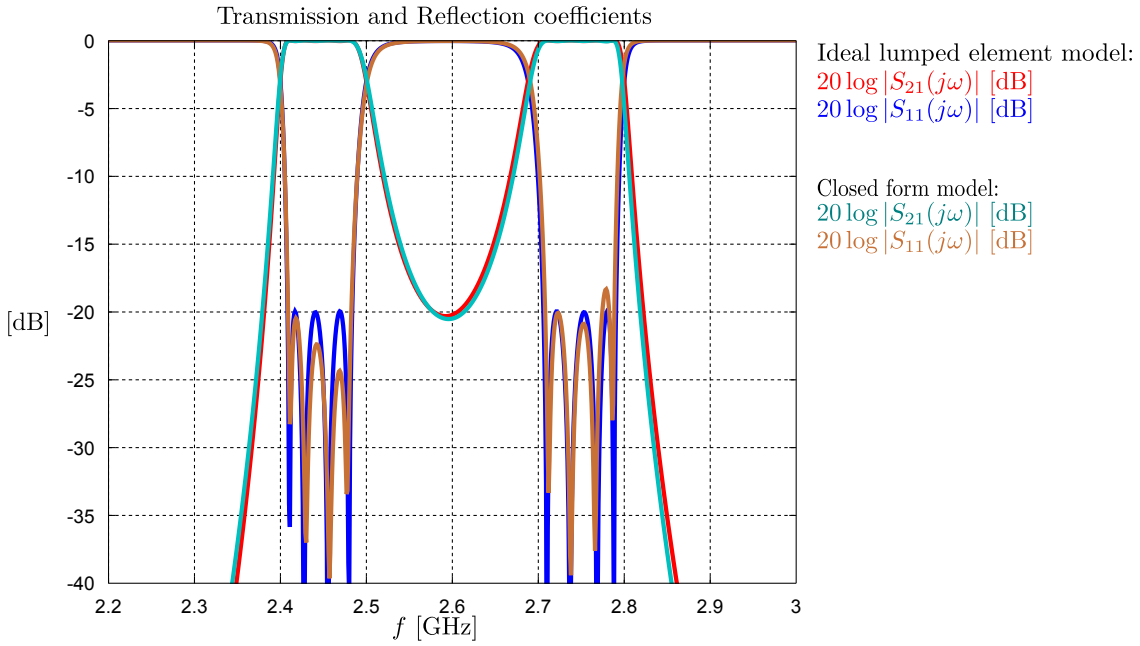

Figure 8.7: The frequency response of the ideal lumped element coupled resonator circuit (figure 8.2) is compared to the frequency response of the closed form model (figure 8.6).

8.3.3 Electromagnetic simulation and port tuning of single-layer stripline filter

We constructed an electromagnetic model in Sonnet. The conducting layer is shown in figure 8.8. The electromagnetic model includes the substrates and the bonding film. We did not include loss in the initial simulations. The frequency response of the initial electromagnetic model is compared to the frequency response of the tuned closed form model in figure 8.9 (a). The discrepancy between the responses is attributed to the inaccuracy of the closed form models and due to the fact that stray couplings are not included in the closed form model. The dimensions of the initial electromagnetic model is now adjusted until a model with a frequency response that meets the design specifications are obtained. In order to achieve this the port tuning procedure introduced in section 7.9.2 is applied. The initial electromagnetic model now becomes the first fine model. A surrogate model can be constructed from the fine model by segmenting the fine model into smaller sections. Each section can be simulated on its own and be represented by an s-parameter matrix. The different matrices can then be connected together using closed form models in Microwave Office. The closed form models can then be used to tune the dimensions of the fine model. Simulating the surrogate model is computationally inexpensive in the optimisation loop. A surrogate model associated with the circuit in figure 8.8 is shown in figure 8.10. Each black box in figure 8.10 represents a separate Sonnet simulation. Note that the conductors inside each of the Sonnet simulations are moved sufficiently far away from the simulation walls to prevent coupling. De-embedding is then used to correct the phase shift.

The initial filter cannot be segmented arbitrarily. A guideline in choosing segmentation positions is that conductors in different segments cannot couple energy to each other. Also, one should try to segment the resonators so that it would be possible to tune their centre frequencies. Sections of coupled lines can be segmented but through experimentation it was found that for all-pole filters it is usually sufficient to tune only the resonant frequencies of the stepped impedance resonators in order to obtain the desired frequency response.

Figure 8.9 (b) compares the frequency responses of the initial fine model and the initial surrogate model. The two are identical as the surrogate model has not been tuned. The surrogate model is now tuned until it meets the design specifications. Figure 8.9 (c) compares the frequency response of the tuned surrogate model with that of the ideal lumped element model. The tuned surrogate model meets the design specifications. A second fine model can now be constructed from the surrogate model. This is done by updating the resonator lengths in the electromagnetic model according to the predictions of the surrogate model. Figure 8.9 (d) shows a comparison of the second fine model and the first surrogate model. It is clear that the surrogate model accurately predicts the behaviour of the electromagnetic model when its resonator lengths are changed. Figure 8.9 (e) compares the frequency response of the second fine model to the ideal lumped element model. The second fine model meets the design specifications.

The port tuning procedure is considered to be complete. The filter will be packaged inside a metal box. The circuit will be connected to an outside system via SMA connectors. The next subsection deals with the design of a SMA-to-stripline transition.

8.3.4 Design of SMA-to-stripline transition

A coaxial-to-stripline transition must be designed to minimise the reflections of electromagnetic waves as they enter the filter. It is not sufficient to only ensure that the characteristic impedance of the coaxial line is equal to the characteristic impedance of the stripline on opposing sides of the transition. This is because the field distributions inside the two different transmission line technologies are not the same. A transition is a taper-like section of stripline. It is physically much smaller than a wavelength. The one side of the transition has the same width as the input stripline to the filter. The other side of the transition has a width equal to the width of

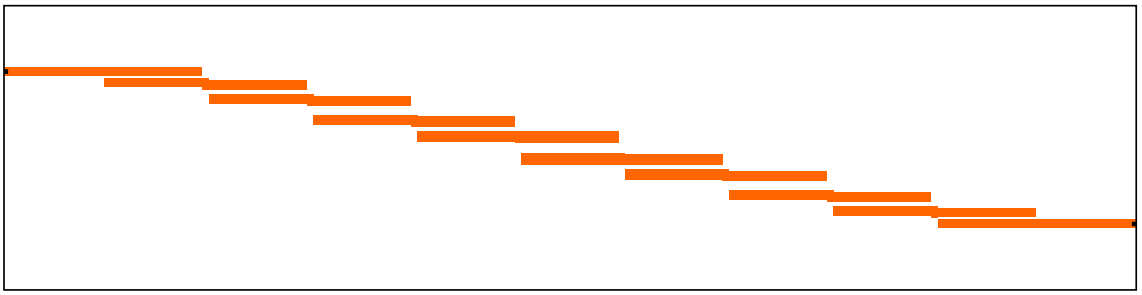

Figure 8.8: The conducting layer of the stripline filter is shown above. The model was constructed and simulated in Sonnet. The conducting layer is positioned between two Rogers 4003C substrates. The two substrates are combined using Arlon's CuClad 6250 bonding film. The top and bottom of the combined structure are connected together to form the ground plane. The electromagnetic model above constitutes the fine model in the space mapping procedure.

Connector dielectric	Teflon
Length of dielectric extension	4.75 mm
Radius of dielectric extension	0.4953 mm
Pin shape	Rectangular
Pin width	0.3048 mm
Pin height	0.1016 mm
Pin length	0.635 mm

Table 8.3: Properties of South Western connector.

the pin of the SMA connector. A transition can be designed using a full-wave electromagnetic simulator such as CST. Figure 8.11 (a) shows a CST model of the connection between a SMA connector and the stripline circuit. The model includes the Rogers substrates and the Arlon bonding film. Figure 8.11 (b) shows the conducting layer. The variable l_t is the length of the transition. The goal is to find the value of l_t that corresponds to the lowest return loss level across the entire band of operation.

The choice of SMA connector depends on the substrate thickness. It is advantageous to ensure that the radius of the connector dielectric is equal to the thickness of the substrate. In such a case the geometries would align and reflections would be minimised. A second point to note is that the difference between the width of the connector pin and width of the input stripline track must be a minimum. It is also advisable to use a SMA where the launch pin has a minimum thickness. When the launch pin is as thin as possible there is a minimum of obstruction to the adhesion of the top substrate to the bottom substrate. A SMA connector from Southwest Microwave, consisting of the 214-520SF jack and 1090-07G pin , was used for all of the planar filter designs in this dissertation. The dimensions of both the jack and the pin are listed in table 8.3. These dimensions where used to model the connector in CST.

The width of the input stripline to the filter is 1.34 mm. A parameter study of the transition in figure 8.11 (b) was performed and it was found that the reflections are a minimum if $l_t = 0.6$ mm. A plot of the associated reflection coefficient is shown in figure 8.11 (c). The transition will obviously influence the performance of the filter. The effect of the transition can be introduced as a s-parameter block in Microwave Office. A final electromagnetic simulation of the filter was performed and losses were included. The frequency response of the lossy electromagnetic model is shown in figure 8.12 (a). The s-parameter models of the SMA-to-stripline transitions were then cascaded with the lossy electromagnetic model to produce a predicted frequency response of the final filter. The predicted frequency response is shown in figure 8.12 (b). It is clear that the SMA-to-stripline transition degrades the $|S_{11}|$ of the filter by up to $5dB$. In the next subsection we shall discuss the manufacturing process and show the measured results.

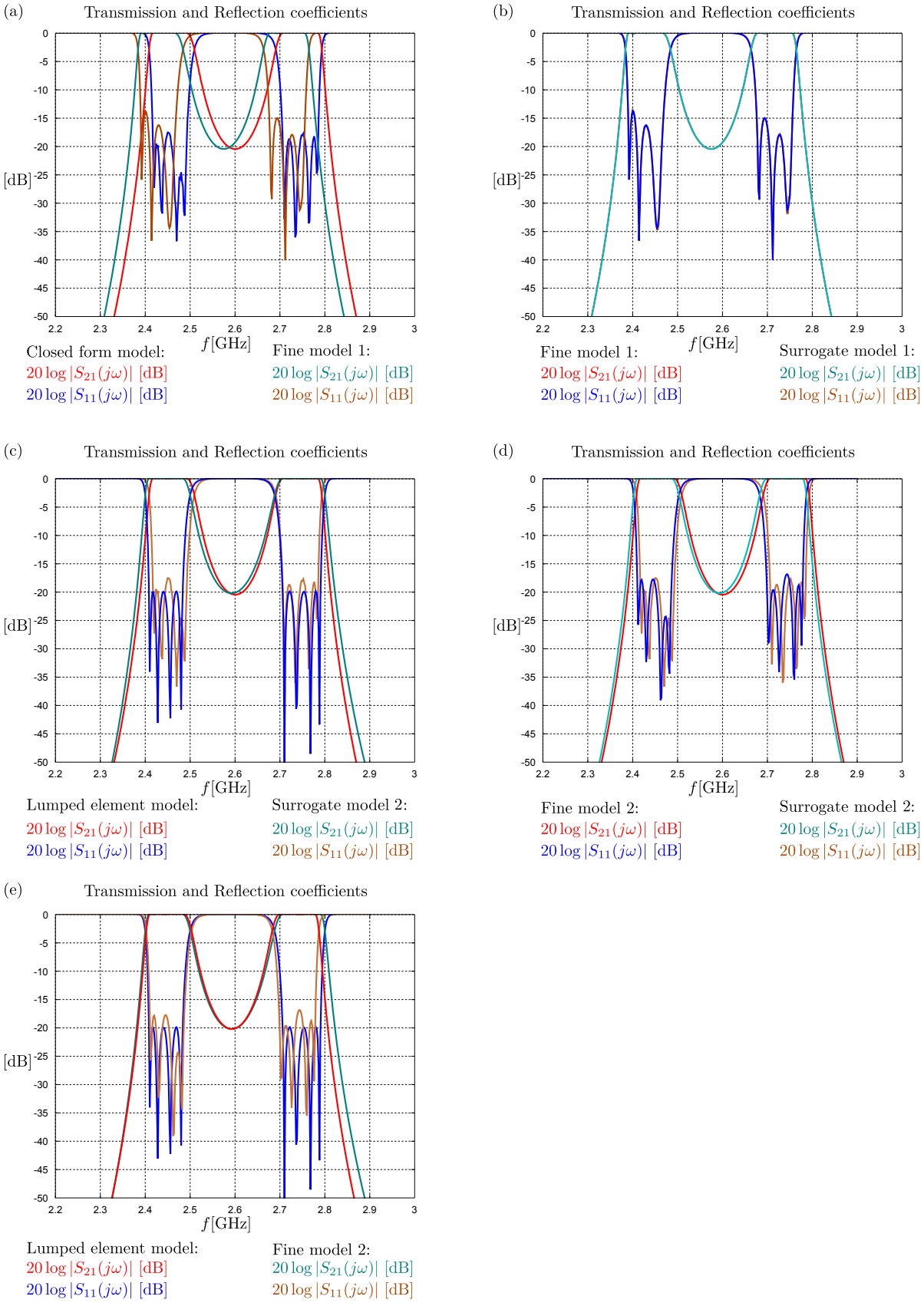

Figure 8.9: The frequency response of the ideal lumped element coupled resonator circuit is compared to the frequency response of the initial electromagnetic model in (a). The frequency response of the surrogate model is compared to the frequency response of the initial electromagnetic simulation in (b). The physical dimensions of the surrogate model are now tuned until it meets the design specifications. The frequency response of the tuned surrogate model is compared to the ideal frequency response in (c). A second electromagnetic model is created from the tuned surrogate model. The frequency response of the new electromagnetic model is compared to the tuned surrogate model in (d). The frequency response of the new electromagnetic model is compared to the ideal response in (e).

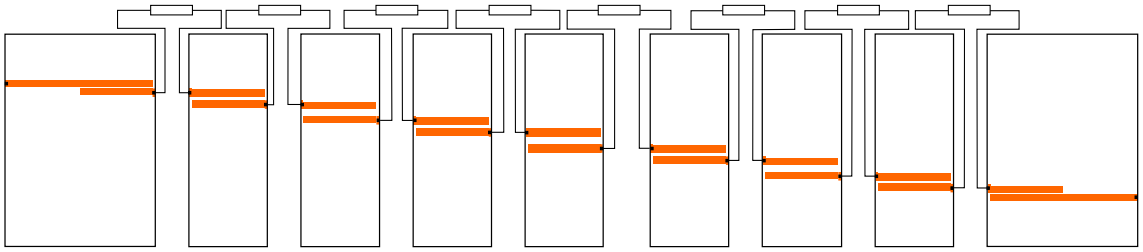

AWR title	Description	Symbol
GM1LIN	Single line on general multi-layer substrate	

Figure 8.10: The surrogate model associated with the fine model in figure 8.8 is shown above. The fine model was divided into smaller electromagnetic models. Each black box refers to a separate electromagnetic model. The models were then connected together using closed form models of transmission line sections in Microwave Office. The Microwave Office element is identified in the table. This element required a general multi-layer substrate definition. All the transmission line sections are tuneable and can be used to change the centre frequencies of the resonators.

8.3.5 Fabrication and measurements

The final dimensions of the filter is provided in figure C.1 in appendix C. The conducting layer of the stripline filter was fabricated using a photo-etching procedure. A metal box with a lid was machined. The bottom layer of the filter was inserted into the box using a conductive adhesive. The connectors were connected through the box walls and soldered onto the tracks. The top layer was then attached using a bonding film. The entire device had to be heated to 250°F for the bonding procedure. The lid was then connected to the ground plane of the top substrate using a conductive adhesive. Photographs of the manufactured filter are shown in figure 8.14. The frequency response of the device was measured and compared to the predicted frequency response. The measured results are shown in figure 8.13. It is clear that the measured frequency response correlate well with the predicted frequency response.

8.4 Summary

In this chapter we illustrated how the theory presented in chapter 3, can be applied in conjunction with well-known concepts from chapters 5 and 7 to design a dual-band all-pole stepped impedance resonator filter using stripline. The filter was manufactured and the measured results correlate well with the ideal frequency response. In order to reduce the loss in the passbands, a multi-layer stripline version of this filter was designed and manufactured and is presented in appendix A.

In the next chapter we shall design a dual-band cascaded triplet filter using polynomial mapping functions. The design is included to serve as a more complex example of the application of the theory.

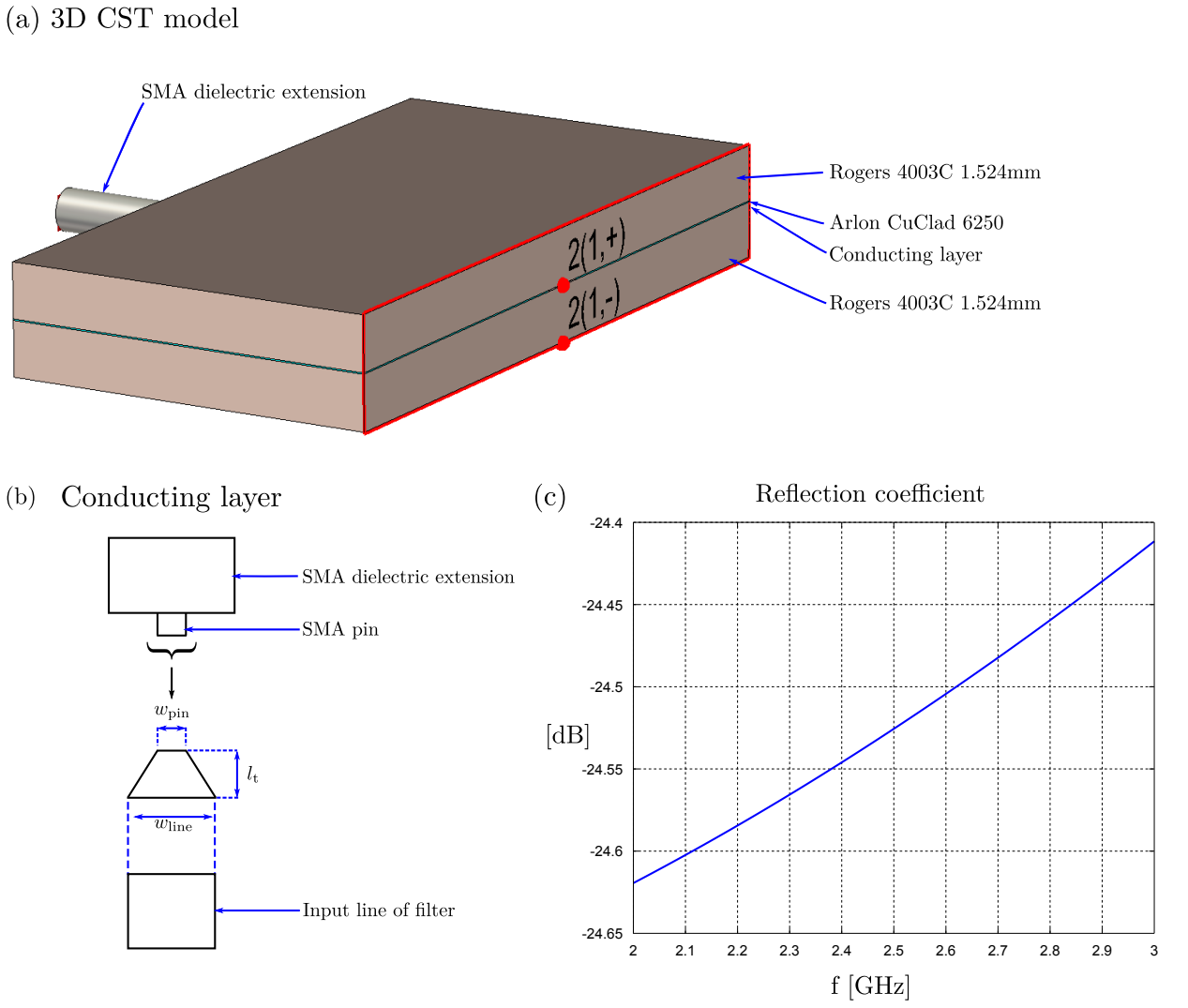

Figure 8.11: The design of the transition is illustrated above. A 3D CST model of the transition is shown in (a). Note that the structure is enclosed inside a metal box. The metal walls are however not shown. The SMA dielectric extension is the part of the SMA that extends through the box wall. The parameterisation of the conducting layer is shown in (b). The length of the transition, l_t, was optimised until the reflections at the input port were at a minimum. The frequency response is shown in (c).

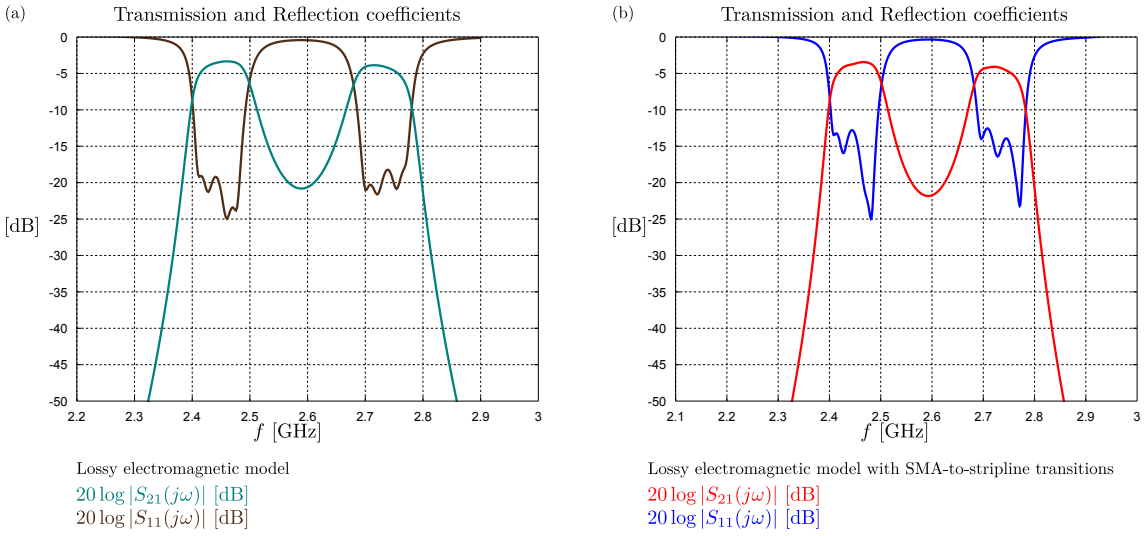

Figure 8.12: The final electromagnetic model was simulated in Sonnet and losses were included. The frequency response of the lossy electromagnetic model is shown in (a). The SMA-to-stripline transitions were simulated in CST and losses were also included. The mentioned simulations were cascaded in Microwave Office to provide a realistic prediction of the performance of the manufactured filter. The predicted frequency response of the manufactured filter is shown in (b). It is clear that the SMA-to-stripline transition grossly degrades the filter performance.

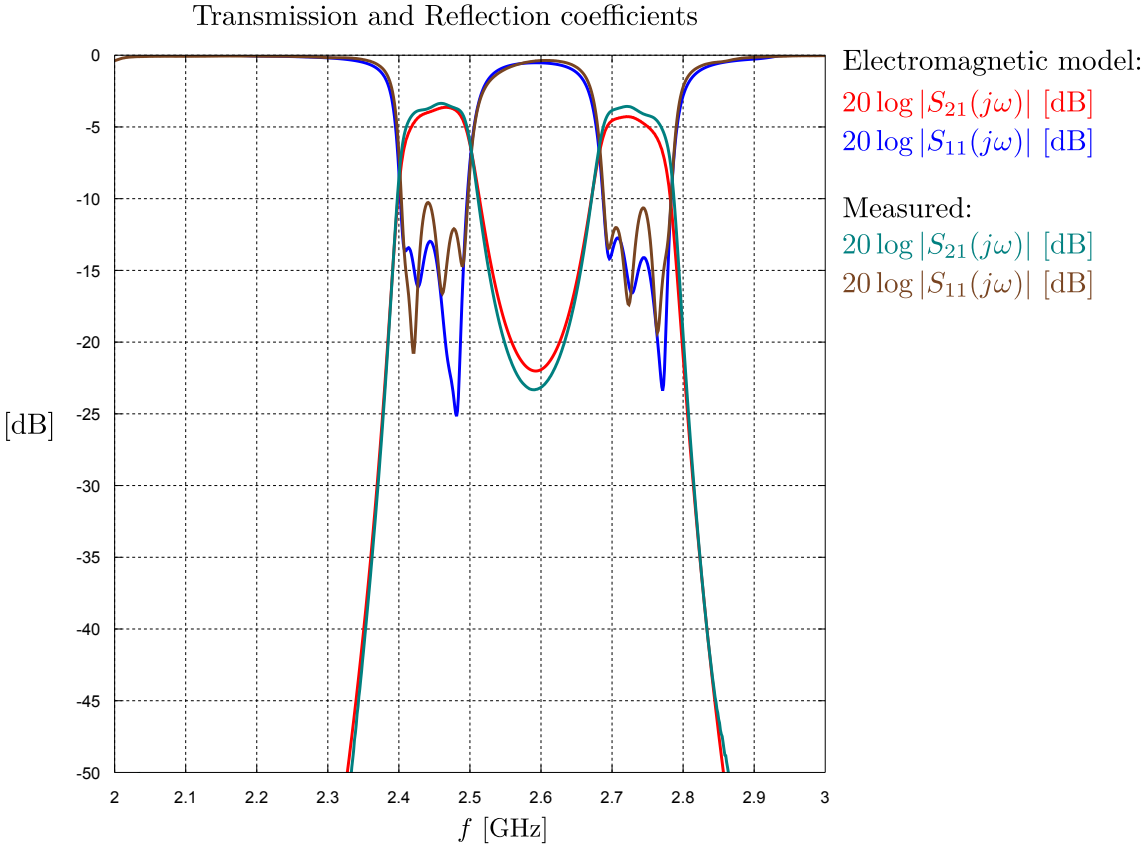

Figure 8.13: A comparison of the measured frequency response of the fabricated filter and the predicted frequency response is shown above. The fabricated filter is the all-pole filter manufactured using single-layer stripline. The predicted frequency response is a lossy electromagnetic model that includes the SMA-to-stripline transitions. There is a good correlation between the predicted performance and the measured results.

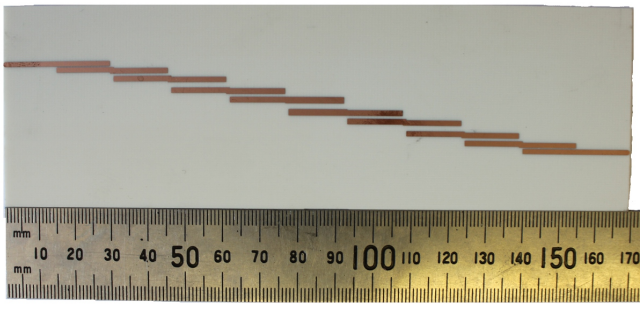

(a)

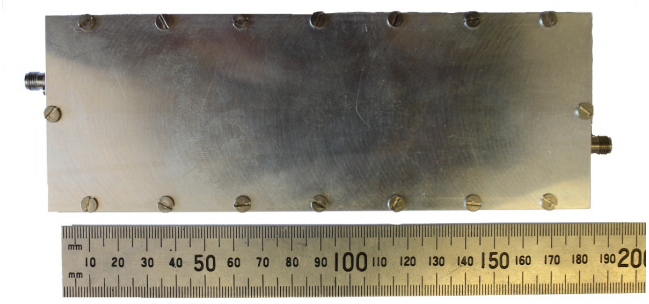

(b)

Figure 8.14: The conducting layer was manufactured using a photo-etching procedure. The conducting layer is shown in (a). The circuit was built into a metal enclosure as shown in (b). The top and bottom ground planes are connected to the metal enclosure to ensure a ground connection at the SMA ports.

Chapter 9

Designs: Dual-band cascaded triplet filters

In the previous chapter a polynomial mapping technique was used to construct an all-pole multi-band filter which was then synthesised. For a more complicated case study this chapter presents the design of a filter with a non-symmetric intermediate frequency axis.

9.1 Specifications

Our goal is to design a dual-band cascaded triplet filter, using a polynomial mapping function, with the following specifications:

- Half power passband 1: 5.15 GHz to 5.35 GHz.
- Half power passband 2: 5.75 GHz to 5.95 GHz.
- Return loss in passband: 20 dB.
- Order of filter: 4.
- Two transmission zeros must be located between the passbands for isolation.

The passbands correspond to frequency bands that are allocated for WiMAX in some European countries [1]. Note that the passband specification will inadvertently lead to a prototype circuit with an asymmetric frequency response. In the next sections we consider the approximation and synthesis procedures.

9.2 Approximation and synthesis

The procedure described in section 8.2 was followed to identify the following prototype specifications:

- Passband 1: $\Omega \in [-1\ ;\ -0.5476]$.
- Passband 2: $\Omega \in [0.7575\ ;\ 1]$.
- Return loss in passband: 20 dB.
- Order of dual-band filter: 4.
- The filter should have finite frequency transmission zeros at $\Omega = 0.1752$ and $\Omega = 0.3725$.

A polynomial mapping function for the bandwidth specification above was constructed in example 2 in section 3.7.1, and was then used to construct the required dual-band characteristic polynomials from a second-order generalised Chebyshev polynomial that has a finite frequency transmission zero at 2 rad/s. The final dual-band characteristic polynomials are as follows:

$$\begin{aligned} E(S) &= S^4 + (1.0701 - 0.2122j)\,S^3 + (1.9257 - 0.4080j)\,S^2 \\ &\quad + (0.6604 - 0.4899j)\,S + 0.3762 - 0.1903j \\ F(S) &= S^4 - 0.2122j\,S^3 + 1.3531\,S^2 - 0.1749jS + 0.4195 \\ jP(S) &= j\,S^2 + 0.5477\,S - 0.0653j \\ \epsilon &= 1.5615 \\ \epsilon_r &= 1 \end{aligned} \tag{9.1}$$

In order to obtain a lumped element filter design in the cascaded triplet topology, an $N+2 \times N+2$ coupling matrix must be synthesised using the method presented in section 5.6. Example 2 in section 5.6.3 illustrates the coupling matrix synthesis procedure for the the characteristic polynomials in equation 9.1. The coupling matrix must now be transformed into the wheel topology using the algorithm defined in section 5.7.2. The example in section 5.7.2 shows how to transform the transversal coupling matrix, obtained during the previous step, into a coupling matrix that is arranged in the wheel topology. The coupling matrix in the wheel topology must next be transformed into a coupling matrix in the cascaded triplet topology using the technique presented in section 5.7.3. The example in section 5.7.3 shows how the wheel prototype that we obtained during the previous step can be converted into a cascaded triplet filter. The coupling matrix obtained in section 5.7.3 is as follows:

$$\mathbf{M}_{N+2\times N+2} = \begin{array}{c|cccccc} & S & 1 & 2 & 3 & 4 & L \\ \hline S & 0 & -0.0923 & 0.7256 & 0 & 0 & 0 \\ 1 & -0.0923 & -0.0733 & -0.8017 & 0 & 0 & 0 \\ 2 & 0.7256 & -0.8017 & -0.0310 & -0.6078 & 0 & 0 \\ 3 & 0 & 0 & -0.6078 & 0.3504 & -0.6929 & 0.7259 \\ 4 & 0 & 0 & 0 & -0.6929 & -0.4584 & 0.0900 \\ L & 0 & 0 & 0 & 0.7259 & 0.0900 & 0 \end{array}$$

The coupling matrix has the property that if one multiplies all the elements in row i and in column i by -1, the resulting matrix will have the same frequency response. The effect is that all the elements in row i and in column i, except for the main diagonal element, will invert their signs. This property is valid for $i = 1, \ldots N$. This property can be proven using similarity transformations [26]. If we invert the elements in row and column 1 and in row and column 3, the resultant matrix is as follows:

$$\mathbf{M}_{N+2\times N+2} = \begin{array}{c|cccccc} & S & 1 & 2 & 3 & 4 & L \\ \hline S & 0 & 0.0923 & 0.7256 & 0 & 0 & 0 \\ 1 & 0.0923 & -0.0733 & 0.8017 & 0 & 0 & 0 \\ 2 & 0.7256 & 0.8017 & -0.0310 & 0.6078 & 0 & 0 \\ 3 & 0 & 0 & 0.6078 & 0.3504 & 0.6929 & -0.7259 \\ 4 & 0 & 0 & 0 & 0.6929 & -0.4584 & 0.0900 \\ L & 0 & 0 & 0 & -0.7259 & 0.0900 & 0 \end{array} \tag{9.2}$$

The circuit will be realised as a stepped impedance coupled resonator filter. As the stepped impedance resonators exhibit a shunt type resonance, the coupling matrix in equation 9.2 is represented as a prototype circuit in

(a) Prototype circuit

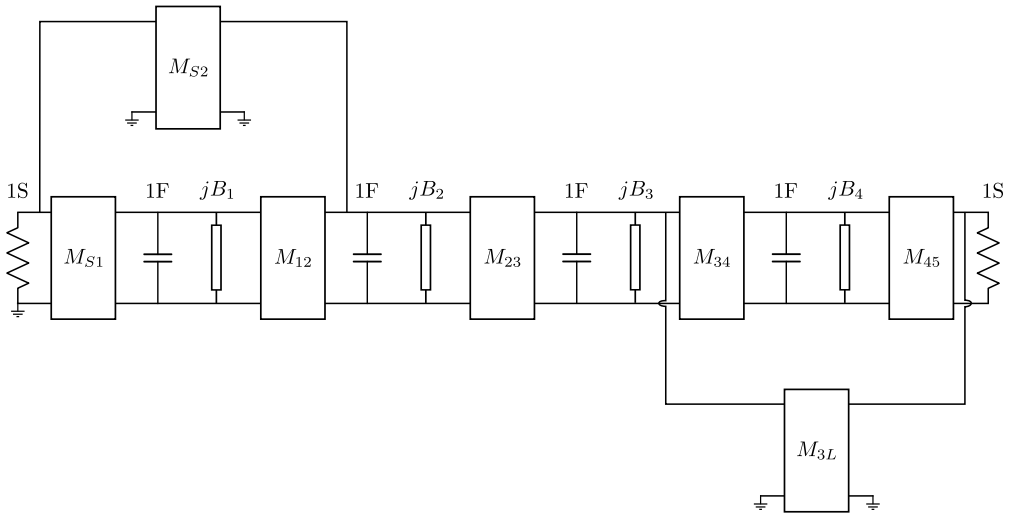

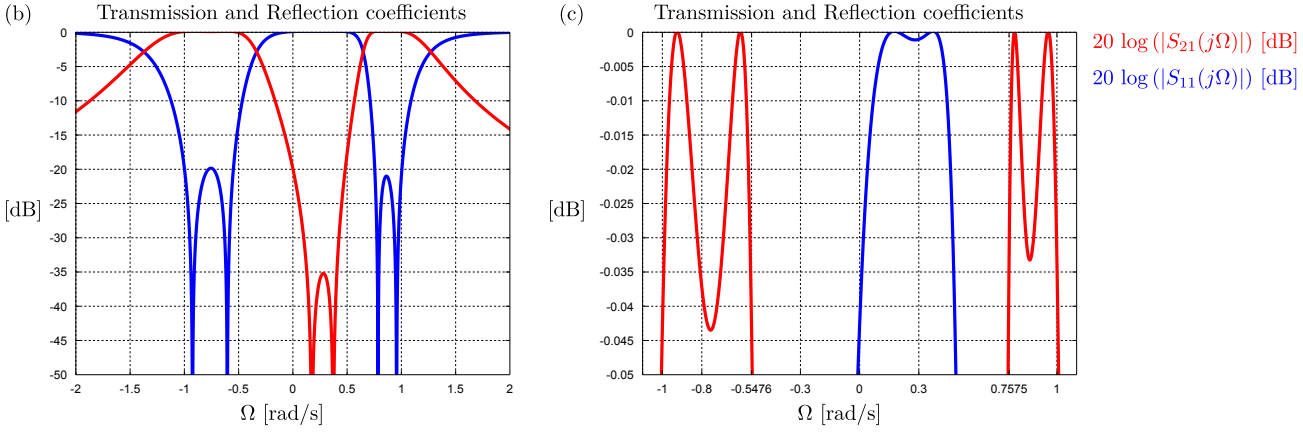

Figure 9.1: The coupling matrix represented as an admittance prototype is shown in (a). The values of the admittance inverters refer to the coupling matrix elements in equation 9.2. The FIR elements correspond to the main diagonal entries in equation 9.2. The frequency response in the prototype frequency domain is shown in (b). The ripple bandwidth is shown in (c). The ripple passbands are defined as $\Omega \in [-1; -0.5476] \cap [0.7575; 1]$. Note that the two passbands have different equal ripple levels.

the admittance form as shown in figure 9.1. The prototype circuit can now be denormalised using the technique presented in section 7.1. The centre frequency is calculated as $f_0 = 5.5507$ GHz. The fractional bandwidth is calculated as $\Delta = 0.1092$. The impedance level at the ports were taken as $50\,\Omega$. The denormalised lumped element circuit is shown in figure 9.2. Note that we included phase-reversing transformers in figure 9.2 to ensure that the lumped element circuit has a phase shift over its resonators similar to that of a half-wavelength distributed resonator. This is important as we use phase relationships to realise the cross-couplings. Both the ripple passbands and the half-power passbands of the denormalised lumped element circuit are shown in figure 9.2. It is clear that the filter has the required half-power bandwidths.

9.3 Realisation

The coupling matrix in equation 9.2 will now be realised as a cascaded triplet filter consisting of stepped impedance resonators. We shall systematically design the single-layer stripline filter using the technique described in section 7.8.2.

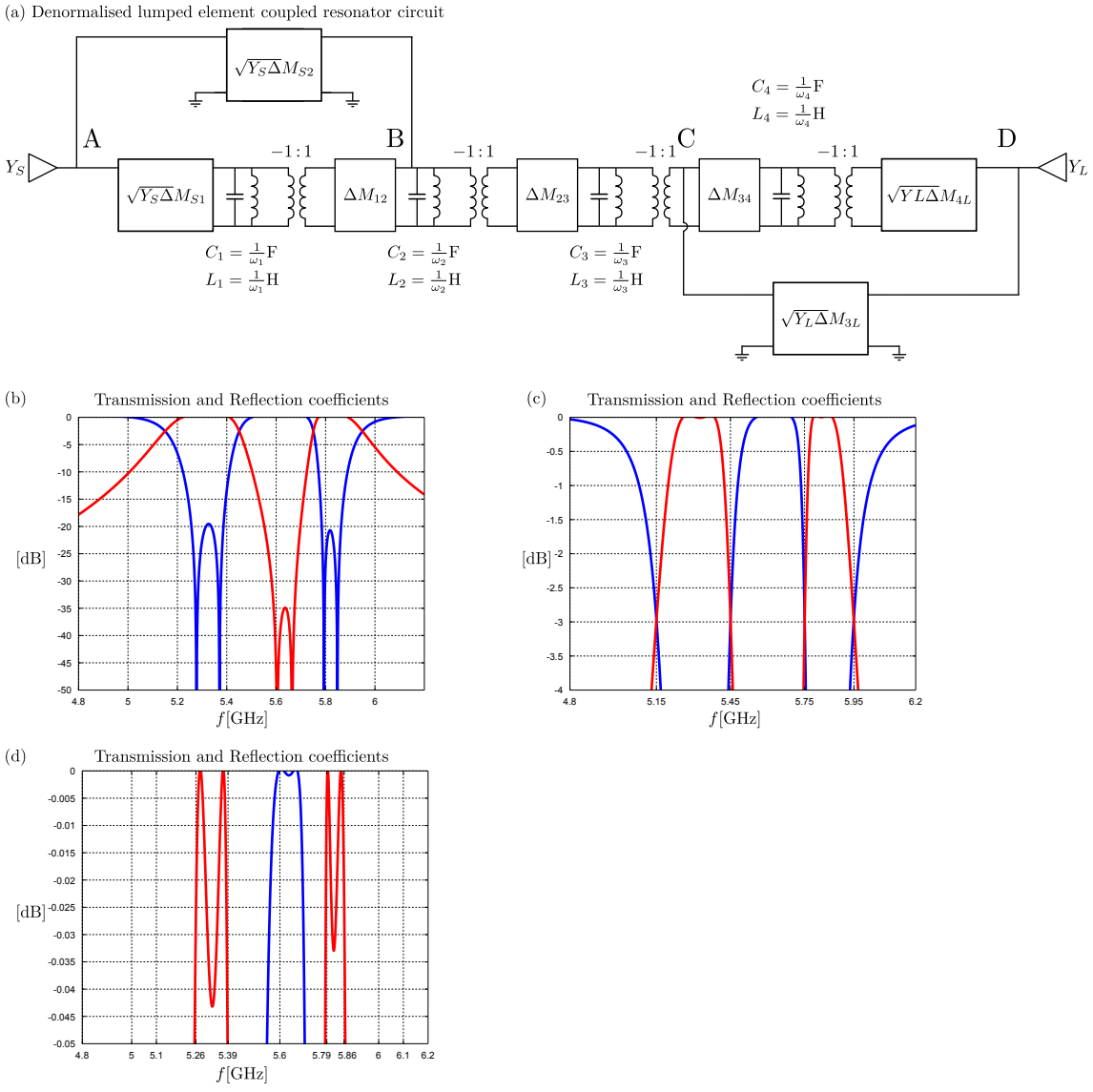

Figure 9.2: The denormalised lumped element coupled resonator circuit is shown in (a). The frequency response is shown in (b). The half-power bandwidth is shown in (c). The first half-power passband extends from 5.15 GHz to 5.45 GHz. The second half-power passband extends from 5.75 GHz to 5.95 GHz. The ripple bandwidth is shown in (d). The first ripple passband extends from 5.255 GHz to 5.387 GHz. The second ripple passband extends from 5.79 GHz to 5.86 GHz.

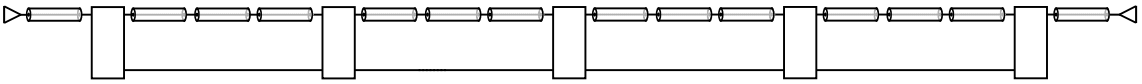

AWR title	Description	Symbol
TLIN	Section of ideal transmission line	
PORT	Port	
N/A	Admittance inverter circuit	

Figure 9.3: The main coupling path of the cross-coupled filter is realised as an all-pole filter using stepped impedance resonators. The resonators exhibit a shunt type resonance and are therefore coupled to each other through admittance inverters. The resonators are asynchronously tuned. The central part of each stepped impedance resonator is used to tune the centre frequencies of the resonators. A table defining the Microwave Office elements is provided.

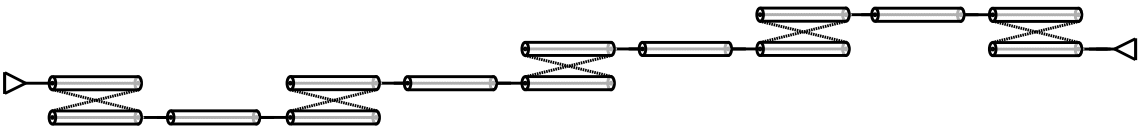

AWR title	Description	Symbol
CLIN	Section of ideal coupled transmission lines	
TLIN	Section of ideal transmission line	
PORT	Port	

Figure 9.4: The main coupling path of the cross-coupled filter is realised as an all-pole filter using stepped impedance resonators. The resonators are coupled to each other using ideal coupled transmission lines. The resonators are asynchronously tuned. The central part of each stepped impedance resonator is used to tune the centre frequencies of the resonators. A table defining the Microwave Office elements is provided.

9.3.1 Ideal transmission line model

The coupling matrix in equation 9.2 has a topology similar to the circuit illustrated in figure 7.13. An ideal transmission line model is constructed for the main coupling path of the filter. The main coupling path is indicated in blue in figure 7.13. We realise the main coupling path of the coupling matrix in equation 9.2 as the circuit in figure 9.3. This circuit is an all-pole filter that was realised using stepped impedance resonators. Each resonator consists of three ideal transmission line sections. The stepped impedance resonators are coupled to each other using admittance inverters. The entire circuit is defined by the characteristic impedances and electrical lengths of the transmission line sections and by the values of the admittance inverters. Each coupled section in the filter is 45° in length at f_0 to ensure that resonant frequencies and couplings can be tuned independently. The defining parameters of the filter can be calculated using the technique described in section 7.6. The circuit in figure 9.3 can be transformed into the transmission line model in figure 9.4 using the technique described in section 7.6. The frequency response of the ideal model in figure 9.2, with all the cross-couplings removed, is compared to the frequency response of the transmission line model in figure 9.4. The comparison is shown in figure 9.5.

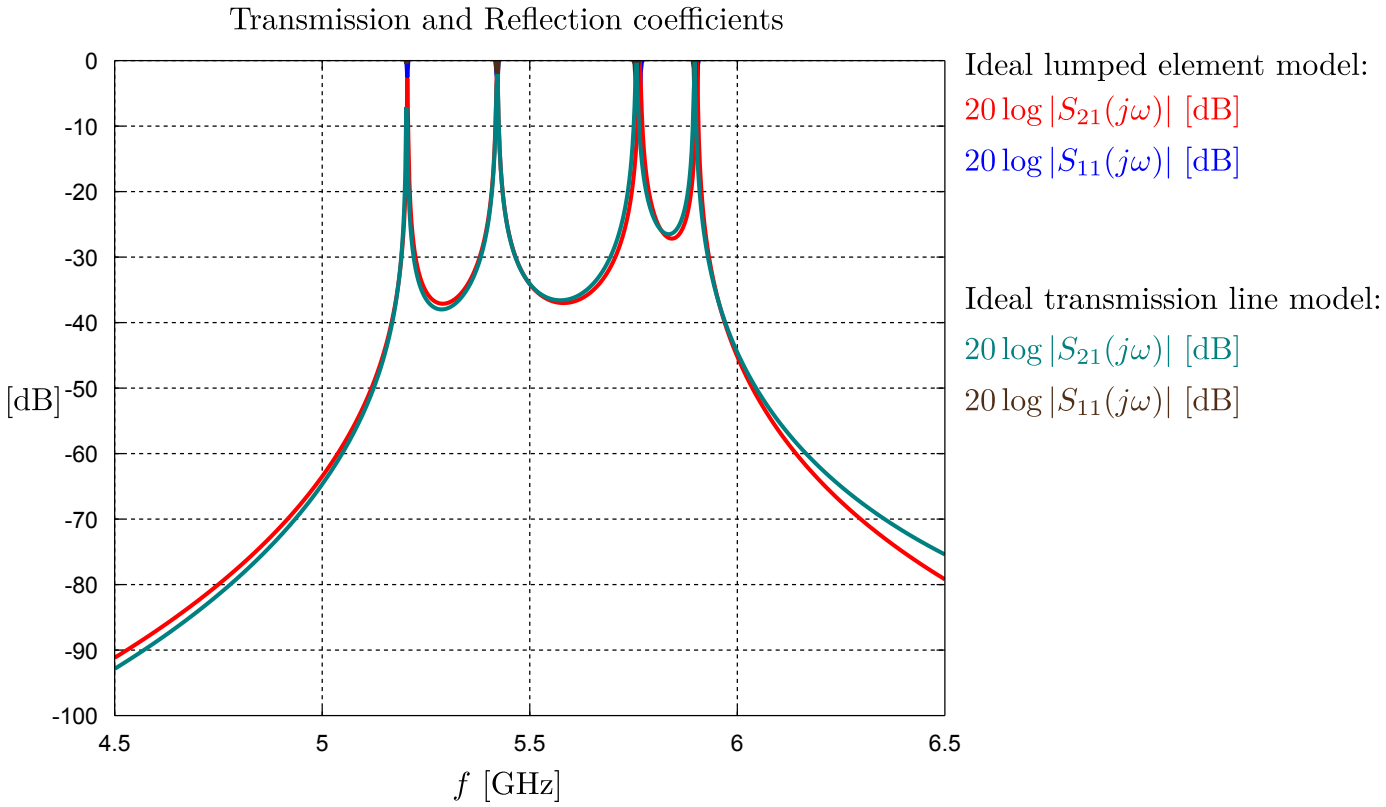

Figure 9.5: The frequency response of the ideal model in figure 9.2, with all the cross couplings removed, is compared to the frequency response of the transmission line model in figure 9.4. Both circuits are asynchronously tuned. The frequency responses of the circuits correlate well over a narrow bandwidth.

9.3.2 Delay lines for cross-couplings

The technique described in section 7.8.1 is employed to calculate the lengths of the delay lines required to introduce the desired cross-couplings. Our filter has the same topology as the circuit depicted in figure 7.14. Suppose all the cross-couplings in 9.2 are disconnected. We must calculate the phase of the transfer admittance Y_{AB} along the main coupling path. The phase of the transfer admittance from A to B is shown together with $|S_{21}|$ in figure 9.6 (a). We now reintroduce the cross-coupling from A to B. Again we measure the phase of the transfer admittance from A to B together with $|S_{21}|$. These are shown figure 9.6 (b). It is clear the phase changes from $+90°$ to $-90°$ at the frequency of the transmission zero associated with the cross-coupling. The phase along the main coupling path was $+90°$. The phase shift along the cross-coupling path must be $-90° \pm 360k$ where $k \in \mathbb{Z}$. It is important to note that the capacitive coupling of the delay line to the position B will introduce a $-90°$ phase shift. Our delay line from A to B must therefore be $360°k$, $k \in \mathbb{Z}$ in length.

The required length of the delay line between C and D can be determined using a similar technique. The phase of the transfer admittance from C to D, when the cross-coupling from C to D is disconnected, is shown in figure 9.6 (c) together with $|S_{21}|$. The cross-coupling from C to D is then reintroduced and the phase of the transfer admittance from C to D and $|S_{21}|$ are measured again and are shown in figure 9.6 (d). It is clear the phase changes from $-90°$ to $+90°$ at the frequency of the transmission zero associated with the cross-coupling. The phase shift along the main coupling path was $-90°$. The phase shift along the cross-coupling path must be $+90° \pm 360k$ where $k \in \mathbb{Z}$. Again the capacitive coupling of the delay line to the position C will introduce a $-90°$ phase shift. Our delay line from C to D must therefore be $180° \pm 360k$, $k \in \mathbb{Z}$ in length.

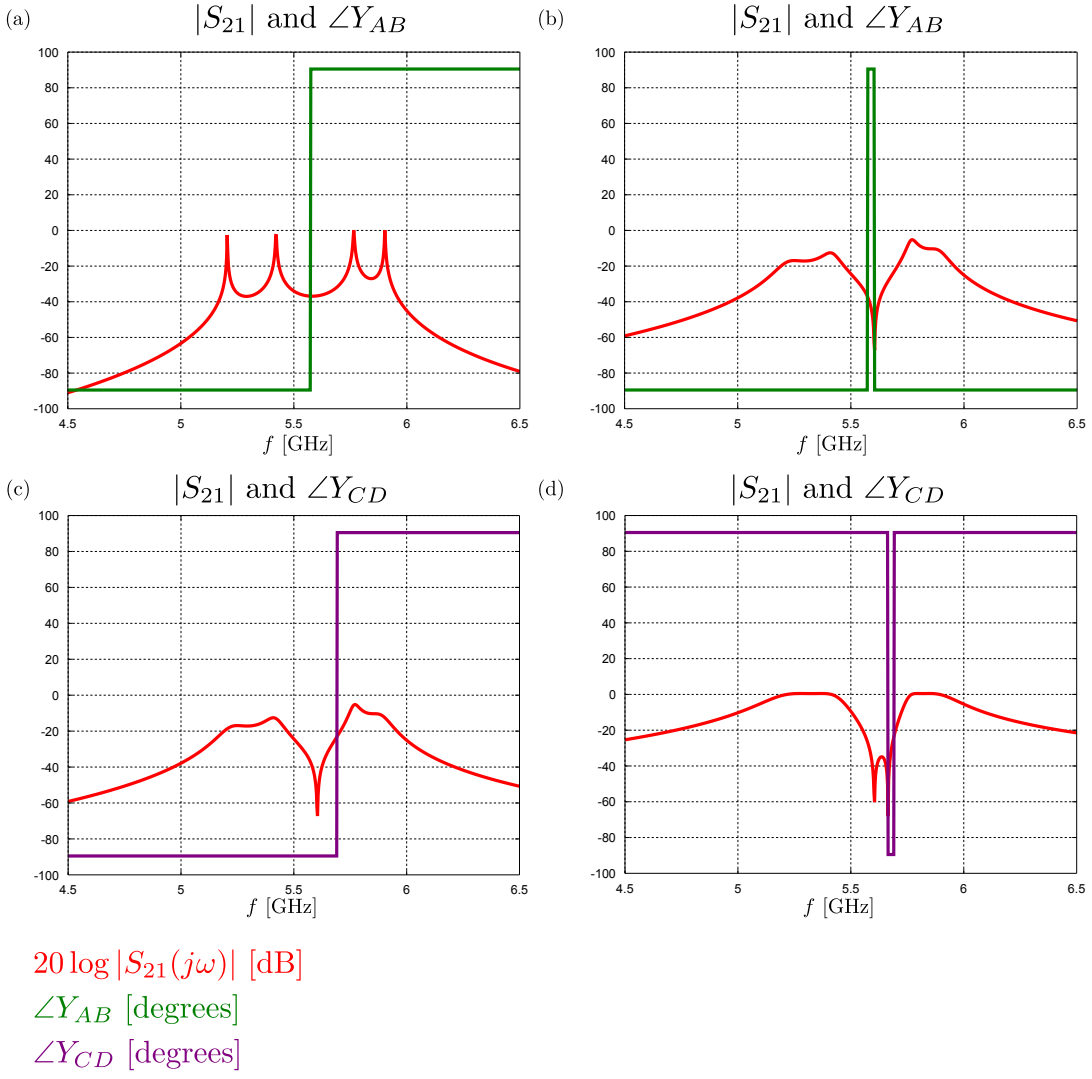

Figure 9.6: The reader is referred to figure 7.14. All the cross-couplings are disconnected and the phase of Y_{AB} as well as the magnitude of S_{21} are measured and shown in (a). The cross coupling from A to B is then inserted and the phase of Y_{AB} and the magnitude S_{21} are measured again. These are shown in (b). Next the phase of Y_{CD} as well as the magnitude of S_{21} are measured and shown in (c). The cross coupling from C to D is then inserted and the phase of Y_{CD} and the magnitude of S_{21} are measured again. These are shown in (d). From these measurements the lengths of the delay lines can be calculated.

9.3.3 Closed form model of single-layer stripline filter

The procedure described in section 8.3 is followed here to design the main coupling path of the closed form model of the cascaded triplet filter. The physical length of the cross-coupling paths must now be determined from the electrical lengths identified in the previous section. The impedance of the delay lines can be arbitrarily chosen. This can be used during the optimisation procedure to fine tune the cross-coupling. The width of the delay lines were chosen as 0.4 mm as this dimension agrees well with the discretisation grid in Sonnet. The delay lines must be positioned in such a manner that they do not couple energy into unwanted places and that they remain as straight as possible as straight delay lines produce fewer reflections. The initial coupling gaps at the end of the delay lines were both chosen as 0.25 mm. A complete closed form model of the filter is shown in figure 9.7. We extensively used the extraction feature in Microwave Office to associate closed form models with electromagnetic simulation data. This is an necessity if one wants to accurately model bends and other discontinuities (refer to section A.1.2). Initially the closed form model of the filter does not produce the required frequency response. The procedure discussed in section 7.8.2 must be used to ensure that the circuits in figures 9.7 and 9.2 have the same frequency response over a narrow bandwidth: First all the cross-couplings are removed and the main coupling path is tuned on its own. The group delay method discussed in section 7.9.1 can be used for the main coupling path. Then the first triplet is inserted and only the delay line, the capacitive gap at the end of the delay line and the centre frequency of the resonator being coupled to are tuned. The same procedure is applicable to the remaining triplet. Following this procedure, the closed form model can be tuned until it has the desired frequency response. The frequency response of the tuned closed form model is compared to the ideal frequency response in figure 9.8.

9.3.4 Electromagnetic simulation and port tuning of single-layer stripline filter

An electromagnetic model is now constructed for the filter in Sonnet. The conducting layer of the filter is shown in figure 9.9. The electromagnetic model includes the effects of the substrates and of the bonding films. Again the frequency response of the initial electromagnetic model is compared to the ideal frequency response and the port tuning procedure from section 7.9.2 has to be applied to until a model is found that meets the design specifications. The initial electromagnetic model becomes the first fine model and a surrogate model can be constructed from the fine model by segmenting the fine model into smaller sections. Each section can be simulated on its own and be represented by an s-parameter matrix. The different matrices are connected together using closed form models in Microwave Office. The closed form models can then be used to tune the dimensions of the fine model. A surrogate model associated with the circuit in figure 9.9 is shown in figure 9.10 . Each black box in figure 9.10 represents a separate Sonnet simulation. Note that the conductors inside each of the Sonnet simulations are moved sufficiently far away from the simulation walls to prevent coupling.

The initial filter cannot be segmented arbitrarily. Each resonator, delay line and capacitive gap at the end of a delay line should span over at least two segments. Closed form models can then be embedded into these lines to render them tuneable. In this manner all the cross-couplings and all the resonant frequencies become tuneable. The surrogate model with the embedded closed form models is shown in figure 9.10.

The procedure described in section 8.3.3 was followed here to obtain the final dimensions of the filter. The results of the tuning procedure is summarised in figure 9.11.

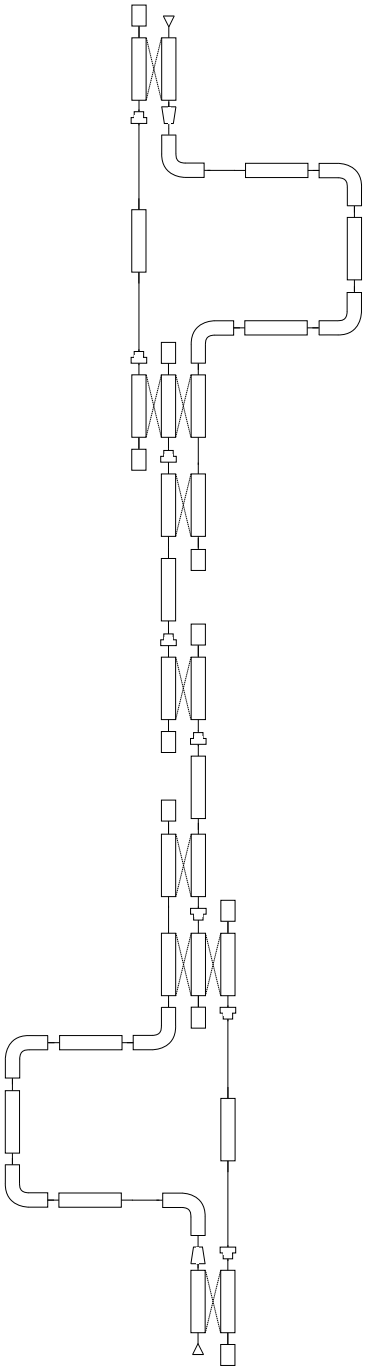

AWR title	Description	Symbol
GMCLIN	Multiple coupled lines on general multi-layer substrate	
GMCLIN	Multiple coupled lines on general multi-layer substrate	
GM1LIN	Single line on general multi-layer substrate	
MTAPER	A linear microstrip taper	
MCURVE	Microstrip radiused corner	
PORT	Port	
SSTEP0	Stripline step in conductor width	
SLEF	Open stripline with end effect	

Figure 9.7: A closed form model of a cross-coupled stepped impedance resonator filter is shown above. A table identifying the Microwave Office components is provided. Note that the closed form models also require a general multi-layer substrate definition. Depending on the substrate definition, the circuit above can represent a multi-layer stripline circuit or a normal single-layer stripline circuit.

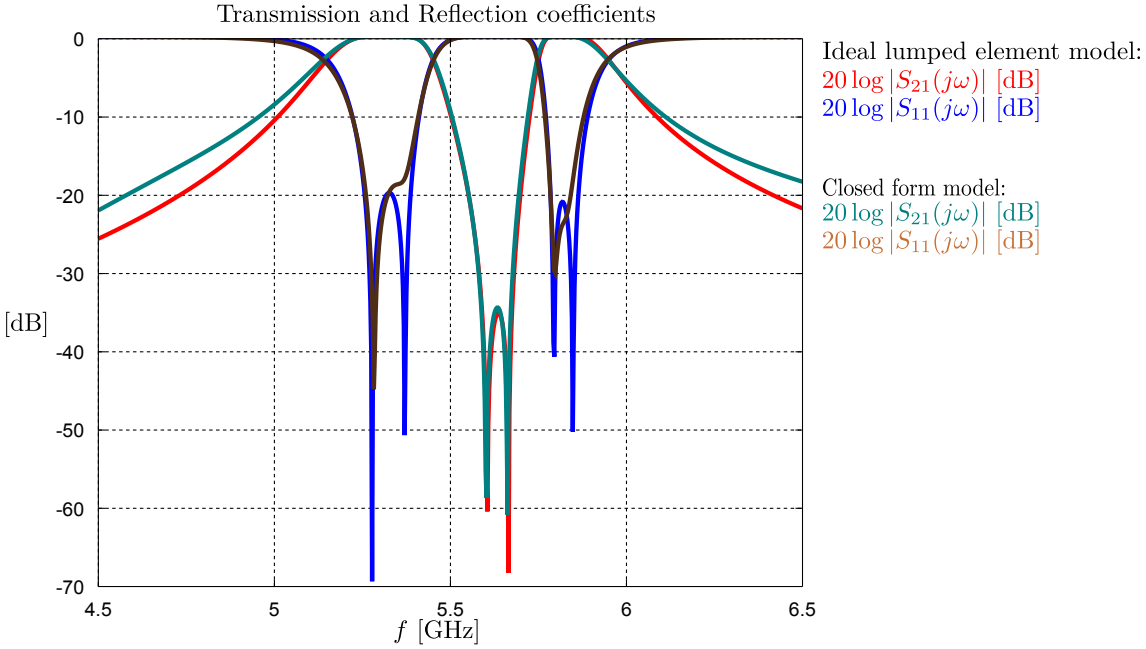

Figure 9.8: The frequency response of the tuned closed form model in figure 9.7 is compared to the ideal frequency response of the lumped element circuit in figure 9.2.

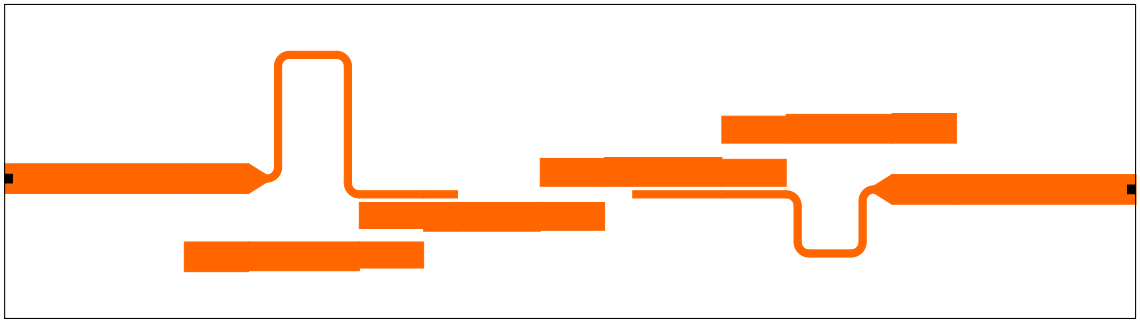

Figure 9.9: The electromagnetic model of the stripline filter is shown above. This model was constructed and simulated in Sonnet. The stripline model constitutes the fine model in the space mapping procedure.

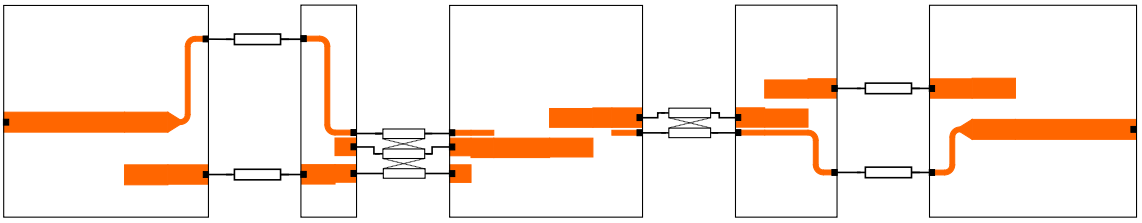

AWR title	Description	Symbol
GMCLIN	Multiple coupled lines on general multi-layer substrate	
GM1LIN	Single line on general multi-layer substrate	

Figure 9.10: The surrogate model associated with the fine model in figure 9.9 is shown above. The fine model was divided into smaller electromagnetic models. Each black box refers to a separate electromagnetic model. The models were then connected together using closed form models of transmission line sections. All the transmission line sections are tuneable and can be used to tune the centre frequencies of the resonators and the values of the cross-couplings.

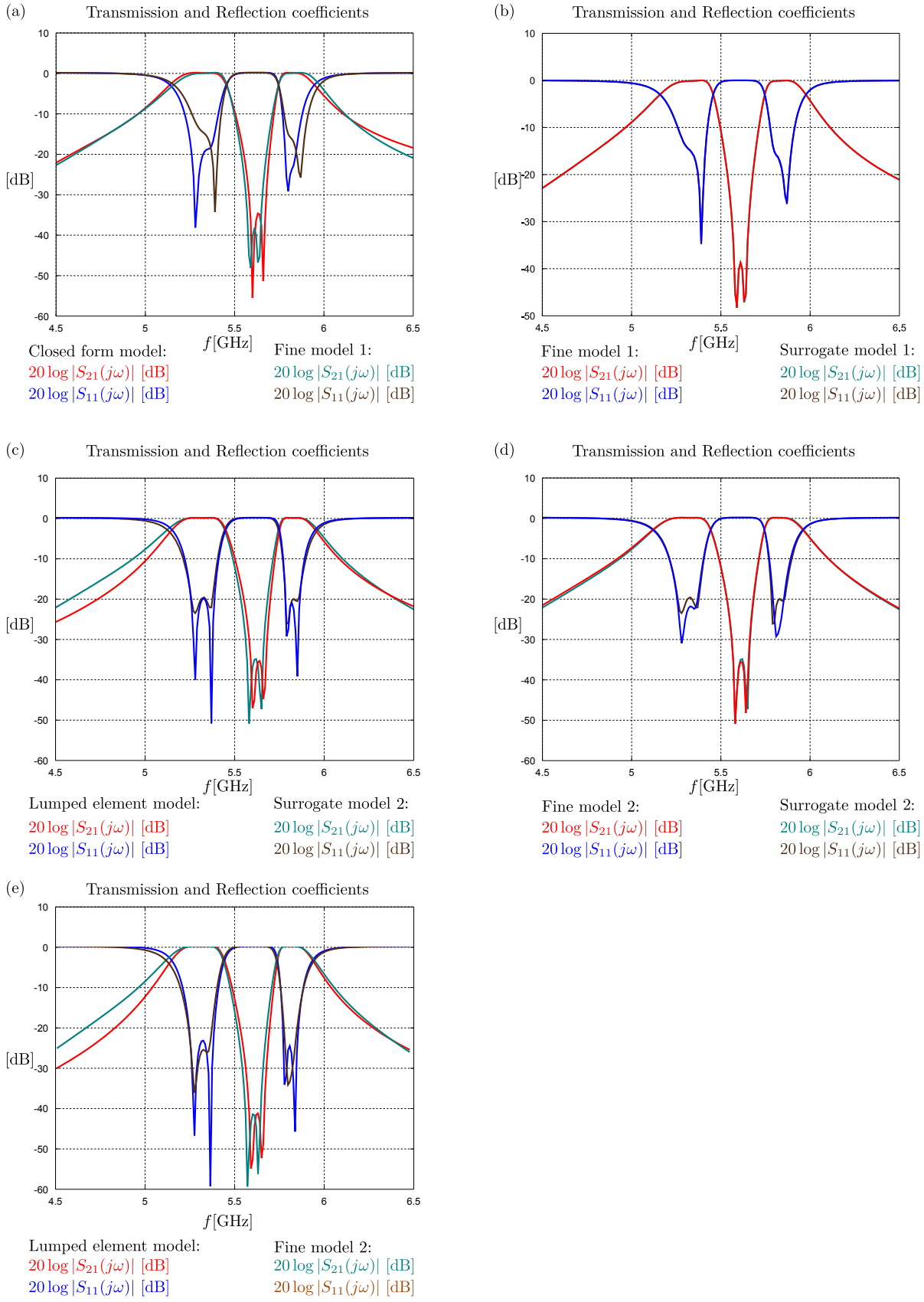

Figure 9.11: The frequency response of the ideal lumped element coupled resonator circuit is compared to the frequency response of the initial electromagnetic model in (a). The frequency response of the surrogate model is compared to the frequency response of the initial electromagnetic simulation in (b). The physical dimensions of the surrogate model are now tuned until it meets the design specifications. The frequency response of the tuned surrogate model is compared to the ideal frequency response in (c). A second electromagnetic model is created from the tuned surrogate model. The frequency response of the new electromagnetic model is compared to the tuned surrogate model in (d). The frequency response of the new electromagnetic model is compared to the ideal response in (e).

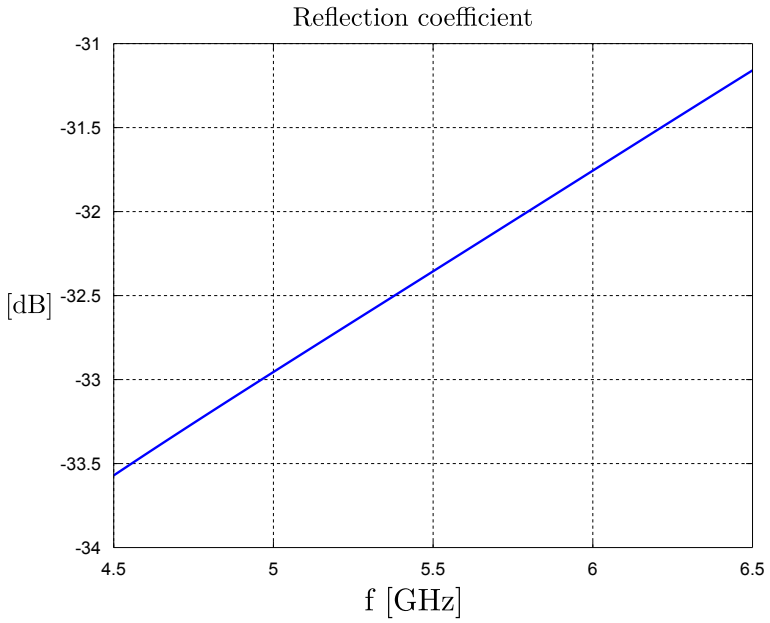

Figure 9.12: The design procedure of the transition for the cross-coupled filter in single-layer stripline is identical to the procedure illustrated in figure 8.11. The final reflection coefficient for $l_t = 0.75$ mm is shown above.

9.3.5 Design of SMA-to-stripline transition

A SMA-to-stripline transition can be designed using the technique described in section 8.3.4. The same connectors are used for all the filters. The only difference in the design is that the width of the input stripline to the filter is 1.65 mm. A parameter study of the transition in figure 8.11 (b) was performed and it was found that the reflections are a minimum if $l_t = 0.75$ mm. A plot of the associated reflection coefficient is shown in figure 9.12. A final electromagnetic simulation of the filter was performed and losses were included. The frequency response of the lossy electromagnetic model is shown in figure 9.13 (a). The s-parameter models of the SMA-to-stripline transitions were then cascaded with the lossy electromagnetic model to produce a predicted frequency response of the final filter. The predicted frequency response is shown in figure 9.13 (b). In the next subsection we shall discuss the manufacturing process and show the measured results.

9.3.6 Fabrication and measurements

The manufacturing procedure of the cross-coupled filter is identical to that described in section 8.3.5. The final dimensions of the filter is provided in figure C.3 in appendix C. Photographs of the manufactured filter are shown in figure 9.14. The frequency response of the device was measured and compared to the predicted frequency response. The measured results are shown in figure 9.15. It is clear that the measured frequency response correlate well with the predicted frequency response. This completes the design of a cascaded triplet filter in stripline.

9.4 Summary

In this chapter we illustrated how the theory presented in chapter 3, can be applied in conjunction with well-known concepts from chapters 5 and 7 to design a dual-band cascaded triplet filter using stripline. The filter was manufactured and the measured results correlate well with the ideal frequency response. In order to

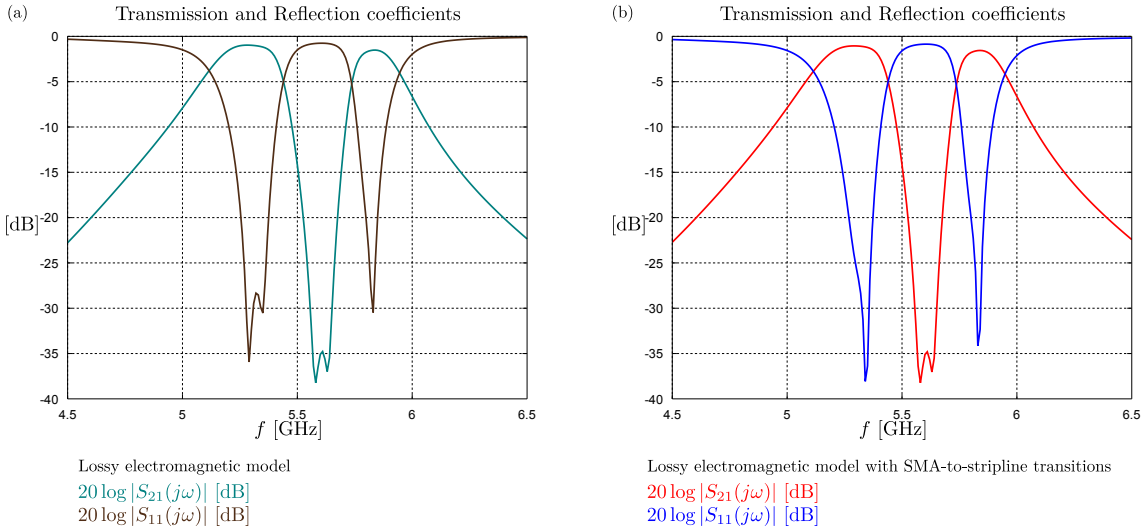

Figure 9.13: The final electromagnetic model was simulated in Sonnet and losses were included. The frequency response of the lossy electromagnetic model is shown in (a). The SMA-to-stripline transitions were simulated in CST and losses were also included. The mentioned simulations were cascaded in Microwave Office to provide a realistic prediction of the performance of the manufactured filter. The predicted frequency response of the manufactured filter is shown in (b). The SMA-to-stripline transition has almost a negligible influence on the frequency response of the filter.

reduce the loss in the passbands, a multi-layer stripline version of this filter was designed and manufactured and is presented in appendix A.2.

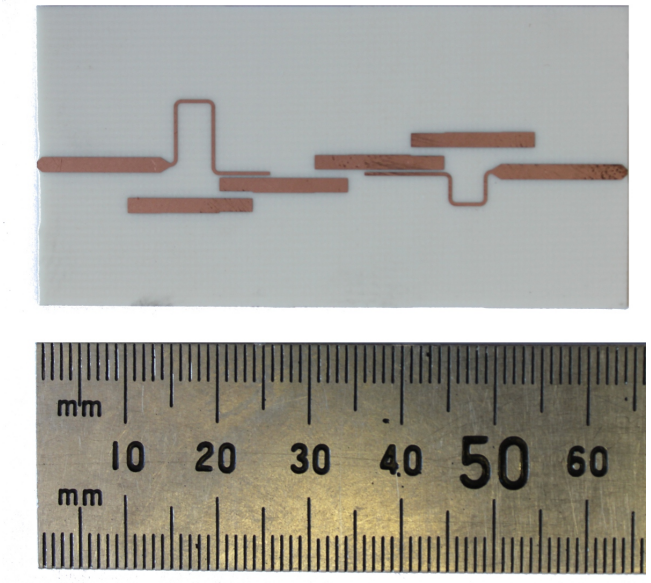

(a)

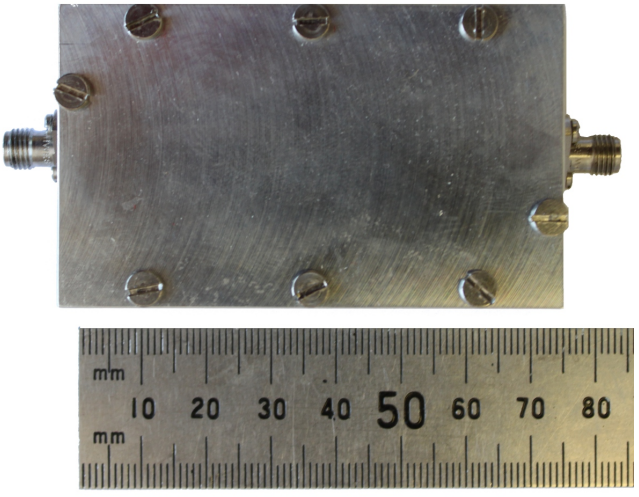

(b)

Figure 9.14: The conducting layer was manufactured using a photo-etching procedure and is shown in (a). The circuit was built into a metal enclosure as shown in (b).

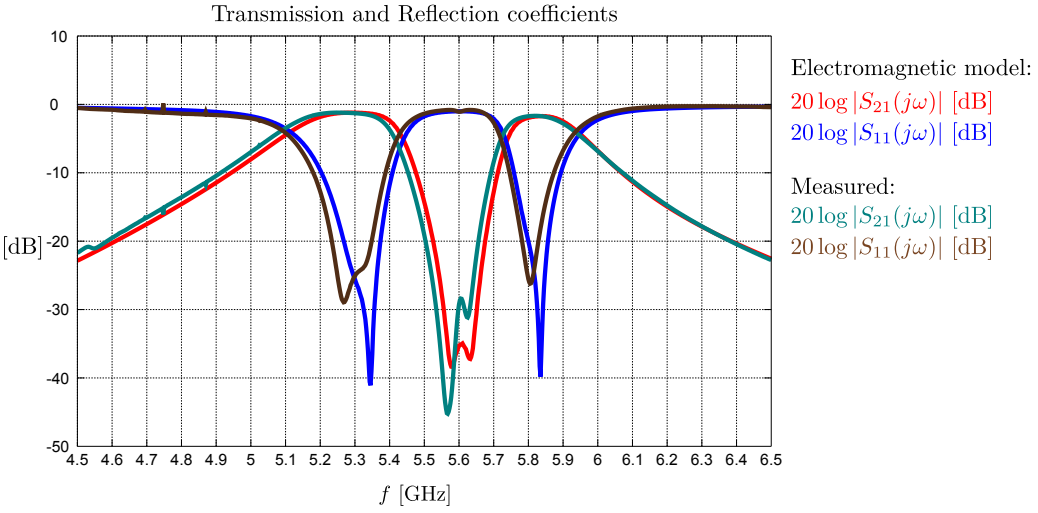

Figure 9.15: A comparison of the measured frequency response of the fabricated filter and the predicted frequency response is shown above. The fabricated filter is the cascaded triplet filter manufactured using single-layer stripline. The predicted frequency response is a lossy electromagnetic model that includes the SMA-to-stripline transitions. There is a good correlation between the predicted performance and the measured results.

Chapter 10

Design: Three-band coaxial resonator filter

A rational mapping function is utilised to design a three-band coaxial resonator filter. The contents of this chapter therefore serves as both a practical example and a validation of the theory presented in chapters 4 and 6. The chapter starts by listing the design specifications. The theory discussed in chapters 4 and 6 is then employed to synthesise a suitable lumped element filter circuit. The lumped element circuit is then realised as a microwave structure. The realisation of coaxial resonator filters have been studied in great detail and there are numerous books and other publications on the matter. We shall rely extensively on the available body of knowledge to realise the three-band filter in this chapter [9, 61, 77, 6, 78, 79, 10]. Some of the available techniques have been discussed in chapter 7.

10.1 Specifications

The goal is to design a three-band filter with the following specifications:

- Passband 1: 1.50 GHz to 1.53 GHz.
- Passband 2: 1.56 GHz to 1.59 GHz.
- Passband 3: 1.62 GHz to 1.65 GHz.
- Order of each passband: 4.
- Minimum return loss in each passband: 20 dB.

In the next section we consider the approximation and synthesis procedures.

10.2 Approximation and synthesis

The filter designed in this chapter is a coupled resonator filter. Both the narrowband and general approximation methods presented in chapter 4 can therefore be applied to the design. Likewise both associated synthesis methods presented in chapter 6 can be used to synthesise the final circuit. For the narrowband formulation, a rational mapping function for the bandwidth specification in section 10.1, was constructed in example 1 in section 4.3.3. The mapping function was then used to design a three-band lumped element filter, adhering to the design specifications in section 10.1, in example 1 in section 6.1.5. Likewise, for the general formulation, a rational mapping function for the bandwidth specification in section 10.1, was constructed in example 1 in section 4.4.3. Said mapping function was then used to design a three-band lumped element filter, adhering

Component	Value	Component	Value
G_S, G_L	0.02 S	C_1	101.2 pF
J_{S1}, J_{4L}	0.03502 S	L_1	101.2 pH
J_{12}, J_{34}	0.05211 S	C_2	101.1 pF
J_{23}	0.04005 S	L_2	101.1 pH
J_a	0.05393 S	C_3	101 pF
J_b	0.04256 S	L_3	101 pH

Table 10.1: Component values for the circuit in figure 10.1. Note that any inductor and capacitor values can be used to construct the resonators, providing that they produce the correct resonant frequencies. The couplings surrounding a resonator must be scaled using the susceptance slope of the resonator – that is dependent on the inductor and capacitor values of said resonator. Both input and output couplings can also be chosen arbitrarily providing that the input and output couplings compensate for the correct loaded quality factors.

to the design specifications in section 10.1, in section 6.2.5. Both design methodologies produced the same result. The final lumped element circuit, with its frequency response, is shown in figure 10.1. This filter meets the design specifications listed in section 10.1. Component values for the circuit elements in figure 10.1 are provided in table 10.1. Note that for coupled resonator filters one has freedom to alter component values and the solution in table 10.1 is only one possible solution of a multitude of solutions.

Next we consider the realisation of the filter.

10.3 Realisation

This section concerns the realisation of the lumped element circuit in figure 10.1 as a coaxial resonator filter. The various topics discussed in this section are introduced in the same chronological order that they were considered during the design procedure.

10.3.1 Filter topology

A graphical representation of the filter is shown in figure 10.1 (c). Resonators are indicated using circles, port terminations are indicated using squares and couplings are indicated using lines. The diagram in figure 10.1 (c) dictates the topology of the filter - i.e. the arrangement of the resonators and the couplings between them. The main coupling path in the filter is formed by resonators R_1,R_2,R_3 and R_4. The main coupling path forms a connection between the source and the load. Each of the resonators in the main coupling path is also the base of a branch coupling path. A branch coupling path is a string of direct coupled resonators. The first branch is R_1, R_{1A} and R_{1B}. The second branch is R_2, R_{2A} and R_{2B}. All of the branches in the filter are identical. The designer has freedom to choose the orientation of each branch in the filter. They can be located at any side of the filter and do not have to form straight lines. All of the branches in the final filter were placed on the same side of the main coupling path as this configuration results in the smallest possible filter. The filter is shown in figure 10.2.

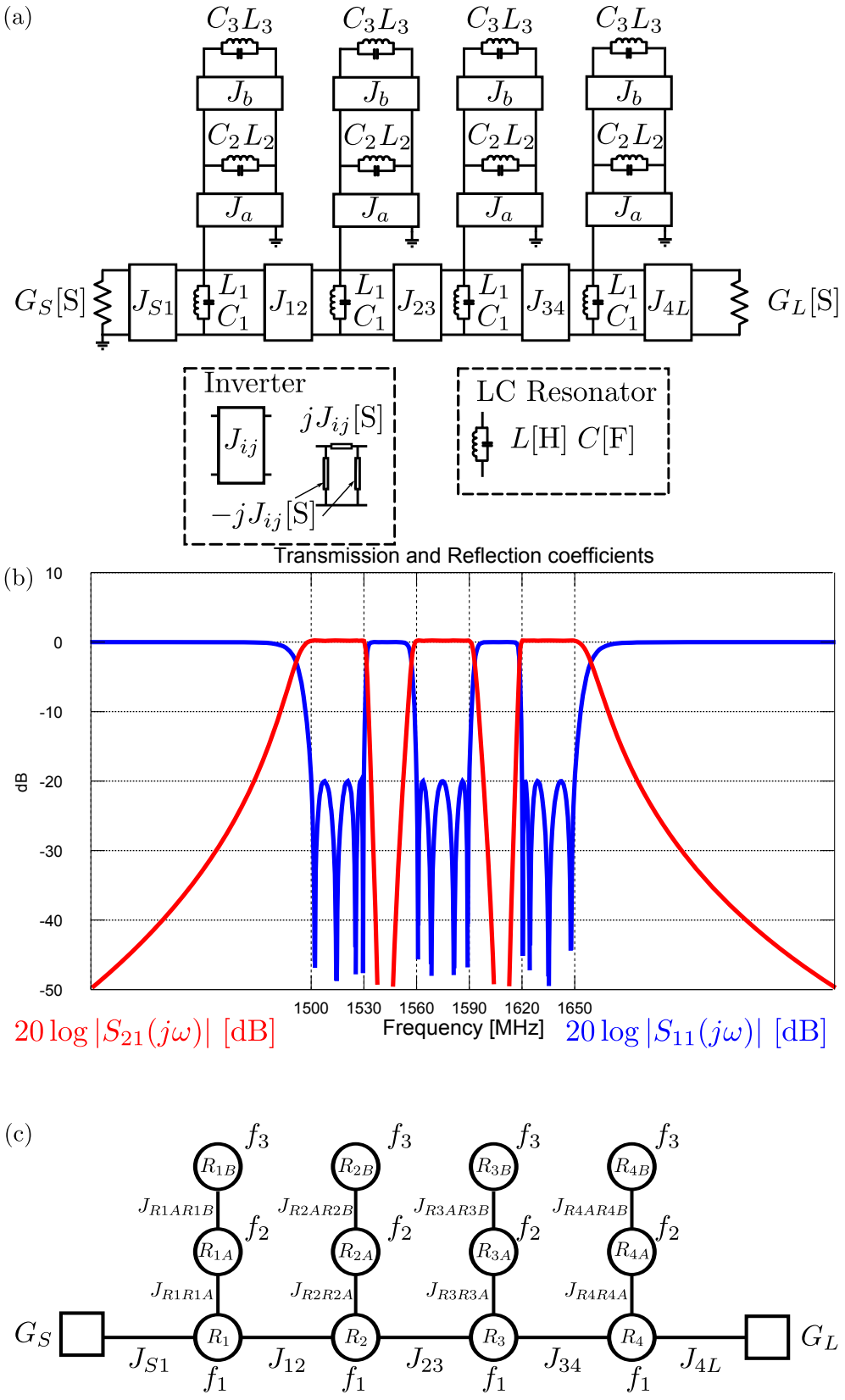

Figure 10.1: The result of the synthesis and approximation procedures is shown above. The synthesised lumped element filter circuit is shown in (a). The frequency response of the circuit in (a) is shown in (b). The circuit topology, with symbols signifying the different resonators and couplings, is shown in (c).

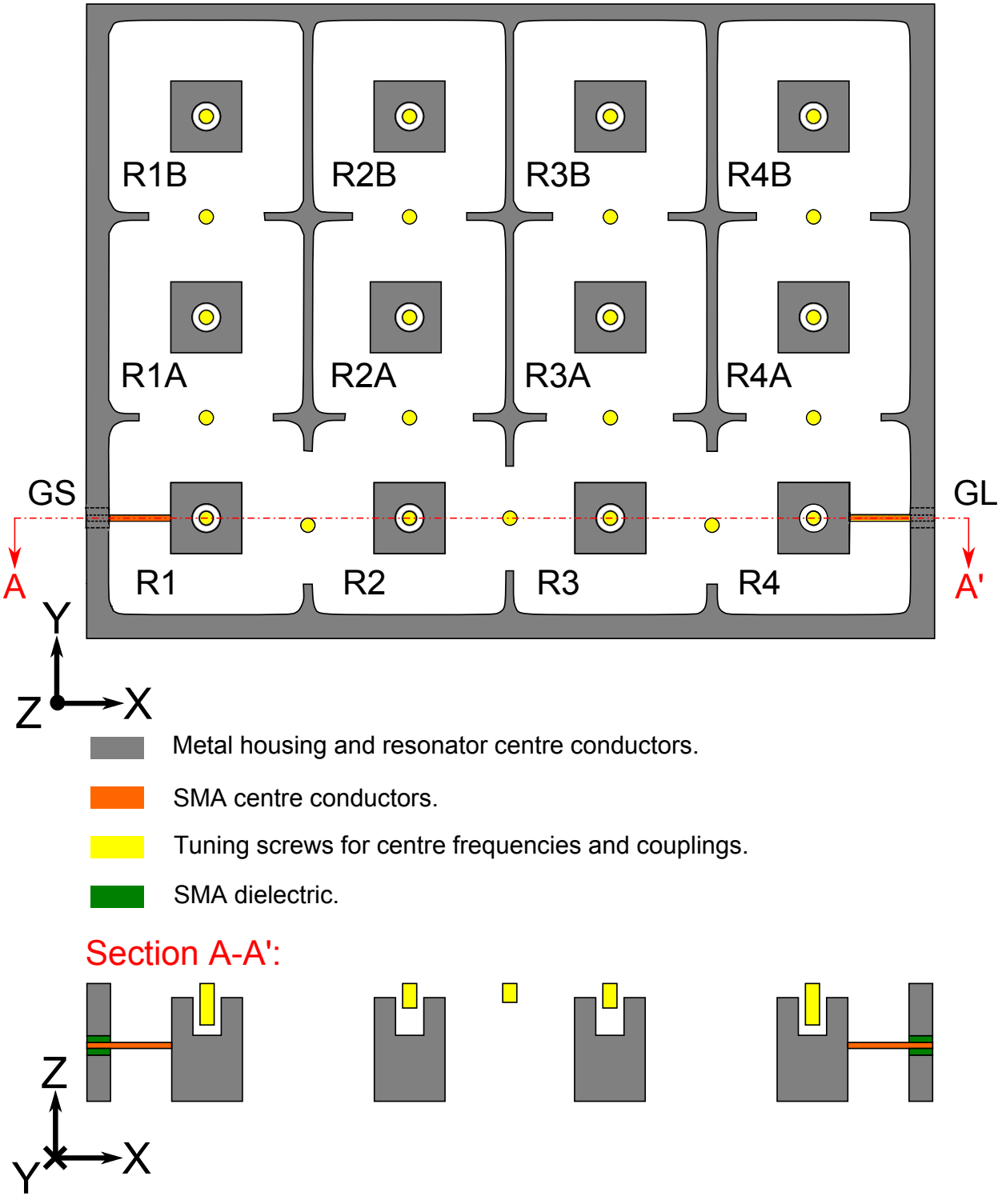

Figure 10.2: The structure of the three-band coaxial resonator filter is shown above. The top image is a top view of the filter. Here the top cover of the filter was removed and the floor of the filter was not drawn. The bottom image is a section taken through the middle of the main coupling path. Here the holes inside the centre conductors and the arrangement of the SMA connectors are visible. Tuning screws were included to tune all of the couplings and all of the resonant frequencies, except for the input and output couplings. All of the tuning screws are 3 mm in diameter and are shown in yellow. Note the resemblance of the circuit shown above and of the circuit shown in figure 10.1 (c).

10.3.2 Initial dimensioning of resonators

The resonators in the filter will be realised as short-circuited, quarter-wavelength coaxial resonators. Both the inner conductor and the outer conductor can have any shape. Rectangular inner conductors and outer conductors are used for the resonator as they are well-suited for electromagnetic simulation. The resonators will be a quarter-wavelength in length as they would then exhibit a shunt-type resonance similar to the resonators in figure 10.1 (a). An experiment was performed in CST and it was found that the maximum coupling ($J_a = J_{R1R1A} = J_{R2R2A} = J_{R3R3A} = J_{R4R4A} = 0.05393$) could be realised using the combline orientation of the resonators. It was thus decided to use the same orientation for all of the resonators in the filter. The couplings where calculated using the two-resonant method described by Hong et al. for asynchronously tuned resonators and listed in equation 7.13 [78].

The relationship between the inner and outer conductors of a coaxial resonator directly influences the unloaded quality factor of the resonator and the range of obtainable couplings . In a normal combline or interdigital filter the distance between consecutive resonators can be used to design the couplings. Large couplings can be achieved by closely spacing the centre conductors of two resonators. In the filter in this chapter the centre conductors of the resonators must be located in the centre of their respective cavities, in both axes. This is to ensure proper coupling along the main path and proper coupling into the respective branches. Furthermore each resonator must be tunable over a wide frequency range using a tuning screw. Numerous experiments where performed in CST to find a set of dimensions where the largest and the smallest couplings could be achieved and where the resonators could be tuned over a wide frequency range. Relatively large coupling irises were assumed between resonators to provide a loading effect on the resonators. The following resonator dimensions were found:

- Each resonant cavity has a square base where each side is 41 mm.
- Centre conductors are squares where each side is 15 mm.
- The centre conductor height is 22 mm for all of the resonators.
- The hole for the tuning screw in each centre conductor is 6 mm in diameter and 8 mm in depth.
- Cavity height is 25 mm for all of the cavities.

Note that the resonators should be designed with the tuning screws. This is to enable adjustment to higher and lower frequencies. The tip of the tuning screw should be located inside the resonator to ensure that tuning of the resonant frequency does not tune the coupling as well. For this filter a good tuning range is a possible adjustment of 500 MHz in both directions for each resonator.

10.3.3 Initial dimensioning of coupling irises

Once the positions of the resonators and their orientations have all been determined, one should find dimensions for the individual coupling irises. For this purpose we use a port tuning procedure as illustrated in figure 10.3 for the coupling J_{R1AR1B}. The procedure to find the dimensions of an iris is as follows:

1. Construct an electromagnetic model of a large portion of the filter. Short-circuit all of the resonators in the filter, except for the two that are coupled by the iris under consideration.
2. Connect the centre conductors of the two resonators that are being coupled to the housing of the filter using internal ports. We shall later use the ports to ensure that the resonators have the correct centre frequencies.

3. Place two normal waveguide ports in the vicinity of the coupled resonators. These ports must be lightly coupled to the resonators and must not load the resonators.
4. Simulate the structure using an electromagnetic simulator such as CST.
5. Import the s-parameters into a circuit simulator such as Microwave Office. Connect capacitors between the ports connected to the centre conductors and ground.
6. Connect normal ports to the probe ports. Suppose that the probe ports are ports 1 and 2.
7. Short-circuit the one capacitor and measure S_{21}. From the peak in S_{21} we can deduce the centre frequency of the uncoupled resonator. Use the remaining capacitor to correct the resonant frequency of the resonator. Repeat this procedure for the other resonator.
8. Measure S_{21} when both resonators have the correct centre frequencies. Note the frequencies of the resonant peaks. Use these frequencies to calculate the coupling between the resonators using equation 7.13.
9. Either increase or decrease the size of the iris and repeat the procedure until the correct coupling value is obtained. This procedure is extremely accurate.

The electromagnetic model of each coupling iris should contain a tuning screw that is already penetrated into the iris. This is to ensure that we can both increase and decrease the size of the couplings in the final filter. The described procedure must be performed for all of the couplings. Due to the symmetry of the filter only half of the couplings need to be dimensioned. The branches are also identical and the dimensions of similar irises in the branches should be very similar - they are usually not identical due to the loading effects of the rest of the filter.

10.3.4 Tuning of the electromagnetic model

Once all of the initial dimensions of the resonators and of the coupling irises have been identified, SMA connectors must be introduced into the electromagnetic model and all of the resonant frequencies of the various resonators must be tuned sequentially. The connector used for this design is the Huber and Suhner 23_SMA-50-0-3/111_N connector. It is flange mounted and has a dielectric extension to prevent reflections as the wave propagates into the resonant cavity. The filter structure is symmetric in the Y-axis (refer to figure 10.2) and we shall therefore only consider half of the filter and tune the filter from the input port. The tuning procedure is as follows:

1. Short-circuit all the resonators (using their tuning screws) except for the input resonator and use the group delay tuning procedure described in section 7.9.1 to find the tap position of the SMA and the depth of the tuning screw of the input resonator.
2. Sequentially tune the resonators in the first branch. Start with R_1 and then tune R_{1A} and later R_{1B}. In each case tune the resonant frequency of the new resonator and the coupling between the new resonator and the last resonator.
3. When the first branch is complete, short-circuit all of the resonators in the first branch again. Then start to sequentially tune the second branch. Start with R_1 and then tune R_2, followed by R_{2A} and R_{2B}.
4. Short-circuit all of the resonators in the branches. Start to sequentially tune the main coupling path using the method presented in section 7.9.1. In theory it should only be necessary to tune J_{23}. The result of this step is shown in figure 10.4. It is clear that the electromagnetic model has the desired frequency response.

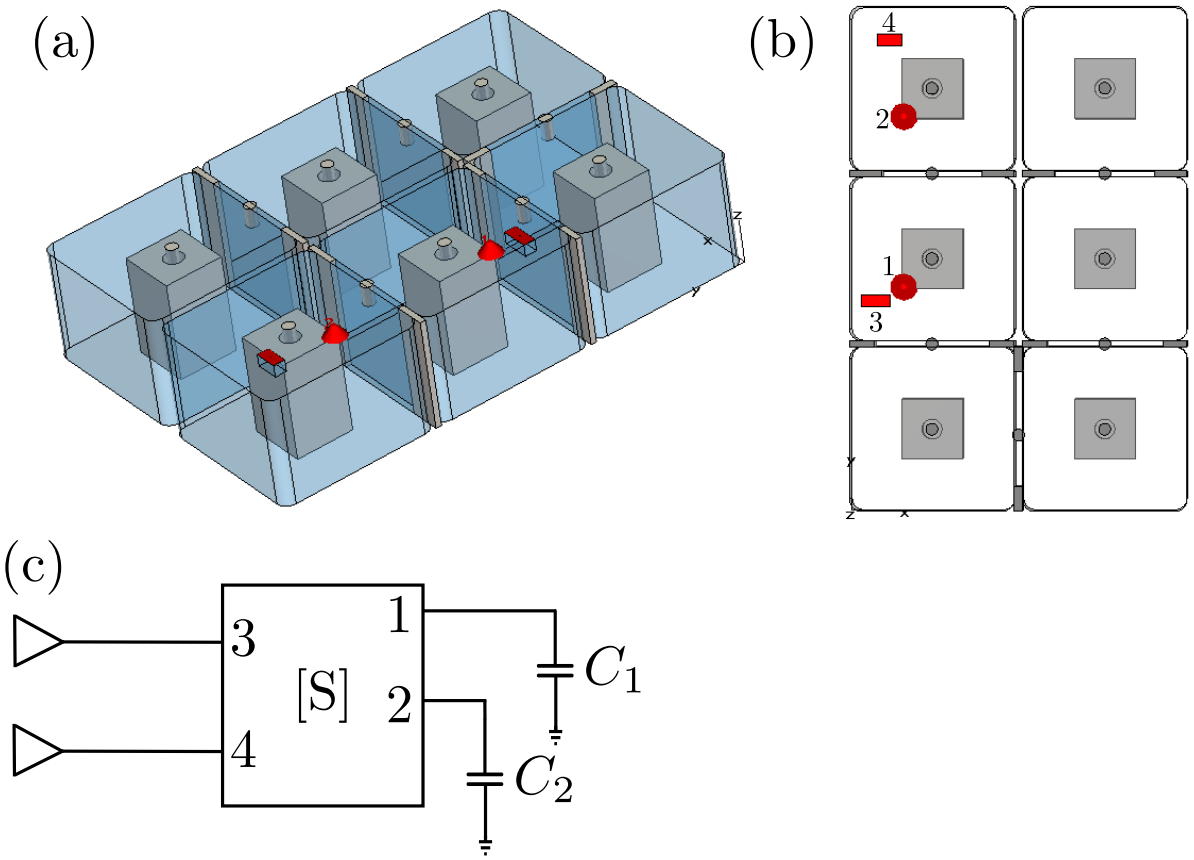

Figure 10.3: The required physical dimensions of the structure to produce a desired coupling value can be determined with a port tuning procedure. A CST model of half of the filter is shown in (a) and (b). The CST model contains four ports. Two of these are used to tune resonant frequencies (ports 1 and 2) and two serve as measurement probes (ports 3 and 4). The calculated S-parameters are connected to tuning elements in AWR Microwave Office as shown in (c). The capacitors are used to ensure that the resonators have the correct centre frequencies. The probes are used to determine the couplings

5. Include resonators R_{1A}, R_{2A}, R_{3A} and R_{4A}. It is simpler to include all of them at once and to then adjust the centre frequencies of the new resonators remembering the symmetry of the circuit. The result of this step is shown in figure 10.5.

6. Include resonators R_{1B}, R_{2B}, R_{3B} and R_{4B}. The result of this step is shown in figure 10.6.

We now have a fully dimensioned electromagnetic model of the three-band coaxial resonator filter. As shown in figure 10.6, the electromagnetic model has the desired frequency response.

10.3.5 Fabrication and tuning of actual filter

The filter was constructed using a milling machine. The manufactured filter consists of two metal parts - the housing and the lid. The housing is a single piece of metal and contains the resonators. The positions of the resonators and the sizes of the coupling irises should therefore be very accurate. The positions of the tuning screws will be more prone to error as they are determined relative to the edge of the lid. Positioning of the SMA connectors could also introduce additional error. Photographs of the manufactured filter is provided in figure 10.10. The various tuning screws are visible. The manufactured filter must now be tuned using the same procedure described in section 10.3.4. The procedure is as follows:

1. Connect the filter to a VNA and short-circuit all of the resonators using the tuning screws.

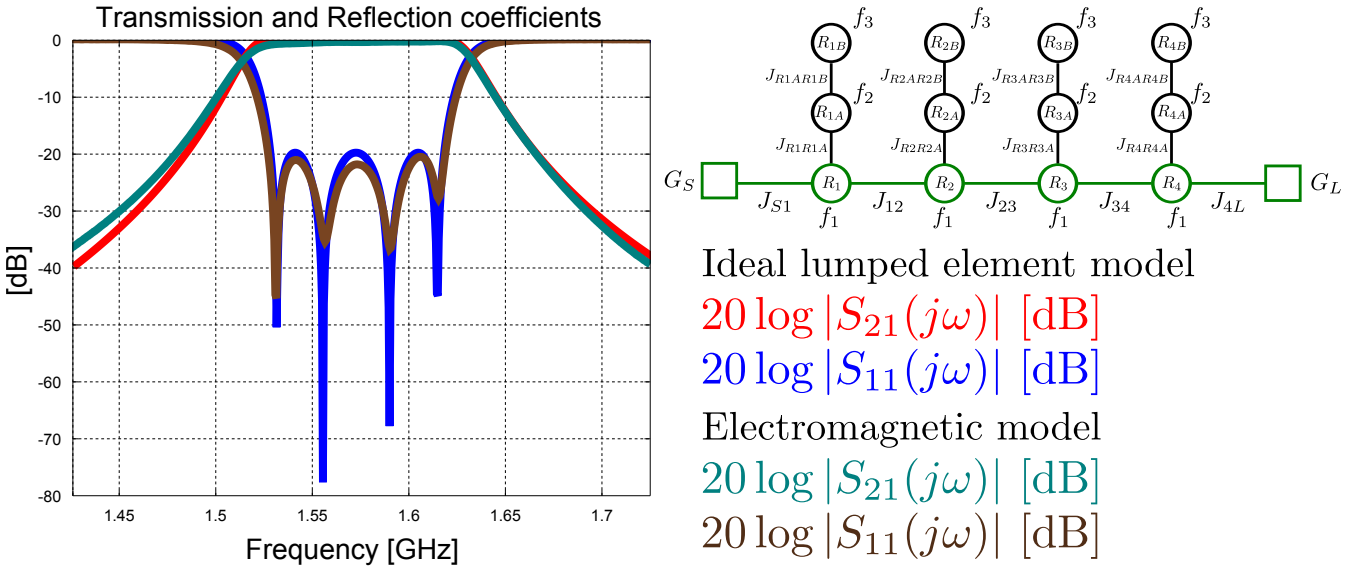

Figure 10.4: The frequency response of the ideal lumped element circuit is compared to the frequency response of the electromagnetic model. All resonators, except those indicated in green, are short-circuited during the simulation. We effectively have a single-band filter.

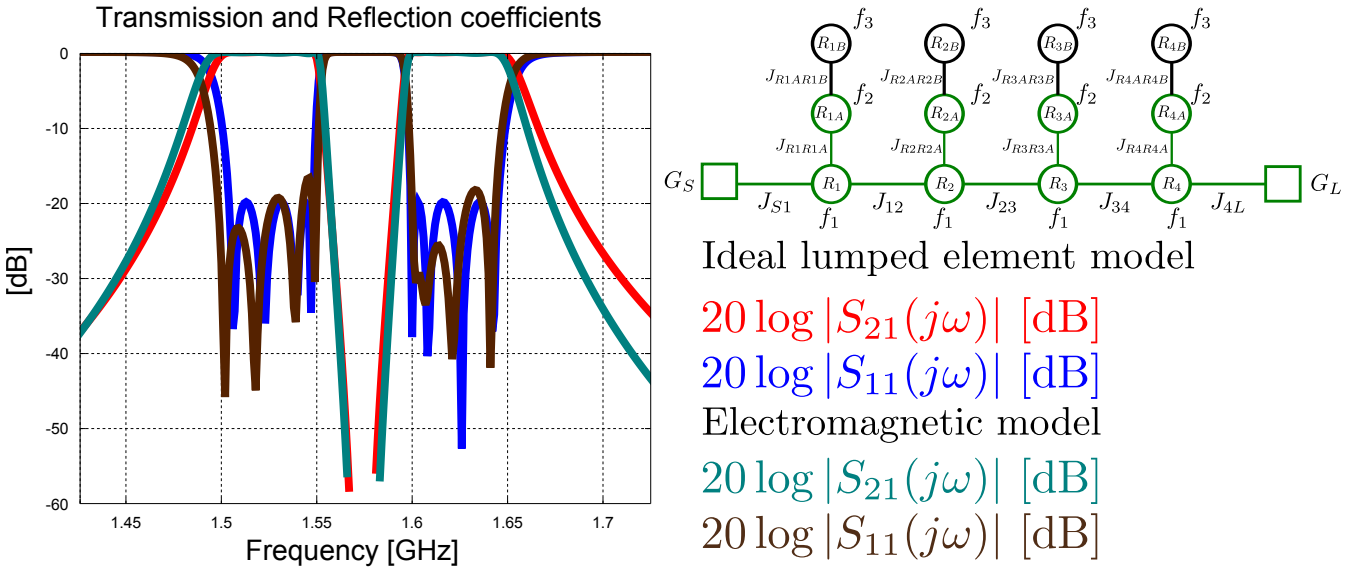

Figure 10.5: The frequency response of the ideal lumped element circuit is compared to the frequency response of the electromagnetic model. All resonators, except those indicated in green, are short-circuited during the simulation. We effectively have a dual-band filter.

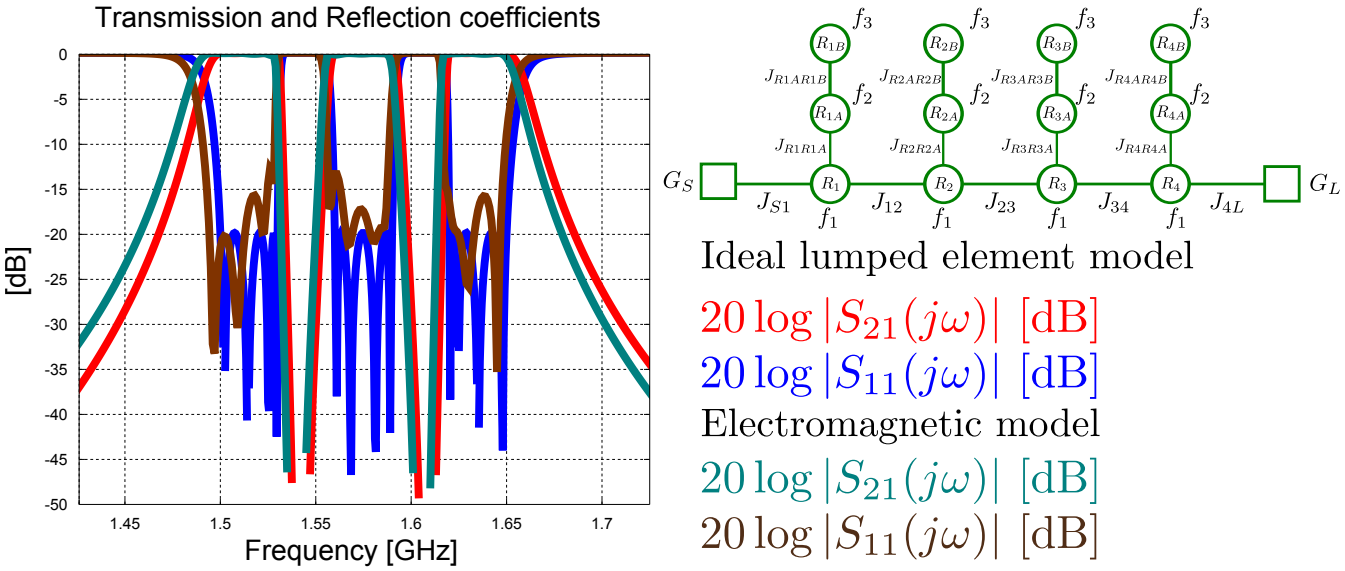

Figure 10.6: The frequency response of the full ideal lumped element circuit is compared to that of the full electromagnetic model

2. The procedure described in section 7.9.1 is employed to tune the main coupling path. The result is shown in figure 10.7. It is clear that the main coupling path in the manufactured filter has an almost perfect frequency response.

3. Tune resonators R_{1A}, R_{2A}, R_{3A} and R_{4A}. The result is shown in figure 10.8. The frequency response of the manufactured filter is not perfect any more. This can be contributed to the sensitivity of the circuit and to manufacturing tolerances.

4. Lastly we include resonators R_{1B}, R_{2B}, R_{3B} and R_{4B}. The result of this step is shown in figure 10.9.

There is good correlation between the frequency response of the manufactured filter and that of the ideal lumped element model. The frequency response of the manufactured filter is however not perfect. The discrepancies can be contributed to the closely spaced asynchronous resonant frequencies of the resonators. Resonators R_1, R_2, R_3 and R_4 are resonant at 1.573 GHz. Resonators R_{1A}, R_{2A}, R_{3A} and R_{4A} are resonant at 1.574 GHz and resonators R_{1B}, R_{2B}, R_{3B} and R_{4B} are resonant at 1.576 GHz. Simulations proved that there is a significant deterioration in the frequency response when even one of the resonators are detuned by as little as 0.1%.

10.4 Summary

In this chapter we illustrated how the theory presented in chapters 4 and 6 can be applied to design a three-band coaxial resonator filter. The filter was manufactured and the measured results correlate well with the ideal frequency response. The discrepancies in the frequency responses of the manufactured filter and that of the ideal lumped element filter is in no way related to the theory presented in chapters 4 and 6. The issues are rather related to the inherent sensitivity of asynchronously tuned coupled resonator filters. The tuning sensitivity issues can possibly be remedied by using tuning screws with a very fine screw thread.

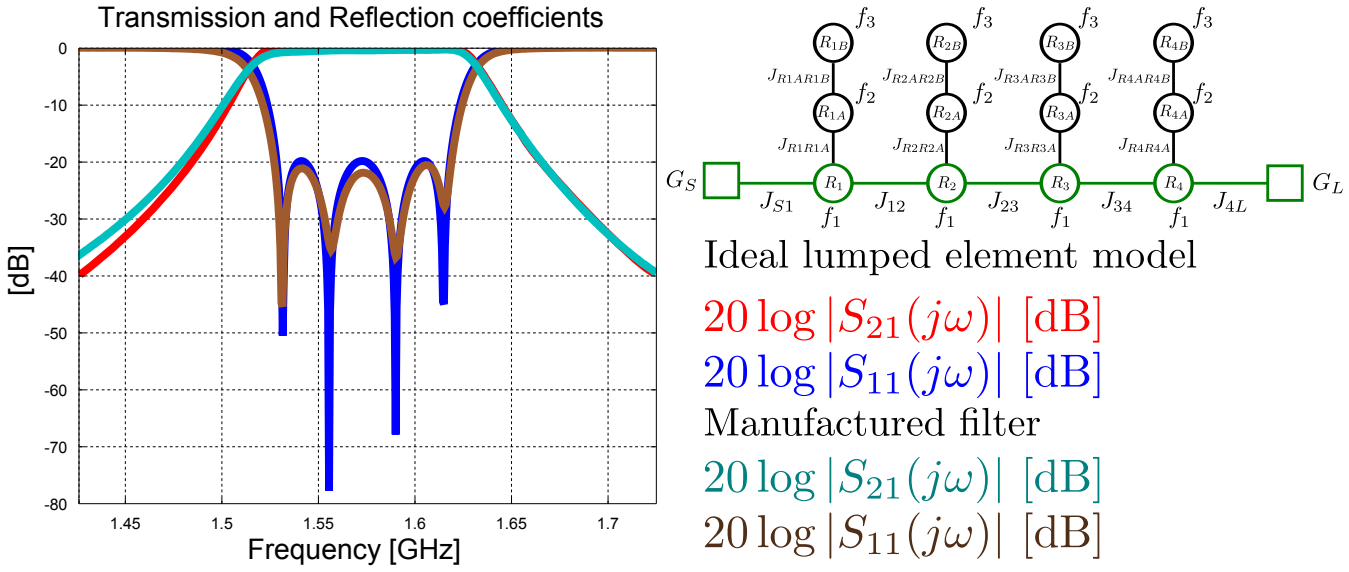

Figure 10.7: The sequential tuning of the manufactured filter is exhibited above. The circuit elements that are green are currently active in both the lumped element filter and in the manufactured circuit. All other resonators are short-circuited in both the lumped element circuit and in the actual manufactured circuit.

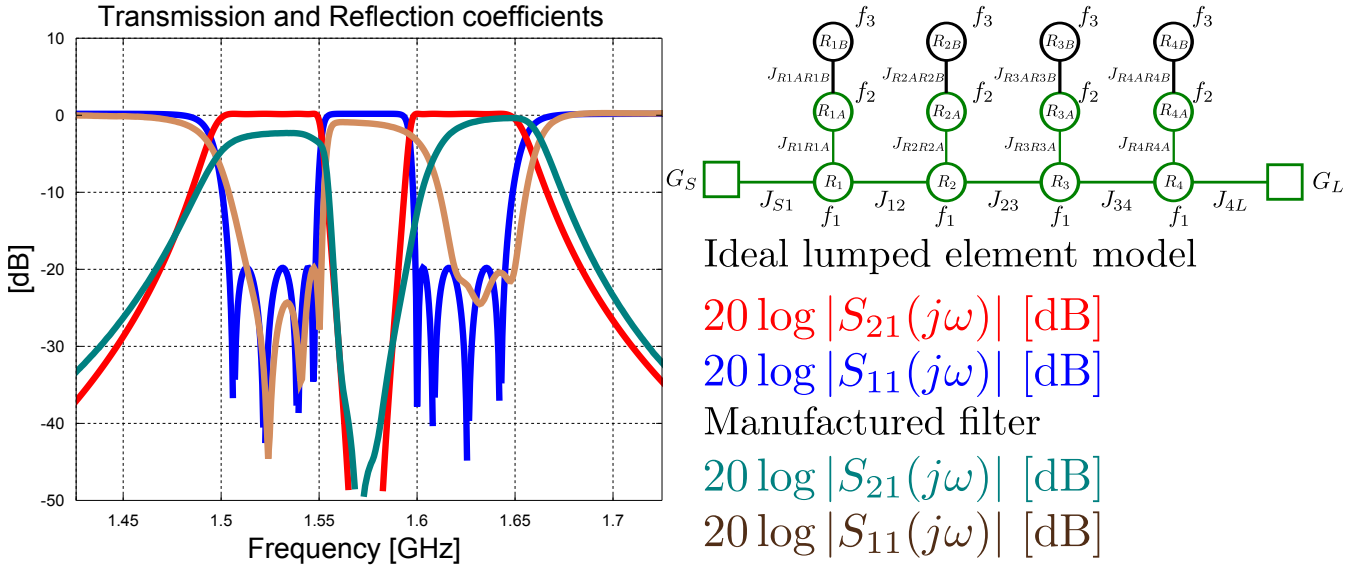

Figure 10.8: The sequential tuning of the manufactured filter is exhibited above. The circuit elements that are green are currently active in both the lumped element filter and in the manufactured circuit. All other resonators are short-circuited in both the lumped element circuit and in the actual manufactured circuit.

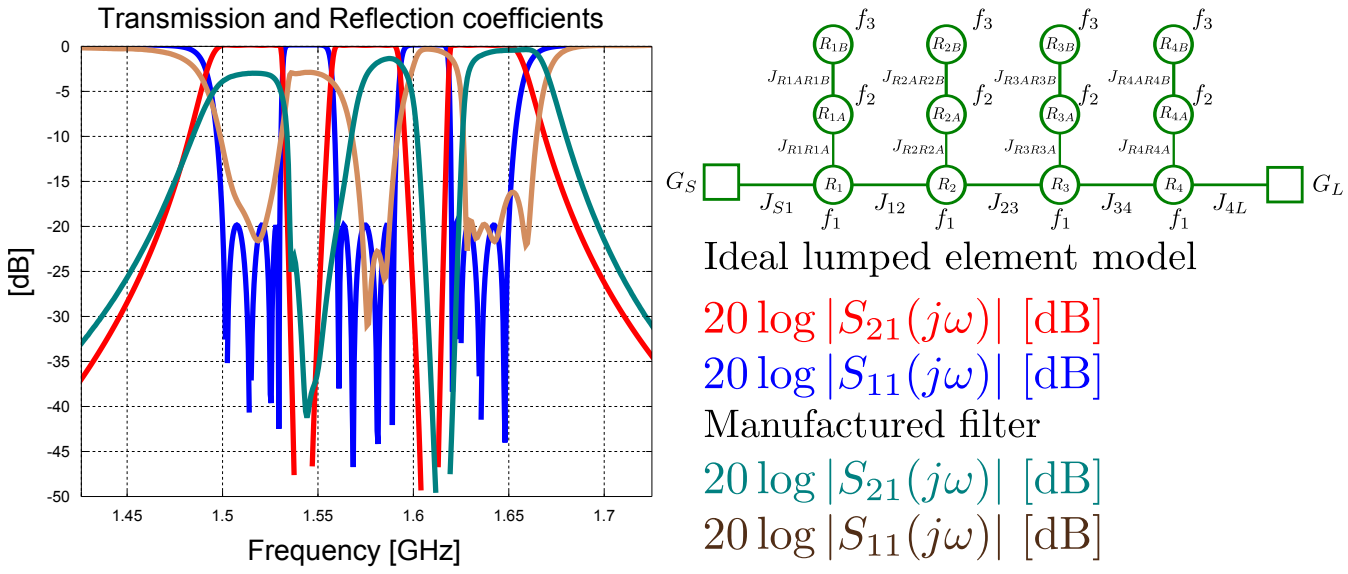

Figure 10.9: The final step in the sequential tuning of the manufactured filter is exhibited above. The frequency response of the lumped element filter (lossless model) is compared to the final measured frequency response of the manufactured filter.

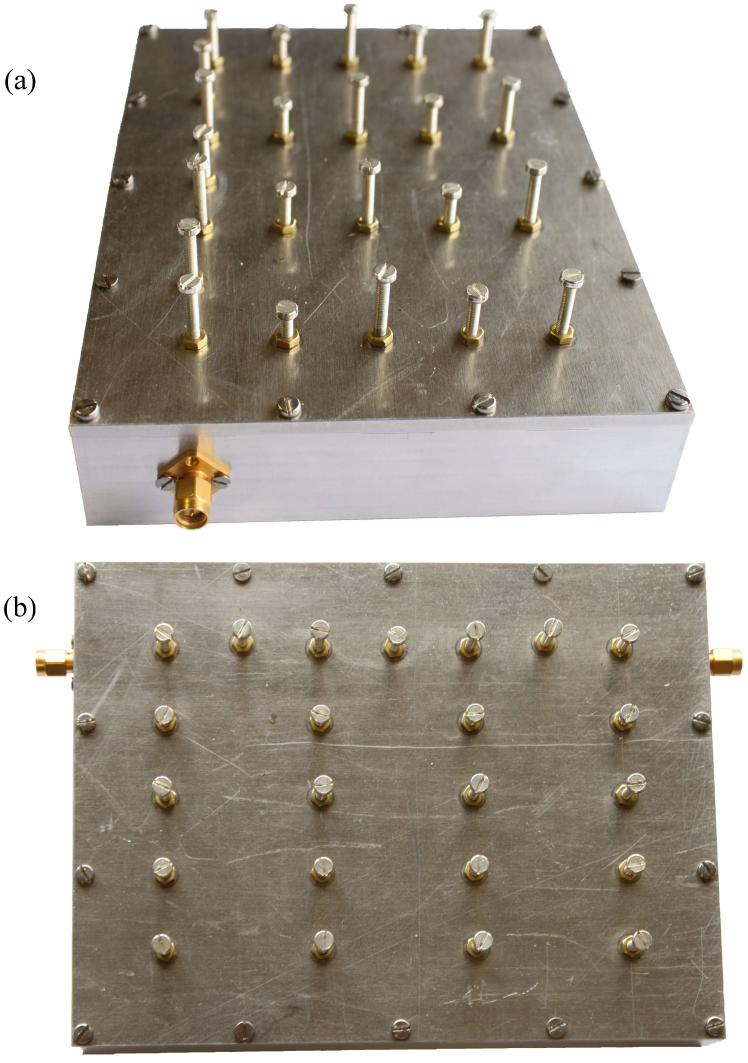

Figure 10.10: Views of the manufactured filter are provided above. The filter was constructed using a milling machine. The side view is shown in (a). The top view is shown in (b). Note that both the tuning screws and the SMA connectors are visible.

Chapter 11

Conclusion

In this dissertation we established the state of the art in the design of multi-band coupled resonator circuits, and then proposed three new design methods for multi-band coupled resonator filters, all based on the frequency mapping principle. The following mapping functions were proposed:

1. Polynomial mapping functions
2. Narrowband rational mapping functions
3. General rational mapping functions

A procedure to construct polynomial mapping functions from a bandwidth specification using Lagrange basis functions was presented. The polynomial mapping functions can be used to construct multi-band transfer functions and these can in turn be used to synthesise multi-band filters using established synthesis theory. The theory is effective for filters with up to three passbands.

A procedure to construct a special class of rational mapping functions was presented. Two formulations for the same theory were provided – the one formulation is only applicable to the design of multi-band narrowband filters and the other is applicable to all multi-band filters. The narrowband theory is applicable to filters with fractional bandwidths less than 15% [1]. Special synthesis procedures were presented for the design of multi-band filters using rational mapping functions. The rational mapping functions have the following advantages:

1. There is no theoretical limit on the number of passbands that can be obtained using this transformation.
2. Each passband in the final multi-band filter will have the exact same reflection and transmission responses as the original lowpass transfer function in terms of amplitude and phase.
3. The centre frequency and bandwidth of each passband can be chosen completely arbitrarily.
4. By simply choosing the correct poles and zeros, or equivalently choosing the passband edges for each band, a valid mapping function can be obtained using a single matrix equation. No optimisation of the final transfer functions are required.
5. Given a lowpass filter function that can be realised with a circuit containing only positive inductors and capacitors, the application of the general rational mapping function, followed by the application of the appropriate denormalisation function, will result in a classical reactance function transformation, and

[1] This is an estimate based on circuit simulation. The bandwidth limitation is not influenced by the number of bands.

will, therefore, guarantee, a multi-band filter function, which can also be realised with positive value inductors and capacitors.

6. The multi-band circuit can simply be realised by replacing each reactive element of any lowpass network with a network obtained by synthesising the mapping function as a scaled impedance or admittance one-port. The process places no restrictions on the lowpass function, therefore any lowpass network can be used.

7. No complicated cross-couplings are incurred by the lowpass to multi-band mapping as each reactive element is realised in isolation.

8. The final multi-band function needs never be synthesised as a whole on its own. The only functions that need to be synthesised are the original lowpass function and the mapping function, in isolation, as a one-port impedance or admittance.

There are two avenues that can be followed when designing a multi-band filter using a frequency mapping function:

1. Frequency mapping functions can be employed to construct a multi-band filtering function out of a single-band filtering function. Multi-band transfer functions can then be constructed from the multi-band filtering function. A multi-band filter can then be synthesised from the multi-band transfer functions directly using standard synthesis methods. For narrowband filters one can employ coupling matrix synthesis methods for this purpose. The coupling matrices can then be rotated to obtain multiple topologies for a given frequency response. Both rational mapping functions and polynomial mapping functions can be employed to design filters in this fashion.

2. Multi-band filters can be synthesised using reactance transformations [2]. The frequency mapping function is considered to be the driving point function of a unit reactance or susceptance in a multi-band filter. The driving point function is then synthesised as normalised lumped element circuits representing multi-band reactances or susceptances. These circuits are said to be frequency transformation subcircuits and scaled versions of them can be substituted into single-band prototype filter circuits in order to obtain multi-band filter circuits.

The most general multi-band circuit topologies can be obtained by synthesising multi-band circuits directly from the multi-band transfer functions. In contrast to this, the topology of a multi-band filter that is designed using reactance transformations is dependent on the topology of the single-band base filter. The direct synthesis procedure result in more general designs because the procedure does not place any additional restrictions on the set of realisable circuit topologies other than those already imposed by the desired multi-band transfer function. That being said, the disadvantage of the direct synthesis method is that the calculations are generally tedious and prone to numerical accuracy issues [3]. In contrast to direct synthesis, the synthesis of circuits using reactance transformations require minimal calculations. For narrowband filters the reactance transformation method results in circuits that have desirable topologies for realisation as coupled resonator circuits. Equivalent direct synthesis methods using coupling matrices generally result in undesirable topologies from a practical perspective and one cannot always obtain desirable topologies using matrix rotations.

[2] Only applicable to rational mapping functions.
[3] Numerical accuracy issues are due to the typical high-order network functions used for multi-band filters.

All of the proposed theory was validated in all cases through the design and manufacture of multi-band coupled resonator filters using different implementation technologies. In each case the measured results correlated with the predictions.

In the light of the work presented in this dissertation, it is clear that the original objectives in section 1.4 were achieved.

11.1 Future work

The possible research directions that could reap results are as follows:

- Investigate the tuning of multi-band coupled resonator filters that were designed using rational mapping functions.
- Develop new topologies for multi-band filters by investigating alternative synthesis possibilities for the driving point functions obtained using the rational mapping functions.

Part IV

Appendices

Appendix A

Additional filter designs

In this section we present two alternative realisations for the filters designed in chapter 8 and 9. The realisations presented here employ multi-layer stripline and were performed to to reduce the passband loss of the filters.

A.1 Dual-band all-pole filter in multi-layer stripline

The lumped element filter presented in figure 8.2 is realised as a multi-layer stripline structure that employs hairpin resonators using the technique described in section 7.6. The various topics discussed in this section are introduced in the same chronological order that they were considered during the design procedure.

A.1.1 Ideal transmission line model

An ideal transmission line model was constructed for the filter from the lumped element circuit. The transmission line model consists of stepped impedance resonators coupled by admittance inverters. The coupled sections in the resonators are 45° in length at f_0 to enable the resonators to be shaped like hairpins – the coupled sections form the sides of the hairpin and the 90° central section form the bend of the hairpin. The admittance inverters are replaced by sections of coupled line using the technique described in section 7.6, to obtain the transmission line circuit in figure A.1.

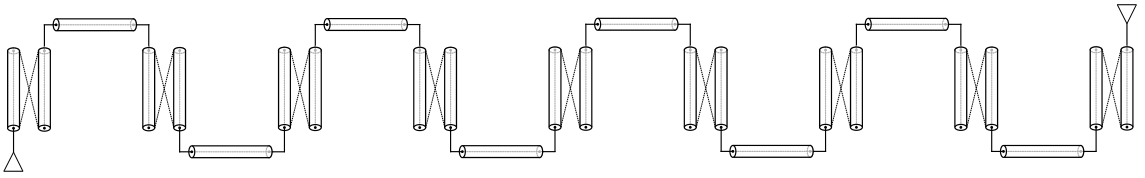

AWR title	Description	Symbol
CLIN	Section of ideal coupled transmission lines	
TLIN	Section of ideal transmission line	
PORT	Port	▷

Figure A.1: An ideal transmission line model of the all-pole SIR filter is shown above. The resonators are shaped as hairpins. The entire circuit is defined by the electrical lengths and characteristic impedances of the of transmission line sections. A table identifying the Microwave Office components are provided.

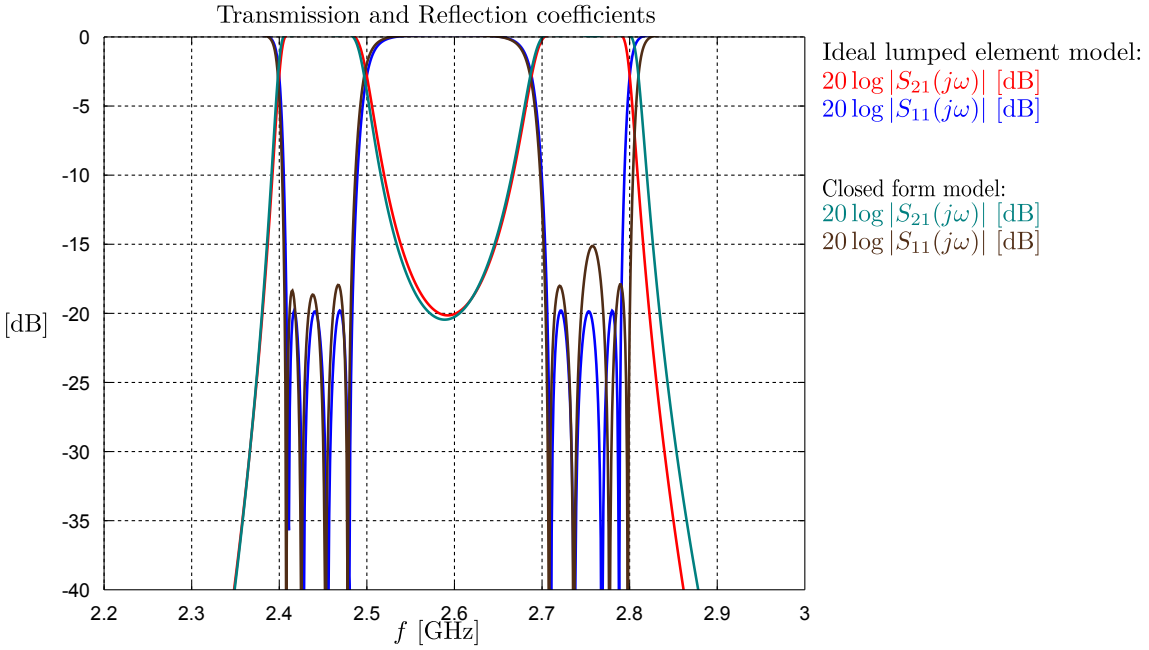

Figure A.2: The frequency response of the ideal lumped element coupled resonator circuit (figure 8.2) is compared to the frequency response of the closed form model (figure A.3). The closed form model approximates the ideal coupled model over the frequency band under consideration.

A.1.2 Closed form model of multi-layer stripline filter

The filter was realised in a Rogers 4003C substrate that has a thickness of 1.524 mm. The substrate is listed in table 8.1. The multi-layer structure is constructed by bonding three Rogers substrates together. The conducting layers are positioned on the inside of the structure, between the substrates. The outside copper cladding on the top and bottom substrates form the ground planes and must be connected together. Arlon's CuClad 6250 was used as bonding film. The electrical properties of the bonding film are listed in table 8.2. A closed form model was constructed from the transmission line model and is shown in figure A.3. The initial simulation of the closed form model does not produce the desired frequency response. The filter dimensions had to be tuned using the group delay tuning procedure that was discussed in section 7.9.1. The frequency response of the tuned closed form model is compared to the ideal frequency response in figure A.2. The ideal response here being the denormalised lumped element circuit in figure 8.2. Next an electromagnetic model is created to verify the filter dimensions using a simulator.

A.1.3 Electromagnetic simulation and port tuning of multi-layer stripline filter

An electromagnetic model was constructed in Sonnet. A 3D model of the filter is shown in figure A.4. The different colours refer to the different conducting layers. The electromagnetic model includes the effects of the substrates and of the bonding films. Loss is not included in the initial simulations. The frequency response of the initial electromagnetic model is compared to the frequency response of the tuned closed form model in figure A.5 (a). The discrepancy between the responses is attributed to the inaccuracy of the closed form models and due to the fact that stray couplings are not included in the closed form model. The dimensions of the initial electromagnetic model is now adjusted until the model meets the design specifications by applying the port tuning procedure discussed in section 7.9.2. The surrogate model associated with the circuit in figure A.4 is shown in figure A.6. Each black box in figure A.6 represents a separate Sonnet simulation. The port tuning

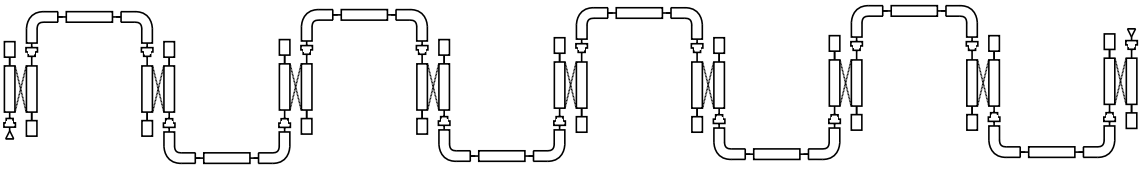

AWR title	Description	Symbol
GMCLIN	Multiple coupled lines on general multi-layer substrate	
GM1LIN	Single line on general multi-layer substrate	
PORT	Port	
SSTEP0	Stripline step in conductor width	
SLEF	Open stripline with end effect	
MCURVE	Microstrip radiused corner	

Figure A.3: A closed form model of the all-pole SIR filter is shown above. The resonators are shaped as hairpins. The closed form models are parameterised by the physical dimensions of the circuit. The impedance steps and stripline corners are extracted as external electromagnetic models to increase the accuracy of the closed form filter model.

procedure is summarised in figure A.5. Once the port tuning procedure is completed the filter is packaged inside a metal enclosure. The next subsection deals with the design of a SMA-to-stripline transition.

A.1.4 Design of SMA-to-stripline transition

A coaxial-to-stripline transition must be designed to minimise the reflections of electromagnetic waves as they enter the filter. The technique described in section 8.3.4 is also applied here to design a transition. It is important now to consider how the filter will be assembled. The filter consists of three substrates that are bonded together. There are two ports and each port is located on different conducting layer. In order to construct this device, one must first position the central substrate inside a box and then solder the two connectors onto the two conducting layers. Then it is necessary to bond the top and bottom substrates onto the central substrate. Considering the minute dimensions of the SMA connector pin (refer to table 8.3), it is clear that the bonding procedure could damage the SMA connectors. A solution to this problem is to include a metal support inside the box. The metal support will be 5 mm wide and will have the height of a single substrate. The metal enclosure with the mentioned support is graphically illustrated in figure A.9. Figure A.7 (a) shows a CST model of the connection between a SMA connector and the stripline circuit. There are only two substrates above the support. Both ports will have the structure depicted in figure A.7 (a). The CST model includes the Rogers substrates and the Arlon bonding film. Figure A.7 (b) shows the conducting layer. The variable w_{pin} is fixed to 0.3048 mm due to the pin width in table 8.3 and the variable w_{line} has the value of 2.14 mm that is equal to the width of the input track. The variables l_{t1}, l_{t2} and w_{mid} can be optimised to minimise the return loss at the coaxial port across the entire band of operation.

A parameter study of the transition in figure A.7 (b) was performed and it was found that the reflections are a minimum if $l_{t1} = 2.5$ mm, $l_{t2} = 5$ mm and $w_{\text{mid}} = 2.14$ mm. A plot of the associated reflection coefficient

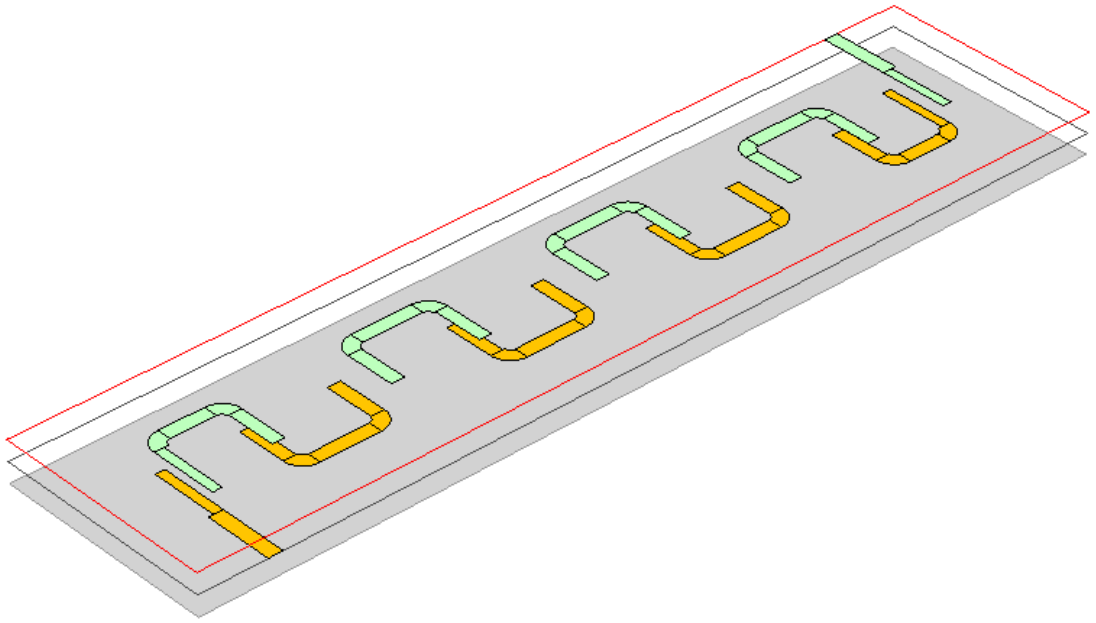

Figure A.4: The electromagnetic model of the multi-layer stripline filter is shown above. This model was constructed and simulated in Sonnet. The multi-layer stripline model constitutes the fine model in the space mapping procedure. The different colours refer to different conducting layers

is shown in figure A.7 (c). A final electromagnetic simulation of the filter was performed and losses were included. The frequency response of the lossy electromagnetic model is shown in figure A.8 (a). The s-parameter models of the SMA-to-stripline transitions were then cascaded with the lossy electromagnetic model to produce a predicted frequency response of the final filter. The predicted frequency response is shown in figure A.8 (b). It is clear that the effect of the SMA-to-stripline transition is almost negligible. In the next subsection we shall discuss the manufacturing process and show the measured results.

A.1.5 Fabrication and measurements

The final dimensions of the filter is provided in figure C.2 in appendix C. The two conducting layers are fabricated using a photo-etching procedure. The two conducting layers are located on the two sides of the central substrate. The top and bottom substrates must be bonded onto the central substrate using Arlon's CuClad 6250. Note that the metal cladding on the top and bottom substrates must be removed on the side facing the conducting layers. The outer sides of the top and bottom substrates form the ground plane and must be connected. A difficulty that arises is that the layout of the filter requires the two connectors to be positioned on two different conducting layers. The required assembly procedure is thus as follows:

1. Place central substrate inside a metal box.
2. Solder the connectors onto the conducting layers. Note that the connectors have dielectric extensions and must be connected through the wall of the metallic enclosure.
3. Bond the top and bottom substrates to the central substrate using bonding film. Note that this requires heating the entire structure to $250°$F.
4. Attach the top and bottom lids and ensure that there is a connection between the ground planes of the substrates and the metal enclosure.

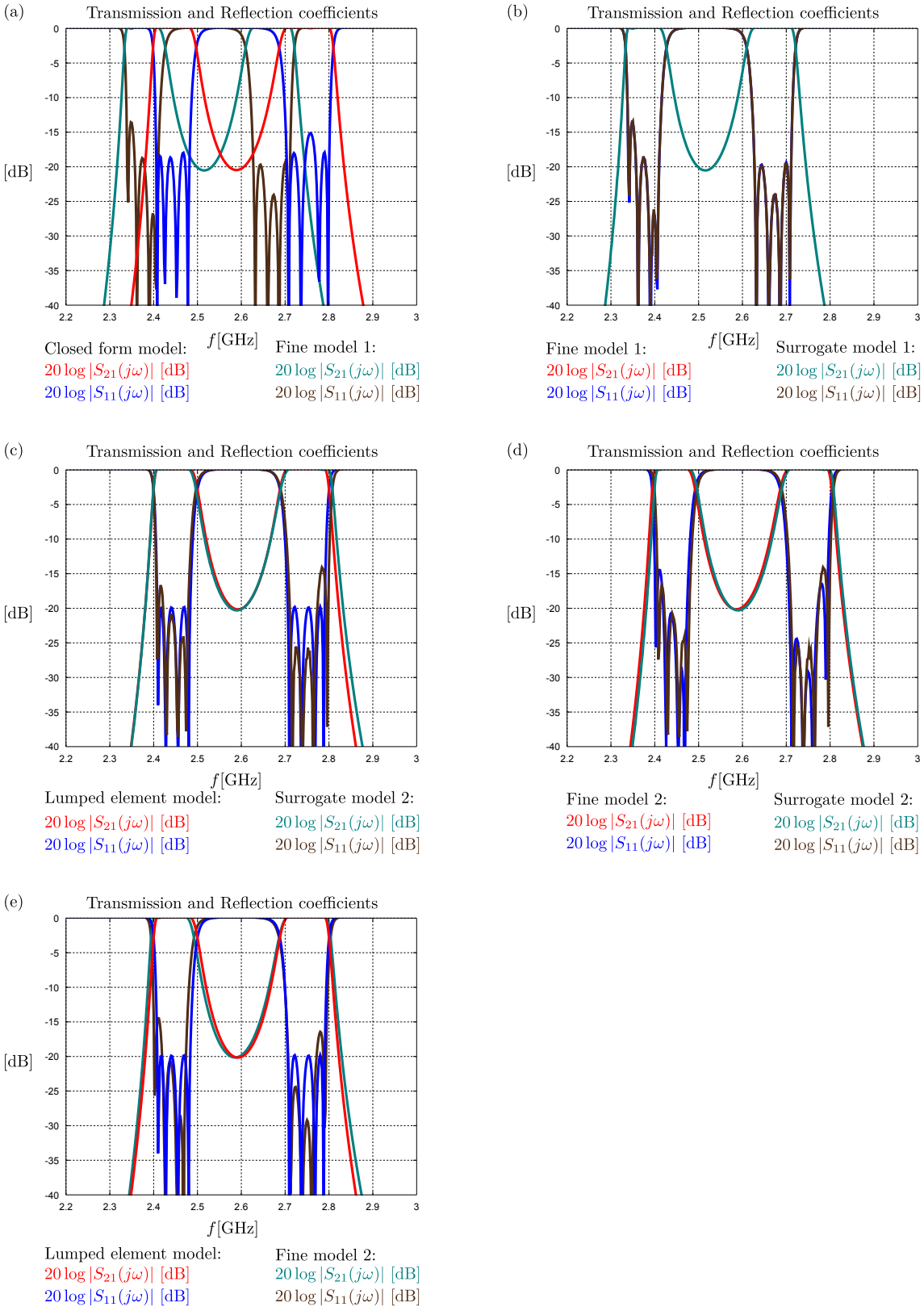

Figure A.5: The frequency response of the ideal lumped element coupled resonator circuit is compared to the frequency response of the initial electromagnetic model in (a). The frequency response of the surrogate model is compared to the frequency response of the initial electromagnetic simulation in (b). The physical dimensions of the surrogate model are now tuned until it meets the design specifications. The frequency response of the tuned surrogate model is compared to the ideal frequency response in (c). A second electromagnetic model is created from the tuned surrogate model. The frequency response of the new electromagnetic model is compared to the tuned surrogate model in (d). The frequency response of the new electromagnetic model is compared to the ideal response in (e).

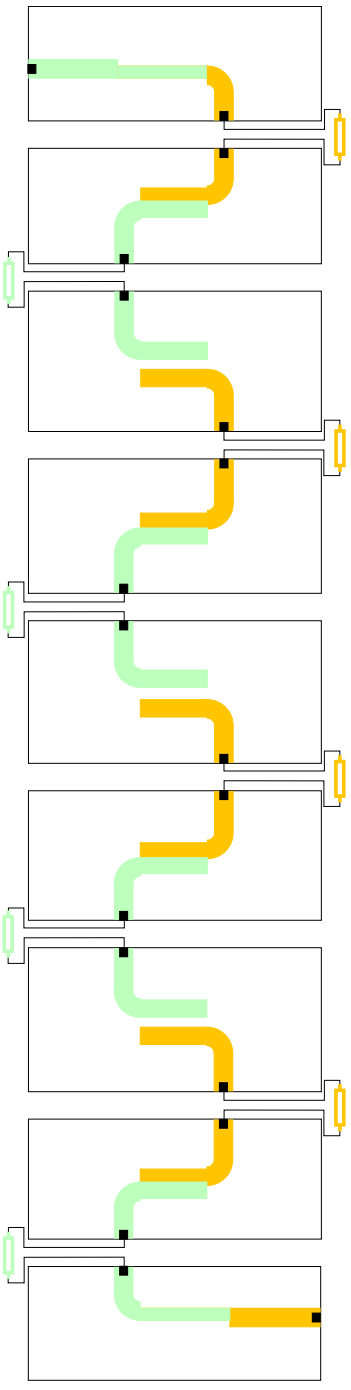

AWR title	Description	Symbol
GM1LIN	Single line on general multi-layer substrate	

Figure A.6: The surrogate model associated with the fine model in figure A.4 is shown above. The fine model was divided into smaller electromagnetic models. Each black box refers to a separate electromagnetic model. The models were then connected together using closed form models of transmission line sections. The different colours refer to different conducting layers. The transmission line sections were defined in such a manner that they correspond to the appropriate conducting layer. All the transmission line sections are tuneable and can be used to change the centre frequencies of the resonators.

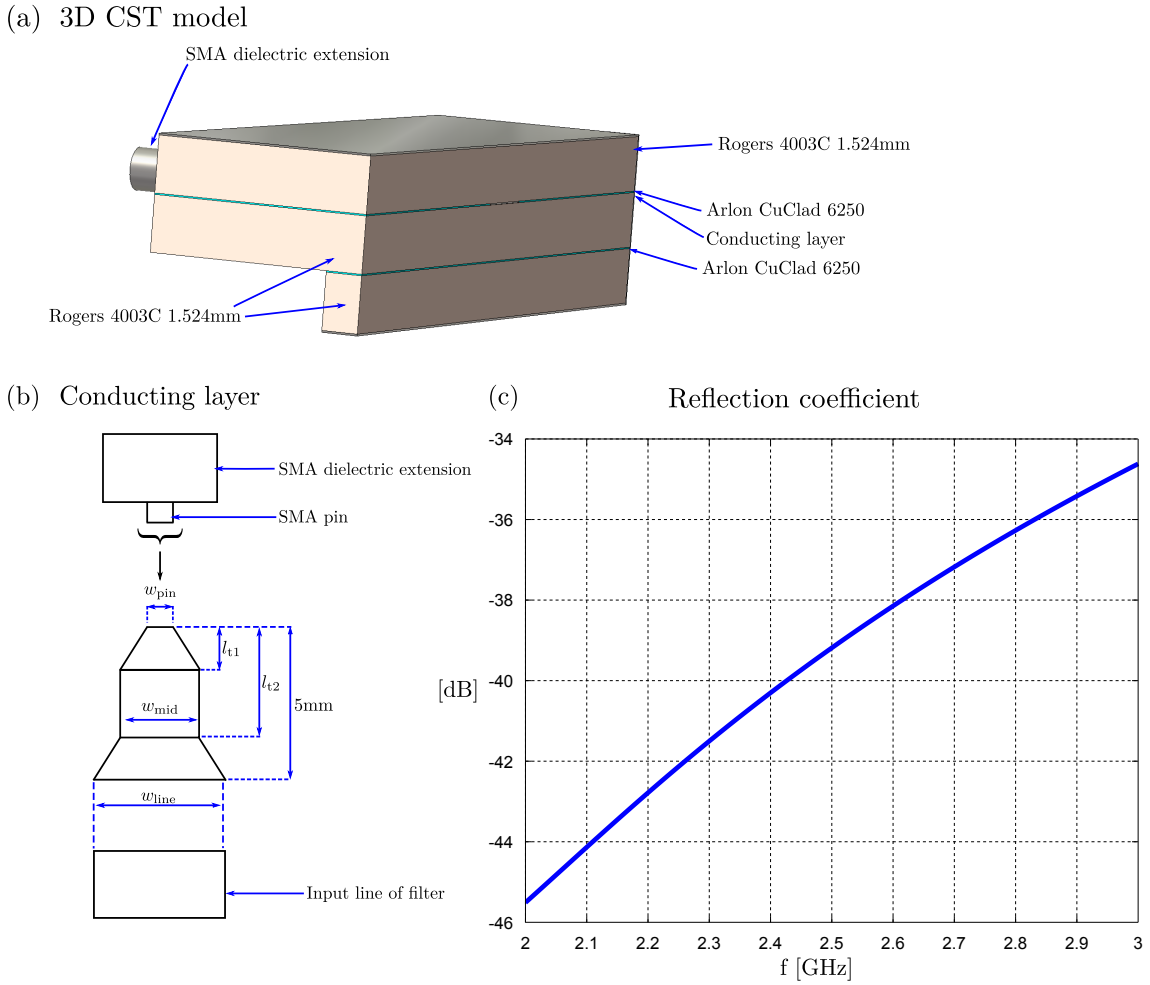

Figure A.7: The design of the transition is illustrated above. A 3D CST model of the transition is shown in (a). Note that the structure is enclosed inside a metal box. The metal walls are however not shown. The SMA dielectric extension is the part of the SMA that extends through the box wall. The parameterisation of the conducting layer is shown in (b). The variables l_{t1}, l_{t2} and w_{mid} were optimised until the reflections at the input port were at a minimum. The frequency response is shown in (c).

As mentioned in section A.1.4, the assembly is a mechanical challenge because the dimensions of the connector pin are minute. A 5 mm ledge was therefore included inside the metal enclosure to support the fragile connector pin. The design of the box is graphically illustrated in figure A.9 (a). A cross-sectional view of the closed box is shown in figure A.9 (b). Photographs of the manufactured filter is shown in figure A.10. The frequency response of the device was measured and compared to the predicted frequency response. The measured results are shown in figure A.11. It is clear that the electromagnetic model predicts transmission zeros above and below the passbands. These transmission zeros are only produced if the SMA-to-stripline transitions are included in the model. The measured frequency response exhibit a transmission zero at $\approx$ 2.85 GHz and a peak at $\approx$ 2.17 GHz. We can conclude that the measured frequency response correlate well with the predicted frequency response. This completes the design of the all-pole multi-layer stripline filter.

A.2 Dual-band cascaded triplet filter in multi-layer stripline

The cascaded triplet filter designed in chapter 9 is realised here using multi-layer stripline.

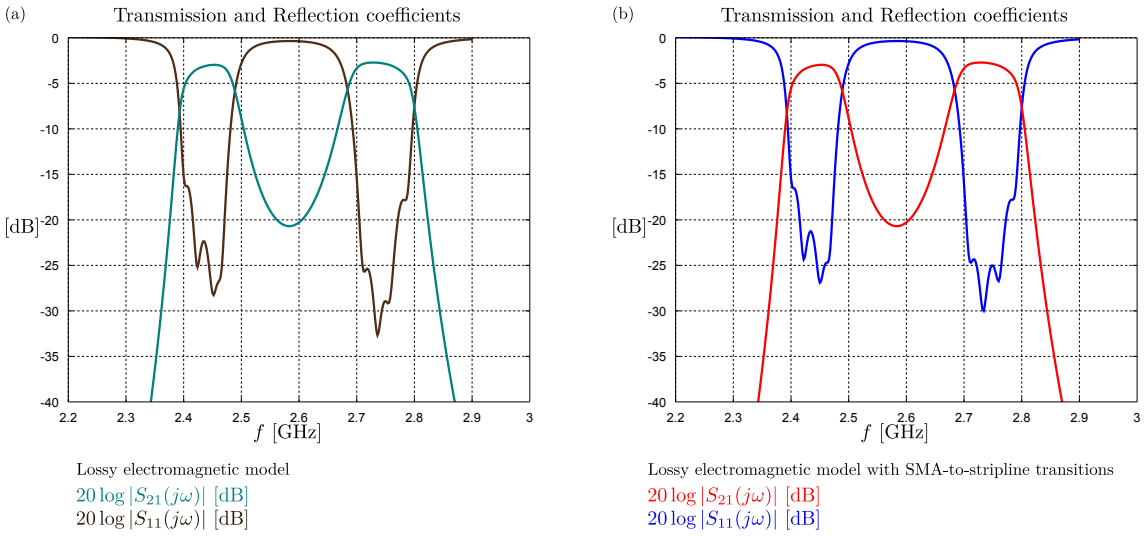

Figure A.8: The final electromagnetic model was simulated in Sonnet and losses were included. The frequency response of the lossy electromagnetic model is shown in (a). The SMA-to-stripline transitions were simulated in CST and losses were also included. The mentioned simulations were cascaded in Microwave Office to provide a realistic prediction of the performance of the manufactured filter. The predicted frequency response of the manufactured filter is shown in (b). The SMA-to-stripline transition has almost a negligible influence on the frequency response of the filter.

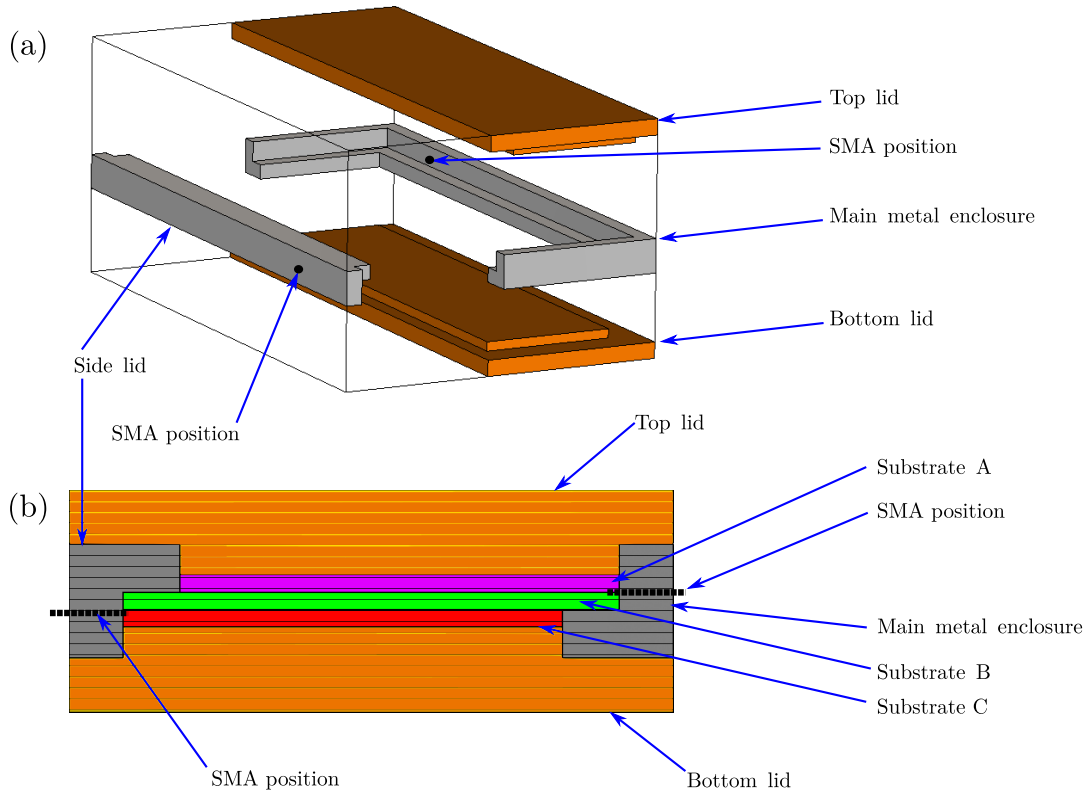

Figure A.9: A graphical representation of the metal enclosure with its three lids is shown in (a). A sectional view of the enclosure is shown in (b).

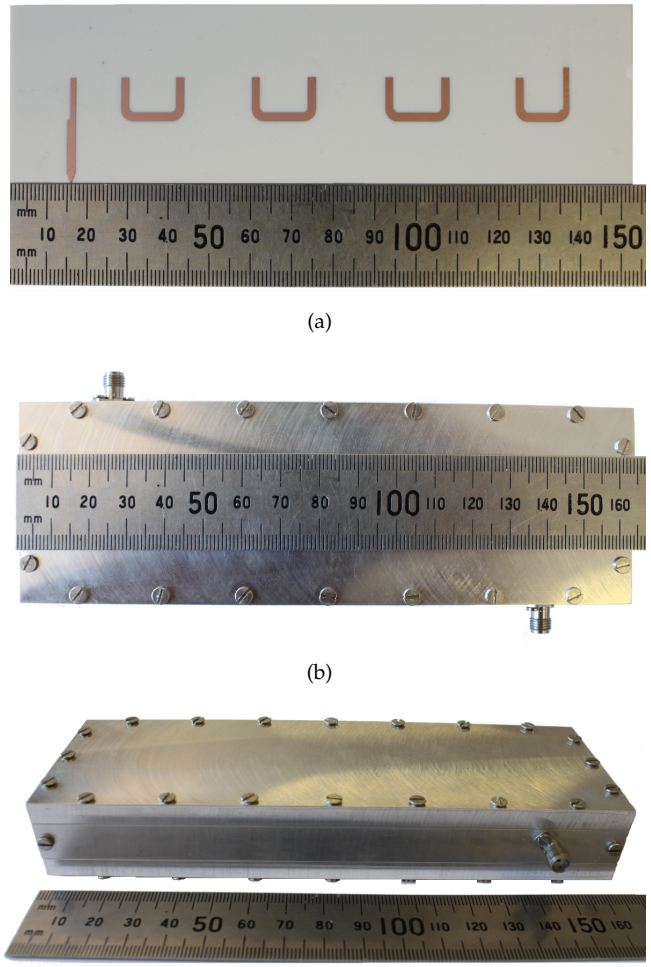

(a)

(b)

(c)

Figure A.10: The conducting layers were manufactured using a photo-etching procedure. The two conducting layers were etched on the two opposing sides of the central substrate. One of the conducting layers is shown in (a). The circuit was built into a metal enclosure as shown in (b). The two ports are not positioned on the same conducting layer. In order to perform the assembly of the filter it was necessary to design an enclosure with three lids. One lid on top, one lid at the bottom and an additional lid at one of the SMA connectors. The lid at one of the SMA connectors is shown in (c).

A.2.1 Closed form model of multi-layer stripline filter

The multi-layer structure is identical to the structure described in section A.1.2 except that the Rogers 4003C substrate for this design has a thickness of 0.508 mm. The procedure described in section 9.3 is followed to find a closed form model for the filter, as shown in figure 9.7.

A.2.2 Electromagnetic simulation and port tuning of multi-layer stripline filter

An electromagnetic model was constructed in Sonnet. A 3D model of the filter is shown in figure A.13. The different colours refer to the different conducting layers. The electromagnetic model includes the effects of the substrates and of the bonding films. Loss is not included in the initial simulations. The frequency response of the initial electromagnetic model is compared to the frequency response of the tuned closed form model in figure A.15 (a). The discrepancy between the responses is attributed to the inaccuracy of the closed form models and due to the fact that stray couplings are not included in the closed form model. The dimensions of

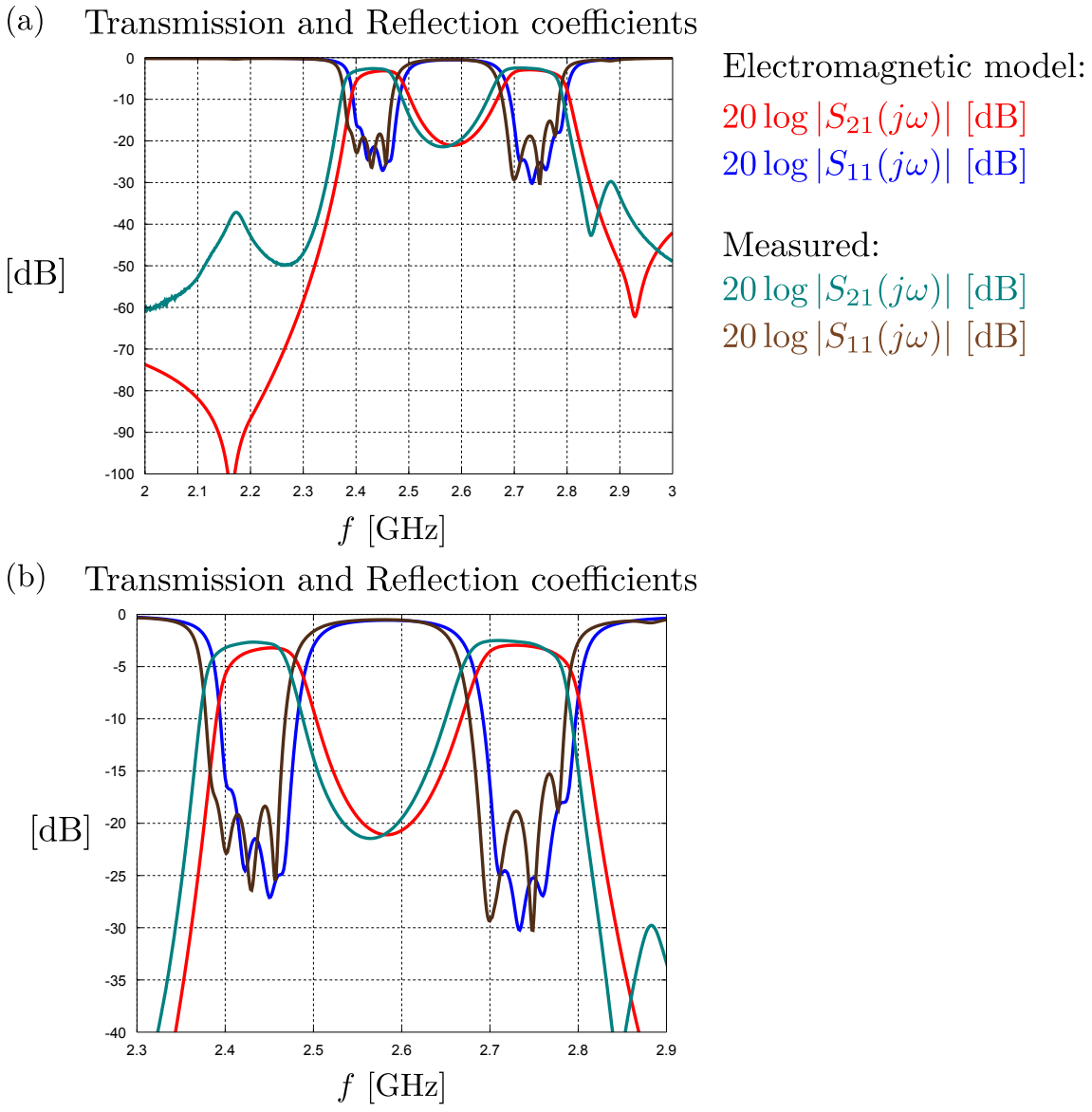

Figure A.11: A comparison of the measured frequency response of the fabricated filter and the predicted frequency response is shown above. The fabricated filter is the all-pole filter manufactured using multi-layer stripline. The predicted frequency response is a lossy electromagnetic model that includes the SMA-to-stripline transitions. There is a good correlation between the predicted performance and the measured results. The frequency response over a relatively wide bandwidth is shown in (a). The frequency response over a narrow bandwidth is shown in (b).

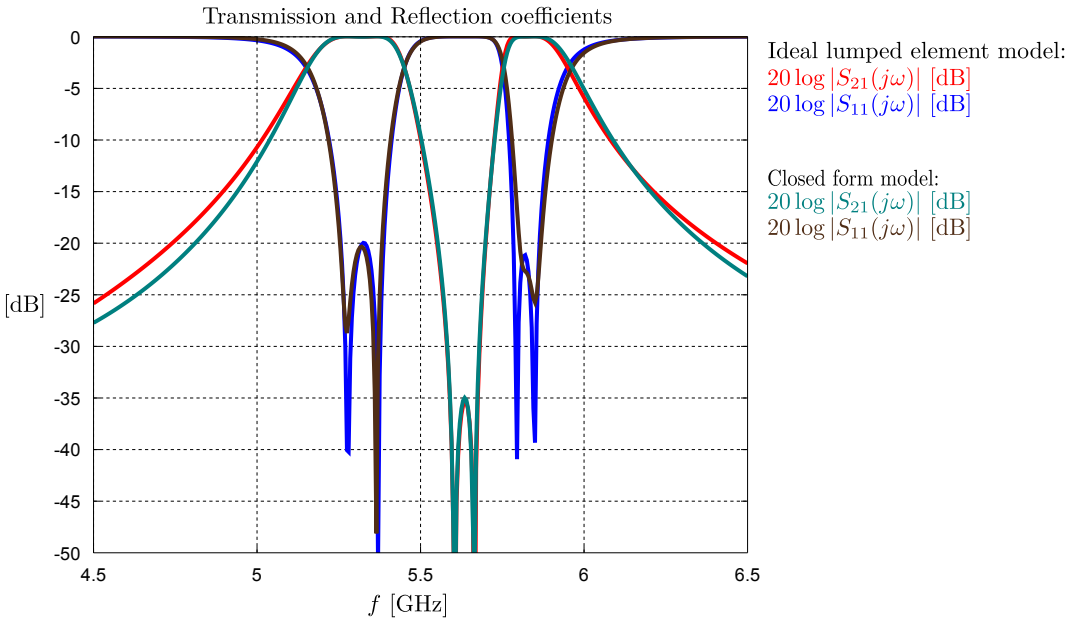

Figure A.12: The frequency response of the tuned closed form model in figure 9.7 is compared to the ideal frequency response of the lumped element circuit in figure 9.2. Here the closed form model has a multi-layer substrate definition.

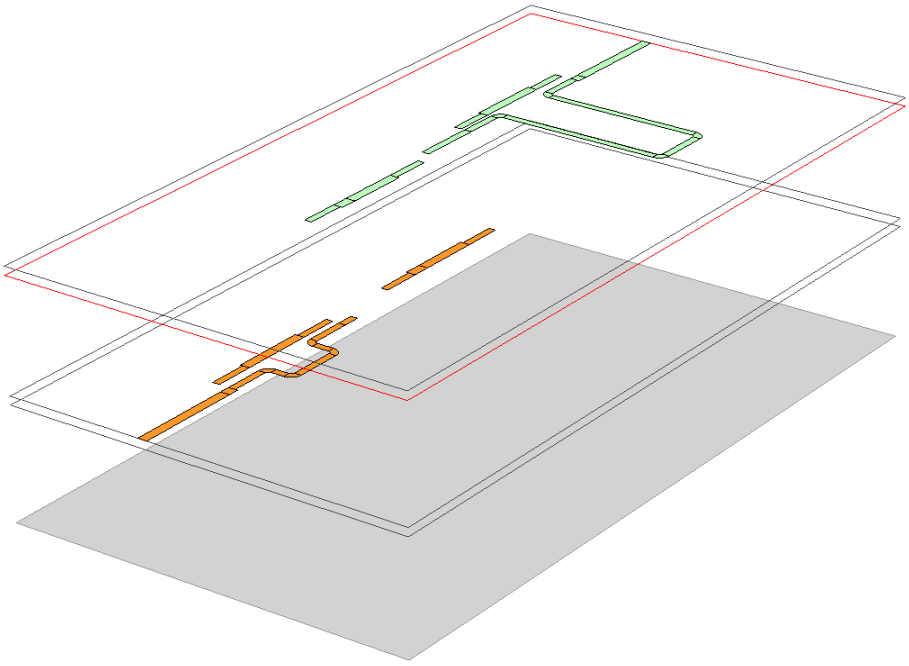

Figure A.13: The electromagnetic model of the multi-layer stripline filter is shown above. This model was constructed and simulated in Sonnet. The multi-layer stripline model constitutes the fine model in the space mapping procedure. The different colours refer to different conducting layers.

the initial electromagnetic model is now adjusted until the model meets the design specifications by applying the port tuning procedure discussed in section 7.9.2. The surrogate model associated with the circuit in figure A.13 is shown in figure A.14. The port tuning procedure is summarised in figure A.15. Once the port tuning procedure is completed the filter is packaged inside a metal enclosure. The next subsection deals with the design of a SMA-to-stripline transition.

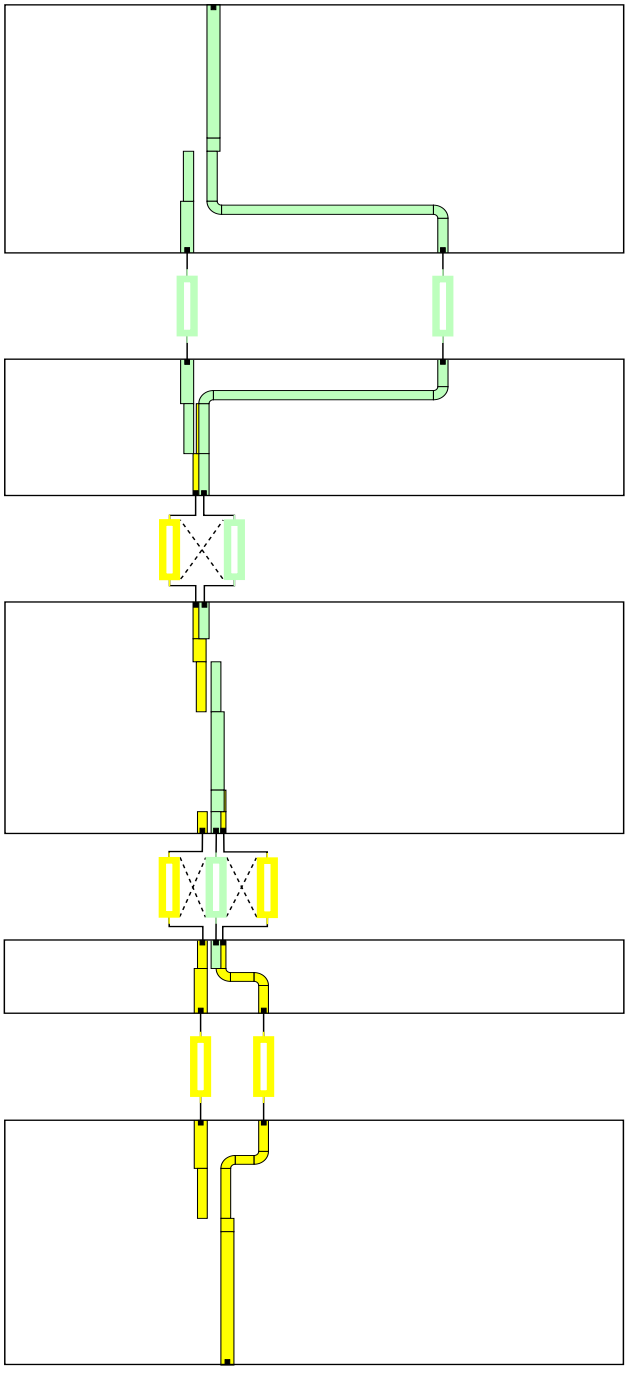

AWR title	Description	Symbol
GMCLIN	Multiple coupled lines on general multi-layer substrate	
GM1LIN	Single line on general multi-layer substrate	

Figure A.14: The surrogate model associated with the fine model in figure A.13 is shown above. The fine model was divided into smaller electromagnetic models. Each black box refers to a separate electromagnetic model. The models were then connected together using closed form models of transmission line sections. The different colours refer to different conducting layers. The transmission line sections were defined in such a manner that they correspond to the appropriate conducting layers. All the transmission line sections are tuneable and can be used to change the centre frequencies of the resonators or the strengths of the cross-couplings.

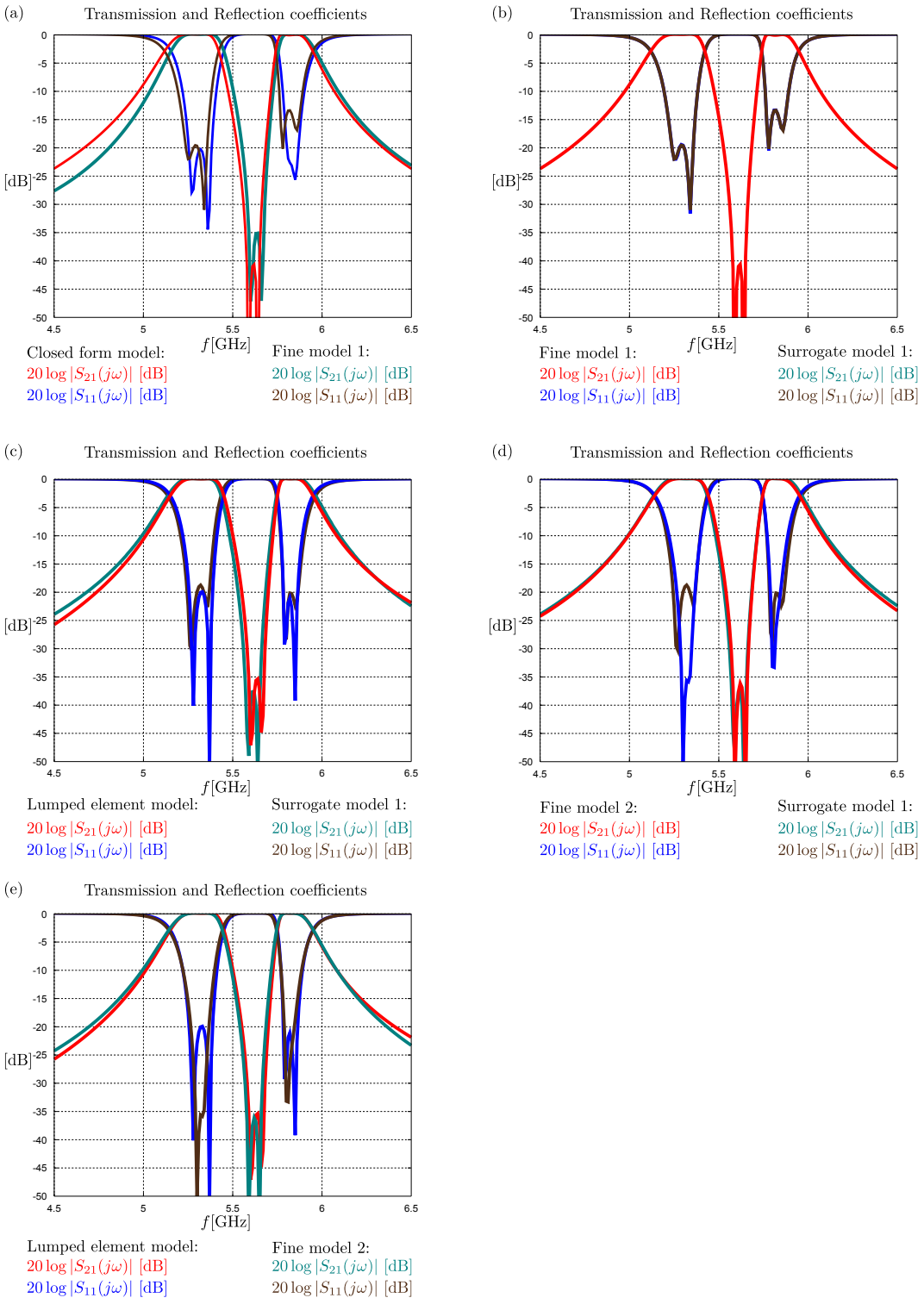

Figure A.15: The frequency response of the ideal lumped element coupled resonator circuit is compared to the frequency response of the initial electromagnetic model in (a). The frequency response of the surrogate model is compared to the frequency response of the initial electromagnetic simulation in (b). The physical dimensions of the surrogate model are now tuned until it meets the design specifications. The frequency response of the tuned surrogate model is compared to the ideal frequency response in (c). A second electromagnetic model is created from the tuned surrogate model. The frequency response of the new electromagnetic model is compared to the tuned surrogate model in (d). The frequency response of the new electromagnetic model is compared to the ideal response in (e).

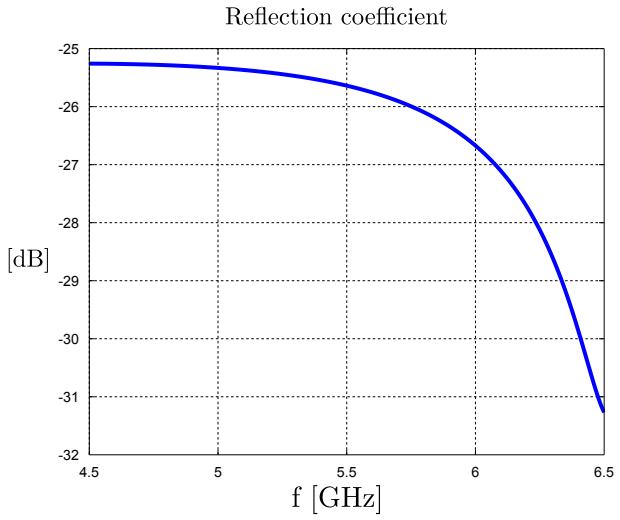

Figure A.16: The design procedure of the transition for the cross-coupled filter in multi-layer stripline is identical to the procedure illustrated in figure A.7. The final reflection coefficient for $l_{t1} = 0.55$ mm, $l_{t2} = 3$ mm and $w_{\text{mid}} = 0.5$ mm is shown above.

A.2.3 Design of SMA-to-stripline transition

A SMA-to-stripline transition can be designed using the technique described in section A.1.4. The same connectors are used for all the filters. The only difference in the design is that the width of the input stripline to the filter is 0.88 mm and that each substrate layer is now 0.508 mm thick. A parameter study of the transition in figure A.7 (b) was performed and it was found that the reflections are a minimum if $l_{t1} = 0.55$ mm, $l_{t2} = 3$ mm and $w_{\text{mid}} = 0.5$ mm. A plot of the associated reflection coefficient is shown in figure A.16. A final electromagnetic simulation of the filter was performed and losses were included. The frequency response of the lossy electromagnetic model is shown in figure A.17 (a). The s-parameter models of the SMA-to-stripline transitions were then cascaded with the lossy electromagnetic model to produce a predicted frequency response of the final filter. The predicted frequency response is shown in figure A.17 (b). In the next subsection we shall discuss the manufacturing process and show the measured results.

A.2.4 Fabrication and measurements

The manufacturing procedure of the multi-layer cross-coupled filter is identical to that described in section A.1.5. Photographs of the manufactured filter are shown in figure A.18. The frequency response of the device was measured and compared to the predicted frequency response. The measured results are shown in figure A.19. The return loss in the second passband did not reach the design specification. It is however still at an acceptable level for the device to be operational.

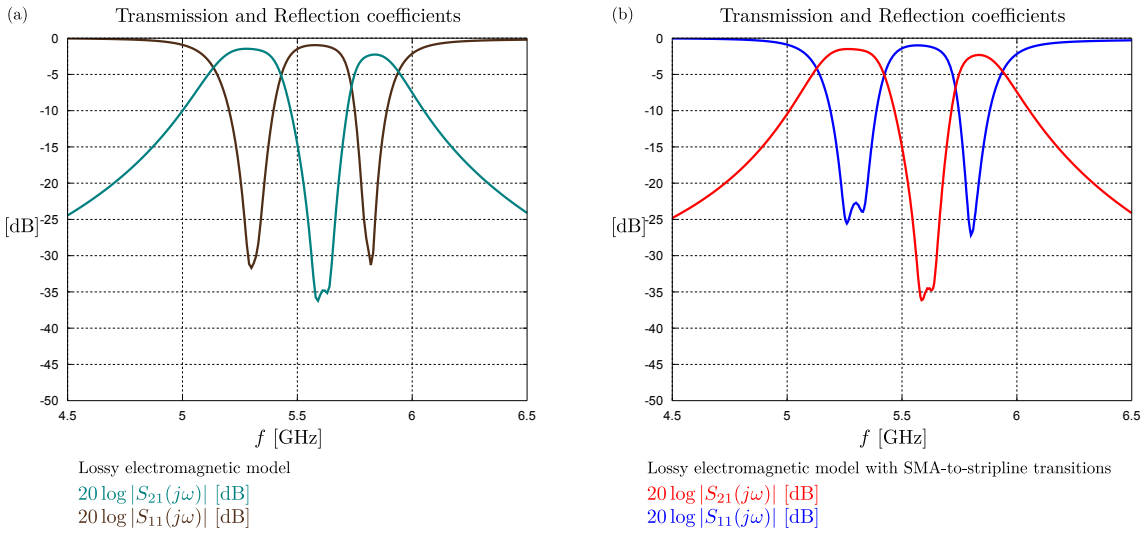

Figure A.17: The final electromagnetic model was simulated in Sonnet and losses were included. The frequency response of the lossy electromagnetic model is shown in (a). The SMA-to-stripline transitions were simulated in CST and losses were also included. The mentioned simulations were cascaded in Microwave Office to provide a realistic prediction of the performance of the manufactured filter. The predicted frequency response of the manufactured filter is shown in (b). The SMA-to-stripline transition has almost a negligible influence on the frequency response of the filter.

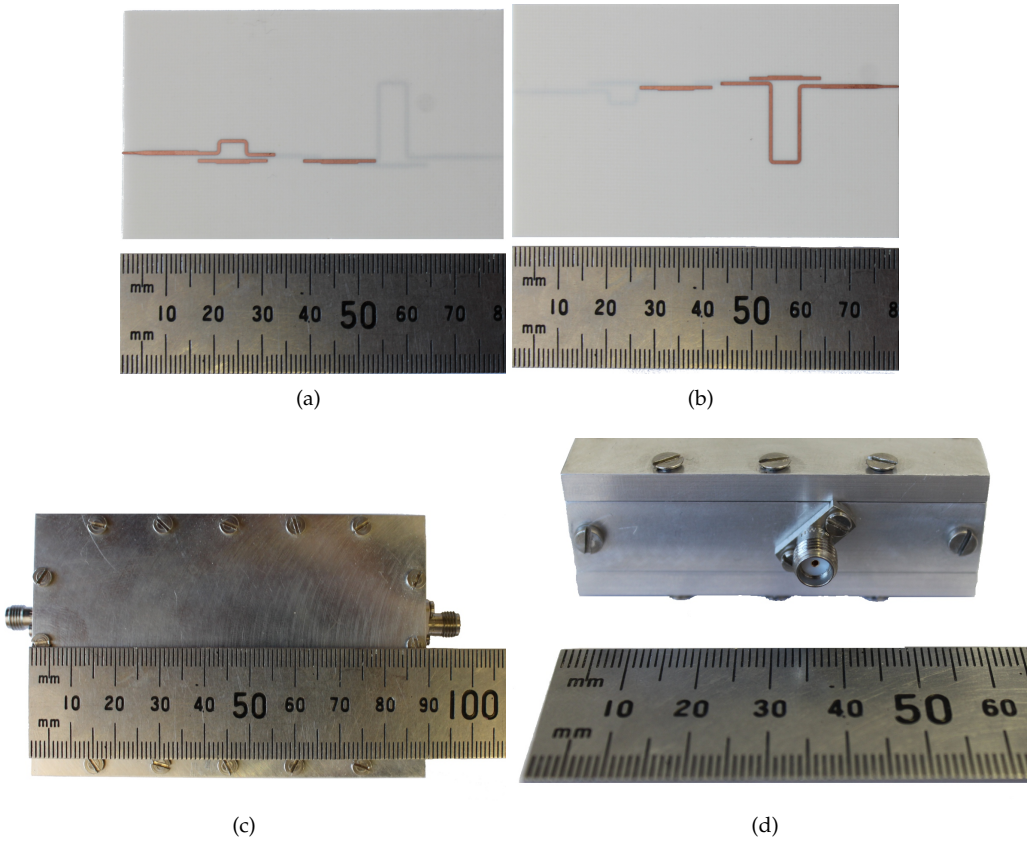

Figure A.18: The conducting layers were manufactured using a photo-etching procedure. The layers were etched onto the opposing sides of the central substrate. The one conducting layer is shown in (a). The other conducting layer is shown in (b). The circuit was built into a metal enclosure as shown in (c). The metal enclosure has a lid on the side to aid the assembly process as shown in (d).

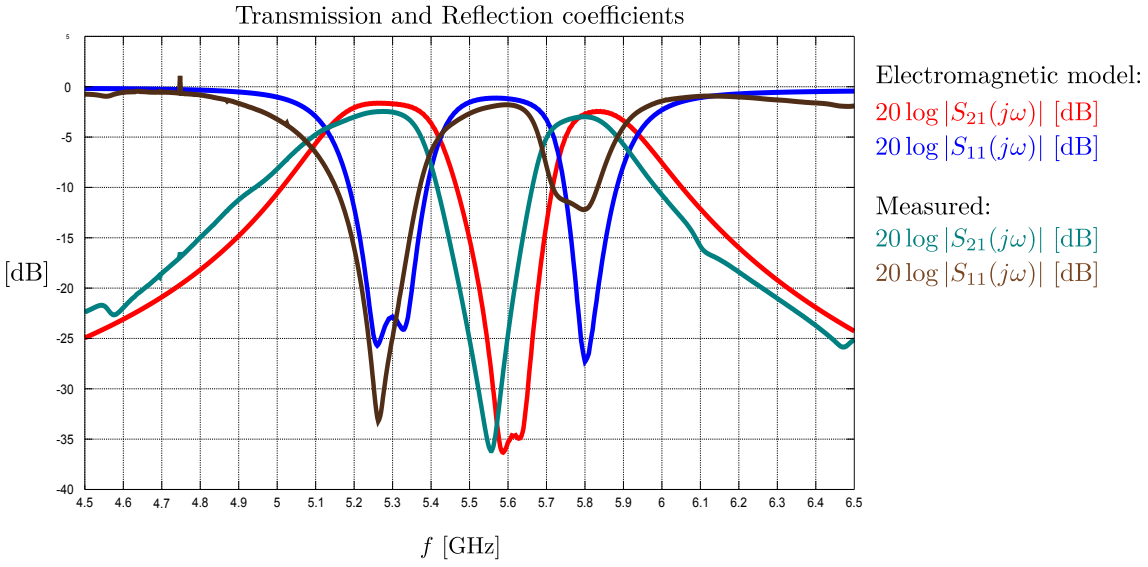

Figure A.19: A comparison of the measured frequency response of the fabricated filter and the predicted frequency response is shown above. The fabricated filter is the cascaded triplet filter manufactured using multi-layer stripline. The predicted frequency response is a lossy electromagnetic model that includes the SMA-to-stripline transitions. There is a good correlation between the predicted performance and the measured results.

Appendix B

Immittance inverters and coupling

In this section we introduce immittance inverters and illustrate why they are used to model coupling between different nodes inside a coupled resonator circuit. We also provide circuits consisting entirely of inductors and capacitors that approximate ideal immittance inverters over finite bandwidths. The theoretical work presented in this section is attributed to Hong and Cameron [78, 61].

B.1 Immittance inverters

Immittance inverters refer to impedance inverters and admittance inverters. Impedance inverters operate like quarter wavelength transmission lines of characteristic impedance K at all frequencies. Likewise, admittance inverters operate like quarter wavelength transmission lines of characteristic admittance J at all frequencies. Consequently, impedance inverters are referred to as K-inverters and admittance inverters are referred to as J-inverters. The inverters and their operation is illustrated in figure B.1. Note that the immittance inverters introduce a 90 degree phase shift. In the next section we shall illustrate why immittance inverters can be used to model coupling in coupled resonator circuits.

B.2 The use of immittance inverters to model coupling

Coupling between resonant nodes inside an $N \times N$ coupled resonator circuit is modelled using mutual inductances. The terminations are coupled to the first and last resonators through ideal transformers. Ideal transformers are also mutually coupled inductors. Coupling using mutual inductance is an abstraction of magnetic field coupling. We shall now illustrate that all the couplings inside an $N \times N$ coupled resonator

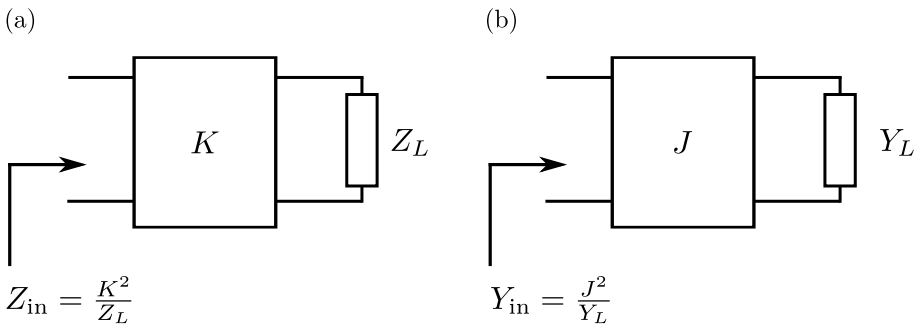

Figure B.1: The definition of an impedance inverter is shown in (a). The definition of an admittance inverter is shown in (b).

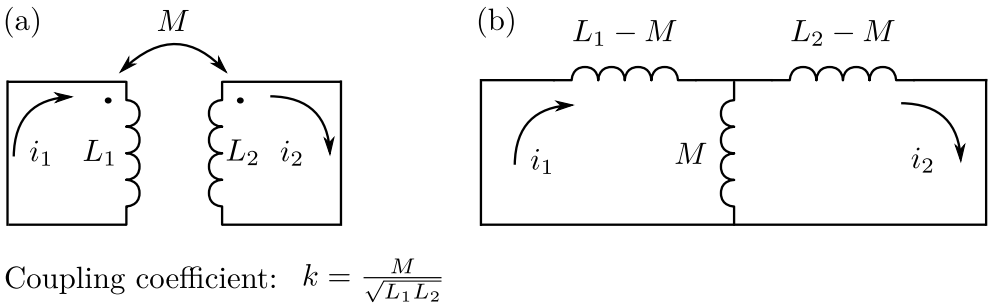

Figure B.2: Resonant nodes inside an $N \times N$ coupled resonator circuit are coupled through mutual inductance. Coupling using mutual inductance is shown in (a). The definition of the coupling coefficient k is also shown. An equivalent circuit for (a) is given in (b). The equivalence can be proven by comparing the loop equations of the circuits in (a) and (b).

circuit can be replaced by appropriate inverters. Figure B.2 (a) contains an illustration of two current loops that are coupled through mutual inductance. This circuit is equivalent to the circuit in figure B.2 (b) due to the equivalence of their loop equations. The loop equations mentioned here are those obtained using Kirchhoff's laws. Suppose we couple energy from a source loop into a loop containing an arbitrary load impedance Z_L. If we assume that the self inductance of our loops is negligible, we can use the equivalent circuit in figure B.3 (a) to describe this situation. The ABCD-parameters of the circuit describing the coupling is given as follows:

$$\begin{bmatrix} V_1 \\ I_1 \end{bmatrix} = \begin{bmatrix} 0 & -j\omega M \\ \frac{1}{j\omega M} & 0 \end{bmatrix} \begin{bmatrix} V_2 \\ I_2 \end{bmatrix} \tag{B.1}$$

The impedance seen from the source loop can now be calculated as follows:

$$\begin{aligned} Z_{\text{in}} &= \frac{V_1}{I_1} \\ &= \frac{j\omega M I_2}{\frac{V_2}{j\omega M}} \\ &= \frac{(\omega M)^2}{Z_L} \end{aligned} \tag{B.2}$$

We now compare equation B.2 with the circuits in figure B.1. It is clear that if two loops are coupled through mutual inductance, the coupling can be modelled using an impedance inverter with $K = \omega M$. The equivalent circuit for inductive coupling using an impedance inverter is shown in figure B.3 (b). Up to this point we only illustrated that magnetic field coupling can be modelled using impedance inverters. It is possible to perform the same derivation using two loops that are coupled using mutual capacitance. Coupling using mutual capacitance is an abstraction of electric field coupling. The result of the analysis is that electric field coupling can be modelled using admittance inverters where $J = \omega C$. In this case C refers to the mutual capacitance between two loops. For most practical situations, coupling between different loops is usually a mixture of electric and magnetic field coupling. Hong proved that mixed coupling is the superposition of electric field coupling and magnetic field coupling. He showed that it is sufficient to model the combined coupling using K inverters for circuits containing series resonators and J inverters for circuits containing shunt resonators.

It is possible to realise immittance inverters using lumped elements. Possible realisations of immittance inverters using capacitors and inductors are provided in figure B.4.

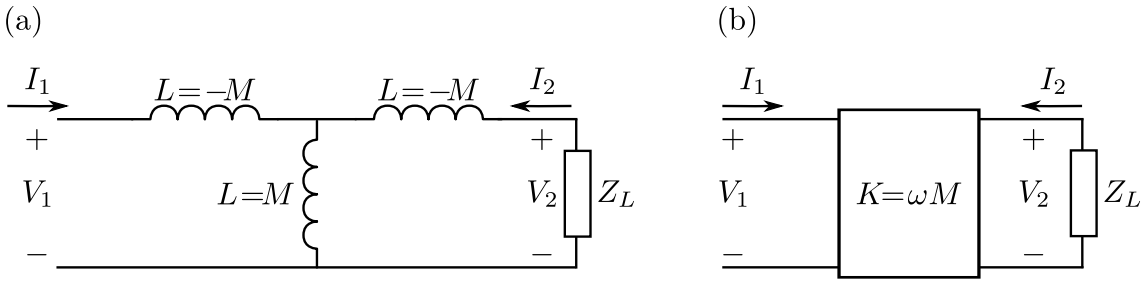

Figure B.3: Energy is coupled through mutual inductance to an arbitrary load impedance. A T-equivalent circuit for the coupling is shown in (a) where it is assumed that the self inductance of the coupling element is zero. An impedance inverter to model the same exchange of energy is shown in (b).

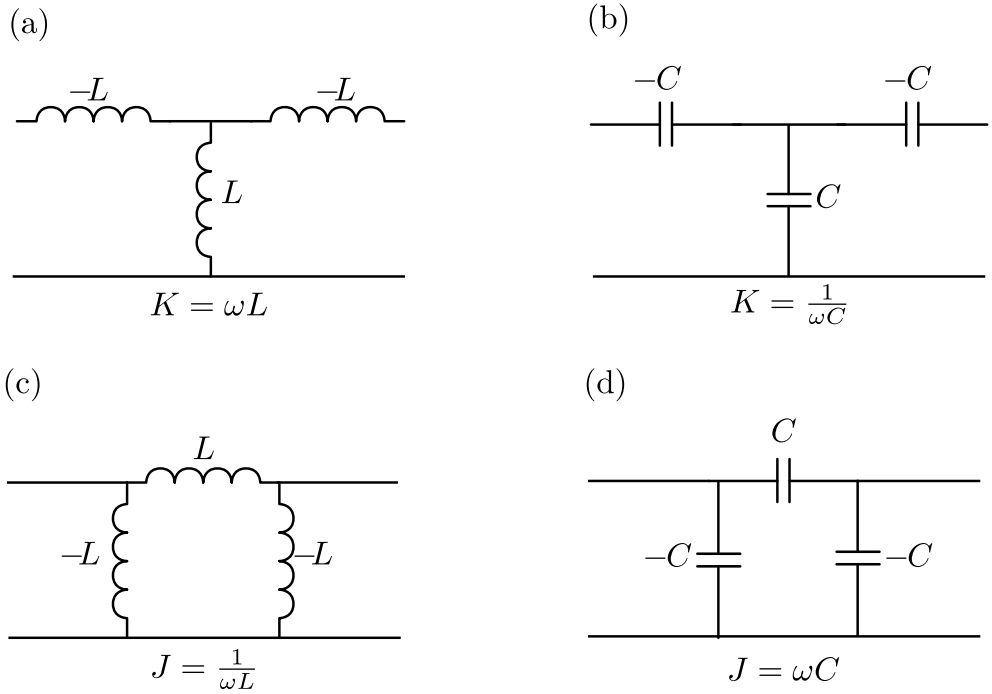

Figure B.4: Practical realisations of the immittance inverters. Impedance inverters are constructed using inductors in (a) and capacitors in (b). Admittance inverters are constructed using inductors in (c) and capacitors in (d).

Appendix C

Filter dimensions

This section contains a listing of the dimensions of the filters designed in this dissertation:

1. Figure C.1 contains the dimensions of the all-pole filter designed in section 8.3.
2. Figure C.2 contains the dimensions of the all-pole filter designed in section A.1.
3. Figure C.3 contains the dimensions of the cross-coupled filter designed in section 9.3.
4. Figure C.4 contains the dimensions of the cross-coupled filter designed in section A.2.
5. Figure C.5 contains the dimensions of the coaxial resonator filter designed in chapter 10.

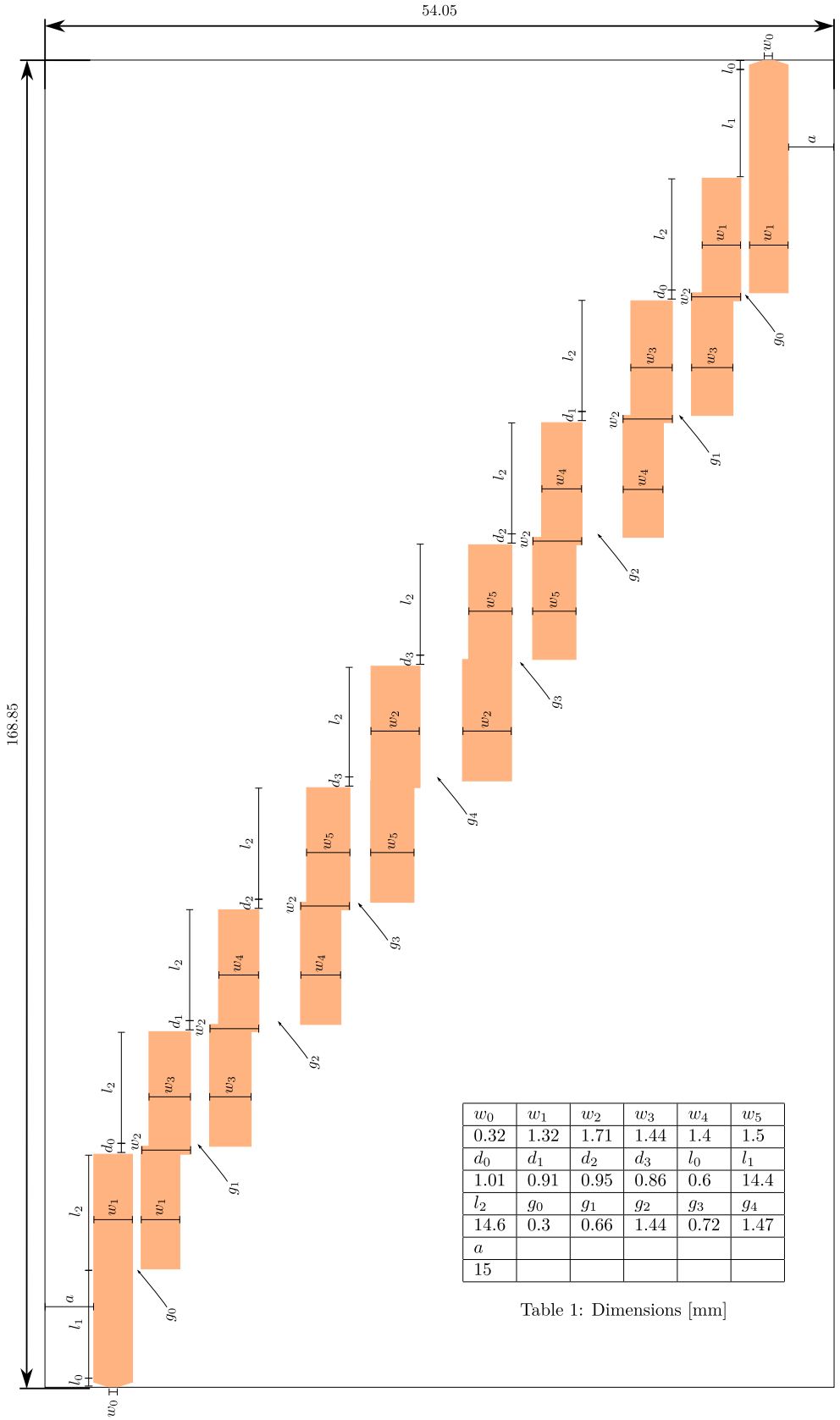

w_0	w_1	w_2	w_3	w_4	w_5
0.32	1.32	1.71	1.44	1.4	1.5
d_0	d_1	d_2	d_3	l_0	l_1
1.01	0.91	0.95	0.86	0.6	14.4
l_2	g_0	g_1	g_2	g_3	g_4
14.6	0.3	0.66	1.44	0.72	1.47
a					
15					

Table 1: Dimensions [mm]

Figure C.1: Dimensions of all-pole filter in stripline is shown above. The substrate used is Rogers 4003C with a thickness of 1.524mm. Copper cladding is 35μm.

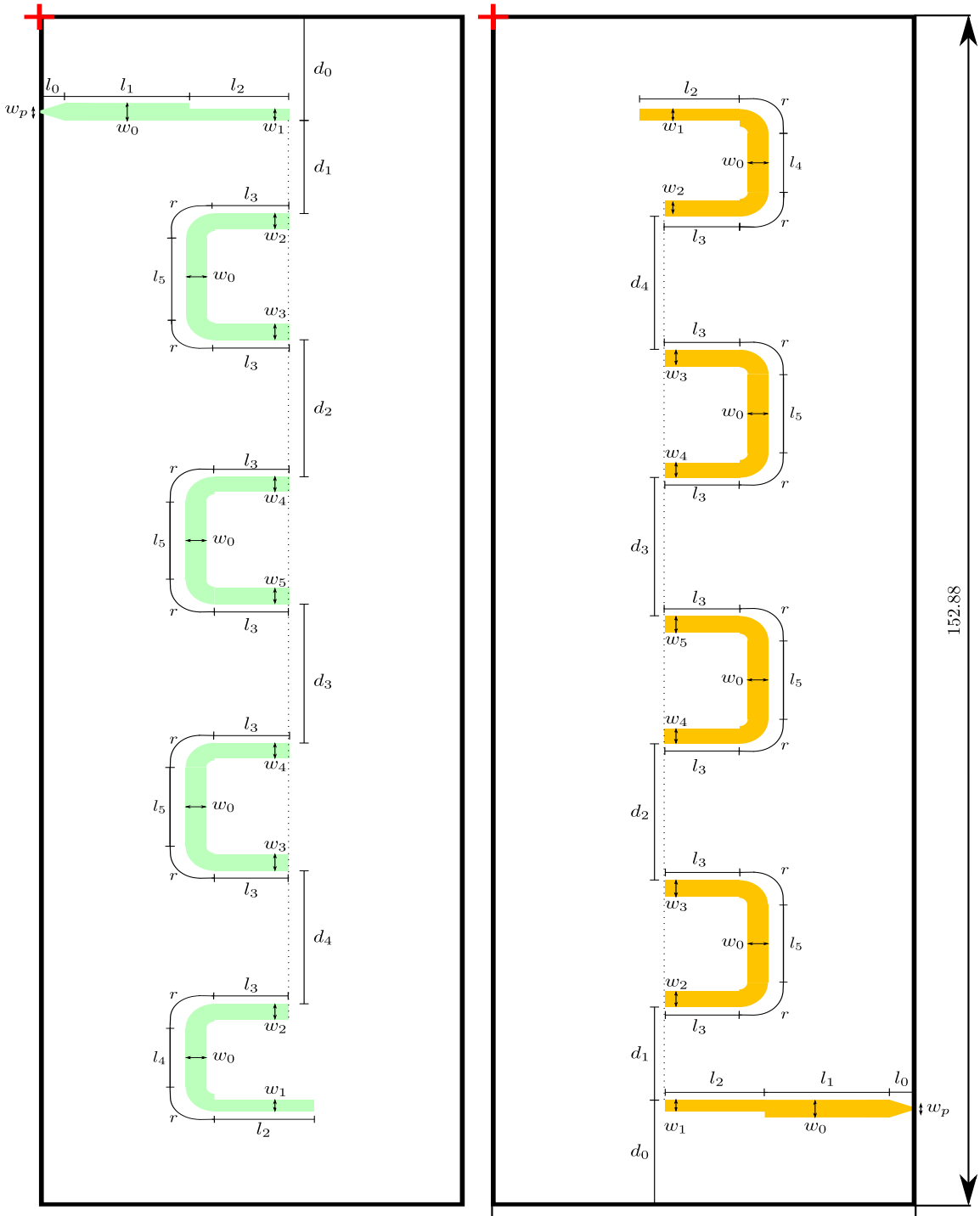

w_p	w_0	w_1	w_2	w_3	w_4
0.32	2.14	1.4	1.9	2	1.84
w_5	l_0	l_1	l_2	l_3	l_4
2	1.23	12.9	10.32	7.7	7.06
l_5	r	d_0	d_1	d_2	d_3
9.52	4.68	17.15	11.22	16.52	16.76
d_4					
16.12					

Table 1: Dimensions [mm]

Figure C.2: Dimensions of the conducting layers of an all-pole filter in multi-layer stripline is shown above. The substrate used is Rogers 4003C with a thickness of 1.524mm. Copper cladding is 35μm. The different colours represent different conducting layers. The green conducting layer is the top layer. The red cross indicates the alignment of the layers.

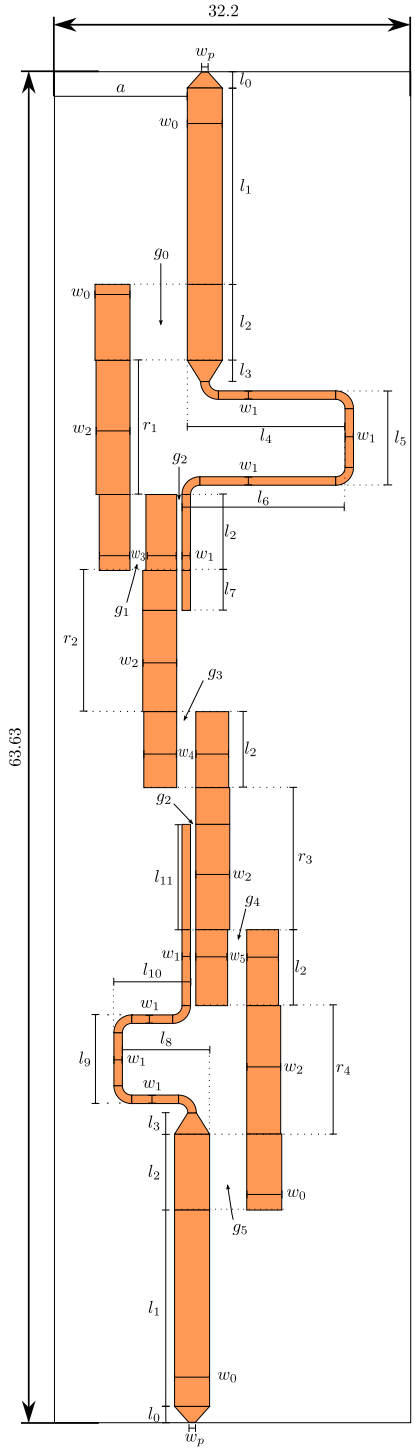

w_p	w_0	w_1	w_2	w_3	w_4	w_5	l_0	l_1
0.31	1.65	0.4	1.6	1.45	1.55	0.9	0.75	9.25
l_2	l_3	l_4	l_5	l_6	l_7	l_8	l_9	l_{10}
3.58	1	7.43	4.45	7.68	1.88	4.11	4.17	3.61
l_{11}	g_0	g_1	g_2	g_3	g_4 g_5	r_1	r_2	r_3
4.96	2.7	0.75	0.25	0.9	0.9	6.32	6.65	6.69
r_4	a							
6.05	14.35							

Table 1: Dimensions [mm]

Figure C.3: Dimensions of cross-coupled filter in stripline is shown above. Substrate used is Rogers 4003C with a thickness of 1.524mm. Copper cladding is 35μm.

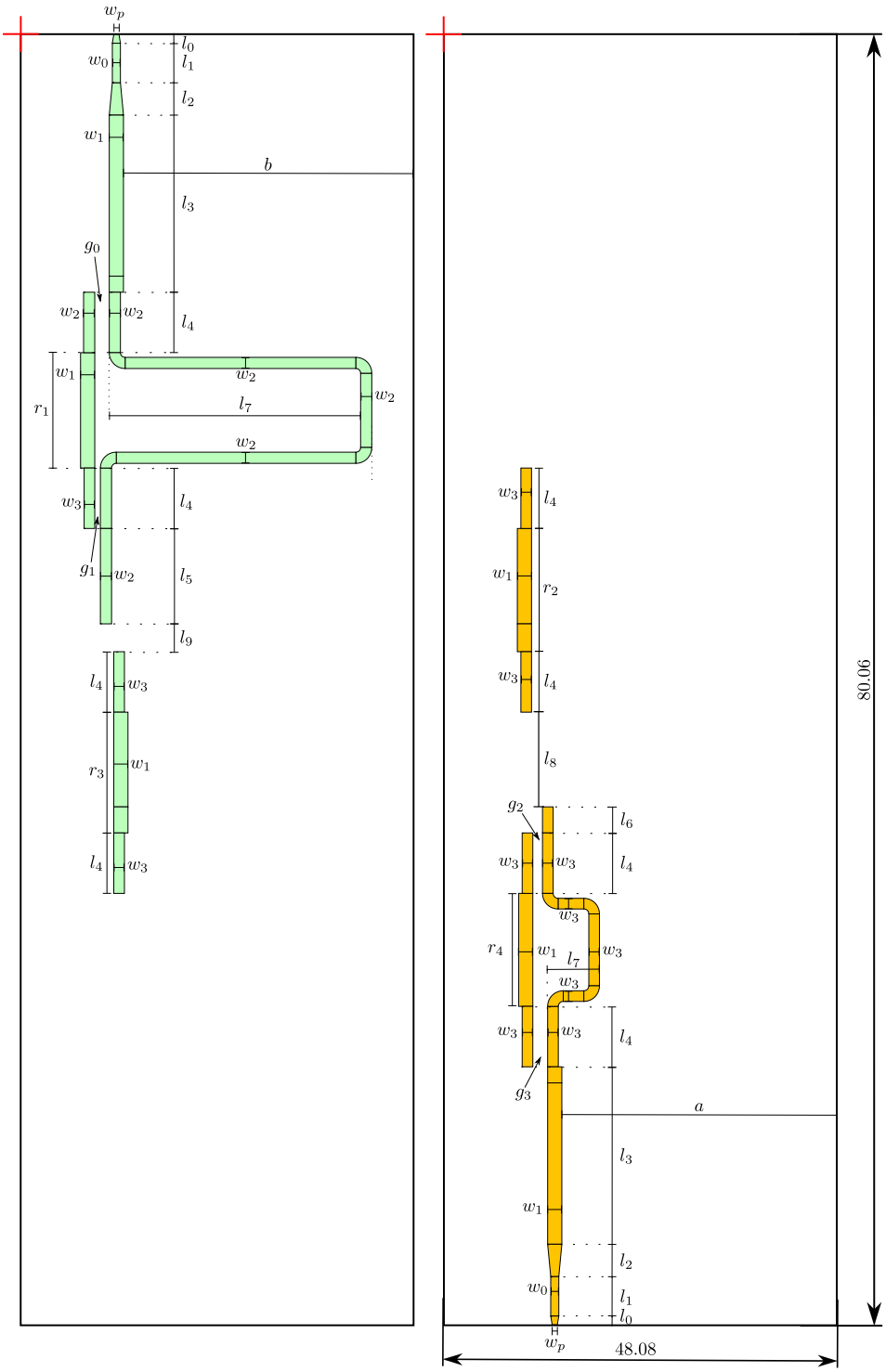

w_p	w_0	w_1	w_2	w_3	r_1	r_2	r_3
0.32	0.5	0.88	0.69	0.66	7.16	7.65	7.49
r_4	g_0	g_1	g_2	l_0	l_1	l_2	l_3
7	0.9	0.35	0.6	0.55	2.45	2	10
l_4	l_5	l_6	l_7	l_8	l_9	a	b
3.75	5.92	1.62	15.59	5.88	1.73	29.47	30.41

Table 1: Dimensions [mm]

Figure C.4: Dimensions of cross-coupled filter in multi-layer stripline is shown above. Substrate used is Rogers 4003C with a thickness of 0.508mm. Copper cladding is 35μm. The different colours represent different conducting layers. The green conducting layer is the top layer. The red cross indicates the alignment of the layers.

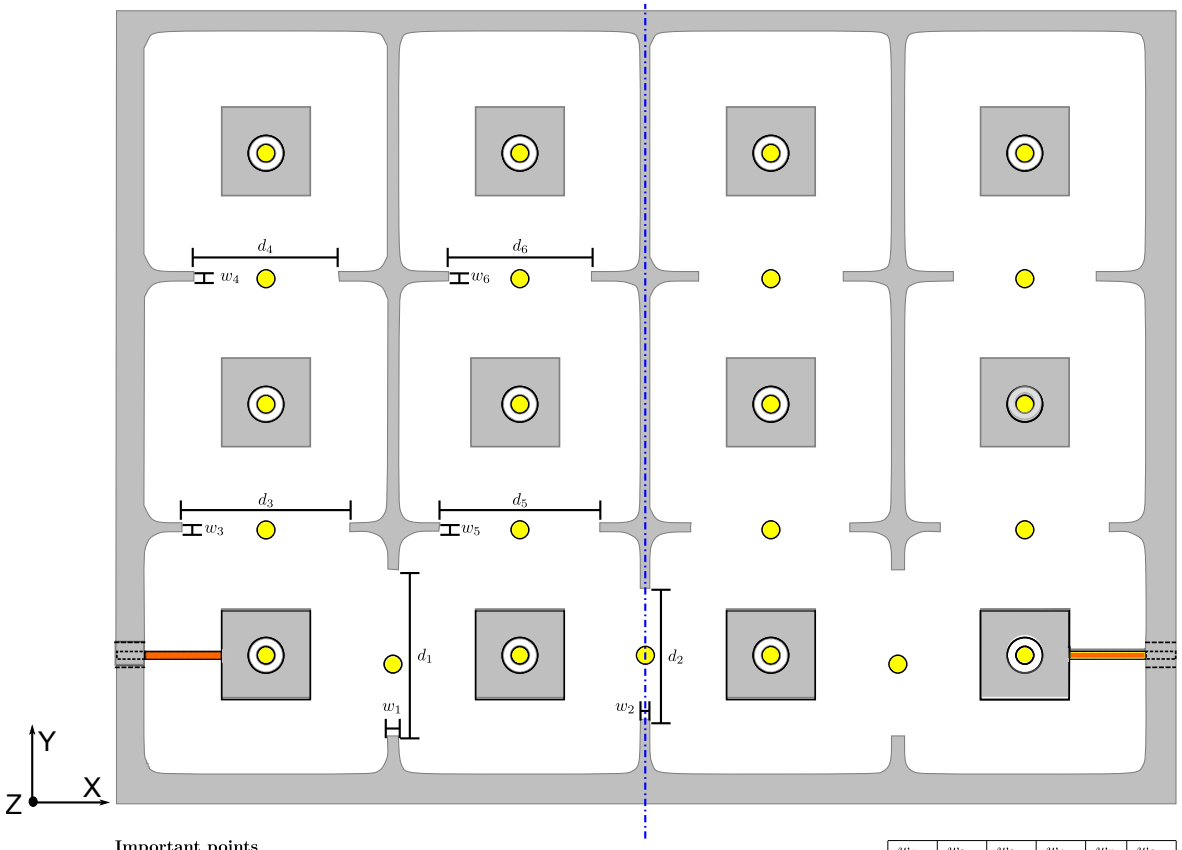

Important points

- All resonators and all cavities are identical. The coupling irises between them are not identical.
- Filter is symmetric around its centre line (refer to figure).
- All internal radii are 3 mm.
- Resonators have a square base and have dimensions: 1.5 cm × 1.5 cm × 2.2 cm.
- All resonators have a cylindrical opening in their centres, that has a diameter of 6 mm, and sinks from the top to a depth of 8 mm. The openings are there for the coupling screws.
- All tuning screws have a diameter of 3 mm.
- Each resonator is located exactly in the centre of its cavity (1.3 cm from the the 4 walls surrounding it).
- All cavities have the same dimensions: 4.1 cm × 4.1 cm × 2.5 cm.
- The dimensions of the coupling irises are indicated on the drawing. All coupling irises have a height of 2.2 cm.
- All tuning screws that are associated with resonators are located exactly in the centre of the resonator in the XY plane.
- All of the tuning screws associated with the couplings are located exactly in the centre of the coupling irises. Their positions can be deduced from the dimensions of the irises.
- The XYZ position of the source SMA is (0 mm, 25.5 mm, 11.85 mm). The SMA connector used for this design is the Huber and Suhner 23_SMA-50-0-3/111_N connector

w_1	w_2	w_3	w_4	w_5	w_6
2	1.5	1.5	1.5	1.5	1.5
d_1	d_2	d_3	d_4	d_5	d_6
28.2	22.2	28.6	24.4	27	24.4

Table 1: Dimensions [mm]

Figure C.5: Dimensions of coaxial resonator filter is shown above. The filter was constructed using a milling machine.

Bibliography

[1] G. R. K. Rao and G. Radhamani, *WiMAX: A Wireless Technology Revolution*. Auerbach Publications, 2007.

[2] D. M. Pozar, *Microwave Engineering*. Wiley, 2004.

[3] V. Belevitch, "Summary of the history of circuit theory," *Proceedings of the IRE*, vol. 50, no. 5, pp. 848 –855, may 1962.

[4] S. Darlington, "A history of network synthesis and filter theory for circuits composed of resistors, inductors, and capacitors," *Circuits and Systems I: Fundamental Theory and Applications, IEEE Transactions on*, vol. 46, no. 1, pp. 4 –13, jan 1999.

[5] R. Foster, "A reactance theorem," *Bell Syst. Tech. J*, vol. 3, no. 2, pp. 259–267, 1924.

[6] M. Dishal, "Design of dissipative band-pass filters producing desired exact amplitude-frequency characteristics," *Proceedings of the IRE*, vol. 37, no. 9, pp. 1050 – 1069, sept. 1949.

[7] G. Matthaei, "Direct-coupled, band-pass filters with resonators," in *IRE International Convention Record*, vol. 6, mar 1958, pp. 98 – 111.

[8] S. Cohn, "Direct-coupled-resonator filters," *Proceedings of the IRE*, vol. 45, no. 2, pp. 187 –196, feb. 1957.

[9] G. Matthaei, L. Young, and E. Jones, *Microwave filters, impedance-matching networks, and coupling structures*, ser. Artech House microwave library. McGraw-Hill, 1964, no. v. 1. [Online]. Available: http://books.google.co.za/books?id=cRMoAQAAMAAJ

[10] A. Williams, "A four-cavity elliptic waveguide filter," *Microwave Theory and Techniques, IEEE Transactions on*, vol. 18, no. 12, pp. 1109 – 1114, dec 1970.

[11] A. Atia and A. Williams, "Narrow-bandpass waveguide filters," *Microwave Theory and Techniques, IEEE Transactions on*, vol. 20, no. 4, pp. 258 – 265, apr 1972.

[12] A. Atia, A. Williams, and R. Newcomb, "Narrow-band multiple-coupled cavity synthesis," *Circuits and Systems, IEEE Transactions on*, vol. 21, no. 5, pp. 649 – 655, sep 1974.

[13] R. Cameron and J. Rhodes, "Asymmetric realisations for dual-mode bandpass filters," in *Microwave symposium Digest, 1980 IEEE MTT-S International*, may 1980, pp. 138 –140.

[14] R. Cameron, "General coupling matrix synthesis methods for chebyshev filtering functions," *Microwave Theory and Techniques, IEEE Transactions on*, vol. 47, no. 4, pp. 433 –442, apr 1999.

[15] ——, "Advanced coupling matrix synthesis techniques for microwave filters," *Microwave Theory and Techniques, IEEE Transactions on*, vol. 51, no. 1, pp. 1 – 10, jan 2003.

[16] J. Lee, M. S. Uhm, and I.-B. Yom, "A dual-passband filter of canonical structure for satellite applications," *Microwave and Wireless Components Letters, IEEE*, vol. 14, no. 6, pp. 271 – 273, june 2004.

[17] S.-F. Chang, Y.-H. Jeng, and J.-L. Chen, "Dual-band step-impedance bandpass filter for multimode wireless lans," *Electronics Letters*, vol. 40, no. 1, pp. 38 – 39, jan. 2004.

[18] L.-C. Tsai and C.-W. Hsue, "Dual-band bandpass filters using equal-length coupled-serial-shunted lines and z-transform technique," *Microwave Theory and Techniques, IEEE Transactions on*, vol. 52, no. 4, pp. 1111 – 1117, april 2004.

[19] X. Guan, Z. Ma, P. Cai, G. Li, Y. Kobayashi, T. Anada, and G. Hagiwara, "A dual-band bandpass filter synthesized by using frequency transformation and circuit conversion technique," in *Microwave Conference Proceedings, 2005. APMC 2005. Asia-Pacific Conference Proceedings*, vol. 4, dec. 2005, p. 4 pp.

[20] G. Macchiarella and S. Tamiazzo, "Design techniques for dual-passband filters," *Microwave Theory and Techniques, IEEE Transactions on*, vol. 53, no. 11, pp. 3265 – 3271, nov. 2005.

[21] J. Lee, M. S. Uhm, and J. H. Park, "Synthesis of a self-equalized dual-passband filter," *Microwave and Wireless Components Letters, IEEE*, vol. 15, no. 4, pp. 256–258, 2005.

[22] M. Mokhtaari, J. Bornemann, K. Rambabu, and S. Amari, "Coupling-matrix design of dual and triple passband filters," *Microwave Theory and Techniques, IEEE Transactions on*, vol. 54, no. 11, pp. 3940–3946, 2006.

[23] X. Guan, Z. Ma, P. Cai, Y. Kobayashi, T. Anada, and G. Hagiwara, "Synthesis of dual-band bandpass filters using successive frequency transformations and circuit conversions," *Microwave and Wireless Components Letters, IEEE*, vol. 16, no. 3, pp. 110–112, 2006.

[24] S. Bila, R. Cameron, P. Lenoir, V. Lunot, and F. Seyfert, "Chebyshev synthesis for multi-band microwave filters," in *Microwave Symposium Digest, 2006. IEEE MTT-S International*, 2006, pp. 1221–1224.

[25] A. Garcia-Lamperez and M. Salazar-Palma, "Dual band filter with split-ring resonators," in *Microwave Symposium Digest, 2006. IEEE MTT-S International*, 2006, pp. 519–522.

[26] J. Lee and K. Sarabandi, "A synthesis method for dual-passband microwave filters," *Microwave Theory and Techniques, IEEE Transactions on*, vol. 55, no. 6, pp. 1163 –1170, june 2007.

[27] S.-H. Han, T.-S. Yun, H. Nam, I.-w. Lee, K.-M. Oh, and J.-C. Lee, "Dual-band bandpass filter using stepped impedance resonator with analytical tapped-line feeding," in *Microwave Conference, 2007. APMC 2007. Asia-Pacific*. IEEE, 2007, pp. 1–4.

[28] A. Garcia Lamperez, "Analytical synthesis algorithm of dual-band filters with asymmetric pass bands and generalized topology," in *Microwave Symposium, 2007. IEEE/MTT-S International*. IEEE, 2007, pp. 909–912.

[29] M. Mokhtaari, J. Bornemann, and S. Amari, "Dual-band stepped-impedance filters for ultra-wideband applications," in *Microwave Conference, 2007. European*. IEEE, 2007, pp. 779–782.

[30] D. Deslandes and F. Boone, "Iterative design techniques for all-pole dual-bandpass filters," *Microwave and Wireless Components Letters, IEEE*, vol. 17, no. 11, pp. 775 –777, nov. 2007.

[31] H.-M. Lee and C.-M. Tsai, "Dual-band filter design with flexible passband frequency and bandwidth selections," *Microwave Theory and Techniques, IEEE Transactions on*, vol. 55, no. 5, pp. 1002–1009, 2007.

[32] G. Macchiarella and S. Tamiazzo, "Dual-band filters for base station multi-band combiners," in *Microwave Symposium, 2007. IEEE/MTT-S International*. IEEE, 2007, pp. 1289–1292.

[33] F. Seyfert and S. Bila, "General synthesis techniques for coupled resonator networks," *Microwave Magazine, IEEE*, vol. 8, no. 5, pp. 98–104, 2007.

[34] A.-S. Liu, T.-Y. Huang, and R.-B. Wu, "A dual wideband filter design using frequency mapping and stepped-impedance resonators," *Microwave Theory and Techniques, IEEE Transactions on*, vol. 56, no. 12, pp. 2921–2929, 2008.

[35] P. K. Singh, S. Basu, and Y.-H. Wang, "Miniature dual-band filter using quarter wavelength stepped impedance resonators," *Microwave and Wireless Components Letters, IEEE*, vol. 18, no. 2, pp. 88–90, 2008.

[36] V. Lunot, F. Seyfert, S. Bila, and A. Nasser, "Certified computation of optimal multiband filtering functions," *Microwave Theory and Techniques, IEEE Transactions on*, vol. 56, no. 1, pp. 105–112, 2008.

[37] S.-G. Mao and M.-S. Wu, "Design of artificial lumped-element coplanar waveguide filters with controllable dual-passband responses," *Microwave Theory and Techniques, IEEE Transactions on*, vol. 56, no. 7, pp. 1684–1692, 2008.

[38] J. Lee and K. Sarabandi, "Design of triple-passband microwave filters using frequency transformations," *Microwave Theory and Techniques, IEEE Transactions on*, vol. 56, no. 1, pp. 187 –193, jan. 2008.

[39] D. Deslandes and F. Boone, "An iterative design procedure for the synthesis of generalized dual-bandpass filters," *International Journal of RF and Microwave Computer-Aided Engineering*, vol. 19, no. 5, pp. 607–614, 2009.

[40] M.-S. Wu, Y.-Z. Chueh, J.-C. Yeh, and S.-G. Mao, "Synthesis of triple-band and quad-band bandpass filters using lumped-element coplanar waveguide resonators," *Progress In Electromagnetics Research B*, vol. 13, pp. 433–451, 2009.

[41] C. Karpuz, A. Gorur, E. Gunturkun, and A. Gorur, "Asymmetric response dual-mode dual-band bandstop filters having simple and understandable topology," in *Microwave Conference, 2009. APMC 2009. Asia Pacific*. IEEE, 2009, pp. 925–928.

[42] C. Karpuz and A. Gorur, "Dual-mode dual-band microstrip filters," in *Microwave Conference, 2009. EuMC 2009. European*. IEEE, 2009, pp. 105–108.

[43] H.-B. Qin, Y.-W. Zhai, and Y.-J. Zhao, "Synthesis method for chebyshev dual-band microwave filters," *Journal of Electromagnetic Waves and Applications*, vol. 24, no. 2-3, pp. 307–317, 2010.

[44] M.-L. Chuang, "Dual-band microstrip coupled filters with hybrid coupling paths," *Microwaves, Antennas & Propagation, IET*, vol. 4, no. 7, pp. 947–954, 2010.

[45] Y.-T. Kuo, J.-C. Lu, C.-K. Liao, and C.-Y. Chang, "New multiband coupling matrix synthesis technique and its microstrip implementation," *Microwave Theory and Techniques, IEEE Transactions on*, vol. 58, no. 7, pp. 1840 –1850, july 2010.

[46] X. Guan, S. Jiang, L. Shen, H. Liu, G. Li, and D. Xu, "A microstrip dual-band bandpass filter based on a novel admittance inverter," in *Microwave and Millimeter Wave Technology (ICMMT), 2010 International Conference on*. IEEE, 2010, pp. 577–580.

[47] S. Luo, L. Zhu, and S. Sun, "A dual-band ring-resonator bandpass filter based on two pairs of degenerate modes," *Microwave Theory and Techniques, IEEE Transactions on*, vol. 58, no. 12, pp. 3427–3432, 2010.

[48] A. Garcia-Lamperez and M. Salazar-Palma, "Single-band to multiband frequency transformation for multiband filters," *Microwave Theory and Techniques, IEEE Transactions on*, vol. 59, no. 12, pp. 3048–3058, 2011.

[49] F. Liang, B. Luo, W. Lu, and X. Wang, "A compact dual-band filter with close passbands using asymmetric $\lambda/4$ resonator pairs with shared via-hole ground," *Journal of Electromagnetic Waves and Applications*, vol. 25, no. 8-9, pp. 1289–1296, 2011.

[50] H.-W. Wu and R.-Y. Yang, "A new quad-band bandpass filter using asymmetric stepped impedance resonators," *Microwave and Wireless Components Letters, IEEE*, vol. 21, no. 4, pp. 203–205, 2011.

[51] A. Mohan, S. Singh, and A. Biswas, "Generalized synthesis and design of symmetrical multiple passband filters," *Progress In Electromagnetics Research B*, vol. 42, pp. 115–139, 2012.

[52] M. T. Doan, W. Che, and W. Feng, "Novel compact dual-band bandpass filter with multiple transmission zeros and good selectivity," in *Microwave and Millimeter Wave Technology (ICMMT), 2012 International Conference on*, vol. 5. IEEE, 2012, pp. 1–4.

[53] X. Yu, X. Tang, F. Xiao, and F. Xu, "A new class of multi-band waveguide filters," in *Microwave and Millimeter Wave Technology (ICMMT), 2012 International Conference on*, vol. 4, 2012, pp. 1–4.

[54] F. Yang, H.-x. Yu, X.-y. He, Y. Zhou, and R.-z. Liu, "Novel multi-band filter design and substrate integrated waveguide filter realization," in *Microwave Symposium Digest (MTT), 2012 IEEE MTT-S International*. IEEE, 2012, pp. 1–3.

[55] Y. Dong, C.-T. Wu, and T. Itoh, "Miniaturised multi-band substrate integrated waveguide filters using complementary split-ring resonators," *IET microwaves, antennas & propagation*, vol. 6, no. 6, pp. 611–620, 2012.

[56] X. Shang, Y. Wang, G. Nicholson, and M. Lancaster, "Design of multiple-passband filters using coupling matrix optimisation," *IET microwaves, antennas & propagation*, vol. 6, no. 1, pp. 24–30, 2012.

[57] J.-K. Xiao and W.-J. Zhu, "Compact split ring sir bandpass filters with dual and tri-band," *Progress In Electromagnetics Research C*, vol. 25, pp. 93–105, 2012.

[58] W. Wang and X. Lin, "A dual-band bandpass filter using open-loop resonator," in *Millimeter Waves (GSMM), 2012 5th Global Symposium on*. IEEE, 2012, pp. 575–578.

[59] A. Genc, R. Baktur, and R. J. Jost, "Dual-bandpass filters with individually controllable passbands."

[60] C.-Y. Hsu, C.-Y. Chen, and H.-R. Chuang, "Microstrip dual-band bandpass filter design with closely specified passbands," 2013.

[61] R. J. Cameron, R. Mansour, and C. M. Kudsia, *Microwave Filters for Communication Systems: Fundamentals, Design and Applications*. Wiley-Interscience, 2007.

[62] G. Temes and J. LaPatra, *Introduction to circuit synthesis and design*. McGraw-Hill, 1977. [Online]. Available: http://books.google.co.za/books?id=T-lSAAAAMAAJ

[63] J. Bell, H.C., "Canonical asymmetric coupled-resonator filters," *Microwave Theory and Techniques, IEEE Transactions on*, vol. 30, no. 9, pp. 1335 –1340, sep. 1982.

[64] S. Tamiazzo and G. Macchiarella, "An analytical technique for the synthesis of cascaded n-tuplets cross-coupled resonators microwave filters using matrix rotations," *Microwave Theory and Techniques, IEEE Transactions on*, vol. 53, no. 5, pp. 1693 – 1698, may 2005.

[65] R. Cameron, M. Yu, and Y. Wang, "Direct-coupled microwave filters with single and dual stopbands," *Microwave Theory and Techniques, IEEE Transactions on*, vol. 53, no. 11, pp. 3288 – 3297, nov. 2005.

[66] Y. Zhang, K. Zaki, J. Ruiz-Cruz, and A. Atia, "Analytical synthesis of generalized multi-band microwave filters," in *Microwave Symposium, 2007. IEEE/MTT-S International*, june 2007, pp. 1273 –1276.

[67] H. C. Bell, "Zolotarev bandpass filters," *IEEE Transactions on Microwave Theory and Techniques*, vol. 49, pp. 2357–2362, 2001.

[68] T. G. Brand, P. Meyer, and R. H. Geschke, "Designing multiband coupled-resonator filters using reactance transformations," *International Journal of RF and Microwave Computer-Aided Engineering*, pp. n/a–n/a, 2014. [Online]. Available: http://dx.doi.org/10.1002/mmce.20826

[69] M. C.-B. e. a. Brand, Geschke, "Advances in multi-band microstrip filters," 2014, cambridge University Press, ISBN 9781107081970, Unpublished at current date. In the process of being edited.

[70] I. C. Hunter, *Theory and Design of Microwave Filters (IEE Electromagnetic Waves Series)*. The Institution of Engineering and Technology, 2001.

[71] J. Rhodes and S. Alseyab, "The generalized chebyshev low-pass prototype filter," *International Journal of Circuit Theory and Applications*, vol. 8, no. 2, pp. 113–125, 1980.

[72] H. Jeffreys and B. Jeffreys, *Methods of Mathematical Physics (Cambridge Mathematical Library)*. Cambridge University Press, 2000.

[73] S. Karni, *Analysis of Electrical Networks*. Wiley, 1986.

[74] R. Baum, "Design of unsymmetrical band-pass filters," *Circuit Theory, IRE Transactions on*, vol. 4, no. 2, pp. 33 – 40, jun 1957.

[75] V. Belevitch, *Classical Network Theory*. Holden-Day, 1968.

[76] D. G. Zill, *Advanced Engineering Mathematics, Third Edition*. Jones and Bartlett Publishers, 2006.

[77] M. Dishal, "Alignment and adjustment of synchronously tuned multiple-resonant-circuit filters," *Proceedings of the IRE*, vol. 39, no. 11, pp. 1448 –1455, nov. 1951.

[78] J.-S. G. Hong and M. J. Lancaster, *Microstrip Filters for RF/Microwave Applications*. Wiley-Interscience, 2001.

[79] J. Meng, S. Koziel, J. Bandler, M. Bakr, and Q. Cheng, "Tuning space mapping: A novel technique for engineering design optimization," in *Microwave Symposium Digest, 2008 IEEE MTT-S International*, june 2008, pp. 991 –994.

[80] A. Simine, V. Piatnitsa, A. Lapshin, E. Jakku, D. Kholodnyak, S. Leppaevuori, and I. Vendik, "Design of quasi-lumped-element ltcc filters and duplexers for wireless communications," in *Microwave Conference, 2003. 33rd European*, oct. 2003, pp. 911 –914.

[81] J. Stewart, *Calculus*. Brooks Cole, 2011. [Online]. Available: http://www.amazon.com/Calculus-James-Stewart/dp/0538497815%3FSubscriptionId%3D0JYN1NVW651KCA56C102%26tag%3Dtechkie-20%26linkCode%3Dxm2%26camp%3D2025%26creative%3D165953%26creativeASIN%3D0538497815

[82] I. Awai, "Meaning of resonator's coupling coefficient in bandpass filter design," *Electronics and Communications in Japan (Part II: Electronics)*, vol. 89, no. 6, pp. 1–7, 2006.

[83] I. Awai and Y. Zhang, "Coupling coefficient of resonators. an intuitive way of its understanding," *Electronics and Communications in Japan (Part II: Electronics)*, vol. 90, no. 9, pp. 11–18, 2007. [Online]. Available: http://dx.doi.org/10.1002/ecjb.20342

[84] M. Makimoto and S. Yamashita, "Bandpass filters using parallel coupled stripline stepped impedance resonators," *Microwave Theory and Techniques, IEEE Transactions on*, vol. 28, no. 12, pp. 1413 – 1417, dec 1980.

[85] B. C. Wadell, *Transmission Line Design Handbook (Artech House Antennas and Propagation Library) (Artech House Microwave Library)*. Artech Print on Demand, 1991.

[86] J.-C. Lu, C.-K. Liao, and C.-Y. Chang, "Microstrip parallel-coupled filters with cascade trisection and quadruplet responses," *Microwave Theory and Techniques, IEEE Transactions on*, vol. 56, no. 9, pp. 2101 – 2110, sept. 2008.

[87] J. Ness, "A unified approach to the design, measurement, and tuning of coupled-resonator filters," *Microwave Theory and Techniques, IEEE Transactions on*, vol. 46, no. 4, pp. 343 –351, apr 1998.